Design and Development of Bis-azo Based Homogeneous 3d-Metal Catalysts for Auto-Tandem Annulation of N-Heterocycles via Oxidative Dehydrogenation

Thesis Submitted for the Degree of

Doctor of Philosophy (Science)

By

Debashis Jana

Department of Chemistry

JADAVPUR UNIVERSITY

Jadavpur, Kolkata – 700 032, India

March, 2025

Prof. Kausikisankar Pramanik,
Professor,
Department of Chemistry

JADAVPUR UNIVERSITY
KOLKATA - 7 0 0 0 3 2, I N D I A
E-mail:
kausikis.pramanik@jadavpuruniversity.in
Mobile: +91-89109 35661

CERTIFICATE FROM THE SUPERVISORS

This is to certify that the thesis entitled "**Design and Development of Bis-azo Based Homogeneous 3d-Metal Catalysts for Auto-Tandem Annulation of N-Heterocycles via Oxidative Dehydrogenation**" submitted by **Mr. Debashis Jana** who got his name registered on **March 22, 2021** for the award of Ph.D. (Science) degree of Jadavpur University, is absolutely based on his own work under my supervision and that neither this thesis nor any part of it has been submitted for either any degree/diploma or any other academic award anywhere before.

Date: 19.03.2025

(Prof. Kausikisankar Pramanik)
Signature of the Supervisor & date with seal
Department of Chemistry
Jadavpur University
Kolkata-700 032

Dr. Kausikisankar Pramanik
Professor of Chemistry
Jadavpur University
Kolkata-700032

Dedicated

To

My Grandfather

PREFACE

The thesis entitled **"Design and Development of Bis-azo Based Homogeneous 3d-Metal Catalysts for Auto-Tandem Annulation of N-Heterocycles via Oxidative Dehydrogenation"** presents a glimpse on recent advances in the field of ligand π radical chemistry derived from tailor-made poly aza chelates. The work initiated with the planned synthesis of novel organic azo molecules in conjugation with aryl/het-aryl groups. These azo-aromatics are successfully employed for the preparation of various 3d-metals compounds of fascinating features and their catalytic behaviour.

The thesis comprises of five chapters.

Chapter 1 gives the general introduction of concise report of this thesis along with brief description of redox-active azoaromatic compounds. A concise literature review of sustainable approaches in transition-metal catalysis for the activation and functionalization of small organic molecules. Physical methods, computational details and equipments used for the characterization of compounds have been accounted in the last section of this chapter.

Chapter 2 highlights the development and application of a homogeneous, isolable, air- and moisture-stable zinc catalyst stabilized by an electron-deficient N^N^N pincer-type ligand. This ternary, penta-coordinated neutral catalyst, [Zn(N^N^N)Cl_2], facilitates the selective synthesis of α-alkylated ketone derivatives (*14 examples*) via a one-pot acceptorless dehydrogenative coupling (ADC) reaction between secondary and primary alcohols, employing the borrowing hydrogen (BH) methodology. The reactions proceed with good to excellent isolated yields, reaching up to 93%. Notably, this catalyst also enables the efficient synthesis of quinoline derivatives (*32 examples*) by utilizing 2-aminobenzyl alcohols as alkylating agents through a sequence of dehydrogenative coupling and N-annulation steps. The catalyst is characterized by its cost-effectiveness, ease of synthesis, and environmentally benign nature, along with remarkable stability during catalytic cycles under open-air conditions. This is evidenced by its high turnover number (~10^4). Activation is achieved under mild conditions with a catalytic amount of base, making this system a robust and practical tool for sustainable synthetic transformations.

Chapter 3 demonstrates Highly efficient Ni-catalyzed C–N/C–C bond formation from amidines during the [3 + 2 + 1] annulation by primary alcohols alone or by primary alcohols with secondary alcohols/phenyl acetylenes has been successfully accomplished toward scaled synthesis of *s*-triazine and pyrimidines, respectively. The reaction takes place efficiently for a wide range of substrates (*76 examples*). This catalyst that promotes this process is has a higher turnover number (TON) than previously methods using homogeneous catalysts. The results of mechanistic studies suggest that the process takes place through a pathway that begins with Ni-catalyzed dehydrogenation of the alcohol, which is followed by sequential condensation, cyclization, and dehydrogenation.

Chapter 4 contains the report of an eco-friendly and efficient method for the synthesis of biologically relevant poly-substituted pyridines, including penta-substituted derivatives, using a nickel-metalloradical catalyst. This strategy employs readily available primary and secondary aryl alcohols and ammonium acetate to achieve polyfunctionalized pyridines through catalytic dehydrogenative alcohol oxidation, affording products in good to excellent yields (68–93%) in. The microwave-assisted, solvent-free domino [2 + 2 + 1 + 1] annulation involves consecutive C–C and C–N bond formations, followed by catalytic dehydrogenative aromatization. The nickel-metalloradical catalyst efficiently serves dual catalytic cycles namely alcohol dehydrogenation and ring aromatization, both via single-electron transfer (SET) pathways. An important aspect of this approach is that it generates only environmentally benign byproducts, such as H_2O and H_2O_2, without requiring external oxidants or additional additives. This green and cost-effective methodology adheres to green chemistry principles, offering simplicity and excellent E-factor values (0.3–0.5), representing a significant advancement in functionalized pyridine synthesis.

Chapter 5 explores a catalytic approach to synthesizing *E*-configured vinylarenes through the dehydrogenative coupling of secondary alcohols or ketones with 2-amino primary alcohol derivatives i.e., Friedländer annulation reactions. A novel penta-coordinated Cu(II) catalyst, stabilized by N^N^N pincer-type ligands, facilitates this reaction, yielding products in high yields and selectivity. The process generates hydrogen peroxide and water as environmentally friendly by-products. This method offers a significant advantage over previous homogeneous catalytic systems, demonstrating a higher TON. Mechanistic studies suggest a pathway involving initial Cu-catalyzed alcohol dehydrogenation, followed by condensation.

ACKNOWLEDGEMENT

My research work will remain incomplete if I do not offer my regards and thanks to those people, who helped me during this venture.

It is a great pleasure to pay my regards and deep sense of gratitude to my supervisor, **Prof. Kausikisankar Pramanik** for giving me the opportunity to work on this topic. His invaluable guidance, outstanding supervision and continuous encouragement inspired me throughout this research work. His excellent forethought and practical approach have been a guiding force behind all my efforts in bringing this thesis to its ultimate goal.

I am indebted to **Dr. Sanjib Ganguly** (St. Xavier's College) and express my deep regards to him for his unstinted advice and constant encouragement. His valuable suggestions and excellent guidance were a genuine motivation to me for carrying out this study.

I express my sincere thanks to **Prof. Kajal Krishna Rajak**, Head of the Department of Chemistry, and **Prof. Partha Roy**, Section-incharge, Inorganic Chemistry Section, for his helpful suggestions and for allowing me to use his laboratory and instruments whenever required.

I also thankful to **Prof. Samaresh Bhattacharya**, Department of Chemistry, Jadavpur University, for providing his laboratory instruments with the necessary facilities to carry out this study.

I express my regards to **Prof. Prabir Kumar Kundu**, Dean of the Faculty of Science, **Prof. Subrata Mukhopadhyay**, **Dr. Bibhuti Bhushan Show**, **Prof. Jnan Prakash Naskar**, **Prof. Sujoy Baitalik**, **Prof. Subratanath Koner** and **Prof. Debajyoti Ghoshal** of Department of Chemistry, Jadavpur University and for their help and encouragement.

I am grateful to **Prof. Chhanda Mukhopadhay**, Department of Chemistry, University of Calcutta, for her continuous support.

I would like to express my heartfelt thanks to my labmate **Gopal Kanrar** (Gopalda**)**. Without his help and support I could not be able to complete my work within time.

I am also thankful to my ex and present labmates **Dr. S. Roy** (Simadi), **Sampad**, **Supriyo** and **Srijita** for their cooperation and friendly atmosphere to preparation of my thesis.

Special thanks go to, **Uday Shee**, **Arijit Maity**, **Soumitra Rana** (University of Calcutta), **Dr. Sourajit Bera** (IIT Roorkee), **Dr. Pradip Bhunia** (Indian Association for Cultivation of science, IACS) for helping me in several ways during my research work.

I thank **UGC**, New Delhi for my fellowship and contingency grants.

I gratefully acknowledge Jadavpur University for providing me the infrastructural facilities for my research.

This acknowledgment would be incomplete without thanking my wonderful, loving co-passenger, my love, **Rupu** who has always been a consistent and loving source of motivation in my research work.

I would like to say my sincere gratitude to **Maa**, **Baba** for their love, affection and infinite patience over the years of my study.

I also acknowledge all my friends, teachers, relatives and well-wishers for their support, whom I could not mention by name.

Lastly, I am thankful to God whose blessings have given me patience and strength to face all the barriers in life.

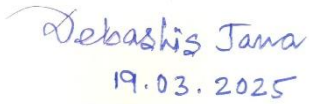

Debashis Jana

CONTENTS

LIST OF ABREVIATIONS

[O]	oxidant
°C	degree Celsius
Ac	acetyl
aq	aqueous
Ar	aryl
BHT	Butylated hydroxytoluene
Bn	benzyl
CF_3	trifluoromethyl
cm	centimeter
CV	cyclic voltammetry
Cy	cyclohexyl
d	doublet
DCM	dichloromethane
DFT	density functional theory
DMF	dimethylformamide
DMSO	dimethylsulfoxide
$E_{1/2}$	half-wave potential
equiv	equivalents
E_{red}	reduction potential
ESI	electrospray ionization
Et	ethyl
Fac	facial
Fc	ferrocene
g	grams
h	hours
HAT	hydrogen atom transfer
Het	heteroarene
HOMO	highest occupied molecular orbital
HRMS	high resolution mass spectroscopy
HT	hydride transfer
Hz	hertz
hν	light
ILCT	intra-ligand charge transfer
IR	infrared
J	coupling constant
L	liters
LMCT	ligand to metal charge transfer
LUMO	lowest occupied molecular orbital
M	molar concentration
m	multiplet
MCR	multi component reaction
Me	methyl
MeCN	acetonitrile
Mes	mesityl
mg	milligrams
MHz	megahertz
min	minutes
mL	milliliters
MLCT	metal to ligand charge transfer
mm	millimeters
mmol	millimoles
mol	moles
mol%	mole percent
MRC	metallo-radical catalysis
MW	molecular weight
nm	nanometers
NMR	nuclear magnetic resonance

O_2	oxygen
PF_6	hexafluorophosphate anion
Ph	phenyl
ppm	parts per million
py	pyridine
q	quartet
rt or RT	room temperature
s	singlet
SET	single electron transfer
t	triplet
TEMPO	(2,2,6,6-Tetramethylpiperidin-1-yl)oxyl
THF	tetrahydrofuran
TON	turn over number
UV	ultraviolet
V	volts
W	watt
δ	chemical shift in parts per million
λ_{max}	maximum wavelength
μL	microliters
μW	microwave

Chapter I

A Concise Literature Review of Sustainable Approaches in Transition-Metal Catalysis for the Activation and Functionalization of Small Organic Molecules

[I.1] General Introduction

The core idea behind sustainable transformation is to develop new synthetic methods for producing essential pharmaceuticals, chemicals, and materials.[1] Consequently, there is considerable interest in establishing modern procedures that address the need for environmentally friendly and durable alternatives to traditional methods.[2] Catalysis is a crucial component of sustainable transformations, as it not only lowers activation energy but also reduces the number of steps needed to synthesize a specific molecule.[3] The production of bulk and fine chemicals, pharmaceuticals, agrochemicals, energy, materials, and even environmental remediation technologies rely heavily on catalysis. Catalysts drive chemical transformations, enabling a faster, simpler, and safer conversion of reactants into target products. Notably, catalysis enhances resource efficiency and minimizes waste, with catalytic processes now responsible for over 75% of modern industrial chemical operations.[4]

Consequently, a key goal in chemical research is to develop catalytic methodologies that are both cost-effective and eco-friendly. Transition metal-catalyzed activation and functionalization of small molecules have garnered significant interest in the sustainable advancement of new catalytic methods for C-X (X = O, N, C, etc.) bond functionalization.[5] This approach is applicable to the synthesis of bioactive natural products, agrochemicals, drug molecules and essential pharmaceuticals.[6] Consequently, transition-metal catalysis has become a prominent research area. Although extensive research has been conducted over recent decades on the use of novel transition metals (such as Pd, Rh, Ir, Ru), the high cost of these metal catalysts restricts their use in large-scale synthesis.[7]Therefore, the use of cost-effective and earth-abundant metals for the activation and functionalization of small molecules presents an ideal alternative in this context.

Traditionally, organic synthesis in laboratories focused on two primary areas: total synthesis[8] and methodology development.[9] However, with the rise of catastrophic diseases worldwide (such as SARS-CoV), the current guiding principle in organic synthesis has shifted towards synthesis for purpose.

The use of advanced techniques for the production of drug derivatives or pharmaceuticals has, therefore, become the most focused area of research in this century.[10]

Alcohols are widely found in biomolecules and present valuable opportunities for building chemical libraries. Furthermore, their significant presence in pharmaceuticals underscores their potential for late-stage modifications. [11] It is widespread and exhibits remarkable structural

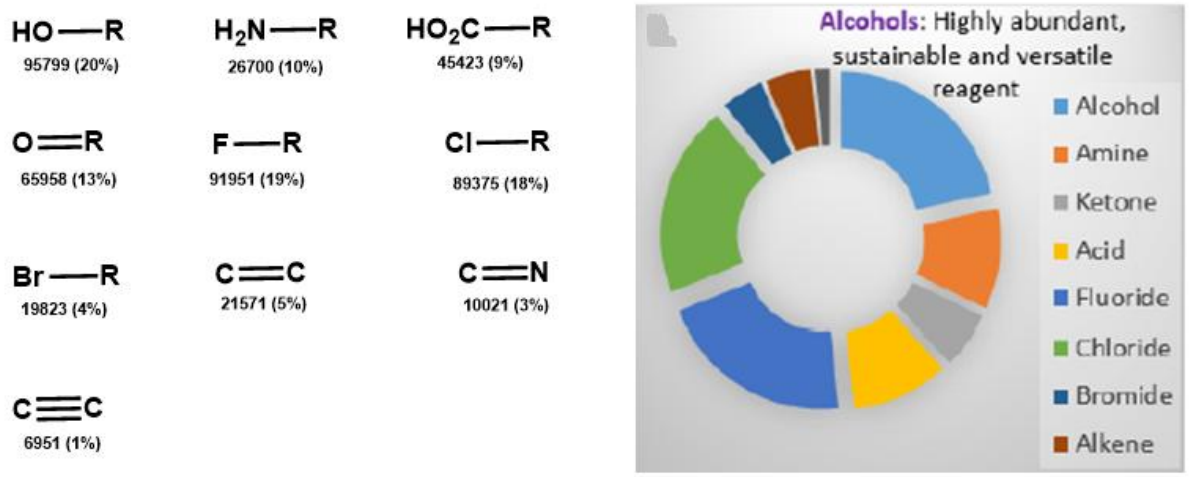

Figure 1: The most prevalent functional groups in the ChEMBL database, with molecule counts and percentages shown below (left), Pie chart of the most common functional groups in the ChEMBL database (right).

diversity, with extensive applications as a native functional group in organic synthesis from a commercial perspective (Figure 1). In the past decade, alcohol has been widely used as a more environmentally benign chemical in numerous organic conversions. [12] As a result, alcohol has become a popular reagent for synthesizing value-added products and developing various sustainable methodologies. Dehydrogenation is a key organic reaction in which adjacent hydrogen atoms are removed to produce a reactive compound (Figure 2A). Though, the overall process is endothermic. [12e] Due to the thermodynamic inefficiency of the reaction, some form of external activation is required. To achieve effective transformation, chemists traditionally used stoichiometric amounts of oxidants, but this approach generated significant amounts of hazardous waste. To develop a sustainable methodology where hydrogen gas, water, hydrogen-peroxide are generated as by-products, an effective combination of catalytic systems is essential.[12c] As we know, hydrogen gas can be used as a power source or as a fertilizer in the agrochemical industry. However, storing hydrogen gas is challenging and requires high-pressure vessels. Alternatively, in-situ generated hydrogen gas can be further utilized in various organic transformations.[13] If an additional nucleophile were introduced into the reaction system, it could lead to the formation of different products.

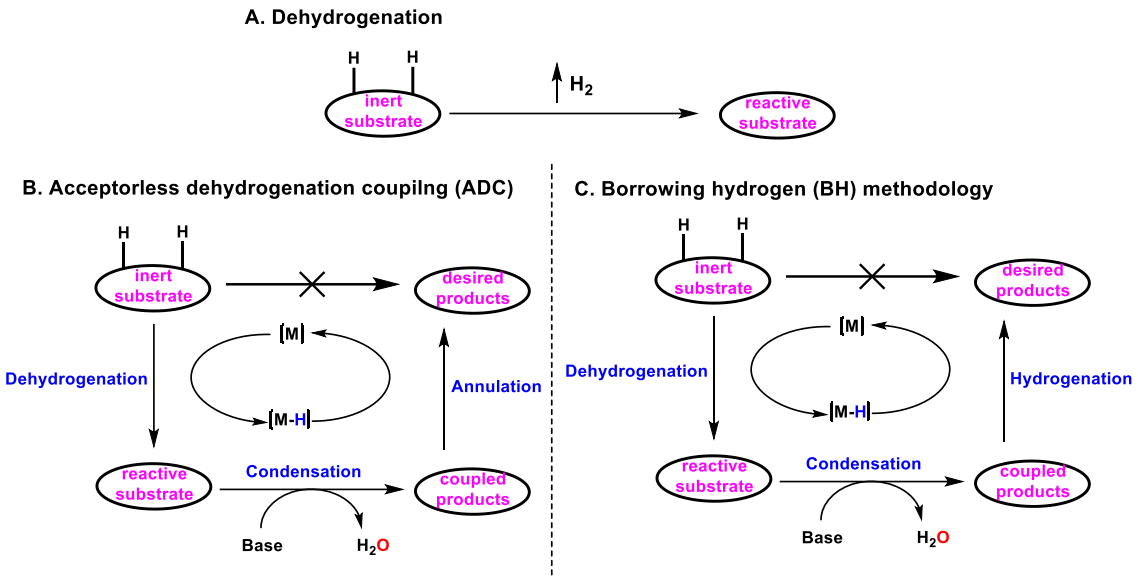

Figure 2: A. Classical dehydrogenation reaction, B. Acceptorless dehydrogenating coupling (ADC), C. Borrowing hydrogen (BH) methodology.

Acceptorless dehydrogenation (AD)[12c] represents a methodology wherein the dehydrogenated intermediate subsequently participates in nucleophilic addition with an external nucleophile, yielding hydrogen gas/water/hydrogen-peroxide as by-products (Figure 2B). Another approach involves the *in-situ* generation of hydrogen atom or hydride by a metal catalyst, which can be returned within a one-pot process. This enables multiple bond-breaking and bond-forming steps that are challenging to achieve even in three separate steps. This overall process is known as the Hydrogen Auto-Transfer process or Hydrogen-Borrowing (HB) methodology (Figure 2C).[12a-b] Throughout my doctoral research, I conducted an in-depth investigation of these catalytic strategies and applied them to activate and functionalize small molecules. The developed strategies include: (a) both BH and AD method for synthesizing homogeneous α-alkylated ketones and N-heterocycles with primary alcohols, (b) Highly efficient Ni-catalyzed C–N/C–C bond formation from amidines during the [3 + 2 + 1] annulation by primary alcohols alone or by primary alcohols with secondary alcohols/phenyl acetylenes, (c) Highly efficient Ni-catalyzed C–N/C–C bond formation from secondary alcohols during the [2 + 2 + 1 + 1] annulation by primary alcohols and ammonium acetate and (d) Cu(II)-catalyzed dehydrogenative coupling of secondary alcohols or ketones with 2-amino primary alcohol derivatives i.e., Friedländer annulation reactions.

[I.1.1] Transition metal-catalyzed α-alkylation of ketone:

The α-alkylation of carbonyl compounds via transition-metal catalysis using renewable resources offers a sustainable method for constructing new C–C bonds.[14] This approach enables access to a variety of functionalized organic compounds widely utilized in agrochemical applications, pharmacology, and materials science. The use of readily available alcohols for the α-alkylation of ketones through the borrowing hydrogen approach eliminates the need for pre-synthesized alkyl halides and cryogenic temperatures, while generating water and hydrogen peroxide as by-products. In this context, transition-metal-catalyzed α-alkylation of ketones and secondary alcohols using alcohol as a sustainable reagent has shown significant potential.

Precious metal-catalyzed *α*-alkylation of ketone:

In 2006, Grigg et al. employed alcohol as an alkylating agent for the microwave-assisted functionalization of 1,3-diethyl barbituric acid (Scheme 1).[15] In 2016, Wang and

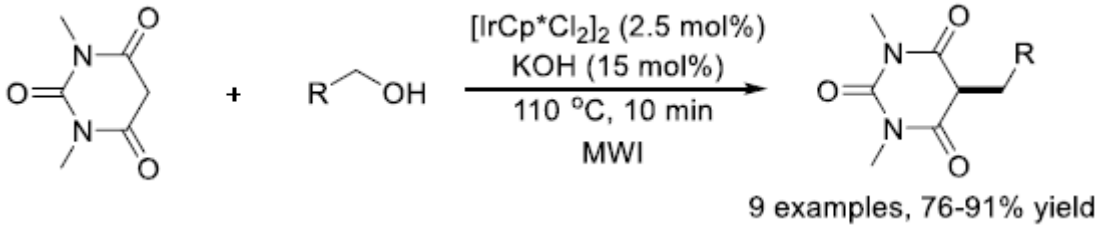

Scheme 1. Ir catalyzed *α*-alkylation of 1,3-diethyl barbituric acid

Shi developed alanine triazole (**L2**) and employed it as a ligand in the Ru-catalyzed α-alkylation of ketones (Scheme 2, method A).[16]

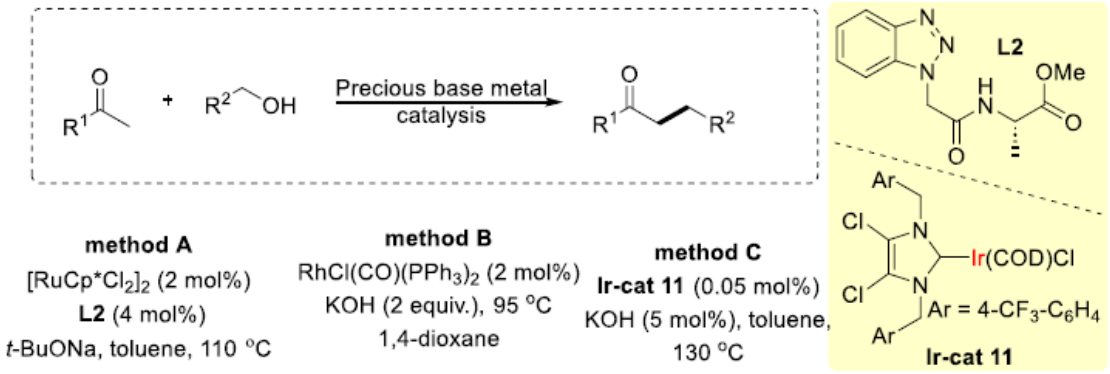

Scheme 2. Precious metal catalyzed *α*-alkylation of ketone

Feng and his group also employed Rh-based catalysis for a similar reaction, where water was the only by-product formed (Scheme 2, method B).[17] Subsequently, Gülecemal and his group introduced Ir-catalyst for the same reaction. They demonstrated that using 0.05 mol% Ir-cat 11,

along with a catalytic amount of base KOH, effectively alkylated a variety of electronically substituted ketones with good yields (Scheme 2, method C).[18] In 2012, Baratta groups demonstrated that the readily available complexes [MCl2(dppf)-(ampy)] (M = Ru, Os; dppf = 1,1′-bis(diphenylphosphine) ferrocene; ampy = 2-aminomethyl pyridine) were effective catalysts for the α-alkylation of α-tetralone in the presence of a base. A TOF of up to 10^5 h^{-1} indicated that the catalyst efficiently facilitated the cleavage of the α-C−H bond of alcohols (Scheme 3, method A).[19] In 2017, Venkatasubbaiah et al. isolated and characterized a

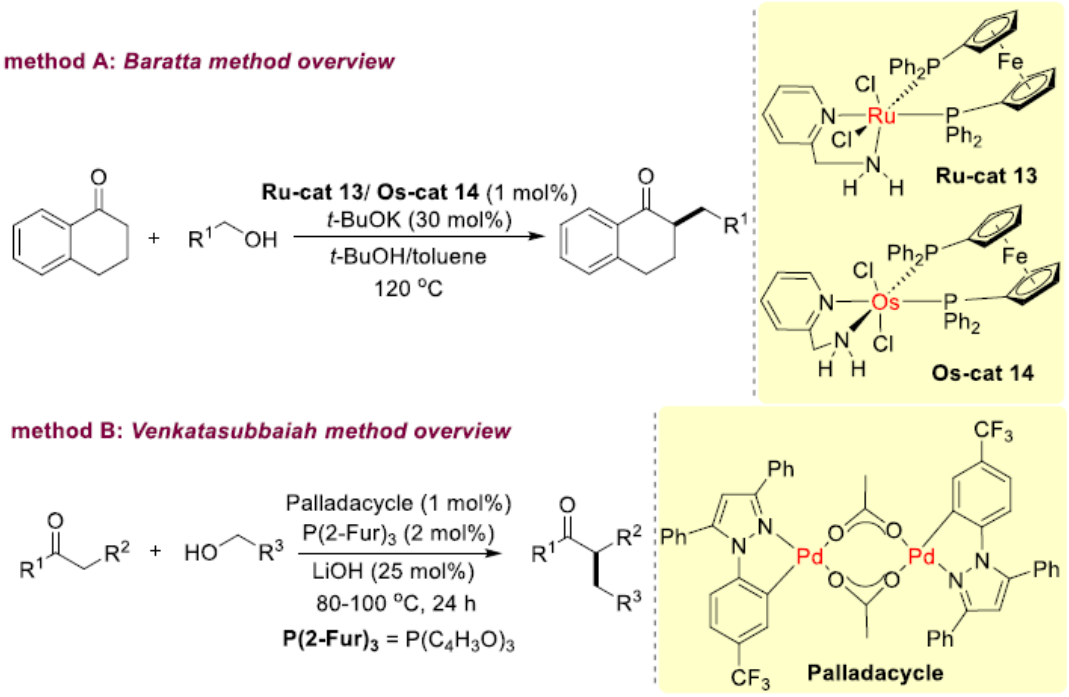

Scheme 3. Precious metal catalyzed *a*-alkylation of ketone

pyrazole-based palladacycle and used this catalyst for the α-alkylation of carbonyl compounds with the aid of the ancillary ligand $P(2\text{-Fur})_3$. Additionally, they demonstrated the synthesis of the drug Donepezil (used for Alzheimer's disease) in a 46% yield (Scheme 3, method B).[20]

Non-precious metal-catalyzed α-alkylation of ketone

In 2016, Darcel et al. developed an iron-catalyzed α-alkylation reaction between ketones and primary alcohols. The use of a Knolker-type Fe-catalyst (Fe-cat 15, 2 mol%) in the presence of Cs2CO3 as a base (10 mol%) was essential for the reaction's effectiveness under hydrogen-borrowing conditions (Scheme 4, method A).[21] Subsequently, Renaud et al. modified the Fe catalyst by incorporating an electron-rich cyclopentadienone ligand, while Zheng et al. introduced the Co-PNP pincer complex for the same reaction. Ketones with both electron-

donating and electron-withdrawing groups reacted efficiently, yielding the product in good yields (Scheme 4, method B).[22] Similarly, Beller et al. demonstrated the alkylation of ketones with various alcohols using Mn-cat 14. The functionalization of several important ketones, including 2-oxindole, estrone 3-methyl ether, and testosterone, was achieved using manganese complexes with non-innocent PNP pincer ligands. Mechanistic studies suggested that the

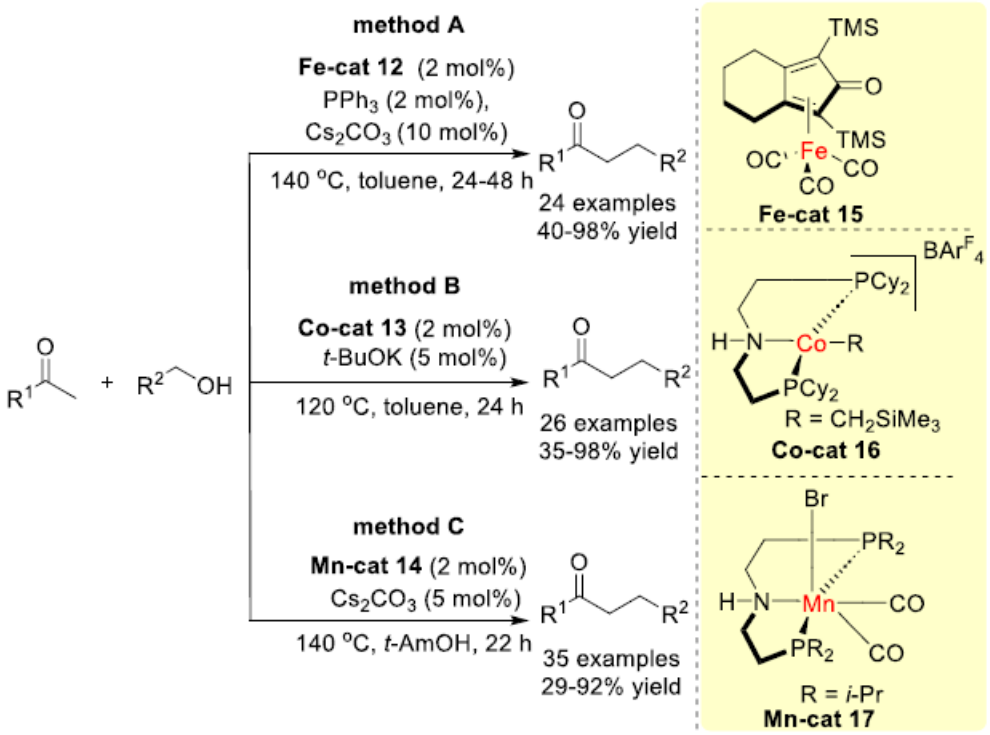

Scheme 4. Non-precious metal catalyzed a-alkylation of ketone

alcohol-dehydrogenation process could be facilitated by an intramolecular amide group (Scheme 4, method C).[23] Alcohols have attracted significant interest as feedstock molecules for both academic and industrial transformations. The process of selectively producing these ketones is highly challenging, and transition metal catalysts have been employed to achieve the anticipated alkylated products.

[I.1.2] Transition metal-catalyzed β-alkylation of alcohol

Alcohols have attracted considerable interest as feedstock molecules for both industrial and academic transformations. The use of readily accessible alcohols for the synthesis of long-chain linear or branched alcohols, known as β-alkylation of alcohols, is simplified through the application of the sustainable hydrogen-borrowing strategy. Selectively synthesizing these alcohols is a complex process, and transition metal catalysts are employed to achieve the required alkylated products.

Precious metal-catalyzed β-alkylation of alcohol

In 2005, Yamaguchi, Fujita, and colleagues presented the first report on Ir-catalyzed β-alkylation of secondary alcohols. According to the mechanistic analysis, the unsaturated enone

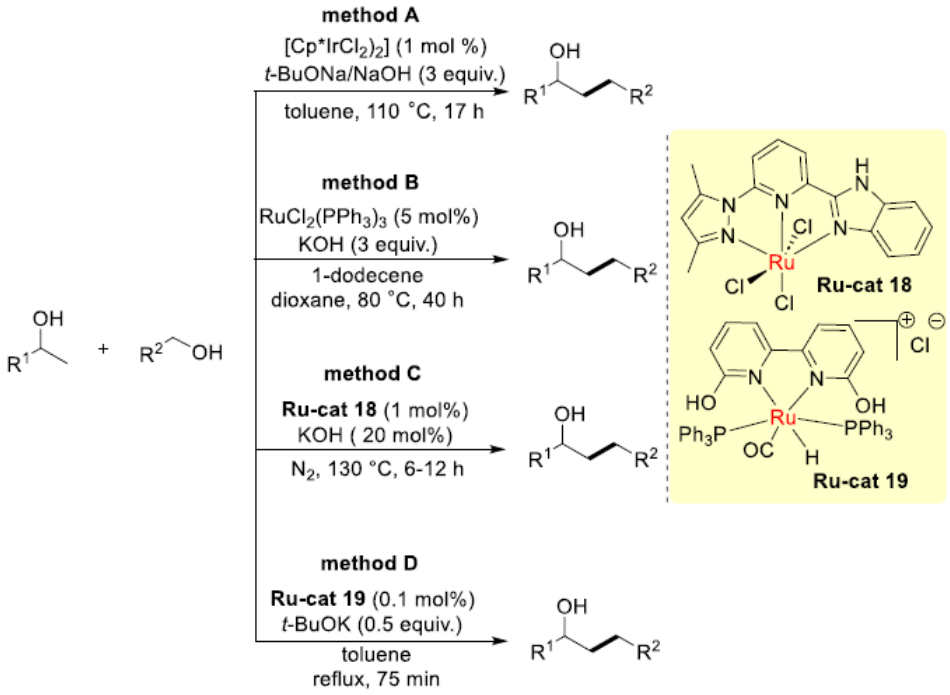

Scheme 5. Non-precious metal catalyzed β-alkylation of alcohol

intermediate was converted to the final alcohol product by the *in-situ* formed iridium hydrido species (Scheme 5, method A).[24] Chao and coworkers demonstrated the cross-coupling of secondary alcohols (carbinols) with primary alcohols in dioxane at 80 °C to produce the corresponding linear secondary alcohols, using $RuCl_2(PPh_3)_3$, KOH, and a sacrificial hydrogen acceptor (Scheme 5, method B).[25] Yu and coworkers introduced a pyridyl-based Ru-NNN pincer catalyst for alcohol cross-coupling. Using 1 mol% catalyst and 20 mol% KOH, they efficiently converted a variety of electronically substituted secondary alcohols into their corresponding β-alkylated products in good yields. Furthermore, they successfully alkylated both β-sites of cyclopentanol from a range of source alcohols (Scheme 5, method C).[26] In 2016, Kundu and coworkers employed a ruthenium complex containing hydroxy bipyridine for the same process. A high turnover frequency of 797.6 h^{-1} was achieved due to low catalyst loading and a relatively short reaction time (Scheme 5, method D).[27]

Non-precious metal-catalyzed β-alkylation of alcohol

In 2018, Yu and coworkers demonstrated that an active Mn-NNN pincer catalyst, incorporating pyridine, pyrazole, and imidazole scaffolds, facilitated the β-alkylation of secondary alcohols with primary alcohols. The reaction, conducted in toluene, required 1 mol% of the Mn-NNN complex and 25 mol% of base under inert conditions. A variety of primary and secondary alcohols (both aryl and alkyl) efficiently participated in the reaction to yield the desired products. Cholesterol was successfully alkylated with good yield, and the synthesis of a flavonoid derivative highlighted the synthetic utility of the method (Scheme 6, method A).[28]

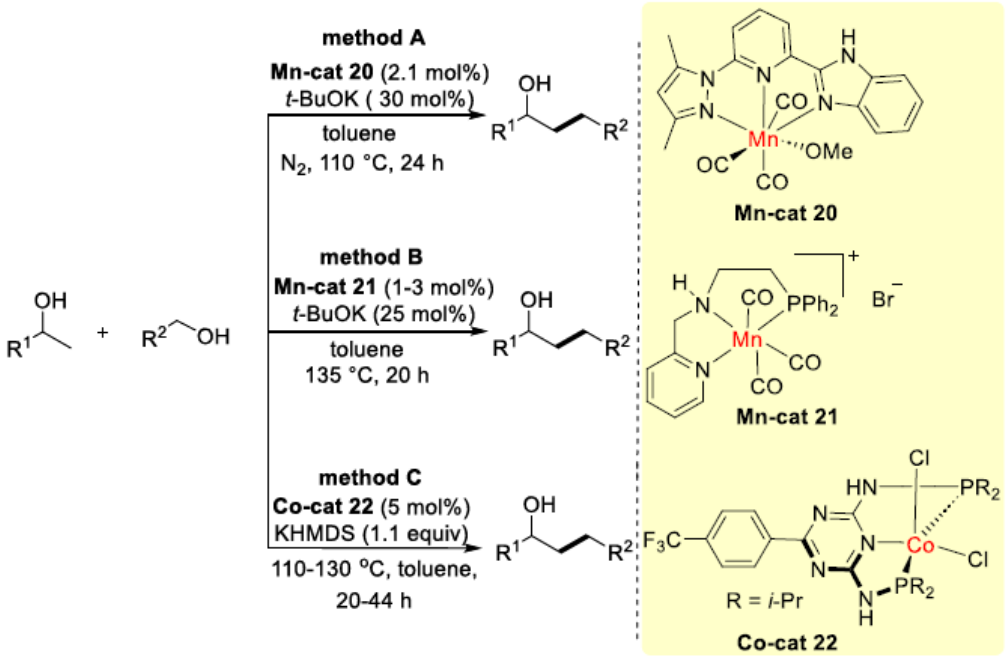

Scheme 6. Non-precious metal catalyzed β-alkylation of alcohol

Reuping et al. introduced a pyridine-based Mn-PNP pincer catalyst for the same reaction. Notably, deuterium scrambling tests indicated that the catalyst functioned via the hydrogen-borrowing methodology, involving the formation of a monohydride metal species and metal-ligand cooperation (Scheme 6, method B).[29] In 2017, Kempe and coworkers reported the first Co-PNP pincer compound based on triazine for the synthesis of β-substituted linear ketones via cross-coupling of secondary alcohols with primary alcohols. The reaction required the use of the strong non-nucleophilic base KHMDS (potassium bis(trimethylsilyl)amide). Various alkyl alcohols, including n-alkyl and cyclopropane alcohols, participated efficiently, leading to β-alkylated alcohols with up to 63% isolated yield (Scheme 6, method C). [30]

[I.1.3] Transition metal-catalyzed quinoline synthesis:

The Friedländer annulation reaction is a popular method for synthesizing quinolines. It involves condensing 2-aminobenzaldehydes with carbonyl compounds containing an active methylene group, using either acid or base as a catalys.[31] Due to the inherent limitations of the Friedländer annulation reaction, various transition metal-catalyzed approaches have been developed to utilize more stable and readily accessible starting materials such as 2-aminoaryl alcohols and ketones.[32] However, many of these methods necessitate the use of large excesses of coupling partners or sacrificial hydrogen acceptors. Subsequently, several greener methodologies have been developed that employ alcohols as coupling partners. This section will discuss recent developments in the field that utilize alcohols as sustainable starting material. A general schematic representation of quinolines synthesized through the acceptorless dehydrogenative coupling (ADC) strategy are illustrated in Scheme 7.

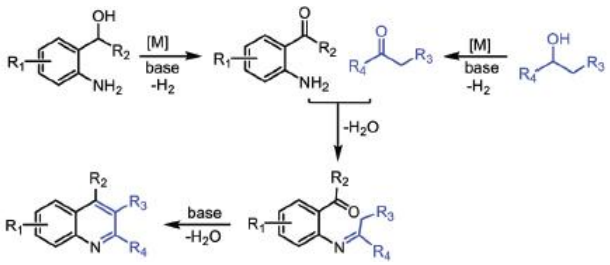

Scheme 7: A general representation of the synthesis of quinoline

Precious metal-catalyzed quinoline synthesis:

In 2014, Kempe and coworkers reported a bidentate PN-ligand-based Ir(I) complex catalyzed acceptorless dehydrogenative coupling of primary amino alcohols and secondary alcohols to synthesize quinolines, liberating H_2 and H_2O (Scheme 8). The reaction proceeded with a low catalyst loading (0.1 mol%) and a catalytic amount of base, although requiring a large excess (5 equiv.) of alcohols.[33]

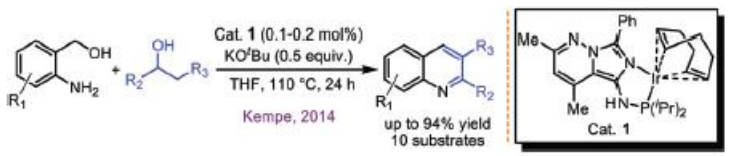

Scheme 8: Ir(I)-Catalyzed synthesis of quinolines.

In 2019, the Sortais group reported a well-defined rhenium complex containing a tridentate diphosphinoamino ligand, which catalyzed the dehydrogenative coupling of o-aminoaryl alcohols and secondary alcohols (Scheme 9). Notably, this was the first report on the synthesis of quinolines using a molecularly defined Re(I) complex in the presence of a catalytic amount

of base (10 mol%). While the method proved effective for aromatic substrates, cyclic alcohols and aliphatic showed no reactivity under the reported conditions.[34]

Scheme 9: (PNP)Re complex catalyzed synthesis of quinolines

In 2019, Kundu and colleagues introduced a sustainable protocol for a similar synthesis conducted in water (Scheme 10). They synthesized and evaluated several new bidentate Ir(III) complexes, identifying a 2-hydroxypyridine-based bifunctional Ir(III) complex **8** as the most reactive. A wide range of quinolines was synthesized directly from 2-aminobenzyl alcohol derivatives, achieving good to excellent yields.[35]

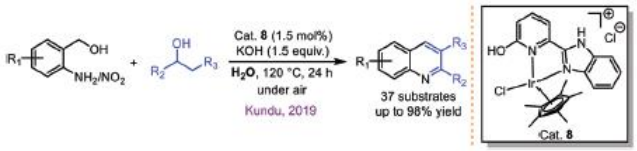

Scheme 10: Ir(III)- catalyzed synthesis of quinolines

Non-precious metal-catalyzed quinoline synthesis:

Paul and co-workers in 2017 reported a nickel-catalyzed synthesis employing a tetra-aza macrocyclic ligand-based Ni(II) complex (Scheme 11). The catalyst demonstrated broad substrate applicability, affording the final products in good to excellent yields. Mechanistic investigations, including several control experiments, provided evidence supporting the proposed pathway, wherein alcohol dehydrogenation proceeds through nickel-hydride intermediates.[36]

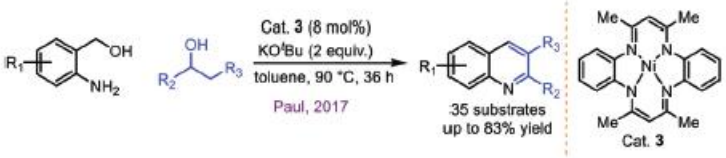

Scheme 11: Ni(II)- catalyzed synthesis of quinolines

Subsequently, in 2016, Kirchner and co-workers reported a similar base-metal-catalyzed synthesis (Scheme 12). The study involved the screening of several pyridine- and triazene-based well-defined tridentate (PNP)-pincer Mn(I) complexes. Among these, catalyst **2** featuring Mn–H exhibited the highest reactivity. Under optimized conditions, various quinoline

derivatives were synthesized in good to excellent yields, employing excess amounts of base as additives.[37]

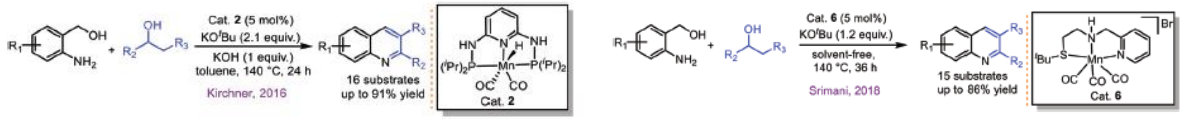

Scheme 12: (a) (PNP)Mn(II)- catalyzed synthesis of quinolines (left), (b) (NNS)Mn(II)-catalyzed synthesis of quinolines (right).

In 2018, Srimani and co-workers reported a quinoline synthesis utilizing an NNS-pincer ligand-based Mn(I)-pincer complex (Scheme 12). The study highlighted solvent-free reaction conditions, enabling the use of alcohols to achieve good to excellent yields of the desired products.[38]

[I.1.4] Transition metal-catalyzed dehydrogenative synthesis of s-triazines and pyrimidines:

The synthesis of nitrogen-containing heterocycles, including triazines, pyrimidines, pyrroles, quinolines, indoles, quinazolines and pyridines from simple alcohols is a growing area of interest in sustainable and eco-friendly organic chemistry.[39]Among these nitrogen-containing heterocycles, the triazine framework is widely found in numerous pharmaceuticals various herbicides, polymers and fungicides.[40] Various other triazines demonstrate a broad spectrum of pharmacological activities, such as antimalarial, anticancer, antiviral, antiprotozoal, antitumor, antimicrobial antituberculosis, anti-HIV, and anti-HSV-1effects.[41] Pyrimidines are fundamental structural units commonly found in pharmaceuticals, natural products, and functional materials.[42] Numerous poly-substituted pyrimidine derivatives exhibit significant biological activities, such as antibacterial, anti-inflammatory, anticancer, and antimicrobial effects.[43] Additionally, pyrimidine-containing polymers play a vital role in functional materials, including fluorescent compounds, semiconductors, and photophysical applications.[44]

Precious metal-catalyzed synthesis of s-triazines:

Li et al. in 2016 reported a cascade dehydrogenative synthesis of triazines from stable aryl-substituted alcohols and amidines catalyzed by an iridium complex [Cp*IrI2]2/Xantphos (Scheme 13). This was the first successful application of an iridium catalyst in such a transformation.[45]

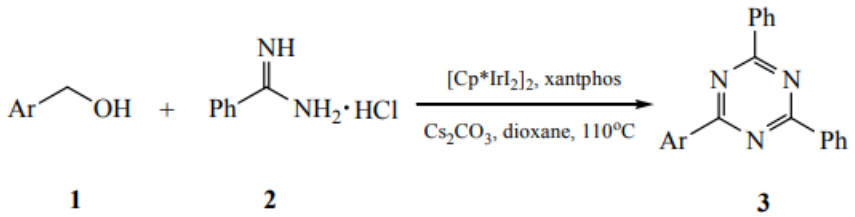

Scheme 13. Precious metal catalyzed synthesis of s-triazine

In 2022, Poly and coworkers demonstrated that an active Pt-nanoparticle catalyst, facilitated the synthesis of triazines from alcohols and amidines. The reaction, conducted in toluene, required 1 mol% of the Pt/Al_2O_3 catalyst and 10 mol% of base under reflux conditions. A variety of primary alcohols (both aryl and alkyl) efficiently participated in the reaction to yield the desired triazines (Scheme 14).[46]

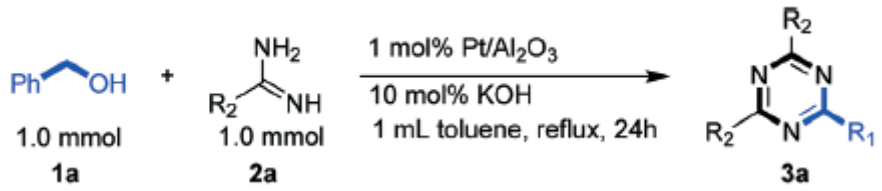

Scheme 14. Precious metal catalyzed synthesis of s-triazine

In 2014, Zhang and coworkers established $[RuCl_2(p\text{-Cymene})]_2/Cs_2CO_3$ as an efficient catalyst system, enabled the synthesis of triazines from alcohols and amidines. The reaction, conducted in DMSO, required 1.5 mol% of catalyst and 1.0 mmol of base at 110 ^{0}C. A variety of primary alcohols and amidines (both aryl and alkyl) efficiently participated in the reaction to yield the desired triazines (Scheme 15).[47]

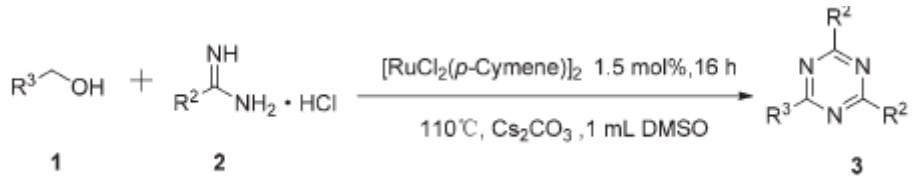

Scheme 15. Precious metal catalyzed synthesis of s-triazine

Precious metal-catalyzed synthesis of pyrimidines:

In 2015, kempe and coworkers established iridium as an efficient catalyst **A**, enabled the synthesis of pyrimidines from alcohols and amidines. The reaction, conducted in tert-amy; alcohol, required 0.5 mol% of catalyst and 1.1 equiv. of base under inert conditions. A variety

of primary alcohols and amidines (only aryl) efficiently participated in the reaction to yield the desired triazines (Scheme 16).[48]

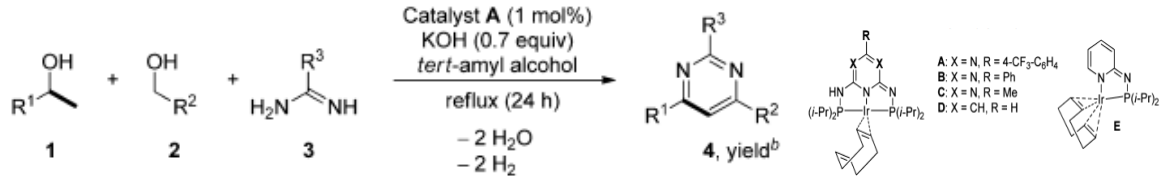

Scheme 16. Precious metal catalyzed synthesis of pyrimidine

In 2018, Shimizu and coworkers established Pt/C as an efficient catalyst, enabled the synthesis of pyrimidines from primary and secondary alcohols and amidines. The reaction, conducted in toluene, required 1.0 mol% of catalyst and 1.1 mmol of base under reflux conditions. A variety of primary alcohols and amidines (only aryl) efficiently participated in the reaction to yield the desired triazines (Scheme 17).[49]

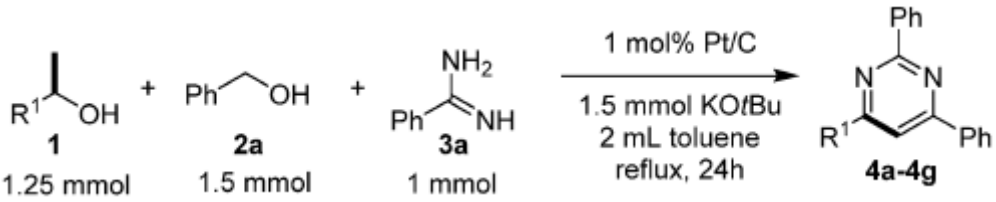

Scheme 17. Precious metal catalyzed synthesis of pyrimidine

Non-precious metal-catalyzed synthesis of s-triazines:

In 2020, Adhikari and coworkers established nickel as an efficient catalyst **1**, enabled the synthesis of triazines from alcohols and amidines. The reaction, conducted in toluene, required 5 mol% of catalyst and 0.5 mmol of base at 80 ^{0}C. A variety of primary alcohols and amidines (only aryl) efficiently participated in the reaction to yield the desired triazines (Scheme 18).[50]

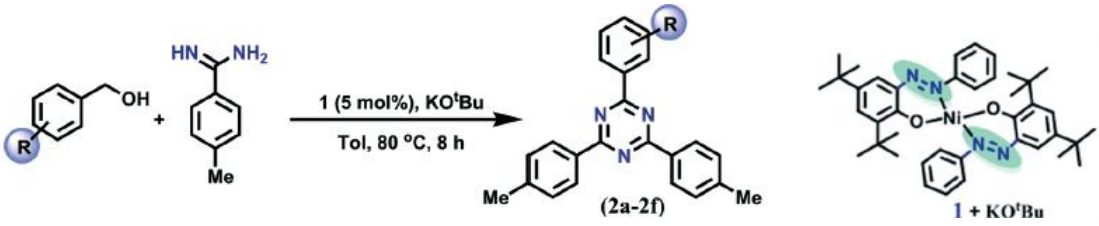

Scheme 18. Non-precious metal catalyzed synthesis of triazine

In 2015, Zhang and groups demonstrated Cu(OAC)2 as an efficient catalyst, enabled the synthesis of triazines from alcohols and amidines. The reaction, conducted in toluene, required 10 mol% of catalyst and 2 equiv of base at 110 ^{0}C. A variety of primary alcohols and amidines

(both aryl and alkyl) efficiently participated in the reaction to yield the desired triazines (Scheme 19).[51]

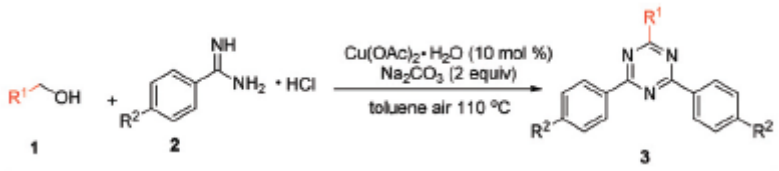

Scheme 19. Non-precious metal catalyzed synthesis of triazine

In 2022, Paul and his groups demonstrated zinc-stabilized azo-anion radical catalyst as an efficient catalyst, enabled the synthesis of triazines from alcohols and amidines. The reaction, conducted in toluene, required 3 mol% of catalyst and 0.5 equiv of base at 100 ^{0}C. A variety of primary alcohols and amidines (both aryl and alkyl) efficiently participated in the reaction to yield the desired triazines (Scheme 20). [52]

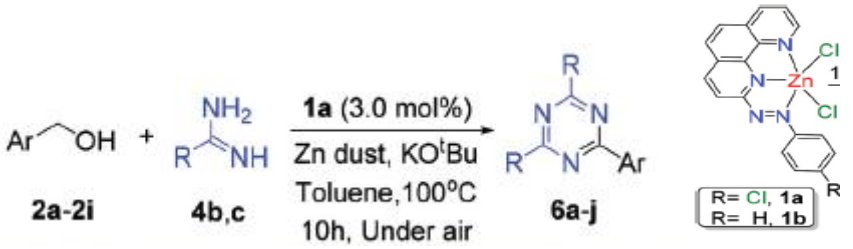

Scheme 20. Non-precious metal catalyzed synthesis of triazine

Non-precious metal-catalyzed synthesis of s-pyrimidines:

In 2016, kirchner and groups demonstrated that an active Mn-PNP pincer catalyst, facilitated multicomponent synthesis of primary alcohols, secondary alcohols with amidines. The reaction, conducted in toluene, required 5 mol% of the Mn-PNP complex and 1.5 mmol of base under inert conditions. A variety of primary and secondary alcohols (only aryl groups) efficiently participated in the reaction to yield the desired product (Scheme 21).[53]

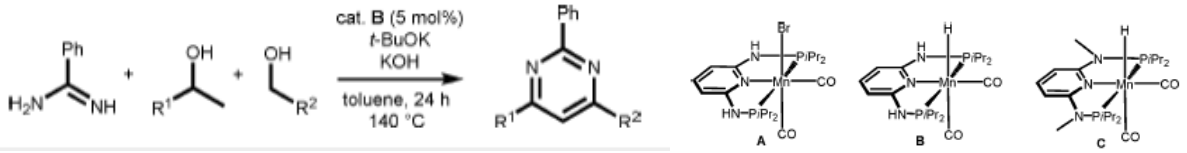

Scheme 21. Non-precious metal catalyzed synthesis of pyrimidine

In 2019, paul and groups demonstrated iron-catalyzed multicomponent dehydrogenative functionalization of alcohols to pyrimidines under atmospheric conditions. Using a well-defined Fe(II)-complex featuring redox noninnocent 2-phenylazo-(1,10-phenanthroline) ligand, as a catalyst. The reaction, conducted in toluene, required 3.0 mol% of the Fe-NNN complex **1b** and 0.5 equiv. of base under inert conditions. A variety of primary and secondary alcohols (both aryl and alkyl groups) efficiently participated in the reaction to yield the desired product (Scheme 22). [54]

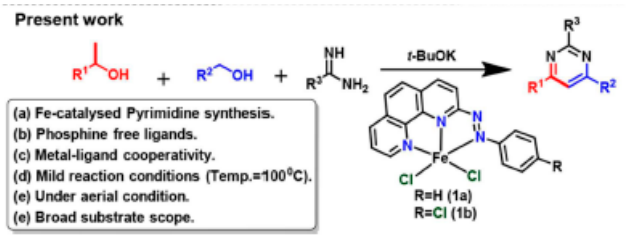

Scheme 22. Non-precious metal catalyzed synthesis of pyrimidine

In 2020, Adhikari and coworkers established nickel as an efficient catalyst **1**, enabled the synthesis of pyrimidines from primary alcohols, secondary alcohols and amidines. The reaction, conducted in toluene, required 5 mol% of catalyst and 0.5 mmol of base at 80 ^{0}C. A variety of primary alcohols and amidines (only aryl) efficiently participated in the reaction to yield the desired triazines (Scheme 23).[50]

Scheme 23. Non-precious metal catalyzed synthesis of pyrimidine

In 2020, Paul and colleagues demonstrated that catalysts **1a** and **1b**, which are tetracoordinate Ni(II) complexes containing two seemingly redox-inactive tetraaza-macrocyclic ligands, and catalysts **2a** and **2b**, which are square planar Ni(II) complexes featuring redox-active diiminosemiquinonato-type scaffolds, effectively facilitated the multicomponent synthesis of pyrimidines from primary alcohols, secondary alcohols, and amidines (Scheme 24).[55]

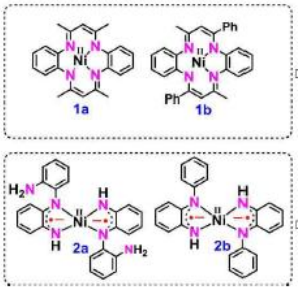

Scheme 24. Non-precious metal catalyzed synthesis of pyrimidine

[I.1.5] Transition metal-catalyzed synthesis of substituted pyridine:

The Chichibabin reaction, which involves the condensation of α, β-unsaturated ketones or aldehydes with ammonia, is widely regarded as a prominent method for the industrial synthesis of pyridine derivatives. Several traditional methods for pyridine synthesis are illustrated in Scheme 25.[56] However, these approaches often involve relatively unstable precursors, require extremely high reaction temperatures, and generate multiple by-products.

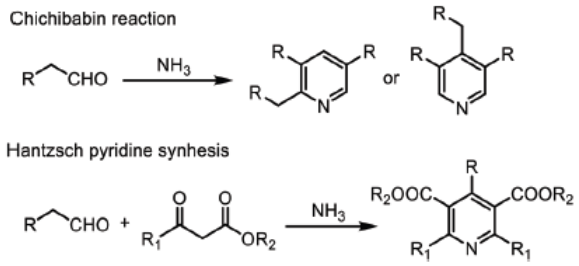

Scheme 25: Traditional method for synthesis of pyridine derivatives.

The use of stable, readily available and renewable substrates is highly desirable for achieving greener synthetic pathways for pyridines. This discussion focuses on recent advances in the synthesis of pyridine derivatives, employing alcohol as a renewable coupling partner. A schematic representation of the dehydrogenative synthesis of quinoline is provided in Scheme 26.

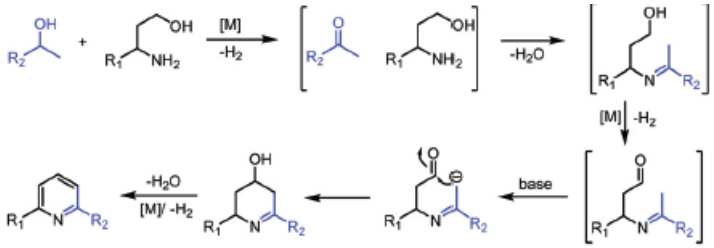

Scheme 26: Schematic pathway for synthesis of pyridine from amino alcohol and secondary alcohol

Precious metal-catalyzed synthesis of pyridines

In 2013, Kempe and co-workers reported the synthesis of various substituted pyridine derivatives using a (PNP)Ir-pincer complex via the coupling of 1,3-amino alcohols with alcohols (Scheme 27).[57] This approach utilized an acceptorless dehydrogenative coupling strategy, resulting in the release of three equivalents of hydrogen and two equivalents of water.

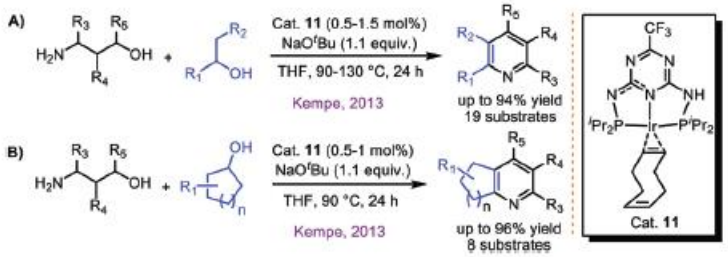

Scheme 27: Ir(I)-Catalyzed synthesis of pyridine derivatives.

In 2013, Milstein and co-workers described a similar two-component reaction involving 1,3-amino alcohols and secondary alcohols catalyzed by a (PNN)Ru complex (Scheme 28). This method primarily yielded fused bicyclic pyridine derivatives in moderate yields.[58] A metal–ligand cooperative mechanism was proposed to explain the dehydrogenative coupling process.

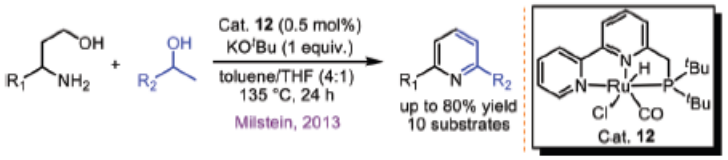

Scheme 28: Ru(II)-Catalyzed synthesis of pyridine derivatives

Non-precious metal-catalyzed synthesis of pyridines

In 2018, the Balaraman group reported a cobalt-catalyzed approach for similar reactions. This method utilized a new phosphine-free, air-stable SNS-pincer ligand-based dimeric Co(II) complex to achieve the direct synthesis of pyridines from amino alcohols and secondary alcohols, delivering moderate to good yields (Scheme 29).[59]

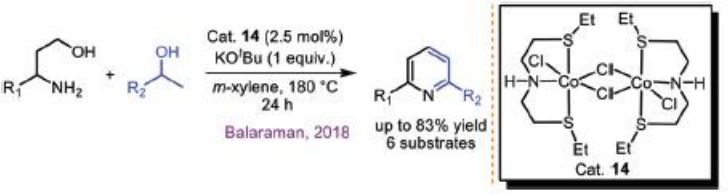

Scheme 29: Co(II)-Catalyzed synthesis of pyridine derivatives

In 2023, Paul and colleagues described a sustainable Zn(II)-catalyzed approach for synthesizing tri- and tetra-substituted pyridines under solvent-free conditions. This method utilizes alcohols as the primary feedstock and NH_4OAc as the nitrogen source for comparable reactions. (Scheme 30)

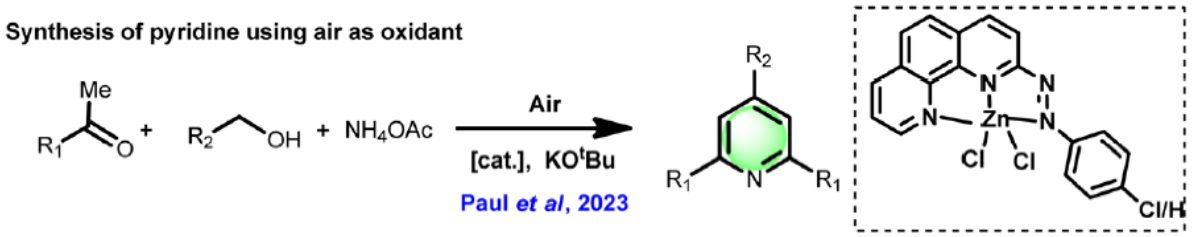

Scheme 30: Zn(II)-Catalyzed synthesis of pyridine derivatives

[I.2] General Introduction of Azo Aromatic Compounds

Acyclic polyaza aromatic compounds, including imine-conjugated aryls, aza-heterocycles and diaryldiazene (azoaromatic) molecules, are among the most extensively utilized ligands in coordination and organometallic chemistry.[60] Azoaromatic compounds, distinguished by their low-lying π* molecular orbitals, have evolved from traditional dye industry applications to become promising materials for optoelectronic and photonic technologies over the past decade.[61] Azoaromatic compounds, characterized by low-lying π* molecular orbitals, function as electron sinks and exhibit cooperative interactions with metals. This property enables their involvement in homogeneous oxidative coupling reactions.[62] Bi- and polydentate azoaromatics that incorporate additional donor groups have garnered significant attention in the fields of coordination and organometallic chemistry. These ligands offer a rich platform for exploring diverse coordination modes and electronic properties, leading to the development of a wide range of metal complexes with potential applications in catalysis, materials science, and medicine. Notable examples embrace the complexes of diphenyldiazene, 2-(arylazo)pyridine, 2,2′-azobispyridine, 2-(phenyldiazenyl)-1,10-phenanthroline, 2,6-bis-phenyldiazenyl)pyridine 1,2-bis-phenyldiazenyl)benzene, 2,2′-phenyldiazenyl)phenyl)diazenyl)pyridine and so forth (Scheme 31).

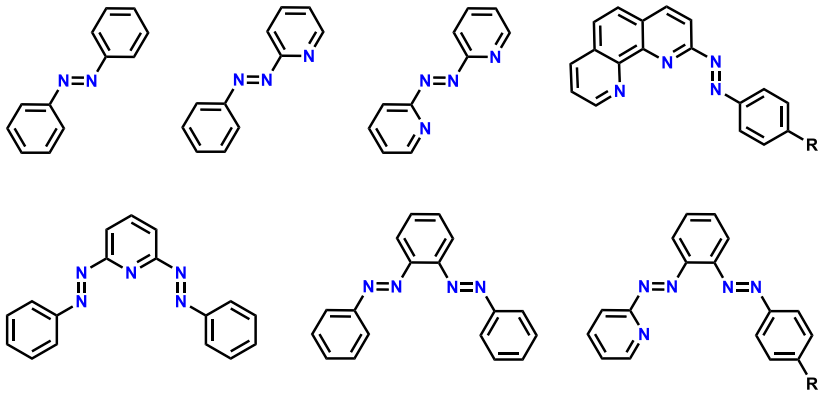

Scheme 31: Motif of different mono and bis-azo-aromatics.

Recent research has focused on the synthesis of transition metal complexes incorporating azo chelates, driven by their potential for diverse coordination modes and intriguing molecular structures. Some of the additional attributes are (i) potential sites of facile electron transfer,[63] (ii) formation of M−C bond,[64] (iii) stabilization of radical compounds,[64] (iv) metal assisted C−E, N−E (E = H, C and N) bond activation,[65] and so forth. These notable attributes have sparked significant interest in this field, driving further exploration of new transition metal-azo systems. The goal is to understand how the ligand environment can modulate electronic and molecular structure, redox properties, optoelectronic behaviour, and reactivity. The chemistry of a metal-ligand complex is significantly influenced by the immediate environment around the metal ion. Strategic modifications to ligand architecture can lead to dramatic changes in the properties of these complexes.

In this context, we aimed to design and synthesize a new class of azo-aromatic chelates containing one or two azo functionalities. By carefully selecting aryl groups, we introduced additional coordination sites and/or pendent arms into the ligand framework to create functional materials. These multidentate azo-aromatics are redox-active, known to stabilize azo anion radical complexes and potentially exhibit rich spectral properties.

Our research focused on investigating the structural, electrochemical, and spectral properties of these new materials, exploring their potential reactivity i.e., catalysis.

[I.3] Present Work

[I.3.1] Our Ligand Systems

This research focuses on designing and synthesizing new organic molecules containing two azo chromophores. To enhance the metal-binding properties of these molecules, nitrogen atoms

were incorporated as additional donor sites. In this thesis, two tridentate NNN donor ligands were employed (Scheme 32).

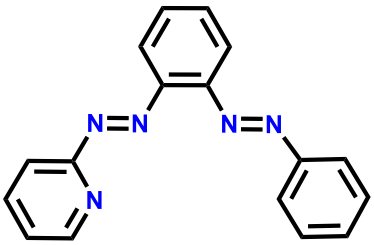

2-(pyridylazo)azobenzene

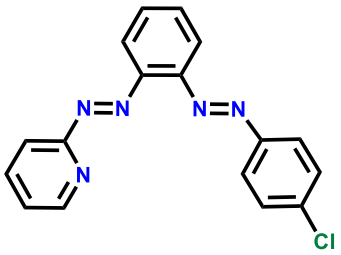

2-(2-pyridylazo)-4-chloroazobenzene

Scheme 32: Structures of the ligands used in this thesis

The polydentate chelators synthesized were redox-active, capable of stabilizing radical intermediates, and exhibited promising spectroscopic properties due to their extended π-electron system. Metal complexes of these chelators with zinc, nickel, and copper were prepared and demonstrated catalytic activity. The entire work is divided into five chapters, each detailing specific complexes and their catalytic properties.

[I.3.2] Experimental Details

[1.3.3] Physical Measurements

Various physical methods were utilized to characterize and elucidate the properties of the synthesized compounds. These techniques are detailed in the subsequent chapters and briefly summarized below.

NMR Spectra. ^{1}H, ^{13}C, ^{19}F NMR data were recorded in DMSO-d_6, $CDCl_3$ at room temperature using tetramethylsilane (TMS) as an internal standard with the help of Bruker 300 and 400 MHz FT spectrometer. Signals are assigned to individual protons on the basis of chemical shifts, spin-spin structure and substituent effects.

Electronic Spectra. Electronic spectra were recorded on Perkin-Elmer LAMBDA EZ-301 and a LAMBDA 25 UV-VIS spectrometer (200-1200 nm). A matched pair of quartz cells of path length 1 cm was used.

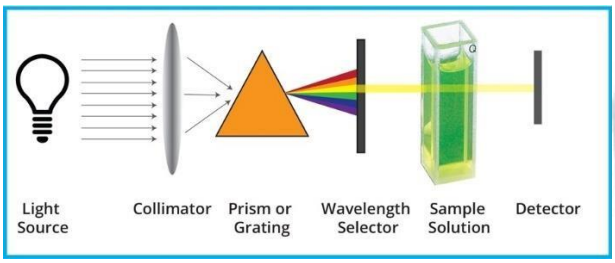

Electrochemical Measurements. CHI 620A electrochemical analyzer was used for electrochemical measurements. All experiments were performed under pure argon atmosphere 298 K. The potentials are referenced to the Ag/AgCl electrode without junction correction.

Mass Spectrometry. Electrospray ionization mass spectra (ESI-MS) (70 eV) were recorded on a Qtof Micro YA263 spectrometer.

Elemental Analysis. The C, H, N analysis of the samples was determined with the help of a Perkin-Elmer 2400 Series II elemental analyzer which utilizes thermal conductivity data for gas (CO_2, H_2O, N_2) analysis. The sample was introduced into the combustion cell usually at a temperature in the range of 900–980 °C. For combustion, pure oxygen was used and pure helium was used as the driving gas.

Infrared Spectra. IR spectra were recorded with the help of a Perkin-Elmer L-0100 spectrometer.

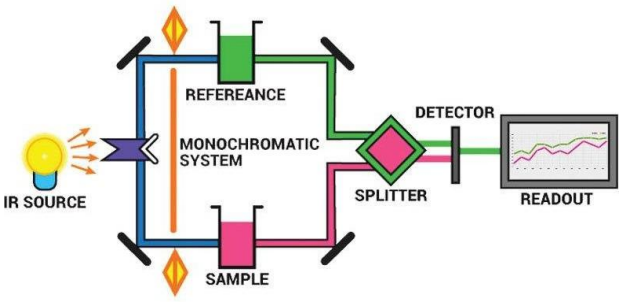

EPR Spectroscopy. EPR spectrum was recorded on a JEOL JES-FA200 spectrometer at X band.

X-ray Structure Determination

X-ray diffraction data were collected on a Bruker D8 QUEST diffractometer using Mo-Kα radiation at 298 K. The structures of all compounds were solved by direct methods using

APPEX 3.0 and OLEX 2.0. Molecular structure plots were drawn using ORTEP. *R1*, *wR2* and goodness-of-fit (GOF) are given by the following equations 1, 2 and 3 respectively.

$R1 = S½½Fo½- ½Fc½½/ S½ Fo½$ (1)

$wR2 = [S[w(Fo2 - Fc2)2] / S[w(Fo2)2]]^{1/2}$ (2)

$GOF = S = [\Sigma [w(Fo2 - Fc2)2] / (n_o - n_p)]^{1/2}$ (3)

n_o = number of reflections

n_p = total number of parameters refined

[I.3.4] Computational Studies

All calculations were performed using the Gaussian 09 program. Geometry optimization of the complexes was carried out at the (R/U)B3LYP level of theory in the gas phase, starting from their crystallographic coordinates. The optimized structural parameters generally agree well with the experimental values, with minor discrepancies attributed to crystal packing effects. The nature of all stationary points was confirmed as true minima by the absence of imaginary frequencies in the vibrational analysis. Time-dependent density functional theory (TD-DFT) calculations were performed to predict the absorption and emission spectra of the optimized geometries in dichloromethane (CH_2Cl_2) solvent. TD-DFT is a well-established method for calculating electronic excitation energies of transition metal complexes within the DFT framework. To gain insight into the nature of electronic transitions, natural transition orbital (NTO) analysis was performed based on the calculated transition density matrices. This method provides a concise representation of the transition density between the ground and excited states by decomposing it into single-particle transitions (hole and electron states). The unoccupied and occupied NTOs are referred to as "electron" and "hole" transition orbitals, respectively. For the metal atoms (zinc, copper, and nickel), a double-ζ basis set with the effective core potential of Hay and Wadt (LANL2DZ) was employed. The 6-311+G(d,p) basis set was used for other elements except hydrogen (6-31G) to optimize the ground-state geometries of the complexes. Electronic density plots for frontier molecular orbitals were generated using GaussView 5.0, and molecular orbital contributions from specific groups or atoms were calculated using GaussSum 2.2.

[I.4.] Outline of thesis

This thesis focuses on the development of homogeneous catalysts for the dehydrogenative coupling (DC) of alcohols, addressing critical limitations associated with existing methodologies. The primary objectives include the design and synthesis of novel homogeneous catalysts for the efficient DC of alcohols and the exploration of dehydrogenative aromatization as a key transformation in contemporary synthetic catalysis. Additionally, investigations into the structure-activity relationships and mechanistic pathways of these catalytic systems are undertaken, aiming to establish a comprehensive design framework for effective homogeneous catalysts that promote sustainable and greener organic synthesis.

Chapter 2 highlights the development and application of a homogeneous, isolable, air- and moisture-stable zinc catalyst stabilized by an electron-deficient N^N^N pincer-type ligand. This ternary, penta-coordinated neutral catalyst, [Zn(N^N^N)Cl_2], facilitates the selective

synthesis of α-alkylated ketone derivatives (*14 examples*) via a one-pot acceptorless dehydrogenative coupling (ADC) reaction between secondary and primary alcohols, employing the borrowing hydrogen (BH) methodology. The reactions proceed with good to excellent isolated yields, reaching up to 93%. Notably, this catalyst also enables the efficient synthesis of quinoline derivatives (*32 examples*) by utilizing 2-aminobenzyl alcohols as alkylating agents through a sequence of dehydrogenative coupling and N-annulation steps. The catalyst is characterized by its cost-effectiveness, ease of synthesis, and environmentally benign nature, along with remarkable stability during catalytic cycles under open-air conditions. This is evidenced by its high turnover number (~10^4). Activation is achieved under mild conditions with a catalytic amount of base, making this system a robust and practical tool for sustainable synthetic transformations.

Chapter 3 demonstrates Highly efficient Ni-catalyzed C–N/C–C bond formation from amidines during the [3 + 2 + 1] annulation by primary alcohols alone or by primary alcohols with secondary alcohols/phenyl acetylenes has been successfully accomplished toward scaled synthesis of *s*-triazine and pyrimidines, respectively. The reaction takes place efficiently for a wide range of substrates (*76 examples*). This catalyst that promotes this process is has a higher turnover number (TON) than previously methods using homogeneous catalysts. The results of mechanistic studies suggest that the process takes place through a pathway that begins with Ni-catalyzed dehydrogenation of the alcohol, which is followed by sequential condensation, cyclization, and dehydrogenation.

Chapter 4 contains the report of an eco-friendly and efficient method for the synthesis of biologically relevant poly-substituted pyridines, including penta-substituted derivatives, using a nickel-metalloradical catalyst. This strategy employs readily available primary and secondary aryl alcohols and ammonium acetate to achieve polyfunctionalized pyridines through catalytic dehydrogenative alcohol oxidation, affording products in good to excellent yields (68–93%) in. The microwave-assisted, solvent-free domino [2 + 2 + 1 + 1] annulation involves consecutive C–C and C–N bond formations, followed by catalytic dehydrogenative aromatization. The nickel-metalloradical catalyst efficiently serves dual catalytic cycles namely alcohol dehydrogenation and ring aromatization, both via single-electron transfer (SET) pathways. An important aspect of this approach is that it generates only environmentally benign byproducts, such as H_2O and H_2O_2, without requiring external oxidants or additional additives. This green and cost-effective methodology adheres to green chemistry principles, offering simplicity and excellent E-factor values (0.3–0.5), representing a significant advancement in functionalized pyridine synthesis.

Chapter 5 explores a catalytic approach to synthesizing *E*-configured vinylarenes through the dehydrogenative coupling of secondary alcohols or ketones with 2-amino primary alcohol derivatives i.e., Friedländer annulation reactions. A novel penta-coordinated Cu(II) catalyst, stabilized by N^N^N pincer-type ligands, facilitates this reaction, yielding products in high yields and selectivity. The process generates hydrogen peroxide and water as environmentally friendly by-products. This method offers a significant advantage over previous homogeneous catalytic systems, demonstrating a higher TON. Mechanistic studies suggest a pathway involving initial Cu-catalyzed alcohol dehydrogenation, followed by condensation.

[I.5] References

1. (a) Rao, R. N.; Jena, S.; Mukherjee, M.; Maiti, B.; *Environ. Chem. Lett.* **2021**, *19*, 3315-3358. (b) Karageorgis, G.; Foley, D. J.; Laraia, L.; Waldmann, H. *Nat. Chem*. **2020**, *12*, 227-235. (c) Kim, Y.; Li, C.-J. *Green. Synth. Catal.* **2020**, *1*, 1-11. (d) Blakemore, D. C.; Castro, L.; Churcher, I.; Rees, D. C.; Thomas, A. W.; Wilson, D. M.; Wood, A. *Nat. Chem.* **2018**, *10*, 383-394. (e) Rotella, D. P. *ACS Chem. Neurosci*. **2016**, *7*, 1315-1316.
2. (a) Lasso, J. D.; Castillo-Pazos, D. J.; Li, C.-J. *Chem. Soc. Rev*. **2021**, *50*, 10955-10982. (b) Zhang, W.; Cue, B. W. *Green Techniques for Organic Synthesis and Medicinal Chemistry,* 2nd Edition.; Pharmaceutical & Medicinal Chemistry, John Wiley & Sons, 2012, ISBN: 978-1-119-28816-9.
3. (a) Amrutkar, R. D.; Bhalerao, S. S.; Bhoir, A. S.; Bhusare, R. H.; Bodhare, S. S.; Borse, J. N. *Curr. Trends. Pharm. Pharm. Chem*. **2022**, *4*, 115-119. (b) Rothenberg, G. *Catalysis: Concepts and Green Applications*, Wiley, 2017.
4. (a) Poovan, F.; Chandrashekhar, V. G.; Natte, K.; Jagadeesh, R. V.. *Catal. Sci. Technol*. **2022**, *12*, 6623-6649. (b) Catlow, C. R.; Davidson, M.; Hardacre, C.; Hutchings, G. J. *Philos. Trans. R. Soc. A*.; **2016**, *374*, 20150089. (c) Negishi, E.-I. *Angew. Chem., Int. Ed*., **2011**, *50*, 6738-6764.
5. (a) Lei, A.; Shi, W.; Liu, C.; Liu, W.; Zhang, H.; He, C. Oxidative Cross-Coupling Reactions. Wiley-VCH: Weinheim, Germany, **2016**. (b) De Meijere, A., Diederich, F., Eds. *Metal-Catalyzed Cross-Coupling Reactions*, Wiley-VCH: Weinheim, Germany, **2004**.
6. (a) Toan, V. N.; Hai, D. S.; Van, H. T. K.; Tri, N. M.; Toan, D. N.; Mai, N. T. T.; Thanh, *RSC Med. Chem.* **2024**, *15*, 3395-3417. (b) Lim, H. Y.; Dolzhenko, A. V. *Eur. J. Med. Chem.* **2024**, *276*, 116680. (c) Tian, T.; Li, Z.; Li, C.-J. *Green Chem.*, **2021**, 23, 6789–6862. (d) Marichev, K. O.; Takacs, J. M. *ACS Catal.* **2016**, *6*, 2205-2210.
7. D. Meijere, A., Diederich, F., Eds. *Metal-Catalyzed Cross-Coupling Reactions*, Wiley-VCH: Weinheim, Germany, **2004**.
8. (a) D. Ainge; V. Luis-Manuel; *Org. Process Res. Dev.*, **2002**, *6*, 811-813. (b) B. Blank; R. Kempe; *J. Am. Chem. Soc.* **2010**, *132*, 924-925. (d) M. Zeng; T. Wang; D. Cui; C. Zhang; *New J. Chem.* **2016**, *40*, 8225-8228. (e) K. O. Marichev; J. M. Takacs; *ACS Catal.* **2016**, *6*, 2205-2210.

9. (a) C. G. Freyschlag; R. J. Madix; *Materials Today* **2011**, *14*, 134-142. (b) E. Chong; H. Wu; J. Lee; K. Forson; N. Haddad; *Org. Process Res. Dev*. **2023**, *27*, 1931-1953.
10. (a) K. C. Nicolaou; *Proc. R. Soc. A*., **2013**, *470*, 1-17. (b) K. C. Nicolaou; S. Rigol; R. Y; Total *CCS Chem*. **2019**, *1*, 3-37. (c) P. S. Baran; *J. Am. Chem. Soc*. **2018**, *140*, 4751-4755.
11. (a) P. J. Parsons; C. S. Penkett; A. J. Shell; *Chem. Rev*. **1996**, *96*, 195-206. (b) Y. Hamada; *Chem Pharm Bull*. **2012**, *60*, 1-20. (c) H. M. L. Davies; J. D. Bois; J.-Q. Yu; *Chem. Soc. Rev*. **2011**, *40*, 1855-1856.
12. (a) C. Gunanathan; D Milstein; *Science* **2013**, *341*, 1229712. (b) G. E. Dobereiner; R. H. Crabtree; *Chem. Rev*. **2010**, *110*, 681-703. (c) G. Guillena; D. J. Ramon; M. Yus; *Chem. Rev*. **2010**, *110*, 1611-1641. (d) A. J. A. Watson; J. M. J. Williams; *Science* **2010**, *329*, 635-636. (e) T Irrgang; R. Kempe; *Chem. Rev*. **2019**, *119*, 2524-2549. (f) B. G. Reed-Berendt; D. E. Latham M. B.Dambatta; L. C. Morril; *ACS Cent. Sci*. **2021**, *7*, 570-585.
13. J. Hwang; K. Maharjan; H. Cho; *Int. J. Hydrog. Energy*. **2023**, *48*, 28629-28648.
14. K. Barta; P. C. Ford; *Acc. Chem. Res*. **2014**, *47*, 1503-1512.
15. C. Lofberg; R. Grigg; A. Keep; A. Derrick; V. Sridharan; C. Kilner, *Chem. Commun*. **2006**, 5000-5002.
16. Y. Yang; A. Qin; K. Zhao; D. Wang; X. Shi; *Adv. Synth. Catal.* **2016**, *358,* 1433-1439.
17. R. Wang; L. Huang; Z. Du; H. Feng; *J. Organomet. Chem.* **2017**, *846*, 40-43.
18. S. Genc; S. Günnaz; B. Çetinkaya; S. Gülcemal; D. Derya Gülcemal; *J. Org. Chem*. **2018**, *83*, 2875-2881.
19. E. Putignano; G. Bossi; P. Rigo; W. Baratta; *Organometallics* **2012**, *31*, 1133-1142.
20. R. Mamidala; S. Samser; N. Sharma; U. Lourderaj; K. Venkatasubbaiah; *Organometallics* **2017**, *36*, 3343-3351.
21. (a) C. Seck; M. D. Mbaye; S. Coufourier; A. Lator; J.-F. Lohier; A. Poater; T. R. Ward; S. Gaillard; J.-L. Renaud; *ChemCatChem* **2017**, *9*, 4410-4416. (b) S. Elangovan; J.-B. Sortais; M. Beller; C. Darcel; *Angew. Chem., Int. Ed*. **2015**, *54*, 14483-14486.
22. G. Zhang; J. Wu; H. Zeng; S. Zhang; Z. Yin; S. Zheng; *Org. Lett.* **2017**, *19*, 1080.
23. M. Peña-López; P. Piehl; S. Elangovan; H. Neumann; M. Beller; *Angew. Chem., Int. Ed.* **2016**, *55*, 14967.
24. I. K. Fujita; C. Asai; T. Yamaguchi; F. Hanasaka; R. Yamaguchi; *Org. Lett.* **2005**, *7*, 4017-4019.
25. C. S. Cho; B. T. Kim; H. -S. Kim; T. -J. Kim; S. C. Shim; *Organometallics.* **2003**, *22*, 3608-3610.
26. B. C. Roy; K. Chakrabarti; S. Shee; S. Paul; S. Kundu; *Chem. - A Eur. J.* **2016**, *22*, 18147-18155.
27. Q. Wang; K. Wu; Z. Yu; *Organometallics* **2016**, *35*, 1251-1256.
28. T. Liu; L. Wang; K. Wu; Z. Yu; *ACS Catal.* **2018**, *8*, 7201-7207.
29. O. El-Sepelgy; E. Matador; A. Brzozowska; M. Rueping; *ChemSusChem* **2019**, *12*, 3099-3102.
30. F. Freitag; T. Irrang; R. Kempe; *Chem. - Eur. J.* **2017**, *23*, 12110.
31. J. Marco-Contelles, E. Pérez-Mayoral, A. Samadi, M. d, C. Carreiras and E. Soriano, *Chem. Rev.*, **2009**, 109, 2652–2671.
32. G. Chelucci; A. Porcheddu; *Chem*. *Rec*., **2017**, 17, 200–216.
33. S. Ruch, T. Irrgang; R. Kempe; *Chem. – Eur. J.*, **2014**, 20, 13279–13285.
34. D. Wei, V. Dorcet, C. Darcel; J.-B. Sortais; *ChemSusChem*, **2019**, 12, 3078–3082.
35. M. Maji, K. Chakrabarti, D. Panja; S. Kundu; *J. Catal*., **2019**, 373, 93–102.
36. S. Parua, R. Sikari, S. Sinha, S. Das, G. Chakraborty; N. D. Paul; *Org*. *Biomol*. *Chem*., **2018**, 16, 274–284.

37. M. Mastalir, M. Glatz, E. Pittenauer, G. Allmaier; K. Kirchner; *J. Am. Chem. Soc.*, **2016**, 138, 15543–15546.
38. K. Das, A. Mondal; D. Srimani; *Chem*. *Commun*., **2018**, 54, 10582–10585.
39. (a) M. J. Climent, A. Corma; S. Iborra; Chem. Rev., 2011, 111, 1072–1133. (b) S. M. A. Hakim Siddiki, T. Toyao; K. I. Shimizu; Green Chem., 2018, 20, 2933–2952. (c) C. Gunanathan; D. Milstein; Science, 2013, 341, 1761–1779. (d) R. H. Crabtree, Chem. Rev., 2017, 117, 9228–9246. (e) T. D. Nixon, M. K. Whittlesey; J. M. J. Williams; Dalton Trans., 2009, 753–762.
40. (a) T. He, L. Liu, G. Wu; P. Chen, *J. Mater. Chem.* A, **2015**, 3, 16235–16241. (b) Z. Zhang, W. Liu, Y. Zhang, J. Bai; J. Liu, *ACS Catal.* **2021**, 11, 313–322. (c) W. Guo, M. Zhao, W. Tan, L. Zheng, K. Tao; X. Fan; *Org. Chem. Front*; **2019**, *6*, 2120–2141. (d) K. Sun, H. Shan, G. Lu, C. Cai; M. Beller; *Angew*. *Chem*., **2021**, *133*, 25392–25406.
41. (a) K. C. Tan; T. He; Y. S. Chua; P. Chen; *J. Phys. Chem*. *C*; ***2021***, *125*, 18553–18566. (b) M. Maji; D. Panja; I. Borthakur; S. Kundu; *Org*. *Chem*. *Front*; **2021**, *8*, 2673–2709. (c) M. Liu, L. Guo, S. Jin; B. Tan; *J. Mater. Chem. A;* **2019**, *7*, 5153–5172.
42. (a) I.M. Lagoja; *Chem. Biodivers*. **2005**, *2*, 1–50; (b) F. Varano; D. Catarzi; F. Vincenzi; M. Betti; M. Falsini; A. Ravani; P.A. Borea; V. Colotta; K. Varani; *J. Med. Chem*. **59** (*2016*) 10564–10576; (c) S. Bag; A. Mondal; R. Jayarajan; U. Dutta; S. Porey; R.B. Sunoj; D. Maiti; *J. Am. Chem. Soc. **2020***, *142,* 12453–12466; (d) R. Mondal; G. Chakraborty; A.K. Guin; S. Sarkar; N.D. Paul; *J. Org. Chem*. **2021,**86, 13186–13197.
43. (a) M. Johar; T. Manning; D.Y. Kunimoto; R. Kumar; *Bioorg. Med. Chem., **2005**,13*,6663–6671; (b) V. Sharma; N. Chitranshi; A.K. Agarwal; *Int. J. Med. Chem*. **2014** (*2014*) 1–31; (c) D. Liu; W. Guo; W. Wu; H. Jiang; *J. Org. Chem*., ***2017,*** *82,* 13609–13616.
44. (a) I.S. Park; H. Komiyama; T. Yasuda; *Chem. Sci*. **2017***, 8*, 953–960; (b) Y.-K. Chen; H.-H. Kuo; D. Luo; Y.-N. Lai; W.-C. Li; C.-H. Chang; D. Escudero; A. K.Y. Jen; L.-Y. Hsu; Y. Chi; *Chem. Mater*. **2018**,*31*, 6453–6464; (c) A.K. Yadav; V.D. Ghule; S. Dharavath; *J. Mater. Chem. A* **2022**,*10*, 12702–12712; (d) C.-H. Chen; S.-C. Lin; B.-Y. Lin; C.-Y. Li; Y.-C. Kong; Y.-S. Chen; S.-C. Fang; C.- H. Chiu; J.-H. Lee; K.-T. Wong; C.-F. Lin; W.-Y. Hung; T.-L. Chiu; *Chem. Eng. J*. **2022**, *442*, 136292.
45. G. Shi; F. He; Y. Che; C. Ni; Y. Li; *Russ. J. Gen. Chem.* **2016**, *86,* 380–386.
46. S. S. Poly; Y. Hashiguchi; I. Nakamura, T. Fujitani; S. M. A. H. Siddiki. *Catal. Sci. Technol.* **2022**, *12*, 4679–4687.
47. F. Xie; M. Chen; X. Wang; H. Jiang; M. Zhang; *Org. Biomol. Chem.*, **2014**, *12*, 2761–2768.
48. N. Deibl, K. Ament, R. Kempe, *J. Am*. *Chem*. *Soc*. **2015**, *137*, 40, 12804–12807.
49. S. S. Poly; S. M. A. H. Siddiki; A. S. Touchy; K. W. Ting; T. Toyao; Z. Maeno; Y. Kanda. K.I Shimizu, *ACS Catal*. **2018**, *8,* 11330−11341.
50. A. K. Bains; D. Adhikari; *Catal. Sci. Technol*., **2020**, *10*, 6309–6318.
51. Q. You; F. Wang; C. Wu; T. Shi; D. Min; H. Chen; W. Zhang; *Org. Biomol. Chem.*, **2015**, *13*, 6723–6727.
52. S. Das; R. Mondal; A. K. Guina; N. D. Paul; *Org*. *Biomol*. *Chem*., **2022**, *20*, 3105-3117.
53. M. Mastalir; M. Glatz; E. Pittenauer; G. Allmaier; K. Kirchner; *J. Am. Chem. Soc.* **2016**, *138*, 15543–15546.
54. R. Mondal; S. Sinha; S. Das; G. Chakraborty; N. D. Paul; *Adv*. *Synth*. *Catal*. **2020**, *362,* 594 – 600.

55. G. Chakraborty; R. Sikari; R. Mondal; S. Mandal; N. D. Paul; *Asian J. Org. Chem*. **2020**, *9,* 431 –436.

56. (a) Y. Higashio; T. Shoj;, *Appl. Catal., A*, **2004**, *260*, 251–259. (b) R. S. Sagitullin, G. P. Shkil, I. I. Nosonov; A. A. Ferber, *Chem. Heterocycl. Compd.*, **1996**, *32*, 127–140.

57. S. Michlik; R. Kempe, *Angew. Chem., Int. Ed.*, **2013**, *52*, 6326–6329.

58. D. Srimani, Y. B. David; D. Milstein; *Chem. Commun.*, **2013**, *49*, 6632–6634.

59. S. P. Midya; V. G. Landge; M. K. Sahoo; J. Rana; E. Balaraman. *Chem. Commun.*, **2018**, *54*, 90–93.

60. (a) D. Astruc; E. Boisselierand; C. Ornelas. *Chem. Rev.,* **2010**, *110*, 1857–1959; (b) E. Coronado; P. Gaviña; S. Tatay; R. Groarkeand; J. G. Vos; *Inorg. Chem*., **2010**, *49*, 6897–6903; (c) J. Albert; R. Bosque; M. Crespo; J. Granell; J. Rodríguez; J. Zafrilla; *Organometallics,* **2010**, *29*, 4619–4627; (d) A. K. Das; B. Sarkar; J. Fiedler; S. Záliš; I. Hartenbach; S. Strobel; G. K. Lahiri; W. Kaim; *J. Am. Chem. Soc*., **2009**, *131*, 8895–8902; (e) A. N. Singh; R. P. Thummel; *Inorg. Chem.*, **2009**, *48*, 6459–6470;(f) S. Patraand; P. Paul; *Dalton Trans*., **2009**, 8683–8695; (g) J. Maurer; M. Linseis; B, Sarkar; B. Schwederski; M. Niemeyer; W. Kaim; S. Záliš; C. Anson; M. Zabel; R. F. Winter; *J. Am. Chem. Soc*., **2008**, *130*, 259–268; (h) D. M. Morales; C. M. Jensen; Eds. The Chemistry of Pincer compounds, Elsevier, Amsterdam, Netherlands, **2007**, 248, 2239–2246; (i) L. Ackermann; N. Chatani; Directed Metallation, Springer, Berlin, **2007**; (j) E. Peris; R. H. Crabtree; *Coord. Chem. Rev*.,**2004**, (k) J. A. McCleverty; T. J. Mayer; Eds. Comprehensive Coordination Chemistry II, Pargamon, Oxford, 2004; (l) S. A. Cotton; Chemistry of Precious Metals, Blackie Academic and Professional, UK, 1997;(m) A. K. Singh; V. Balamurugan; R. Mukherjee; *Inorg. Chem*., **2003**, *42,* 6497–6502; (n) A. K. Bilakhiya; B. Tyagi; P. Paul; P. Natarajan; *Inorg. Chem*., **2002**, *41*, 3830–3842; (o) D. Herebian; E. Bothe; E. Bill; T. Weyhermüllerand; K. Wieghardt, J. Am. Cheīm. *Soc*., **2001**, *123*, 10012–10023.

61. (a) M. S. Yadav; O. D. Tyagi; A Textbook of Synthetic Dyes, 2nd Ed., Anmol Publications Pvt. Ltd, New Delhi, 2004. (b) W. Herbstand K Hunger, 3rd Ed., Industrial organic pigments: production, properties, applications, Wiley-VCH, Weinheim, 2004. (a) E. Westphal; I. H. Bechtold; H. Gallardo; *Macromolecules*, **2010**, *43*, 1319-1328; (b) H. Li; R. Termine; L. Angiolini; L. Giorgini; F. Mauriello; A. Golemme; *Chem. Mater*. **2009**, *21*, 2403–2409; (c) M. Haro; B. Giner; I. Gascon; F. M. Royo; M. C. Lopez; *Macromolecules*, **2007**, *40*, 2058–2069; (d) C. Cojocariu; P. Rochon; *Pure Appl. Chem*.,**2004**, *76*, 1479–1497;(e) A. Natansohn; P. Rochon; *Chem. Rev*. **2002**, *102*, 4139–4176; (f) J. A. Delaire; K. Nakatani; *Chem. Rev*., **2000**, *100*, 1817–1845.

62. (a) S. McCarthy; D. C. Braddock; J. D. E. T. Wilton-Ely; *Coord. Chem. Rev.* **2021,** *442,* 213925. (b) A. Biffis; P. Centomo; A. Del Zotto; M. Zecca; *Chem. Rev.* **2018,** *118,* 2249−2295. (c) N. Hazari; P. R. Melvin; M. M. Beromi. *Nat, Rev. Chem.* **2017,** *1,* 0025. (d) V. R. Landaeta; T. M. Horsley Downie; R. Wolf; *Chem. Rev.* **2024,** *124,* 1323−1463. (e) Q. Yan; X. Wu; H. Jiang; H. Wang; F. Xu; H. Li; H. Zhang; S. Yang; *Coord. Chem. Rev.* **2024**, *502*, 215622. (f) Y. Wang; W. -X. Zhang; Z. Xi; *Chem. Soc. Rev.* **2020**, *49*, 5810–5849.

63. (a) N. Paul; T. Kramer; J. E. McGrady; S. Goswami; *Chem. Commun*., **2010**, *46*, 7124–7126; (b) P. Pattanayak; J. L. Pratihar; D. Patra;S. Mitra; A. Bhattacharyya; H. M. Lee; S. Chattopadhyay, *Dalton Trans*., **2009**, 6220–6230; (c) J. L. Pratihar; B. Shee; P. Pattanayak; D. Patra; A. Bhattacharyya; V. G. Puranik; C. H. Hung; S. Chattopadhyay, *Eur. J. Inorg. Chem*., **2007**, *4272*–4281. (a) U. Das; T. Ghorui; B. Adhikari; S. Roy; S. Pramanik; K. Pramanik; *Dalton Trans*. **2015**, *44*, 8625–8639; (b) S. Pramanik; S. Roy; T. Ghorui; S. Ganguly; K. Pramanik; *Dalton Trans*., **2014**, *43*, 5317–5334; (c) K. Pramanik; U. Das; B.

Adhikari; D. Chopra; H. Stoeckli-Evans; *Inorg*. *Chem*.,**2008**, *47*, 429–438; (d) K. Pramanik; B. Adhikari; *Polyhedron*, **2010**, *29*, 1015−1022.

64. (a) J. Mooibroek; G. Aromi; M. Quesada; O. Roubeau; P. Gamez; S. DeBeer George; J. van Slageren; S. Yasin; E. Ruiz; J. Reedijk, *Inorg*. *Chem*., **2009**, *48*, 10643-10651. (b) I. Aiello; M. Guedini; M. La Deda; J. Luminescence,2002, 96, 249-259. (c) M. Albrecht; *Chem*. *Rev*., **2010**, *110*, 576–623. (d) S.-H; Li C.-W. Yu J.-G. Xu, *Chem*. *Commun*., **2005**, *450*–452.

65. (a) S. Roy; S. Pramanik; T. Ghorui; K. Pramanik; *RSC Adv*., **2015**, *5*, 22544–22559; (b) S. Baksi; D. K. Seth; H. Tadesse; A. J. Blake; S. Bhattacharya; *J*. *Organomet*. *Chem*., **2010**,*695*, 1111–1118; (c) P. Pattanayak; J. L. Pratihar; D. Patra; S. Mitra; A. Bhattacharyya; H. M. Leeand; S. Chattopadhyay; *Dalton Trans*., **2009**, 6220–6230; (d) J. L. Pratihar; S. Bhaduri; P. Pattanayak; D. Patra; S. Chattopadhyay; *J*. *Organomet*. Chem., **2009**, *694*, 3401–3408;(e) S. Baksi; R. Acharyya; S. Dutta; A. J. Blake; M.G.B. Drew; S. Bhattacharya; *J*. *Organomet*. *Chem*., **2007**,*692*, 1025–1032; (f) P. Gupta; S. Dutta; F. Basuli; S-M. Peng; G-H. Lee; M. Nethaji; S. Bhattacharya; *Inorg*. *Chem*., **2006**, *45*, 460–467; (g) J. L. Pratihar; N. Maitiand; S. Chattopadhyay; *Inorg*. *Chem*., **2005**, *44*, 6111–6114.

Chapter II

Potent Pincer-Zinc Catalyzed Homogeneous a-Alkylation and Friedländer Quinoline Synthesis of Secondary alcohols/Ketones with Primary Alcohols

II.1 Introduction

The construction of molecules with diverse functional groups from commonly available small molecules/building blocks by C−C, C−heteroatom bond activations is one of the fundamental aspects of chemical and biochemical syntheses.[1] In reality, majority of classical methods require expensive and environmentally toxic reagents and, discharge hazardous waste even in (over)stoichiometric amounts.[2] Thus, the development of efficient approach is desirable for selective C−C and C−heteroatom formation reactions. Accordingly, beneficial organic compounds with potential applications in the medical, agrochemical and pharmaceutical industries may be synthesized.[3] In this context, conversion of alcohols to C-alkylated derivatives and N-heterocycles *via* acceptorless dehydrogenation coupling (ADC) and borrowed hydrogen (BH)/N-annulation methodologies using homogeneous catalysts have received considerable importance in recent years.[4] Although such transformation reactions can be accomplished with 0.5-5 mol% platinum-group-metal catalysts (e.g., Ru, Rh, Ir, Pd and Pt) in satisfactory yields.[5-9] In general, catalysis by non-precious first-row transition metals with good turnover numbers (TONs) under open-air condition for α-alkylation and Friedländer annulation reactions remains challenging for gram-scale production of high-value bio-active molecules.[10] Nonetheless, a continuous effort has been made with 3d metal catalysts (Mn, Fe, Co, Ni and Cu) with comparable catalyst loading **(**0.5-5 mol%**)** since they provide a more economically viable solution (Scheme 1and 2).[11-15] Only a few examples have recently been reported where analogous reactions can be accomplished with 0.05% or less catalyst loading with Ni(II) and Mn(I), respectively.[16]

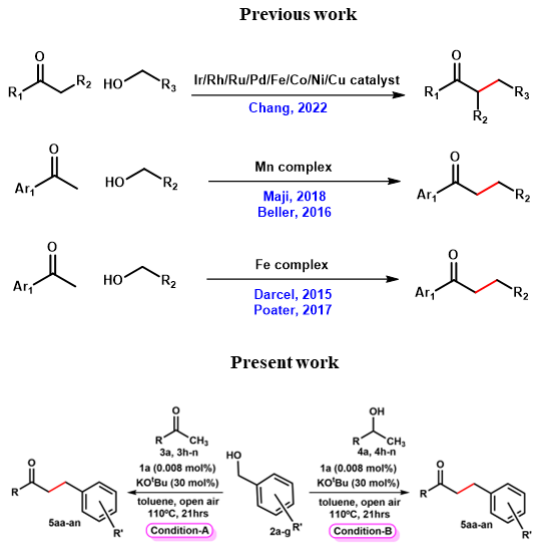

Scheme 1: Selected examples for C–C bond formation reactions.

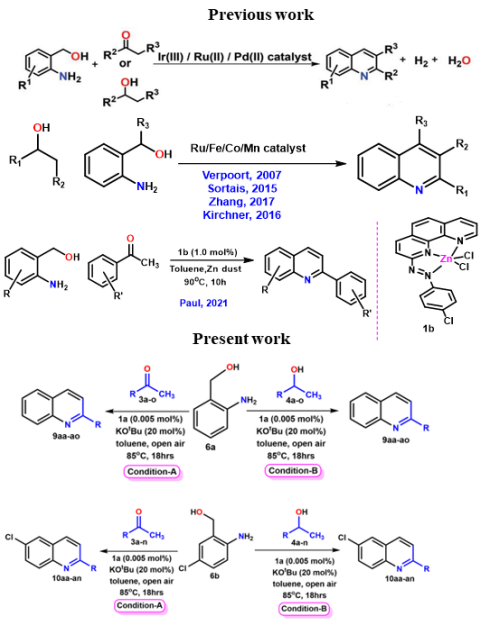

Scheme 2: Selected examples for C–N bond formation reactions.

It is worth noting that the use of zinc(II) is less cited as homogeneous catalysis unlike other 3d metals plausibly due to its closed-shell, electron-rich, redox innocent nature. Only very recently molecular zinc-catalyzed dehydrogenation reactions of secondary alcohol have been documented.[17]

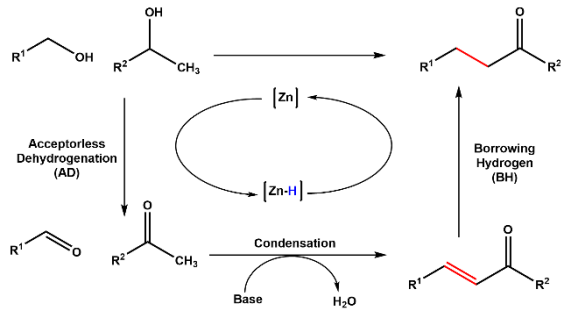

Scheme 3: Plausible mechanistic pathway for α-alkylation of secondary alcohols/ketones with primary alcohols.

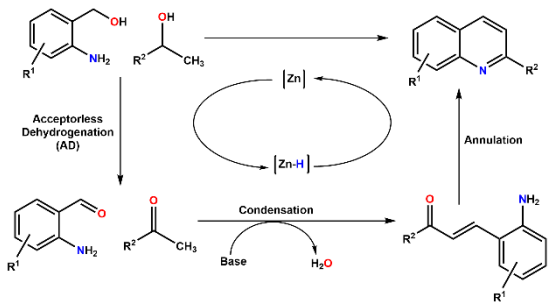

Scheme 4: Plausible mechanistic pathway for dehydrogenative coupling of secondary alcohols/ketones with primary amino alcohols.

Here, dehydrogenation of an alcohol occurred first to produce an aldehyde or ketone that undergoes an *in-situ* condensation reaction with an enolate or amine to form an α, β-unsaturated ketone or imine, where the former is finally reduced to form a new C−C bond (Scheme 3) or the subsequent cyclization of aniline derivatives leads to quinolines because of the aromatization in case of C−N annulation reaction (Scheme 4).

In general, the catalytic performance of homogeneous catalysts is superior to that of heterogeneous catalysts.[18] Nonetheless, the disadvantage of the use of homogeneous catalysts lies in their limited *in-situ* recyclability. The easily available metal catalysts are commonly leached in catalytic cycles. Only homogeneous catalysts of robust nature are the best option to overcome this difficulty. Azo-based N-heterocyclic pincer-type ligands with contiguous chelate rings are particularly useful in imparting better stability to metal complexes and therefore helping to maintain metal-ligand integrity many times during the catalytic cycle.[19] In contrast, typically stoichiometric amount or higher catalyst loading is required for 3d metal catalysts, generated *in-situ* from its simple salt with commonly available coligand(s). Majority of such catalysts suffers from sustainability issue as manifested from their turnover number (TON) *vis-à-vis* catalyst loading in due course of catalytic reactions. Readily available binary, ternary transition metal catalysts of types halides, acetates, carbonyls, phosphines and so forth tend to leach during the catalytic cycle and hence the catalyst loading needs to be enhanced to obtain

the satisfactory result.[10] This creates two additional burdens due to extra costs for the purification process of the substance and accompanying wastage of environmentally hazardous metal catalysts. In the context of scaled production of bioactive molecules, the paucity of environmentally benign homogeneous catalysts containing 3d metals leaves much space for potential improvements.

Herein, we report a convenient strategy to synthesize a compelling homogeneous molecular catalyst incorporating environmentally benign zinc integrated with an archetypal π-acidic pincer. The neutral penta-coordinated [Zn(N^N^N)Cl_2] catalyst **1** have been shown an effective complex to mediate both one-pot C–C (α-alkylation) and C–N (Friedländer annulation) bond formation in good to excellent yields under mild conditions. Furthermore, the use of zinc as a non-precious metal has received significant attention in sustainable chemistry, as it is environmentally friendly, cost-effective and widely accessible compared to other 3d transition metals as well as platinum-group metals.[20] It is worth mentioning that the catalyst loading in our case (C–C and C–N cross coupling) is very small, less than 0.01 mol%.

II.2 Results and discussion

II.2.1. Synthesis of ligands and complexes

First, we synthesized two penta-coordinated Zn(II) complexes, [Zn(L^{Cl})Cl_2] **1a** and [Zn(L^{H})Cl_2] **1b**, by reacting anhydrous $ZnCl_2$ with 2-(2-pyridylazo)-4-chloroazobenzene (L^{Cl}) and 2-(2-pyridylazo)azobenzene (L^{H}), respectively (Scheme 5). The reason behind the use of a strong electron-deficient organic template L lies in the favourable initial attack of nucleophiles (primary/secondary alcohols) at the electron-rich zinc centre, which in turn can facilitate the overall catalytic pathway Scheme 8. Exploration of these pincer complexes toward cross-coupling catalytic activities is reported in this work.

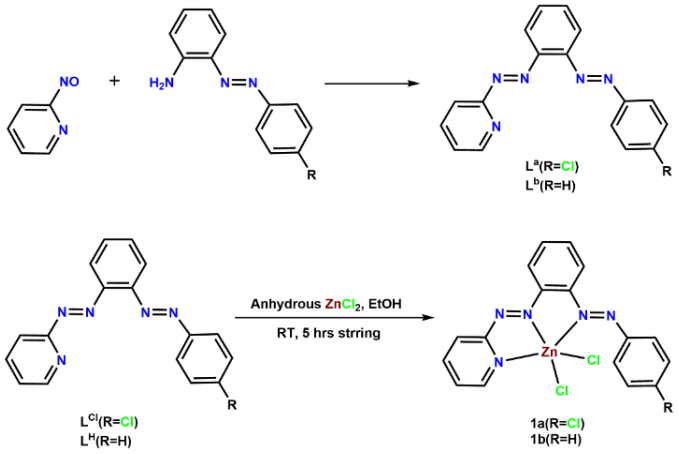

Scheme 5: Synthetic strategy of the zinc catalysts of type [Zn(L)Cl_2] **1**

The organic templates L^{Cl} and L^{H} comprising two electron-deficient azo moieties along with an aromatic heterocyclic group have been prepared by condensation of (E)-2-((4-chlorophenyl)azo)aniline or (E)-2-(phenylazo)aniline with 2-nitrosopyridine using the previously reported procedure.[21a] Stoichiometric reaction of anhydrous $ZnCl_2$ with the respective organic template (L^{Cl} or L^{H}) in ethanolic medium at room temperature for 6 hrs affords two new deep red complexes, **1a** and **1b** in 90% and 92% yields, respectively. Both products are air- and moisture-stable.

II.2.2. IR spectra

Sharp vibrations around 1461, 1417 cm^{-1} and 1467, 1416 cm^{-1} in the infrared spectra of the free ligands were assigned to the $\nu_{N=N}$ stretching for $\mathbf{L^{Cl}}$ and $\mathbf{L^{H}}$ respectively. The observed lowering of $\nu_{N=N}$ values in complexes 1459, 1390 cm^{-1} and 1456, 1397 cm^{-1} as compared to that of free ligand is consistent with the Zn(II) → π*(azo) back-bonding for complex **1a** and **1b** respectively (Figure 1).

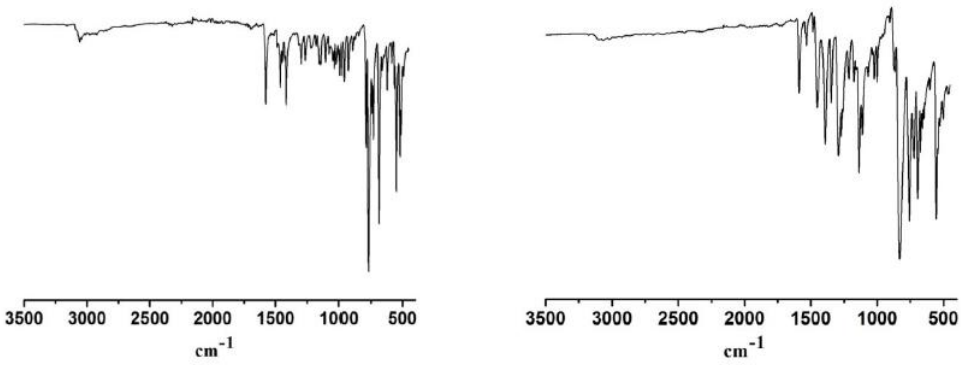

Figure 1: IR spectra of $\mathbf{L^{Cl}}$ (left) and **1a**(right).

II.2.3. NMR spectra

^{1}H and ^{13}C NMR of the ligands and complexes were recorded in CDCl3 with TMS as internal standard. ^{1}H and ^{13}C NMR spectral data provided the support for coordination of the L through the azo chromophores with zinc metal in both $[Zn^{II}(L^{Cl})Cl_2]$ **1a** and $[Zn^{II}(L^{H})Cl_2]$ **1b** complexes. The ligands are coordinated in their pristine neutral form as apparent from their diamagnetic behaviour, though the coordination with other oxidation states (L^{-I}, L^{-II}) was known.[21b] Noticeable variations in chemical shift of the bisazo-pyridine chelates with that of their respective free forms are consistent with their strong bonding with the metal center.[21a] ^{1}H and ^{13}C NMR spectrum of both complexes are pertinent with the expected structure (Figure 3). The most deshielded protons observed at δ 8.76 and 8.75 as doublet can be assigned as the H atoms adjacent to the pyridyl nitrogen atom.

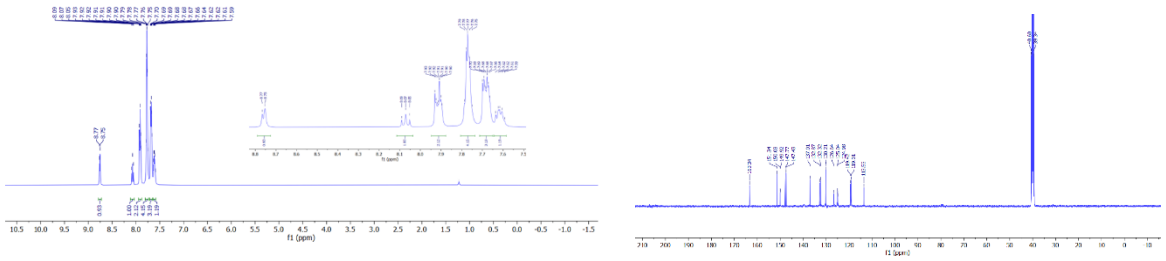

Figure 3: ^{1}H and ^{13}C NMR spectra of complex **1a** (DMSO-d_6).

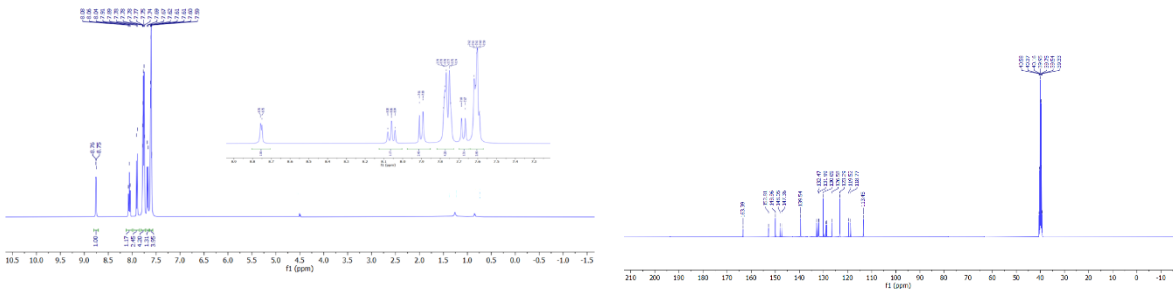

Figure 4: ^{1}H and ^{13}C NMR spectra of complex **1b** (DMSO-d_6).

II.2.4. Crystal Structures

Using the X-ray diffraction technique, the molecular structures of two zinc compounds were determined by growing suitable X-ray quality single crystals from the slow diffusion of respective dichloromethane solutions into n-hexane at room temperature. ORTEP perspectives with selected bond parameters of **1a** and **1b** are given in Figures 5-6.

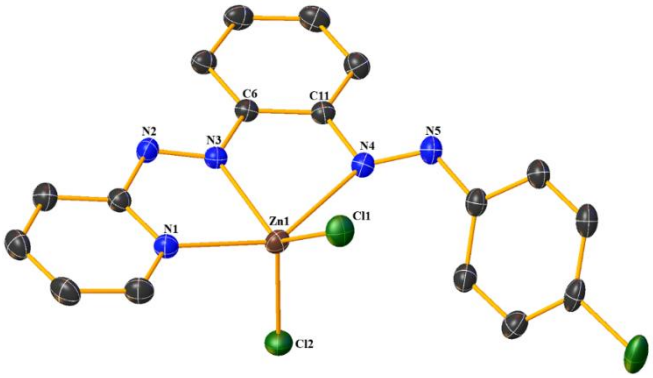

Figure 5: ORTEP view of **1a** (Solvent molecule and hydrogen atoms are omitted for clarity, and thermal ellipsoids are set at 50% probability). Selected bond lengths (Å) and bond angles (deg): Zn1–Cl1 2.2125(9), Zn1–Cl2 2.2272(9), Zn1–N1 2.167(3), Zn1–N3 2.127(2), Zn1–N4 2.466(3), N2–N3 1.260(3), N4–N5 1.263(4), N1–Zn1–N3 73.25(9), N3–Zn1–N4 71.40(9), N4–Zn1–Cl1 94.71(6), Cl1–Zn1–Cl2 123.35(4), Cl1–Zn1–N3 126.89(7), Cl1–Zn1–N1 99.51(9), N1–Zn1–Cl2 100.84(7), N3–Zn1–Cl2 109.54(7), N4–Zn1–Cl2 98.87(6).

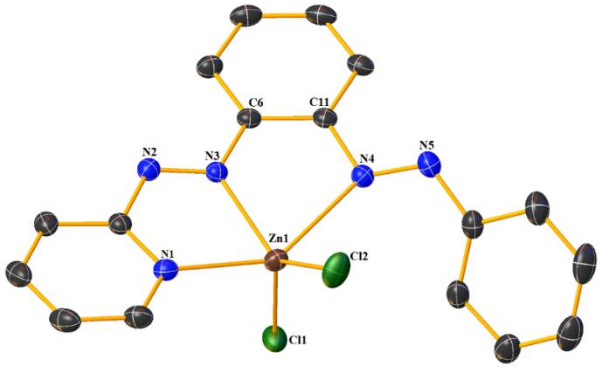

Figure 6: ORTEP view of **1b** (Solvent molecule and hydrogen atoms are omitted for clarity, and thermal ellipsoids are set at 50% probability). Selected bond lengths (Å) and bond angles (av) (deg): Zn1–Cl1 2.221(7), Zn1–Cl2 2.210(7), Zn1–N1 2.170(1), Zn1–N3 2.126(1), Zn1–N4 2.452(1), N2–N3 1.259(2), N4–N5 1.257(3), N1–Zn1–N3 73.14(7), N3–Zn1–N4 72.51(6), N4–Zn1–Cl1 95.78(5), Cl1–Zn1–Cl2 126.54(3), Cl1–Zn1–N3 115.64(5), Cl1–Zn1–N1 99.90(5), N1–Zn1–Cl2 99.98(5), N3–Zn1–Cl2 117.54(5), N4–Zn1–Cl2 96.53(5).

and additional crystallographic information are provided in Table 1 and 2. Complexes **1a** and **1b** crystalize in monoclinic C12/c1 and orthorhombic Pbca space group respectively.

The asymmetric unit of complex **1b** contains two crystallographically independent molecules ($Z' = 8$), with all atoms located in general positions, and the unit cell contains sixteen molecules. The primary valency of Zn(II) is fulfilled by two chlorides, aligned cis to each other to reduce

Table 1: Crystallographic Details of complexes **1a** and **1b**.

	1a	**1b**
Empirical formula	$C_{17}H_{12}N_5Cl_3Zn$	$C_{17}H_{13}N_5Cl_2Zn$
T/K	298K	298K
fw	458.04	847.19
Crystal system	Monoclinic	Orthorhombic
Space Group	C12/c1	Pbca
a/Å	14.0244(8)	13.2739(4)
b/Å	15.2683(9)	13.0215(4)
c/ Å	19.1822(11)	41.0373(12)
α/deg	90	90
β/deg	105.697(2)	90
γ/deg	90	90
V/ $Å^3$	3954.3(4)	7093.1(4)
Z	8	8
D_c/Mgm^{-3}	1.539	1.587
μ/mm^{-1}	1.658	1.696
F(000)	1840	3424
cryst size/mm^3	0.5 × 0.3 × 0.2	0.5 × 0.3 × 0.2

θ/deg	2.091 – 25.712	2.405 – 28.733
Measured reflns	9889	9139
Unique reflns	3912	10062
[a]GOF on F^2	1.117	1.191
R1[b], wR2[c][$I>2\sigma(I)$]	0.0425, 0.0986	0.0368, 0.0827
R1, wR2	0.0521, 0.1045	0.0423, 0.0858

[a]GOF = $\{\Sigma[w(F_o{}^2-F_c{}^2)2]/(n-p)\}^{1/2}$. [b]R1 = $\Sigma\,[|F_o|-|F_c|]/\,\Sigma\,|F_o|$.
[c]wR2 = $[\Sigma\,[w(F_o{}^2-F_c{}^2)^2]/\,\Sigma\,[w(F_o{}^2)^2]]^{1/2}$ where $w = 1/[\,\sigma^2(F_o{}^2)+(aP)^2+bP]$, $P = (F_o{}^2+2F_c{}^2)/3$.

overall steric encumbrance. The ligand L and two Cl atoms furnish distorted penta-coordinated geometry around Zn(II), while tridentate coordination was found through $N_{pyridyl}$, $N_{azopyridyl}$ and and $N_{azophenyl}$ atoms to form two juxtaposed five-membered rings in due course of chelation. This typical class of ligand with appreciable π-acidity ensures strong coordination through back-bonding with the metal centre, and thus leads to a robust class of coordinatively unsaturated zinc compounds. These two features are indispensable for a metal catalyst to be a good candidate in homogeneous catalysis with sustainable character. For precise determination of geometry between square pyramid and trigonal bipyramid of penta-coordinated complexes, the largest (N1−Zn1−N4 143.59Å) and second-largest (N3−Zn1−Cl1 126.89Å) angles are used to calculate the τ value as 0.278 for **1a** and similar calculation for **1b** results τ value as 0.225.

Table 2: Selected Experimental and Theoretical Bond Parameters of **1a** and **1b** complex.

1a			**1b**		
Parameter	**Expt.**	**Theo.**	**Parameter**	**Expt.(average)**	**Theo.**
Zn1–Cl1	2.2125(9)	2.349	Zn1–Cl1	2.221(7)	2.299
Zn1–Cl2	2.2272(9)	2.355	Zn1–Cl2	2.210(7)	2.283
Zn1–N1	2.167(3)	2.228	Zn1–N1	2.170(19)	2.279
Zn1–N3	2.127(2)	2.245	Zn1–N3	2.126(17)	2.246
Zn1–N4	2.466(3)	2.593	Zn1–N4	2.452(17)	2.451
N2–N3	1.260(3)	1.261	N2–N3	1.259(2)	1.261
N4–N5	1.263(4)	1.263	N4–N5	1.257(3)	1.265
Cl1Zn1Cl2	123.35(4)	129.99	Cl1Zn1Cl2	126.54(3)	132.27
Cl1Zn1N4	94.71(6)	97.82	Cl1Zn1N4	95.78(5)	100.58
Cl2Zn1N4	98.87(6)	96.67	Cl2Zn1N4	96.53(5)	96.89
N1Zn1Cl1	99.51(7)	99.76	N1Zn1Cl1	99.90(5)	97.66
N1Zn1Cl2	100.84(7)	99.57	N1Zn1Cl2	99.98(5)	96.39
N1Zn1N4	143.59(9)	139.22	N1Zn1N4	143.54(6)	140.26
N3Zn1Cl1	126.89(7)	127.45	N3Zn1Cl1	115.64(5)	107.27
N3Zn1Cl2	109.54(7)	102.35	N3Zn1Cl2	117.54(5)	120.41
N3Zn1N1	73.25(9)	71.54	N3Zn1N1	73.14(7)	70.10
N3Zn1N4	71.40(9)	68.88	N3Zn1N4	72.51(6)	70.86
C1N1Zn1	128.9(2)	127.08	C1N1Zn1	128.99(17)	126.89

C5N1Zn1	113.5(2)	114.02	C5N1Zn1	113.04(2)	114.16
N3N2C5	113.6(2)	114.92	N3N2C5	113.30(17)	114.25
C6N3Zn1	123.02(19)	123.35	C6N3Zn1	122.48(13)	120.81
N2N3C6	116.0(2)	117.11	N2N3C6	116.38(17)	117.51
N2N3Zn1	120.85(19)	119.38	N2N3Zn1	120.73(13)	121.50
C11N4Zn1	110.28(18)	110.20	C11N4Zn1	110.11(12)	112.27
N5N4C11	112.4(3)	113.42	N5N4C11	113.04(18)	113.33
N5N4Zn1	135.2(2)	133.11	N5N4Zn1	134.57(15)	132.25
N4N5C12	116.6(3)	118.24	N4N5C12	116.34(19)	118.41

So, they are best described as distorted square pyramid and not as trigonal bipyramid. The bond lengths Zn–N_{py} and Zn–N_{azopy} are 2.167(3) and 2.127(2) Å in 1a and 2.170(2) and 2.126(2) Å in **1b** and these are quite expected for typical Zn–N bonding.[17b,22] In the contrary, Zn–N_{azoph} distances are significantly longer by 0.04 Å for the reported complexes and lie near 2.46 Å, indicating the natural preference of the Zn(II) centre towards the tetra-coordinated species. As a result, fascinating structural types have been achieved and these can be beneficial in catalysis because the flexible-dentate nature of the organic scaffolds plays an important role towards the metal-substrate bond-making/breaking processes during catalysis.

II.2.5. Absorption spectra

Both complexes are soluble in polar and nonpolar solvents, e.g., dichloromethane, ether, acetonitrile ethanol and toluene and so forth, and producing a blood-red solution. A fascinating aspect of Zn(II) compounds, the typical d^{10} electronic configuration devoid of any d-d transition, is the intense red colouration. This is apparent from the well-stretched window above 600 nm in the observed spectra (Figure 7). In order to understand the origin of the red coloration we performed theoretical studies which reveals that lower energy bands are mainly composed of intraligand charge-transfer (ILCT) of π to π^* character and thereby absorbing the blue-green region of the visible region.

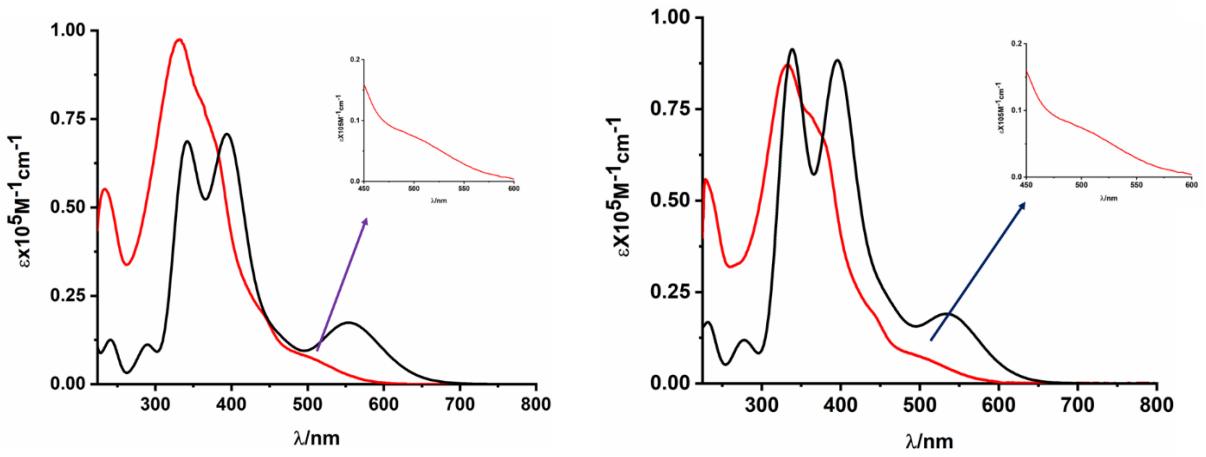

Figure 7: Experimental (red) and theoretical (black) absorption spectrum of **1a**(left) **&** **1b**(right) complex in CH_2Cl_2 solution at 298 K.

II.2.6. Electronic Structure and FMOs

The singlet ground state (S_0) and excited state molecular geometries of synthesised complex **1a** and **1b** were computed by DFT method by employing (R)B3LYP in GAUSSIAN 09 programme package. The solution phase optimised geometries of the complexes were found without applying any geometry constraints. In order to verify all stationary points as the true minima in potential energy surface, frequency calculation was executed. The absence of any imaginary frequency (NImag = 0) indicates that all the obtained stationary points are indeed the true minima in potential energy surface. The X-Ray positional coordinates of complex **1a** and **1b** were directly used as the initial input for geometry optimisation calculation. By using these ground state optimised geometries as well as excited state geometries, we performed subsequent Single Point Energy and TD-DFT calculation. In TD-DFT calculation we employ conductor like continuum model (CPCM) and dichloromethane (CH_2Cl_2) as solvent to simulate absorption spectra in dichloromethane solvent. The lowest 100 singlet-singlet transitions in absorption and emission processes for the complex **1a** and **1b** were evaluated gradually. The experimental results and the results obtained from TD calculations were qualitatively comparable. Presently the approach of TD-DFT is documented as a rigorous formalism for the electronic excitation energies among the DFT framework for calculating spectral properties of many transitions metal complexes. In order to acquire the information and nature of absorption and emission processes natural transition orbital (NTO) analysis was executed. This method delivers the most accurate representation of the transition density between the ground and excited states in terms of an expansion into single-particle transitions (hole and electron states

for each given excitation). we refer to the unoccupied and occupied NTOs as “electron” and “hole” transition orbitals. The computed vertical transitions were calculated at the equilibrium geometry of the S_0 state and described in terms of one-electron excitations of molecular orbitals of the corresponding S_0 geometry. The calculated transitions with moderate intensities ($f \geq 0.02$) can be envisaged going from the lower to the higher energy region of the spectrum. The zinc atom was described by a double-ζ basis set with the effective core potential of Hay and Wadt (LANL2DZ)[15,16], and the 6-311++G(d,p) basis set was used for the other elements except hydrogen atom (6-31G) present in the complexes to optimize the ground state geometries. The calculated electronic density plots for frontier molecular orbitals were prepared by using the GaussView 6.0 software. GaussSum program, version 3.2, was used to calculate the molecular orbital contributions from groups or atoms.

Table 3: Frontier Molecular Orbital Composition (%) in the Ground State for **1a** complex.

Orbital	MO	Energy (eV)	Composition						Contribution
			Zn	Azo1	Azo2	Cl	Py	Ph	
112	L+5	-0.80	0	0	4	0	3	93	π^* (Ph)
111	L+4	-0.82	0	0	5	0	2	93	π^* (Ph)
110	L+3	-1.27	0	5	1	0	55	39	π^* (Py + Ph)
109	L+2	-2.01	0	2	0	0	94	4	π^* (Py)
108	L+1	-3.05	1	4	46	1	3	45	π^* (Azo + Ph)
107	LUMO	-3.99	0	44	5	1	25	24	π^* (Azo +Py +Ph)
106	HOMO	-6.54	1	1	22	31	1	43	lp (Azo) + π (Cl + Ph)
105	H–1	-6.67	1	0	1	95	0	3	π (Cl + Ph)
104	H–2	-6.73	1	0	1	93	1	4	π (Cl)
103	H–3	-6.78	5	1	0	90	2	3	π (Cl)
102	H–4	-6.90	9	0	4	63	0	24	π (Cl + Ph + Py + Azo)
101	H–5	-7.39	3	8	38	20	3	28	π (Azo + Ph + Cl)

Table 4: Frontier Molecular Orbital Composition (%) in the Ground State for **1b** complex.

Orbital	MO	Energy (eV)	Composition						Contribution
			Zn	Azo1	Azo2	Cl	Py	Ph	
104	L+5	-0.54	0	0	3	0	0	97	π^* (Ph)
103	L+4	-0.67	0	1	7	0	5	87	π^* (Ph)
102	L+3	-1.14	0	4	1	0	55	39	π^* (Py + Ph + Azo)
101	L+2	-1.82	0	1	0	0	94	4	π^* (Py)

100	L+1	-2.97	1	5	45	1	3	45	π^* (Azo + Ph)
99	LUMO	-3.85	0	44	6	1	24	25	π^* (Azo +Py +Ph)
98	HOMO	-6.53	2	1	19	44	1	32	lp (Azo) + π (Cl + Ph)
97	H–1	-6.67	2	0	4	88	1	5	π (Cl)
96	H–2	-6.73	1	0	4	85	1	10	π (Cl)
95	H–3	-6.79	3	1	0	90	2	4	π (Cl)
94	H–4	-6.91	9	1	6	58	1	26	π (Cl + Ph + Azo)
93	H–5	-7.24	1	2	1	8	0	88	π (Ph + Cl)

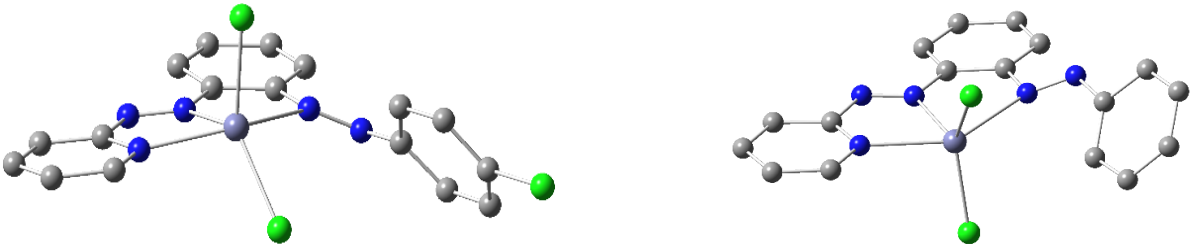

Figure 8: Solvent phase optimised geometry of **1a** (left) and **1b** (right) complex (H's are omitted for clarity) calculated at B3LYP/6-311+G(d,p) level of theory.

Table 5: Main Optical Transition at the TD-DFT/B3LYP/6-31+G(d,p) Level for the complex **1a** with composition in terms of Molecular Orbital Contribution of the Transition, Computed Vertical Excitation Energies, and Oscillator Strength in Dichloromethane.

Transition	**CI**	**Composition**	**E (eV)**	**Oscillator Strength (*f*)**	**λ_{theo} (nm)**
$S_0 \rightarrow S_1$	0.63460	HOMO → LUMO (81%)	2.23654	0.1586	554.39
$S_0 \rightarrow S_3$	0.51482	HOMO → L+1 (53%)	2.7684	0.0243	447.86
$S_0 \rightarrow S_7$	0.55532 0.32956	H-5→LUMO (62%) H-4→LUMO (22%)	3.0766	0.1091	402.99
$S_0 \rightarrow S_8$	0.42948 0.40887	H-2→LUMO (37%) H-3→LUMO (33%)	3.1584	0.4438	392.56
$S_0 \rightarrow S_{12}$	0.42254 0.35229	H-1→L+1 (36%) H-2→L+1 (25%)	3.6283	0.3418	341.71
$S_0 \rightarrow S_{14}$	0.48405 0.38441	H-1→L+1 (47%) H-3→L+1 (30%)	3.7226	0.1571	333.05
$S_0 \rightarrow S_{15}$	0.67201	H-4→L+1 (90%)	3.7960	0.0121	326.62
$S_0 \rightarrow S_{17}$	0.66652	H-5→L+1 (89%)	3.8345	0.0315	323.34
$S_0 \rightarrow S_{30}$	0.52252 0.27871	HOMO→L+4 (55%) HOMO→L+3 (16%)	5.0444	0.0282	245.79
$S_0 \rightarrow S_{38}$	0.50026 -0.43140	H-5→L+2 (50%) H-2→L+2 (37%)	5.2230	0.0294	237.38
$S_0 \rightarrow S_{41}$	0.61394	HOMO→L+5 (75%)	5.3973	0.0176	229.72

Table 6: Main Optical Transition at the TD-DFT/B3LYP/6-31+G(d,p) Level for the complex **1b** with composition in terms of Molecular Orbital Contribution of the Transition, Computed Vertical Excitation Energies, and Oscillator Strength in Dichloromethane.

Transition	CI	Composition	E (eV)	Oscillator Strength (*f*)	λ_{theo} (nm)
$S_0 \rightarrow S_1$	0.61198	HOMO → LUMO (75%)	2.3093	0.1272	536.90
$S_0 \rightarrow S_3$	0.48488	HOMO → L+1 (47%)	2.8147	0.0180	440.49
$S_0 \rightarrow S_6$	0.64522	H-4 → LUMO (83%)	3.1318	0.0125	395.88
$S_0 \rightarrow S_{11}$	0.56551	H-1 → L+1 (64%)	3.6127	0.1311	343.19
$S_0 \rightarrow S_{12}$	0.49452 -0.31640	H-2→L+1 (49%) H-1→L+1 (20%)	3.6914	0.3604	335.87
$S_0 \rightarrow S_{26}$	0.65379	HOMO→L+2 (85%)	4.7083	0.0162	263.33
$S_0 \rightarrow S_{35}$	0.49423 0.39368	HOMO→L+4 (49%) H-4→L+2 (31%)	5.3128	0.0216	233.37

Table 7: Natural transition orbitals (NTOs) for complex **1a** illustrating the nature of singlet excited states in the absorption bands in the range 200–700 nm. For each state, the respective number of the state, transition energy (eV), and the oscillator strength (in parentheses) are listed. Shown are only occupied (holes) and unoccupied (electrons) NTO pairs that contribute more than 15% to each excited state.

Wavelength	Transition	Hole	electron
500 nm	S1 w = 0.8055 *f* = 0.1586 554.39 nm	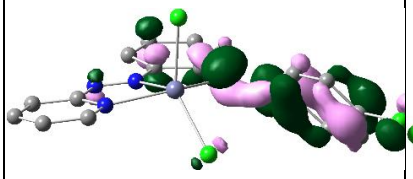	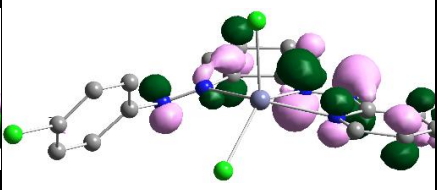
	S3 w = 0.5300 *f* = 0.0243 447.86 nm	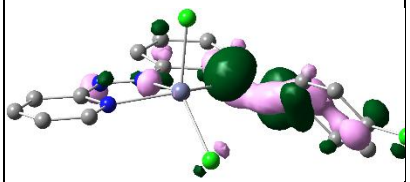	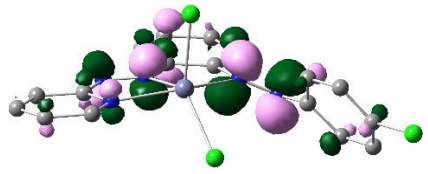
360 nm	S7 w = 0.6167 *f* = 0.1091 402.99 nm		

		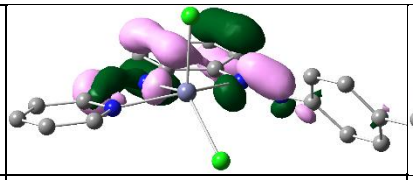	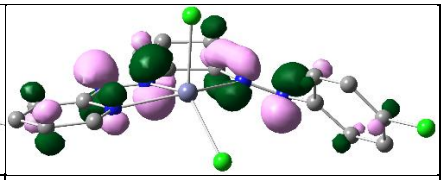
	S7 w = 0.2172 *f* = 0.1091 402.99 nm	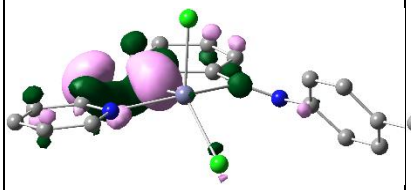	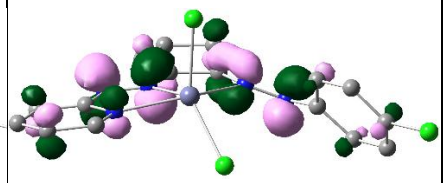
	S8 w = 0.3689 *f* = 0.4438 392.56 nm	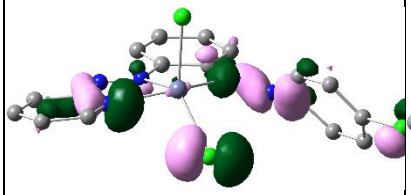	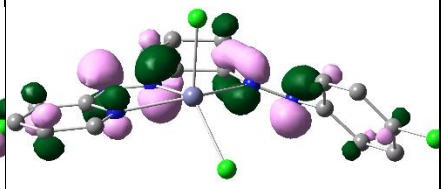
	S8 w = 0.3343 *f* = 0.4438 392.56 nm	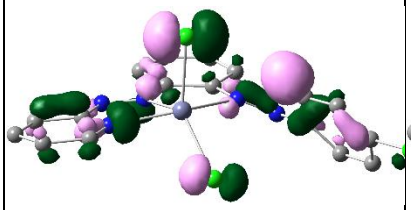	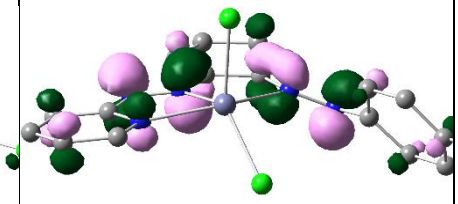
333 nm	S12 w = 0.3570 *f* = 0.1571 341.71 nm	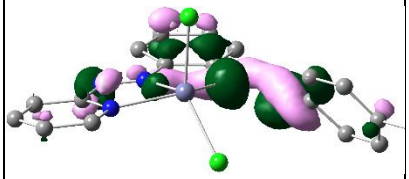	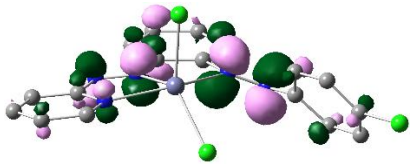
	S14 w = 0.4686 *f* = 0.1571 333.05 nm	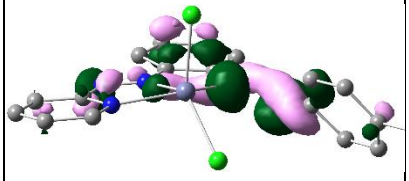	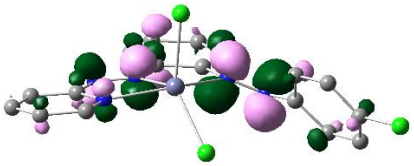
	S14 w = 0.2955 *f* = 0.1571 333.05 nm	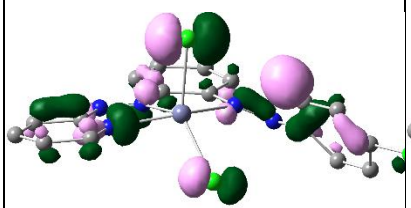	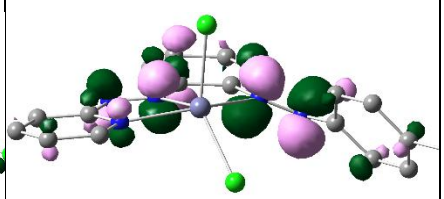

	S15 w = 0.9031 *f* = 0.0121 326.62 nm	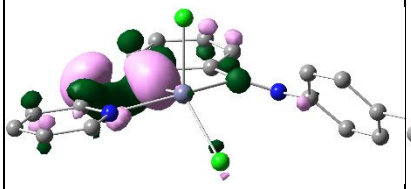	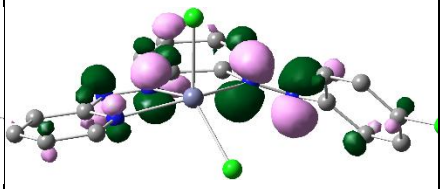
	S17 w = 0.8885 *f* = 0.0315 323.34 nm	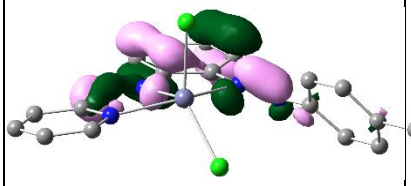	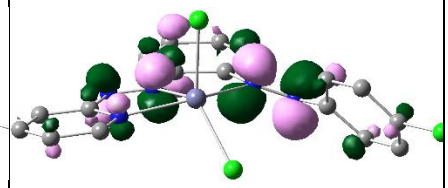
236 nm	S30 w = 0.5460 *f* = 0.0282 245.79 nm	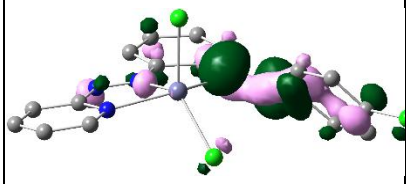	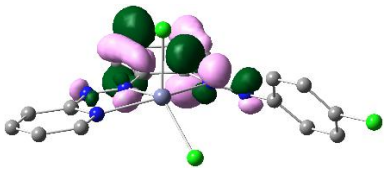
	S30 w = 0.1553 *f* = 0.0282 245.79 nm	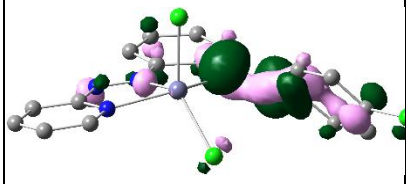	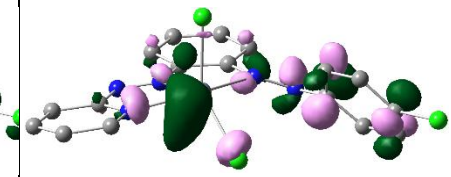
	S38 w = 0.5005 *f* = 0.0294 237.38 nm	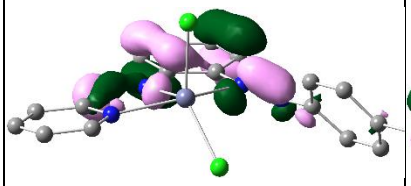	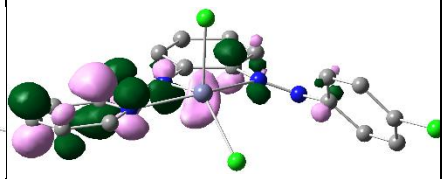
	S38 w = 0.3722 *f* = 0.0294 237.38 nm	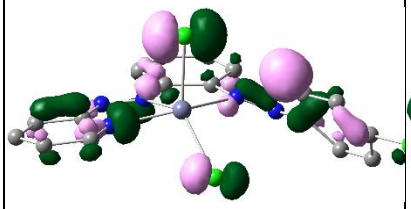	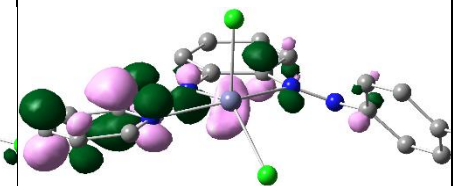

Table 8: Natural transition orbitals (NTOs) for complex **1b** illustrating the nature of singlet excited states in the absorption bands in the range 200–700 nm. For each state, the respective number of the state, transition energy (eV), and the oscillator strength (in parentheses) are listed. Shown are only occupied (holes) and unoccupied (electrons) NTO pairs that contribute more than 15% to each excited state.

Wavelength	Transition	Hole	Electron
499 nm	S1 w = 0.7490 *f* = 0.1272 536.90 nm	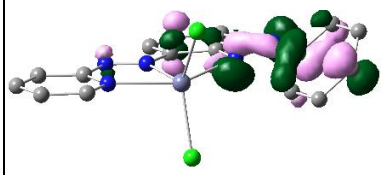	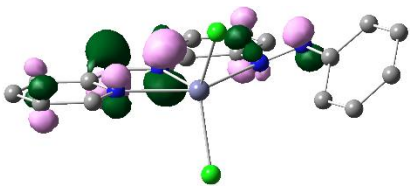
	S3 w = 0.4702 *f* = 0.0180 440.49 nm	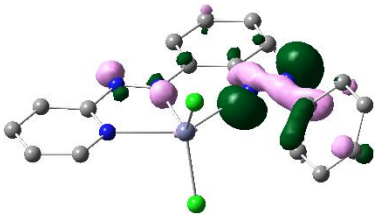	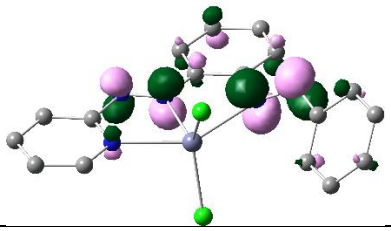
365 nm	S6 w = 0.8326 *f* = 0.0125 395.88 nm	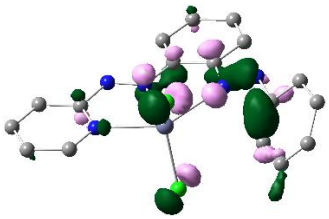	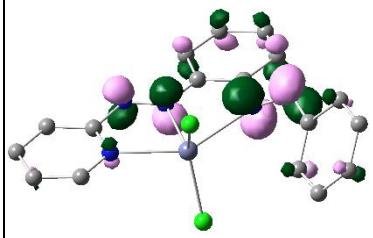
	S11 w = 0.6396 *f* = 0.1311 343.19 nm	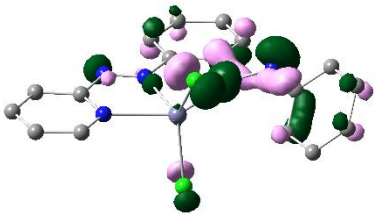	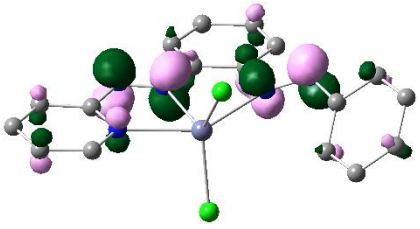
335 nm	S12 w = 0.4891 *f* = 0.3604 335.87 nm	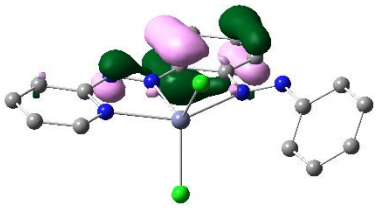	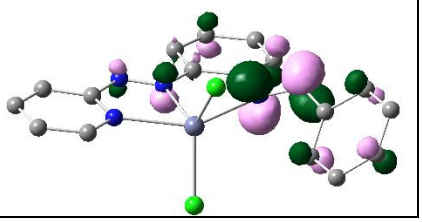

	S12 w = 0.2002 *f* = 0.3604 335.87 nm	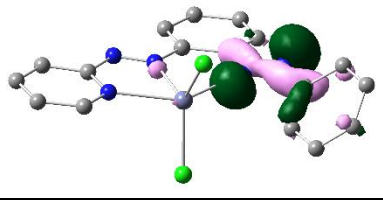	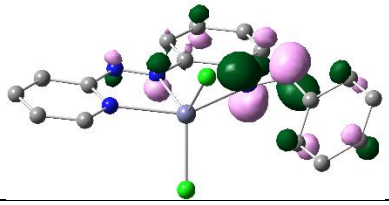
235 nm	S26 w = 0.8548 *f* = 0.0162 263.33 nm	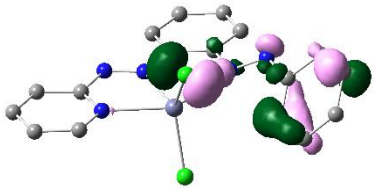	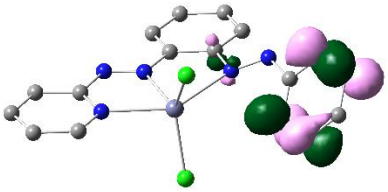
	S35 w = 0.4885 *f* = 0.0216 233.37 nm	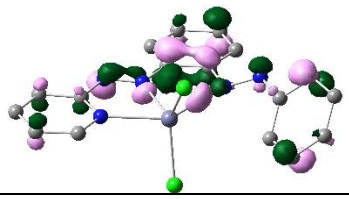	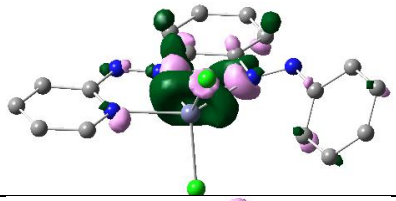
	S35 w = 0.3099 *f* = 0.0216 233.37 nm	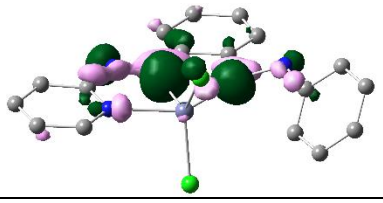	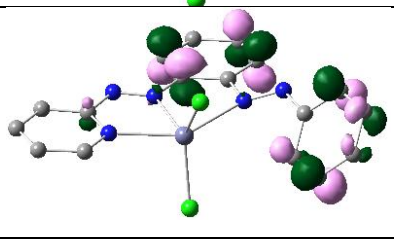

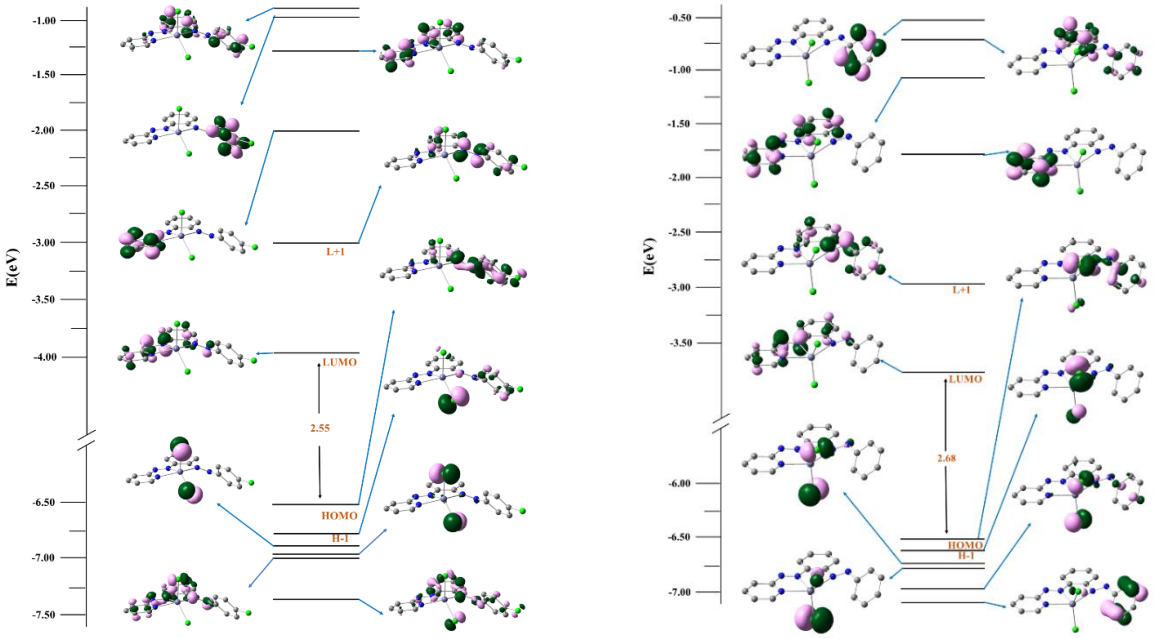

Figure 9: Partial MO diagram and isodensity surface plots (isovalue = 0.06) for selected FMOs of the complexes **1a** (left) and **1b** (right). The arrows are used to highlight the HOMO–LUMO energy gaps. All the DFT energy values are given in eV.

II.2.7. Catalytic Activity

Herein, we perform two distinctly different types of catalytic reactions: the first is an α-alkylation of secondary alcohols/ketones with primary alcohols and the second one is dehydrogenative coupling of secondary alcohols/ketones with 2-aminobenzyl alcohol derivatives using the synthesized stable penta-coordinated Zn(II) complexes as catalysts.

II.2.7.1. α-alkylated ketones synthesis

To optimize the reaction conditions of α-alkylation of secondary alcohols/ketones with primary alcohols have been carried out in presence of acetophenone **3a** (1.00 mmol), 1-phenylethanol **4a** (1.00 mmol) and benzyl alcohol **2a** (1.00 mmol) as benchmark substrates. Preliminary experiments have been carried out with 1.00 mol% of **1a**, 100 mol% of bases (KO^{t}Bu) under open air condition at 110 ºC in 87 and 86% yield of 5aa through condition **A** and condition **B**, respectively (Table 9, entry 1). Reactions were implemented by decreasing the catalyst loading up to 0.008 mol% and observed almost unaltered yield of the desired product (Table 9, entry 2-3,5). Upon lowering the catalyst loading to 0.005 mol%, yield of 5aa drastically reduced to 45 (A) and 38% (B), respectively (Table 9, entry 4).

Table 9: Reaction of **2a** with **3a** and **4a**: optimization of α-alkylation reactions

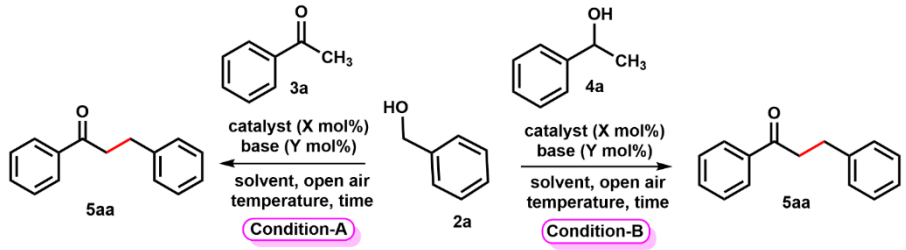

Entry	Catalyst (X mol%)	Solvent	Base (Y mol%)	Temp (ºC)	Yield^{A,b} (%)	Yield^{B,b} (%)
1	**1a** (1.00 mol%)	Toluene	KO^{t}Bu (100)	110	87	86
2	**1a** (0.1 mol%)	Toluene	KO^{t}Bu (100)	110	88	86
3	**1a** (0.01 mol%)	Toluene	KO^{t}Bu (100)	110	87	85
4	**1a** (0.005 mol%)	Toluene	KO^{t}Bu (100)	110	45	38
5	**1a** (0.008 mol%)	Toluene	KO^{t}Bu (100)	110	88	85
6	**1a** (0.008 mol%)	Toluene	KO^{t}Bu (50)	110	87	74
7	**1a** (0.008 mol%)	Toluene	KO^{t}Bu (10)	110	36	trace
8	**1a (0.008 mol%)**	**Toluene**	**KO^{t}Bu (30)**	**110**	**88**	**65**
9	**1a (0.008 mol%)**	**Toluene**	**KO^{t}Bu (60)**	**110**	**88**	**86**
10	**1a** (0.01 mol%)	Toluene	KO^{t}Bu (60)	110	88	87
11	**1a** (0.008 mol%)	Toluene	NaO^{t}Bu (30)	110	75	48
12	**1a** (0.008 mol%)	Toluene	KOH (30)	110	70	42
13	**1a** (0.008 mol%)	Toluene	NaOH (30)	110	65	36

14	**1a** (0.008 mol%)	Toluene	K_2CO_3 (30)	110	49	19
15	**1a** (0.008 mol%)	Toluene	Na_2CO_3 (30)	110	50	18
16	**1a** (0.008 mol%)	xylene	KO^{t}Bu (30)	110	78	50
17	**1a** (0.008 mol%)	THF	KO^{t}Bu (30)	70	69	38
18	**1a** (0.008 mol%)	EtOH	KO^{t}Bu (30)	80	NR	NR
19[c]	**1a** (0.008 mol%)	Toluene	KO^{t}Bu (30)	RT	NR	NR
20	**1a** (0.008 mol%)	Toluene	KO^{t}Bu (30)	100	54	30
21	**1a** (0.008 mol%)	Mesitylene	KO^{t}Bu (30)	150	87	64
22	$ZnCl_2$(1.00 mol%)	Toluene	KO^{t}Bu (30)	110	trace	NR
23	$ZnCl_2$:ligand (1:1)	Toluene	KO^{t}Bu (30)	110	trace	trace
24	ligands	Toluene	KO^{t}Bu (30)	110	NR	NR
25	**1a** (0.008 mol%)	Neat	KO^{t}Bu (30)	110	NR	NR
26[d]	**1a** (0.008 mol%)	Toluene	KO^{t}Bu (30)	110	trace	trace
27[e]	**1a** (0.008 mol%)	Toluene	KO^{t}Bu (30)	110	60	25
28		Toluene	KOtBu (30)	110	trace	NR
29	**1a** (0.008 mol%)	Toluene		110	NR	NR
30	**1b** (0.008 mol%)	Toluene	KOtBu (30)	110	78	49

[a]Reaction Conditions: (mono-dehydrogenation: condition-**A**): Benzyl alcohol **2a** (1.00 mmol), acetophenone **3a** (1.00 mmol). (double-dehydrogenation: condition-**B**): Benzyl alcohol **2a** (1.00 mmol), 1-phenylethanol **4a** (1.00 mmol), Base, solvent (5mL), Reaction time 21 hrs, open air, [b]Isolated yield after coloumn chromatography, [c]RT = Room Temperature, [d]Under Argon atmosphere, [e]Reaction time 8 hrs, NR = No Reaction. [A]represents mono-dehydrogenative coupling product and [B]represents double-dehydrogenative coupling product.

Hence, it could be concluded that optimum catalyst loading was 0.008 mol%. Now, upon lowering the base loading up to 30 mol%, the yield of the expected products remains almost unchanged (Table 9, entry 5-6, 8). Further lowering of base loading to 10 mol%, yield of products decreased severely (Table 9, entry 7). An increase in base loading to 60 mol% and enduring the reaction with **2a** and **4a** the yield of the desired **5aa** increases significantly to 86% (Table 9, entry 9). Nevertheless, when the catalyst loading was increased to 0.01 mol% with condition **B**, the yield of **5aa** did not significantly improve (Table 9, entry 10). Among the series of trial bases *e.g.*, NaO^{t}Bu, KOH, NaOH, K_2CO_3, Na_2CO_3, KO^{t}Bu, the maximum yield of the desired **5aa** was found when the reaction was accomplished with 30 mol% of KO^{t}Bu and 0.008 mol% catalyst (Table 9, entry 11-15). Notably, KO^{t}Bu was found to most efficient for this type of reaction and afforded with **5aa** in excellent yields. The reaction efficiency was found to be maximum in aprotic solvents like xylene, toluene, THF and so forth. But in protic solvent such as ethanol, the yield of the intended products drastically reduced (Table 9, entry 16-18). The yield of **5aa** drops dramatically when the temperature is lowered from 110 to 100 ºC and at room temperature no reaction occurred. However, the yield did not increase appreciably when the reaction was performed at an elevated temperature (Table 9, entry 19-21). Notably, the azo-chromophores play crucial role for the activity of the catalyst because

when commercially available $ZnCl_2$ was used as the catalyst, no activity was observed even at prolonged reaction time (Table 9, entry 22). However, practically no catalytic product was formed, when coupling was carried out by the ligand system itself but only at trace amount of **5aa** formed when ligand: $ZnCl_2$ (1:1) was employed (Table 9, entry 23-24). Indeed, no coupling occurred in the absence of zinc catalyst **1a** or KO^{t}Bu, or when the reaction was performed in neat conditions (Table 9, entry 25, 28, 29). The reaction was also performed in an argon atmosphere but with a trace amount of desired product formed (Table 9, entry 26). Upon lowering the reaction time 8 hrs product formation was decreased to 60% (Table 1, entry 27). Remarkably, **1a** showed higher activity in this catalytic reaction compare to **1b** (Table 9, entry 30) probably because of an electron withdrawing group (Cl *vs* H) made the former complex more electron-deficient.

Finally, optimized condition achieved when the reaction of **2a** (1.00 mmol), **3a** (1.00 mmol) and **4a** (1.00 mmol) in presence of complex **1a** (0.008 mol%) and KO^{t}Bu (30 mol%) as base in toluene medium at 110ºC resulted maximum yield 87% (condition **A**), 65% (condition **B**) yield of **5aa** respectively (Table 9, entry 8).

Table 10: Scope of various secondary alcohols and ketones and various primary alcohols with catalyst **1a**

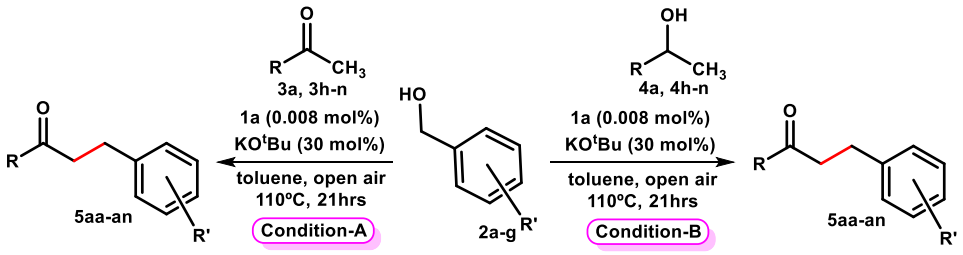

Once the optimum conditions have been established, we evaluated the variety of substrates both primary and secondary alcohols/ketones facilitating the synthesis of α-alkylated ketone derivatives in good to excellent yields (Table 10). In our methodology, both electron-rich or electron-deficient primary alcohols and secondary alcohols/ketones have been used effectively. Several functional groups performed well in the present catalytic system producing the corresponding α-alkylated ketones as final product in 52–93% isolated yields and with good to excellent TON values ranging from 6500 to 11600 (Table 2). Presence of electron-rich functional groups in secondary alcohols/ketones and electron-deficient functional groups in primary alcohols produced relatively higher yields of the desired α-alkylated ketone derivatives during the isolation process. A fascinating finding was that *ortho*-, *meta*- and *para*-substitution of the secondary alcohols/ketones by electron-rich groups such as 4–Me, 3–Me, 2–Me, 4–OMe

and 3–OMe were well tolerated under the optimized reaction conditions, resulting in the isolated **5ab**, **5ac**, **5ad**, **5ak** and **5al** in good to excellent (70–93%, TON 8750–11625) yields. (Table 10). In contrast, secondary alcohols/ketones possessing an electron-deficient group such as 4–F and 4–Br were producing **5am** and **5an** with relatively lower yields as compare to primary alcohols (52-68%, TON 6500-8500) under both conditions **A** and **B** (Table 10).

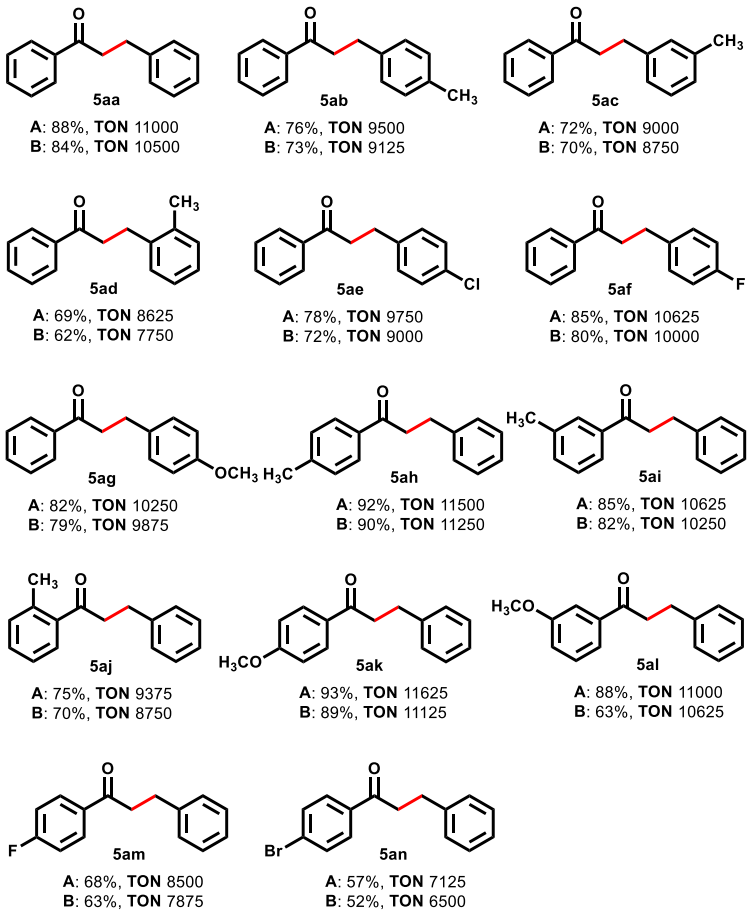

[a]Reaction Conditions: (mono-dehydrogenation reaction: condition-**A**): Benzyl alcohol derivatives (**2a–g**) (1.00 mmol); ketones (**3a, 3h–n**) (1.00 mmol); base (30 mol%). (double-dehydrogenation reaction: condition-**B**): Benzyl alcohol derivatives (**2a–g**) (1.00 mmol); secondary alcohols (**4a, 4h–n**) (2.00 mmol); base (60 mol%). [b]Isolated yields after column chromatography. 5.0 mL toluene. open air. [A]represents the yield of the mono-dehydrogenation reaction product i.e. the yield of the products between benzyl alcohol derivatives (**2a-g**) (1.00 mmol) and ketones (**3a, 3h–n**) (1.00 mmol). [B]represents the yield of the double-dehydrogenation reaction product i.e. the yield of the products between benzyl alcohol derivatives (**2a–g**) (1.00 mmol) and secondary alcohols (**4a, 4h–n**) (2.00 mmol).

Next, the suitability of numerous primary alcohols for this C–C bond forming reaction was assessed. Under both reaction conditions A and B, alkylating agents with structural variations in primary alcohols were chosen and results of this experiment summarises in Table 2. Notably, reducible halogen functional groups at 4-position of the benzyl alcohol, such as fluoro and chloro were well tolerated and resulted in 72–85% yields of **5ae** and **5af** (Table 10). Furthermore, benzyl alcohol derivatives containing electron-rich –Me group at *ortho*-, *meta*-

and *para*-positions and –OMe at *para*- and *meta*- positions were also found to be good coupling partners delivering the products in 62–82% yields (Table 10).

II.2.7.2. Friedländer quinoline synthesis

The Zn(II) based catalyst **1a** also revealed efficient activity for dehydrogenative coupling in one-pot cascade synthesis of quinoline derivatives when 2-aminobenzyl alcohol (**6a**) was utilised as the coupling partner. Conventionally, Friedländer annulation reactions rely on the condensation of 2-aminobenzaldehydes with ketones in basic or acidic environments.[1d] These reactions frequently encounter problems due to the somewhat limited stability of 2-aminobenzaldehydes, self-condensations and other related issues.[23] An eco-friendly synthesis of quinolines have been developed here *via* acceptorless dehydrogenative coupling (ADC), utilising catalytic amounts of base and relatively more stable 2-aminobenzyl alcohol and its derivatives. According to our hypothesis, α, β-unsaturated ketones would be formed by alcohols dehydrogenation *via* base-promoted cross-aldol condensation. These ketones proceed through intramolecular cyclodehydration to produce compatible quinoline derivatives (Scheme 3). Using this mechanistic approach, the reaction between 2-aminobenzyl alcohol **6a** and acetophenone **3a** was scrutinized as the model substrates to determine the optimum condition for the mono-dehydrogenative cyclization in order to produced quinoline derivatives. The prospect of double-dehydrogenative cyclization of secondary alcohols and 2-aminobenzyl alcohols was then determined to investigate. Fortunately, we noticed the reaction employing 1-phenylethanol **4a** and **6a** as the benchmark substrates to produced quinoline derivatives as shown in Table 11.

Table 11: Optimization of the reaction conditions for the zinc catalyzed acceptorless mono- and double-dehydrogenative coupling of 2-aminobenzylalcohol (**6a**) with acetophenone (**3a**) and 1-phenylethanol (**4a**)[a]

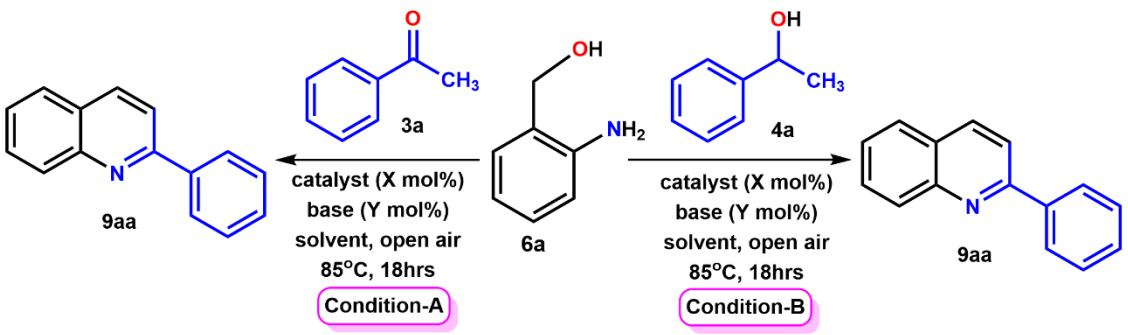

Entry	Catalyst (X mol%)	Solvent	Base (Y mol%)	Temp (°C)	Yield[b,f] (%)	Yield[b,g] (%)
1	**1a** (1.00 mol%)	Toluene	KO^{t}Bu (100)	85	92	90
2	**1a** (0.1 mol%)	Toluene	KO^{t}Bu (100)	85	91	90
3	**1a** (0.01 mol%)	Toluene	KO^{t}Bu (100)	85	92	91
4	**1a** (0.005 mol%)	Toluene	KO^{t}Bu (100)	85	92	87
5	**1a** (0.001 mol%)	Toluene	KO^{t}Bu (100)	85	53	47
6	**1a** (0.005 mol%)	Toluene	KO^{t}Bu (50)	85	92	87
7	**1a (0.005 mol%)**	**Toluene**	**KO^{t}Bu (20)**	**85**	**92**	**60**
8	**1a (0.005 mol%)**	**Toluene**	**KO^{t}Bu (40)**	**85**	**92**	**90**
9	**1a** (0.005 mol%)	Toluene	$NaBH_4$ (20)	85	74	42
10	**1a** (0.005 mol%)	Toluene	NaO^{t}Bu (20)	85	85	57
11	**1a** (0.005 mol%)	Toluene	NaOH (20)	85	90	59
12	**1a** (0.005 mol%)	Toluene	KOH (20)	85	90	57
13	**1a** (0.005 mol%)	Toluene	K_2CO_3 (20)	85	52	19
14	**1a** (0.005 mol%)	Xylene	KO^{t}Bu (20)	85	82	55
15	**1a** (0.005 mol%)	THF	KO^{t}Bu (20)	85	45	23
16	**1a** (0.005 mol%)	EtOH	KO^{t}Bu (20)	85	NR	NR
17[c]	**1a** (0.005 mol%)	Toluene	KO^{t}Bu (20)	RT	NR	NR
18	**1a** (0.005 mol%)	Toluene	KO^{t}Bu (20)	100	90	58
19	$ZnCl_2$ + Ligand (1:1)	Toluene	KO^{t}Bu (20)	85	Trace	NR
20	$ZnCl_2$ (0.005 & 1 mol%)	Toluene	KO^{t}Bu (20)	85	NR	NR
21	Ligand (1 mol%)	Toluene	KO^{t}Bu (20)	85	NR	NR
22		Toluene	KO^{t}Bu (20)	85	NR	NR
23[d]	**1a** (0.005 mol%)	Toluene	KO^{t}Bu (20)	85	trace	trace
24[e]	**1a** (0.005 mol%)	Toluene	KO^{t}Bu (20)	85	68	37
25	**1a** (0.005 mol%)	Neat	KO^{t}Bu (20)	85	45	trace
26	**1b** (0.005 mol%)	Toluene	KO^{t}Bu (20)	85	87	59

[a]Reaction Conditions: mono-dehydrogenation: condition **A**: 2-Amino benzyl alcohol **6a** (1.00 mmol), acetophenone **3a** (1.00 mmol). Double-dehydrogenation: condition **B**: 2-Amino benzyl alcohol **6a** (1.00 mmol), 1-phenylethanol **4a** (1.00 mmol), Base, 5.0 ml toluene, Reaction time 18 hrs, open air.
[b]Isolated yield after coloumn chromatography.
[c]RT = Room Temperature.
[d]Under an argon atmosphere.
[e]Reaction time 6 hrs, NR = No Reaction.
[f]represents the yield of the mono-dehydrogenative coupling reaction.
[g]represents the yield of the double-dehydrogenative coupling reaction.

It is worth noting that the exclusively quinoline-based derivatives i.e., the envisioned cyclization products were obtained under the optimum reaction conditions with no self-condensed side products of 2-aminobenzaldehydes. Furthermore, unreacted alcohols or ketones have been found in petite amount in all cases.

Table 12: Screening of various secondary alcohols and ketones for dehydrogenative coupling reaction with **1a**

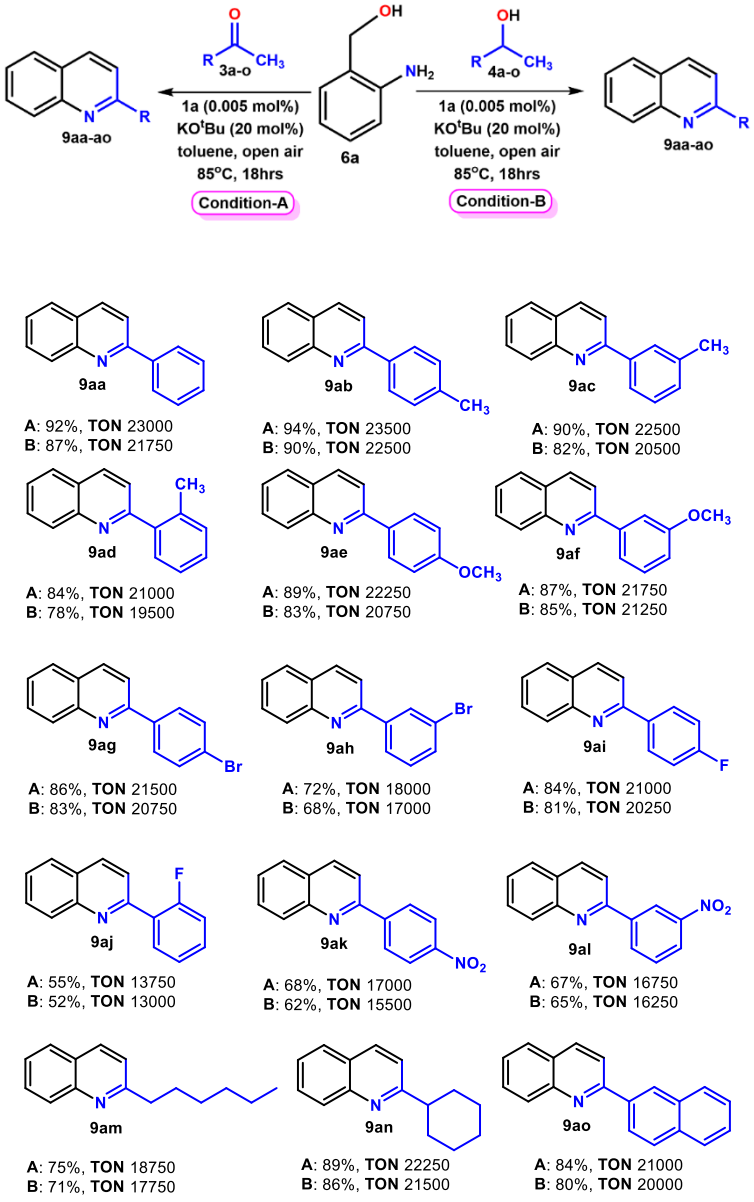

[a]Reaction Conditions: (mono-dehydrogenation reaction: condition **A**): 2-Aminobenzyl alcohol (**6a**) (1.00 mmol); ketone (**3a–o**) (1.00 mmol); base (20 mol%). (double-dehydrogenation reaction: condition **B**): 2-Aminobenzyl alcohol (**6a**) (1.00 mmol); secondary alcohols (**4a–o)** (2.00 mmol); base (40 mol%). [b]Isolated yields after column chromatography. 5.0 mL toluene. open air. [A]represents the yield of the mono-dehydrogenation reaction product i.e. the yield of the products between 2-Aminobenzyl alcohol (**6a**) (1.00 mmol) and ketones (**3a–o**) (1.00 mmol). [B']represents the yield of the double-dehydrogenation reaction product i.e. the yield of the products between 2-Aminobenzyl alcohol (**6a**) (1.00 mmol) and secondary alcohols (**4a–o)** (2.00 mmol)

As optimal conditions were established, the scope for dehydrogenative cyclization of 2-aminobenzyl alcohol **6a** and ketones was elaborately scrutinized starting with ketones. A wide range of functional groups, including aryl, alkyl, and naphthyl functionalities, were well

tolerated. It has been found that, under optimum condition **A**, acetophenones with both electron withdrawing and electron donating groups could be compatible with **6a** as coupling partners. Superior yields of the corresponding quinolines were found while acetophenones containing electron-donating groups at the *para*-, *meta*- and *ortho*- positions of the phenyl ring were employed (Table 12, **9ab**-**af**). For example, the corresponding quinolines **9ab**, **9ac**, and **9ad** were produced in 94, 90 and 84% isolated yields under condition **A**, respectively, by the reaction of 1-(*p*-tolyl)ethan-1-one **3b,** 1-(*m*-tolyl)ethan-1-one **3c** and 1-(*o*-tolyl)ethan-1-one **3d** with **6a**. Moreover, reactions continued with acetophenones containing halogens as the electron-withdrawing groups, producing the corresponding quinolines in 55–86% isolated yields (Table 3, **9ag-aj**). Nevertheless, in the presence of strong electron withdrawing group like nitro, the desired quinolines were isolated in moderate yields (Table 12, **9ak**-**al**). Additionally, aliphatic ketones were also used as coupling partners in order to examine the substrate scope further. Notably, it has been found that the corresponding quinolines **9am** and **9an** were produced in 75 and 89% isolated yields, respectively (Table 12). This result differs greatly from the rhenium catalyst developed by Sortais, where aliphatic alcohols were unable to produce any quinoline products.[24] Furthermore, naphthyl ketone was used as coupling partner in order to test the substrate scope. For example, the corresponding quinolines, **9ao** was produced in 84% isolated yield, by the reaction of 1-(naphthalen-2-yl)ethan-1-one **3o** with **6a**.

To assess the adaptability of the zinc catalysed dehydrogenative cyclization processes, the substrate range of the double dehydrogenative coupling of 2-aminobenzyl alcohols and secondary alcohols was also explored. The coupling partners of **6a** were evaluated with a range of substituted secondary alcohols (**4a-o**) in reaction condition **B** (Table 3). The corresponding quinolines were produced in moderate to high isolated yields by the reaction of 1-phenylethanol having electron-donating groups at the *ortho*-, *meta*- or *para*-positions of the phenyl ring. The reaction of **6a** with 1-(*p*-tolyl)ethanol **4b,** 1-(*m*-tolyl)ethanol **4c** and 1-(*o*-tolyl)ethanol **4d** afforded the corresponding quinolines **9ab**, **9ac** and **9ad** in 90, 82 and 78% yields respectively. 1-phenylethanol with electron-withdrawing groups was also compatible, although it required a longer reaction time and produced lower yields. Aliphatic alcohols were also found to be good coupling partners even though they had a lower yield and required a longer reaction time. This might be attributed to the decreased reactivity of the aliphatic alcohols to form the corresponding ketones *via* acceptorless dehydrogenation.

Table 13: Screening of various secondary alcohols and ketones with 2-amino-5-chloro benzyl alcohol **6b** for dehydrogenative coupling reaction with zinc catalyst **1a**

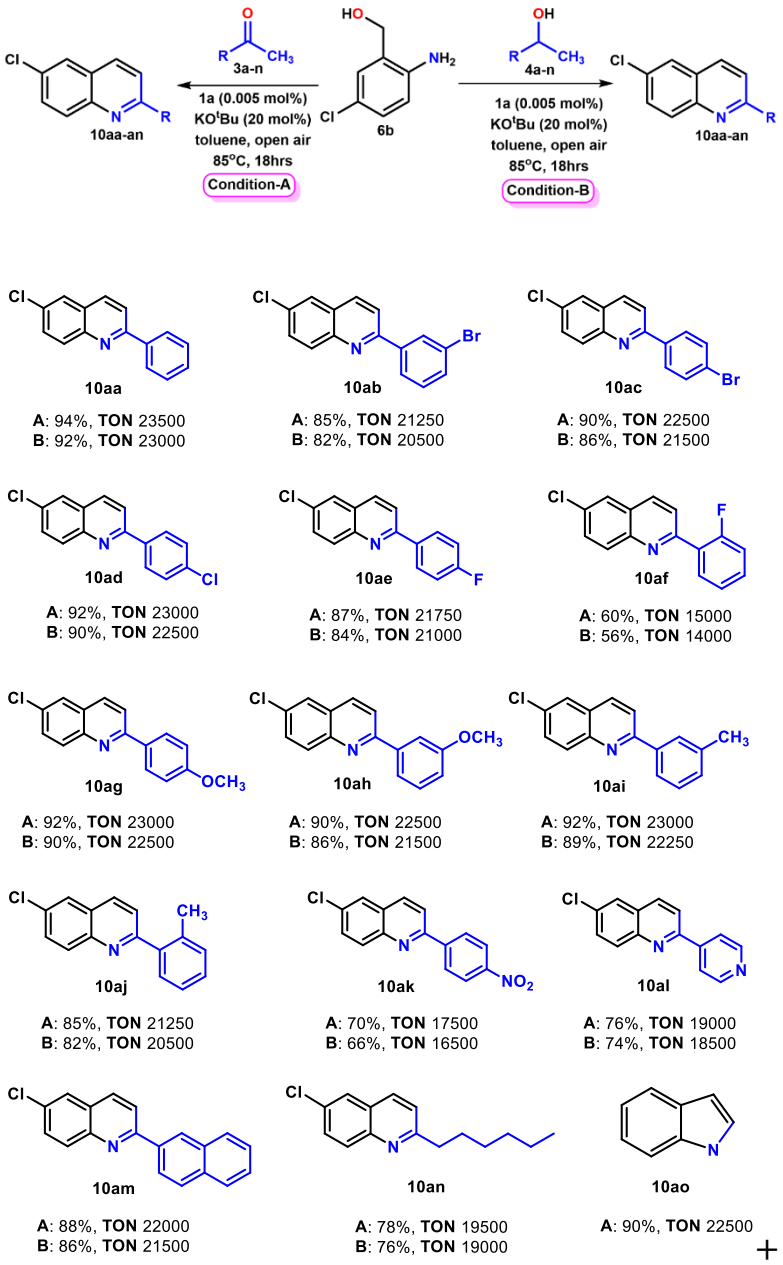

[a]Reaction Conditions: (mono-dehydrogenation reaction: condition **A**): 2-amino-5-chloro benzyl alcohol **6b** (1.00 mmol); ketone **3a–n** (1.00 mmol); base (20 mol%). (double-dehydrogenation reaction: condition **B**): 2-amino-5-chloro benzyl alcohol **6b** (1.00 mmol); secondary alcohols **4a–n** (2.00 mmol); base (40 mol%). [b]Isolated yields after column chromatography. 5.0 mL toluene. open air. [A]represents the yield of the mono-dehydrogenation reaction product i.e. the yield of the products between 2-amino-5-chloro benzyl alcohol **6a** (1.00 mmol) and ketones **3a–n** (1.00 mmol). [B]represents the yield of the double-dehydrogenation reaction product i.e. the yield of the products between 2-amino-5-chloro benzyl alcohol **6b** (1.00 mmol) and secondary alcohols **4a–n** (2.00 mmol)

In order to broaden the scope of the substrate, one substituted 2-aminobenzyl alcohol was investigated as potential coupling partners with acetophenone **3a** and 1-phenylethanol **4a**. **3a**

and **4a** bearing both electron donating and withdrawing groups were found to be compatible coupling partners with 2-amino-5-chloro benzyl alcohol **6b** furnishing the corresponding quinolines in 56–92% isolated yields (Table 13).

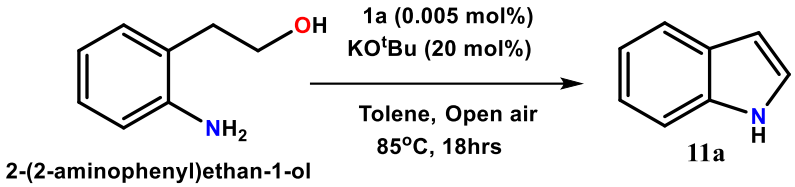

Scheme 6: Intramolecular dehydrogenative cyclization with zinc catalyst **1a**

Intramolecular cyclization reactions can also be performed with catalyst **1a** (Scheme 6). Intramolecular dehydrogenative cyclization of 2-(2-aminophenyl)ethan-1-ol produced 1*H*-indole **11a** in 90% yield under our standard experimental setup with an excellent TON value of 22500.

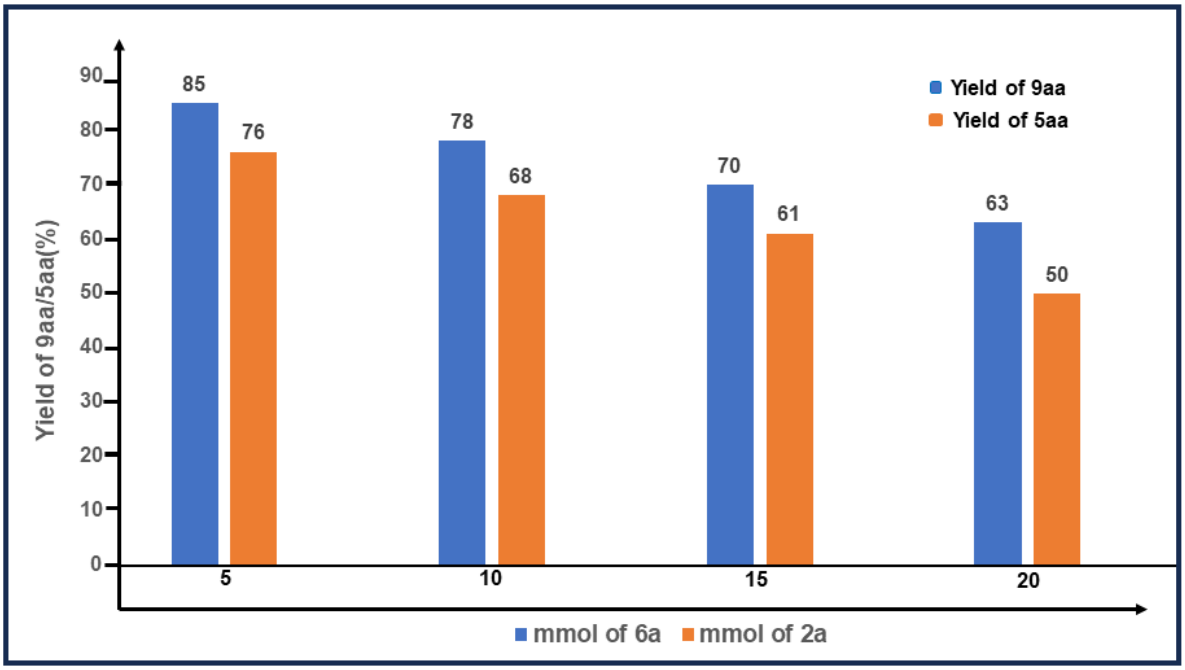

Figure 10: Graphical representation of gram-scale catalytic reaction with **1a**

To illustrate the usefulness of this methodology, four set of gram scale syntheses were carried out with **6a** [0.616 gm (5 mmol), 1.232 gm (10 mmol), 1.848 gm (15 mmol) and 2.463 gm (20 mmol) respectively] and **2a** [0.541 gm (5 mmol), 1.081 gm (10 mmol), 1.622 gm (15 mmol) and 2.162 gm (20 mmol) respectively] under optimized reaction conditions. The

reaction generates the intended products **9aa** and **5aa** in good percentage of yields as anticipated. Figure 10 displays a graphical illustration of the gram-scale reaction.

II.2.7.3. Mechanistic Investigation

A mercury poisoning test was conducted in an attempt to understand the uniformity of catalytic conversions and the role of catalysts. Mercury did not alter the dehydrogenation of alcohol or the coupling reaction that followed. After scrutinising the substrate range, we proceeded to examine the conceivable mechanism of the current Zn-catalysed dehydrogenation of aromatic primary alcohols to the corresponding aromatic aldehydes.

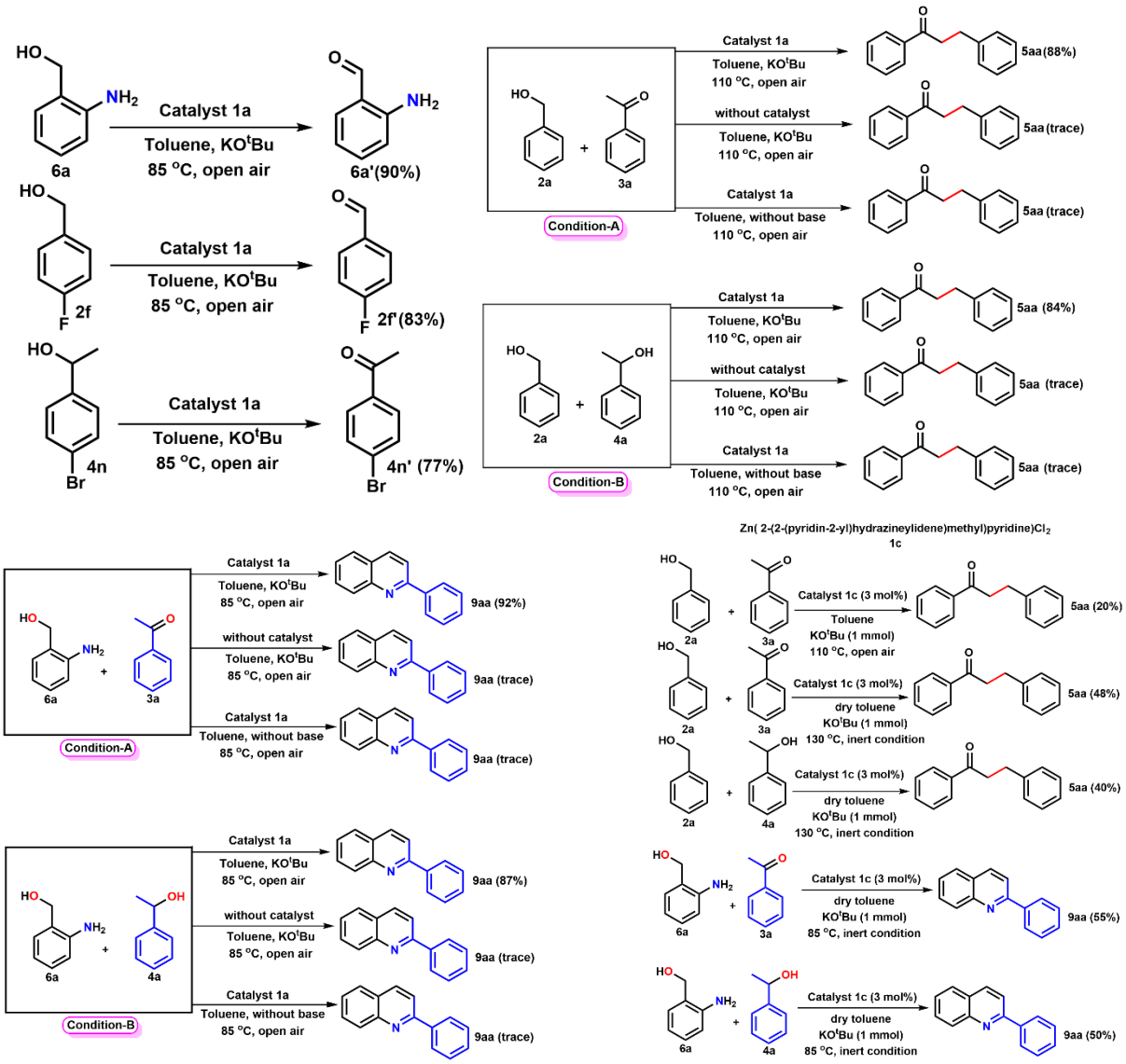

Figure 11: Some control experiments for both C–C and C–N catalytic reactions.

When **6a**, **2f** and **4n** were reacted under optimal reaction condition without any coupling partner, the corresponding carbonyls **6a'**, **2f'** and **4n'** produced in 90, 83 and 77% yield respectively (Figure 11), indicated the possibility of a probable conversion both primary and secondary alcohols as intermediates. Notably, reaction of **6a** with base has been performed without catalyst **1a**, only a trace amount of **6a'** was produced. To further clarify our mechanistic study, we reacted **2a** with **3a** and **4a** using both reaction condition-**A** and -**B** to produce **5aa** with a 92 and 87% yield respectively. The intended product **5aa** wasn't produced when the reaction was carried out without catalyst **1a** or base. These findings proved that alcohols could be oxidized to carbonyls only in the presence of catalyst **1a**. Similar results were found in case of quinoline synthesis reaction (Figure 11). Some control experiments were also carried out using a Schiff-base pincer ligand with zinc metal, i.e., complex **1c**, instead of the azo pincer ligand for both C–C (α-alkylation) and C–N (Friedländer annulation) coupling reactions. Under open air condition, the reaction between **2a** and **3a** using catalysts **1c** (3 mol%), KO^{t}Bu (100 mol%), and **5aa** was produced in 20%. Notably, under inert conditions, the reaction of **2a** with **3a** and **4a** produced **5aa** in 48% and 40% of yield, respectively. Similarly, under inert conditions, the reaction of **6a** with **3a** and **4a** using catalyst **1c** produced the desired product **9aa** in 55 and 50% yield, respectively (Figure 11).[25] Dehydrogenation of cyclobutanol (radical clock substrate) was carried out under optimised circumstances utilising **1a** as catalyst in order to validate the viability of one-electron hydrogen atom transfer (HAT) *vs* two-electron hydride transfer (HT) pathway (involving an intermittent zinc hydride intermediate). The observed HRMS data at 420.9877 and 543.0594 (m/z) of the reaction mixture indicated the formation of a zinc hydride intermediate corresponding to [**I2**]$^+$ and an intermediate adduct [**I4**]$^+$, respectively, when the reaction was carried out with 1-phenylethanol and catalyst **1a** in presence of base as shown in Figure 12.

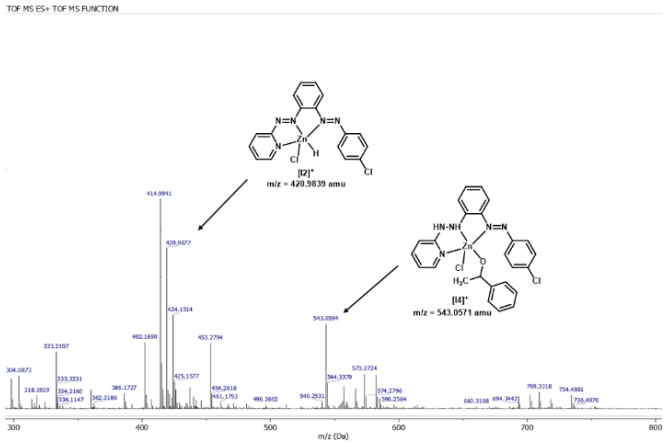

Figure 12: HRMS of intermediates **[I2]$^+$, [I4]$^+$**: when the reaction was carried out with 1-phenylethanol and catalyst **1a** in presence of base.

Synthesis of cyclobutanone as the dehydrogenated product, which indicates the involvement of the two-electron hydride transfer process and rules out the viability of the HAT process involving ketyl radical intermediate (Scheme 7). To understand the redox behaviour of **1a**, we have performed electrochemical study. Two cathodic responses around −0.3 and −1.2 V have observed in agreement with two azo chromophores (Figure 13).[17a,22]

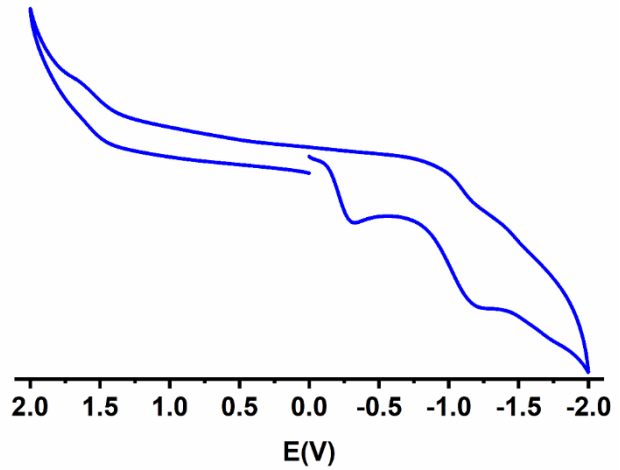

Figure 13: Cyclic voltammogram of **1a** in CH_3CN using 0.1 M Bu_4NPF_6 using a Pt working electrode at 50 mV s^{-1} with respect to Ag/AgCl reference electrode.

The irreversible nature of both reductive couples most plausibly accounts for adoption of a non-radical pathway during the catalytic cycle. ^{1}H NMR spectrum was found to be consistent with the *in situ* exclusive formation of cyclobutanone as the end product with catalyst **1a** (Figure 14).[26]

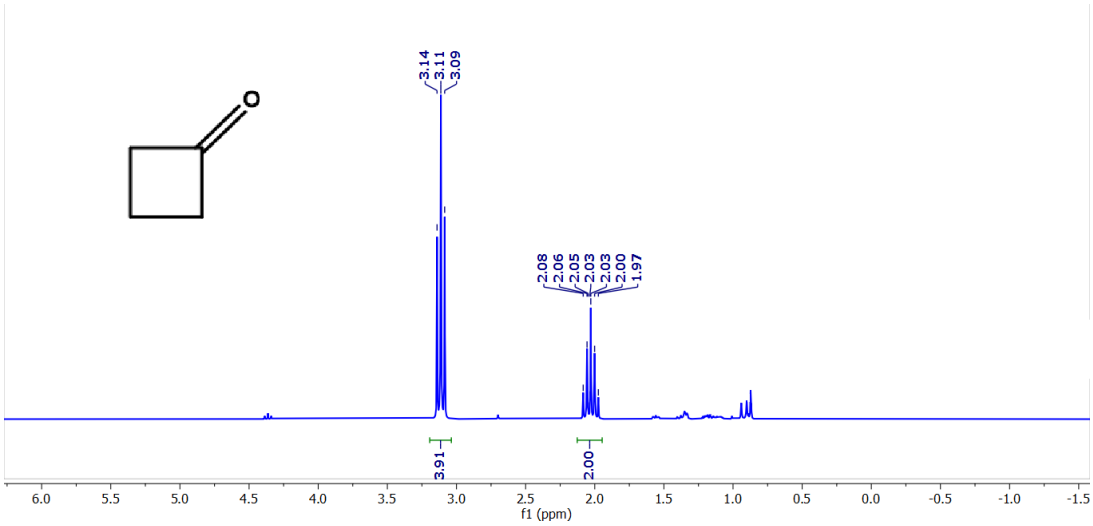

Figure 14: ^{1}H NMR spectrum of cyclobutanone (300 MHz, $CDCl_3$).

It is worth mentioning that the mixture of substrate, catalyst **1** and base resulted in a sharp single line EPR spectrum near g ≈ 2 with small signal width (ΔH ≈ 3 mT) at room temperature,

indicating the *in-situ* generation of an organic radical. But this does not necessarily imply the formation of a zinc-coordinated anion radical since a similar attribution was also observed in the absence of zinc catalyst **1**. Furthermore, the catalyst does not give any EPR signal with base alone. Thus, the EPR experiment indubitably shows that organic radical species are not associated with catalyst **1** and this finding is consistent with the reported non-radical pathway (Scheme 8). It is apparent that the bisazo-pyridine based Zn(II) catalyst is reluctant to follow the radical pathway, possibly due to its electron-rich nature, despite coordination to the strong π-acidic pyridylazo ligand.

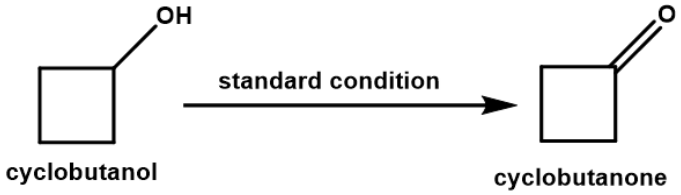

Scheme 7: Investigation of active participation of non-radical intermediate during catalytic transformation Dehydrogenation of cyclobutanol with catalyst **1a**

Even when they do not form radicals, bisazo-pyridine ligands can act as electron sinks in a chemical reaction pertaining azo-hydrazo redox pair.[17a] Thus, 1-phenylethanol and deuterated 1-phenylethanol were exposed to stoichiometric dehydrogenation under optimal conditions in the presence of argon in order to examine the potential participation of the azo-chromophore. The IR spectra of reaction mixtures show ν_{N-H} vibrational modes at 3029 and 3063 cm^{-1} and N–D stretching at 2107 and 2131 cm^{-1}, respectively, suggesting the active participation of the coordinated azo-aromatic template in due course of the dehydrogenation of deuterated 1-phenylethanol and non-deuterated 1-phenylethanol (Figure 15).[27,17b]

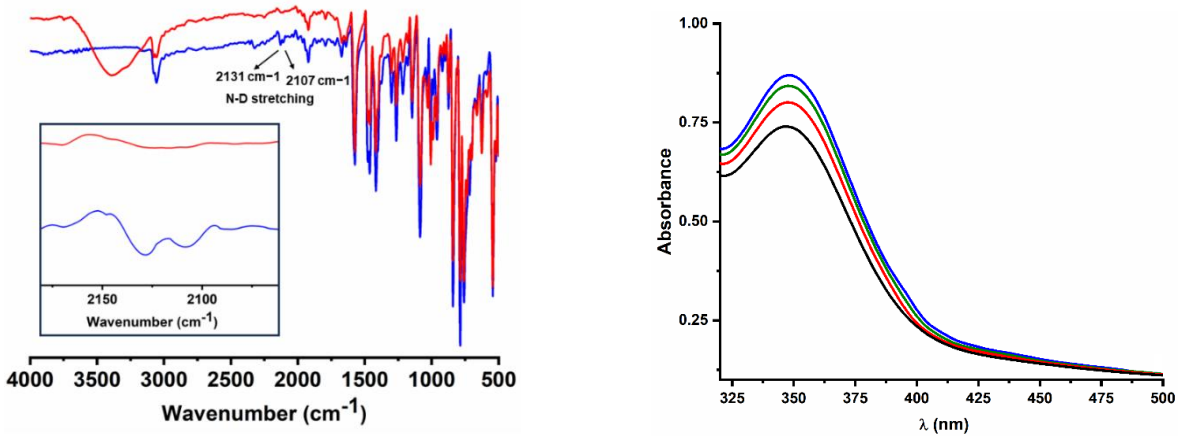

(a) **(b)**

Figure 15: (a) IR spectrum of reaction mixture showing N-D stretching during dehydrogenation of non-deuterated 1-phenylethanol (red) and deuterated 1-phenylethanol

(blue). (b) Electronic spectra of the formation of I_3^- ion in presence of H_2O_2 (detection of H_2O_2 was achieved as described in the text).

After performing these control experiments, we report a probable catalytic cycle for this reaction mechanism as shown in Scheme 8. Mechanistic research pertaining to α-alkylation

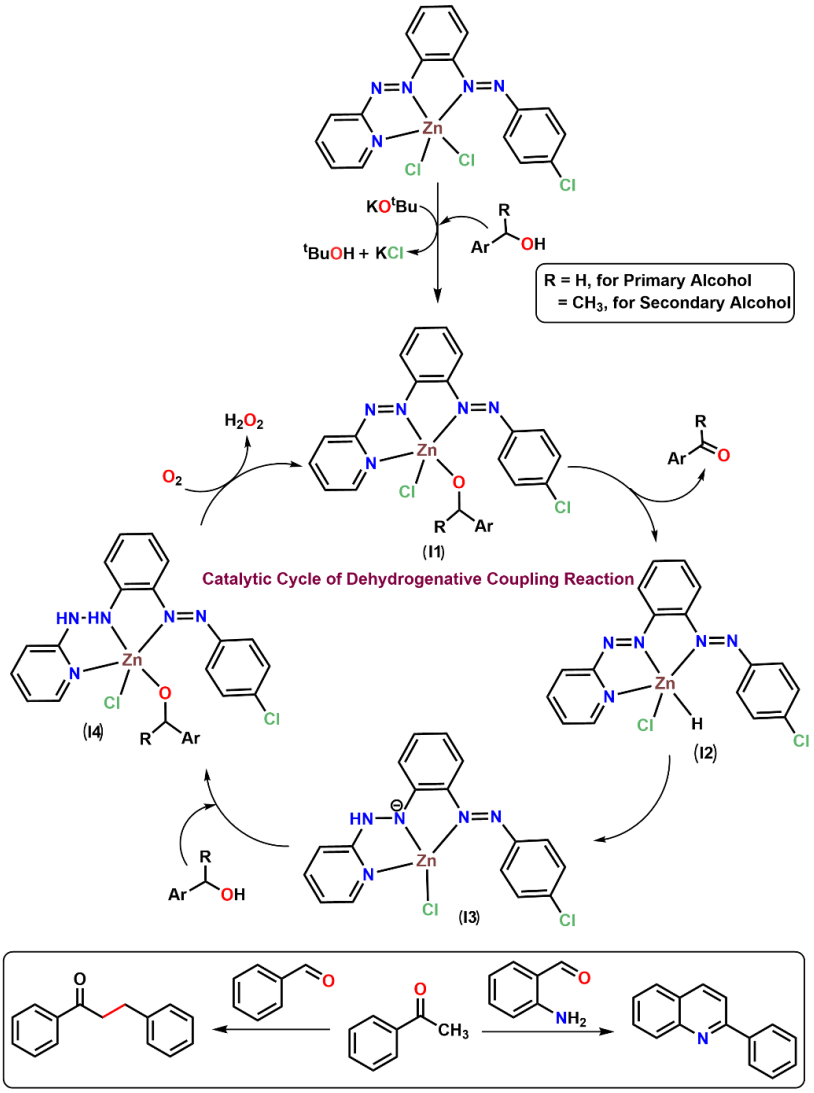

Scheme 8: Proposed reaction mechanism for Zn(II)-mediated alcohol dehydrogenation reaction.

of secondary alcohols/ketones with primary alcohols using catalyst **1a** have reported similar findings as mention in Scheme 1. This would give α, β-unsaturated ketones as intermediate *via* classical aldol condensation and dehydration, which hydrogenated to give final C–C bonded alkylated product *via* well-known borrowing-hydrogen (BH) mechanism.

II.3 Conclusion

In summary, we have developed a simple, sustainable, and scalable dehydrogenative cross-coupled strategy by employing a novel electron deficient robust pincer N^N^N-zinc catalyst. The highly electron-deficient bisazo-pyridine template is likely advantageous for the overall catalytic cycle by facilitating the initial nucleophilic coordination of alcohols in the catalytic cycles. This neutral coordinatively unsaturated square pyramidal [Zn^{II}(N^N^N)Cl_2] catalyst exhibit excellent stability *vis-à-vis in-situ* recyclability as well, which is manifested by its remarkably high turnover numbers (up to 23,000 using a 0.005 mol% catalyst loading) apart from low base loading (20 mol% KO^{t}Bu) under homogeneous aerobic conditions. Both C-alkylation of secondary alcohols/ketones with primary alcohols and C–N Friedländer annulation to quinoline derivatives occurred *via* hydride transfer (HT) under open-air homogeneous reaction conditions in presence of catalytic amounts (~30 mol%) of base, KO^{t}Bu. Production of α-alkylated ketones and quinoline derivatives are accomplished by acceptorless dehydrogenative coupling followed by hydrogen borrowing/N-annulation, respectively, in one-pot procedure. Notably, the dual role of the catalyst was found in nucleophilic aromatic substitution reaction and α-alkylation with primary alcohols. In both cases, respective desired catalytic products are formed without any noticeable self-condensed side products and the reaction byproducts are highly benign in nature. Lower (metal) catalyst, and base loading are challenging but indispensable in terms of green and sustainable chemistry because of minimal release of hazardous metal wastes and toxic byproducts to the environment. A non-radical pathway following a hydride transfer mechanism is presented for the Zn(II)-mediated alcohol dehydrogenation reaction and substantiated by certain control studies. This urbane method shows a broad substrate tolerance using aliphatic, aromatic and hetero aromatic alcohols to produce wide range of C–C/C–N cross-coupled products under mild conditions with highest TON reported so far among homogeneous zinc catalysts.

II.4 Experimental Section

II.4.1 General Information

Except where emphasised, all manipulations have been carried out in an argon atmosphere. Prior to use, solvents were dried using conventional techniques and afterwards distilled under argon. Anhydrous zinc chloride, benzyl alcohol and its derivatives and acetophenone and its derivatives were bought from Sigma Aldrich chemical company. Additional chemicals and solvents were bought from Merck India, Ranchem Private Limited, TCI Chemicals (India) Pvt. Ltd., Alfa Aesar and dried before use using well-known methods. FT-IR spectra have been

measured using a Perkin-Elmer L1600300 spectrometer. TMS was used as the internal reference for ^{1}H, ^{13}C & ^{19}F NMR spectra measurements on Bruker FT 300 & 400 MHz spectrometers. Electronic spectra were recorded using a Perkin-Elmer LAMDA 25 spectrophotometer and a dichloromethane solution with a solute concentration of approximately 10^{-5} M.

II.4.2. Synthesis

Synthesis of ligands

The organic ligands L^{Cl} and L^{H} comprising two electron-deficient azo moieties along with an aromatic heterocyclic group have been prepared by condensation of (*E*)-2-((4-chlorophenyl)azo)aniline or (*E*)-2-(phenylazo)aniline with 2-nitrosopyridine using the previously reported procedure.[21a]

Synthesis of complexes

[Zn(L^{Cl})Cl_2] 1a Anhydrous $ZnCl_2$ (136 mg, 1.00 mmol) was added to a solution of (L^{Cl}) (354 mg, 1.10 mmol) in ethanol (25 mL) under open air. The reaction mixture was stirred at room temperature for 6 hrs. The solvent was removed under reduced pressure. Slow diffusion of the dichloromethane solution of the complex into n-hexane led to the crystallisation of **1a** as rod-shaped crystals. Yield and characterization data: Blood-red crystal, Yield 90% (412 mg). Anal. Calcd. for $C_{17}H_{12}N_5Cl_3Zn$: C 44.58, H 2.64, N 15.29; Found C 44.98, H 2.69, N 15.16%. ^{1}H-NMR (400 MHz, DMSO-d_6): δ (ppm) 8.76 (d, *J* = 5.4 Hz, 1H), 8.07 (t, *J* = 7.8 Hz, 1H), 7.93-7.90 (m, 2H), 7.79-7.75 (m, 4H), 7.70-7.64 (m, 3H), 7.62-7.59 (m, 1H). ^{13}C-NMR (100 MHz, DMSO-d_6): δ (ppm) 163.3, 151.3, 150.0, 149.9, 147.8, 147.4, 137.0, 132.9, 132.3, 130.2, 126.6, 125.0, 124.9, 119.4, 119.0, 113.5. FT-IR (cm^{-1}): 1459, 1390 ($\nu_{N=N}$).

[Zn(L^{H})Cl_2] 1b The former procedure has been applied with same stoichiometrically amount to synthesised complex **1b**. Yield and characterization data: Blood-red crystal, Yield 85% (360 mg). Anal. Calcd. for $C_{17}H_{13}N_5Cl_2Zn$: C 48.20, H 3.09, N 16.53; Found C 48.61, H 3.13, N 16.41%. ^{1}H-NMR (400 MHz, DMSO-d_6): *δ* (ppm) 8.75 (d, *J* = 5.4 Hz, 1H), 8.06 (t, *J* = 7.8 Hz, 1H), 7.90 (d, *J* = 7.7 Hz, 2H), 7.79-7.74 (m, 4H), 7.68 (d, *J* = 8.1 Hz, 1H), 7.62-7.59 (m, 4H). ^{13}C-NMR (100 MHz, DMSO-d_6): *δ* (ppm) 163.4, 152.8, 149.9, 148.0, 147.4, 139.5, 132.8, 132.5, 131.9, 130.0, 129.1, 128.7, 126.6, 123.3, 119.5, 118.8, 113.4. FT-IR (cm^{-1}): 1456, 1397 ($\nu_{N=N}$).

General procedure for synthesis of α-alkylated ketone derivatives

In aerial condition, a mixture of catalyst **1a** (0.008 mol%), KO^{t}Bu (30 mol%), secondary alcohols/ketones (1.0 mmol), and primary alcohols (1.0 mmol) had been placed into a 50.0 ml round-bottom flask. The reaction mixture was then placed in a preheated oil bath at 110 °C prior 5.0 ml of toluene was added to it. The reaction was continuing for 21 hrs. Following the reaction, the resulting mixture was vacuum-concentrated and purified using column chromatography on silica gel 60-120 mesh (hexane/ethyl acetate) to afford the desired product.

General procedure for Friedländer quinoline synthesis

Catalyst **1a** (0.005 mol%), KO^{t}Bu (20 mol%), secondary alcohols/ketones (1.0 mmol), and 2-aminobenzyl alcohol derivatives (1.0 mmol) were added to a 50.0 ml round-bottom flask under aerial condition. The reaction mixture was then placed in an oil bath that had been heated to 85 °C before 5.0 ml of toluene was added to it. The reaction continued for 18 hrs. The resulting mixture was subsequently concentrated under vacuum and purified using column chromatography on silica gel 60-120 mesh (hexane/ethyl acetate) to afford the desired product.

Detection of hydrogen peroxide in the catalytic reaction

The production of H_2O_2 as a byproduct during the catalytic process was developed spectrophotometrically by the typical band for I_3^- (λ_{max} = 350 nm) upon reaction with KI.[27] Applying our developed procedure, 0.008 mmol catalyst **1a** and 20 mol% KO^{t}Bu were added to a round-bottom flask containing 1 mmol of benzyl alcohol in 5 ml of dry toluene. Following 2 hrs of reaction, the reaction mixture was extracted using dichloromethane, and an equal volume of water was added. To prevent further oxidation, the aqueous layer was acidified with H_2SO_4 to pH 2, and then 1 ml of a 10% KI solution and 3 drops of a 3% ammonium molybdate solution were added. $H_2O_2 + 2I^- + 2H^+ \rightarrow 2H2O + I_2$ is the process that takes place when hydrogen peroxide is present, while I_2 (aq) + $I^- \rightarrow I_3^-$ is the reaction that forms when there is an excess of iodide ions. By adding an ammonium molybdate solution, the reaction becomes almost instantaneous albeit it starts out slowly and increases as the acid concentration increases.

II.4.3. Characterization data of Zn catalyzed compounds:

All the reactions were carried out in 1.0 mmol scale of reactant and according to the general procedure for synthesis of α-alkylated ketone derivatives.

1,3-diphenylpropan-1-one (5aa): Eluent: Hexane/Ethyl acetate (20:1). White solid (yield = 88%, 185mg). ^{1}H NMR (300 MHz, $CDCl_3$): δ (ppm) 8.00 (d, J = 7.4 Hz, 2H) 7.59 (t, J = 7.3 Hz, 1H), 7.49 (t, J = 7.5 Hz, 2H), 7.37 – 7.22 (m, 5H), 3.34 (t, J = 7.7 Hz, 2H), 3.11 (t, J = 7.7 Hz, 2H). ^{13}C NMR (75 MHz, $CDCl_3$): δ (ppm) 199.3, 141.3, 136.9, 133.0, 128.6, 128.5, 128.4, 128.0, 126.2, 40.5, 30.1.

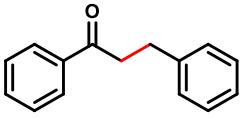

1-phenyl-3-(p-tolyl)propan-1-one (5ab): Eluent: Hexane/Ethyl acetate (20:1). White solid (yield = 76%, 170 mg).^{1}H NMR (300 MHz, $CDCl_3$): δ (ppm) 8.09 – 8.05 (m, 2H), 7.64 – 7.60 (m, 1H), 7.56 – 7.52 (m, 2H), 7.29 – 7.25 (m, 4H), 3.37 – 3.31 (m, 2H), 3.19 – 3.14 (m, 2H), 2.45 (s, 3H).^{13}C NMR (75 MHz, $CDCl_3$): δ (ppm) 198.9, 143.9, 141.4, 134.4, 129.3, 128.5, 128.4, 128.2, 126.1, 40.4, 30.2, 21.7.

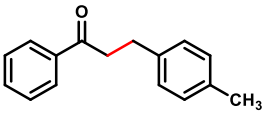

1-phenyl-3-(m-tolyl)propan-1-one (5ac): Eluent: Hexane/Ethyl acetate (20:1). White solid (yield = 72%, 161 mg). ^{1}H NMR (300 MHz, $CDCl_3$): δ (ppm) 7.99 (d, J = 8.6 Hz, 2H), 7.61- 7.56 (m, 1H), 7.51-7.45 (m, 2H), 7.22 (t, J = 7.1 Hz, 1H), 7.11-7.04 (m, 3H), 3.32 (dd, J = 8.5, 6.4 Hz, 2H). 3.09-3.03 (m, 2H), 2.36 (s, 3H). ^{13}C NMR (75 MHz, $CDCl_3$): δ (ppm) 199.4, 141.2, 138.1, 136.9, 133.0, 129.2, 128.6, 128.1, 126.9, 125.4, 40.6, 30.1, 21.4.

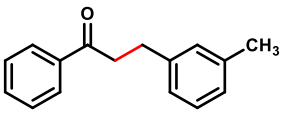

1-phenyl-3-(o-tolyl)propan-1-one (5ad): Eluent: Hexane/Ethyl acetate (20:1). White solid (yield = 69%, 155 mg). ^{1}H NMR (300 MHz, $CDCl_3$): δ (ppm) 8.01- 7.98 (m, 2H), 7.62-7.57 (m, 1H), 7.51-7.45 (m, 2H), 7.21-7.16 (m, 4H), 3.31-3.26 (m, 2H). 3.11-3.06 (m, 2H), 2.38 (s, 3H). ^{13}C NMR (75 MHz, $CDCl_3$): δ (ppm) 199.4, 139.5, 136.9, 136.0, 133.2, 130.5, 129.4, 128.9, 128.7, 128.2, 126.4 (d, J = 10.4 Hz), 39.2, 27.6, 19.5.

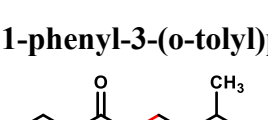

3-(4-chlorophenyl)-1-phenylpropan-1-one (5ae): Eluent: Hexane/Ethyl acetate (20:1). White solid (yield = 78%, 191 mg). ^{1}H NMR (300 MHz, $CDCl_3$): δ (ppm) 7.99-7.96 (m, 2H), 7.60-7.56 (m, 1H), 7.51-7.48 (m, 2H), 7.28-7.20 (m, 4H), 3.33-3.28 (m, 2H), 3.09-3.04 (m, 2H). ^{13}C NMR (75 MHz, $CDCl_3$): δ (ppm) 198.9, 139.8, 136.8, 133.2, 131.9, 129.8, 128.7, 128.6, 128.0, 40.1, 29.4.

3-(4-fluorophenyl)-1-phenylpropan-1-one (5af): Eluent: Hexane/Ethyl acetate (20:1). White solid (yield = 85%, 194 mg). ^{1}H NMR (300 MHz, $CDCl_3$): δ (ppm) 7.99-7.96 (m, 2H), 7.61-7.56 (m, 1H), 7.50-7.45 (m, 2H), 7.25-7.21 (m, 2H), 7.03-6.97 (m, 2H), 3.31 (t, J = 7.5 Hz, 2H), 3.07 (t, J = 7.5 Hz, 2H). ^{13}C NMR (75 MHz, $CDCl_3$): δ (ppm) 199.0, 163.0, 159.8, 136.8, 133.1, 129.9, 129.8, 128.6, 128.0, 115.4, 115.1, 40.4, 29.3. ^{19}F NMR (282 MHz, $CDCl_3$): δ = -117.3 (s, 1F).

3-(4-methoxyphenyl)-1-phenylpropan-1-one (5ag): Eluent: Hexane/Ethyl acetate (20:1). White solid (yield = 82%, 197mg). ^{1}H NMR (300 MHz, $CDCl_3$): δ (ppm) 8.00-7.97 (m, 2H), 7.61-7.56 (m, 1H), 7.50-7.46 (m, 2H), 7.22-7.19 (m, 2H), 6.89-6.85 (m, 2H), 3.81 (s, 3H), 3.30 (t, J = 7.6 Hz, 2H), 3.04 (t, J = 7.6 Hz, 2H). ^{13}C NMR (75 MHz, $CDCl_3$): δ (ppm) 199.4, 158.0, 136.9, 133.3, 133.0, 129.4, 128.6, 128.0, 113.9, 55.3, 40.7, 29.3.

3-phenyl-1-(p-tolyl)propan-1-one (5ah): Eluent: Hexane/Ethyl acetate (20:1). Colourless liquid (yield = 92%, 206mg). ^{1}H NMR (300 MHz, $CDCl_3$): δ (ppm) 7.92 (d, J = 8.0 Hz, 2H), 7.39-7.26 (m, 7H), 3.33 (t, J = 7.7 Hz, 2H), 3.12 (t, J = 7.7 Hz, 2H). ^{13}C NMR (75 MHz, $CDCl_3$): δ (ppm) 198.9, 143.9, 141.5, 134.5, 129.4, 128.6, 128.5, 128.3, 126.2, 40.4, 30.3, 21.7.

3-phenyl-1-(m-tolyl)propan-1-one (5ai): Eluent: Hexane/Ethyl acetate (20:1). White solid (yield = 85%, 190 mg). ^{1}H NMR (300 MHz, $CDCl_3$): δ (ppm) 7.80-7.76 (m, 2H), 7.39-7.29 (m, 7H), 3.32 (t, J = 8.1 Hz, 2H), 3.12-3.07 (m, 2H), 2.43 (s, 3H) ^{13}C NMR (75 MHz, $CDCl_3$): δ (ppm) 199.5, 141.4, 138.4, 136.9, 133.8, 128.6, 128.4, 128.5, 128.4, 126.1, 125.3, 40.5, 30.2, 21.3.

3-phenyl-1-(o-tolyl)propan-1-one (5aj): Eluent: Hexane/Ethyl acetate (20:1). Colorless liquid (yield = 75%, 168mg). ^{1}H NMR (300 MHz, $CDCl_3$): δ (ppm) 7.62 (d, J = 7.0 Hz, 1H), 7.27-7.21 (m, 8H), 3.25 (t, J = 7.6 Hz, 2H), 3.07 (t, J = 7.6 Hz, 2H), 2.49 (s, 3H). ^{13}C NMR (75 MHz, $CDCl_3$): δ (ppm) 203.41, 141.2, 138.1, 136.4, 136.2, 131.9, 129.4, 128.5, 128.4, 126.1, 125.7, 125.2, 43.2, 30.4, 21.3.

1-(4-methoxyphenyl)-3-phenylpropan-1-one (5ak): Eluent: Hexane/Ethyl acetate (20:1). White solid (yield = 93%, 223mg). ^{1}H NMR (300 MHz, $CDCl_3$): δ (ppm) 7.97 (d, J = 8.8 Hz, 2H), 7.23 (d, J = 6.9 Hz, 1H), 7.17 (d, J = 7.0 Hz, 1H), 6.95 (d, J = 8.8 Hz, 2H), 3.89 (s, 3H),3.28 (t, J = 7.6 Hz, 2H), 3.09 (t, J = 7.6 Hz, 2H). ^{13}C NMR (75 MHz, $CDCl_3$): δ (ppm) 197.9, 163.3, 141.5, 130.5, 129.0, 128.5, 128.4, 126.2, 113.6, 55.4, 40.1, 30.4.

1-(3-methoxyphenyl)-3-phenylpropan-1-one (**5al**): Eluent: Hexane/Ethyl acetate (20:1).

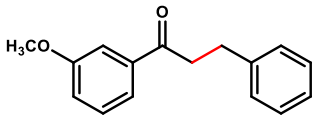

White solid (yield = 88%, 211mg). ^{1}H NMR (300 MHz, $CDCl_3$): δ (ppm) 7.58-7.52 (m, 2H), 7.41-7.30 (m, 5H), 7.19-7.15 (m, 2H), 3.88 (s, 3H), 3.33 (t, J = 7.7 Hz, 2H), 3.10 (t, J = 7.7 Hz, 2H). ^{13}C NMR (75 MHz, $CDCl_3$): δ (ppm) 199.1, 159.9, 141.3, 138.3, 129.6, 128.6, 128.5, 126.2, 120.7, 119.6, 112.3, 55.5, 40.6, 30.2.

1-(4-fluorophenyl)-3-phenylpropan-1-one (**5am**): Eluent: Hexane/Ethyl acetate (20:1).

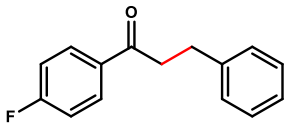

White solid (yield = 68%, 155mg). ^{1}H NMR (300 MHz, $CDCl_3$): δ (ppm) 8.05-8.00 (m, 2H), 7.38-7.24 (m, 5H), 7.19-7.12 (m, 2H), 3.31 (t, J = 7.6 Hz, 2H) 3.12 (t, J = 7.6 Hz, 2H). ^{13}C NMR (75 MHz, $CDCl_3$): δ (ppm) 197.6, 167.0, 164.5, 141.2, 133.47, 133.3, 130.71 (d, J = 9.3 Hz), 128.55 (d, J = 13.0 Hz), 115.71 (d, J = 21.8 Hz), 40.4, 30.1. ^{19}F NMR (282 MHz, $CDCl_3$): δ = -105F.2 (s, 1F).

1-(4-Bromophenyl)-3-phenylpropan-1-one (**5an**): Eluent: Hexane/Ethyl acetate (20:1).

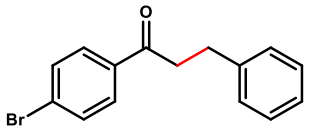

White solid (yield = 57%, 165mg). ^{1}H NMR (300 MHz, $CDCl_3$): δ (ppm) 7.84 (d, J = 8.6 Hz, 2H), 7.61 (d, J = 8.6 Hz, 2H), 7.33-7.30 (m, 2H), 7.25-7.21 (m, 3H), 3.32-3.26 (m, 2H), 3.11-3.06 (m, 2H). ^{13}C NMR (75 MHz, $CDCl_3$): δ (ppm) 198.2, 141.0, 135.6, 131.9, 129.6, 128.9, 128.6, 128.5, 128.5, 128.4, 128.2, 126.4, 126.2, 40.4, 30.0.

All the reactions were carried out in 1.0 mmol scale of reactant and according to the general procedure for Friedländer quinoline synthesis.

2-phenyl quinoline (**9aa**): Eluent: Hexane/Ethyl acetate (20:1). Fawn solid (yield = 92%,

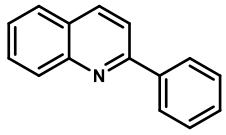

189mg). ^{1}H NMR (300 MHz, $CDCl_3$): δ (ppm) 8.26-8.18 (m,4H), 7.92-7.84 (m, 2H), 7.78-7.73 (m,1H), 7.59-7.47 (m,4H). ^{13}C NMR (75 MHz, $CDCl_3$): δ (ppm) 157.4, 148.3, 139.7, 136.8, 129.8, 129.7, 129.4, 128.9, 127.6, 127.5, 127.2, 126.3, 119.1.

2-(p-tolyl)quinoline (9ab): Eluent: Hexane/Ethyl acetate (20:1). Fawn solid (yield = 94%,

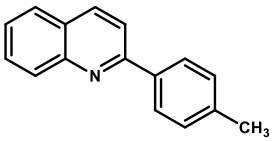

207mg). ^{1}H NMR (300 MHz, $CDCl_3$): δ (ppm) 8.21 (d, J = 8.5 Hz, 2H), 8.11 (d, J = 8.2 Hz, 2H), 7.89-7.82 (m,2H), 7.78-7.72 (m,1H), 7.57-7.51(m, 1H), 7.37(d, J = 7.8 Hz, 2H), 2.47 (s, 3H). ^{13}C NMR (75 MHz, $CDCl_3$): δ (ppm) 157.4, 148.3, 139.4, 136.8 (d, J = 16.6 Hz), 129.6 (d, J = 5.7 Hz), 129.3, 128.5, 127.5, 127.1, 126.1, 118.9, 21.4.

2-(m-tolyl)quinoline (**9ac**): Eluent: Hexane/Ethyl acetate (20:1). Yellowish Liquid (yield = 90%, 197mg). 1H NMR (300 MHz, $CDCl_3$): δ (ppm) 8.25-8.20 (m, 2H), 7.95 (d, *J* = 7.7 Hz, 1H), 7.85 (d, *J* = 6.6 Hz, 1H), 7.80-7.73 (m, 2H), 7.55 (t, *J* = 6.9 Hz, 1H), 7.47-7.37(m, 2H), 7.31 (d, *J* = 6.7 Hz, 1H), 2.51 (s, 3H). ^{13}C NMR (75 MHz, $CDCl_3$): δ (ppm) 157.6, 148.3, 138.5, 136.7, 133.8, 130.1, 129.7, 129.6, 128.7, 128.4, 128.3, 127.4, 126.2, 124.7, 119.1, 21.6.

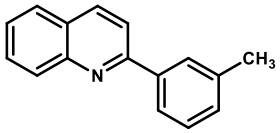

2-(o-tolyl)quinoline (9ad): Eluent: Hexane/Ethyl acetate (20:1). Fawn solid (yield = 84%, 185mg). ^1H NMR (300 MHz, $CDCl_3$): δ (ppm) 8.22 (dd, J = 15.9, 8.5 Hz, 2H), 7.89 (dd, *J* = 8.2, 1.5 Hz, 1H), 7.77 (m,1H), 7.62-7.51 (m,3H), 7.40-7.31 (m, 3H), 2.44 (s, 3H). ^{13}C NMR (75 MHz, $CDCl_3$): δ (ppm) 160.3, 147.9, 140.8, 136.1, 136.0, 130.9, 129.7, 129.6, 128.5, 127.5, 126.8, 126.4, 126.0, 122.4, 20.4.

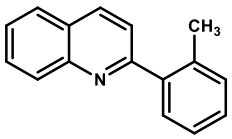

2-(4-methoxyphenyl)quinoline (9ae): Eluent: Hexane/Ethyl acetate (20:1). White solid (yield = 89%, 209mg). ^1H NMR (300 MHz, $CDCl_3$): δ (ppm) 8.22-8.15 (m, 4H), 7.88-7.82 (m, 2H), 7.73 (t, *J* = 6.9 Hz, 1H), 7.52 (t, *J* = 7.5 Hz, 1H),7.08 (d, *J* = 8.9 Hz, 2H), 3.92 (s, 3H). ^{13}C NMR (75 MHz, $CDCl_3$): δ (ppm) 160.8, 157.0, 148.3, 136.7, 132.3, 129.6, 129.5, 128.9, 127.4, 126.9, 125.9, 118.6, 114.2, 55.4.

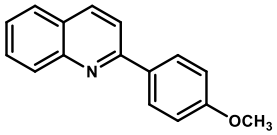

2-(3-methoxyphenyl)quinoline (9af): Eluent: Hexane/Ethyl acetate (20:1). White solid (yield = 87%, 205mg). ^1H NMR (300 MHz, $CDCl_3$): δ (ppm) 8.24-8.20 (m, 2H), 7.89-7.81 (m, 3H), 7.78-7.72 (m, 2H), 7.57-7.51 (m, 2H), 7.07-7.03 (m, 1H), 3.95 (s, 3H). ^{13}C NMR (75 MHz, $CDCl_3$): δ (ppm) 160.2, 159.8, 148.2, 141.2, 136.8, 129.8, 129.8, 129.7, 127.5, 126.4, 120.0, 119.1, 115.4, 112.8, 55.4.

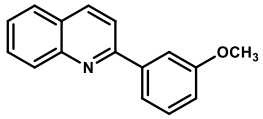

2-(4-bromophenyl)quinoline (9ag): Eluent: Hexane/Ethyl acetate (20:1). Beige solid (yield = 86%, 245mg). ^1H NMR (300 MHz, $CDCl_3$): δ (ppm) 8.26 (d, *J* = 7.8 Hz, 1H), 8.18 (dd, *J* = 8.5, 1.0 Hz, 1H), 8.08 (d, *J* = 8.6 Hz,2H), 7.87 (d, *J* = 8.6 Hz,2H), 7.79-7.74(m, 1H), 7.68(d, *J* = 8.6 Hz, 2H), 7.57 (t, *J* = 6.9 Hz,1H). ^{13}C NMR (75 MHz, $CDCl_3$): δ (ppm) 156.1, 148.3, 138.5, 137.0, 132.0, 131.4, 129.9, 129.7, 129.1, 127.5, 127.3, 126.6, 123.9, 118.5.

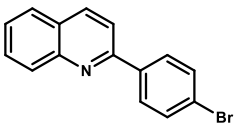

2-(3-bromophenyl)quinoline (9ah): Eluent: Hexane/Ethyl acetate (20:1). Beige solid (yield = 72%, 204mg). ^1H NMR (300 MHz, $CDCl_3$): δ (ppm) 8.38 (s, 1H), 8.26-8.18 (m, 2H), 8.10(s, 1H), 7.85 (d, *J* = 8.0 Hz, 2H), 7.76 (t, *J* = 7.8 Hz, 1H), 7.59 (t, *J* = 8.4 Hz, 2H), 7.43-7.33 (m, 1H). ^{13}C NMR (75 MHz, $CDCl_3$): δ (ppm) 155.6, 148.2, 141.7, 137.0, 132.2, 131.4, 130.6, 130.3, 129.9, 129.8, 127.5, 126.7, 126.0, 123.2, 118.7

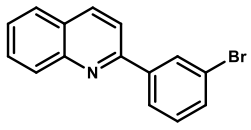

2-(4-fluorophenyl)quinoline (9ai): Eluent: Hexane/Ethyl acetate (20:1). Beige solid (yield = 84%, 188mg). ^{1}H NMR (300 MHz, $CDCl_3$): δ (ppm) 8.26-8.16 (m, 4H), 7.86 (d, *J* = 8.6 Hz, 2H), 7.76 (t, *J* = 6.9 Hz, 1H), 7.56 (t, *J* = 7.5 Hz, 1H), 7.27-7.21(m, 2H). ^{13}C-NMR (75 MHz, $CDCl_3$): δ (ppm) 165.5, 162.2, 156.3, 148.2, 136.9, 135.9, 129.8, 129.5, 129.4, 127.5, 126.4, 118.7, 115.9, 115.7. ^{19}F NMR (282 MHz, CDCl3): δ = -117.3 (s, 1F)

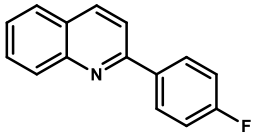

2-(2-fluorophenyl)quinoline (9aj): Eluent: Hexane/Ethyl acetate (20:1). Fawn Liquid (yield = 55%, 123mg). ^{1}H NMR (300 MHz, $CDCl_3$): δ (ppm) 8.32-8.29 (m, 1H), 8.09-8.05 (m, 2H), 8.0-7.97 (m, 1H), 7.87-7.84 (m, 1H), 7.80-7.74 (m, 1H), 7.61-7.55 (m, 1H), 7.42-7.34 (m, 1H), 7.13-7.10 (m, 1H), 7.02-6.96 (m, 1H). ^{13}C NMR (75 MHz, $CDCl_3$): δ (ppm) 161.0, 158.0, 144.8, 137.7, 132.1, 130.5, 127.6 (d, *J* = 4.3 Hz), 127.0, 126.7, 118.7 (d, *J* = 6.3 Hz), 117.3. ^{19}F NMR (282 MHz, CDCl3): δ = -117.3 (s, F).

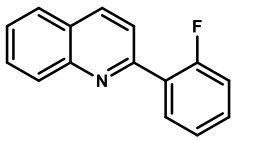

2-(4-nitrophenyl)quinoline (9ak): Eluent: Hexane/Ethyl acetate (20:1). Pastel orange solid (yield = 81%, 203mg). ^{1}H NMR (300 MHz, $CDCl_3$): δ (ppm) 8.43-8.36 (m, 4H), 8.35-8.32 (m, 1H), 8.24-8.20 (m, 1H), 7.96 (d, *J* = 8.6 Hz, 1H), 7.92-7.89 (m, 1H), 7.84-7.78 (m, 1H), 7.65-7.60 (m, 1H). ^{13}C NMR (75 MHz, $CDCl_3$): δ (ppm) 157.6, 148.4, 148.3, 145.5, 137.4, 130.3, 130.0, 128.4, 128.2, 127.6, 127.3, 124.1, 118.8.

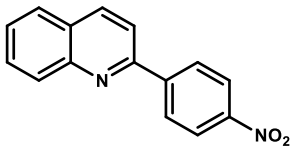

2-(3-nitrophenyl)quinoline (9al): Eluent: Hexane/Ethyl acetate (20:1). Pastel orange solid (yield = 67%, 168mg). ^{1}H NMR (300 MHz, $CDCl_3$): δ (ppm) 9.07 (s, 1H), 8.58 (d, *J* = 7.8 Hz, 1H), 8.33 (d, *J* = 8.2 Hz, 2H), 8.22 (d, *J* = 8.5 Hz, 1H), 7.97 (d, *J* = 8.6 Hz, 1H), 7.90 (d, *J* = 6.7 Hz, 1H), 7.83-7.70 (m, 2H), 7.61 (t, *J* = 6.9 Hz, 1H). ^{13}C NMR (75 MHz, $CDCl_3$): δ (ppm) 154.5, 148.9, 148.3, 141.3, 137.5, 133.3, 130.2, 129.9, 129.8, 129.0, 127.6, 127.1, 123.9, 122.5, 118.4.

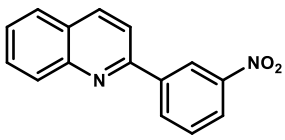

2-hexylquinoline (9am): Eluent: Hexane/Ethyl acetate (20:1). Colorless Liquid (yield = 85%, 182mg). ^{1}H NMR (300 MHz, $CDCl_3$): δ (ppm) 8.06 (t, *J* = 8.1 Hz, 2H), 7.76 (dd, *J* = 8.1, 1.5 Hz, 1H), 7.68 (ddd, *J* = 8.5, 6.8, 1.5 Hz, 1H)), 7.47 (ddd, *J* = 8.1, 6.8, 1.2 Hz, 1H), 7.29 (d, *J* = 8.5 Hz, 1H), 3.00 – 2.95 (m, 2H), 1.87 – 1.77 (m, 2H), 1.37-1.27 (m, 6H), 0.93-0.87 (m, 3H). ^{13}C NMR (75 MHz, $CDCl_3$): δ (ppm) 163.1, 147.9, 136.1, 129.3, 128.8, 127.5, 126.7, 125.6, 121.3, 39.3, 31.7, 30.0, 29.2, 22.6, 14.1.

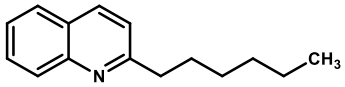

2-cyclohexylquinoline (9an): Eluent: Hexane/Ethyl acetate (20:1). Yellowish Oil (yield = 89%, 188mg). 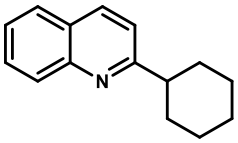 ^{1}H NMR (300 MHz, $CDCl_3$): δ (ppm) 8.11 (d, *J* = 3.0 Hz, 1H), 8.08 (d, *J* = 3.4 Hz, 1H), 7.79 (dd, *J* = 8.1, 1.5 Hz, 1H), 7.70 (ddd, *J* = 8.5, 6.9, 1.5 Hz, 1H), 7.50 (ddd, *J* = 8.1, 6.9, 1.2 Hz, 1H), 7.36 (d, *J* = 8.6 Hz, 1H), 2.99-2.93 (m, 1H), 2.09-2.03 (m, 3H), 1.95-1.90 (m, 2H), 1.69-1.48 (m, 5H). ^{13}C NMR (75 MHz, $CDCl_3$): δ (ppm) 166.8, 147.9, 136.2, 129.2, 129.0, 128.2, 127.4, 125.6, 119.6, 47.62, 32.8, 28.5, 26.6, 26.2, 25.7.

2-(naphthalen-2-yl)quinoline (9ao): Eluent: Hexane/Ethyl acetate (20:1). White solid (yield = 84%, 213mg). 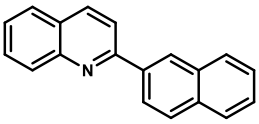 ^{1}H NMR (300 MHz, $CDCl_3$): δ (ppm) 8.65 (s, 1H), 8.41 (dd, *J* = 8.6, 1.8 Hz, 1H), 8.27 (dd, *J* = 8.5, 4.6 Hz, 2H), 8.07 – 8.02 (m, 3H), 7.94 – 7.92 (m, 1H), 7.87 (d, *J* = 6.7, Hz, 1H), 7.80 – 7.76 (m, 1H), 7.59 – 7.54 (m, 3H). ^{13}C NMR (75 MHz, $CDCl_3$): δ (ppm) 157.2, 148.4, 137.0, 136.8, 133.9, 133.5, 129.8, 129.7, 128.8, 128.6, 128.3, 127.7. 127.5, 127.3, 127.2, 126.7, 126.4, 125.1, 119.2.

6-chloro-2-phenylquinoline (10aa): Eluent: Hexane/Ethyl acetate (20:1). White solid (yield = 94%, 225mg). 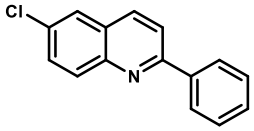 ^{1}H NMR (300 MHz, $CDCl_3$): δ (ppm) 8.19-8.12(m, 4H), 7.92 (d, *J* = 8.7 Hz, 1H), 7.83 (d, *J* = 2.3 Hz, 1H), 7.68 (dd, *J* = 9.0, 2.3 Hz, 1H), 7.59-7.47 (m, 3H). ^{13}C NMR (75 MHz, $CDCl_3$): δ (ppm) 157.6, 146.7, 139.2, 135.9, 131.9, 131.3, 130.6, 129.6, 128.9, 127.7, 127.5, 126.2, 119.8.

6-chloro-2-(3-bromophenyl)quinoline (10ab): Eluent: Hexane/Ethyl acetate (20:1). White solid (yield = 92%, 252mg). 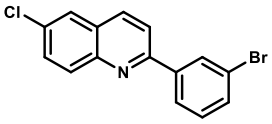 ^{1}H NMR (300 MHz, $CDCl_3$): δ (ppm) 8.17-8.09 (m, 4H), 7.89-7.83 (m, 2H), 7.69 (dd, *J* = 9.0, 2.3 Hz, 1H), 7.54-7.50 (m, 2H). ^{13}C NMR (75 MHz, $CDCl_3$): δ (ppm) 156.2, 146.6, 137.6, 136.1, 135.8, 132.2, 131.3, 130.8, 129.1, 128.8, 127.8, 126.2, 119.4. MS (ESI+): $C_{15}H_{10}BrClN$ ([M+H]+
); calculated: 317.96, found: 317.98.

6-chloro-2-(4-bromophenyl)quinoline (10ac): Eluent: Hexane/Ethyl acetate (20:1). White solid (yield = 92%, 252mg). 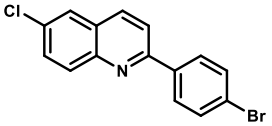 ^{1}H NMR (300 MHz, $CDCl_3$): δ (ppm) 8.17-8.09 (m, 4H), 7.89-7.83 (m, 2H), 7.69 (dd, *J* = 9.0, 2.3 Hz, 1H), 7.54-7.50 (m, 2H). ^{13}C NMR (75 MHz, $CDCl_3$): δ (ppm) 156.2, 146.6, 137.6, 136.1, 135.8, 132.2, 131.3, 130.8, 129.1, 128.8, 127.8, 126.2, 119.4. MS (ESI+): $C_{15}H_{10}BrClN$ ([M+H]+); calculated: 317.96, found: 317.98.

6-chloro-2-(4-chlorophenyl)quinoline (10ad): Eluent: Hexane/Ethyl acetate (20:1). White solid (yield = 92%, 252mg). ^{1}H NMR (300 MHz, $CDCl_3$): δ (ppm) 8.17-8.09 (m, 4H), 7.89-7.83 (m, 2H), 7.69 (dd, *J* = 9.0, 2.3 Hz, 1H), 7.54-7.50 (m, 2H). ^{13}C NMR (75 MHz, $CDCl_3$): δ (ppm) 156.2, 146.6, 137.6, 136.1, 135.8, 132.2, 131.3, 130.8, 129.1, 128.8, 127.8, 126.2, 119.4.

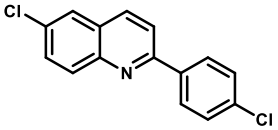

6-chloro-2-(4-fluorophenyl)quinoline (10ae): Eluent: Hexane/Ethyl acetate (20:1). White solid (yield = 87%, 224mg). ^{1}H NMR (300 MHz, $CDCl_3$): δ (ppm) 8.20-8.08 (m, 4H), 7.88-7.82 (m, 2H), 7.68 (dd, *J* = 9.0, 2.4 Hz, 1H), 7.26-7.20 (m, 2H). ^{13}C NMR (75 MHz, $CDCl_3$): δ (ppm) 165.6, 162.3, 156.4, 146.6, 135.9, 132.0, 131.2, 130.7, 129.5, 129.3, 127.6, 126.2, 119.4, 116.0, 115.7. ^{19}F NMR (282 MHz, $CDCl_3$): δ = -111.9 (s, 1F). MS (ESI+): $C_{15}H_{10}ClFN$ ([M+H]+); calculated: 258.04, found: 258.06.

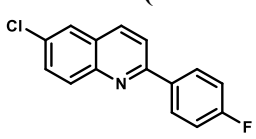

6-chloro-2-(2-fluorophenyl)quinoline (10af): Eluent: Hexane/Ethyl acetate (20:1). White solid (yield = 60%, 154mg). ^{1}H NMR (300 MHz, $CDCl_3$): δ (ppm) 8.16-8.10 (m, 3H), 7.94 (dd, *J* = 8.6, 2.6 Hz, 1H), 7.85 (d, *J* = 2.3 Hz, 1H), 7.69 (dd, *J* = 9.0, 2.3 Hz, 1H), 7.49-7.44 (m, 1H), 7.34 (td, *J* = 7.5, 1.2 Hz, 1H), 7.23 (ddd, J = 11.4, 8.2, 1.2 Hz, 1H). ^{13}C NMR (75 MHz, $CDCl_3$): δ (ppm) 162.1, 159.6, 154.3 (d, *J* = 2.0 Hz), 146.7, 135.3, 132.4, 131.43 (d, *J* = 2.9 Hz), 131.3, 131.1 (d, *J* = 8.6 Hz), 130.6, 127.8, 126.2, 124.8 (d, *J* = 3.4 Hz), 123.3 (d, J = 8.4 Hz), 116.3 (d, *J* = 22.8 Hz). ^{19}F NMR (282 MHz, CDCl3): δ = -117.0 (s, 1F) MS (ESI+): $C_{15}H_{10}ClFN$ ([M+H]+); calculated: 258.04, found: 258.06.

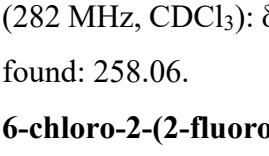

6-chloro-2-(4-methoxyphenyl)quinoline (10ag): Eluent: Hexane/Ethyl acetate (20:1). White solid (yield = 92%, 245mg). ^{1}H NMR (300 MHz, $CDCl_3$): δ (ppm) 8.17-8.07 (m, 4H), 7.87 (d, *J* = 8.7 Hz, 1H), 7.80 (d, *J* = 2.3 Hz, 1H), 7.66 (dd, *J* = 9.0, 2.4 Hz, 1H), 7.07 (d, *J* = 8.9 Hz, 2H), 3.91 (s, 1H). ^{13}C NMR (75 MHz, $CDCl_3$): δ (ppm) 161.0, 157.1, 146.7, 135.7, 131.8, 131.5, 131.1, 130.5, 128.9, 127.5, 126.1, 119.4, 114.3, 55.4. MS (ESI+): $C_{16}H_{13}ClNO$ ([M+H]+); calculated: 270.06, found: 270.07.

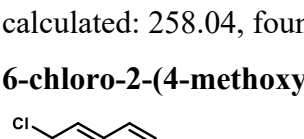

6-chloro-2-(3-methoxyphenyl)quinoline (10ah): Eluent: Hexane/Ethyl acetate (20:1). White solid (yield = 90%, 240mg). ^{1}H NMR (300 MHz, $CDCl_3$): δ (ppm) 8.13-8.07 (m, 2H), 7.86 (d, *J* = 9.6 Hz, 1H), 7.79-7.76 (m, 2H), 7.71-7.67 (m, 2H), 7.44 (t, *J* = 7.9 Hz, 1H), 7.04 (dd, *J* = 8.2, 2.5 Hz, 1H), 3.94 (s, 3H).^{13}C NMR (75 MHz, $CDCl_3$): δ (ppm) 160.2, 157.3, 146.6, 140.6, 135.8, 131.9,

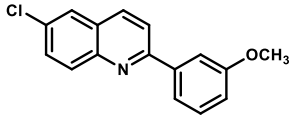

131.3, 130.6, 129.9, 127.8, 126.1, 119.9, 119,8, 115.6, 112.7, 55.4. MS (ESI+): $C_{16}H_{13}ClNO$ ([M+H]+); calculated: 270.06, found: 270.07.

6-chloro-2-(m-tolyl)quinoline (10ai): Eluent: Hexane/Ethyl acetate (20:1). White solid (yield = 92%, 233mg). ^{1}H NMR (300 MHz, $CDCl_3$): δ (ppm) 8.12-8.06 (m, 4H), 7.88 (d, *J* = 8.7 Hz, 1H), 7.80 (d, *J* = 2.4 Hz, 1H), 7.66 (dd, *J* = 9.0, 2.4 Hz, 1H), 7.38-7.34 (m, 2H), 2.46 (s, 3H).^{13}C NMR (75 MHz, $CDCl_3$): δ (ppm) 157.5, 146.7 139.7, 136.4, 135.7, 131.7, 131.3, 130.5, 129.7, 129.3, 128.5, 127.6, 127.4, 126.1, 119.7, 21.4. MS (ESI+): $C_{16}H_{13}ClN$ ([M+H]+); calculated: 254.07, found: 254.09.

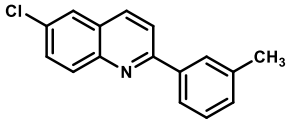

6-chloro-2-(o-tolyl)quinoline (10aj): Eluent: Hexane/Ethyl acetate (20:1). White solid (yield = 86%, 218mg). ^{1}H NMR (300 MHz, $CDCl_3$): δ (ppm) 8.13 (t, *J* = 8.1 Hz, 2H), 7.87 (d, *J* = 2.4 Hz, 1H), 7.69 (dd, *J* = 9.0, 2.3 Hz, 1H), 7.59 (d, *J* = 8.5 Hz, 1H), 7.53-7.50 (m, 1H), 7.41-7.32 (m, 3H) 2.44 (s, 3H). ^{13}C NMR (75 MHz, $CDCl_3$): δ (ppm) 160.5, 146.3, 140.3, 136.0, 132.1, 131.2, 130.9, 129.7, 128.7, 127.3, 126.2, 126.1, 123.3, 20.4. MS (ESI+): $C_{16}H_{13}ClN$ ([M+H]+); calculated: 254.07, found: 254.09.

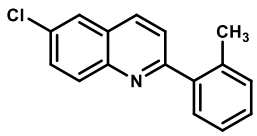

6-chloro-2-(4-nitrophenyl)quinoline (10ak): Eluent: Hexane/Ethyl acetate (20:1). White solid (yield = 70%, 198mg). ^{1}H NMR (300 MHz, $CDCl_3$): δ (ppm) 8.23 (d, *J* = 8.7 Hz, 2H), 7.96 (d, *J* = 8.6 Hz, 2H), 7.86 (d, *J* = 2.3 Hz, 2H), 7.74 (d, *J* = 2.3 Hz, 1H), 7.45 (d, *J* = 2.5 Hz, 1H), 6.63 (d, *J* = 8.8 Hz, 1H). ^{13}C NMR (75 MHz, $CDCl_3$): δ (ppm) 154.7, 148.5, 146.4, 144.7, 136.6, 133.2, 131.4, 129.3, 128.4, 128.1, 126.3, 124.1, 119.7. MS (ESI+): $C_{15}H_9ClN_2O_2$ ([M]+); calculated: 284.03, found: 284.06.

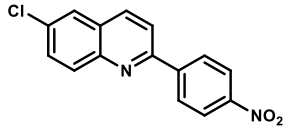

6-chloro-2-(pyridin-4-yl)quinoline (10al): Eluent: Hexane/Ethyl acetate (20:1). White solid (yield = 76%, 182mg). ^{1}H NMR (300 MHz, $CDCl_3$): δ (ppm) 8.73 (d, J = 5.1 Hz, 2H), 8.24 – 8.06 (m, 2H), 8.01 – 7.99 (m, 2H), 7.84 (dd, *J* = 8.7, 3.0 Hz, 1H), 7.78 – 7.72 (m, 1H), 7.67 – 7.63 (m, 1H). ^{13}C NMR (75 MHz, $CDCl_3$): δ (ppm) 154.5, 150.4, 146.6, 137.3, 136.3, 132.9, 131.5, 131.0, 130.1, 129.9. 128.3, 127.6, 126.2, 121.5, 119.2. MS (ESI+): $C_{14}H_9ClN_2$ ([M]+); calculated: 240.04, found: 240.07.

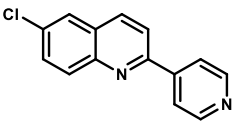

6-chloro-2-(naphthalen-2-yl)quinoline (10am): Eluent: Hexane/Ethyl acetate (20:1). White solid (yield = 88%, 253mg). ^{1}H NMR (300 MHz, $CDCl_3$): δ (ppm) 8.61 (s, 1H), 8.37 (dd, *J* = 8.6, 1.8 Hz, 1H), 8.16 (dd, *J* = 8.8, 4.1 Hz, 2H), 8.06 – 7.98 (m, 3H), 7.95 – 7.89 (m, 1H), 7.83 (d, *J* = 2.4 Hz, 1H), 7.70

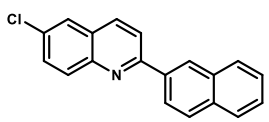

(dd, *J* = 9.0, 2.4 Hz, 1H), 7.59 – 7.54 (m, 2H). ^{13}C NMR (75 MHz, $CDCl_3$): δ (ppm) 157.4, 149.8, 136.5, 135.9, 133.9, 133.5, 131.9, 131.3, 130.7, 128.9, 128.7, 127.8. 127.2, 126.9, 126.5, 126.2, 124.9, 119.9. MS (ESI+): $C_{19}H_{12}ClN$ ([M]+); calculated: 289.06, found: 289.08.

6-chloro-2-hexylquinoline (10an): Eluent: Hexane/Ethyl acetate (20:1). Colorless Oil (yield = 78%, 193mg). ^{1}H NMR (300 MHz, $CDCl_3$): δ (ppm) 8.00-7.92 (m, 2H), 7.77-7.71 (m, 1H), 7.64-7.53 (m, 1H), 7.34-7.28 (m, 1H), 2.97 (dd, *J* = 8.6, 7.2 Hz, 2H), 1.86-1.76 (m, 2H), 1.46-1.40 (m, 5H), 0.97-0.87 (m, 4H). ^{13}C NMR (75 MHz, $CDCl_3$): δ (ppm) 163.5, 146.2, 135.3, 131.2, 130.4, 130.2, 127.3, 126.1, 122.3, 39.3, 31.7, 29.9, 29.2, 22.6, 14.1. MS (ESI+): $C_{15}H_{19}ClN$ ([M+H]+); calculated: 248.120, found: 248.125.

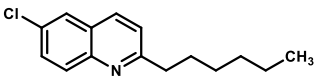

1H-indole (11a): Eluent: Hexane/Ethyl acetate (20:1). Colorless Liquid (yield = 90%, 105mg). ^{1}H NMR (300 MHz, $CDCl_3$): δ (ppm) 8.17 (s, 1H), 7.70 (dd, *J* = 7.8, 1.2 Hz, 1H), 7.45-7.41(m, 1H), 7.25-7.16(m, 3H), 6.61-6.59(m, 1H). ^{13}C NMR (75 MHz, $CDCl_3$): δ (ppm) 135.8, 127.9, 124.1, 122.0, 120.7, 119.8, 111.0, 102.6.

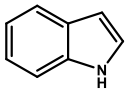

II.4.4. NMR spectra of selected compounds

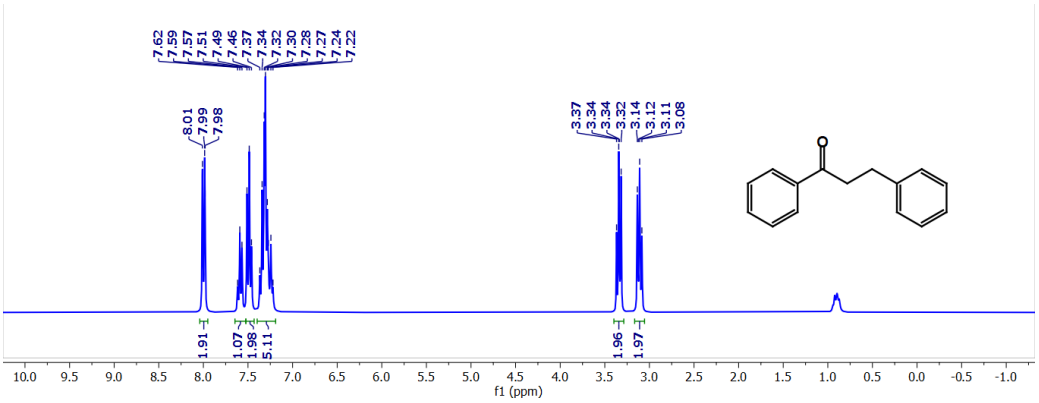

Figure 16: ^{1}H NMR spectrum of compound **5aa** (300 MHz, $CDCl_3$).

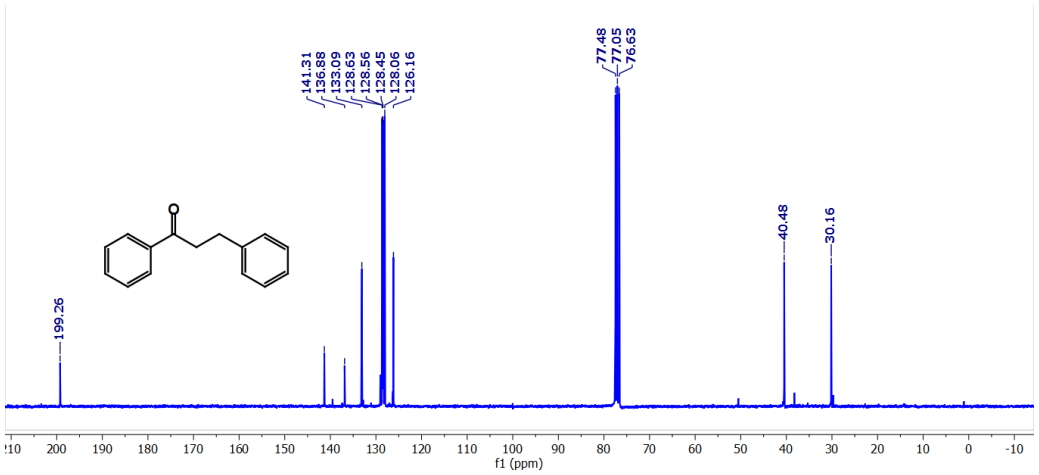

Figure 17: ^{13}C NMR spectrum of compound **5aa** (75 MHz, $CDCl_3$).

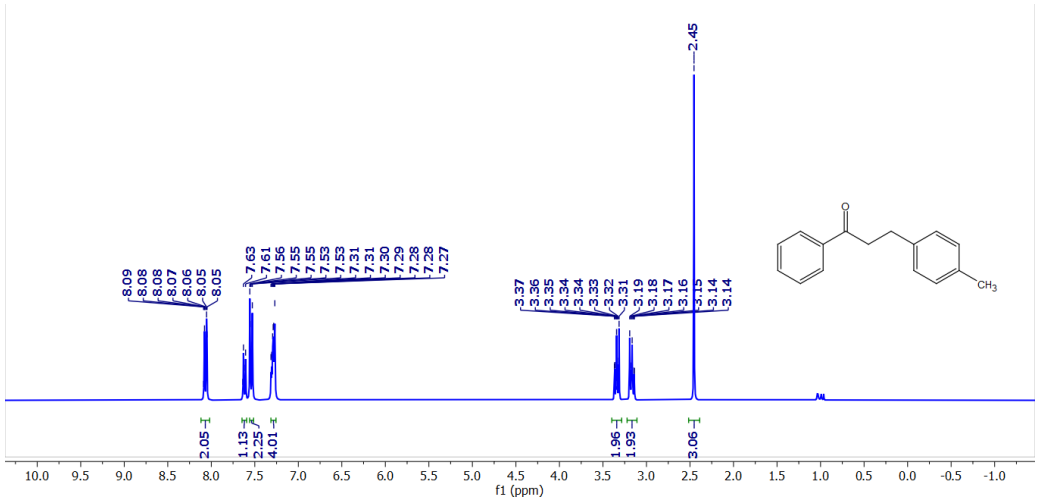

Figure 18: ^{1}H NMR spectrum of compound **5ab** (300 MHz, $CDCl_3$).

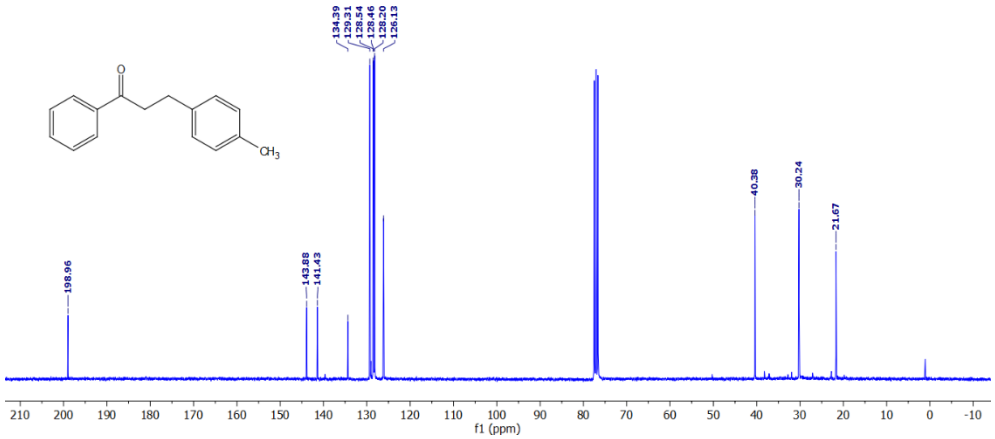

Figure 19: ^{13}C NMR spectrum of compound **5ab** (75 MHz, $CDCl_3$).

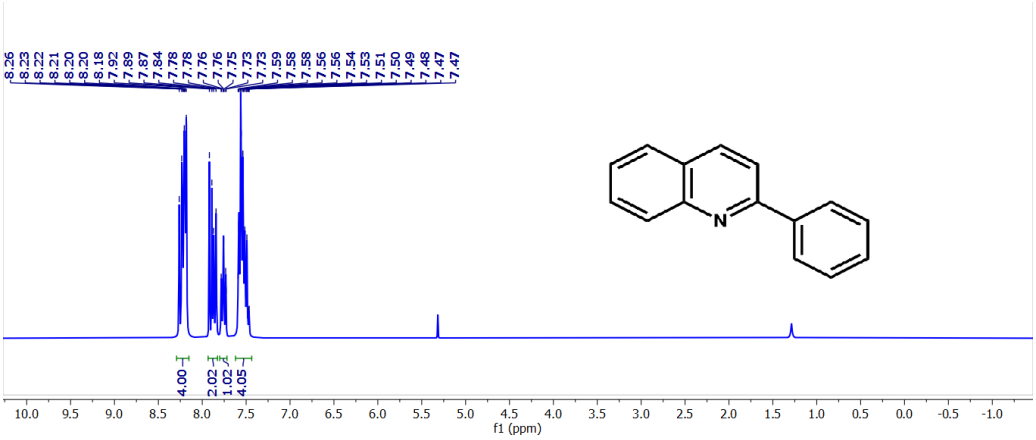

Figure 20: ^{1}H NMR spectrum of compound **9aa** (300 MHz, $CDCl_3$).

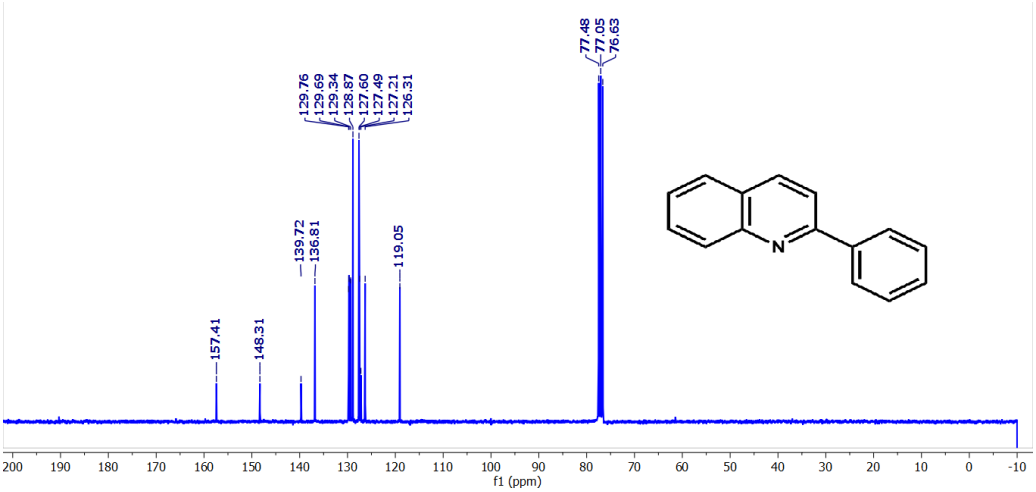

Figure 21: ^{13}C NMR spectrum of compound **9aa** (75 MHz, $CDCl_3$).

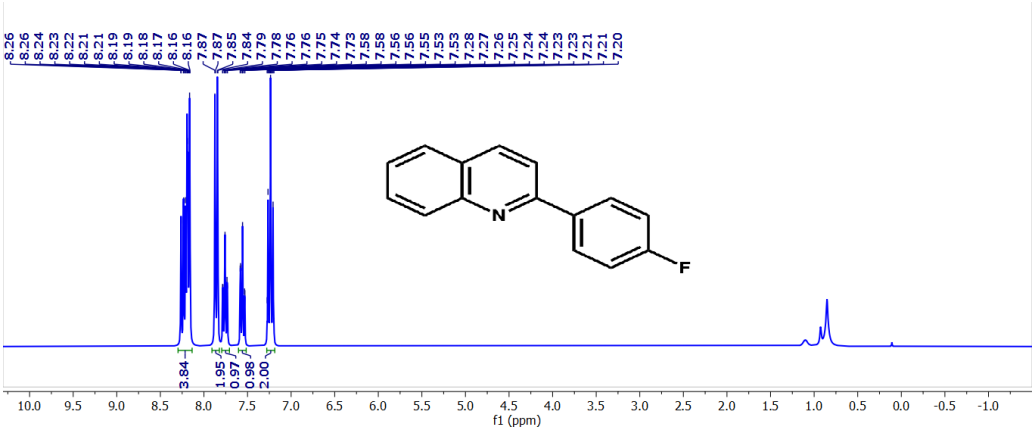

Figure 22: ^{1}H NMR spectrum of compound **9ai** (300 MHz, $CDCl_3$).

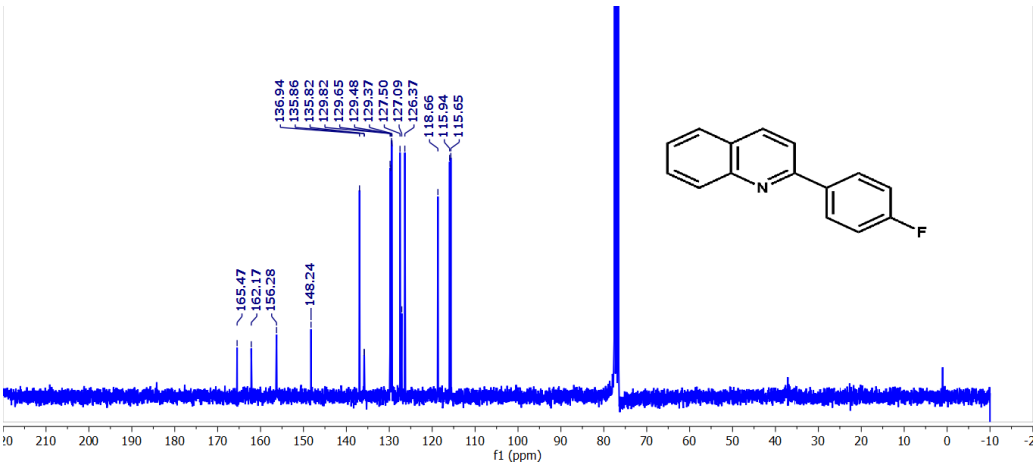

Figure 23: ^{13}C NMR spectrum of compound **9ai** (75 MHz, $CDCl_3$).

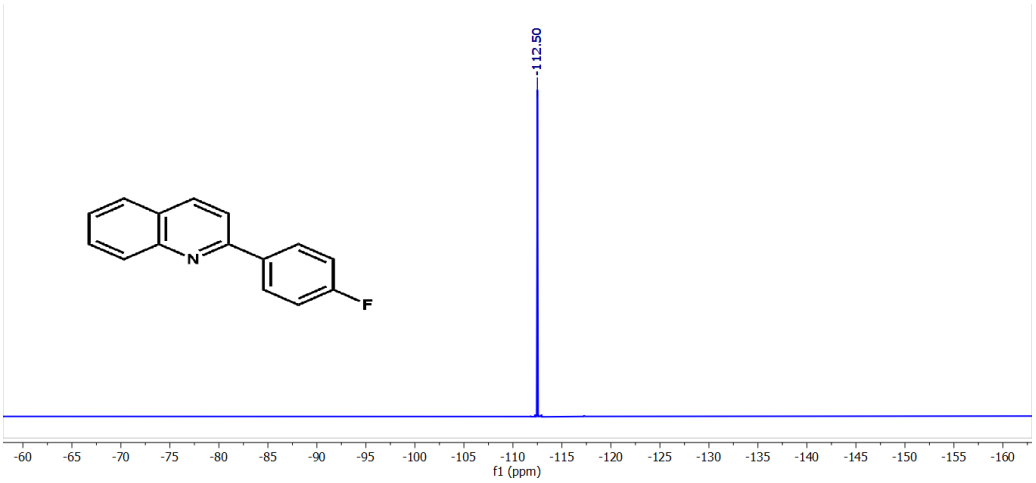

Figure 24: ^{19}F NMR spectrum of compound **9ai** (282 MHz, $CDCl_3$).

II.5. References

1. (a) G. Brachmachari, *CRC Press*, 2007; (b) A. Ricci, *Wiley-VCH*, 2008; (c) J. Hartwig, *University Science Books*, 2009. (d) J. Marco-Contelles, E. Pérez-Mayoral, A. Samadi, M. C. Carreiras and E. Soriano, *Chem. Rev.*, 2009, **109**, 2652–2671; (e) K. Natte, H. Neumann, M. Beller and R. V. Jagadeesh, *Angew. Chem., Int. Ed*., 2017, **56**, 6384−6394; (f) R. H. Crabtree, *Chem. Rev.*, 2017, **117**, 9228–9246; (g) G. A. Filonenko, R. van Putten, E. J. M. Hensen and E. A. Pidko, *Chem. Soc. Rev.*, 2018, **47**, 1459-1483; (h) Z. Chen, M. Y. Rong, J. Nie, X. F. Zhu, B. F. Shi and J. A. Ma, *Chem. Soc. Rev.*, 2019, **48**, 4921–4942; (i) L. Alig, M. Fritz and S. Schneider, *Chem. Rev.*, 2019, **119**, 2681−2751; (j) D-Y. Yang, H. Wang and C-R. Chang, *Adv. Synth. Catal*., 2022, **364**, 3100–3121; (k) A. A. Swatiputra, D. Mukherjee, S. Dinda, S. Roy, K. Pramanik and S. Ganguly, *Dalton Trans.* 2023, **52**, 15627-15646. (l) L. M. Kabadwal, A. Bera, D. Banerjee, Direct synthesis of gem-β, β′-bis(alkyl) alcohols using nickel catalysis via sequential DCR approach, *ACS Catal.*, 2024, **14**, 4018–4029; (m) F. Doraghia, F. Gilaninezhad, S. Karimianc, A. M. Mahdavian, B. Larijani and M. Mahdavi, *Adv. Synth. Catal.*, 2024, **366**, 1–24.
2. (a) M. S. Kwon, N. Kim, S. H. Seo, I. S. Park, R. K. Cheedrala and J. Park, Angew. Chem. Int. Ed., 2005, **44**, 6913−6915; (b) G. Xu, Q. Li, J. Feng, Q. Liu, Z. Zhang, X. Wang, X. Zhang and X. Mu, *ChemSusChem*, 2014, **7**, 105−109; (c) F. Huang, Z. Liu and Z. Yu, *Angew. Chem. Int. Ed.*, 2016, ***55***, 862–875; (d) P. Liu, R. Liang, L. Lu, Z. Yu and F. Li, *J. Org. Chem*., 2017, **82**, 1943–1950; (d) S. Genç, B. Arslan, S. Gülcemal, S. Günnaz, B. Çetinkaya and D. Gülcemal, *J. Org. Chem.*, 2019, **84**, 6286–6297; (e) C. Teja, F. Rahman and N. Khan, *ACS Omega*, 2019, **4**, 8046–8055; (f) R. Mondal and D. E. Herbert, *Organometallics*, 2020, **39**, 1310−1317; (g) Y. Hu, J. Nan, J. Yin, G. Huang, X. Ren and Y. Ma, *Organic Letters*, 2021, **23**, 8527-8532; (h) D. Yang, H. Wang, C. Liuc and C-R. Chang, *Catal. Sci. Technol.*, 2023, **13**, 3174-3181; (i) K. Rupa, D. Yadagiri and P. Anbarasan, *J. Org. Chem.*, 2023, **88**, 9077-9086; (j) C. Zhang, K. Xu, Y. Liao, L.Zhao, S. Jin, X. Lu, J. Wang, L. Ding and J. Zhang, *J. Org. Chem.*, 2023, **88**, 3436-3450.
3. (a) A. Maji, A. Singh, N. Singh and K. Ghosh, *ChemCatChem*, 2020, **12**, 3108−3125. (b) S. Dey, A. Patel, N. Haloi, S. Srimayee, S. Paul and G. K. Barik, N. Akhtar, D. Shaw, G. Hazarika, B. M. Prusty, M. Kumar, M. K. Santra, E. Tajkhorshid, S. Bhattacharjee and D. Manna, *J. Med. Chem.* 2023, **66**, 11078−11093. (c) S. Ghosh, Md. U. Arshi, S. Ghosh, M. Jash, S. Sen, K. Mamchaoui, S. Bhattacharyya, N. K. Rana and S. Ghosh, *J. Med. Chem.* 2024, doi.org/10.1021/acs.jmedchem.4c00398.
4. (a) U. K. Das, Y. Ben-David, Y. Diskin-Posner and D. Milstein, *Angew. Chem. Int. Ed.*, 2018, **57**, 2179 – 2182; (b) A. Corma, J. Navas and M. J. Sabater, *Chem. Rev.*, 2018, **118**, 1410−1459; (c) T. Irrgang and R. Kempe, *Chem. Rev.*, 2019, **119**, 2524−2549; (d) A. M. Pandey, N. K. Digrawal, N. Mohanta, A. B. Jamdade, M. B. Chaudhari, G. S. Bisht and B. Gnanaprakasam, *J. Org. Chem.*, 2021, **86**, 8805–8828; (e) N. Hofmann and K. C. Hultzsch, *Eur. J. Org. Chem.*, 2021, **2021**, 6206–6223; (f) K. Sun, H. Shan, G-P. Lu, C. Cai and M. Beller, *Angew. Chem. Int. Ed.*, 2021, **60**, 25188– 25202; (g) A. Cicolella, M. C. D′Alterio, J. Duran, S. Simon, G, Talarico and A. Poater, *Adv. Theory Simul.*, 2022, **5**, 2100566; (h) A. Banik, P. Datta and S. K. Mandal, *Org. Lett.*, 2023, **25**, 1305–1309. (i) Md. Bakibillah, S. Reja, K. Sarkar, D. Mukherjee, D. Sarkar, S. Roy, T. M. Almutairi, Md. S. Islam and R. K. Das, *Org. Biomol. Chem.*, 2024, **22**, 4704-4719.
5. (a) C. Schlepphorst, B. Maji and F. Glorius, *ACS Catal.*, 2016, **6**, 4184–4188; (b) A. R. Sahoo, G. Lalitha, V. Murugesh, C. Bruneau, G. V. M. Sharma, S. Suresh and M. Achard, *J. Org. Chem.*, 2017, **82**, 10727–

10731; (c) D. Bhattacharyya, B. K. Sarmah, S. Nandi, H. K. Srivastava and A. Das, *Org. Lett.*, 2021, **23**, 869−875; (d) N. Kumar, R. V. Sankar and C. Gunanathan, *J. Org. Chem.*, 2023, **88**, 17155–17163.

6. (a) P. Satyanarayana, G. M. Reddy, H. Maheswaran and M. L. Kantam, *Adv. Synth. Catal*., 2013, **355**, 1859−1867; (b) L. K. M. Chan, D. L. Poole, D. Shen, M. P. Healy and T. J. Donohoe, *Angew. Chem. Int. Ed*., 2014, **53**, 761-765; (c) R. Wang, L. Huang, Z. Du and H. Feng, *J. Organomet. Chem*., 2017, **846**, 40-43; d) D. Wang, R. T. McBurney, I. Pernik and B. A. Messerle, *Dalton Trans*., 2019, **48**, 13989-13999.
7. (a) S. Genç, S. Günnaz, B. Cetinkaya, S. Gülcemal and D. Gülcemal, *J. Org. Chem*., 2018, **83**, 2875–2881; (b) Y. Wang, Z. Huang, G. Liu and Z. Huang, *Acc. Chem. Res*., 2022, **55**, 2148–2161.
8. (a) B. W. J. Chen, L. L. Chng, J. Yang, Y. Wei, J. Yang and J. Y. Ying, *ChemCatChem*, 2013, **5**, 277–283; (b) R. Mamidala, S. Samser, N. Sharma, U. Lourderaj and K. Venkatasubbaiah, *Organometallics*, 2017, **36**, 3343−3351; (c) S. P. Kavina and R. Ramesh, *Dalton Trans*., 2023, **52**, 10038-10044.
9. J.-J. Zhong, W.-P. To, Y. Liu, W. Lu and C.-M. Che, *Chem. Sci*., 2019, **10**, 4883–4889.
10. (a) M. North, *Royal Society of Chemistry*, 2015; (b) T. J. Brown, M. Cumbes, L. J. Diorazio, G. J. Clarkson and M. Wills, *J. Org. Chem.*, 2017, **82**, 10489−10503; (c) D-W. Tan, H-X. Li, D-L. Zhu, H-Y, Li, D. J. Young, J-L. Yao and J-P. Lang, *Org. Lett*., 2018, **20**, 608–611; (d) M. K. Barman, A. Jana and B. Maji, *Adv. Synth. Catal*., 2018, **360**, 3233 – 3238; (e) J. Das, K. Singh, M. Vellakkaran and D. Banerjee, *Org. Lett*., 2018, **20**, 5587–5591; (f) K. Polidano, J. M. J. Williams and L. C. Morrill, *ACS Catal.*, 2019, **9**, 8575−8580; (g) Y-Y. Liu, Y. Wei, Z-H. Huanga and Y. Liu, *Org. Biomol. Chem.*, 2021, **19**, 659-666; (h) L. Lu, J. Luo and D. Milstein, *ACS Catal.*, 2023, **13**, 5949–5954; (x) A. Maji, S. Gupta, M. Maji and S. Kundu, *J. Org. Chem*., 2022, **87**, 8351–8367; (i) D. Pal, A. Mondal, R. Sarmah and D. Srimani, *Org. Lett.*, 2024, **26**, 514–518.
11. (a) S. Chakraborty, P. Daw, Y. Ben-David and D. Milstein, *ACS Catal.*, 2018, **8**, 10300–10305; (b) J. Tang, J. He, S.-Y. Zhao and W. Li, *Angew. Chem. Int. Ed*., 2023, **135**, e202215882; (c) S. Jalwal, A. Regina, V. Atreya, M. Paranjothy and S. Chakraborty, *Dalton Trans.*, 2024, **53**, 3236-3243.
12. (a) S. Elangovan, J.-B. Sortais, M. Beller and C. Darcel, Angew. Chem. Int. Ed., 2015, **54**, 14483–14486.
13. (a) S. P. Midya, V. G. Landge, M. K. Sahoo, J. Rana and E. Balaraman, *Chem. Commun.*, 2018, **54**, 90-93; (b) B. Pandey, S. Xu and K. Ding, *Org. Lett.*, 2019, **21**, 7420–7423; (c) B. Goswami, M. Khatua, R. Chatterjee, Kamal and S. Samanta, *Organometallics*, 2023, **42**, 1854–1868.
14. (a) R. Babu, M. Subaramanian, S. P. Midya and E. Balaraman, *Org. Lett.*, 2021, **23**, 3320–3325; (b) A. K. Bains, A. Biswas and D. Adhikari, *Adv. Synth. Catal*., 2022, **364**, 47–52; (c) M. Sk, A. Bera and D. Banerjee, *ChemCatChem,* 2023, **15**, e2023004; (d) S. Bansal and B. Punji, *Chem. Eur. J*., 2024, **30**, e2023040.
15. (a) J. Xu, Q. Chen, Z. Luo, X. Tang and J. Zhao, *RSC Adv.*, 2019, **9**, 28764–28767; (b) M. Karuppasamy, B. S. Vachan and V. Sridharan, *Copper in N-Heterocyclic Chemistry*, 2021, 249-288.
16. (a) V. Arora, H. Narjinari and A. Kumar, *Organometallics*, 2021, **40**, 2870–2880; (b) S. Nandi, I. Borthakur, K. Ganguli and S. Kundu, *Organometallics*, 2023, **42**, 1793–1802.
17. (a) R. Pramanick, R. Bhattacharjee, D. Sengupta, A. Datta and S. Goswami, *Inorg. Chem.*, 2018, **57**, 6816–6824; (b) S. Das, R. Mondal, G. Chakraborty, A. K. Guin, A. Das and N. D. Paul, *ACS Catal*., 2021, **11**, 7498−7512; (c) S. Chakraborty, R. Mondal, S. Pal, A. K. Guin, L. Roy and N. D. Paul, *J. Org. Chem.*, 2023, **88**, 771–787; (d) S. Pal, S. Das, S. Chakraborty, S. Khanra and N. D. Paul, *J. Org. Chem.*, 2023, **88**, 3650–

3665 (e) A. Samanta, P. Behera, A. Chaubey, A. Mondal, D. Pal, K. Mohar, L. Roy and D. Srimani, *Chem. Commun*., 2024, **60**, 4056-4059.

18. X. Zhang, G.-P. Lu, K. Wang, Y. Lin, P. Wang and W. Yi, *Nano Res.*, 2022, **15**, 1874–1881.
19. S. Roy, S. Pramanik, T. Ghorui and K. Pramanik, *RSC Adv.*, 2015, **5**, 22544–22559.
20. (a) X.-F. Wua and H. Neumann, *Adv. Synth. Catal.*, 2012, **354**, 3141–3160; (b) S. Enthaler, *ACS Catal.*, 2013, **3**, 150−158; (c) L. A. López and J. González, *Zinc Catalysis: Applications in Organic Synthesis*, 2015, 149-178.
21. (a) S. Roy, S. Pramanik, S. C. Patra, B. Adhikari, A. Mondal, S. Ganguly and K. Pramanik, *Inorg. Chem.*, 2017, **56**, 12764–12774. (b) The occurrence of dianionic L^{2-} has been confirmed from the successful isolation of $\{Co^{III}–L^{-II}\}$ coordination and remains an unpublished result.
22. I. Chatterjee, M. Chakraborty, P. Ghosh and S. Goswami, *J. Indian Chem. Soc.*, 2018, **95**, 771-780.
23. In all cases, unreacted alcohols or ketones had been identified during the TLC screening of the reaction mixture. Additionally, all yields listed here were isolated yields. Thus, it was likewise impossible to completely rule out the chance of product loss during workup and column chromatographic separation of desired products from the reaction mixture.
24. D. Wei, V. Dorcet, C. Darcel and J. B. Sortais, *ChemSusChem*, 2019, **12**, 3078−3082.
25. The higher catalytic efficiency of penta-coordinated complex **1**, $[Zn(N_{py}\text{^}N_{azo}\text{^}N_{azo})Cl_2]$, compared to $[Zn(N_{py}\text{^}N_{inime}\text{^}N_{py})Cl_2]$ **1c** of similar type with pyridylimine ligand ($N_{py}\text{^}N_{inime}\text{^}N_{py}$ = py−CH=N−NH−py) can be demonstrated by comparing analogous catalytic reactions (Fig. 5). The formula of the latter compound was confirmed from MS (ESI+) ($C_{11}H_9N_3ZnCl_2$ $[M–Cl]^+$; calculated: 296.99, found: 296.94).
26. (a) Y. Ma, Z. Du, J. Liu, F. Xia and J. Xu, *Green Chem.*, 2015, **17**, 4968−4973; (b) R. Ray, S. Chandra, D. Maiti and G. K. Lahiri, *Chem. Eur. J.*, 2016, **22**, 8814−8822; (c) W. Ai, R. Zhong, X. Liu and Q. Liu, *Chem. Rev.*, 2019, **119**, 2876−2953.
27. D. Sengupta, R. Bhattacharjee, R. Pramanick, S. P. Rath, N. Saha Chowdhury, A. Datta and S. Goswami, *Inorg. Chem.*, 2016, **55**, 9602−9610.
28. (a) E. Monzani, G. Battaini, A. Perotti, L. Casella, M. Gullotti, L, Santagostini, G. Nardin, L. Randaccio, S. Geremia, P. Zanello and G. Opromolla, *Inorg. Chem.* 1999, **38**, 5359−5369; (b) J. Ackermann, F Meyer, E. Kaifer and H. Pritzkow, *Chem. Eur. J*., 2002, **8**, 247−258.

Chapter III

One-pot cascade [3 + 2 + 1] annulation: synthesis and mechanistic insight of s-triazines and pyrimidines using azo-supported metalloradical nickel catalyst

III.1 Introduction

Metal-organic catalysts have played an important role in achieving numerous synthetically valuable organic and biomolecules that are otherwise challenging to achieve in realism. Remarkably, palladium continues to rule the field in fine organic synthesis when compared to other metals because it validates reliability and uniformity in metal-mediated catalysis and exhibits a wide substrate tolerance.[1] However, the substantial expense associated with palladium has limited its commercial adequacy, thereby motivating the exploration of catalysts based on earth-abundant, low-cost metals. Being the sibling, cost-effective nickel is the most viable option. Furthermore, they show striking resemblance in a number of organic catalytic transformation.[2] Nevertheless, they differ in many instances as well due to their innate physicochemical aspects. The recent development of homogeneous catalysis using 3d metals in organic synthesis is highly promising as it has only lately begun to challenge the abiding supremacy of late and mostly noble metals in this field and they hold the potency of being able to encompass large-scale synthesis with substantial turnover number (TON).[3]

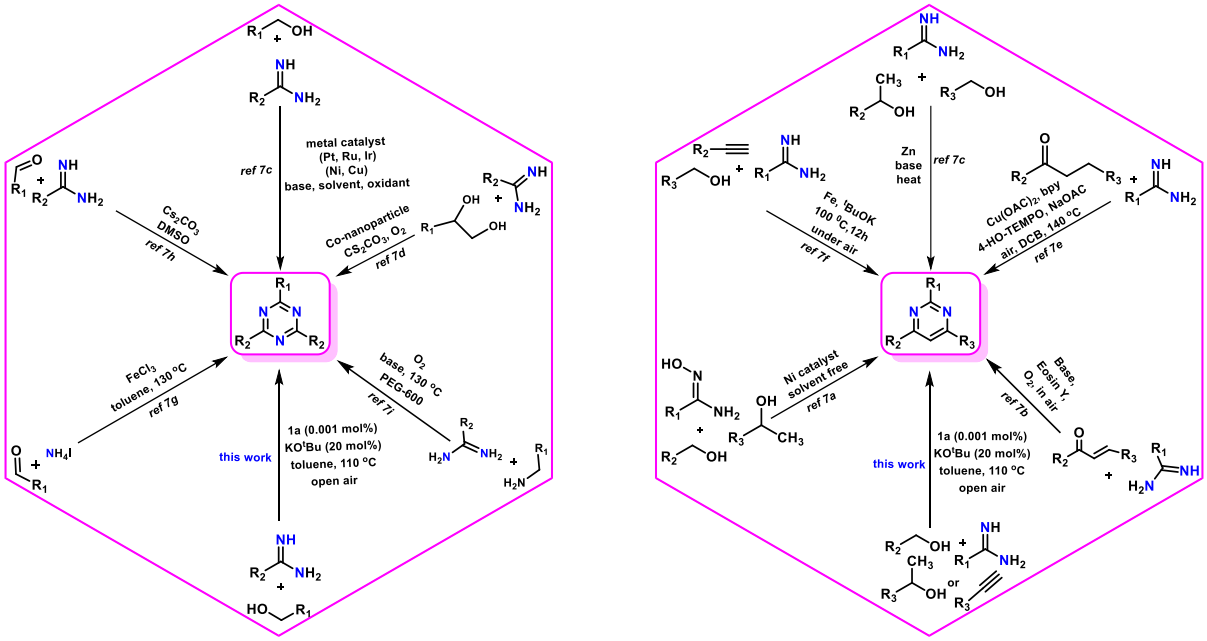

Scheme 1. Synthesis of *s*-triazines and pyrimidines by various synthetic protocols.

The synthesis of bio-active poly-azaheterocycles such as pyrroles, pyridines, imidazoles, pyrimidines and triazines procured from common alcohols is a rapidly expanding area of interest for green sustainable chemistry.[4] Among these N-heterocycles, the pyrimidine and *s*-triazine are found in a wide range of bio-relevant molecules and are crucial structural motifs found in many pharmacological, enzyme inhibitor, antifungal, anticancer, antitubercular

activity, argochemicals.[5-6] In fact, a variety of synthetic procedures have been cited in the literature depending on the substrates, reagents and reaction conditions; where metal-mediated homogeneous catalysis emerging as a versatile and valuable synthetic protocol due to their gradual improvising catalytic efficiency, sustainability and atom-economy (Schemes 1).[7] Nevertheless, such methods in general suffer from the complications of physical separation of product(s), formation of hazardous by-products, use of stoichiometric or high amounts of base and low TON i.e., high catalyst loading. The primary drawback of homogeneous catalysts is that they cannot be efficiently reinstated after the reaction cycle, which makes cost reduction challenging in industrial applications.[8] It is worth noting that nickel catalysts generated *in-situ* from commercially available simple salts typically require (over)stoichiometric amounts catalyst loading and hence suffer from sustainability issues with low TON.[9] Therefore, it is highly desirable to design a more practical and eco-friendly catalytic systems for the synthesis of substituted pyrimidines and triazines from readily available starting materials.

This has prompted us to explore the catalytic efficiency with the first member of nickel-triad owing to its easy availability and affordability. We focused here on the development of a robust pincer-type Ni(II) catalyst with a distinctly redox-active organic template. The advantage of employing highly π-acidic redox non-innocent ligands relies on their active participation to facilitate the facile electron transfer process, which is one of the most crucial aspects of bond-breaking and bond-making processes. Such electron deficient ligand with low-energy acceptor orbitals demonstrates dual functionality viz. they readily convert to anion-radical species, thereby acting as good electron-sources and have potency to furnish robust metal-ligand bonding through double bond character. To retain their efficiency, organometallic catalysts need to be fabricated with a typical multidentate ligand with strong π-acceptor donors so that they can sustain the harsh condition during catalytic cycles.

One-pot synthesis of N-heterocycles has become more popular due to its time-efficient, high-yield products, minimal and eco-friendly waste. In this context, it is still demanding to have a simple and efficient process to synthesize bio-relevant heterocycles such as pyrimidines and triazines from basic and easily accessible starting materials. Ni-catalyzed annulation reactions for synthesizing pyrimidines and triazines, as reported by the Adhikari[7h] and Paul[7j] groups, typically require catalyst loadings of 3-5 mol%. Notably, the use of lower alcohols as C1 or C2 synthons in these transformations remains unexplored. It is worth noting that the earth-abundant 3d metal-catalysed multicomponent reactions (MCRs) under mild conditions are highly desirable for synthesizing such heterocycles with improved control over catalyst and

base loading. We started our exploration with various annulation reactions, where nickel-catalysed scaled cascade [3 + 2 + 1] annulation reactions are successfully accomplished to afford high-yield aromatic azaheterocycles with appreciably low (0.001 mol%) catalyst loading, viz. (i) amalgamation of amidines and primary alcohols with/without phenyl acetylenes/secondary alcohols affording pyrimidines (*43 examples*) and *s*-triazines (*37 examples*) in excellent yields, respectively. The synthesis of novel bioactive poly-aza heterocycles through C–C/C–N bond formation, using the partial oxidation of methanol or ethanol (C1 or C2 sources), presents an intriguing yet challenging process. Therefore, exploration of methanol/ethanol as a safe, readily available, and cost effective C1/C2 synthon has attracted significant global attention.[10] Notably, formaldehyde is the simplest aldehyde and has widespread applications across various fields. Traditionally, silver and iron-molybdenum oxides are used as catalysts to convert methanol to formaldehyde at higher temperatures (600 °C and 250-400 °C, respectively).[11] However, this work highlights the superior efficiency of an Ni-based auto-tandem catalyst, which readily converts methanol/ethanol to formaldehyde/acetaldehyde even under mild conditions.

III.2 Result and Discussion

III.2.1 Synthesis of ligands and complexes

The organic template L, consisting of two electron-deficient azo chromophores and an electron-poor aromatic heterocyclic ring, was synthesized by the previously reported Baeyer-Mills condensation of (E)-2-(phenylazo)aniline with 2-nitrosopyridine.[12] Two hexa-coordinated Ni(II) complexes, $[Ni(L)Cl_2(H_2O)]$ **1a** and $[Ni_2(L)_2(\mu\text{-}Cl)_2Cl_2]$ **1b**, were synthesized in good yields (80 and 84% respectively) by reacting strongly electron deficient *NNN*-pincer ligand,

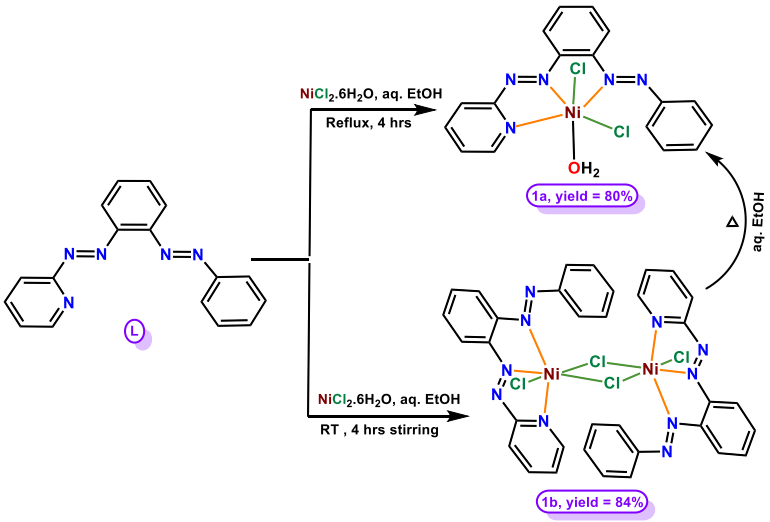

Scheme 2. Synthetic strategy of $[Ni(L)Cl_2(H_2O)]$ **1a** and $[Ni_2(L)_2(\mu\text{-}Cl)_2Cl_2]$ **1b**.

2-(2-pyridylazo)azobenzene, L with $NiCl_2.6H_2O$ in stoichiometric ratio in ethanol under varying reaction conditions (Scheme 2).The reddish-brown mononuclear complex **1a** is formed under reflux conditions, whereas the deep brown dinuclear complex **1b** is produced by stirring at room temperature. Notably, the transfusion from the dinuclear to the mononuclear form can be thermally induced at elevated temperatures. Both complexes exhibit excellent stability in the presence of air and moisture and demonstrate high solubility in polar solvents such as dichloromethane, acetonitrile, and ethanol, while displaying limited solubility in non-polar solvents like toluene. UV-vis and IR spectral data, along with elemental analysis, corroborate the coordination of ligand L with the nickel metal in both complexes via the azo chromophores.

III.2.2. IR spectra

Sharp vibrations around 1455, 1397 cm^{-1} and 1457, 1392 cm^{-1} in the infrared spectra of complex **1a** and **1b** were assigned to the $\nu_{N=N}$ stretching respectively (Figure 1).

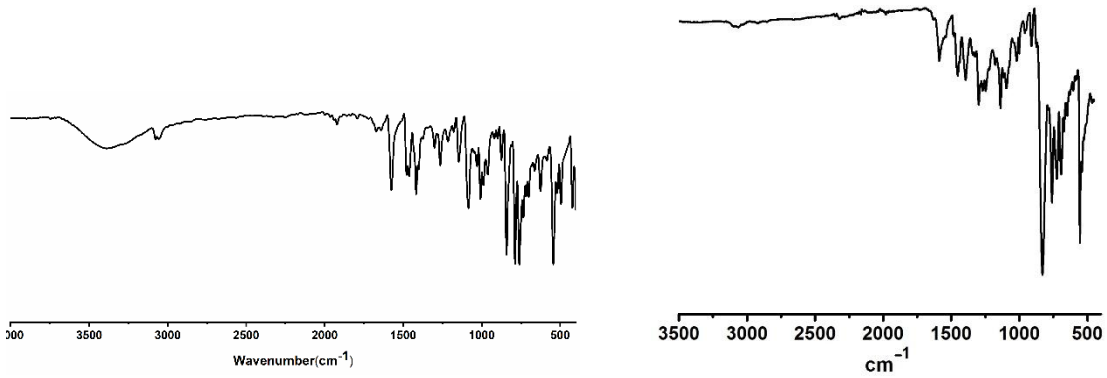

Figure 1. IR spectra of **1a** (left) and **1b**(right).

III.2.3. Crystal Structures

Hexa-coordination around the nickel atom was authenticated by X-ray crystallographic analysis (*vide infra*), and advanced spectroscopic techniques were utilized to characterize the isolated compounds. Both complexes crystallise in the monoclinic crystal system with space group $P2_1/c$. The structural analysis reveals that complex **1a** has a mononuclear structure, while complex **1b** is dinuclear. Each nickel centre is coordinated through N_{py}, N_{pyazo} and N_{phazo} in meridional fashion with comparable Ni–N_{py} and Ni–N_{pyazo} distances ranging 1.987(3)-2.098(3) Å, while Ni–N_{phazo} length is somewhat elongated and lies near 2.20-2.40 Å. The N–N azo distances in complexes lie near 1.26 Å signifies Ni(d) → azo(π*) back-bonding as the corresponding distance in analogous free ligand is 1.24 Å.[13] Theoretical analysis indicates that

this conclusion could be further supported by the nearly identical average azo lengths of 1.26 Å and 1.25 Å calculated in the coordinated and free ligand, respectively (Table 2).

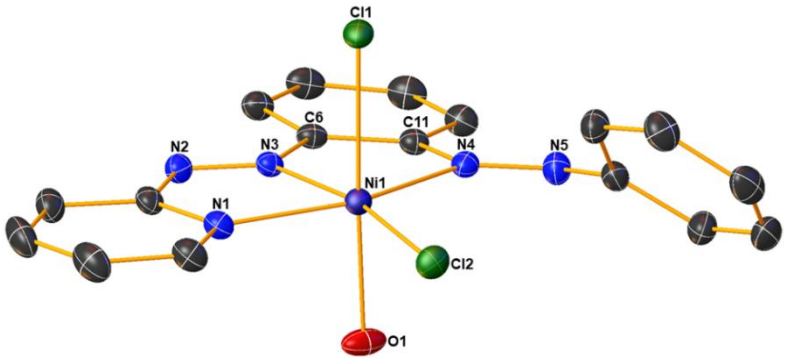

Figure 2. ORTEP depiction of complex **1a** (Solvent molecules and hydrogen atoms have been omitted for clarity, with thermal ellipsoids displayed at a 50% probability level). Selected bond lengths (Å) and bond angles (deg): Ni1–Cl1 2.392(1), Ni1–Cl2 2.023(3), Ni1–O1 2.082(3), Ni1–N1 2.081(3), Ni1–N3 1.987(3), Ni1–N4 2.192(3), N2–N3 1.260(5), N4–N5 1.261(5), Cl2–Ni1–Cl1 99.75(10), Cl2–Ni1–O1 84.76(13), Cl2–Ni1–N1 95.80(14), Cl2–Ni1–N4 108.09(13), O1–Ni1–Cl1 173.21(11), O1–Ni1–N4 84.58(14), N1–Ni1–Cl1 91.92(9), N1–Ni1–O1 92.67(15), N1–Ni1–N4 155.55(12), N3–Ni1–Cl1 88.66(9), N3–Ni1–Cl2 168.91(13), N3–Ni1–O1 87.54(12), N3–Ni1–N1 76.57(13), N3–Ni1–N4 79.03(12), N4–Ni1–Cl 1 89.17(8).

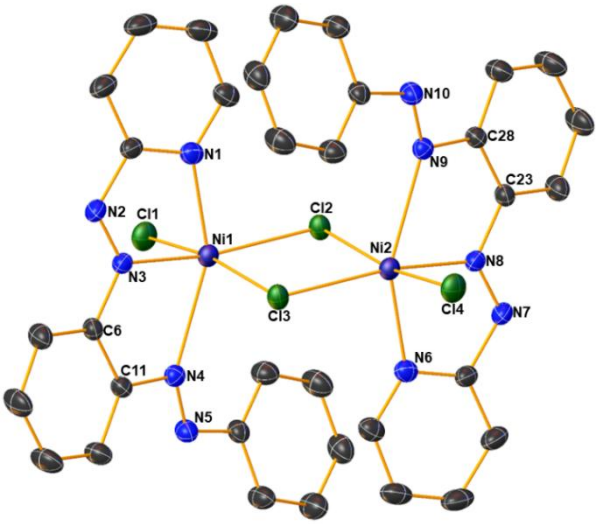

Figure 3. ORTEP representation of complex **1b** (Solvent molecules and hydrogen atoms have been omitted for clarity, and thermal ellipsoids are depicted at a 50% probability level to enhance visualization.). Selected bond lengths (Å) and bond angles (deg): Ni1–Cl1 2.325(1), Ni1–Cl2 2.397(1), Ni1–Cl3 2.429(1) Ni1–N1 2.098(4), Ni1–N3 2.014(3), Ni1–N4 2.387(3), N2–N3 1.252(5), N4–N5 1.254(5), N1–Ni1–N4 151.15(13), N1–Ni1–N3 75.83(14), N3–Ni1–Cl3 89.29(9), N3–Ni1–N4 75.34(12), N4–Ni1–Cl2 115.05(8), Cl1–Ni1–N3 93.92(10), N1–Ni1–Cl2 93.69(11), Cl2–Ni1–Cl3 84.87(4), Cl2–Ni1–N4 82.94(8), Cl1–Ni1–Cl2 93.92(4), Cl1–Ni1–Cl3 169.15(5), Cl1–Ni1–N4 87.85(9), N1–Ni1–Cl1 92.83(10), N1–Ni1–Cl3 98.02(10), N3–Ni1–Cl2 167.20(10), Ni1–Cl2–Ni2 95.13(4).

It is worth noting that the aforesaid azo bond lengths clearly indicate that the ligands are coordinated in their pristine neutral form.

Table 1. Crystallographic Details of complexes **1a** and **1b**.

	1a	**1b**
Empirical formula	$C_{17}H_{15}N_5Cl_2ONi$	$C_{34}H_{26}N_{10}Cl_4Ni_2$
T/K	298K	298K
fw	434.95	833.83
Crystal system	Monoclinic	Monoclinic
Space Group	$P2_1/c$	$P2_1/c$
a/Å	11.5517(9)	10.4657(5)
b/*Å*	13.0793(11)	11.2362(6)
c/ *Å*	13.0431(10)	15.4896(8)
α/deg	90	90
β/deg	90.415(3)	109.160(2)
γ/deg	90	90
V/ *Å*^{3}	1970.6(3)	1720.59(15)
Z	4	4
D_c/mgm^{-3}	1.466	1.610
μ/mm^{-1}	1.271	1.448
F(000)	888	848
cryst size/mm^3	0.45 × 0.36 × 0.21	0.41× 0.32 × 0.23
θ/deg	3.485 – 25.732	2.74 – 26.87
Measured reflns	9941	9812
Unique reflns	3938	3945
[a]GOF on F^2	1.070	1.041
R1[b], wR2[c][*I>2σ(I)*]	0.0566, 0.1656	0.0586, 0.1561
R1, wR2	0.0622, 0.1721	0.0636, 0.1608

[a]GOF = $\{\Sigma[w(F_o{}^2-F_c{}^2)2]/(n-p)\}^{1/2}$. [b]R1 = $\Sigma\,[|F_o|-|F_c|]/\,\Sigma\,|F_o|$.

[c]wR2 = $[\Sigma\,[w(F_o{}^2-F_c{}^2)^2]/\,\Sigma\,[w(F_o{}^2)^2]]^{1/2}$ where $w = 1/[\,\sigma^2(F_o{}^2)+(aP)^2+bP]$, $P = (F_o{}^2+2F_c{}^2)/3$.

Table 2. Selected Experimental and Theoretical Bond Parameters of **1a** and **1b** complex.

1a			**1b**		
Parameter	**Expt.**	**Theo.**	**Parameter**	**Expt.**	**Theo.**
Ni1–Cl1	2.392(1)	2.421	Ni1–Cl1	2.325 (1)	2.396
Ni1–Cl2	2.023(3)	2.420	Ni1–Cl2	2.397 (1)	2.430
Ni1–O1	2.082(3)	2.184	Ni1–Cl3	2.429(1)	2.534
Ni1–N1	2.081(3)	2.129	Ni1–N1	2.098(4)	2.128
Ni1–N3	1.987(3)	2.056	Ni1–N3	2.014(3)	2.040
Ni1–N4	2.192(3)	2.316	Ni1–N4	2.387(3)	2.307
N2–N3	1.260(5)	1.255	N2–N3	1.252(5)	1.254
N4–N5	1.261(5)	1.258	N4–N5	1.254(5)	1.256
Cl1Ni1Cl2	99.75(10)	99.73	Cl1Ni1Cl2	93.92(10)	100.14
Cl2Ni1O1	84.76(13)	81.60	Cl2Ni1Cl3	84.87(4)	83.84
Cl1Ni1N4	89.17(8)	91.03	Cl1Ni1N4	87.85(9)	89.55
Cl2Ni1N4	108.09(13)	112.31	Cl2Ni1N4	82.94(8)	87.15
N1Ni1Cl1	91.92(9)	92.54	N1Ni1Cl1	92.83(10)	95.54
N1Ni1Cl2	95.80(14)	94.80	N1Ni1Cl2	93.69(11)	96.24
N1Ni1N4	155.55(12)	151.60	N1Ni1N4	151.15(13)	152.00
N3Ni1Cl1	88.66(9)	91.23	N3Ni1Cl1	93.92(10)	90.53
N3Ni1Cl2	168.91(13)	165.77	N3Ni1Cl2	167.20(10)	166.08
N3Ni1N1	76.57(13)	75.53	N3Ni1N1	75.83(14)	75.47
N3Ni1N4	79.03(12)	76.23	N3Ni1N4	75.34(12)	76.95
C1N1Ni1	130.8(3)	130.00	C1N1Ni1	130.8(3)	128.97
C5N1Ni1	111.1(3)	111.20	C5N1Ni1	111.5(3)	110.83
N3N2C5	113.3(1)	113.43	N3N2C5	112.4(3)	112.70
C6N3Ni1	122.5(1)	120.15	C6N3Ni1	121.7(2)	119.27
N2N3C6	111.7(3)	119.23	N2N3C6	116.4(3)	119.38
N2N3Ni1	121.8(3)	120.60	N2N3Ni1	121.7(3)	121.29
C11N4Ni1	109.2(2)	109.08	C11N4Ni1	106.8(2)	107.85
N5N4C11	112.1(3)	113.26	N5N4C11	110.9(3)	112.44
N5N4Ni1	138.0(3)	135.82	N5N4Ni1	142.2(3)	139.40
N4N5C12	116.34(19)	119.54	N4N5C12	119.7(4)	121.04

However, coordination in other oxidation states (L^{-I} and L^{-II}) has been identified.[12, 14] In **1a**, two chlorides disposed *cis* to one another along with a highly labile water molecule in the apical position. In contrast, two bridging chlorides furnishes the dinuclear integrity in **1b**, while the remaining two chloride atoms are terminally coordinated. In both complexes, they satisfy the primary valency of Ni(II), while tridentate coordination was found through $N_{pyridyl}$, $N_{azopyridyl}$, and and $N_{azophenyl}$ atoms to form two juxtaposed five-membered rings during the course of chelation. This usual class of ligand with significant π-acidity corroborates strong coordination through back-bonding with the metal centre, and a robust class of coordinatively unsaturated nickel complex is produced by the extremely labile water molecule.

III.2.4. Absorption Spectra

The electronic spectra of compounds **1a** and **1b** were recorded in dichloromethane at room temperature and are presented in Figure 4, along with the reduced species of **1a**. The bathochromically shifted structured profiles observed for the complexes may be attributed to

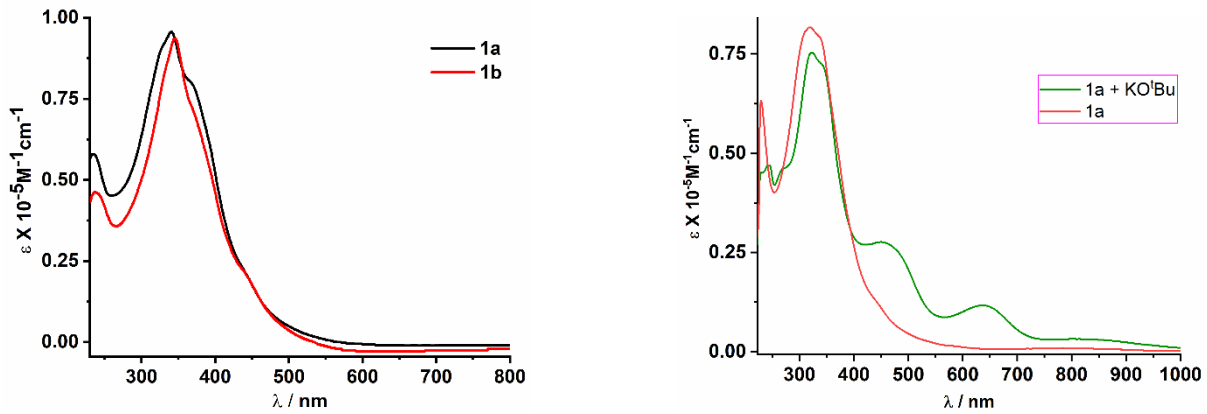

Figure 4. Experimental absorption spectra of **1a** and **1b** in dichloromethane (left) and absorption spectra of the catalyst **1a**, in the presence of KO^{t}Bu (right).

the increased electronic asymmetry introduced by the electron-accepting bis-azo ligand. Multiple transitions, characteristic of these complexes, are primarily associated with charge-transfer transitions within the tri-coordinated bis-azo ligand. To investigate the origin of the orange-red coloration, we conducted theoretical studies, which indicate that the lower energy bands are predominantly characterized by intraligand charge-transfer (ILCT) transitions of π to π* type. These transitions result in absorption within the blue-green region of the visible spectrum.[13]

III.2.5. Electronic Structure and FMOs

The singlet ground state (S_0) and excited state molecular geometries of synthesised complex **1a** and **1b** were computed by DFT method by employing (R)B3LYP[1,2] in GAUSSIAN 09[3] programme package. The solution phase optimised geometries of the complexes were found without applying any geometry constraints. In order to verify all stationary points as the true minima in potential energy surface, frequency calculation was executed. The absence of any imaginary frequency (NImag = 0) indicates that all the obtained stationary points are indeed the true minima in potential energy surface. The X-Ray positional coordinates of complex **1a** and **1b** were directly used as the initial input for geometry optimisation calculation. By using these ground state optimised geometries as well as excited state geometries, we performed subsequent Single Point Energy and TD-DFT[4-7]calculation. In TD-DFT calculation we employ conductor like continuum model (CPCM) [8-10] and dichloromethane (CH_2Cl_2) as solvent to simulate absorption spectra in dichloromethane solvent. The lowest 100 singlet-singlet transitions in absorption and emission processes for the complex **1a** and **1b** were evaluated gradually. The experimental results and the results obtained from TD calculations were qualitatively comparable. Presently the approach of TD-DFT is documented as a rigorous formalism for the electronic excitation energies among the DFT framework for calculating spectral properties of many transitions metal complexes[11-14]. In order to acquire the information and nature of absorption and emission processes natural transition orbital (NTO) analysis was executed. This method delivers the most accurate representation of the transition density between the ground and excited states in terms of an expansion into single-particle transitions (hole and electron states for each given excitation). we refer to the unoccupied and occupied NTOs as “electron” and “hole” transition orbitals. The computed vertical transitions were calculated at the equilibrium geometry of the S_0 state and described in terms of one-electron excitations of molecular orbitals of the corresponding S_0 geometry. The calculated transitions with moderate intensities ($f \geq 0.02$) can be envisaged going from the lower to the higher energy region of the spectrum. The zinc atom was described by a double-ζ basis set with the effective core potential of Hay and Wadt (LANL2DZ)[15,16], and the 6-311++G(d,p)[17,18] basis set was used for the other elements except hydrogen atom (6-31G) present in the complexes to optimize the ground state geometries. The calculated electronic density plots for frontier molecular orbitals were prepared by using the GaussView 6.0 software. GaussSum program, version 3.2[19], was used to calculate the molecular orbital contributions from groups or atoms.

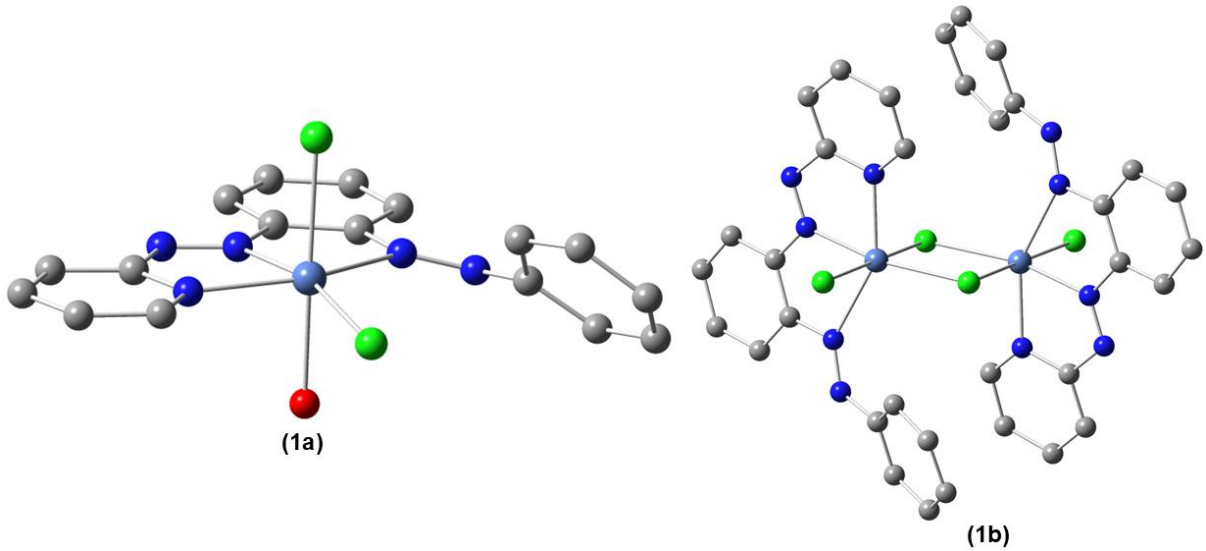

Figure 5. Solvent phase optimised geometry of **1a** (left) and **1b** (right) complex (H's are omitted for clarity) calculated at B3LYP/6-311+G(d,p) level of theory.

Table 3. Coordinates of Optimised structure of complex **1a**.

Tag	Symbol	X	Y	Z
1	Ni	8.011004	9.822242	3.765901
2	Cl	6.933146	10.16802	1.625147
3	Cl	10.30331	9.561243	3.03245
4	O	8.929697	9.458083	5.713733
5	H	8.680037	8.690555	6.243447
6	H	9.852089	9.333489	5.437854
7	N	8.176399	11.91378	4.127466
8	N	6.050182	11.49599	5.10279
9	N	6.280945	10.3091	4.765671
10	N	6.934141	7.788113	4.026944
11	N	7.267419	6.576433	3.967222
12	C	9.141573	12.76611	3.792423
13	H	10.00481	12.33319	3.300874
14	C	9.051667	14.13558	4.059001
15	H	9.862185	14.79185	3.767279
16	C	7.917913	14.62626	4.696293
17	H	7.81979	15.68272	4.916629
18	C	6.905096	13.7371	5.049528
19	H	5.999943	14.0609	5.547281
20	C	7.077075	12.39017	4.743111
21	C	5.341436	9.319108	5.066307
22	C	4.118424	9.583376	5.699192
23	H	3.875269	10.60307	5.967745
24	C	3.246665	8.542432	5.967625
25	H	2.298703	8.742703	6.453546

26	C	3.585919	7.232189	5.601167
27	H	2.895613	6.420408	5.801436
28	C	4.792088	6.961927	4.970959
29	H	5.044657	5.95465	4.669253
30	C	5.694129	7.99958	4.704014
31	C	8.33231	6.193746	3.145544
32	C	8.972864	4.99226	3.500058
33	H	8.667361	4.481498	4.406421
34	C	9.986759	4.488273	2.698047
35	H	10.49855	3.575023	2.980621
36	C	10.3237	5.144952	1.509935
37	H	11.09627	4.735773	0.867582
38	C	9.655964	6.312801	1.136307
39	H	9.907736	6.806438	0.20416
40	C	8.669788	6.853314	1.952498
41	H	8.134692	7.746959	1.657353

Table 4. Coordinates of Optimised structure of complex **1b**.

Tag	Symbol	X	Y	Z
1	Ni	4.413579	6.280003	7.42835
2	Cl	2.956366	4.555175	8.578448
3	Cl	5.88927	7.922665	6.497565
4	N	4.349552	7.479906	9.398755
5	N	5.951921	5.480315	8.504988
6	N	3.706158	8.424638	9.919652
7	N	5.342684	4.906995	6.093232
8	N	6.735899	4.642612	7.9978
9	C	6.102132	5.834222	9.849118
10	C	5.249212	6.853012	10.32524
11	C	2.886255	9.252968	9.145134
12	C	6.453631	4.3854	6.640697
13	C	7.028816	5.217804	10.70125
14	H	7.66444	4.439295	10.29948
15	C	5.350583	7.235761	11.66886
16	H	4.709801	8.026525	12.03332
17	C	5.113837	4.715643	4.798051
18	H	4.212566	5.175314	4.40893
19	C	1.933829	9.980318	9.884245
20	H	1.874378	9.81971	10.95505
21	C	7.366838	3.623452	5.91636
22	H	8.241756	3.225962	6.415485
23	C	5.986305	3.984033	3.990379
24	H	5.76733	3.861651	2.936233
25	C	3.032107	9.482481	7.767844
26	H	3.819819	8.994169	7.210378
27	C	7.106847	5.604574	12.02672
28	H	7.818699	5.126636	12.69089

29	C	7.126136	3.426901	4.560245
30	H	7.822354	2.853517	3.95792
31	C	1.095168	10.88098	9.245978
32	H	0.35286	11.43075	9.815134
33	C	6.263113	6.614892	12.50783
34	H	6.324806	6.919622	13.54738
35	C	1.230971	11.09682	7.871327
36	H	0.590631	11.81686	7.371377
37	C	2.204305	10.40967	7.146019
38	H	2.325605	10.5946	6.08435
39	Ni	1.006662	4.980095	7.246348
40	Cl	2.433185	6.666999	6.074
41	Cl	-0.43661	3.331315	8.18493
42	N	1.01856	3.73993	5.210052
43	N	-0.54845	5.74723	6.192994
44	N	1.650325	2.808369	4.653063
45	N	0.061966	6.351017	8.610405
46	N	-1.33953	6.572505	6.710606
47	C	-0.71945	5.415305	4.841275
48	C	0.109121	4.398018	4.321445
49	C	2.480063	1.967423	5.406644
50	C	-1.06616	6.833681	8.067141
51	C	-1.65585	6.061813	4.021534
52	H	-2.27269	6.839054	4.453238
53	C	-0.0276	4.048098	2.971149
54	H	0.596003	3.258003	2.576318
55	C	0.28127	6.538725	9.907294
56	H	1.19663	6.106081	10.29539
57	C	3.406338	1.229801	4.646322
58	H	3.440623	1.388007	3.573922
59	C	-2.00728	7.559537	8.794328
60	H	-2.89611	7.928246	8.297569
61	C	-0.61689	7.233487	10.71971
62	H	-0.40432	7.355653	11.77535
63	C	2.368454	1.745137	6.788117
64	H	1.604046	2.248232	7.364208
65	C	-1.76803	5.707906	2.689568
66	H	-2.48764	6.211487	2.053235
67	C	-1.77464	7.755502	10.15179
68	H	-2.49101	8.30007	10.75726
69	C	4.250852	0.320765	5.265943
70	H	4.972011	-0.23914	4.679605
71	C	-0.9491	4.698443	2.166013
72	H	-1.03712	4.418993	1.121226
73	C	4.14926	0.111463	6.644209
74	H	4.794711	-0.61367	7.130093
75	C	3.20363	0.813269	7.392549
76	H	3.109731	0.635136	8.4582

Table 5. Frontier β-Molecular Orbital Composition (%) in the Ground State for **1a** complex.

Orbital	MO	Energy (eV)	Composition						
			Ni	Cl	H_2O	pyazo	phazo	py	ph
111	L+5	-1.09	1	0	0	3	2	50	45
110	L+4	-1.68	51	3	0	3	2	35	5
109	L+3	-1.69	32	6	0	3	0	55	3
108	L+2	-1.89	76	10	2	0	2	9	1
107	L+1	-3.03	2	1	0	8	41	5	43
106	LUMO	-3.78	2	1	0	39	9	23	27
105	HOMO	-5.92	3	95	0	3	1	0	-1
104	H–1	-6.02	4	91	0	0	3	0	2
103	H–2	-6.28	5	79	0	0	4	0	12
102	H–3	-6.45	9	89	2	0	0	0	0
101	H–4	-6.78	7	14	0	2	18	2	57
100	H–5	-7.07	25	70	0	2	-2	0	7

III.2.6. Electrochemistry and EPR

The electron-transfer property of the complex **1a** was examined using cyclic voltammetry in an acetonitrile solution (0.2 M Bu_4NPF_6) with a platinum working electrode. Complex **1a** exhibited well-defined reductive responses at −0.34 V (ΔEp = 120 mV) and −1.40 V (ΔEp = 130 mV) vs. ferrocenium/ferrocene (Fc^+/Fc) reference couple (Figure 6), indicating its strong electron-accepting capability. The redox potentials are referenced to the (Fc^+/Fc). The value of the Fc^+/Fc couple under similar experimental conditions is found to be 0.46 V vs Ag/AgCl. To investigate the origin of the electron transfer process, we conducted

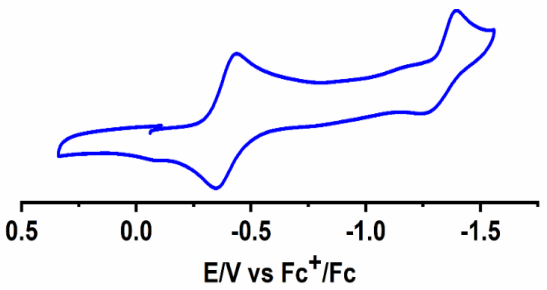

Figure 6. Cyclic voltammogram of **1a** in CH_3CN/0.2 M Bu_4NPF_6 using a Pt working electrode at 100 mV s^{-1}.

DFT calculations at the (U)B3LYP/6-311+G(d,p) level of theory. The computational analysis demonstrates that the LUMO is largely localized on the tridentate ligand backbone, with a significant contribution of 62% attributed to the pyridyl-azo moiety, Figure 7 and Table 5. The LUMO +1 is composed primarily (~80%) of the phenylazo moiety, indicating that the second reduction event occurs at the azo group linked to the phenyl ring. In contrast, the metal orbitals

contribute minimally (2%) to the LUMO, corroborating the fact that the redox event is primarily ligand-centered. The position of the redox couple of such chelated radical anion

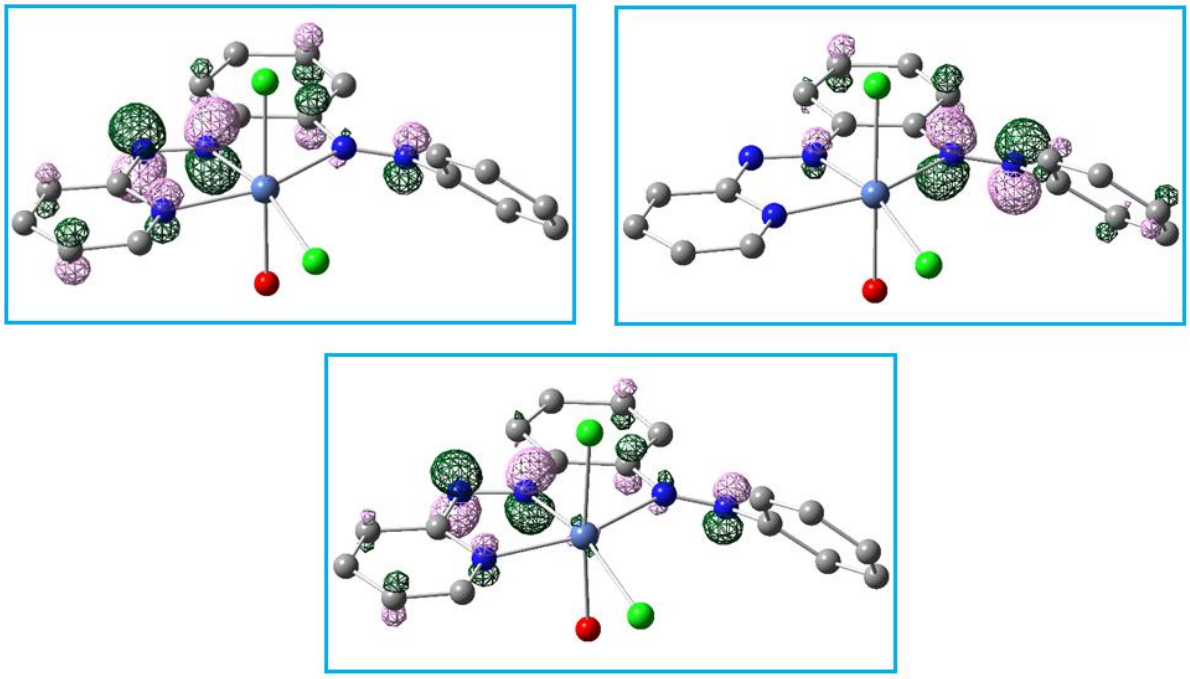

Figure 7. LUMO (left) and LUMO+1 of **1a** (right), and SOMO of one-electron reduced form, **1a**$^{\bullet-}$ (bottom).

ligand directly reflects their ability to stabilize the trapped electron.[11] In particular, the redox potential value in [$Ni^{II}(L^{\bullet-})Cl_2(H_2O)$] suggests its suitability as an electron reservoir, capable of releasing the electron during catalytic processes when necessary. To further substantiate the existence of the ligand-bound odd electron, EPR studies were conducted in a fluid solution. The mixture of the substrate, catalyst 1a, and base produced a sharp, single-line isotropic EPR spectrum at g = 1.998 with a narrow signal width ($\Delta H \approx$ 1.5 mT) at room temperature, indicating the in-situ generation of an organic radical. Notably, the formation of a nickel-bound azo-anion radical is evident, as this signal was not observed in the absence of the nickel catalyst **1a**. Additionally, the catalyst alone also generates an analogous EPR signal in the presence of the base. These observations conclusively demonstrate that the organic radical species is associated with the Ni catalyst, consistent with the reported radical pathway during

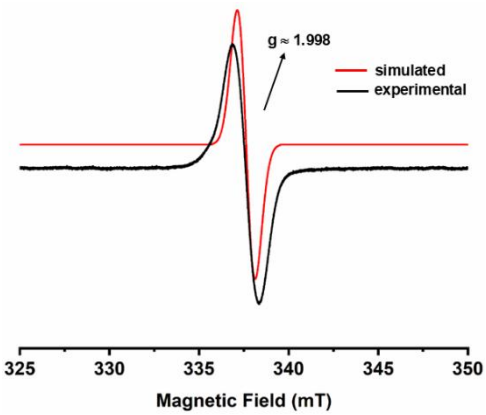

Figure 8. X-band EPR spectrum of **1a**$^{\bullet-}$ in toluene (experimental: black, simulated: red). Conditions: frequency 9.436 GHz, power 1 mW, modulation 1.0 mT, T = 298 K.

cascade annulation reactions (Scheme 7).[12,15] The strongly π-accepting pyridylazo-based Ni(II) catalyst demonstrates a superior tendency for electron acceptance, as evidenced by cyclic voltammetry studies (*vide supra*). During this process, we also noted that the azo radical was generated by a relatively mild reductant, such as KO^{t}Bu, which was made feasible by the low-lying π* orbital (calculated as –3.78 eV) of the nickel-coordinated azo moiety, Table 5.

III.2.7. Catalytic Activity

III.2.7.1. Synthesis of *s*-triazines

In this study, we explore a two-component coupling reaction of primary alcohols with amidines, alongside a three-component coupling involving primary alcohols and secondary alcohols or alkynes in conjunction with amidines. This process is followed by dehydrogenation and subsequent C–N annulation, leading to the formation of *s*-triazine and pyrimidine derivatives. The reactions are catalyzed by an air- and moisture-stable hexa-coordinated Ni(II) complex **1**. The aim of the present work is to investigate the catalytic annulation efficiency of such pincer complexes. The strategic use of a robust, electron-deficient bis-azo based organic template L is warranted due to its ability to enhance the initial nucleophilic attack of primary and secondary alcohols at the electron-rich nickel center, thereby propelling the entire catalytic process (Scheme 7). Moreover, such electron-sink moiety would play a key role in the dehydrogenative oxidation process, where alcohols are oxidized to their corresponding carbonyl compounds by removing hydrogen atoms, likely through electron transfer. Aryl-substituted 1,3,5-triazine derivatives are recognized for their diverse biological activities. To assess the feasibility of the proposed synthetic procedure, benzamidine **2a** and benzyl alcohol **3a** were employed as model substrates. Initial reactions were conducted at 110 °C for 10 hrs

Table 6. synthesis of 2,4,6-triphenyl-1,3,5-triazine **4aa**: optimization of reaction conditions.[a]

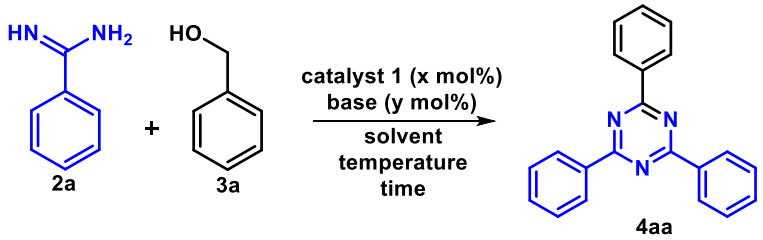

Entry	Catalyst (X mol%)	Solvent	Base (Y mol%)	Temp (°C)	Yield[b] (%)
1		Toluene	KO^{t}Bu (100)	110	NR
2	**1a** (1.00 mol%)	Toluene	KO^{t}Bu (100)	110	90
3	**1a** (1.00 mol%)	Toluene	NaO^{t}Bu (100)	110	81
4	**1a** (1.00 mol%)	Toluene	KOH (100)	110	70
5	**1a** (1.00 mol%)	Toluene	NaOH (100)	110	62
6	**1a** (1.00 mol%)	Toluene	K_2CO_3 (100)	110	45
7	**1a** (1.00 mol%)	Toluene	Na_2CO_3 (100)	110	35
8	**1a** (1.00 mol%)	Toluene	$NaBH_4$ (100)	110	50
9	**1a** (1.00 mol%)	Toluene	NEt_3 (100)	110	30
10	**1a** (1.00 mol%)	Toluene	KO^{t}Bu (60)	110	90
11	**1a** (1.00 mol%)	Toluene	KO^{t}Bu (20)	110	90
12	**1a** (0.1 mol%)	Toluene	KO^{t}Bu (20)	110	90
13	**1a (0.001 mol%)**	**Toluene**	**KO^{t}Bu (20)**	**110**	**90**
14	**1a** (0.0001 mol%)	Toluene	KO^{t}Bu (20)	110	41
15	**1a** (0.001 mol%)	Xylene	KO^{t}Bu (20)	110	84
16	**1a** (0.001 mol%)	Mesitylene	KO^{t}Bu (20)	110	85
17	**1a** (0.001 mol%)	THF	KO^{t}Bu (20)	65	70
18	**1a** (0.001 mol%)	EtOH	KO^{t}Bu (20)	75	trace
19	**1a** (0.001 mol%)	Toluene	KO^{t}Bu (20)	60	56
20[c]	**1a** (0.001 mol%)	Toluene	KO^{t}Bu (20)	RT	NR
21	**1a** (0.001 mol%)	Mesitylene	KO^{t}Bu (20)	150	85
22	$NiCl_2.6H_2O$ (1.00 mol%)	Toluene	KO^{t}Bu (20)	110	NR
23	**1a** (0.001 mol%)		KO^{t}Bu (20)	110	trace
24		Toluene	KO^{t}Bu (20)	110	NR
25	**1a** (0.001 mol%)	Toluene		110	NR
26[d]	**1a** (0.001 mol%)	Toluene	KO^{t}Bu (20)	110	45
27	**L** : NiCl2.6H2O (1:1)	Toluene	KO^{t}Bu (20)	110	trace
28[e]	**1a** (0.001 mol%)	Toluene	KOtBu (20)	110	40
29	**1b** (0.001 mol%)	Toluene	KOtBu (20)	110	84

[a]Reaction Conditions: benzamidine **2a** (2.00 mmol), benzyl alcohol **3a** (1.10 mmol), base (20 mol%), solvent (5 ml), reaction time (10 hrs), open air. [b]isolated yield after coloumn chromatography. [c]Room temperature (RT). [d]Reaction time (5 hrs), NR = No Reaction. [e]Under Argon atmosphere.

using 100 mol% KO^{t}Bu in toluene; however, no traces of the desired product were detected (Table 6, entry 1). Remarkably, upon the addition of 1.00 mol% of complex **1a** to the reaction mixture, a significant yield of 90% of the expected product was achieved under the same reaction conditions (Table 6, entry 2). A thorough examination of common reaction parameters, including bases, solvents, and reaction temperature were conducted using standard substrates. Screening of various organic and inorganic bases in toluene revealed that KO^{t}Bu produced a notably higher product yield, while organic bases were ineffective in forming product **4aa** (Table 6, entries 3-9). Upon reducing the amount of KO^{t}Bu to 20 mol%, unaltered yields of **4aa** were observed (Table 6, entries 10-11). Notably, decreasing the catalyst loading to 0.001 mol% did not affect the yield of **4aa**, yielding an excellent TON value of 90,000. However, further reduction in catalyst loading led to a significant drop in yield to 41% (Table 6, entries 12-14). Upon evaluating the efficacy of various polar and nonpolar solvents, it was found that their performance was inferior to that of toluene. (Table 6, entries 15-18). A reduction in reaction temperature from 110 °C to 60 °C led to a considerable decrease in yield to 56%, with no reaction occurring at room temperature. Additionally, no increase in activity was noticed at elevated temperatures (Table 6, entries 19-21). Therefore, KO^{t}Bu was selected as the preferred base and toluene as the preferred solvent for the aforesaid catalytic reactions. Further optimization of the base and catalyst loading was pursued using the selected base, solvent, and catalyst. The optimal catalyst loading was determined to be 0.001 mol%. Notably, the commercially available $NiCl_2 \cdot 6H_2O$ was tested as a catalyst, but showed no activity even after prolonged reaction times (Table 6, entry 22). Moreover, conducting the reactions under solvent-free conditions or without complex **1a** and base resulted in either trace amounts or no detectable coupling products (Table 6, entries 23-25). A significant reduction in product formation to 45% was observed when the reaction time was shortened to 5 hrs (Table 1, entry 26). Furthermore, only trace amounts of **4aa** were detected when coupling was attempted using an equimolar mixture of L and $NiCl_2 \cdot 6H_2O$ (Table 6, entry 27). Notably, conducting the reaction under an argon atmosphere led to a reduced yield of 40% of **4aa** under optimized conditions (Table 6, entry 28). Finally, the reaction of **2a** (1.00 mmol) and **3a** (1.10 mmol) in 5 ml of toluene at 110 °C, utilizing catalyst **1b** (0.001 mol%) and 20 mol% KOtBu as the base, resulted in the highest yield of 84% of **4aa**, with a TON value of 84,000, indicating somewhat lower activity in this catalytic reaction compared to catalyst **1a** (Table 6, entry 29).

Utilizing the optimal reaction conditions detailed in Table 6, we investigated the synthesis of *s*-triazine derivatives through the reaction of a diverse array of primary alcohols

and amidines as starting materials. The representative outcomes of these reactions are presented in Table 7.

Table 7. Scope of primary alcohols.[a,b]

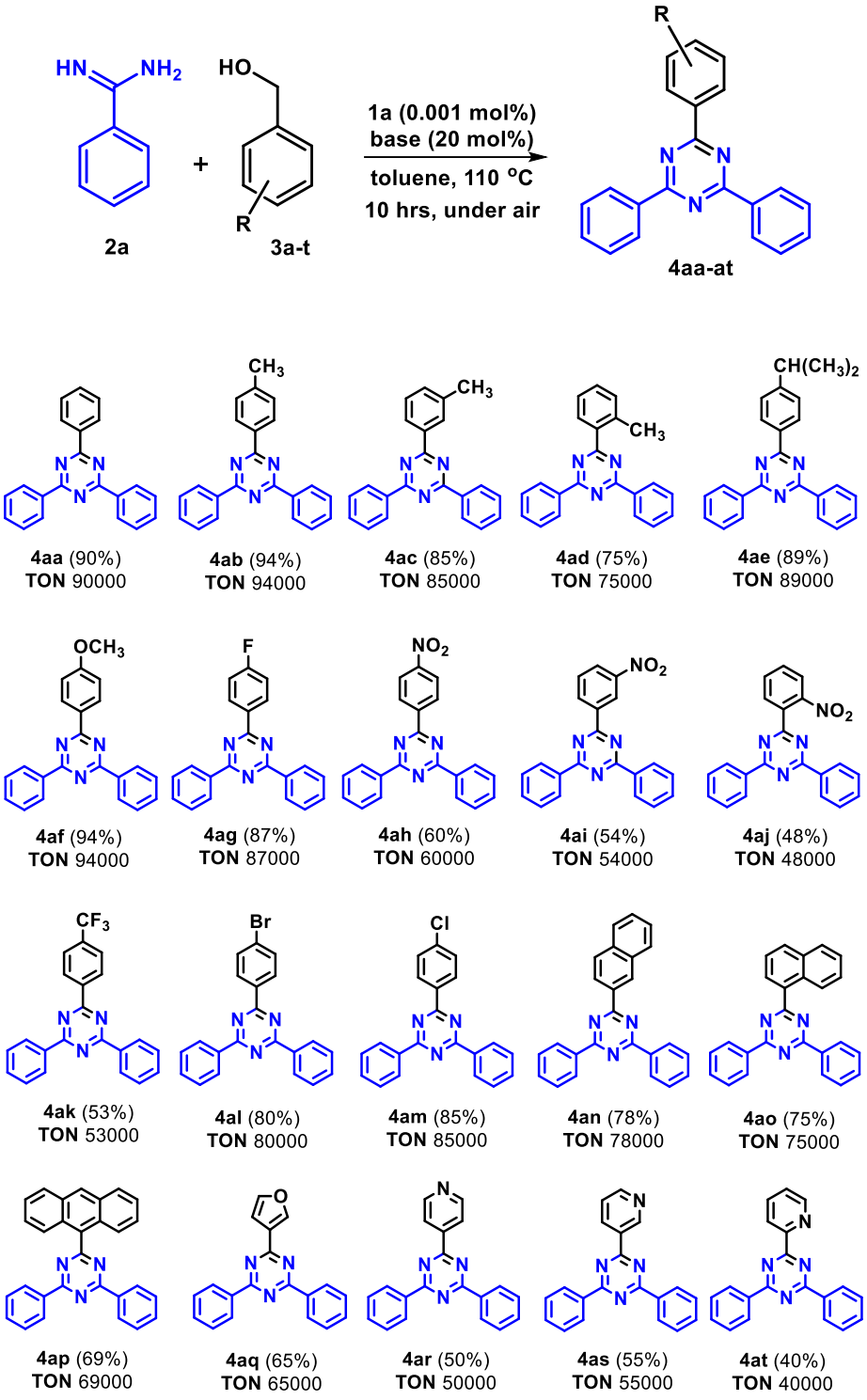

[a]Reaction conditions: benzamidine **2a** (2.00 mmol); primary alcohols **3a**–**t** (1.10 mmol); base (20 mol%), 5.0 ml toluene, open air. [b]Isolated yields after column chromatography.

The corresponding *s*-triazine compounds were obtained in moderate to excellent yields (40–94%) by a variety of functional groups at the ortho-, meta-, and para-positions of the benzyl alcohols. These groups included both electron-donating and electron-withdrawing substituents such as methyl, methoxy, isopropyl, fluoro, nitro, trifluoromethyl and so forth (Table 7, **4ab-am**). Electron-donating substituents, such as methyl, isopropyl, and methoxy, facilitated the formation of the desired products in higher isolated yields (Table 7, **4ab-af**).

Table 8. Scope of aliphatic primary alcohols.[a,b]

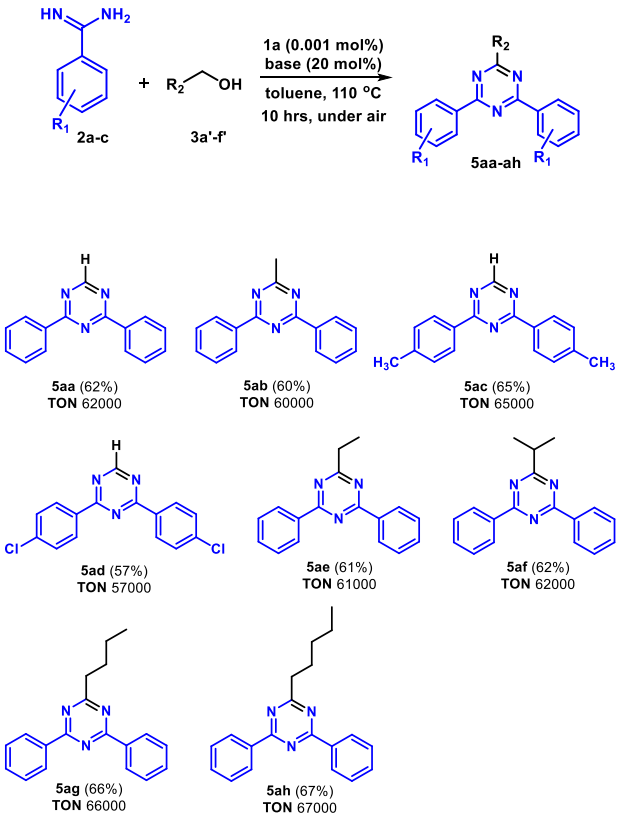

[a]Reaction conditions: amidines **2a-c** (2.00 mmol); aliphatic primary alcohols **3a′-f′** (1.10 mmol); base (20 mol%), 5.0 ml toluene, open air. [b]Isolated yields after column chromatography.

This trend is consistent with the observation that electron-rich substrates, such as 4-methoxy benzylic alcohol, tend to produce comparatively greater yields due to their enhanced nucleophilicity, which likely promotes more efficient reaction pathways (Table 7, **4af**). When alcohols were substituted with electron-withdrawing groups such as $–NO_2$ and $–CF_3$, lower yields were observed (Table 7, **4ah-ak**); for example, the presence of a nitro group reduced the yield to 48%. In contrast, halogen substituents such as -F, -Br, and -Cl resulted in the formation of the corresponding products in very high yields (Table 7, **4ag**, **4al**, and **4am**). Additionally,

steric hindrance significantly impacted the reaction outcomes. Para- and meta-substituted compounds generally provided higher yields compared to ortho-substituted derivatives, as demonstrated in methyl-substituted benzyl alcohols (Table 7, **4ab-ad**). Sterically hindered alcohols, such as 2-naphthalenemethanol, 1-naphthalenemethanol, and anthracen-9-ylmethanol, were also efficiently participated in the transformations, yielding the desired pyrimidines in 78%, 75%, and 69% yields, respectively (Table 7, **4an-ap**). Subsequently, primary alcohols containing heteroatoms were explored, including furan-3-ylmethanol, pyridine-2-methanol, pyridine-3-methanol, and pyridine-4-methanol (Table 7, **4aq-at**). All reactions proceeded efficiently, resulting in good product yields.

Simple alcohols are comparatively more challenging to dehydrogenate than benzylic alcohols.[16] Notably, when primary aliphatic alcohols such as methanol, ethanol, and higher alcohols were examined under standard reaction conditions, reasonably good results were obtained (Table 8, **5aa-ah**).

Table 9. Scope of amidines.[a,b]

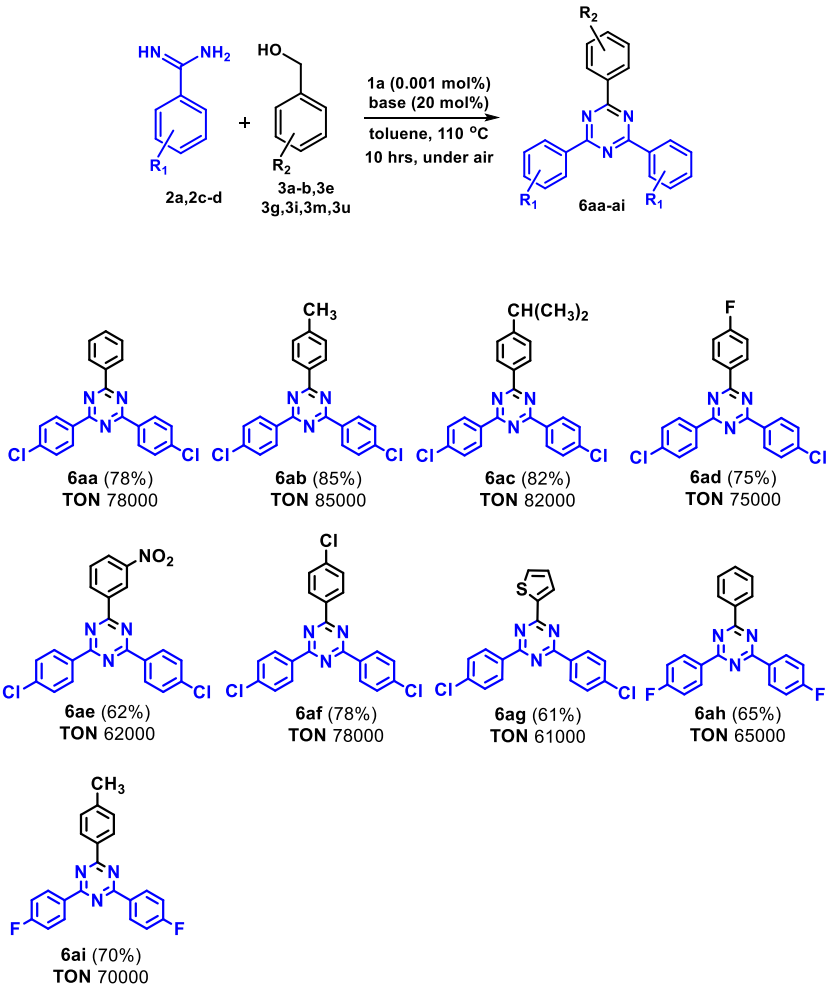

[a]Reaction conditions: amidines **2a**, **2c-d** (2.00 mmol); primary alcohols **3a–b, 3e, 3g, 3i, 3m, 3u** (1.10 mmol); base (20 mol%), 5.0 ml toluene, open air. [b]Isolated yields after column chromatography.

Subsequently, the reactions between various substituted primary aryl alcohols and aryl amidines were investigated. All reactions involving aryl amidines proceeded smoothly, yielding the desired products in moderate to good isolated yields ranging from 61% to 85% (Table 9, **6aa-ai**). An apparent substitution effect was observed with the amidines; specifically, the reaction of **3a** with 4-fluorobenzamidine **2d** resulted in lower yields of *s*-triazines, whereas the reaction with 4-chlorobenzamidine **2c** afforded the desired product in a higher yield (Table 9, **6aa** and **6ah**).

III.2.7.2. Synthesis of Pyrimidines

we found that pyrimidine could be synthesized via an analogous three-component coupling that occurs through two distinct pathways utilizing **1a**. The first pathway (Condition **A**) involves the dehydrogenative coupling of primary and secondary alcohols with amidines. The alternative pathway (Condition **B**) proceeds through the dehydrogenative coupling of primary alcohols with alkynes and amidines. To optimize the reaction conditions for synthesizing the desired products via both pathways, various parameters were varied, including solvent, base, catalyst loading, temperature, and reaction time (Table 10).

Table 10. Optimization of the reaction conditions for the nickel catalyzed 2,4,6-trisubstituted pyrimidine synthesis[a]

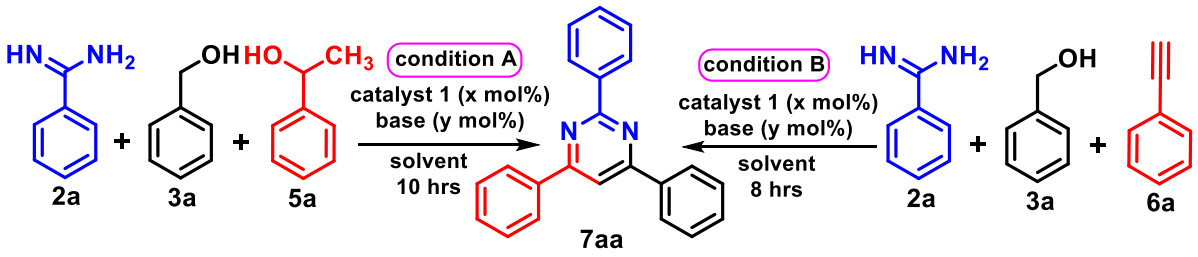

Entry	Catalyst (X mol%)	Solvent	Base (Y mol%)	Temp (°C)	Yield[b] (%) Condition A	Yield[b] (%) Condition B
1		Toluene	KO^{t}Bu (100)	110	NR	NR
2	**1a** (1.00 mol%)	Toluene	KO^{t}Bu (100)	110	87	90
3	**1a** (1.00 mol%)	Toluene	NaO^{t}Bu(100)	110	76	80
4	**1a** (1.00 mol%)	Toluene	KOH (100)	110	68	70
5	**1a** (1.00 mol%)	Toluene	NaOH (100)	110	60	63

6	**1a** (1.00 mol%)	Toluene	K_2CO_3 (100)	110	40	41
7	**1a** (1.00 mol%)	Toluene	Na_2CO_3 (100)	110	32	35
8	**1a** (1.00 mol%)	Toluene	$NaBH_4$ (100)	110	42	45
9	**1a** (1.00 mol%)	Toluene	NEt_3 (100)	110	25	26
10	**1a** (1.00 mol%)	Toluene	KO^tBu (50)	110	87	90
11	**1a** (1.00 mol%)	Toluene	KO^tBu (20)	110	87	90
12	**1a** (1.00 mol%)	Toluene	KO^tBu (10)	110	70	72
13	**1a** (0.1 mol%)	Toluene	KO^tBu (20)	110	87	90
14	**1a** (0.01 mol%)	Toluene	KO^tBu (20)	110	86	90
15	**1a (0.001 mol%)**	**Toluene**	**KO^tBu (20)**	**110**	**87**	**90**
16	**1a** (0.0001 mol%)	Toluene	KO^tBu (20)	110	45	50
17	**1a** (0.001 mol%)	Xylene	KO^tBu (20)	110	82	85
18	**1a** (0.001 mol%)	Mesitylene	KO^tBu (20)	110	83	85
19	**1a** (0.001 mol%)	THF	KO^tBu (20)	65	75	78
20	**1a** (0.001 mol%)	EtOH	KO^tBu (20)	75	trace	trace
21	**1a** (0.001 mol%)	Mesitylene	KO^tBu (20)	150	85	88
22	**1a** (0.001 mol%)	Toluene	KO^tBu (20)	60	trace	trace
23[c]	**1a** (0.001 mol%)	Toluene	KO^tBu (20)	RT	NR	NR
24	$NiCl_2$. $6H_2O$(1.00 mol%)	Toluene	KO^tBu (20)	110	NR	NR
25	**1a** (0.001 mol%)		KO^tBu (20)	110	trace	trace
26		Toluene	KO^tBu (20)	110	NR	NR
27	**1a** (0.001 mol%)	Toluene		110	NR	NR
28[d]	**1a** (0.001 mol%)	Toluene	KO^tBu (20)	110	47	50
29[e]	**1a** (0.001 mol%)	Toluene	KO^tBu (20)	110	trace	trace
30	$\mathbf{L^H}$: $NiCl_2.6H_2O$ (1:1)	Toluene	KO^tBu (20)	110	trace	trace
31	**1b** (0.001 mol%)	Toluene	KO^tBu (20)	110	81	84

[a]Reaction Conditions: for condition **A**: benzamidine **2a** (1.00 mmol), benzyl alcohol **3a** (1.10 mmol), 1-phenylethanol **5a** (1.10 mmol), reaction time (10 hrs); for condition **B**: benzamidine **2a** (1.00 mmol), benzyl alcohol **3a** (1.10 mmol), phenylacetylene **6a** (1.10 mmol), reaction time (8 hrs); base (20 mol%), solvent (5mL), open air, [b]isolated yields after column chromatography, [c]room temperature, [d]reaction time (5 hrs), [e]under argon atmosphere, NR = No Reaction

After establishing the optimal conditions, we investigated the breadth and versatility of this transformation by testing a range of substituted primary alcohols.

Table 11. Scope of aryl/het-aryl primary alcohols.[a,b]

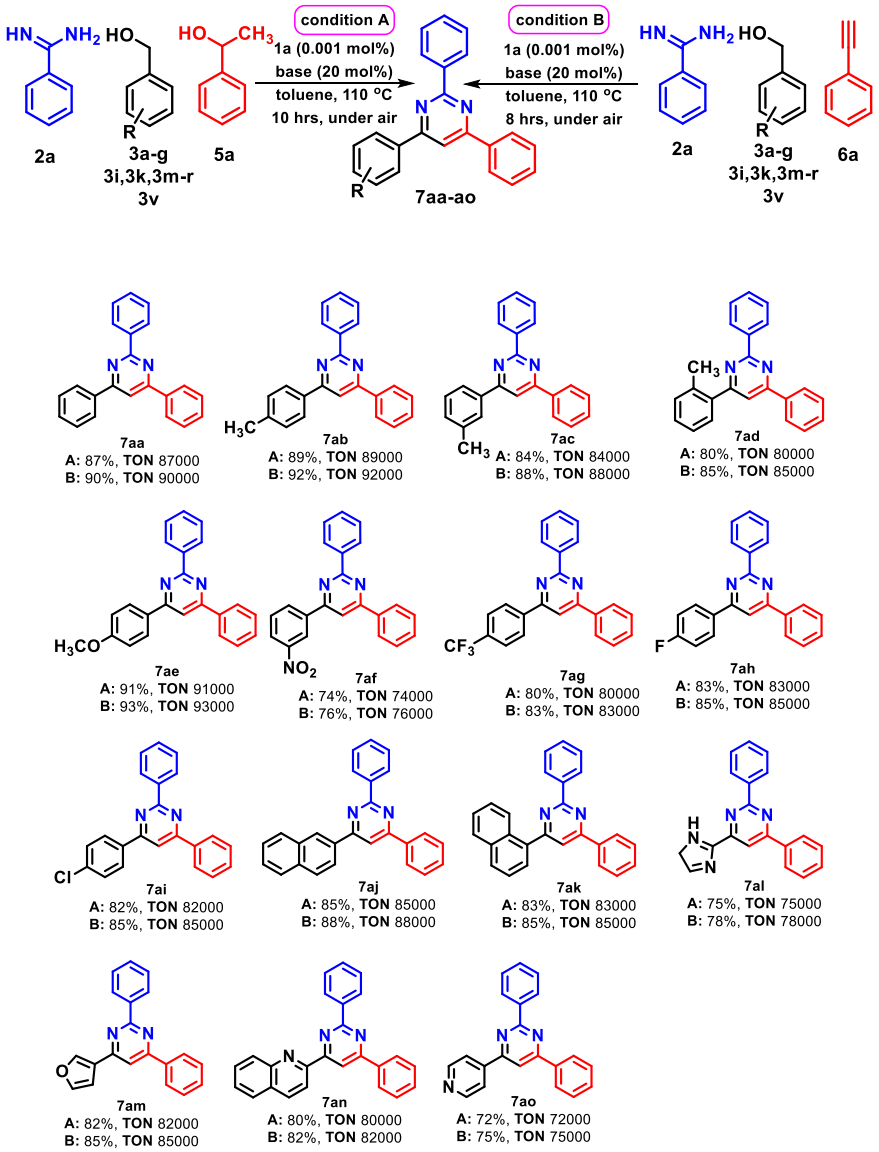

[a]Reaction conditions: for condition **A**: benzamidine **2a** (1.00 mmol), aryl/het-aryl primary alcohols **3a-d, 3f-g, 3i, 3k, 3m-r, 3v** (1.10 mmol), 1-phenylethanol **5a** (1.10 mmol), reaction time (10 hrs); for condition **B**: benzamidine **2a** (1.00 mmol), aryl/het-aryl primary alcohols **3a-d, 3f-g, 3i, 3k, 3m-r, 3v** (1.10 mmol), phenylacetylene **6a** (1.10 mmol), reaction time (8 hrs); base (20 mol%), 5.0 ml toluene, open air. [b]Isolated yields after column chromatography.

We began by exploring various primary alcohols under both Condition **A** and Condition **B** (Table 11). All selected primary alcohols were able to couple smoothly with benzamidine **2a**,

1-phenylethanol **5a** and phenyl acetylene **6a** via condition **A** and condition **B** respectively, resulting in the formation of trisubstituted pyrimidines with good to excellent yields ranging

Table 12. Scope of secondary alcohols and alkynes.[a,b]

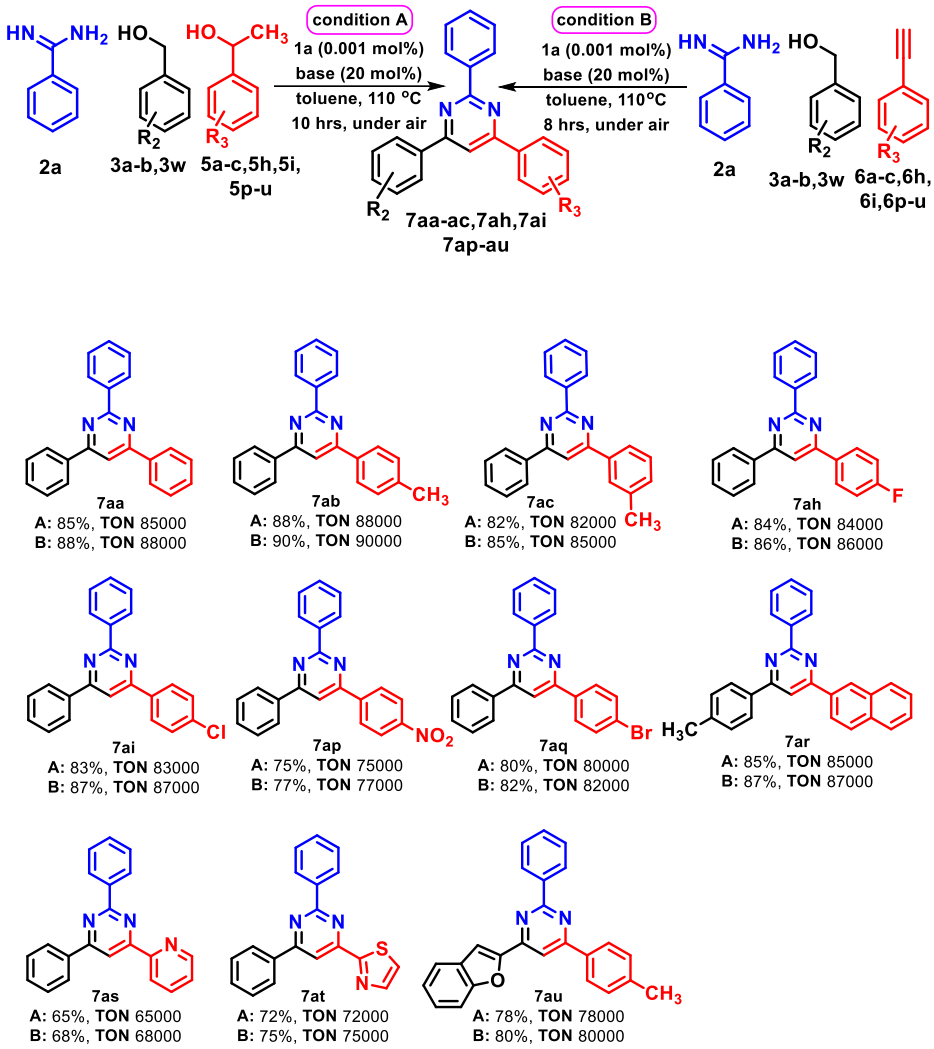

[a]Reaction conditions: for condition **A**: benzamidine **2a** (1.00 mmol), benzyl alcohol **3a-b, 3w** (1.10 mmol), 1-phenylethanol **5a-c, 5h, 5i, 5p-u** (1.10 mmol), reaction time (10 hrs); for condition **B**: benzamidine **2a** (1.00 mmol), benzyl alcohol **3a-b** (1.10 mmol), phenylacetylene **6a-c, 6h, 6i, 6p-u** (1.10 mmol), reaction time (8 hrs); base (20 mol%), 5.0 ml toluene, open air. [b]Isolated yields after column chromatography.

from 72% to 93%. The yields of various pyrimidines produced via both conditions were nearly comparable, indicating that both approaches are equally efficient. A range of electron-donating groups (–Me, –OMe) and electron-withdrawing groups (–NO_2, –CF_3, –F, –Cl) at the para-position of the phenyl ring of benzyl alcohol substituents successfully generated trisubstituted pyrimidine derivatives (**7ab**, **7ae-ai**) with good to excellent yields varying from 74% and 93%.

Similarly, moderate isolated yields of the corresponding pyrimidine **7ac** were obtained with a meta-position substituent on the phenyl ring of benzyl alcohol (Condition **A**: 84%; Condition

Table 13. Scope of amidines.[a,b]

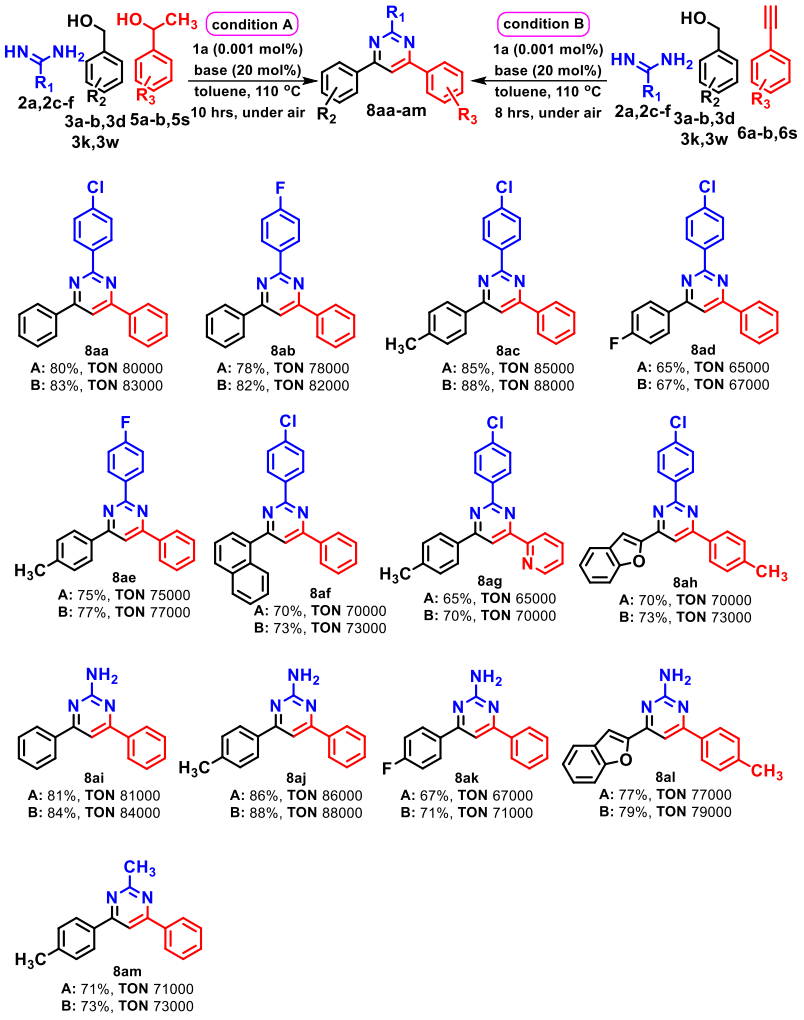

[a]Reaction conditions: for condition **A**: amidines **2c-f** (1.00 mmol), benzyl alcohol **3a-b, 3d, 3k, 3w** (1.10 mmol), 1-phenylethanol **5a-b, 5s** (1.10 mmol), reaction time (10 hrs); for condition **B**: amidines **2a-f** (1.00 mmol), benzyl alcohol **3a-b, 3d, 3k, 3w** (1.10 mmol), phenylacetylene **6a-b, 6s** (1.10 mmol), reaction time (8 hrs); base (20 mol%), 5.0 ml toluene, open air. [b]Isolated yields after column chromatography.

B: 88%). In contrast, a slightly lower yield was observed with the ortho-substituted (**7ad**, Condition **A**: 80%; Condition **B**: 85%). Additionally, sterically hindered alcohols such as 2-naphthalenemethanol and 1-naphthalenemethanol were well-tolerated under the standard conditions, yielding the anticipated products **7aj-ak**. Furthermore, under optimal conditions, heteroaromatic alcohols produced the expected products **7al-ao** with good yields ranging from

72% to 85%. Subsequently, **2a** and **3a** were selected as benchmark substrates to examine the reactivity of secondary alcohols under Condition **A** and alkynes under Condition **B**, respectively. The substitution patterns on the aryl acetylenes or secondary alcohols exhibited a similar trend in the variation of yields for the various pyrimidines, consistent with the observations made using primary alcohols. Under optimum conditions, reactions with diverse substituted secondary alcohols and aryl acetylenes containing both electron-withdrawing and electron-donating groups proceeded well, producing the corresponding pyrimidine derivatives in moderate to good yields (Table 12, **7aa-aq**). Functional group tolerance was also investigated by simultaneously altering substitutions on primary and secondary alcohols/aryl acetylenes (Table 12, **7ar**). Both conditions led to the formation of the corresponding pyrimidines, yielding 65-80% when secondary alcohols or aryl acetylenes with heteroaryl groups were employed as the coupling partners (Table 12, **7as-au**).

Table 14. Scope of aliphatic primary alcohols.[a,b]

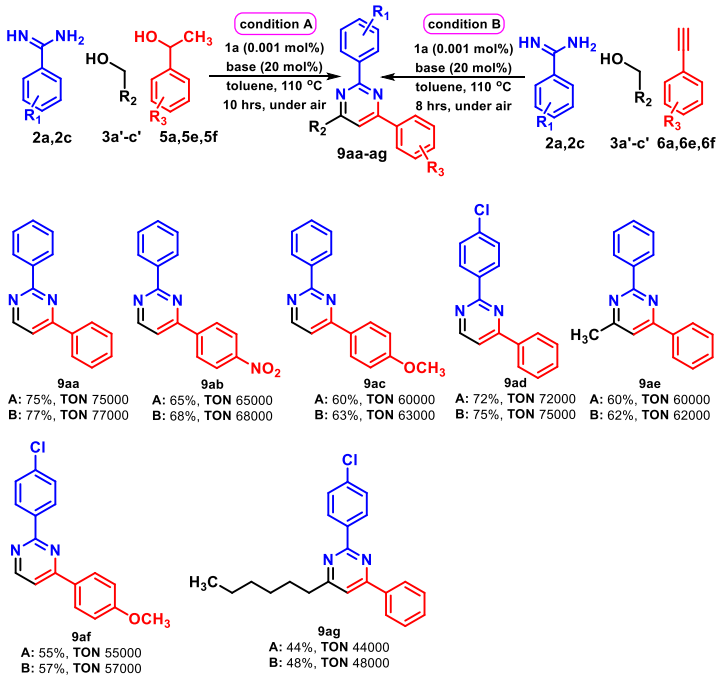

[a]Reaction conditions: for condition **A**: amidines **2a, 2c** (1.00 mmol), primary alcohols **3a′-c′** (1.10 mmol), 1-phenylethanol **5a, 5e, 5f** (1.10 mmol), reaction time (10 hrs); for condition **B**: amidines **2a, 2c** (1.00 mmol), primary alcohols **3a′-c′** (1.10 mmol), arylalkynes **6a, 6e, 6f** (1.10 mmol), reaction time (8 hrs); base (20 mol%), 5.0 ml toluene, open air. [b]Isolated yields after column chromatography.

Furthermore, numerous amidines were investigated using primary alcohols, and secondary alcohols/aryl acetylenes as coupling partners, resulting in desired pyrimidine

derivatives in good yields (Table 13). It was noticed that amidines containing electron-withdrawing groups were viable in the reaction, producing yields of 65–88% for the corresponding products **8aa**–**al** under both condition **A** and condition **B**. Notably, the reactions of guanidine **2e** and acetamidine **2f** under both conditions afforded the desired products in moderate to good yields (Table 13, **8ai-am**).

Additionally, challenging aliphatic alcohols including methanol, ethanol and so forth were successfully utilized in this protocol. Methanol was exploited as the methylene bridge in order to generate the C–C and C–N bonds. Under standard reaction conditions, amidines and secondary alcohols/aryl alkynes showed good tolerance to aliphatic alcohols. Remarkably, compared to substrates with electron-donating substituents on the secondary alcohols/aryl alkynes scaffolds, those with electron-withdrawing groups exhibited higher activity when coupled with aliphatic alcohols, producing yields of 44-77% (Table 14, **9aa-ag**).

Table 15. Scope of both aliphatic primary and secondary alcohols.[a,b]

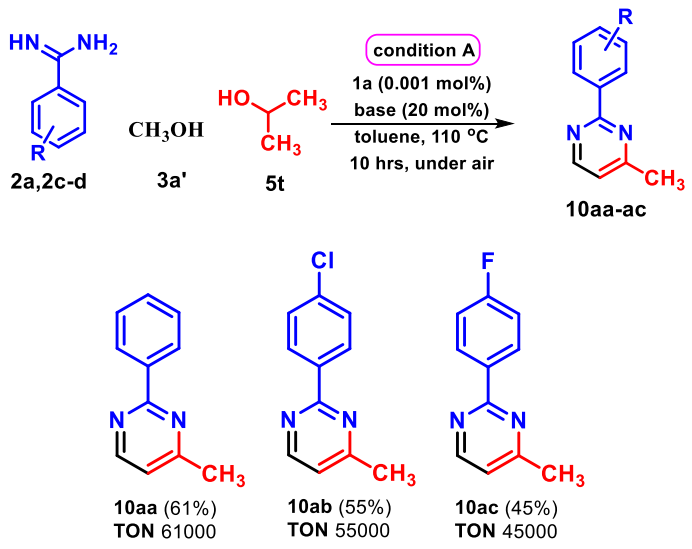

[a]Reaction conditions: amidines **2a**, **2c-d** (1.00 mmol), methanol **3a′** (1.10 mmol), isopropanol **5t** (1.10 mmol), reaction time (10 hrs), base (20 mol%), 5.0 ml toluene, open air. [b]Isolated yields after column chromatography.

A range of trisubstituted pyrimidines were produced in moderate isolated yields, ranging from 45-61%, through the well-established reactions between amidines and various simple primary and secondary aliphatic alcohols using only condition **A** (Table 15, **10aa-ac**).

In order to show the synthetic and industrial utility of this developed methodology, we scaled up the synthesis of both *s*-triazines and pyrimidines (Scheme 3). Under standard conditions, we synthesized *s*-triazines *via* the reaction of benzamidine **2a** (10.00 mmol) with

benzyl alcohol **3a** (5.10 mmol) and 4-methoxybenzyl alcohol **3f** (5.10 mmol), which proceeded smoothly to produce 1.21 g (79%) and 1.42 g (84%) yields of **4aa** and **4af,** respectively.

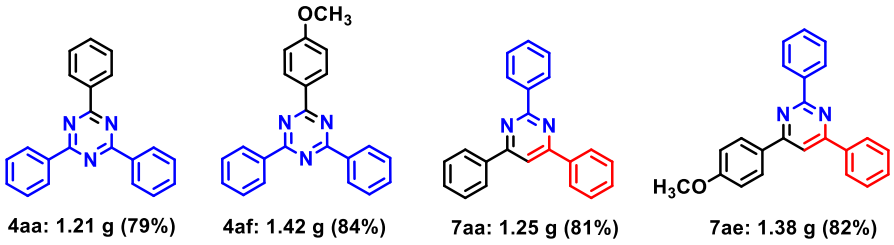

Scheme 3. Gram scale synthesis of triazines and pyrimidines.

Additionally, we successfully synthesized pyrimidines on a gram scale using 5.0 mmol of benzamidine **2a**, benzyl alcohol **3a** (5.10 mmol)/4-methoxybenzyl alcohol **3f** (5.10 mmol) and 1-phenyl ethanol **5a** (5.10 mmol) resulting in 1.25 g (81%)/1.38 g (82%) yields of **7aa**/**7ae**, respectively. The aforementioned two examples demonstrate its potential for industrial application.

III.2.7.3. Mechanistic Investigation

After thoroughly evaluating a broad substrate scope, attention was directed towards elucidating the mechanism behind the Ni-catalyzed two- and three-component synthesis of *s*-triazines and pyrimidines. Systematic control experiments were conducted to clarify the specific role of each reaction component and to gain insights into the reaction mechanism.

Control Experiments

Homogeneity Test

A mercury poisoning test was performed to probe the nature of the catalysis and assess the uniformity of catalytic process. The results indicated that the alcohol dehydrogenation and subsequent coupling reactions were unaffected by mercury, suggesting the absence of metallic nanoparticles as active species (Scheme 4). In a 50 mL oven dried round bottom flask, benzamidine **2a** (2.00 mmol), benzyl alcohol **3a** (1.10 mmol), KO^{t}Bu (20 mol%), and **1a** (0.001 mol%) were dissolved in 5.0 mL of toluene. To this, Hg (0) (200 mg, 1.00 mmol) was added and the resulting reaction mixture was heated at 110 °C in a preheated oil bath for 10 hrs in a closed system. The reaction mixture was cooled to room temperature and vacuum-

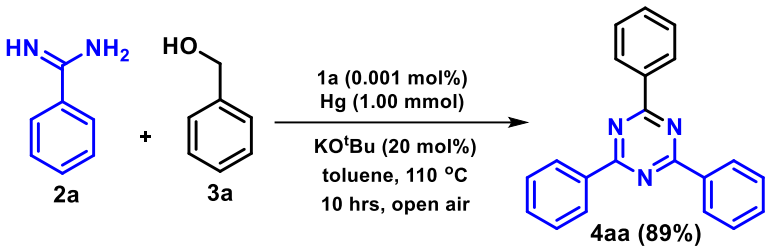

Scheme 4. Mercury poisoning experiment.

concentrated. The crude reaction mixture was then purified through column chromatography on silica gel-60-120 mesh using hexane/ethyl acetate as eluent to afford desired pure products **4aa**. This indicated the homogeneous nature of both the catalyst and the reaction.

Radical Quenching Experiment

Additional control experiments were conducted in order to have a better understanding of the mechanism underlying the catalytic process. To investigate the involvement of a radical pathway, we performed model reactions with radical inhibitors, TEMPO (2 equiv) or BHT (2 equiv).

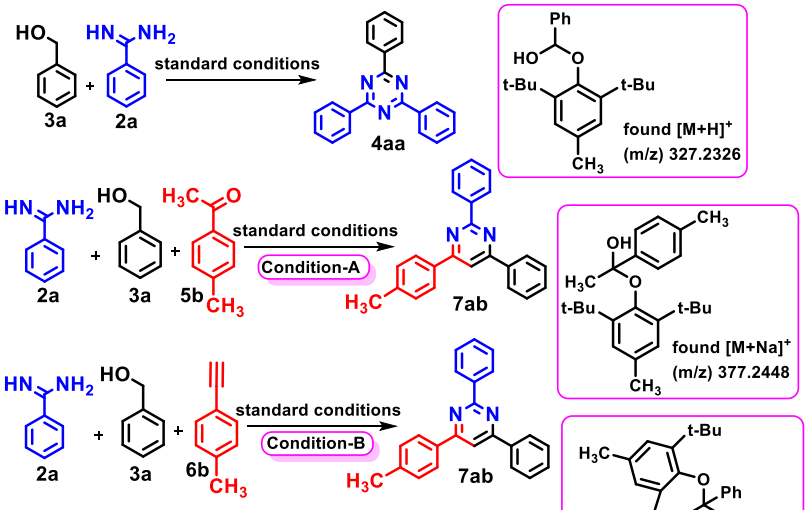

products	without radical scavenger	with radical scavenger (BHT)
4aa	90%	0%
7ab (condition-A)	88%	0%
7ab (condition-B)	90%	0%

Scheme 5. Radical quenching control experiments.

We successfully trapped the BHT radical adduct generated during the reaction and identified it *via* high-resolution mass spectrometry (HRMS).

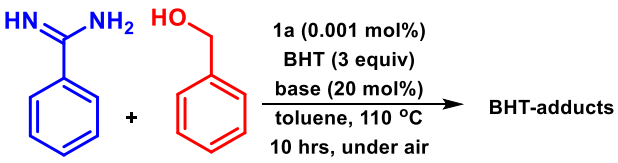

Scheme 6. Radical quenching and radical trapping experiment.

In a 50 mL oven dried round bottom flask, benzamidine **2a** (0.5 mmol), benzyl alcohol **3a** (0.275 mmol), KO^{t}Bu (20 mol%), **1a** (0.001 mol%) and radical scavenger (BHT) (0.75 mmol) were dissolved in toluene 5.0 mL. The resulting reaction mixture was heated at 110 °C in a preheated oil bath for 10 hrs in an open system. The reaction mixture was cooled to room temperature and vacuum-concentrated. In presence of BHT, diminished or no product formation was observed (Scheme 6), possible indication of radical process. To trap the in situ formed radicals, reaction mixtures with 3 equiv. of BHT in standard conditions were analyzed immediately after the completion of the reaction in a high-resolution mass spectrometer. In presence of BHT, HRMS spectra have shown mass (m/z) = 327.2324 which corresponds to the calculated mass value $[M+H]^+$ (m/z) = 327.2326 of BHT adduct of benzyl alcohol (Figure 9). Similarly, HRMS spectra have shown mass (m/z) = 552.2995 which corresponds to the calculated mass value $[M+Na]^+$ (m/z) = 552.2991 of BHT adduct of 2,4,6-triphenyl-1,2-dihydro-1,3,5-triazine (Figure 9)

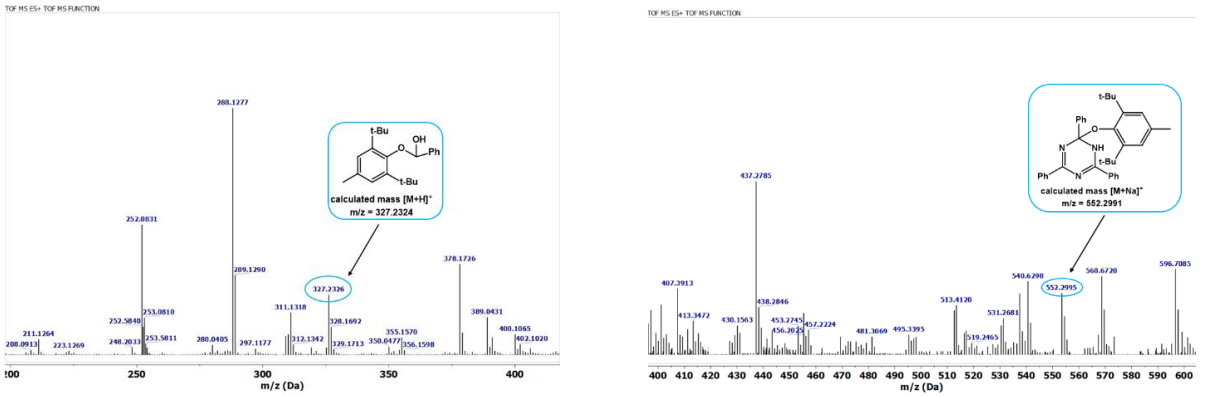

Figure 9. BHT adduct of benzyl alcohol (left) and BHT adduct of 2,4,6-triphenyl-1,2-dihydro-1,3,5-triazine (right)

A 25 mL round bottom flask was charged with benzamidine **2a** (0.25 mmol), benzyl alcohol **3a** (0.275 mmol), 1-(p-tolyl)ethan-1-ol **5b** (0.275 mmol), KO^{t}Bu (20 mol%), and **1a** (0.001 mol%) in 5 mL toluene in an open air. The resulting reaction mixture was stirred at 110 °C for 12 hrs. Once the reaction completed, the mixture was cooled to room temperature and

concentrated in *vacuo*. In presence of radical scavenger, diminished or no product formation was observed (Scheme S2b), possible indication of radical process.

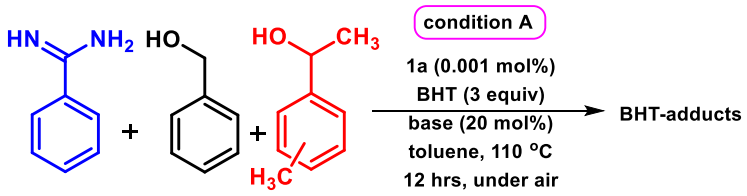

To trap the in situ formed radicals, reaction mixtures with 3 equiv. of BHT in standard conditions were analyzed immediately after the completion of the reaction in a high-resolution mass spectrometer. In presence of BHT, HRMS spectra have shown mass (m/z) = 377.2448 which corresponds to the calculated mass value $[M+Na]^+$ (m/z) = 377.2457 of BHT adduct of 1-(p-tolyl)ethan-1-ol (Figure 10). Similarly, HRMS spectra have shown mass (m/z) = 543.3384 which corresponds to the calculated mass value $[M+H]^+$ (m/z) = 543.3375 of BHT adduct of 2,6-diphenyl-4-(p-tolyl)-1,2-dihydropyrimidine (Figure 10)

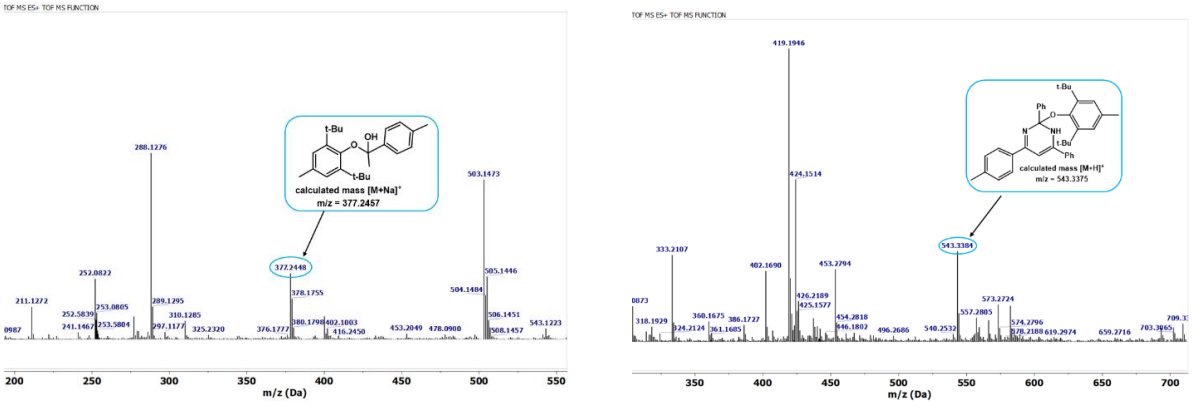

Figure 10. BHT adduct of 1-(p-tolyl)ethan-1-ol (left) and BHT adduct of 2,6-diphenyl-4-(p-tolyl)-1,2-dihydropyrimidine (right)

Electron Paramagnetic Resonance (EPR) study

Several control experiments utilizing EPR spectroscopy were conducted to confirm the presence of radicals in the reaction mixture. A 25 mL oven-dried round-bottom flask was charged with benzamidine **2a** (0.5 mmol), benzyl alcohol **3a** (0.275 mmol), KO^{t}Bu (20 mol%), and **1a** (0.001 mol%) in 1 mL of toluene under open air condition.

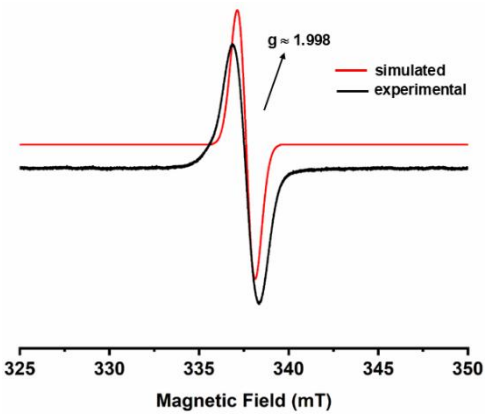

Figure 11. X-band EPR spectrum of **1a**$^{\bullet-}$ in toluene (experimental: black, simulated: red). Conditions: frequency 9.436 GHz, power 1 mW, modulation 1.0 mT, T = 298 K.

The reaction mixture was stirred at 110 °C for 2 hrs. Subsequently, the mixture was transferred to an EPR tube, and the EPR analysis was performed at room temperature. The EPR spectrum showed a sharp peak with a g-value of 1.998, which is consistent with the presence of a nickel-bound organic free radical, ruling out the involvement of Ni(III) or Ni(I) species as reported in the literature (Figure 11). The EPR spectrum of compound **1a** in toluene alone showed no signal. However, when 1a (0.001 mol%) and KO^{t}Bu (20 mol%) were stirred in toluene at 110 °C for 2 hrs, the EPR spectrum exhibited a sharp peak with a g-value of 1.998, indicating the formation of an azo-anion nickel radical intermediate. In contrast, stirring **1a** (0.001 mol%) with benzyl alcohol (0.275 mmol) in toluene under identical conditions did not show any EPR activity. When **1a**, KO^{t}Bu, and **3a** were combined and stirred at 110 °C, EPR activity was observed, highlighting the essential role of the Ni-catalyst in generating ketyl radicals. The formation of pyrimidines also follows a similar radical pathway.

The alcohol oxidation is proposed to proceed through a radical mechanism involving hydrogen atom transfer (HAT), facilitated by the two azo moieties in close proximity to nickel atom in complex **1a** (Scheme 4). A series of control experiments, supported by EPR analysis, were conducted to elucidate the distinct role of each reaction component. For instance, the EPR signal detected in the presence of catalyst **1a** and the base KO^{t}Bu suggests the formation of an azo-anion radical complex as an intermediate species.

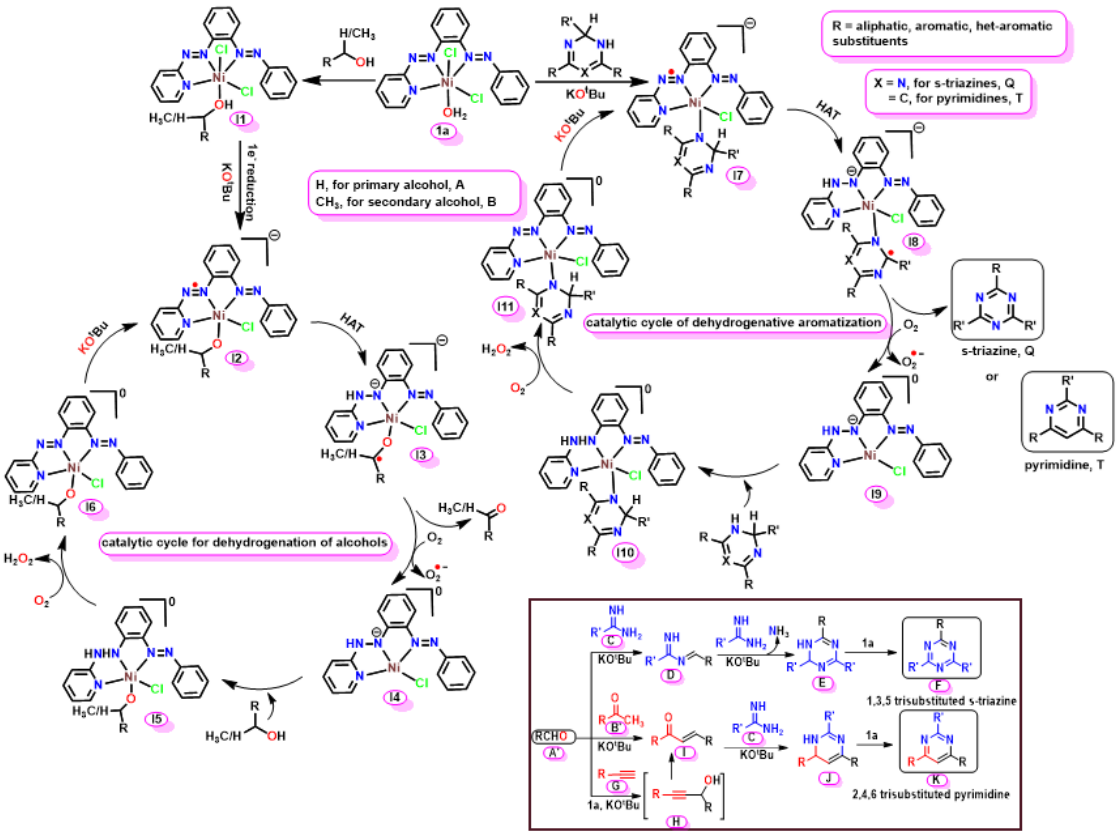

Scheme 7. Proposed reaction mechanism for Ni(II)-mediated annulation reactions.

To elucidate the mechanism and confirm the involvement of radical intermediates, cyclobutanol, a radical clock substrate, was subjected to the standard reaction conditions. The formation of multiple ring-cleavage products is indicative of a one-electron hydrogen atom transfer (HAT) pathway rather than a two-electron hydride transfer (HT) mechanism, further supporting the radical nature of the reaction (Figure 12).

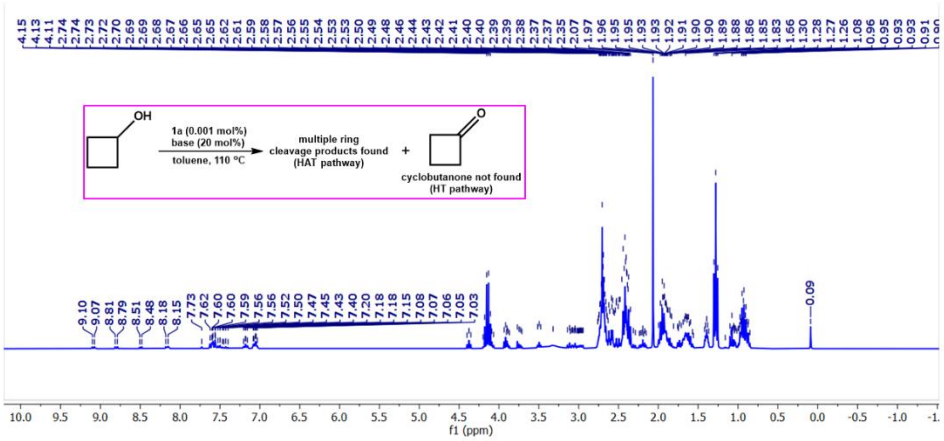

Figure 12. ^{1}H NMR spectrum of reaction mixture of dehydrogenation of cyclobutanol (300 MHz, $CDCl_3$).

The reaction proceeds with the dehydrogenation of alcohols to the corresponding aldehyde with catalyst **1a** and KO^{t}Bu. As an example, under optimized conditions, benzaldehyde **3a′** has been produced in 90% yield by dehydrogenating benzyl alcohol **3a** (Scheme 8). Amidine **C** was

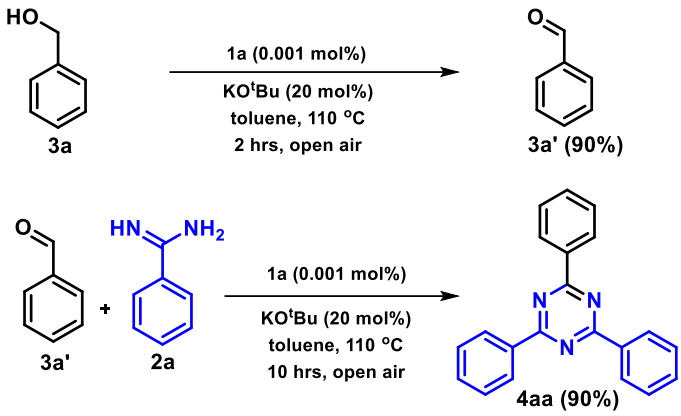

Scheme 8. Control experiments performed for triazine synthesis.

neutralized from its hydrochloride salt using KO^{t}Bu, leading to its condensation with the in-situ generated aldehyde **A′**, resulting in the formation of azadiene **D**. Subsequently, the amino group of **C** underwent nucleophilic addition to the electrophilic carbon of **D**. This process released ammonia and dihydrotriazine E via a thermodynamically favourable deamination reaction. Finally, stable triazine **F** was produced as the sole product through a thermodynamically favorable dehydrogenation step catalyzed by **1a** (Scheme 4). For instance, under optimized conditions, the reaction between **3a′** and **2a** followed this pathway, yielding the desired product **4aa** (Scheme 6).

A plausible mechanistic pathway for the synthesis of pyrimidines from primary and secondary alcohols, along with amidines, is illustrated in Scheme 4. Initially, both types of alcohols undergo dehydrogenation to yield the corresponding carbonyls, a process catalyzed by 1a. For example, 1-phenylethanol **5a** is dehydrogenated to produce acetophenone **5a′** as the dehydrogenation product, which serves to facilitate the subsequent pyrimidine synthesis under condition **A** (Scheme 7). This mechanism highlights the role of the catalyst in promoting the conversion of alcohols into reactive intermediates, which are crucial for the formation of the desired pyrimidine structures.

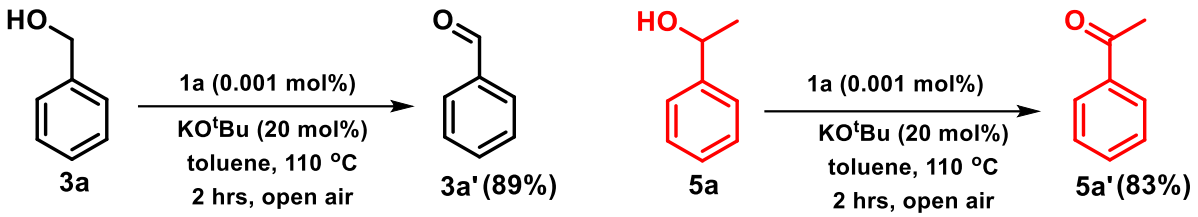

Scheme 9. Dehydrogenation of alcohols.

Subsequently, in the presence of a base, the α,β-unsaturated ketone **I** was formed. The amino group of **C** then underwent nucleophilic addition to the electrophilic carbon core of **I**, resulting in the production of dihydropyrimidine **J**. Finally, stable pyrimidine **K** was generated through a thermodynamically favorable dehydrogenation step catalyzed by **1a** (Scheme 4). The reactions

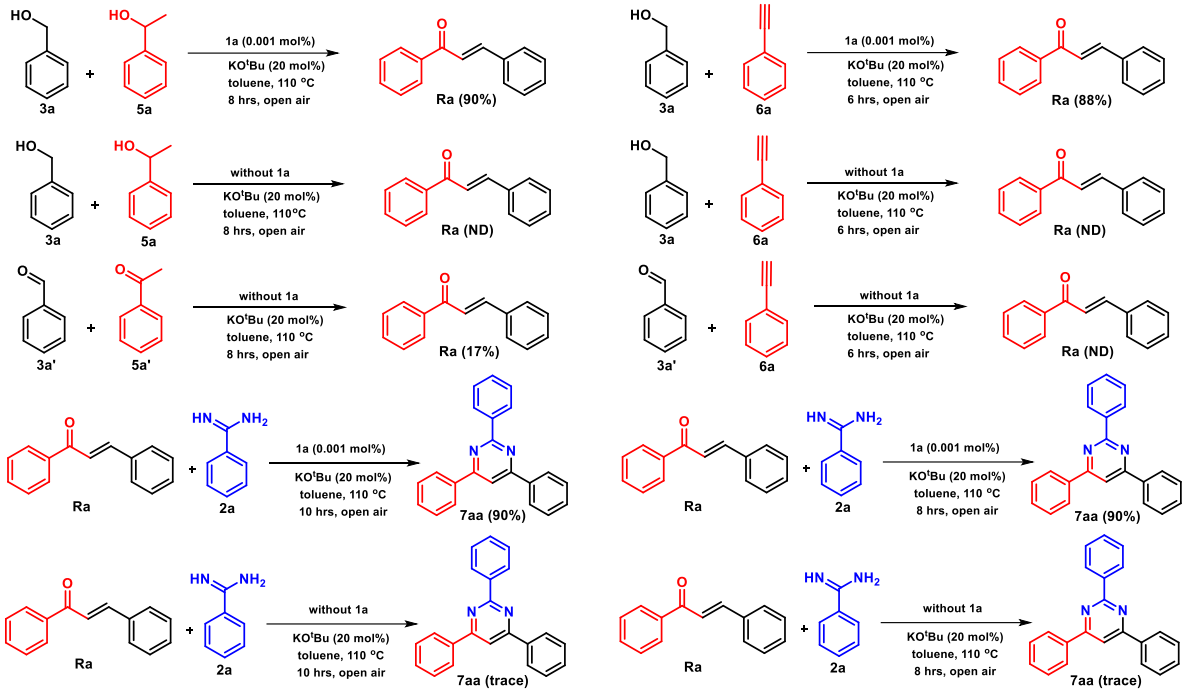

Scheme 10. Control experiments performed for pyrimidine synthesis via condition **A** (left) and condition **B** (right).

of **3a** and **5a** yielded the α,β-unsaturated ketone **Ra** in 90%, whereas in the absence of catalyst **1a**, **Ra** was not formed (Scheme 9). However, when the reaction was performed with **3a′** and **5a′** in the presence of the base alone, without catalyst **1a, Ra** was produced only in 17% yield (Scheme 9). The subsequent reaction of **Ra** with **2a** yielded the desired product, **7aa**, with a 90% yield under optimized conditions. Notably, **7aa** was isolated at only trace amount in the

absence of catalyst **1a** under standard conditions starting from **Ra**, indicating the significant role of catalyst **1a** in enhancing the yield of **7aa** during this condensation step (Scheme 9). Thus, we concluded that catalyst **1a** is crucial for the dehydrogenative aromatization of 1,2-dihydropyrimidine, demonstrating its effectiveness in facilitating these transformations.[17]

Additionally, a mechanistic analysis was carried out to examine the plausible reaction sequence for condition **B**. Initially, the primary alcohol **A** was dehydrogenated to the corresponding aldehyde **A′**, facilitated by catalyst **1a** (Scheme 7). Following this, **A′** condensed with **G** to yield the α,β-unsaturated ketone **I** under our optimized reaction conditions.[18] The remaining steps were executed according to condition **A** (Scheme 7).

The mechanistic investigation revealed that dehydrogenation occurred *via* a one-electron reduced azoaromatic chromophore, which facilitated the removal of the β-hydrogen from the Ni(II)-coordinated alcohol **I2** through a one-electron HAT pathway, ultimately generating a ketyl-type radical intermediate that led to the formation of carbonyls. Upon condensation with amidines, the aldehydes produced during the dehydrogenation of alcohols resulted in the formation of the desired *s*-triazine and its derivatives.

Moreover, the aldehydes and ketones formed during the dehydrogenation of alcohols reacted to produce α,β-unsaturated ketone **I** *via* condensation reactions for both conditions **A** and B. These intermediates subsequently reacted with amidines through sequential C–C and C–N bond formation, catalyzed by **1a**, to generate the desired pyrimidine derivatives. The entire catalytic cycle operates exclusively through ligand-centered redox event, with nickel serving primarily as a spectator.

This mechanistic insight aligns with previous studies that have highlighted the role of radical pathways and ligand-centered events in metal-catalyzed transformations.[7h, 19]

Interestingly, spectrophotometric analysis of the reaction mixture with KI and ammonium molybdate revealed the formation of I_3^- (Table 16), which confirmed the presence of H_2O_2.[20]

Table 16. Quantification of H_2O_2 for the synthesis of **4aa** and **7aa** (both condition **A** and **B**).

Entry	Reaction	Absorption spectral data observed during formation of I_3^- in the presence of H_2O_2.	Amount of H_2O_2 (w.r.t limiting reagent)
1	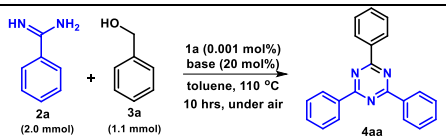	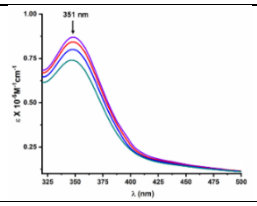	0.039 equiv.
2	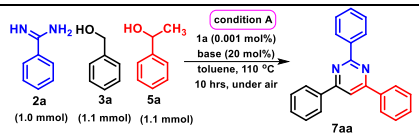	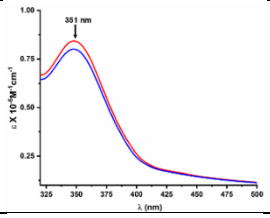	0.037 equiv.
3	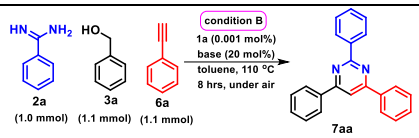	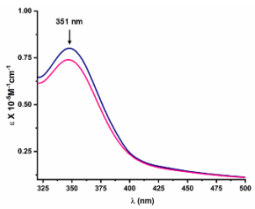	0.038 equiv.

III.3. Conclusions

A *cis*-[Ni(N^N^N)Cl_2(H_2O)] compound, featuring an bis-azo based pincer-type scaffold, has been synthesized and successfully introduced as an auto-tandem catalyst for inducing the [3 + 2 + 1] annulation reaction. This work is an excellent example of the creative application of hybrid organometallic–ligand-radical catalysis in organic transformations, enabling the one-pot synthesis of bio relevant N-heterocycles from amidines and alkyl/aryl/het-aryl alcohols. The process involves C–C and C–N bond formation, followed by oxidative annulation reactions. The dehydrogenation of methanol or ethanol as C1/C2 source under mild reaction conditions is challenging. However, *in-situ* generated formaldehyde or acetaldehyde is effectively utilized to react with amidines resulting in the formation of *s*-triazines. Additionally, this HAT-based partial oxidative approach enables the synthesis of various pyrimidines when similar reactions are carried out in the presence of secondary alcohols or alkynes. It is worth mentioning that the final step, involving dehydrogenative aromatization followed by ring closure through C–N bond formation, is primarily driven by the same metal catalyst. This is evidenced by the fact that sub-stoichiometric amounts of base (*ca*. 20 mol%) are sufficient to achieve excellent yields of N-heterocycles within a short residence time at moderately low temperature. The strongly π-acidic pyridyl-bis-azo scaffold promotes the formation of azo

anion radicals, as demonstrated by spectral, electrochemical, and theoretical studies, thereby initiating MRC. This mechanistic attribute offers a distinct advantage in addressing the challenge of controlling stereoselection. The Ni-catalyzed cascade reaction strategy demonstrates great potential for advancing green chemistry in the synthesis of N-heterocycles, offering advantages over traditional methods: (1) the use of earth-abundant Ni-catalyst, (2) very low catalyst loading (0.001 mol%) with high TON ($\approx 10^4$), (3) scaled synthesis, (4) minimal base loading (20 mol%), (5) good to excellent isolated yields even with challenging substrates, (6) without any supplementary sacrificial acceptor and (7) environmentally benign by-products. This economically and ecologically viable multi-component approach utilizing one-pot AD strategy with ligand radical catalyst enables the efficient synthesis of poly-azaheterocycles. This method offers new perspectives into the development of associated domino reactions.

III.4. Experimental Section

III.4.1. General Information

Except where emphasised, all manipulations have been carried out in an argon atmosphere. Prior to use, solvents were dried using conventional techniques and afterwards distilled under argon. nickel chloride hexahydrate, benzyl alcohol and its derivatives and acetophenone and its derivatives were bought from Sigma Aldrich chemical company. Additional chemicals and solvents were bought from Merck India, Ranchem Private Limited, TCI Chemicals (India) Pvt. Ltd., Alfa Aesar and dried before use using well-known methods. FT-IR spectra have been measured using a Perkin-Elmer L1600300 spectrometer. TMS was used as the internal reference for ^{1}H, ^{13}C & ^{19}F NMR spectra measurements on Bruker FT 300 & 400 MHz spectrometers. Electronic spectra were recorded using a Perkin-Elmer LAMDA 25 spectrophotometer and a dichloromethane solution with a solute concentration of approximately 10^{-5} M.

III.4.2. Synthesis

Synthesis of ligands

The organic ligands L^{Cl} and L^{H} comprising two electron-deficient azo moieties along with an aromatic heterocyclic group have been prepared by condensation of (*E*)-2-((4-chlorophenyl)azo)aniline or (*E*)-2-(phenylazo)aniline with 2-nitrosopyridine using the previously reported procedure.[21a]

Synthesis of complexes:

[Ni(L^H)Cl_2(H2O)] 1a $NiCl_2.6H_2O$ (237.7 mg, 1.00 mmol) was added to a solution of (L^H) (316 mg, 1.10 mmol) in aqueous EtOH (30 mL) under an open air with reflux for 6 hrs. The solvent was evaporated under vacuum. The slow diffusion of a dichloromethane solution of the complex into n-hexane enabled the crystallization of **1a** in the form of block-shaped crystals. Yield and characterization data: Deep-brown crystal, Yield 80% (360 mg). Anal. Calcd. for $C_{17}H_{15}N_5Cl_2NiO$: C 46.95, H 3.48, N 16.10; Found C 47.16, H 3.51, N 16.03%. UV/Vis spectrum (CH_2Cl_2): λ_{max} (nm) 340, 368, 480 nm. FT-IR (cm^{-1}): 1455, 1397 ($\nu_{N=N}$). HRMS (ESI) m/z Calcd. for $C_{17}H_{13}N_5Cl_2Ni$ [M – H_2O] 414.9901, found 414.9916.

[Ni_2(L^H)$_2$(μ-Cl)$_2$$Cl_2$] 1b $NiCl_2.6H_2O$ (237.7 mg, 1.00 mmol) was added to a solution of (L^H) (316 mg, 1.10 mmol) in EtOH (30 mL) while stirring under ambient air conditions. The resultant reaction mixture was then allowed to stir for 4 hrs at room temperature. Solvent was evaporated under vacuum. The slow diffusion of a dichloromethane solution of the complex into toluene enabled the crystallization of **1b** in the form of needle-shaped crystals. Yield and characterization data: Deep-brown crystal, Yield 84% (352 mg). Anal. Calcd. for $C_{34}H_{26}N_{10}Cl_4Ni_2$: C 48.98, H 3.14, N 16.80; Found C 48.77, H 3.23, N 16.87%. UV/Vis spectrum (CH_2Cl_2): λ_{max} (nm) 337, 370, 478 nm. FT-IR (cm^{-1}): 1457, 1392 ($\nu_{N=N}$). HRMS (ESI) m/z calcd for $C_{17}H_{13}N_5ClNi$ [M/2 – Cl]$^+$ 380.1213, found 380.1238.

General procedure for the synthesis of *s*-triazine derivatives:

A 25 mL oven-dried round bottom flask was charged with primary alcohols **3** (1.10 mmol), amidines **2** (2.00 mmol), KO^{t}Bu (20 mol%), and **1a** (0.001 mol%) in 5 mL toluene in an open air. The resulting reaction mixture was stirred at 110 °C for 10 hrs. Once the reaction completed, the mixture was cooled to room temperature and vacuum-concentrated. The crude reaction mixture was then purified through column chromatography on silica gel-100-200 mesh using hexane/ethyl acetate as eluent to afford desired pure products **4-6**. ^{1}H, ^{13}C and ^{19}F NMR spectroscopies were utilized to characterize the desired product.

General procedure for the synthesis of pyrimidine derivatives (condition A)

A 25 mL round bottom flask was charged with secondary alcohols **5** (1.10), primary alcohols **3** (1.10 mmol) and amidines **2** (1.00 mmol), KO^{t}Bu (20 mol%), and **1a** (0.001 mol%) in 5 mL toluene in an open air. The resulting reaction mixture was stirred at 110 °C for 10 hrs. Once the reaction completed, the mixture was cooled to room temperature and concentrated in *vacuo*.

The crude reaction mixture was then purified through column chromatography on silica gel-100-200 mesh using hexane/ethyl acetate as eluent to afford desired pure products **7-10**. ^{1}H, ^{13}C and ^{19}F NMR spectroscopies were utilized to characterize the desired product.

General procedure for the synthesis of pyrimidine derivatives (condition B)

A 25 mL round bottom flask was charged with alkynes **6** (1.10), primary alcohols **3** (1.10 mmol) and amidines **2** (1.00 mmol), KO^{t}Bu (20 mol%), and **1a** (0.001 mol%) in 5 mL toluene in an open air. The resulting reaction mixture was stirred at 110 °C for 8 hrs. Once the reaction completed, the mixture was cooled to room temperature and concentrated in *vacuo*. The crude reaction mixture was then purified through column chromatography on silica gel-100-200 mesh using hexane/ethyl acetate as eluent to afford desired pure products **7-9**. ^{1}H, ^{13}C and ^{19}F NMR spectroscopies were utilized to characterize the desired product.

General procedure for gram-scale synthesis of *s*-triazine derivatives:

A 25 mL oven-dried round bottom flask was charged with benzamidine **2a** (10.00 mmol, 1.566 g), benzyl alcohol **3a** (5.10 mmol, 552 mg), and benzamidine **2a** (10.00 mmol, 1.566 g), 4-methoxybenzyl alcohol **3f** (5.10 mmol, 705 mg), KO^{t}Bu (20 mol%), and **1a** (0.001 mol%) in 5 mL toluene in an open air. The resulting reaction mixture was stirred at 110 °C for 10 hrs. Once the reaction completed, the mixture was cooled to room temperature and vacuum-concentrated. The crude reaction mixture was then purified through column chromatography on silica gel-100-200 mesh using hexane/ethyl acetate as eluent to afford desired pure products: **4aa** (1.21 g, 79%) and **4af** (1.42 g, 84%). ^{1}H and ^{13}C NMR spectroscopies were utilized to characterize the desired product.

General procedure for gram-scale synthesis of pyrimidine derivatives (condition A):

A 25 mL oven-dried round bottom flask was charged with benzamidine **2a** (5.00 mmol, 783 mg), benzyl alcohol **3a** (5.10 mmol, 552 mg), 1-phenyl ethanol **5a** (5.10 mmol, 622 mg) and benzamidine **2a** (5.00 mmol, 783 g), 4-methoxybenzyl alcohol **3f** (5.10 mmol, 705 mg), 1-phenyl ethanol **5a** (5.10 mmol, 622 mg), KO^{t}Bu (20 mol%), **1a** (0.001 mol%) in 5 mL toluene in an open air. The resulting reaction mixture was stirred at 110 °C for 10 hrs. Once the reaction completed, the mixture was cooled to room temperature and vacuum-concentrated. The crude reaction mixture was then purified through column chromatography on silica gel-100-200 mesh using hexane/ethyl acetate as eluent to afford desired pure products: **7aa** (1.25 g, 81%) and **7ae** (1.38 g, 82%). ^{1}H and ^{13}C NMR spectroscopies were utilized to characterize the desired product.

III.4.3. Characterization data of Ni(II)-catalyzed compounds

All the reactions were carried out in 1.0 mmol scale of reactant and according to the general procedure for the synthesis of triazine derivatives.

2,4,6-triphenyl-1,3,5-triazine (4aa):

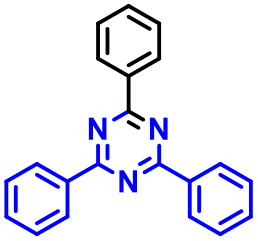

Eluent: Hexane/Ethyl acetate (50:1). White solid (yield = 90%, 278 mg). ^{1}H NMR (300 MHz, $CDCl_3$): δ (ppm) 8.83 – 8.79 (m, 6H), 7.65 – 7.59 (m, 9H). ^{13}C NMR (101 MHz, $CDCl_3$): δ (ppm) 171.70, 136.28, 132.17, 128.99, 128.65.

2,4-diphenyl-6-(p-tolyl)-1,3,5-triazine (4ab):

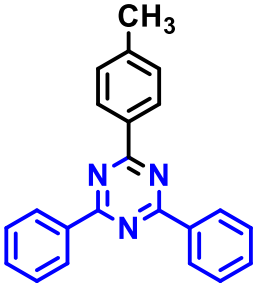

Eluent: Hexane/Ethyl acetate (50:1). White solid (yield = 94%, 303 mg). ^{1}H NMR (400 MHz, $CDCl_3$): δ (ppm) 8.80 (dt, J = 6.4, 1.7 Hz, 4H), 8.70 (d, J = 8.3 Hz, 2H), 7.64 – 7.58 (m, 6H), 7.40 (d, J = 8.0 Hz, 2H), 2.51 (s, 3H). ^{13}C NMR (101 MHz, $CDCl_3$): δ (ppm) 171.58, 143.11, 136.41, 133.60, 132.49, 132.40, 129.41, 128.99, 128.96, 128.60, 21.73.

2,4-diphenyl-6-(m-tolyl)-1,3,5-triazine (4ac):

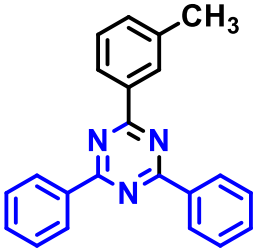

Eluent: Hexane/Ethyl acetate (50:1). White solid (yield = 85%, 274 mg). ^{1}H NMR (300 MHz, $CDCl_3$): δ (ppm) 8.84 – 8.80 (m, 4H), 8.63 – 8.60 (m, 2H), 7.64 – 7.59 (m, 6H), 7.50 – 7.47 (m, 2H), 2.56 (s, 3H). ^{13}C NMR (101 MHz, $CDCl_3$): δ (ppm) 171.80, 171.61, 138.33, 136.32, 133.36, 132.49, 132.18, 129.46, 129.13, 128.99, 128.65, 126.24, 21.60.

2,4-diphenyl-6-(o-tolyl)-1,3,5-triazine (4ad):

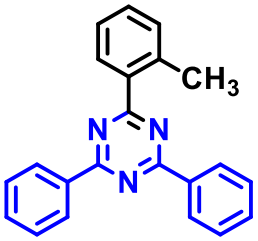

Eluent: Hexane/Ethyl acetate (50:1). White solid (yield = 75%, 242 mg). ^{1}H NMR (300 MHz, $CDCl_3$): δ (ppm) 8.84 – 8.80 (m, 4H), 8.40 – 8.37 (m, 1H), 7.61 – 7.56 (m, 6H), 7.47 – 7.42 (m, 3H), 2.88 (s, 3H). ^{13}C NMR (101 MHz, $CDCl_3$): δ (ppm) 174.58, 171.70, 139.08, 136.29, 132.51, 131.27, 129.44, 128.99, 128.68, 128.65, 127.19, 126.08, 22.70.

2-(4-isopropylphenyl)-4,6-diphenyl-1,3,5-triazine (4ae):

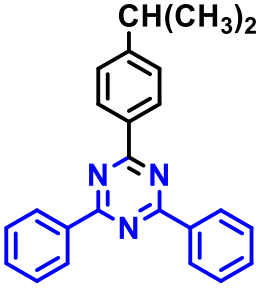

Eluent: Hexane/Ethyl acetate (50:1). White solid (yield = 89%, 312 mg). ^{1}H NMR (400 MHz, $CDCl_3$): δ (ppm) 8.82 (dd, J = 7.9, 1.8 Hz, 4H), 8.73 (d, J = 8.1 Hz, 2H), 7.65 – 7.59 (m, 6H), 7.47 (d, J = 8.0 Hz, 2H), 3.08 (p, J = 6.9 Hz, 1H), 1.38 (d, J = 6.9 Hz, 6H). ^{13}C NMR (101 MHz, $CDCl_3$): δ (ppm) 171.71, 171.55, 153.93, 136.42, 134.00, 132.41, 129.16, 128.98, 126.79, 34.34, 23.85.

2-(4-methoxyphenyl)-4,6-diphenyl-1,3,5-triazine (4af):

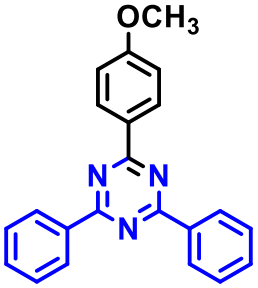

Eluent: Hexane/Ethyl acetate (50:1). White solid (yield = 94%, 319 mg). ^{1}H NMR (300 MHz, $CDCl_3$): δ (ppm) 8.82 – 8.74 (m, 6H), 7.64 – 7.58 (m, 6H), 7.12 – 7.07 (m, 2H), 3.95 (s, 3H). ^{13}C NMR (75 MHz, $CDCl_3$): δ (ppm) 171.39, 163.35, 136.45, 132.36, 130.89, 129.44, 128.92, 128.80, 128.60, 113.97, 55.47.

2-(4-fluorophenyl)-4,6-diphenyl-1,3,5-triazine (4ag):

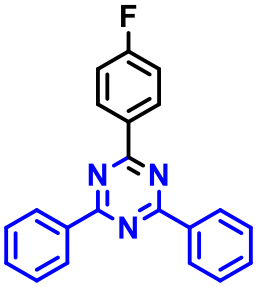

Eluent: Hexane/Ethyl acetate (50:1). White solid (yield = 87%, 284 mg). ^{1}H NMR (300 MHz, $CDCl_3$): δ (ppm) 8.81 (ddt, J = 17.0, 8.3, 1.4 Hz, 6H), 7.65 – 7.59 (m, 6H), 7.30 – 7.27 (m, 2H). ^{13}C NMR (75 MHz, $CDCl_3$): δ (ppm) 171.67, 170.68, 167.50, 136.13, 132.61, 132.53, 132.19, 131.31 (J = 9.0 Hz), 128.97, 128.67, 115.72 (J = 21.7 Hz). ^{19}F NMR (282 MHz, $CDCl_3$): δ = -107.13 (s, 1F).

2-(4-nitrophenyl)-4,6-diphenyl-1,3,5-triazine (4ah):

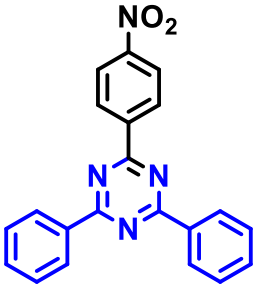

Eluent: Hexane/Ethyl acetate (30:1). White solid (yield = 60%, 212 mg). ^{1}H NMR (400 MHz, $CDCl_3$): δ (ppm) 8.97 (d, J = 8.7 Hz, 2H), 8.82 – 8.79 (m, 4H), 8.44 (d, J = 8.8 Hz, 2H), 7.66 – 7.62 (m, 6H). ^{13}C NMR (101 MHz, $CDCl_3$): δ (ppm) 172.13, 169.81, 150.40, 142.05, 135.68, 133.00, 129.87, 129.08, 128.81, 123.76.

2-(3-nitrophenyl)-4,6-diphenyl-1,3,5-triazine (4ai):

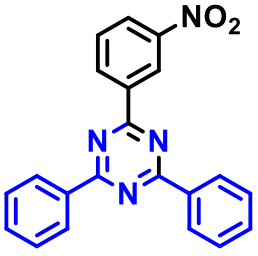

Eluent: Hexane/Ethyl acetate (30:1). White solid (yield = 54%, 191 mg). ^{1}H NMR (300 MHz, $CDCl_3$): δ (ppm) 9.54 (s, 1H), 9.08 (dt, J = 7.8, 1.4 Hz, 1H), 8.77 (dt, J = 6.7, 1.7 Hz, 4H), 8.46 (ddd, J = 8.2, 2.4, 1.1 Hz, 1H), 7.76 (t, J = 8.0 Hz, 1H), 7.69 – 7.57 (m, 6H). ^{13}C NMR (101 MHz, $CDCl_3$): δ (ppm) 171.93, 169.550, 138.10, 135.52, 133.78, 132.19, 129.86, 129.60, 128.25, 128.23, 127.92, 122.92.

2-(2-nitrophenyl)-4,6-diphenyl-1,3,5-triazine (4aj):

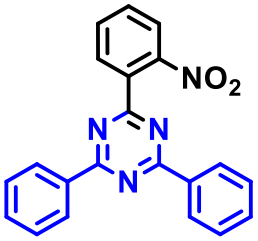

Eluent: Hexane/Ethyl acetate (30:1). White solid (yield = 48%, 170 mg). ^{1}H NMR (400 MHz, $CDCl_3$): δ (ppm) 8.81 (d, J = 9.7 Hz, 2H), 8.70 – 8.63 (m, 3H), 7.80 – 7.59 (m, 9H). ^{13}C NMR (101 MHz, $CDCl_3$): δ (ppm) 171.92, 171.69, 150.79, 136.28, 135.52, 132.95, 132.51, 129.17, 128.99, 128.79, 128.65, 123.88.

2,4-diphenyl-6-(4-(trifluoromethyl)phenyl)-1,3,5-triazine (4ak):

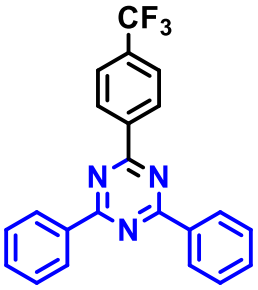

Eluent: Hexane/Ethyl acetate (50:1). White solid (yield = 53%, 200 mg). ^{1}H NMR (300 MHz, $CDCl_3$): δ (ppm) 8.88 (d, J = 8.3 Hz, 1H), 8.80 – 8.76 (m, 4H), 7.84 (d, J = 7.8 Hz, 3H), 7.64 – 7.60 (m, 5H). ^{13}C NMR (101 MHz, $CDCl_3$): δ (ppm) 171.90, 170.43, 139.57, 135.87, 133.62, 132.80, 129.24, 129.02, 128.72, 125.55 (q, J = 3.8 Hz), 122.21. ^{19}F NMR (282 MHz, $CDCl_3$): δ = -62.55 (s, 3F).

2-(4-bromophenyl)-4,6-diphenyl-1,3,5-triazine (4al):

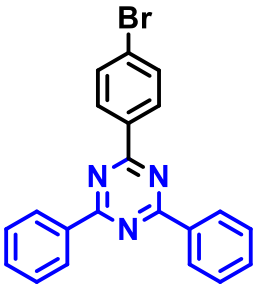

Eluent: Hexane/Ethyl acetate (50:1). White solid (yield = 80%, 310 mg). ^{1}H NMR (400 MHz, $CDCl_3$): δ (ppm) 8.80 – 8.76 (m, 4H), 8.68 – 8.65 (m, 2H), 7.74 – 7.71 (m, 2H), 7.65 – 7.58 (m, 6H). ^{13}C NMR (101 MHz, $CDCl_3$): δ (ppm) 171.79, 170.89, 136.07, 135.25, 132.63, 131.91, 130.48, 128.99, 128.67, 127.47.

2-(4-chlorophenyl)-4,6-diphenyl-1,3,5-triazine (4am):

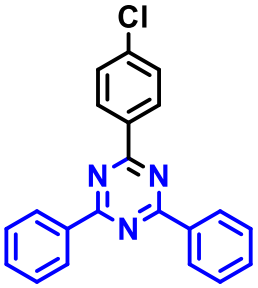

Eluent: Hexane/Ethyl acetate (50:1). White solid (yield = 85%, 291 mg). ^{1}H NMR (400 MHz, $CDCl_3$): δ (ppm) 8.76 – 8.74 (m, 4H), 8.72 – 8.69 (m, 2H), 7.57 – 7.54 (m, 2H), 7.53 (d, J = 1.8 Hz, 1H), 7.51 – 7.48 (m, 5H). ^{13}C NMR (101 MHz, $CDCl_3$): δ (ppm) 171.68, 170.67, 145.04, 138.79, 136.04, 134.74, 132.76, 132.15, 130.28, 129.13, 128.98.

2-(naphthalen-2-yl)-4,6-diphenyl-1,3,5-triazine (4an):

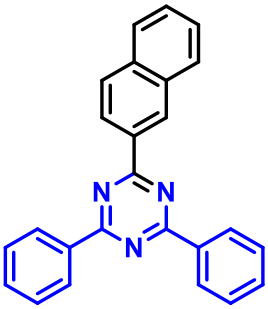

Eluent: Hexane/Ethyl acetate (50:1). White solid (yield = 78%, 280 mg). ^{1}H NMR (300 MHz, $CDCl_3$): δ (ppm) 9.35 (s, 1H), 8.87 – 8.82 (m, 5H), 8.04 (d, J = 8.6 Hz, 2H), 7.66 – 7.60 (m, 9H). ^{13}C NMR (101 MHz, $CDCl_3$): δ (ppm) 171.69, 136.31, 135.71, 133.64, 133.14, 132.54, 129.70, 129.58, 129.03, 128.68, 128.56, 127.87, 126.48, 125.15.

2-(naphthalen-1-yl)-4,6-diphenyl-1,3,5-triazine (4ao):

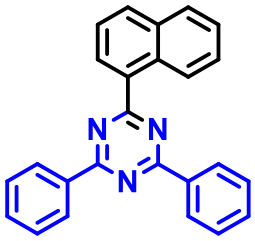

Eluent: Hexane/Ethyl acetate (50:1). White solid (yield = 75%, 269 mg). ^{1}H NMR (300 MHz, $CDCl_3$): δ (ppm) 9.22 (dd, J = 8.6, 1.2 Hz, 1H), 8.87 – 8.83 (m, 4H), 8.59 (dd, J = 7.3, 1.4 Hz, 1H), 8.11 (d, J = 8.2 Hz, 1H), 8.03 – 8.00 (m, 1H), 7.73 – 7.60 (m, 9H). ^{13}C NMR (101 MHz, $CDCl_3$): δ (ppm) 174.43, 171.55, 136.25, 134.30, 134.05, 132.62, 132.31, 131.43, 130.75, 129.10, 128.73, 127.24, 126.17, 126.08, 125.17.

2-(anthracen-9-yl)-4,6-diphenyl-1,3,5-triazine (4ap):

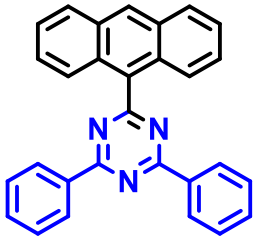

Eluent: Hexane/Ethyl acetate (50:1). White solid (yield = 69%, 282 mg). ^{1}H NMR (400 MHz, $CDCl_3$): δ (ppm) 8.80 – 8.78 (m, 4H), 8.67 (s, 1H), 8.13 (d, J = 8.4 Hz, 2H), 7.97 (d, J = 8.7 Hz, 2H), 7.65 – 7.48 (m, 10H). ^{13}C NMR (75 MHz, $CDCl_3$): δ (ppm) 175.67, 171.95, 135.89, 132.89, 131.44, 129.62, 129.29, 129.01, 128.96, 128.79, 128.70, 126.62, 125.57, 125.35. HRMS (ESI) m/z calcd for $C_{29}H_{20}N_3$ $[M + H]^+$ 410.1657, found 410.1653.

2-(furan-3-yl)-4,6-diphenyl-1,3,5-triazine (4aq):

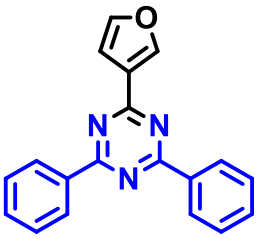

Eluent: Hexane/Ethyl acetate (30:1). White solid (yield = 65%, 194 mg). ^{1}H NMR (300 MHz, $CDCl_3$): δ (ppm) 8.75 – 8.72 (m, 4H), 8.57 (dd, J = 1.7, 0.7 Hz, 1H), 7.62 – 7.58 (m, 7H), 7.47 – 7.42 (m, 1H). ^{13}C NMR (75 MHz, $CDCl_3$): δ (ppm) 171.50, 168.48, 144.16, 136.06, 132.78, 132.51, 132.18, 129.13, 128.90, 128.62.

2,4-diphenyl-6-(pyridin-4-yl)-1,3,5-triazine (4ar):

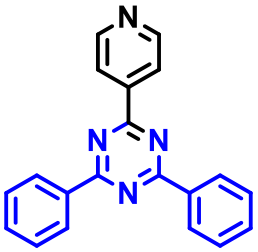

Eluent: Hexane/Ethyl acetate (50:1). White solid (yield = 50%, 155 mg). ^{1}H NMR (300 MHz, $CDCl_3$): δ (ppm) 8.81 (dd, J = 7.9, 1.9 Hz, 2H), 7.69 (dd, J = 7.0, 1.5 Hz, 4H), 7.63 – 7.60 (m, 4H), 7.53 – 7.48 (m, 4H). 7.47 – 7.44 (m, 1H). ^{13}C NMR (101 MHz, $CDCl_3$): δ (ppm) 171.69, 151.83, 139.28, 136.28, 132.75, 132.17, 129.12, 128.65, 118.82. HRMS (ESI) m/z calcd for $C_{20}H_{15}N_4$ $[M + H]^+$ 311.1297, found 311.1295.

2,4-diphenyl-6-(pyridin-3-yl)-1,3,5-triazine(4as):

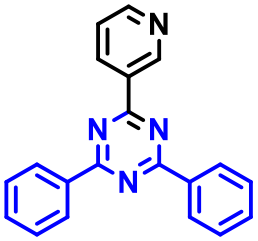

Eluent: Hexane/Ethyl acetate (50:1). White solid (yield = 55%, 178 mg). ^{1}H NMR (300 MHz, $CDCl_3$): δ (ppm) 9.29 (s, 1H), 8.83 (d, J = 1.6 Hz, 2H), 8.80 (d, J = 2.0 Hz, 2H), 8.41 – 8.36 (m, 2H), 7.65 – 7.61 (m, 7H). ^{13}C NMR (75 MHz, $CDCl_3$): δ (ppm) 171.68, 171.38, 166.76, 145.04, 136.27, 132.53, 128.99, 128.92, 128.78, 128.66, 127.21.

2,4-diphenyl-6-(pyridin-2-yl)-1,3,5-triazine (4at):

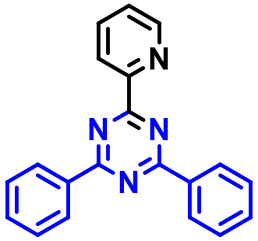

Eluent: Hexane/Ethyl acetate (50:1). White solid (yield = 40%, 124 mg). ^{1}H NMR (300 MHz, $CDCl_3$): δ (ppm) 8.83 – 8.80 (m, 4H), 7.70 – 7.67 (m, 3H), 7.64 – 7.60 (m, 5H), 7.51 (d, J = 7.9 Hz, 2H).^{13}C NMR (101 MHz, $CDCl_3$): δ (ppm) 171.65, 154.64, 149.36, 137.37, 137.18, 132.53, 130.69, 128.87, 127.48, 125.32.

2,4-diphenyl-1,3,5-triazine (5aa):

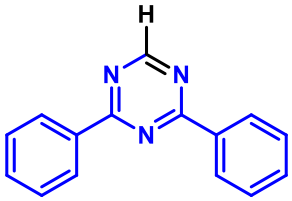

Eluent: Hexane/Ethyl acetate (50:1). White solid (yield = 62%, 144 mg). ^{1}H NMR (300 MHz, $CDCl_3$): δ (ppm) 9.28 (s, 1H), 8.69 – 8.65 (m, 4H), 7.64 – 7.55 (m, 6H). ^{13}C NMR (101 MHz, $CDCl_3$): δ (ppm) 171.36, 166.75, 135.61, 132.82, 129.93, 128.76.

2-methyl-4,6-diphenyl-1,3,5-triazine (5ab):

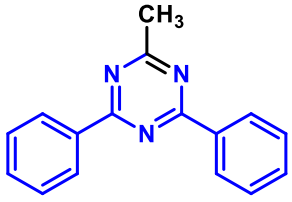

Eluent: Hexane/Ethyl acetate (50:1). White solid (yield = 60%, 148 mg). ^{1}H NMR (300 MHz, $CDCl_3$): δ (ppm) 8.69 – 8.65 (m, 4H), 7.62 – 7.56 (m, 6H), 2.82 (s, 3H). ^{13}C NMR (75 MHz,

$CDCl_3$): δ (ppm) 177.10, 171.28, 135.98, 132.78, 132.48, 132.18, 129.13, 128.90, 128.66, 26.11.

2,4-di-p-tolyl-1,3,5-triazine (5ac):

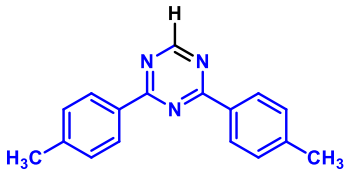

Eluent: Hexane/Ethyl acetate (50:1). White solid (yield = 65%, 170 mg). ^{1}H NMR (300 MHz, $CDCl_3$): δ (ppm) 9.22 (s, 1H), 8.55 (d, J = 8.3 Hz, 4H), 7.37 (d, J = 8.1 Hz, 4H), 2.49 (s, 6H). ^{13}C NMR (101 MHz, $CDCl_3$): δ (ppm) 171.22, 166.51, 143.51, 132.92, 129.54, 128.92, 21.75.

2,4-bis(4-chlorophenyl)-1,3,5-triazine (5ad):

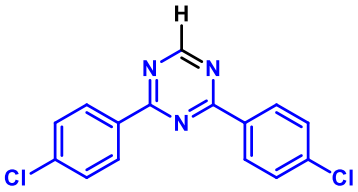

Eluent: Hexane/Ethyl acetate (50:1). White solid (yield = 57%, 172 mg). ^{1}H NMR (300 MHz, $CDCl_3$): δ (ppm) 9.26 (s, 1H), 8.60 (d, J = 8.5 Hz, 4H), 7.55 (d, J = 8.6 Hz, 4H). ^{13}C NMR (101 MHz, $CDCl_3$): δ (ppm) 170.58, 166.85, 139.38, 133.90, 130.26, 129.13. HRMS (ESI) m/z calcd for $C_{15}H_{10}Cl_2N_3$ $[M + H]^+$ 302.0252, found 302.0255.

2-ethyl-4,6-diphenyl-1,3,5-triazine (5ae):

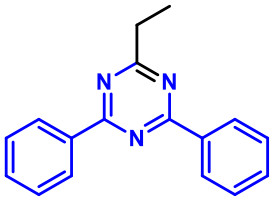

Eluent: Hexane/Ethyl acetate (50:1). White solid (yield = 61%, 159 mg). ^{1}H NMR (400 MHz, $CDCl_3$): δ (ppm) 8.73 – 8.66 (m, 4H), 7.63 – 7.54 (m, 6H), 2.85 (q, J = 9.1, 8.4 Hz, 2H), 1.39 (t, J = 7.7 Hz, 3H). ^{13}C NMR (75 MHz, $CDCl_3$): δ (ppm) 180.85, 169.66, 136.53, 132.23, 128.90, 128.84, 32.51, 12.70. HRMS (ESI) m/z calcd for $C_{17}H_{16}N_3$ $[M + H]^+$ 262.1344, found 262.1348

2-isopropyl-4,6-diphenyl-1,3,5-triazine (5af):

Eluent: Hexane/Ethyl acetate (50:1). White solid (yield = 62%, 171 mg). ^{1}H NMR (300 MHz, $CDCl_3$): δ (ppm) 8.74 – 8.69 (m, 4H), 7.62 – 7.56 (m, 6H), 3.29 (p, J = 6.9 Hz, 1H), 1.51 (dd, J = 6.9, 0.7 Hz, 1H). ^{13}C NMR (75 MHz, $CDCl_3$): δ (ppm) 184.01, 171.24, 136.32, 132.83, 132.34, 128.92, 128.78, 128.61, 37.56, 21.17.

2-butyl-4,6-diphenyl-1,3,5-triazine (5ag):

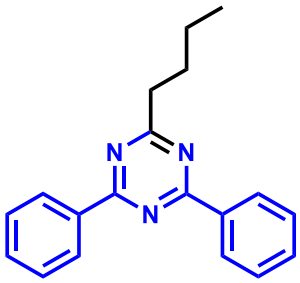

Eluent: Hexane/Ethyl acetate (50:1). White solid (yield = 66%, 191 mg). ^{1}H NMR (400 MHz, $CDCl_3$): δ (ppm) 8.71 – 8.66 (m, 4H), 7.62 – 7.54 (m, 6H), 3.05 – 3.02 (m, 2H), 2.04 – 1.96 (m, 2H), 1.49 – 1.46 (m, 2H), 0.97 (t, J = 6.8 Hz, 3H). ^{13}C NMR (75 MHz, $CDCl_3$): δ (ppm) 180.21, 170.91, 136.13, 132.38, 128.97, 128.66, 38.26, 30.61, 22.53, 14.04. HRMS (ESI) m/z calcd for $C_{19}H_{20}N_3$ $[M + H]^+$ 290.1657, found 290.1651

2-pentyl-4,6-diphenyl-1,3,5-triazine (5ah):

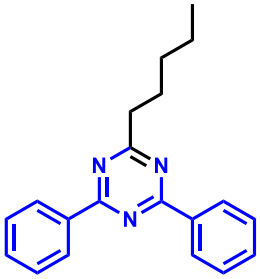

Eluent: Hexane/Ethyl acetate (50:1). White solid (yield = 67%, 203 mg). ^{1}H NMR (400 MHz, $CDCl_3$): δ (ppm) 8.70 – 8.68 (m, 4H), 7.65 – 7.57 (m, 6H), 3.10 – 3.00 (m, 2H), 2.04 – 1.96 (m, 2H), 1.50 – 1.46 (m, 2H), 1.37 – 1.32 (m, 2H), 0.97 (t, J = 6.9 Hz, 3H). ^{13}C NMR (101 MHz, $CDCl_3$): δ (ppm) 180.22, 171.19, 136.18, 132.38, 128.91, 128.63, 39.24, 31.61, 27.42, 22.56, 14.06. HRMS (ESI) m/z calcd for $C_{20}H_{22}N_3$ $[M + H]^+$ 304.1814, found 304.1818

2,4-bis(4-chlorophenyl)-6-phenyl-1,3,5-triazine (6aa):

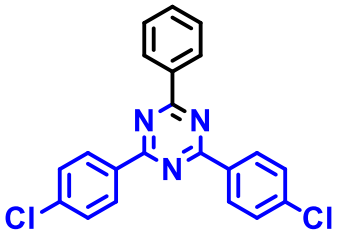

Eluent: Hexane/Ethyl acetate (50:1). White solid (yield = 78%, 295 mg). ^{1}H NMR (400 MHz, $CDCl_3$): δ (ppm) 8.76 – 8.70 (m, 6H), 7.64 – 7.55 (m, 7H). ^{13}C NMR (101 MHz, $CDCl_3$): δ (ppm) 171.81, 170.82, 138.98, 134.54, 133.37, 132.82, 131.19, 130.31, 128.99, 128.74.

2,4-bis(4-chlorophenyl)-6-(p-tolyl)-1,3,5-triazine (6ab):

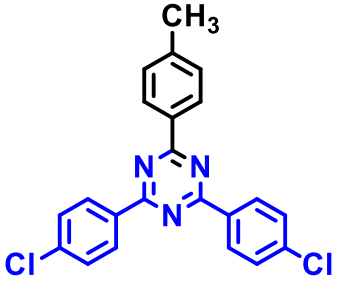

Eluent: Hexane/Ethyl acetate (50:1). White solid (yield = 85%, 333 mg). ^{1}H NMR (300 MHz, $CDCl_3$): δ (ppm) 8.71 (d, J = 8.6 Hz, 4H), 8.64 (d, J = 8.1 Hz, 2H), 7.56 (d, J = 8.6 Hz, 4H), 7.39 (d, J = 8.0 Hz, 2H), 2.51 (s, 3H). ^{13}C NMR (101 MHz, $CDCl_3$): δ (ppm) 171.82, 170.73, 134.68, 134.55, 133.17, 130.83, 130.29, 129.70, 128.95, 128.64, 21.79.

2,4-bis(4-chlorophenyl)-6-(4-isopropylphenyl)-1,3,5-triazine (6ac):

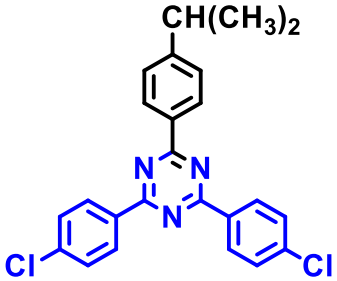

Eluent: Hexane/Ethyl acetate (50:1). White solid (yield = 82%, 344 mg). ^{1}H NMR (400 MHz, $CDCl_3$): δ (ppm) 8.66 (d, J = 8.0 Hz, 6H), 7.65 – 7.60 (m, 4H), 7.45 (d, J = 8.2 Hz, 2H), 3.06 (p, J = 6.9 Hz, 1H), 1.36 (d, J = 6.9 Hz, 6H). ^{13}C NMR (101 MHz, $CDCl_3$): δ (ppm) 171.84, 170.84, 170.72, 154.31, 138.98, 135.86, 134.68, 134.56, 132.80, 130.31, 129.15, 128.99, 128.73, 126.87, 34.34, 23.81. HRMS (ESI) m/z calcd for $C_{24}H_{20}Cl_2N_3$ $[M + H]^+$ 420.1034, found 420.1030.

2,4-bis(4-chlorophenyl)-6-(4-fluorophenyl)-1,3,5-triazine (6ad):

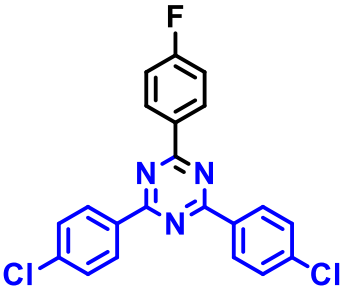

Eluent: Hexane/Ethyl acetate (50:1). White solid (yield = 75%, 297 mg). ^{1}H NMR (400 MHz, $CDCl_3$): δ (ppm) 8.79 – 8.75 (m, 2H), 8.72 – 8.68 (m, 3H), 7.67 – 7.55 (m, 4H), 7.29 – 7.25 (m, 3H). ^{13}C NMR (101 MHz, $CDCl_3$): δ (ppm) 172.84, 170.84, 164.70, 139.08, 134.43, 131.41, 131.32, 130.29, 129.01, 128.73, 115.94, 115.72. ^{19}F NMR (282 MHz, $CDCl_3$): δ = -106.50 (s, 1F). HRMS (ESI) m/z calcd for $C_{21}H_{13}Cl_2FN_3$ $[M + H]^+$ 396.0471, found 396.0468.

2,4-bis(4-chlorophenyl)-6-(3-nitrophenyl)-1,3,5-triazine (6ae):

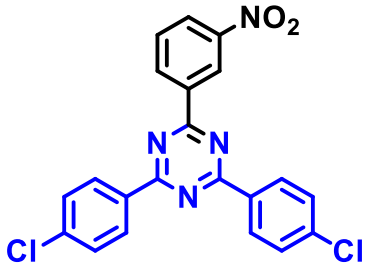

Eluent: Hexane/Ethyl acetate (50:1). White solid (yield = 62%, 262 mg). ^{1}H NMR (300 MHz, $CDCl_3$): δ (ppm) 9.52 (t, J = 1.9 Hz, 1H), 9.06 (dt, J = 7.8, 1.4 Hz, 1H), 8.70 (d, J = 8.6 Hz, 4H), 8.49 (ddd, J = 8.2, 2.4, 1.1 Hz, 1H), 7.79 (t, J = 8.0 Hz, 1H), 7.60 – 7.54 (m, 4H). ^{13}C NMR (75 MHz, $CDCl_3$): δ (ppm) 171.25, 169.83, 148.81, 139.56, 137.76, 134.53, 133.89, 130.40, 129.80, 129.15, 127.05, 123.83. HRMS (ESI) m/z calcd for $C_{21}H_{13}Cl_2N_4O_2$ $[M + H]^+$ 423.0416, found 423.0413.

2,4,6-tris(4-chlorophenyl)-1,3,5-triazine (6af):

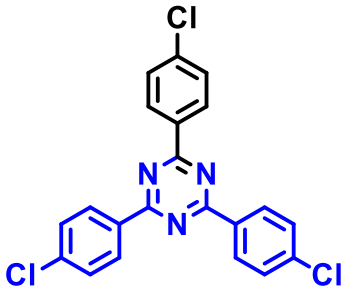

Eluent: Hexane/Ethyl acetate (50:1). White solid (yield = 78%, 321 mg). ^{1}H NMR (400 MHz, $CDCl_3$): δ (ppm) 8.77 – 8.70 (m, 6H), 7.62 – 7.56 (m, 6H). ^{13}C NMR (101 MHz, $CDCl_3$): δ (ppm) 171.67, 136.27, 132.53, 128.99, 128.66.

2,4-bis(4-chlorophenyl)-6-(thiophen-2-yl)-1,3,5-triazine (6ag):

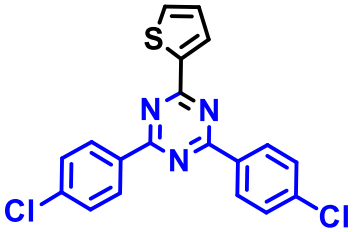

Eluent: Hexane/Ethyl acetate (50:1). White solid (yield = 61%, 234 mg). ^{1}H NMR (400 MHz, $CDCl_3$): δ (ppm) 8.75 (d, J = 7.5 Hz, 2H), 8.65 (d, J = 8.3 Hz, 4H), 8.36 (d, J = 3.7 Hz, 1H),

7.69 – 7.60 (m, 3H), 7.27 – 7.25 (m, 1H). ^{13}C NMR (101 MHz, $CDCl_3$): δ (ppm) 170.84, 170.71, 168.19, 141.73, 134.25, 132.58, 131.82, 130.29, 128.96, 128.73, 128.60.

2,4-bis(4-fluorophenyl)-6-phenyl-1,3,5-triazine (6ah):

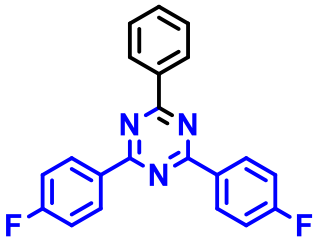

Eluent: Hexane/Ethyl acetate (50:1). White solid (yield = 65%, 224 mg). ^{1}H NMR (400 MHz, $CDCl_3$): δ (ppm) 8.83 – 8.75 (m, 6H), 7.66 – 7.59 (m, 3H), 7.30 – 7.25 (m, 4H). ^{13}C NMR (101 MHz, $CDCl_3$): δ (ppm) 171.67, 170.68, 167.54, 136.00, 133.73, 132.69, 131.37, 131.25, 130.20, 128.95, 128.70, 128.51, 115.90, 115.61. ^{19}F NMR (282 MHz, $CDCl_3$): δ = -106.95 (s, 1F).

2,4-bis(4-fluorophenyl)-6-(p-tolyl)-1,3,5-triazine (6ai):

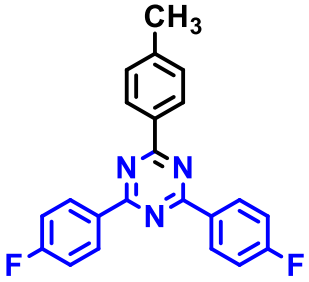

Eluent: Hexane/Ethyl acetate (50:1). White solid (yield = 70%, 258 mg). ^{1}H NMR (300 MHz, $CDCl_3$): δ (ppm) 8.71 (d, J = 8.5 Hz, 4H), 8.65 (d, J = 8.0 Hz, 2H), 7.56 (d, J = 8.6 Hz, 4H), 7.40 (d, J = 8.0 Hz, 2H), 2.51 (s, 3H). ^{13}C NMR (101 MHz, $CDCl_3$): δ (ppm) 171.80, 170.71, 143.53, 138.86, 134.66, 133.14, 130.29, 129.51, 129.00, 128.95, 21.81. ^{19}F NMR (377 MHz, $CDCl_3$): δ = -106.50 (s, 2F). HRMS (ESI) m/z calcd for $C_{22}H_{16}F_2N_3$ $[M + H]^+$ 360.1312, found 360.1315.

All the reactions were carried out in 1.0 mmol scale of reactant and according to the general procedure for the synthesis of pyrimidine derivatives

2,4,6-triphenylpyrimidine (7aa):

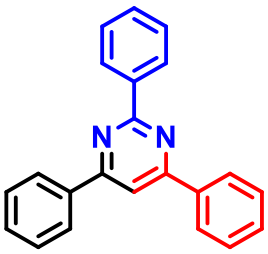

Eluent: Hexane/Ethyl acetate (60:1). White solid (yield: condition **A** = 87%, 268 mg; condition **B** = 90%, 277 mg). ^{1}H NMR (400 MHz, $CDCl_3$): δ (ppm) 8.82 (d, J = 6.4 Hz, 2H), 8.79 – 8.74 (m, 2H), 8.36 – 8.32 (m, 2H), 8.05 (s, 1H), 7.65 – 7.54 (m, 9H). ^{13}C NMR (101 MHz, $CDCl_3$): δ (ppm) 164.80, 164.55, 137.59, 132.51, 130.79, 128.94, 128.65, 128.46, 127.31, 110.33.

2,4-diphenyl-6-(p-tolyl)pyrimidine (7ab):

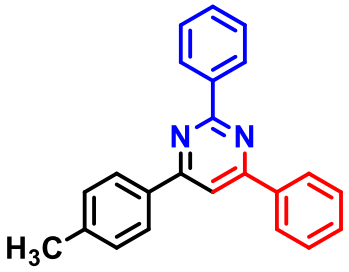

Eluent: Hexane/Ethyl acetate (60:1). White solid (yield: condition **A** = 89%, 286 mg; condition **B** = 92%, 296 mg). ^{1}H NMR (300 MHz, $CDCl_3$): δ (ppm) 8.80 – 8.74 (m, 2H), 8.35 – 8.30 (m, 2H), 8.25 – 8.21 (m, 2H), 8.02 (s, 1H), 7.60 – 7.57 (m, 6H), 7.40 (d, J = 5.0 Hz, 2H), 2.49 (s, 3H). ^{13}C NMR (75 MHz, $CDCl_3$): δ (ppm) 164.69, 164.62, 164.44, 141.18, 137.66, 136.38, 134.72, 132.44, 129.67, 128.97, 128.63, 128.50, 128.46, 127.31, 127.21, 109.97, 21.53.

2,4-diphenyl-6-(m-tolyl)pyrimidine (7ac):

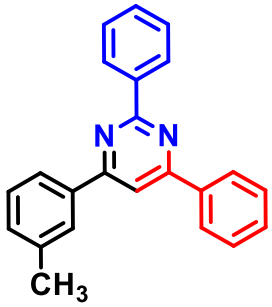

Eluent: Hexane/Ethyl acetate (60:1). White solid (yield: condition **A** = 84%, 270 mg; condition **B** = 88%, 283 mg). ^{1}H NMR (300 MHz, $CDCl_3$): δ (ppm) 8.83 – 8.81 (m, 2H), 8.37 – 8.32 (m, 2H), 8.01 (s, 1H), 7.66 – 7.60 (m, 7H), 7.52 – 7.47 (m, 2H), 7.41 – 7.38 (m, 1H), 2.56 (s, 3H). ^{13}C NMR (75 MHz, $CDCl_3$): δ (ppm) 164.89, 164.61, 164.47, 138.61, 138.31, 137.59, 137.51, 136.35, 132.50, 131.63, 130.80, 130.68, 129.04, 128.94, 128.66, 128.59, 127.95, 127.35, 110.35, 21.70.

2,4-diphenyl-6-(o-tolyl)pyrimidine (7ad):

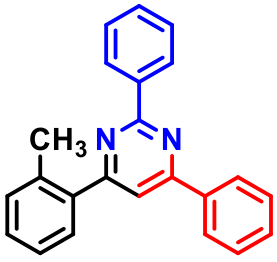

Eluent: Hexane/Ethyl acetate (60:1). White solid (yield: condition **A** = 80%, 258 mg; condition **B** = 85%, 274 mg). ^{1}H NMR (300 MHz, $CDCl_3$): δ (ppm) 8.80 – 8.77 (m, 2H), 8.35 – 8.29 (m, 2H), 7.78 (s, 1H), 7.63 – 7.55 (m, 7H), 7.44 – 7.39 (m, 3H), 2.62 (s, 3H). ^{13}C NMR (75 MHz, $CDCl_3$): δ (ppm) 164.79, 164.20, 164.06, 138.64, 138.12, 137.38, 136.55, 132.56, 131.32, 130.69, 129.69, 129.01, 128.98, 128.71, 128.52, 127.31, 127.21, 114.41, 20.78.

4-(4-methoxyphenyl)-2,6-diphenylpyrimidine (7ae):

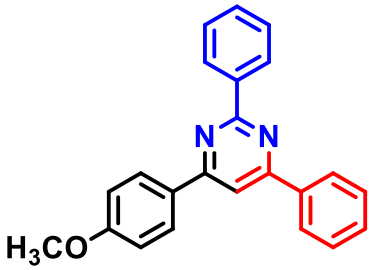

Eluent: Hexane/Ethyl acetate (60:1). White solid (yield: condition **A** = 91%, 307 mg; condition **B** = 93%, 314 mg). ^{1}H NMR (300 MHz, $CDCl_3$): δ (ppm) 8.78 – 8.75 (m, 2H), 8.34 – 8.28 (m, 4H), 7.97 (s, 1H), 7.59 – 7.55 (m, 6H), 7.09 (d, J = 8.9 Hz, 2H), 3.93 (s, 3H). ^{13}C NMR (75 MHz, $CDCl_3$) δ 164.50, 164.37, 164.22, 161.94, 138.33, 137.74, 130.66, 130.55, 129.98, 128.92, 128.81, 128.60, 128.47, 128.43, 127.27, 114.27, 113.98, 109.44, 55.47.

4-(3-nitrophenyl)-2,6-diphenylpyrimidine (7af):

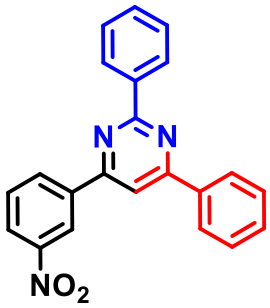

Eluent: Hexane/Ethyl acetate (60:1). White solid (yield: condition **A** = 74%, 261 mg; condition **B** = 76%, 268 mg). ^{1}H NMR (300 MHz, $CDCl_3$): δ (ppm) 9.13 (t, J = 2.0 Hz, 1H), 8.77 – 8.73 (m, 2H), 8.34 – 8.31 (m, 2H), 8.70 – 8.66 (m, 1H), 8.44 – 8.40 (m, 1H), 8.35 – 8.32 (m, 2H), 8.08 (s, 1H), 7.78 (t, J = 8.0 Hz, 1H), 7.62 – 7.57 (m, 6H). ^{13}C NMR (75 MHz, $CDCl_3$): δ (ppm) 165.55, 164.90, 162.25, 157.87, 148.89, 139.36, 137.60, 137.01, 133.11, 131.24, 131.07, 130.01, 129.06, 128.61, 128.55, 127.38, 125.26, 122.18, 110.29.

2,4-diphenyl-6-(4-(trifluoromethyl)phenyl)pyrimidine: (7ag):

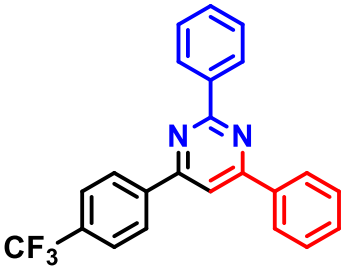

Eluent: Hexane/Ethyl acetate (60:1). White solid (yield: condition **A** = 80%, 300 mg; condition **B** = 83%, 312 mg). ^{1}H NMR (300 MHz, $CDCl_3$): δ (ppm) 8.88 (d, J = 8.3 Hz, 2H), 8.80 – 8.76 (m, 4H), 8.03 (s, 1H), 7.61 – 7.56 (m, 8H). ^{13}C NMR (75 MHz, $CDCl_3$) δ 165.21, 164.74, 163.27, 137.81, 137.19, 135.87, 132.80, 130.99 (d, J = 12.1 Hz), 129.24, 129.02, 128.72, 128.54, 128.51, 125.86 (d, J = 3.9 Hz), 125.55 (d, J = 3.8 Hz), 110.54. ^{19}F NMR (282 MHz, $CDCl_3$): δ = -62.70 (s, 1F).

4-(4-fluorophenyl)-2,6-diphenylpyrimidine (7ah):

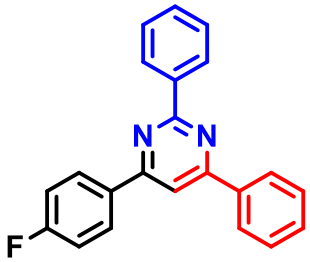

Eluent: Hexane/Ethyl acetate (60:1). White solid (yield: condition **A** = 83%, 270 mg; condition **B** = 85%, 277 mg). ^{1}H NMR (300 MHz, $CDCl_3$): δ (ppm) 8.77 – 8.73 (m, 2H), 8.34 – 8.28 (m, 4H), 7.94 (s, 1H), 7.60 – 7.56 (m, 6H), 7.27 – 7.22 (m, 2H). ^{13}C NMR (75 MHz, $CDCl_3$): δ (ppm) 164.79, 164.47, 163.56, 162.95, 138.05, 137.41, 132.60, 130.81 (d, J = 9.6 Hz), 129.32 (d, J = 8.6 Hz), 128.95, 128.49, 128.40, 127.29, 115.94 (d, J = 21.7 Hz), 109.83. ^{19}F NMR (282 MHz, $CDCl_3$): δ = -110.72 (s, 1F).

4-(4-chlorophenyl)-2,6-diphenylpyrimidine (7ai):

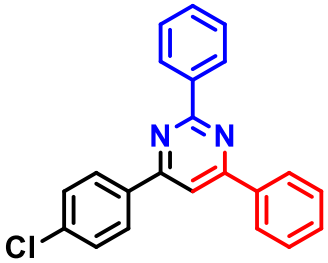

Eluent: Hexane/Ethyl acetate (60:1). White solid (yield: condition **A** = 82%, 280 mg; condition **B** = 85%, 291 mg). ^{1}H NMR (300 MHz, $CDCl_3$): δ (ppm) 8.77 – 8.69 (m, 3H), 8.30 – 8.27 (m, 2H), 8.22 (d, J = 8.6 Hz, 2H), 7.91 (s, 1H)), 7.59 – 7.55 (m, 7H), ^{13}C NMR (75 MHz, $CDCl_3$): δ (ppm) 164.84, 164.48, 163.37, 137.97, 137.31, 136.98, 135.87, 132.65, 130.93, 130.80, 129.13, 128.95, 128.56, 128.51, 127.30, 109.87.

4-(naphthalen-2-yl)-2,6-diphenylpyrimidine (7aj):

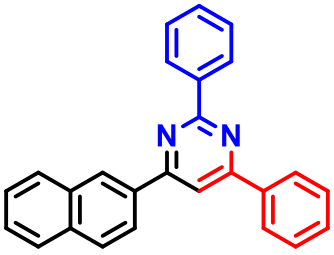

Eluent: Hexane/Ethyl acetate (60:1). White solid (yield: condition **A** = 85%, 304 mg; condition **B** = 88%, 315 mg). ^{1}H NMR (300 MHz, $CDCl_3$): δ (ppm) 8.85 – 8.79 (m, 3H), 8.10 (s, 1H), 8.08 – 8.06 (m, 3H), 7.92 – 7.88 (m, 3H), 7.62 – 7.54 (m, 8H). ^{13}C NMR (101 MHz, $CDCl_3$): δ (ppm) 164.73, 164.53, 164.50, 138.27, 136.31, 135.71, 134.92, 134.62, 133.34, 130.64, 130.04, 129.70, 129.03, 128.68, 128.56, 127.88, 127.30, 126.58, 124.34, 110.24.

4-(naphthalen-1-yl)-2,6-diphenylpyrimidine (7ak):

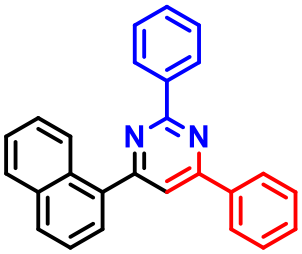

Eluent: Hexane/Ethyl acetate (60:1). White solid (yield: condition **A** = 83%, 297 mg; condition **B** = 85%, 304 mg). ^{1}H NMR (400 MHz, $CDCl_3$): δ (ppm) 8.87 – 8.75 (m, 2H), 8.50 – 8.44 (m, 1H), 8.38 (t, J = 7.7 Hz, 2H), 8.08 – 8.00 (m, 2H), 7.96 (s, 1H), 7.86 (td, J = 7.3, 3.3 Hz, 1H), 7.70 – 7.56 (m, 9H). ^{13}C NMR (75 MHz, $CDCl_3$): δ (ppm) 167.55, 164.48, 164.39, 138.17, 137.35, 136.93, 134.13, 131.01, 130.94, 130.85, 130.27, 129.06, 128.70, 128.63, 128.00, 127.44, 126.31, 125.57, 125.42, 115.44.

4-(1H-imidazol-2-yl)-2,6-diphenylpyrimidine (7al):

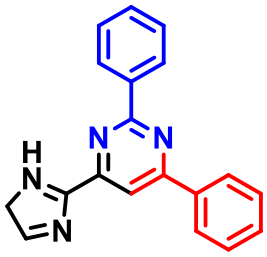

Eluent: Hexane/Ethyl acetate (60:1). White solid (yield: condition **A** = 75%, 224 mg; condition **B** = 78%, 233 mg). ^{1}H NMR (400 MHz, $CDCl_3$): δ (ppm) 8.64 (dd, J = 6.8, 3.0 Hz, 2H), 8.48 (s, 1H), 8.36 (dd, J = 6.6, 3.0 Hz, 2H), 7.58 – 7.54 (m, 6H), 7.35 (s, 1H). ^{13}C NMR (101 MHz, $CDCl_3$): δ (ppm) 165.13, 164.27, 155.20, 144.99, 137.60, 136.83, 131.14, 130.88, 129.07, 128.93, 128.52, 128.33, 127.40, 109.29. HRMS (ESI) m/z calcd for $C_{19}H_{15}N_4$ $[M + H]^+$ 299.1297, found 299.1295.

4-(furan-3-yl)-2,6-diphenylpyrimidine (7am):

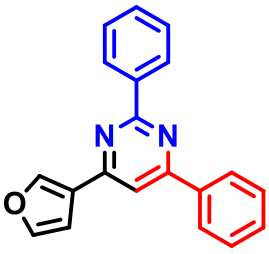

Eluent: Hexane/Ethyl acetate (60:1). White solid (yield: condition **A** = 82%, 244 mg; condition **B** = 85%, 253 mg). ^{1}H NMR (300 MHz, $CDCl_3$): δ (ppm) 8.75 – 8.72 (m, 2H), 8.30 – 8.26 (m, 2H), 7.71 (s, 1H), 7.61 (s, 1H), 7.57– 7.53 (m, 8H). ^{13}C NMR (75 MHz, $CDCl_3$): δ (ppm) 167.46, 164.29, 158.63, 157.86, 144.21, 137.85, 137.52, 132.52, 130.54, 128.90, 128.62, 128.45, 127.23, 113.76, 109.66, 108.48.

2-(2,6-diphenylpyrimidin-4-yl)quinoline (7an):

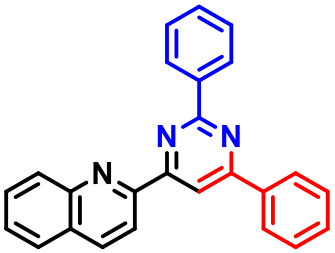

Eluent: Hexane/Ethyl acetate (60:1). White solid (yield: condition **A** = 80%, 288 mg; condition **B** = 82%, 295 mg). ^{1}H NMR (400 MHz, $CDCl_3$): δ (ppm) 9.00 (s, 1H), 8.90 (d, J = 8.5 Hz, 1H), 8.81 (d, J = 7.2 Hz, 2H), 8.47 (d, J = 7.3 Hz, 2H), 8.41 (d, J = 8.6 Hz, 1H), 8.30 (d, J = 9.1 Hz, 1H), 7.95 (d, J = 8.2 Hz, 1H), 7.83 (t, J = 7.7 Hz, 1H), 7.65– 7.55 (m, 7H). ^{13}C NMR (75 MHz, $CDCl_3$): δ (ppm) 165.10, 164.32, 154.74, 147.96, 138.07, 137.45, 137.09, 132.55, 130.90, 130.74, 130.06, 129.90, 128.99, 128.91, 128.68, 128.56, 128.47, 127.77, 127.52, 119.21, 111.21. HRMS (ESI) m/z calcd for $C_{25}H_{18}N_3$ $[M + H]^+$ 360.1501, found 360.1356.

2,4-diphenyl-6-(pyridin-4-yl)pyrimidine (7ao):

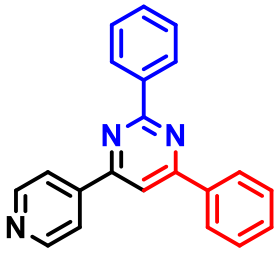

Eluent: Hexane/Ethyl acetate (60:1). White solid (yield: condition **A** = 72%, 222 mg; condition **B** = 75%, 232 mg). ^{1}H NMR (300 MHz, $CDCl_3$): δ (ppm) 8.83 – 8.74 (m, 4H), 8.34 – 8.31 (m, 4H), 8.06 (s, 1H), 7.59– 7.54 (m, 6H). ^{13}C NMR (75 MHz, $CDCl_3$): δ (ppm) 164.85, 164.81, 157.76, 150.30, 138.19, 137.57, 133.82, 131.17, 131.10, 130.24, 128.95, 128.51, 127.33, 114.60, 110.35.

4-(4-nitrophenyl)-2,6-diphenylpyrimidine (7ap):

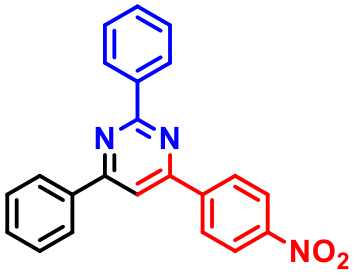

Eluent: Hexane/Ethyl acetate (30:1). White solid (yield: condition **A** = 75%, 265 mg; condition **B** = 77%, 271 mg). ^{1}H NMR (400 MHz, $CDCl_3$): δ (ppm) 8.75 – 8.71 (m, 2H), 8.34 – 8.31 (m, 2H), 8.08 (s, 1H), 7.68 – 7.56 (m, 10H). ^{13}C NMR (75 MHz, $CDCl_3$): δ (ppm) 165.55, 164.90, 148.89, 139.36, 137.60, 137.01, 131.24, 131.07, 130.01, 129.06, 128.96, 128.61, 128.55, 127.38, 125.26, 110.29.

4-(4-bromophenyl)-2,6-diphenylpyrimidine (7aq):

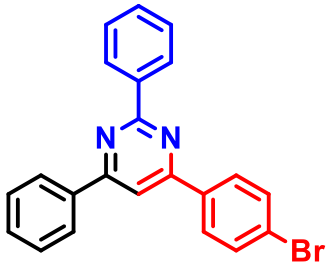

Eluent: Hexane/Ethyl acetate (40:1). White solid (yield: condition **A** = 80%, 309 mg; condition **B** = 82%, 317 mg). ^{1}H NMR (300 MHz, $CDCl_3$): δ (ppm) 8.65 (d, J = 8.6 Hz, 3H), 8.21 – 8.16 (m, 2H), 7.98 (s, 1H), 7.70 (d, J = 2.6 Hz, 2H), 7.60 – 7.55 (m, 7H). ^{13}C NMR (75 MHz, $CDCl_3$): δ (ppm) 164.98, 164.59, 163.56, 136.02, 135.19, 132.67, 131.91, 130.48, 128.99, 128.81, 128.69, 128.51, 128.49, 127.31, 125.45, 109.93.

4-(naphthalen-2-yl)-2-phenyl-6-(p-tolyl)pyrimidine (7ar):

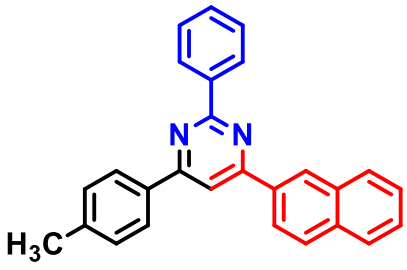

Eluent: Hexane/Ethyl acetate (30:1). White solid (yield: condition **A** = 85%, 316 mg; condition **B** = 87%, 323 mg). ^{1}H NMR (300 MHz, $CDCl_3$): δ (ppm) 8.41 (dd, J = 8.6, 1.8 Hz, 1H), 8.26 (d, J = 8.2 Hz, 2H), 8.01 (s, 1H), 7.98 – 7.88 (m, 4H), 7.61 – 7.58 (m, 7H), 7.40 (d, J = 8.0 Hz, 2H), 2.50 (s, 3H). ^{13}C NMR (101 MHz, $CDCl_3$): δ (ppm) 164.67, 164.46, 141.20, 138.30, 134.91, 134.62, 133.34, 133.13, 130.63, 129.67, 129.59, 128.31, 127.87, 127.81, 127.39, 127.26, 126.57, 126.46, 125.16, 124.30, 110.12, 21.58.

2,4-diphenyl-6-(pyridin-2-yl)pyrimidine (7as):

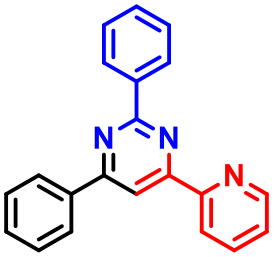

Eluent: Hexane/Ethyl acetate (40:1). White solid (yield: condition **A** = 65%, 200 mg; condition **B** = 68%, 210 mg). ^{1}H NMR (300 MHz, $CDCl_3$): δ (ppm) 8.80 – 8.74 (m, 5H), 8.44 – 8.39 (m, 2H), 7.93 (td, *J* = 7.7, 1.8 Hz, 1H), 7.61– 7.55 (m, 6H), 7.45 (ddd, *J* = 7.5, 4.7, 1.3 Hz, 1H). ^{13}C NMR (75 MHz, $CDCl_3$): δ (ppm) 165.15, 164.25, 163.59, 154.68, 149.41, 138.10, 137.38, 137.12, 130.87, 130.68, 128.86, 128.51, 128.45, 127.47, 125.30, 121.96, 110.61.

2-(2,6-diphenylpyrimidin-4-yl)thiazole (7at):

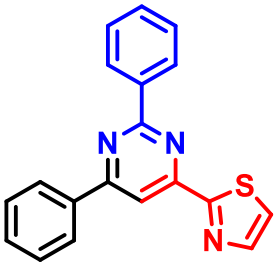

Eluent: Hexane/Ethyl acetate (30:1). White solid (yield: condition **A** = 72%, 226 mg; condition **B** = 75%, 236 mg). ^{1}H NMR (300 MHz, $CDCl_3$): δ (ppm) 8.74 – 8.69 (m, 2H), 8.47 (s, 1H), 8.41 – 8.35 (m, 2H), 8.08 (d, *J* = 3.2 Hz, 1H), 7.63-7.54 (m, 7H). ^{13}C NMR (75 MHz, $CDCl_3$) δ 168.11, 165.41, 164.59, 158.47, 144.67, 137.31, 136.89, 131.19, 131.01, 128.96, 128.56, 128.47, 127.44, 123.00, 108.90.

4-(benzofuran-2-yl)-2-phenyl-6-(p-tolyl)pyrimidine (7au):

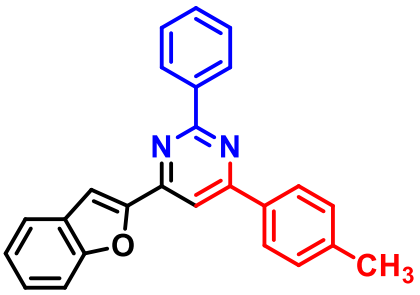

Eluent: Hexane/Ethyl acetate (60:1). White solid (yield: condition **A** = 78%, 282 mg; condition **B** = 80%, 290 mg). ^{1}H NMR (300 MHz, $CDCl_3$): δ (ppm) 8.75 – 8.70 (m, 2H), 8.26 (d, *J* = 8.2 Hz, 2H), 8.09 (s, 1H), 7.83 (s, 1H), 7.74 (dd, *J* = 8.3, 1.1 Hz, 1H), 7.65 – 7.57 (m, 4H), 7.47 – 7.33 (m, 4H), 2.49 (s, 3H). ^{13}C NMR (101 MHz, $CDCl_3$): δ (ppm) 164.86, 164.43, 156.33, 155.72, 154.10, 141.43, 137.95, 134.34, 130.71, 129.65, 128.51, 128.47, 127.26, 126.17, 123.52, 122.27, 111.70, 108.68, 107.96, 21.55.

2-(4-chlorophenyl)-4,6-diphenylpyrimidine (8aa):

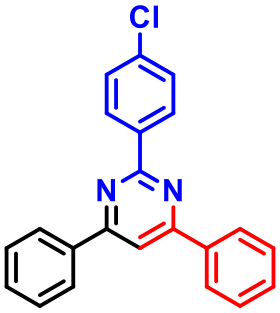

Eluent: Hexane/Ethyl acetate (60:1). White solid (yield: condition **A** = 80%, 274 mg; condition **B** = 83%, 284 mg). ^{1}H NMR (300 MHz, $CDCl_3$): δ (ppm) 8.72 – 8.67 (m, 2H), 8.33 – 8.27 (m, 4H), 8.04 (s, 1H), 7.63 – 7.57 (m, 6H), 7.55 – 7.50 (m, 2H). ^{13}C NMR (75 MHz, $CDCl_3$): δ (ppm) 164.88, 163.54, 137.30, 136.88, 136.57, 130.96, 129.88, 128.99, 128.68, 127.34, 110.54.

2-(4-fluorophenyl)-4,6-diphenylpyrimidine (8ab):

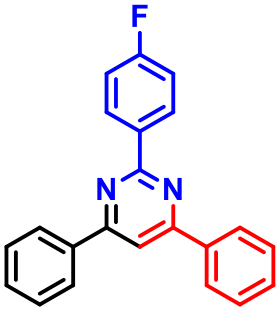

Eluent: Hexane/Ethyl acetate (60:1). White solid (yield: condition **A** = 78%, 254 mg; condition **B** = 82%, 267 mg). ^{1}H NMR (400 MHz, $CDCl_3$): δ (ppm) 8.32 – 8.29 (m, 4H), 8.04 (s, 1H), 7.94 – 7.88 (m, 3H), 7.52 (d, J = 4.0 Hz, 2H), 7.39 (d, J = 4.4 Hz, 5H). ^{13}C NMR (75 MHz, $CDCl_3$): δ (ppm) 167.19, 164.58, 164.51, 154.53, 137.83, 130.61, 130.10, 129.62, 128.87, 127.22 (d, J = 6.9 Hz), 115.85 (d, J = 21.9 Hz), 110.32. ^{19}F NMR (282 MHz, $CDCl_3$): δ = -110.72 (s, 1F).

2-(4-chlorophenyl)-4-phenyl-6-(p-tolyl)pyrimidine (8ac):

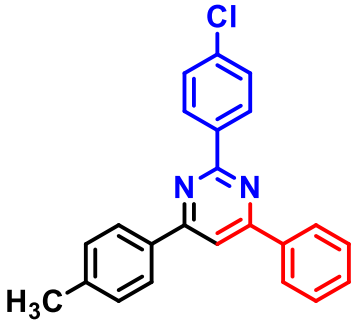

Eluent: Hexane/Ethyl acetate (60:1). White solid (yield: condition **A** = 85%, 302 mg; condition **B** = 88%, 313 mg). ^{1}H NMR (300 MHz, $CDCl_3$): δ (ppm) 8.31 – 8.28 (m, 2H), 8.21 (d, J = 8.2 Hz, 2H), 8.02 (s, 1H), 7.56 – 7.51 (m, 5H), 7.40 (d, J = 6.5 Hz, 4H), 2.49 (s, 3H). ^{13}C NMR (101 MHz, $CDCl_3$): δ (ppm) 164.81, 163.50, 143.52, 138.87, 136.75, 134.54, 130.84, 130.29,

129.83, 129.50, 129.01, 128.65, 127.28. 127.20, 110.15, 21.79. HRMS (ESI) m/z calcd for $C_{25}H_{18}ClN_2$ $[M + H]^+$ 357.1159, found 357.1156.

2-(4-chlorophenyl)-4-(4-fluorophenyl)-6-phenylpyrimidine (8ad):

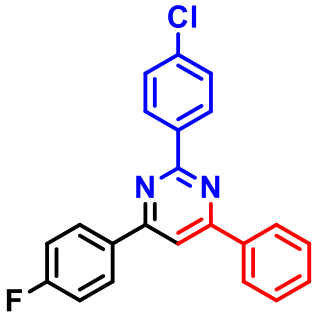

Eluent: Hexane/Ethyl acetate (60:1). White solid (yield: condition **A** = 65%, 234 mg; condition **B** = 67%, 241 mg). ^{1}H NMR (400 MHz, $CDCl_3$): δ (ppm) 8.66 (d, J = 8.1 Hz, 2H), 8.24 (d, J = 7.6 Hz, 4H), 7.91 (s, 1H), 7.58 – 7.50 (m, 5H), 7.07 (d, J = 8.5 Hz, 2H). ^{13}C NMR (101 MHz, $CDCl_3$): δ (ppm) 164.46, 164.20, 163.32, 162.01, 137.49, 136.81, 136.66, 130.76, 129.80, 129.70, 128.90, 128.77, 128.59, 127.23, 114.74, 114.27, 109.49. ^{19}F NMR (282 MHz, $CDCl_3$): δ = -109.56 (s, 1F). HRMS (ESI) m/z calcd for $C_{22}H_{14}ClFN_2$ $[M + H]^+$ 361.0920, found 360.1356.

2-(4-fluorophenyl)-4-phenyl-6-(p-tolyl)pyrimidine (8ae):

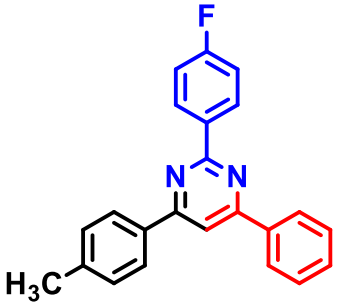

Eluent: Hexane/Ethyl acetate (60:1). White solid (yield: condition **A** = 75%, 255 mg; condition **B** = 77%, 262 mg). ^{1}H NMR (300 MHz, $CDCl_3$): δ (ppm) 8.71 (d, J = 8.9 Hz, 2H), 8.31 – 8.28 (m, 2H), 8.21 (d, J = 8.2 Hz, 2H), 7.95 (s, 1H), 7.62 – 7.55 (m, 3H), 7.38 (d, J = 7.9 Hz, 2H), 7.10 – 7.05 (m, 2H), 2.48 (s, 3H). ^{13}C NMR (75 MHz, $CDCl_3$): δ (ppm) 164.58, 164.51, 164.24, 161.79, 141.04, 137.83, 134.90, 131.04, 130.61, 130.10, 129.62, 128.87, 127.27, 127.17, 113.75, 109.32, 21.50. ^{19}F NMR (282 MHz, $CDCl_3$): δ = -110.82 (s, 1F). HRMS (ESI) m/z calcd for $C_{22}H_{14}ClFN_2$ $[M + H]^+$ 340.1376, found 340.1321.

2-(4-chlorophenyl)-4-(naphthalen-1-yl)-6-phenylpyrimidine (8af):

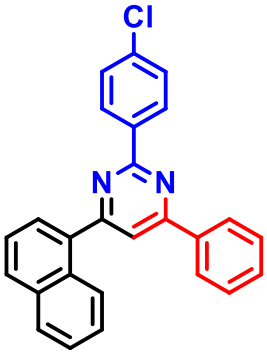

Eluent: Hexane/Ethyl acetate (60:1). White solid (yield: condition **A** = 70%, 275 mg; condition **B** = 73%, 287 mg). ^{1}H NMR (300 MHz, $CDCl_3$): δ (ppm) 8.70 (d, J = 8.6 Hz, 2H), 8.39 – 8.31 (m, 3H), 8.06 – 7.98 (m, 2H), 7.94 (s, 1H), 7.83 (dd, J = 7.1, 1.3 Hz, 1H), 7.68 – 7.51 (m, 8H). ^{13}C NMR (75 MHz, $CDCl_3$): δ (ppm) 167.56, 164.43, 163.49, 137.12, 136.69, 134.09, 131.04, 130.83, 130.29, 129.96, 129.02, 128.75, 128.65, 127.94, 127.36, 127.00, 126.27, 125.38, 125.33, 115.52. HRMS (ESI) m/z calcd for $C_{26}H_{18}ClN_2$ $[M + H]^+$ 393.1159, found 393.1150.

2-(4-chlorophenyl)-4-(pyridin-2-yl)-6-(p-tolyl)pyrimidine (8ag):

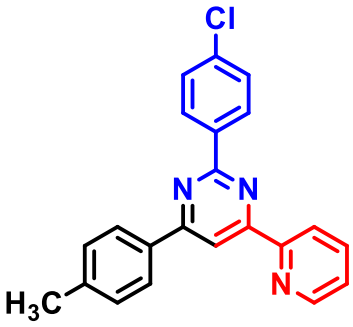

Eluent: Hexane/Ethyl acetate (60:1). White solid (yield: condition **A** = 65%, 232 mg; condition **B** = 70%, 250 mg). ^{1}H NMR (300 MHz, $CDCl_3$): δ (ppm) 8.81 – 8.78 (m, 1H), 8.73 – 8.67 (m, 4H), 8.29 (d, J = 8.2 Hz, 2H), 7.94 (td, J = 7.7, 1.8 Hz, 1H), 7.56 – 7.51 (m, 2H), 7.46 (ddd, J = 7.5, 4.8, 1.2 Hz, 1H), 7.38 (d, J = 7.6 Hz, 2H), 2.48 (s, 3H). ^{13}C NMR (101 MHz, $CDCl_3$): δ (ppm) 165.20, 163.49, 163.23, 154.60, 149.44, 141.40, 137.13, 136.75, 136.68, 134.38, 129.76, 129.62, 128.67, 127.36, 125.32, 121.90, 110.41, 21.52. HRMS (ESI) m/z calcd for $C_{22}H_{17}ClN_3$ $[M + H]^+$ 358.1111, found 358.1109.

4-(benzofuran-2-yl)-2-(4-chlorophenyl)-6-(p-tolyl)pyrimidine (8ah):

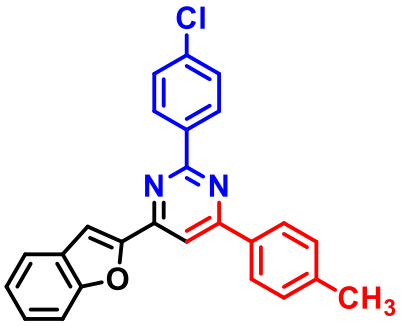

Eluent: Hexane/Ethyl acetate (60:1). White solid (yield: condition **A** = 70%, 277 mg; condition **B** = 73%, 289 mg). ^{1}H NMR (300 MHz, $CDCl_3$): δ (ppm) 8.69 – 8.63 (m, 2H), 8.27 – 8.23 (m, 2H), 8.14 (s, 1H), 7.84 (s, 1H), 7.75 (ddd, J = 7.8, 1.4, 0.7 Hz, 1H), 7.64 (dq, J = 8.3, 0.9 Hz, 1H), 7.55 – 7.50 (m, 2H), 7.48 – 7.31 (m, 4H), 2.50 (s, 3H). ^{13}C NMR (101 MHz, $CDCl_3$): δ (ppm) 164.76, 163.31, 156.23, 155.67, 153.83, 141.54, 136.81, 136.35, 134.03, 129.74, 129.63, 128.58, 128.41, 127.17, 126.23, 123.53, 122.26, 111.68, 108.67, 108.03, 21.56. HRMS (ESI) m/z calcd for $C_{25}H_{18}ClN_2O$ $[M + H]^+$ 397.1108, found 397.1105.

4,6-diphenylpyrimidin-2-amine (8ai):

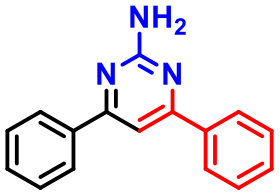

Eluent: Hexane/Ethyl acetate (10:1). White solid (yield: condition **A** = 81%, 200 mg; condition **B** = 84%, 208 mg). ^{1}H NMR (300 MHz, $CDCl_3$): δ (ppm) 8.07 – 8.04 (m, 4H), 7.57 – 7.52 (m, 6H), 7.46 (s, 1H), 5.88 (s, 2H). ^{13}C NMR (75 MHz, $CDCl_3$): δ (ppm) 166.29, 163.69, 137.74, 130.52, 128.82, 127.20, 104.35.

4-phenyl-6-(p-tolyl)pyrimidin-2-amine (8aj):

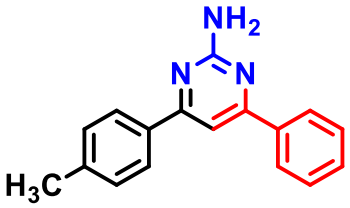

Eluent: Hexane/Ethyl acetate (10:1). White solid (yield: condition **A** = 86%, 225 mg; condition **B** = 88%, 230 mg). ^{1}H NMR (300 MHz, $CDCl_3$): δ (ppm) 8.06 – 8.03 (m, 2H), 7.97 (d, J = 8.2 Hz, 2H), 7.52 (d, J = 6.5 Hz, 2H), 7.42 (s, 1H), 7.34 – 7.25 (m, 3H), 5.68 (s, 2H), 2.45 (s, 3H). ^{13}C NMR (75 MHz, $CDCl_3$): δ (ppm) 166.34, 166.28, 163.63, 140.90, 137.69, 134.73, 130.47, 129.53, 128.77, 127.27, 127.19, 104.32, 21.46.

4-(4-fluorophenyl)-6-phenylpyrimidin-2-amine (8ak):

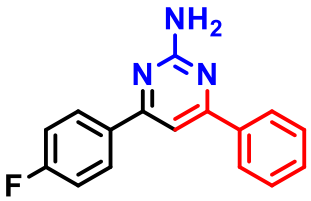

Eluent: Hexane/Ethyl acetate (10:1). White solid (yield: condition **A** = 67%, 178 mg; condition **B** = 71%, 188 mg). ^{1}H NMR (400 MHz, $CDCl_3$): δ (ppm) 8.13 (d, J = 7.8 Hz, 2H), 8.06 – 7.99 (m, 2H), 7.63 (t, J = 7.4 Hz, 1H), 7.55 – 7.52 (m, 1H), 7.49 (s, 1H), 7.38 – 7.33 (m, 1H), 7.23 – 7.12 (m, 2H), 6.02 (s, 2H). ^{13}C NMR (75 MHz, $CDCl_3$): δ (ppm) 166.71, 165.41, 164.51, 163.55, 163.41, 137.35 (d, J = 10.2 Hz), 133.60, 132.79 (d, J = 9.4 Hz), 130.17, 129.00, 128.82, 128.46, 127.41, 115.98, 115.69, 104.50. ^{19}F NMR (282 MHz, $CDCl_3$): δ = -109.96 (s, 1F).

4-(benzofuran-2-yl)-6-(p-tolyl)pyrimidin-2-amine (8al):

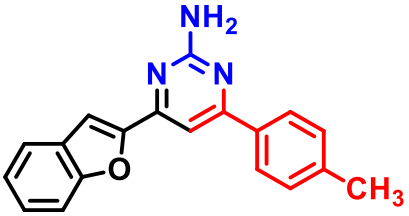

Eluent: Hexane/Ethyl acetate (10:1). White solid (yield: condition **A** = 77%, 232 mg; condition **B** = 79%, 238 mg). ^{1}H NMR (400 MHz, $CDCl_3$): δ (ppm) 8.03 (d, J = 7.8 Hz, 2H), 7.69 (d, J = 7.8 Hz, 1H), 7.62 (d, J = 7.5 Hz, 2H), 7.58 (s, 1H), 7.41 (t, J = 7.8 Hz, 1H), 7.33 (t, J = 7.5 Hz, 3H), 5.36 (s, 2H), 2.46 (s, 3H). ^{13}C NMR (75 MHz, $CDCl_3$): δ (ppm) 166.47, 163.38, 157.07, 155.55, 153.74, 141.18, 134.40, 129.55, 128.34, 127.12, 126.13, 123.44, 122.11, 111.75, 107.57, 102.98, 21.48. HRMS (ESI) m/z calcd for $C_{19}H_{16}N_3O$ $[M + H]^+$ 302.1293, found 302.1289.

2-methyl-4-phenyl-6-(p-tolyl)pyrimidine (8am):

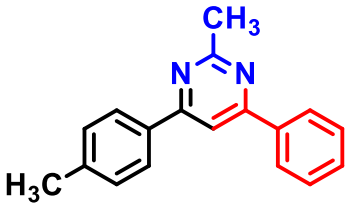

Eluent: Hexane/Ethyl acetate (10:1). White solid (yield: condition **A** = 71%, 185 mg; condition **B** = 73%, 190 mg). ^{1}H NMR (300 MHz, $CDCl_3$): δ (ppm) 8.16 – 8.13 (m, 2H), 8.06 (d, J = 8.2 Hz, 2H), 7.88 (s, 1H), 7.58 – 7.53 (m, 3H), 7.35 (d, J = 7.8 Hz, 2H), 2.89 (s, 3H), 2.46 (s, 3H). ^{13}C NMR (75 MHz, $CDCl_3$): δ (ppm) 168.49, 164.80, 141.02, 137.65, 134.67, 130.57, 129.69, 128.93, 127.27, 127.18, 109.75, 26.53, 21.47.

2,4-diphenylpyrimidine (9aa):

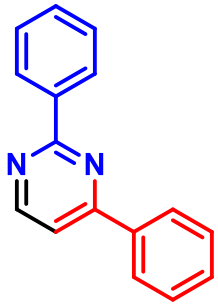

Eluent: Hexane/Ethyl acetate (30:1). White solid (yield: condition **A** = 75%, 174 mg; condition **B** = 77%, 178 mg). ^{1}H NMR (300 MHz, $CDCl_3$): δ (ppm) 8.87 (d, J = 5.2 Hz, 1H), 8.63 – 8.60 (m, 2H), 8.29 – 8.25 (m, 2H), 7.63 (d, J = 5.3 Hz, 1H), 7.64 – 7.53 (m, 6H). ^{13}C NMR (75 MHz, $CDCl_3$): δ (ppm) 164.61, 163.88, 157.88, 137.92, 136.98, 131.00, 130.76, 128.97, 128.59, 128.35, 127.25, 114.55.

4-(4-nitrophenyl)-2-phenylpyrimidine (9ab):

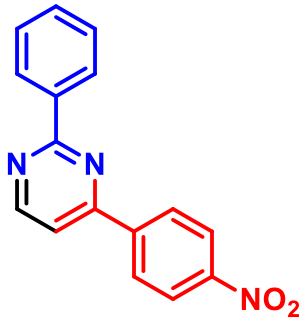

Eluent: Hexane/Ethyl acetate (30:1). White solid (yield: condition **A** = 65%, 180 mg; condition **B** = 68%, 188 mg). ^{1}H NMR (300 MHz, $CDCl_3$): δ (ppm) 8.97 (dd, J = 5.2, 1.3 Hz, 1H), 8.62 – 8.57 (m, 2H), 8.42 (d, J = 1.3 Hz, 4H), 7.69 (dd, J = 5.2, 1.3 Hz, 1H), 7.59 – 7.54 (m, 3H). ^{13}C NMR (75 MHz, $CDCl_3$): δ (ppm) 165.05, 161.51, 158.61, 149.36, 142.87, 137.28, 131.18, 128.70, 128.37, 128.17, 124.15, 115.15.

4-(4-methoxyphenyl)-2-phenylpyrimidine (9ac):

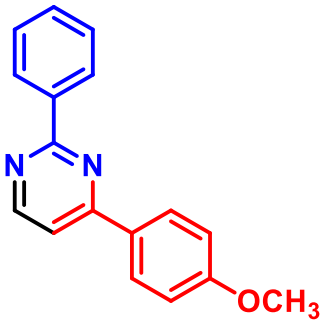

Eluent: Hexane/Ethyl acetate (30:1). White solid (yield: condition **A** = 60%, 157 mg; condition **B** = 63%, 165 mg). ^{1}H NMR (300 MHz, $CDCl_3$): δ (ppm) 8.80 (d, J = 5.3 Hz, 1H), 8.61 – 8.58 (m, 2H), 8.24 (d, J = 8.9 Hz, 2H), 7.56 – 7.52 (m, 4H), 7.07 (d, J = 8.9 Hz, 2H), 3.92 (s, 3H). ^{13}C NMR (101 MHz, $CDCl_3$): δ (ppm) 164.45, 163.39, 162.09, 157.57, 138.04, 130.62, 129.41, 128.77, 128.52, 128.26, 114.31, 113.69, 55.46.

2-(4-chlorophenyl)-4-phenylpyrimidine (9ad):

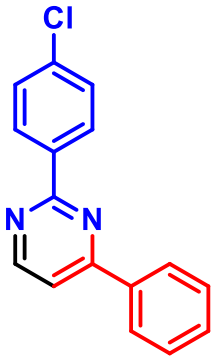

Eluent: Hexane/Ethyl acetate (30:1). White solid (yield: condition **A** = 72%, 192 mg; condition **B** = 75%, 200 mg). ^{1}H NMR (300 MHz, $CDCl_3$): δ (ppm) 8.84 (d, J = 5.3 Hz, 1H), 8.56 (d, J = 8.6 Hz, 2H), 8.26 – 8.24 (m, 2H), 7.63 (d, J = 5.3 Hz, 1H), 7.58 – 7.55 (m, 3H), 7.51 (d, J =

8.6 Hz, 2H). ^{13}C NMR (75 MHz, $CDCl_3$): δ (ppm) 164.00, 163.66, 157.89, 136.94, 136.79, 136.37, 131.11, 129.66, 129.00, 128.77, 127.22, 114.72.

4-methyl-2,6-diphenylpyrimidine (9ae):

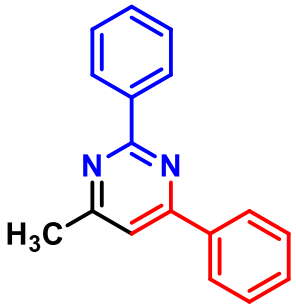

Eluent: Hexane/Ethyl acetate (30:1). Colourless oil (yield: condition **A** = 60%, 148 mg; condition **B** = 62%, 153 mg). ^{1}H NMR (300 MHz, $CDCl_3$): δ (ppm) 8.49 – 8.47 (m, 4H), 7.50 – 7.45 (m, 6H), 6.85 (s, 1H), 2.51 (s, 3H). ^{13}C NMR (101 MHz, $CDCl_3$): δ (ppm) 166.74, 164.11, 161.80, 138.15, 130.29, 128.94, 128.63, 128.45, 128.26, 117.99, 24.14.

2-(4-chlorophenyl)-4-(4-methoxyphenyl)pyrimidine (9af):

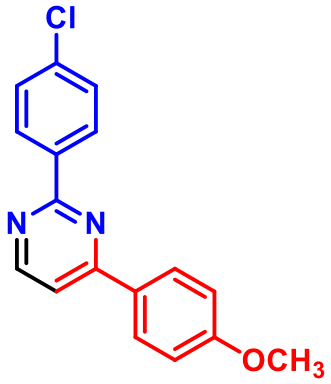

Eluent: Hexane/Ethyl acetate (30:1). White solid (yield: condition **A** = 55%, 163 mg; condition **B** = 57%, 169 mg). ^{1}H NMR (300 MHz, $CDCl_3$): δ (ppm) 8.78 (d, J = 5.3 Hz, 1H), 8.53 (d, J = 8.6 Hz, 2H), 8.21 (d, J = 8.9 Hz, 2H), 7.55 (d, J = 5.4 Hz, 1H), 7.50 (d, J = 8.7 Hz, 2H), 7.07 (d, J = 8.9 Hz, 2H), 3.92 (s, 3H). ^{13}C NMR (101 MHz, $CDCl_3$): δ (ppm) 163.47, 162.18, 157.58, 136.80, 136.52. 129.61, 129.18, 128.77, 128.71, 114.34, 113.84, 55.47.

2-(4-chlorophenyl)-4-hexyl-6-phenylpyrimidine (9ag):

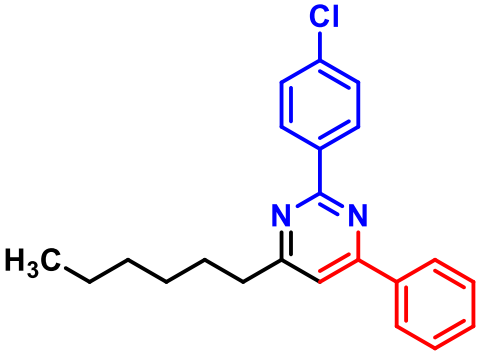

Eluent: Hexane/Ethyl acetate (10:1). Colourless oil (yield: condition **A** = 44%, 139 mg; condition **B** = 48%, 152 mg). ^{1}H NMR (300 MHz, $CDCl_3$): δ (ppm) 8.58 (d, J = 8.6 Hz, 2H), 8.24 – 8.21 (m, 2H), 7.55 – 7.47 (m, 6H), 2.92 – 2.87 (m, 2H), 1.93 – 1.81 (m, 2H), 1.42 – 1.35 (m, 6H), 0.94 – 0.91 (m, 3H). ^{13}C NMR (101 MHz, $CDCl_3$): δ (ppm) 164.89, 163.79, 163.29, 137.29, 136.80, 136.58, 130.73, 129.75, 128.90, 128.62, 127.21, 113.62, 38.26, 31.70, 29.08, 28.87, 22.60, 14.11. HRMS (ESI) m/z calcd for $C_{22}H_{24}ClN_2$ $[M + H]^+$ 351.1628, found 351.1620.

4-methyl-2-phenylpyrimidine (10aa):

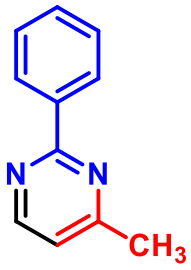

Eluent: Hexane/Ethyl acetate (10:1). Colourless oil (yield = 61%, 103 mg). ^{1}H NMR (300 MHz, $CDCl_3$): δ (ppm) 8.63 (d, J = 5.1 Hz, 1H), 8.50 – 8.45 (m, 2H), 7.54 – 7.49 (m, 3H), 7.01 (d, J = 5.1 Hz, 1H), 2.57 (s, 3H). ^{13}C NMR (101 MHz, $CDCl_3$): δ (ppm) 167.27, 164.37, 156.79, 137.86, 130.56, 128.54, 128.21, 118.63, 24.40. HRMS (ESI) m/z calcd for $C_{11}H_{11}N_2$ $[M + H]^+$ 171.0922, found 171.0929.

2-(4-chlorophenyl)-4-methylpyrimidine (10ab):

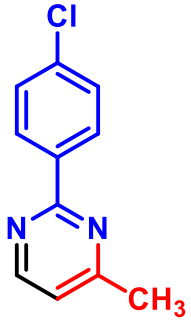

Eluent: Hexane/Ethyl acetate (10:1). Colourless oil (yield = 65%, 133 mg). ^{1}H NMR (300 MHz, $CDCl_3$): δ (ppm) 8.65 (d, J = 5.1 Hz, 1H), 8.44 – 8.39 (m, 2H), 7.50 – 7.43 (m, 2H), 7.07 (d, J = 5.0 Hz, 1H), 2.60 (s, 3H). ^{13}C NMR (101 MHz, $CDCl_3$): δ (ppm) 167.41, 163.41, 156.83, 136.77, 136.32, 129.54, 128.73, 118.79, 24.39. HRMS (ESI) m/z calcd for $C_{11}H_{10}ClN_2$ $[M + H]^+$ 205.0533, found 205.0528.

2-(4-fluorophenyl)-4-methylpyrimidine (10ac):

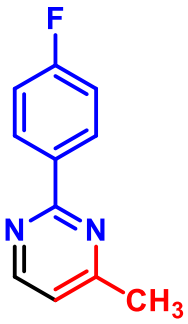

Eluent: Hexane/Ethyl acetate (10:1). Colourless oil (yield = 45%, 85 mg). ^{1}H NMR (300 MHz, $CDCl_3$): δ (ppm) 8.64 (d, J = 5.1 Hz, 1H), 8.49 – 8.44 (m, 2H), 7.22 – 7.19 (m, 2H), 7.07 (d, J = 5.1 Hz, 1H), 2.60 (s, 3H). ^{13}C NMR (101 MHz, $CDCl_3$): δ (ppm) 167.38, 165.85, 163.42 (d, J = 10.6 Hz), 156.81, 134.01, 130.30 (d, J = 8.6 Hz), 127.77, 115.45 (d, J = 21.6 Hz), 24.40. ^{19}F NMR (282 MHz, $CDCl_3$): δ = -110.72 (s, 1F). HRMS (ESI) m/z calcd for $C_{11}H_{10}FN_2$ $[M + H]^+$ 189.0828, found 189.0818.

III.4.4. NMR spectra of selected compounds:

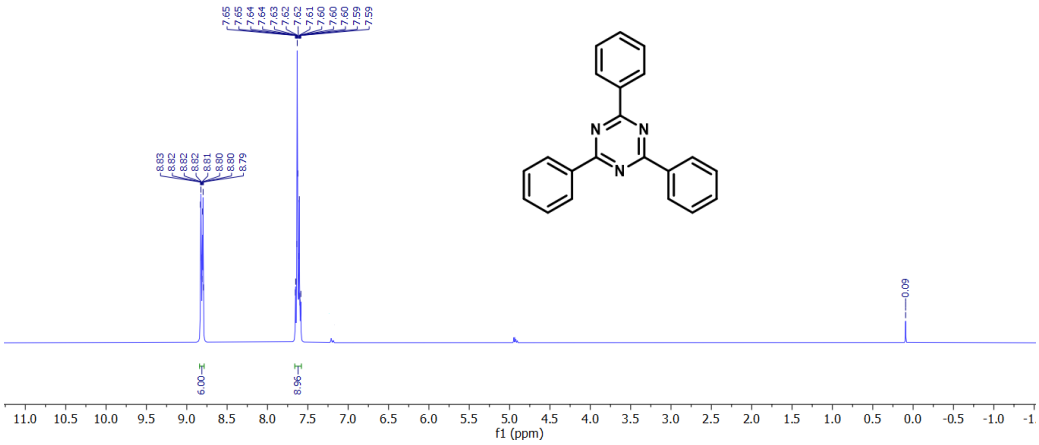

Figure 13. ^{1}H NMR spectrum of compound **4aa** (300 MHz, $CDCl_3$).

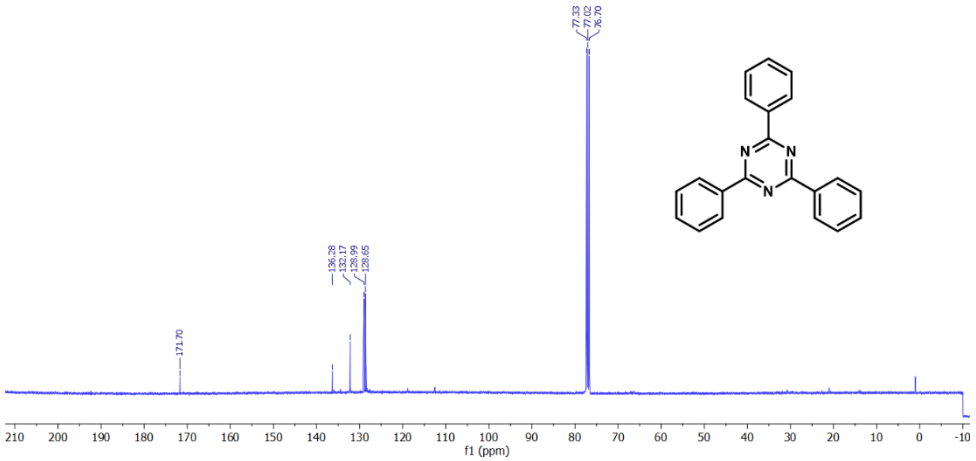

Figure 14. ^{13}C NMR spectrum of compound **4aa** (101 MHz, $CDCl_3$).

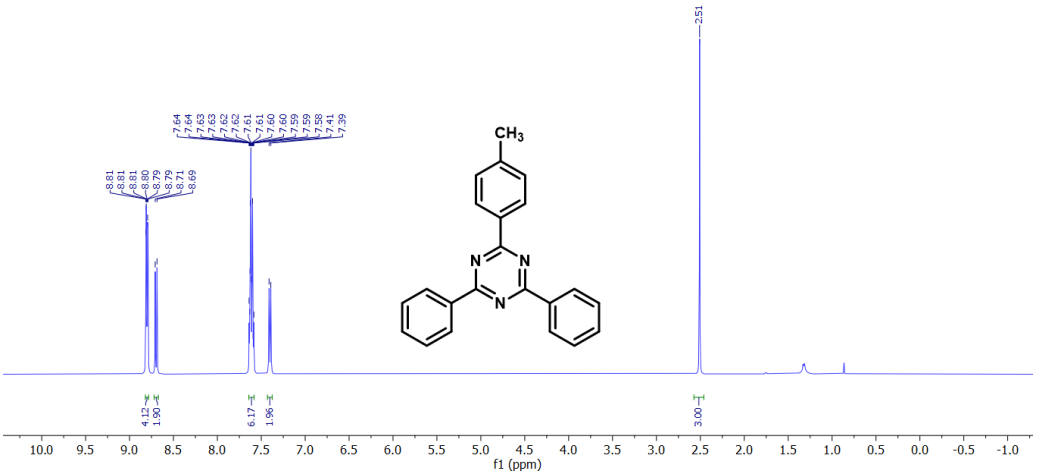

Figure 15. ^{1}H NMR spectrum of compound **4ab** (400 MHz, $CDCl_3$).

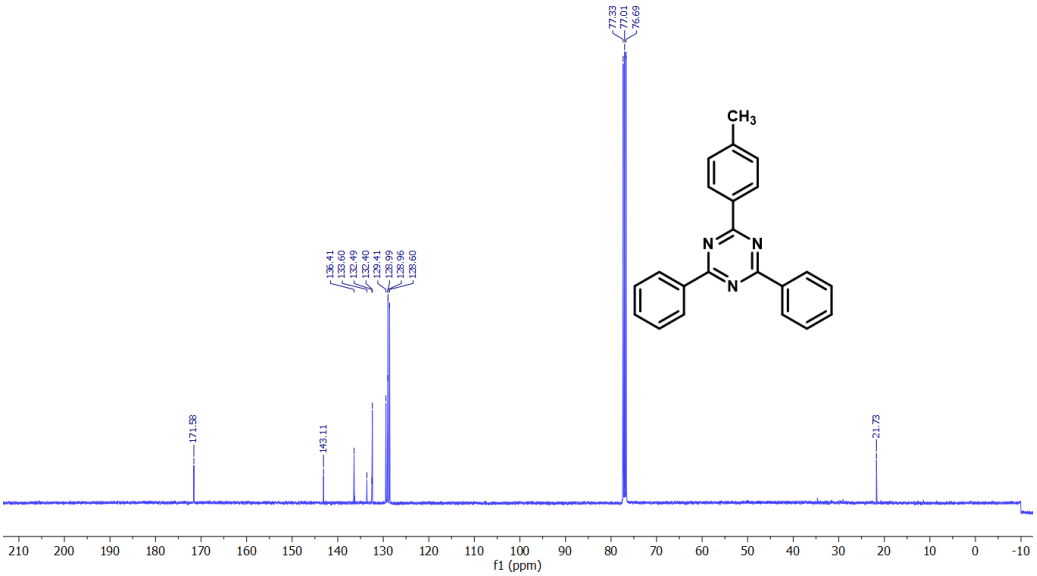

Figure 16. ^{13}C NMR spectrum of compound **4ab** (101 MHz, $CDCl_3$).

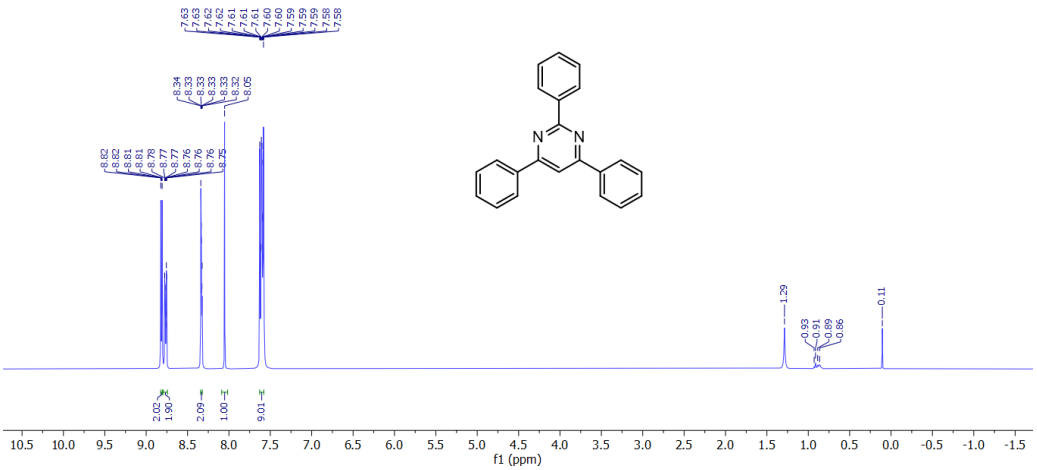

Figure 17. ^{1}H NMR spectrum of compound **7aa** (400 MHz, $CDCl_3$).

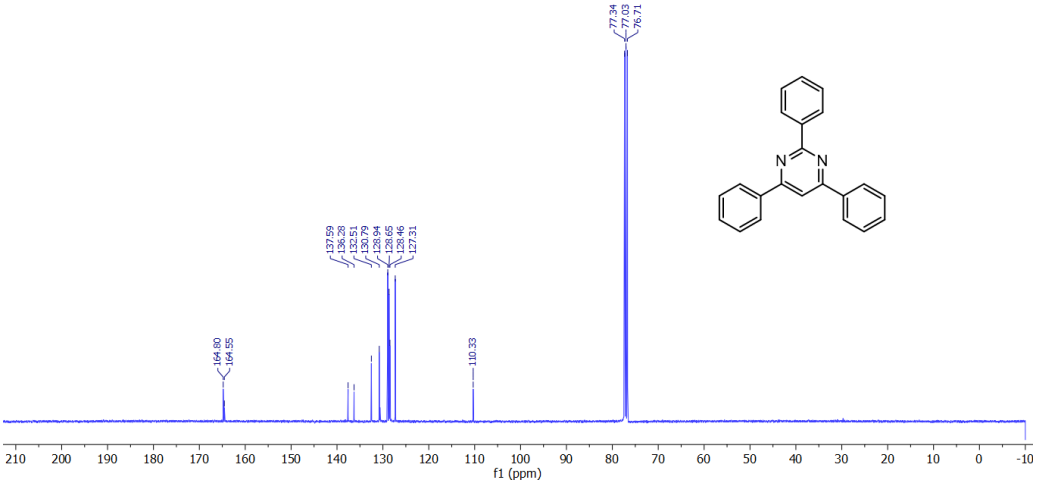

Figure 18. ^{13}C NMR spectrum of compound **7aa** (101 MHz, $CDCl_3$).

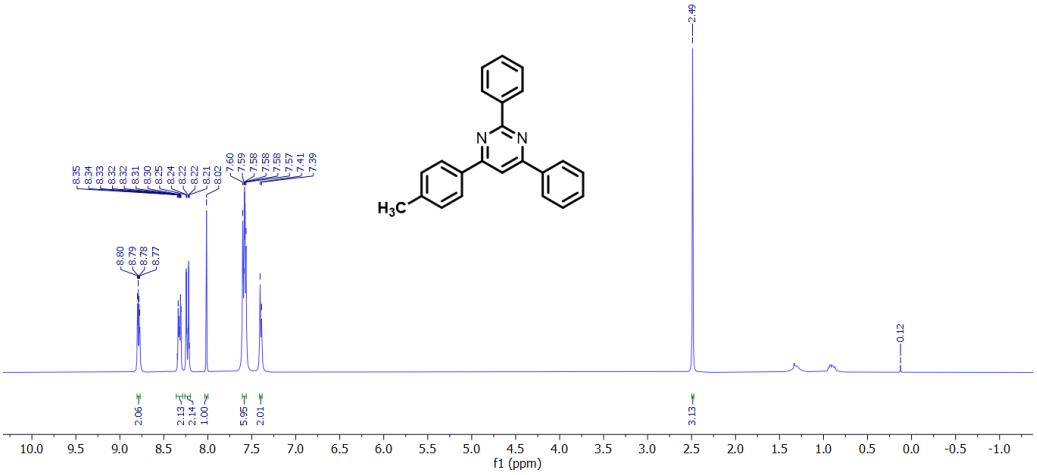

Figure 19. ^{1}H NMR spectrum of compound **7ab** (300 MHz, $CDCl_3$).

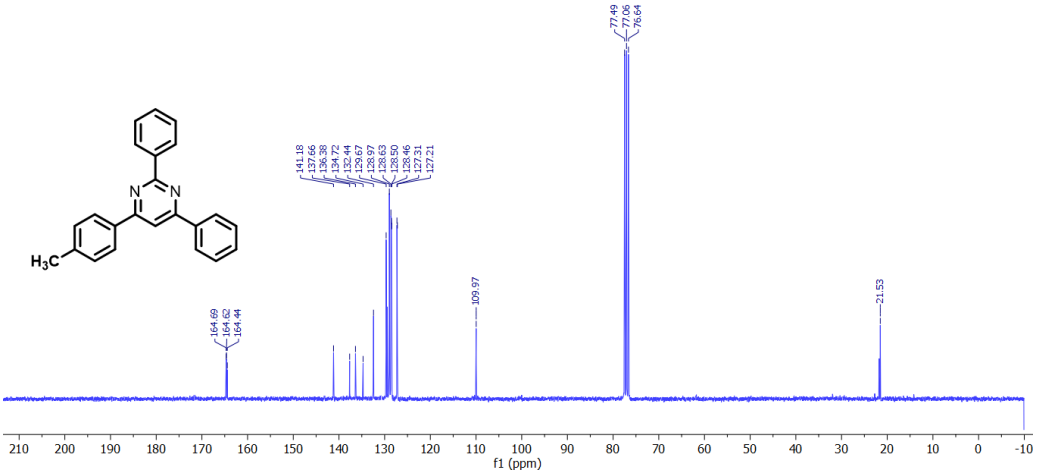

Figure 20. ^{13}C NMR spectrum of compound **7ab** (75 MHz, $CDCl_3$).

III.5. References

1. (a) A. K. Bodnar, S. M. Szewczyk, Y. Sun, Y. Chen, A. X. Huang, T. R. Newhouse, *J. Org. Chem.* **2024,** *89,* 3123–3132. (b) S. McCarthy, D. C. Braddock, J. D. E. T. Wilton-Ely, *Coord. Chem. Rev.* **2021,** *442,* 213925. (c) J. Rayadurgam, S. Sana, M. Sasikumar, Q. Gu, *Org. Chem. Front.* **2021,** *8,* 384–414. (d) A. Biffis, P. Centomo, A. Del Zotto, M. Zecca, *Chem. Rev.* **2018,** *118,* 2249−2295. (e) D. Wang, A. B. Weinstein, P. B. White, S. S. Stahl, *Chem. Rev.* **2018,** *118,* 2636−2679. (f) C. C. C. Johansson Seechurn, M. O. Kitching, T. J. Colacot, V. Snieckus, *Angew. Chem. Int. Ed.* **2012,** *51,* 5062−5085.
2. (a) T. G. Santiago, P. Palma, J. Cámpora, *Adv. Organomet. Chem.* **2024,** *81,* 1–179. (b) V. M. Chernyshev, V. P. Ananikov, *ACS Catal.* **2022,** *12,* 1180−1200. (c) A. K. Coopera, P. M. Burton, D. J. Nelson, *Synthesis* **2020,** *52,* 565–573. (d) M. R. Kwiatkowski, E. J. Alexanian, *Acc. Chem. Res.* **2019,** *52,* 1134–1144. (e) R. Shi, Z. Zhang, X. Hu, *Acc. Chem. Res.* **2019,** *52,* 1471–1483. (f) D. Balcells, A. Nova, *ACS Catal.* **2018,** *8,* 3499−3515. (g) N. Hazari, P. R. Melvin, M. M. Beromi. *Nat, Rev. Chem.* **2017,** *1,* 0025. (h) S. Z. Tasker, E. A. Standley, T. F. Jamison, *Nature* **2014,** *509,* 299−309.
3. (a) V. R. Landaeta, T. M. Horsley Downie, R. Wolf, *Chem. Rev.* **2024,** *124,* 1323−1463. (b) A. A. Swatiputra, D. Mukherjee, S. Dinda, S. Roy, K. Pramanik, S. Ganguly, *Dalton Trans.* **2023,** *52,* 15627–15646. (c) A. Rajeev, M. Balamurugan, M. Sankaralingam, *ACS Catal.* **2022,** *12,* 9953–9982. (d) F. Agbossou-Niedercorn, C. Michon, *Coord. Chem. Rev.* **2020,** *425,* 213523. (e) W. Guo, M. Zhao, W. Tan, L. Zheng, K. Tao, X. Fan, *Org. Chem. Front.* **2019,** *6,* 2120–2141. (f) A. Fürstner, *ACS Cent. Sci.* **2016,** *2,* 778−789.
4. (a) Q. Yan, X. Wu, H. Jiang, H. Wang, F. Xu, H. Li, H. Zhang, S. Yang, *Coord. Chem. Rev.* **2024**, *502*, 215622. (b) S. Majee, Shilpa, M. Sarav, B. K. Banik, D. Ray, *Pharmaceuticals* **2023**, *16*, 873. (c) K. L. Ameta, R. Kant, A. Penoni, A. Maspero, L. Scapinello, N-Heterocycles: Synthesis and Biological Evaluation, Springer: Berlin/Heidelberg, Germany, **2022**, ISBN 978-981-19083-2-3. (d) L. A. Aronica, G. Albano, *Catalysts* **2022**, *12*, 68. (e) J. Feng, W. -C. Geng, H. Jiang, B. Wu, *Biotechnol. Adv.* **2022**, *54*, 107813. (f) M. Maji, D. Panja, I. Borthakur, S. Kundu, *Org. Chem. Front.* **2021**, *8*, 2673–2709. (g) N. Hofmann, K. C. Hultzsch, *Eur. J. Org. Chem.* **2021**, 6206–6223. (h) A. Bera, S. Bera, D. Banerjee, *Chem. Commun.* **2021**, *57*, 13042–13058. (i) K. Sun, H. Shan, G. -P. Lu, C. Cai, M. Beller, *Angew. Chem.* **2021**, *133*, 25392–25406. (j) A. Mondal, R. Sharma, D. Pal, D. Srimani, *Eur. J. Org. Chem.* **2021**, 3690 – 3720. (k) T. Nagata, Y. Obora, *Asian J. Org. Chem.* **2020**, *9*, 1532−1547. (l) Y. Wang, W. -X. Zhang, Z. Xi, *Chem. Soc. Rev.* **2020**, *49*, 5810–5849.
5. (a) H. Y. Lim, A. V. Dolzhenko, *Eur. J. Med. Chem.* **2024,** *276,* 116680. (b) H. Su, Y. Xu, H. Yu, N. Han, Y. Zeng, X. -Q. Hao, J. Shi, M. Wang, *Inorg. Chem.* **2023,** *62,* 7795–7802. (c) E. K. Apartsin, N. Knauer, U. D. Kahlert, A.-M. Caminade, *Pharmaceutics* **2022,** *14,* 393. (d) F. Xie, Y. Hao, J. Liu, J. Bao, T. Ni, Y. Liu, X. Chi, T. Wang, S. Yu, Y. Jin, L. Li, D. Zhang, L. Yan, *Pharmaceutics* **2022,** *14,* 2334. (e) E. Havránková, J. Csöllei, D. Vullo, V. Garaj, P. Pazdera, C. T. Supuran, *Bioorg. Chem.* **2018**, *77*, 25–37.
6. (a) V. N. Toan, D. S. Hai, H. T. K. Van, N. M. Tri, D. N. Toan, N. T. T. Mai, N. D. Thanh, *RSC Med. Chem.* **2024**, *15*, 3395-3417. (b) S. K. Rastogi, S. Khanka, S. Kumar, A. Lakra, R. Rathur, K. Sharma, A. C. Bisen, R. S. Bhatta, R. Kumar, D. Singh, A. K. Sinha, *RSC Med. Chem.* **2024**, *15*, 677–694. (c) C. Li, X. Tian, Z. Huang, X. Gou, B. Yusuf, C. Li, Y. Gao, S. Liu, Y. Wang, T. Yang, Z. Liu, Q. Sun, T. Zhang,

Y. Luo, *J. Med. Chem.* **2023**, *66,* 2699−2716. (d) B. Toviwek, J. Riley, N. Mutter, M. Anderson, L. Webster, I. Hallyburton, D. Gleeson, K. D. Read, M. P. Gleeson, *RSC Med. Chem.* **2022**, *13,* 1587–1604. (e) W. Kim, J.-A. Kang, M. Park, P.-H. Jeong, Y. J. Kim, Y. Cho, S.-G. Park, Y.-C. Kim, *J. Med. Chem.* **2021**, *64*, 5500−5518. (f) J. Zhuang, S. Ma, *ChemMedChem* **2020**, *15*, 1875–1886.

7. (a) J. Li, W. Zeng, L. Wang, G. Shi, D. Wang, *Chem. Eng. J.* **2023**, *474*, 145642. (b) J. Liu, J. Zhuo, Q. Tan, M. Zhou, L. Ma, M. Zhang, *Org. Biomol. Chem.* **2023**, *21*, 3411–3416. (c) S. Das, R. Mondal, A. K. Guin, N. D. Paul, *Org. Biomol. Chem.* **2022**, *20*, 3105–3117. (d) F. Wang, Z. Deng, Y. Wang, F. Yuan, X. Zhan, G-P. Lu, N. Fu, Y. Lin, *Tetrahedron*, **2022**, *123*, 132985. (e) X. Zhang, H. Liu, X. Sheng, X. Mai, S. Hou, B. Li, X. Chen, Y. Li, F. Xie, *J. Catal.* **2022**, *408*, 227–235. (f) Z. Qin, Y. Ma, F. Li, *J. Org. Chem.* **2021**, *86*, 13734–13743. (g) R. Mondal, G. Chakraborty, A. K. Guin, S. Sarkar, N. D. Paul, *J. Org. Chem.* **2021**, *86,* 13186–13197. (h) A. K. Bains, D. Adhikari, *Catal. Sci. Technol.* **2020**, *10*, 6309–6318. (i) J. Zhang, T. Zheng, J. Zhang, *Eur. J. Org. Chem.* **2020,** 860–865. (j) G. Chakraborty, R. Sikari, R. Mondal, S. Mandal, N. D. Paul, *Asian J. Org. Chem.* **2020**, *9*, 431 – 436. (k) S. S. Poly, S. M. A. H. Siddiki, A. S. Touchy, K. W. Ting, T. Toyao, Z. Maeno, Y. Kanda, K. Shimizu, *ACS Catal.* **2018**, *8*, 11330–11341. (l) A. R. Tiwari, B. M. Bhanage, *Green Chem.* **2016,** 18, 144–149. (m) M. Zeng, T. Wang, D-M. Cui, C. Zhang, *New J. Chem.* **2016**, *40*, 8225−8228. (n) Q. You, F. Wang, C. Wu, T. Shi, D. Min, H. Chen, W. Zhang, *Org. Biomol. Chem.* **2015**, *13*, 6723–6727. (o) A. R. Tiwari, T. Akash, B. M. Bhanage, *Org. Biomol. Chem.* **2015**, *13*, 10973-10976.

8. (a) F. Doraghi, F. Gilaninezhad, S. Karimian, A. M. Mahdavian, B. Larijani, M. Mahdavi, *Adv. Synth. Catal.* **2024,** *366*, 2142–2164. (b) S. S. Poly, Y. Hashiguchi, I. Nakamura, T. Fujitani, S. M. A. H. Siddiki, *Catal. Sci. Technol.* **2022,** *12*, 4679–4687. (c) J. Xiao, S. Ren, Q. Liu, *RSC Adv.* **2020,** *10*, 22230–22233. (d) R. Mondal, I. B. Lozada, O. Stotska, D. E. Herbert, *J. Org. Chem.* **2020,** *85*, 13747–13756. (e) J. Zhang, B. Guo, D. J. Young, H.-Xi Li, *Dalton Trans.* **2020,** *49*, 15527–15547. (f) F. -L. Hong, L. -Wu Ye, *Acc. Chem. Res.* **2020,** *53*, 2003−2019.

9. (a) K. Li, B. Zu, C. Mazet, *Org. Lett.* **2024,** *26*, 6047−6052. (b) L. -M. Chen, S. E. Reisman, *Acc. Chem. Res.* **2024,** *57*, 751−762. (c) C. S. Selvan, R. Rengan, J. G. Malecki, *J. Org. Chem.* **2024**, *89*, 11148−11160. (d) J. Davies, J. R. Lyonnet, B. Carvalho, B. Sahoo, C. S. Day, F. Juliá-Hernández, Y. Duan, Á. Velasco-Rubio, M. Obst, P. -O. Norrby, H. Kathrin, R. M. Hopmann, *J. Am. Chem. Soc.* **2024,** *146*, 1753−1759. (e) Y. Zhang, Q. Cao, Y. Xi, X. Wu, J. Qu, Y. Chen, *J. Am. Chem. Soc.* **2024,** *146*, 7971−7978. (f) C. Wen, T. Li, Z. Huang, Q. K. Kang, *Chem. Rec.* **2023,** *23*, e202300146. (g) V. Arora, H. Narjinari, P. G. Nandi, A. Kumar, *Dalton Trans.* **2021**, *50*, 3394–3428.

10. (a) Y. Zhang, X. Yang, S. Liu, J. Liu, S. Pang, *Chem. Commun.* **2024,** *60*, 4121–4139. (b) S. Sheetal, P. Mehara, P. Das, *Coord. Chem. Rev.* **2023,** *475*, 214851. (c) H. -T. Tang, Y. -Z. Pan, Y. -M. Pan, *Green Chem.* **2023,** *25*, 8313–8327. (d) C. C. Meyer, N. P. Stafford, M. J. Cheng, M. J. Krische, *Angew. Chem.* **2021,** *133,* 10636–10640.

11. (a) Y. Ayub, J. Ren, C. He, *Energy* **2024,** *299,* 131482. (b) S. Mehta, M. Kasabe, S. Umbarkar, K. Joshi, *Appl. Surf. Sci.* **2024,** *669,* 160527. (c) Q. Liu, J. Lin, H. Cheng, L. Wei, F. Wang, *Angew. Chem. Int. Ed.* **2023,** *135,* e202218720. (d) H. I. Mahdi, N. N. Ramlee, D. H. S. Santos, D. A. Giannakoudakis, L. H. de Oliveira, R. Selvasembian, N. I. W. Azelee, A. Bazargan, L. Meili, *Mol. Catal.* **2023,** *537,* 112944. (e) M.

Karatok, M. G. Sensoy, E. I. Vovk, H. Ustunel, D. Toffoli, E. Ozensoy, *ACS Catal.* **2021,** *11*, 6200–6209. (f) M. I. Malik, N. Abatzoglou, I. E. Achouri, *Catalysts* **2021,** *11*, 893.

12. S. Roy, S. Pramanik, S. C. Patra, B. Adhikari, A. Mondal, S. Ganguly, K. Pramanik, *Inorg. Chem.* **2017,** *56*, 12764–12774.
13. (a) D. Jana, S. Roy, S. Naskar, S. Halder, G. Kanrar, K. Pramanik, *Org. Biomol. Chem.* **2024,** *22*, 6393–6408. (b) S. Pramanik, S. Roy, T. Ghorui, S. Ganguly, K. Pramanik, *Inorg. Chem.* **2016,** *55*, 1461–1468. (c) S. Roy, S. Pramanik, T. Ghorui, K. Pramanik, *RSC Adv.* **2015,** *5*, 22544–22559.
14. The occurrence of dianionic L^{-2} has been confirmed from the successful isolation of $\{Co^{III}–L^{-II}\}$ coordination and remains an unpublished result.
15. (a) L. M. Kabadwal, A. Bera, D. Banerjee, *ACS Catal.* **2024,** *14*, 4018−4029. (b) W. Gao, L. Xin, Z. Hao, G. Li, J.-H. Su, L. Zhou, Y. Mu. *Chem. Commun.* **2015,** *51*, 7004−7007.
16. F. Xie, M. Chen, X. Wang, H. Jiang, M. Zhang, *Org. Biomol. Chem.* **2014,** *12*, 2761–2768.
17. (a) S. S. Poly, Y. Hashiguchi, A. Sultana, I. Nakamura, K.-I. Shimizu, S. Yasumura, T. Fujitani, *Appl. Catal. A: Gen.* **2021,** *619*, 118158. (b) M. Maji, S. Kundu, *Dalton Trans.* **2019,** *48*, 17479–17487. (c) N. Deibl, R. Kempe, *Angew. Chem. Int. Ed.* **2017,** *56*, 1663–1666. (d) M. Mastalir, M. Glatz, E. Pittenauer, G. Allmaier, K. Kirchner, *J. Am. Chem. Soc.* **2016,** *138*, 15543–15546.
18. (a) N. Mameda, S. Peraka, S. Kodumuri, D. Chevella, R. Banothu, V. Amrutham, N. Nama, *RSC Adv.* **2016,** *6*, 58137–58141. (b) M. Naresh, P. Swamy, M. M. Reddy, K. Srujana, C. Durgaiah, N. Narender, *Appl. Catal. A: Gen.* **2015,** *505*, 213. (c) R. Casado, M. Contel, M. Laguna, P. Romero, S. Sanz, *J. Am. Chem. Soc.* **2003,** *125*, 11925.
19. (a) V. Vermaak, H. C. M. Vosloo, A. J. Swarts, *Coord. Chem. Rev.* **2024,** *507*, 215716. (b) S. Bansal, R. G. Gonnade, B. Punji, *Catal. Sci. Technol.* **2023,** *13*, 2705–2713. (c) R. Sikari, G. Chakraborty, A. K. Guin, N. D. Paul, *J. Org. Chem.* **2021,** *86*, 279−290. (d) A. K. Bains, A. Biswas, D. Adhikari, *Chem. Commun.* **2020,** *56*, 15442–15445. (e) D. Sengupta, R. Bhattacharjee, R. Pramanick, S. P. Rath, N. Saha Chowdhury, A. Datta, S. Goswami, *Inorg. Chem.* **2016,** *55*, 9602–9610.
20. (a) S. Pal, A. K. Guin, S. Chakraborty, N. D. Paul, *ChemCatChem* **2024**, *16*, e202400026. (b) R. Mondal, S. Sinha, S. Das, G. Chakraborty, N. D. Paul, *Adv. Synth. Catal.* **2020**, *362*, 594 – 600.

Chapter IV

Microwave-Driven Solvent-free [2 + 2 + 1 + 1] Cascade Annulation for Poly-Substituted Pyridine Synthesis Catalyzed by a Nickel Metalloradical

IV.1. Introduction

The pyridine scaffold, a privileged structure in medicinal chemistry (Figure 1), is renowned for its pivotal role in drug discovery, biosynthesis, and various biological activities.[1] Poly-substituted pyridines highly sought-after synthetic targets, prompting significant efforts to develop efficient and modular synthetic methodologies.[2]

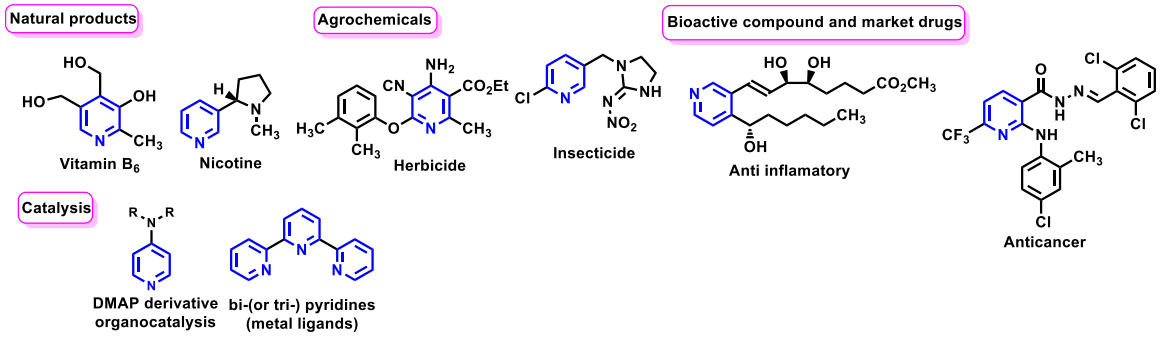

Figure 1. Representative pyridine derivatives and their chemical application domains.

Therefore, considerable efforts have been devoted to developing innovative methods for synthesizing substituted pyridines, utilizing a range of synthetic protocols. Traditional approaches often involve metal-catalyzed cycloadditions.[3] A diverse range of both costly, heavier transition metals (e.g., Ru, Pd, Rh, Ir)[4] and earth-abundant first-row transition metals (e.g., Mn, Fe, Ni, Cu, Zn)[5] are effective for this task. Despite recent advancements in using low-cost, eco-friendly, and accessible metal catalysts,[6] achieving a one-pot MCR (Multi Component Reaction) for the synthesis of highly substituted pyridines from readily available starting materials in a greener manner remains a significant challenge.

While metal-catalyzed cross-coupling strategies have led to notable progress in modifying the prevailing pyridine frameworks, a more versatile and efficient approach involves the multicomponent cascade annulation-based synthesis. Among these, two-component [4+2]/[3+3][7] and three-component [3+2+1]/[2+2+2][8] cycloadditions are commonly employed, offering direct and practical synthetic routes (Scheme 1). Despite significant

Recent Previous work	Limitations
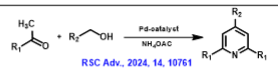 RSC Adv., 2024, 14, 10761	Costly metal catalyst Long residence time (24 hrs) High temperature (150 °C)
 Adv. Synth. Catal. 2024, 366, 1–13	Precious noble metal High temperature (140 °C) Long residence time (24 hrs)
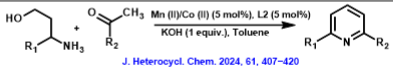 J. Heterocycl. Chem. 2024, 61, 407–420	In-situ generated catalyst Less substituted products Low atom-economy
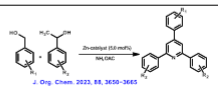	High catalyst loading Low atom-economy Long residence time (24 hrs)
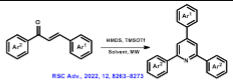	Pre-fuctionalized starting materials Low atom-economy High temperature (150 °C)
 Organometallics 2020, 39, 1310−1317	Precious noble metal Long residence time (24 hrs) Limited substrate scope
Present work	**Advantages**
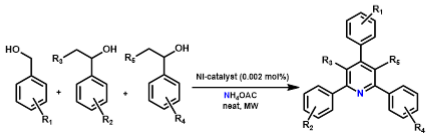	• Non-precious metal catalyst (Ni) • high TON i.e., low catalyst loading • Microwave-assisted greener approach • Low atom-economy • Short residence time (2 hrs) • Broad substrate scope

Scheme 1. Synthesis of substituted pyridine derivatives by various synthetic methods.

advancements in multicomponent annulation strategies, the development of [2 + 2 + 1 + 1] N-annulation remains largely unexplored.[9] Four-component reactions (4CRs) facilitate enhanced functionalization with highest possible substituted derivatives, improved atom economy, and greater structural diversity by integrating multiple reactive units into a single transformation. However, achieving seamless integration and compatibility of four distinct reactants while ensuring regioselective formation of two C−C and two C−N bonds in a one-pot transformation remains a key challenge. Notably, four-component cycloadditions remain scarce, particularly for the synthesis of penta-substituted pyridines.[10] To the best of our knowledge, no precedent exists in the literature for a [2 + 2 + 1 + 1] aza-annulation involving four components under microwave-assisted conditions.[11] Importantly, alcohols, due to their diverse reactivity and cost-effectiveness, have emerged as valuable precursors for constructing cyclic carbon frameworks.[12] One advantage of using an increasing number of components in cycloaddition reactions is the enhanced flexibility in preparing a wide variety of substituted derivatives, including those with the maximum possible substitution. A key challenge associated with multi-component cycloaddition strategies is the generation of multiple by-products, which complicates purification and often leads to reduced yields. Achieving high yields despite these intricacies remains a considerable hurdle in current research.

In addition, the use of metalloradicals in catalysis has gained attention for facilitating challenging transformations via radical-induced single-electron transfer (SET) pathways.X Metalloradicals are particularly effective in promoting annulation reactions, including various two- and three-component [4+2] or [2+2+2] pathways, enabling the synthesis of heterocyclic compounds under mild conditions.[13] These catalysts are especially efficient in oxidation reactions, e.g., oxidative dehydrogenation, using environmentally friendly oxidants like molecular oxygen.

Effective waste management in chemical industries is crucial for sustainability, reducing hazardous byproducts, energy consumption, and reliance on toxic reagents in catalysis. Catalysts with high in situ recyclability, solvent-free conditions, and waste-to-value strategies enhance atom economy and minimize environmental impact. Microwave irradiation under neat conditions offers a sustainable solution by eliminating hazardous solvents, improving safety, simplifying work-up, reducing costs, and enabling scalable synthesis. This methodology/approach improves reaction efficiency while significantly lowering the E-factor, a measure of waste per kilogram of product, by minimizing waste and advancing eco-friendly synthesis.[14] Microwave-assisted synthesis, leveraging high-energy electromagnetic radiation, has become a key tool in organic transformations, addressing limitations of conventional methods. In green chemistry, combining oxygen as an oxidant with microwave processes may provide an eco-friendly and cost-effective route for the oxidative dehydrogenation of primary/secondary alcohols to aldehydes/ketones using metalloradical catalysts. Notably, the microwave-assisted cascade [2 + 2 + 1 + 1] annulation for synthesizing poly-substituted pyridines with a pincer-Ni catalyst remains unexplored.

We have synthesized a bis-complex with a cis-dichloro-configured nickel compound, using a typical electron-deficient azo-pyridyl chelating ligand. The intention behind employing an electron-poor π-acidic environment is to facilitate the generation of a pro-radical species. Herein, we demonstrate the successful isolation and use of this species as a metalloradical catalyst to achieve a four-component domino synthesis of high-yield, multi-substituted bio-relevant pyridines, including penta-substituted ones. Notably, our approach overcomes the limitations of multi-component synthesis, including the formation of multiple products and the reduced yield of the targeted species, achieving excellent yields despite the four-component [2+2+1+1] cyclization. Furthermore, these domino reactions catalyzed by the Ni-metalloradical furnish substituted pyridines in excellent yields under solvent-free microwave conditions.

IV.2 Result and Discussion

IV.2.1 Synthesis of ligands and complexes

Two hexa-coordinated Ni(II) complexes, $[Ni(L)_2Cl_2]$ **1a** and $[Ni(L)_2]^{2+}[2(PF_6^-)$ **[1b]$^{2+}$**, were synthesized in high yields (82% and 86%, respectively) through the reaction of the electron-deficient NNN-pincer ligand 2-(2-pyridylazo)azobenzene **L** with $NiCl_2(PPh_3)_2$ in toluene and $Ni(NO_3)_2.6H_2O$ in ethanol respectively under stoichiometric conditions. This study aims to evaluate the catalytic annulation efficiency of pincer complexes. The strategic utilization of a robust, electron-deficient bis-azo-based organic template (L) is justified by its ability to facilitate the initial nucleophilic attack of primary and secondary alcohols at the electron-rich nickel center, thereby driving the overall catalytic process (Scheme 5). Furthermore, this electron-sink moiety is expected to play a crucial role in the dehydrogenative oxidation process, facilitating the oxidation of alcohols to their corresponding carbonyl compounds by removing hydrogen atoms, likely via an electron transfer mechanism.[15] Both complexes exhibit remarkable stability under ambient conditions, maintaining their integrity in the presence of air and moisture. Moreover, they demonstrate high solubility in polar solvents such as dichloromethane, acetonitrile, and ethanol, while their solubility remains limited in non-polar solvents like toluene. HRMS, IR, and UV-Vis spectral data, along with elemental analysis, validate the coordination of ligand L to the nickel center in both complexes via the azo chromophores.

IV.2.2. IR spectra

Sharp vibrations around 1451, 1395 cm^{-1} and 1448, 1389 cm^{-1} in the infrared spectra of complex **1a** and **1b** were assigned to the $\nu_{N=N}$ stretching respectively (Figure 2).

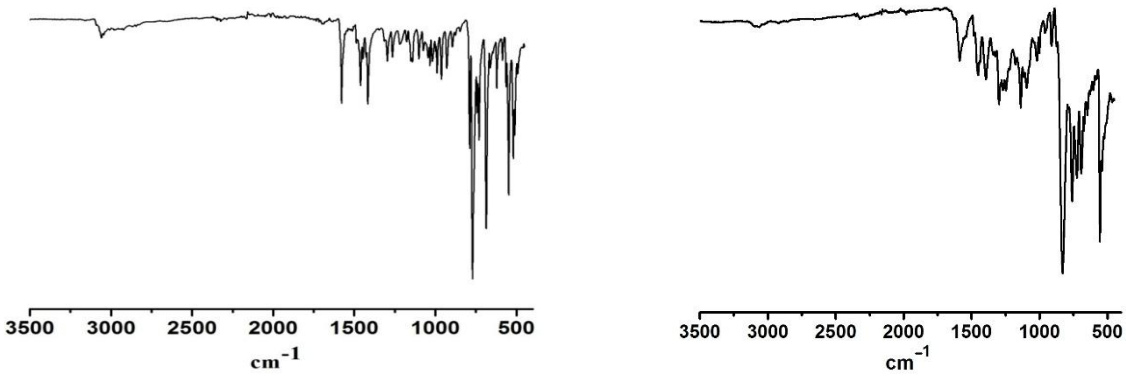

Figure 2. IR spectra of **1a** (left) and **1b**(right).

IV.2.3. Crystal structures

Hexa-coordination around the nickel center was confirmed by X-ray crystallographic analysis (*vide infra*). Complexes **1a** and **1b** crystallize in the monoclinic crystal system, adopting the space groups C2/c and P21/c, respectively. In complex **1a**, the primary valency of Ni(II) is satisfied through bidentate coordination via the $N_{pyridyl}$ and $N_{azopyridyl}$ atoms, forming two juxtaposed five-membered rings upon chelation, with two chloride ligands positioned cis to each other, whereas in complex **1b**, the primary valency of Ni(II) is balanced by two hexafluorophosphate anions as counterions,

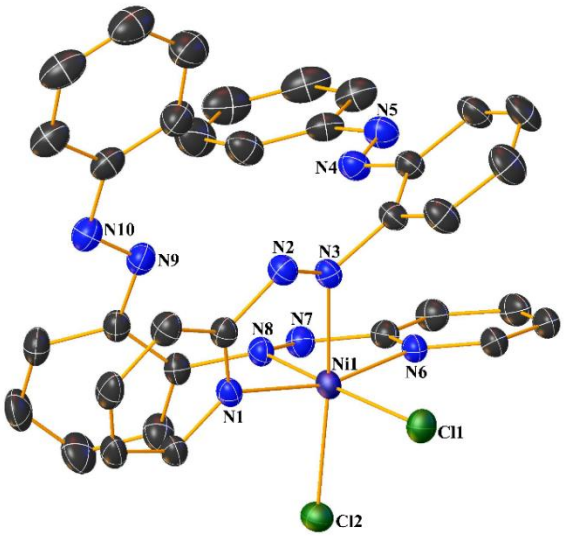

Figure 3: ORTEP view of **1a** (Solvent molecule and hydrogen atoms are omitted for clarity, and thermal ellipsoids are set at 50% probability).

while tridentate coordination through the $N_{pyridyl}$, $N_{azopyridyl}$, and $N_{azophenyl}$ atoms results in the formation of four juxtaposed five-membered rings during chelation.

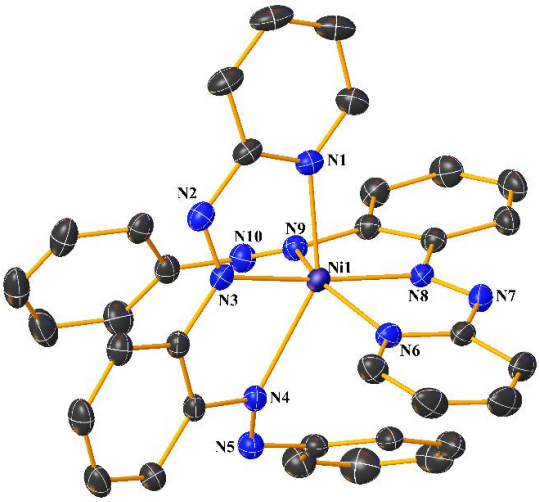

Figure 4: ORTEP view of **1b** (Solvent molecule and hydrogen atoms are omitted for clarity, and thermal ellipsoids are set at 50% probability).

Table 1. Crystallographic Details of complexes **1a** and **1b**.

	1a	**1b**
Empirical formula	$C_{34}H_{26}N_{10}Cl_2Ni$	$C_{34}H_{26}N_{10}F_{12}P_2Ni$
T/K	298K	298K
Fw	704.26	923.30
Crystal system	Monoclinic	Monoclinic
Space Group	C 2/c	$P2_1/n$
a/Å	14.1874(11)	9.9901(5)
b/*Å*	15.9076(12)	16.0963(8)
c/ *Å*	14.6290(11)	25.2883(12)
α/deg	90	90
β/deg	102.102(3)	93.765(2)
γ/deg	90	90
V/ *Å*^{3}	3228.2(4)	4057.7(3)
Z	4	4
D_c/mgm^{-3}	1.449	1.511
μ/mm^{-1}	0.809	0.652
F(000)	1448	1864
cryst size/mm^3	0.37 × 0.26 × 0.16	0.5× 0.4 × 0.2
θ/deg	2.56 – 24.53	2.25 – 25.64
Measured reflns	9936	9245
Unique reflns	3579	5656
[a]GOF on F^2	1.034	1.087
R1[b], wR2[c][$I>2\sigma(I)$]	0.0339, 0.0704	0.0728, 0.1421
R1, wR2	0.0505, 0.0774	0.1013, 0.1549
[a]GOF = $\{\Sigma[w(F_o{}^2-F_c{}^2)2]/(n-p)\}^{1/2}$. [b]R1 = $\Sigma\,[\lvert F_o\rvert-\lvert F_c\rvert]/\,\Sigma\,\lvert F_o\rvert$. [c]wR2 = $[\Sigma\,[w(F_o{}^2-F_c{}^2)^2]/\,\Sigma\,[w(F_o{}^2)^2]]^{1/2}$ where w = 1/[$\sigma^2(F_o{}^2)+(aP)^2+bP$], P = $(F_o{}^2+2F_c{}^2)/3$.		

Table 2. Selected Experimental and Theoretical Bond Parameters of **1a** and **1b** complex.

1a			**1b**		
Parameter	**Expt.**	**Theo.**	**Parameter**	**Expt.**	**Theo.**
Ni1–Cl1	2.376(5)	2.421	Ni1–N1	2.060(4)	2.140
Ni1–Cl1a	2.376(5)	2.421	Ni1–N3	2.013(4)	2.043
Ni1–N1	2.067(6)	2.089	Ni1–N4	2.196(4)	2.279
Ni1–N1a	2.067(5)	2.089	Ni1–N6	2.062(4)	2.142
Ni1–N3	2.148(4)	2.224	Ni1–N8	1.995(4)	2.043
Ni1–N3a	2.148(4)	2.224	Ni1–N9	2.191(4)	2.282
N2–N3	1.259(2)	1.252	N2–N3	1.260(5)	1.257
N4–N5	1.250(2)	1.256	N4–N5	1.267(5)	1.257

Cl1Ni1Cl1a	93.08(3)	94.08	N7–N8	1.256(5)	1.257
N1Ni1Cl1	93.88(4)	91.76	N9–N10	1.263(5)	1.257
N1aNi1Cl1a	93.88(4)	91.76	N1Ni1N4	153.27(15)	152.59
N1aNi1Cl1	96.34(5)	95.99	N1Ni1N6	90.13(15)	95.01
N1Ni1Cl1a	96.34(5)	95.99	N1Ni1N9	88.20(15)	86.65
N1Ni1N1a	165.13(9)	168.61	N3Ni1N1	76.74(15)	75.74
N1aNi1N1	165.13(9)	168.61	N3Ni1N4	77.01(15)	76.94
N1Ni1N3	74.82(6)	74.77	N3Ni1N6	96.35(14)	97.68
N1aNi1N3a	74.82(6)	74.77	N3Ni1N9	108.99(15)	109.17
N1Ni1N3a	95.67(6)	97.90	N6Ni1N4	87.77(14)	86.62
N1aNi1N3	95.67(6)	97.90	N6Ni1N9	153.47(15)	152.61
N3Ni1Cl1	170.08(4)	170.10	N8Ni1N1	95.34(15)	97.39
N3aNi1Cl1a	170.08(4)	170.10	N8Ni1N3	169.34(15)	170.24
N3Ni1Cl1a	83.21(4)	82.83	N8Ni1N4	109.98(15)	109.47
N3aNi1Cl1	83.21(4)	82.83	N8Ni1N6	76.31(15)	75.78
N3Ni1N3a	101.89(8)	101.73	N8Ni1N9	77.48(16)	76.89
C1N1Ni1	128.03(14)	127.38	N9Ni1N4	105.13(14)	104.29
C1aN1aNi1	128.03(14)	127.38	C1N1Ni1	130.7(3)	131.24
C5N1Ni1	114.34(12)	113.93	N2N3Ni1	120.4(3)	120.74
C5aN1aNi1	114.34(12)	113.93	N7N8Ni1	122.2(3)	120.69

IV.2.4. Absorption spectra

The electronic spectra of compounds **1a** and **1b** (figure 5) exhibit bathochromically shifted profiles due to the electron-accepting bis-azo ligand. Theoretical studies suggest that the orange-red coloration arises from intraligand charge-transfer (ILCT) π→π* transitions, leading to absorption in the blue-green region of the visible spectrum.

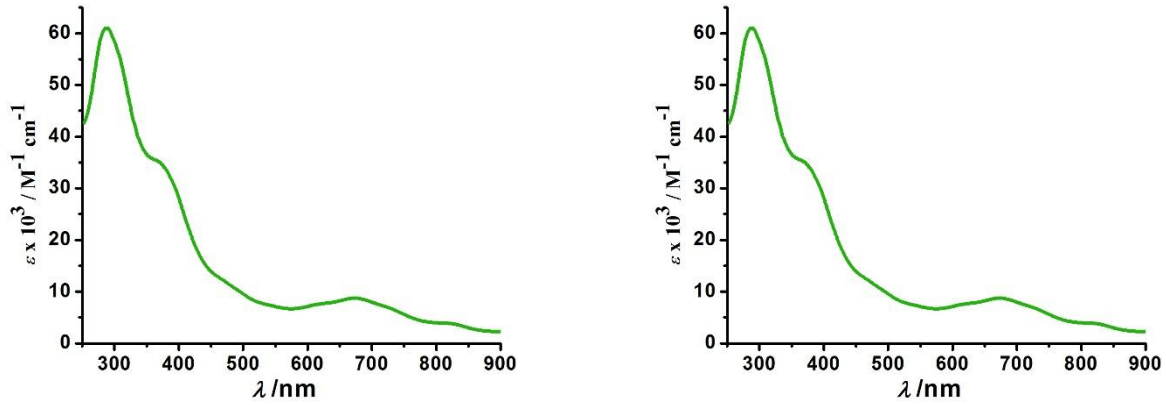

Figure 5. Experimental absorption spectra of **1a** (left) and **1b** (right) in dichloromethane.

IV.2.5. Electronic Structure and FMOs

The singlet ground state (S_0) and excited state molecular geometries of synthesised complex **1a** and **1b** were computed by DFT method by employing (R)B3LYP in GAUSSIAN 09 programme package. The solution phase optimised geometries of the complexes were found without applying any geometry constraints. In order to verify all stationary points as the true minima in potential energy surface, frequency calculation was executed. The absence of any imaginary frequency (NImag = 0) indicates that all the obtained stationary points are indeed the true minima in potential energy surface. The X-Ray positional coordinates of complex **1a** and **1b** were directly used as the initial input for geometry optimisation calculation.

Table 3. Coordinates of Optimised structure of complex **1a**.

Tag	Symbol	X	Y	Z
1	Ni	6.326945	9.590997	3.575985
2	Cl	4.546986	7.920241	3.349381
3	N	6.169119	9.798236	5.649192
4	N	8.161125	11.07991	5.380222
5	N	7.95439	10.99485	4.148457
6	N	7.66951	12.89844	2.075517
7	N	7.595381	13.61227	1.045072
8	C	5.257969	9.245865	6.450846
9	H	4.493535	8.656167	5.959665
10	C	5.294166	9.403226	7.838074
11	H	4.531712	8.935487	8.448556
12	C	6.319548	10.1487	8.407878
13	H	6.378491	10.28158	9.481715
14	C	7.280504	10.71541	7.573821
15	H	8.110372	11.29424	7.958203
16	C	7.159402	10.52025	6.201991
17	C	9.074724	11.39703	3.356118
18	C	10.32354	10.83862	3.65085
19	H	10.40054	10.14409	4.477053
20	C	11.42695	11.13322	2.861042
21	H	12.38751	10.6858	3.091089
22	C	11.2933	12.0007	1.773435
23	H	12.15428	12.23988	1.158735
24	C	10.06168	12.56983	1.484238
25	H	9.955585	13.26855	0.665054
26	C	8.931833	12.27493	2.262935
27	C	6.385471	14.31355	0.845533
28	C	6.267482	14.95497	-0.39582
29	H	7.079582	14.86487	-1.10892
30	C	5.124397	15.68872	-0.69868
31	H	5.034664	16.17862	-1.66213

32	C	4.101154	15.79882	0.243201
33	H	3.212441	16.37744	0.014341
34	C	4.223263	15.17107	1.487978
35	H	3.429463	15.26747	2.221237
36	C	5.355764	14.42821	1.794561
37	H	5.455447	13.94513	2.757823
38	Cl	8.106938	7.920281	3.802599
39	N	6.484744	9.79819	1.502779
40	N	4.492717	11.07983	1.771754
41	N	4.699487	10.99482	3.003517
42	N	4.984446	12.8983	5.076509
43	N	5.058639	13.61207	6.106991
44	C	7.395872	9.245787	0.701124
45	H	8.160342	8.656142	1.192315
46	C	7.359606	9.403043	-0.68611
47	H	8.122044	8.935279	-1.29659
48	C	6.334175	10.14845	-1.25592
49	H	6.275177	10.28124	-2.32977
50	C	5.373245	10.7152	-0.42186
51	H	4.543343	11.29397	-0.80625
52	C	5.494414	10.52013	0.949975
53	C	3.579166	11.397	3.795877
54	C	2.330348	10.83859	3.501162
55	H	2.253321	10.14408	2.674948
56	C	1.226954	11.13319	4.290998
57	H	0.266386	10.68578	4.060961
58	C	1.360627	12.00064	5.378621
59	H	0.499664	12.23981	5.993347
60	C	2.592258	12.56975	5.667808
61	H	2.698384	13.26845	6.487016
62	C	3.722087	12.27487	4.889075
63	C	6.268513	14.31344	6.306431
64	C	6.386623	14.95474	7.547837
65	H	5.574628	14.8645	8.261038
66	C	7.529695	15.68853	7.850612
67	H	7.619524	16.17834	8.814105
68	C	8.552804	15.79881	6.90861
69	H	9.441505	16.37748	7.13741
70	C	8.430572	15.17118	5.663783
71	H	9.224267	15.26772	4.930427
72	C	7.298084	14.42827	5.357278
73	H	7.198309	13.94528	4.393981

Table 4. Coordinates of Optimised structure of complex **1b**.

Tag	Symbol	X	Y	Z
1	Ni	7.073017	11.48773	8.299386
2	N	5.544258	11.04927	6.863782
3	N	7.052212	13.52	8.092883
4	N	8.590022	11.88376	6.841982
5	N	7.084465	9.449589	8.158448
6	N	7.817939	14.08984	7.274512
7	N	8.766737	10.88382	9.700685
8	N	6.314003	8.856158	7.361692
9	N	5.388091	12.1329	9.697393
10	N	9.773676	11.49206	10.14327
11	N	4.39085	11.53443	10.17377
12	C	8.693855	13.21219	6.615281
13	C	6.090497	14.27619	8.768775
14	C	4.725033	11.84845	6.180977
15	H	4.83303	12.91437	6.341252
16	C	5.438423	9.714767	6.677399
17	C	8.937527	9.46564	9.650722
18	C	9.407643	11.0649	6.180902
19	H	9.300769	10.00423	6.373531
20	C	8.04415	8.712076	8.857453
21	C	5.205767	13.54666	9.593806
22	C	9.685762	12.85763	10.42937
23	C	4.49661	10.18293	10.51559
24	C	9.617509	13.75985	5.730541
25	H	9.648451	14.83265	5.590424
26	C	5.965819	15.66636	8.640139
27	H	6.649711	16.20229	7.995382
28	C	8.544341	13.45627	10.98717
29	H	7.668355	12.85645	11.1977
30	C	4.217709	14.23282	10.3068
31	H	3.556366	13.68145	10.96119
32	C	5.648288	9.62456	11.09357
33	H	6.515957	10.24574	11.27464
34	C	8.158217	7.317226	8.780851
35	H	7.466926	6.762333	8.160466
36	C	10.36578	11.52959	5.276108
37	H	11.00496	10.82049	4.765593
38	C	8.584342	14.79765	11.34655
39	H	7.717701	15.25608	11.80927
40	C	3.763587	11.35776	5.293492
41	H	3.123134	12.05201	4.764481
42	C	4.511849	9.141634	5.812122
43	H	4.479627	8.065139	5.704291
44	C	9.924271	8.799889	10.38449
45	H	10.59273	9.370984	11.01428
46	C	4.97297	16.32761	9.342655

47	H	4.87361	17.40286	9.252539
48	C	3.654115	9.985196	5.109091
49	H	2.918705	9.574262	4.428078
50	C	10.86818	13.59994	10.26607
51	H	11.75147	13.10721	9.87635
52	C	10.47389	12.89618	5.05076
53	H	11.20708	13.28692	4.355613
54	C	4.103409	15.61047	10.1769
55	H	3.336258	16.13571	10.73413
56	C	5.628432	8.299007	11.50915
57	H	6.50306	7.87261	11.9872
58	C	9.149716	6.675766	9.503407
59	H	9.24087	5.597162	9.453661
60	C	10.88028	14.95087	10.5847
61	H	11.78259	15.53261	10.43465
62	C	3.324061	9.418408	10.38857
63	H	2.432537	9.881865	9.982024
64	C	9.741091	15.5501	11.12952
65	H	9.763436	16.59734	11.41001
66	C	10.02834	7.417536	10.30604
67	H	10.79443	6.908181	10.87925
68	C	3.332281	8.08203	10.76355
69	H	2.437803	7.481899	10.64167
70	C	4.481803	7.522069	11.3282
71	H	4.475251	6.4872	11.65206

Table 5. Frontier α-Molecular Orbital Composition (%) in the Ground State for **1a** complex.

Orbital	MO	Energy (eV)	Composition					
			Ni	Cl	pyazo	phazo	py	ph
183	L+5	-1.47	0	0	3	1	94	2
182	L+4	-1.49	0	0	4	0	96	0
181	L+3	-2.72	0	0	14	36	10	40
180	L+2	-2.73	0	1	13	35	13	39
179	L+1	-3.28	0	2	39	14	24	21
178	LUMO	-3.31	2	2	38	14	25	19
177	HOMO	-5.57	2	94	4	0	0	0
176	H–1	-5.88	12	67	14	1	2	4
175	H–2	-5.89	2	96	2	0	0	0
174	H–3	-5.99	5	90	5	0	0	0
173	H–4	-6.03	10	90	0	0	0	0
172	H–5	-6.37	13	47	6	2	24	8

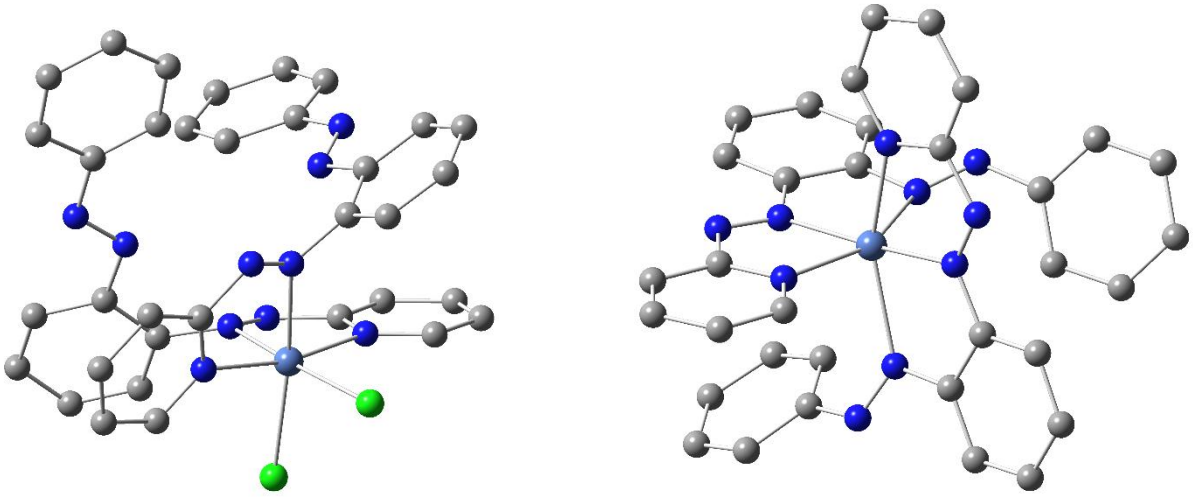

Figure 6. Solvent phase optimised geometry of **1a** (left) and **1b** (right) complex (H's are omitted for clarity) calculated at B3LYP/6-311+G(d,p) level of theory.

IV.2.6. Electrochemistry and EPR

The electron-transfer properties of complex **1a** were investigated via cyclic voltammetry in acetonitrile (0.2 M Bu_4NPF_6) using a platinum working electrode. The voltammogram of **1a** displayed well-defined reductive responses at −0.37 V (ΔEp = 130 mV) vs. ferrocenium/ferrocene (Fc^+/Fc) reference couple (Figure 7), demonstrating its significant electron-accepting capability. Additionally, DFT calculations [(U)B3LYP/6-311+G(d,p)] reveal that the LUMO is predominantly localized on the ligand framework, especially with the pyridyl-azo moiety contributing around 60%, while metal orbital participation remains minimal (5%), corroborating a ligand-centered redox process (Table 5). The redox potential of $[Ni^{II}(L^{\bullet-})(L)Cl_2]^-$ highlights its role as an electron

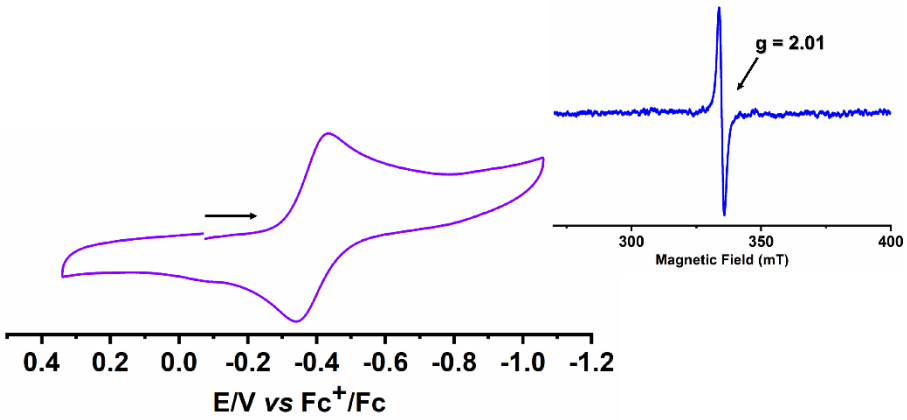

Figure 7. Cyclic voltammogram of **1a** in CH_3CN/0.4 M Bu_4NPF_6 (Pt electrode, 100 mV s^{-1}). Inset: X-band EPR of $\mathbf{1a}^{\bullet-}$ in toluene (9.43 GHz, 1 mW, 1.0 mT mod., 100 kHz mod. freq., 298 K).

reservoir in catalysis. EPR studies confirm ligand-centered radical formation (g = 2.01, ΔH ≈ 2 mT), which is absent without Ni catalyst **1a**, indicating a nickel-bound azo-anion radical (inset of figure 7). The catalyst alone also produces a similar signal in the presence of a base, supporting a radical pathway in cascade annulation (Scheme 5). The π-accepting pyridylazo-based Ni(II) catalyst exhibits strong electron affinity, with the azo radical forming even under mild reduction (KOtBu), facilitated by its low-lying π* orbital (−3.78 eV, Table 5).

IV.2.7. Catalytic Activity

Over the past four years, pincer complexes, including both noble-metal and base-metal variants, have gained prominence in organometallic chemistry and organic synthesis, particularly for their catalytic applications in (de)hydrogenation and transfer (de)hydrogenation reactions.[16]

IV.2.7.1. Synthesis of pyridines

Here, we proposed that alcohol dehydrogenation, followed by sequential C–C and C–N bond construction, could lead to the formation of dihydropyridines. These intermediates may subsequently undergo *in-situ* dehydrogenation to yield pyridines, facilitated by the remarkable catalytic dehydrogenation efficiency of complex **1a**. Bergman and Ellman groups[17] described a two-step approach for synthesizing pyridines through dihydropyridine intermediates. In this approach, dihydropyridines are initially generated via rhodium-catalyzed C–H activation and electrocyclization, then converted to pyridines through Pd/C-catalyzed air oxidation in acetic acid. Developing a single catalyst capable of both forming the dihydropyridine intermediate and dehydrogenating it to the final pyridine in a single reaction step would be a valuable advancement. In pursuit of optimal conditions for synthesizing 2,4,6-triarylpyridines, various reaction parameters were evaluated using a model reaction involving 1-phenyl ethanol **3a**, benzyl alcohol **2a**, ammonium acetate, and catalyst **1**. The main objective of our optimization study was to maximize the isolated yield of desired pyridine by exploring systematic variations in catalysts, reaction conditions, and solvents. Using conventional method, initial reactions at 110 °C for 12 hrs with 100 mol% KO*t*Bu in toluene yielded no detectable traces of the desired product **6aa** (Table 6, entry 1). The addition of 1.00 mol% of complex **1a** to the reaction mixture under the same conditions resulted in a substantial yield of 82% of **6aa** along with numerous side products (entry 2). Even after substituting toluene with xylene as the reaction medium, we were unable to reduced side products (entries 3–5).

Table 6. Optimization of the reaction conditions for Ni(II) catalyzed 2,4,6-trisubstituted pyridine synthesis[a]

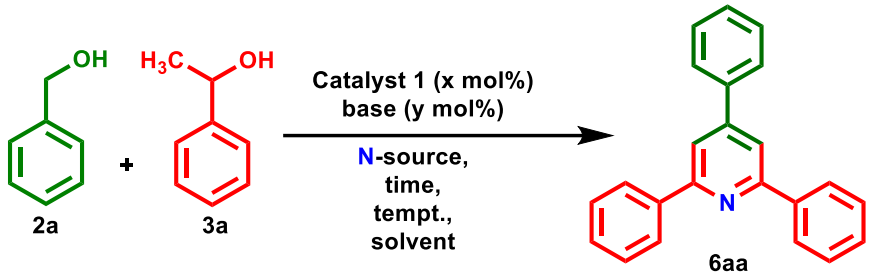

Entry	Catalyst (X mol%)	Solvent	Base (Y mol%)	Temp (°C)	Time (hrs)	Yield[b] (%)
1		Toluene	KO*t*Bu (100)	110	12	trace
2	**1a** (1.00 mol%)	Toluene	KO*t*Bu (100)	110	12	82
3	**1a** (1.00 mol%)	Xylene	KO*t*Bu(100)	110	12	78
4	**1a** (1.00 mol%)	Methanol	KO*t*Bu(100)	60	12	trace
5	**1a** (1.00 mol%)	DMSO	KO*t*Bu(100)	110	12	trace
6	**1a** (1.00 mol%)	Toluene	K_2CO_3 (100)	110	12	51
7	**1a** (1.00 mol%)	Toluene	NEt_3(100)	110	12	46
8	**1a** (1.00 mol%)	Neat	KO*t*Bu(100)	110, MW	2	91
9	**1a** (1.00 mol%)	Neat	KO*t*Bu(100)	80, MW	2	91
10	**1a** (1.00 mol%)	Neat	K_2CO_3 (100)	80, MW	2	49
11	**1a** (1.00 mol%)	Neat	NEt_3(100)	80, MW	2	43
12	**1a** (1.00 mol%)	Neat	KO*t*Bu (50)	80, MW	2	90
13	**1a** (1.00 mol%)	Neat	KO*t*Bu (20)	80, MW	2	91
14	**1a** (0.1 mol%)	Neat	KO*t*Bu (20)	80, MW	2	91
15	**1a** (0.01 mol%)	Neat	KO^{t}Bu (20)	80, MW	2	91
16	**1a (0.002 mol%)**	**Neat**	**KO*t*Bu (20)**	**80, MW**	**2**	**91**
17	**1a** (0.001 mol%)	Neat	KO*t*Bu (20)	80, MW	2	79
18	**1a** (0.002 mol%)	Neat	KO*t*Bu (20)	70, MW	2	84
19	**1a** (0.002 mol%)	Neat	KO*t*Bu (20)	50, MW	2	32
20[c]	**1a** (0.002 mol%)	Neat	KO*t*Bu (20)	RT, MW	2	ND
21	**1a** (0.002 mol%)	Neat		80, MW	2	ND
22		Neat	KO*t*Bu (20)	80, MW	2	ND
23	**1b** (0.002 mol%)	Neat	KO*t*Bu (20)	80, MW	2	trace
24	$NiCl_2$. $6H_2O$(1.00 mol%)	Neat	KO*t*Bu (20)	80, MW	2	trace
25	$\mathbf{L^H}$: $NiCl_2.6H_2O$ (1:1)	Neat	KO*t*Bu (20)	80, MW		trace

[a]Reaction Conditions: benzyl alcohol **2a** (1.10 mmol), 1-phenyl ethanol **3a** (2.00 mmol), ammonium acetate (4.00 mmol), reaction time (2 hrs), base (20 mol%), neat conditions, MW: microwave reactions are performed under air in a sealed tube closed vessel system., [b]isolated yields after column chromatography, [c]room temperature, ND = Not Detected.

Therefore, to improve the yield of **6aa**, the reaction was conducted in polar solvents such as methanol, DMSO, and DMF; however, no detectable amount of the desired product was formed (entries 4 and 5). Furthermore, to address the formation of multiple side products during the reaction, we opted to use a weak base like K_2CO_3. However, the yield drastically reduced when K_2CO_3 was used (entry 6). When an organic base triethylamine i.e., NEt_3 was used as a base the yield of the desired product also decreased (entry 7). As part of our ongoing efforts to develop environmentally sustainable methods, we chose to carry out the reaction using microwave reactor under solvent-free conditions. In this instance, the reaction mixture comprising **2a**, **3a** and ammonium acetate was subjected to microwave reactor (50 W) in the presence of 100 mol% KO*t*Bu for 2 hrs (entry 8). Notably, the improvement in the isolated yield enthused us to further explore the solvent-free, microwave-assisted domino reaction using a variety of reagents. Various bases, including KO*t*Bu, NaO*t*Bu, KOH, NaOH, Cs_2CO_3, K_2CO_3, Na_2CO_3, NEt_3 and pyridine, were evaluated revealing that strong bases, particularly KO*t*Bu, were most effective in achieving high product yields, while weaker bases exhibited lower activity under microwave conditions (entries 9–11). Fortunately, lowering KO*t*Bu to 20 mol% demonstrated excellent reactivity in the cascade reaction, leading to the formation of **6aa** with yield to 91% (entries 12 *vs* 13) under microwave assisted solvent-free condition in 2 hrs. A decrease in catalyst loading from 1 mol% to 0.1 mol%, 0.01 mol%, or 0.002 mol% yielded comparable yields of **6aa**, while significantly increasing the TONs (entries 14–16). Further lowering the catalyst loading to 0.001 mol% the yield of the desired product decreased (entry 17). Reducing the reaction temperature from 110 °C to 80 °C had minimal impact (entries 8 *vs* 9); however, at 80 °C temperature and with a 0.001 mol% loading of **1a**, the yield of **6aa** decreased from 91% to 79% (entries 16 *vs* 17). The reaction with catalyst **1b** resulted in a trace amount of yield of the desired pyridine compared to catalyst **1b** (entries 16 *vs* 23). Notably, blank experiment established that both the catalyst and the base are crucial for the progression of the ADC reaction (entries 21, 22). Consequently, the optimized reaction conditions were determined to be 0.002 mol% of catalyst **1a**, 50 mol% of KO*t*Bu, at 80 °C for 2 hrs under solvent-free microwave conditions (entry 16).

Using the optimized conditions, we efficiently synthesized various symmetrical and unsymmetrical pyridine derivatives, including 2,4,6-trisubstituted, 2,3,4,6-tetrasubstituted, and 2,3,4,5,6-pentasubstituted compounds, through a multicomponent dehydrogenative coupling reaction involving primary and secondary alcohols, with NH_4OAc as the nitrogen source. We began by assessing the performance of different aryl primary alcohols in this synthesis (Table

7). Various benzylic alcohols demonstrated good reactivity, providing the corresponding trisubstituted pyridines with isolated yields of 71–91%. Benzyl alcohols with both electron-donating and electron-withdrawing groups reacted efficiently, yielding the desired products in 71–91% (Table 7, 6ab–ak). For instance, Benzyl alcohol substituted with 4-Me, 4-OMe, 3-Me,

Table 7. Three-component 2,4,6-trisubstituted pyridines: scope of primary alcohols

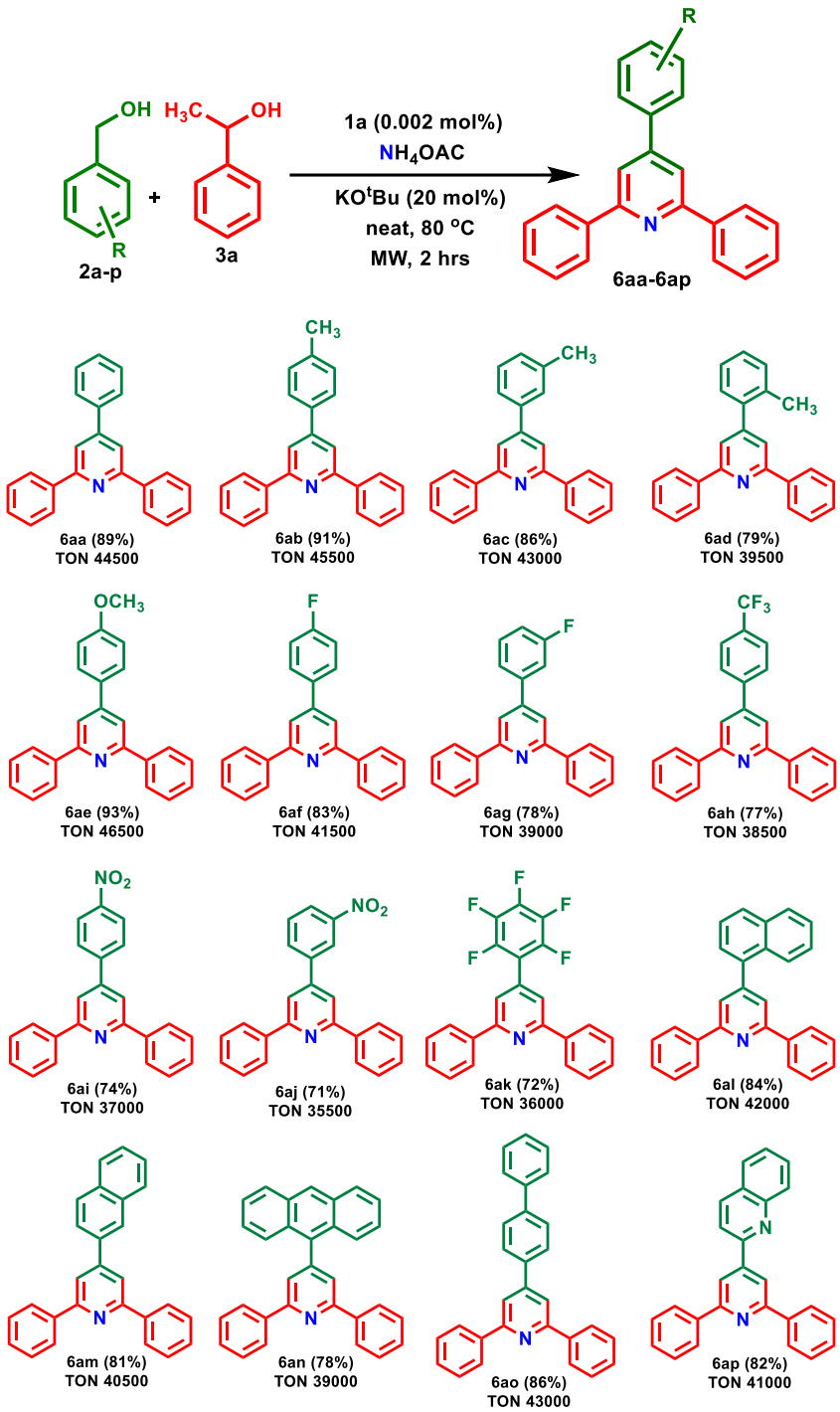

[a]Reaction conditions: primary alcohols **2a-p** (1.10 mmol); 1-phenyl ethanol **3a** (2.00 mmol); base (20 mol%), neat condition, microwave-assisted. [b]Isolated yields after column chromatography.

2-Me group also selectively yielded the anticipated product with good to excellent yield (Table 7, 6ab-ae). Halogen-substituted benzyl alcohols reacted smoothly, affording the desired products (Table 7, 6af-ah and 6ak). Interestingly, challenging nitro-benzyl alcohols[18] also selectively yielded the corresponding pyridine with this methodology (Table 7, 6ai-aj).

After investigating various primary alcohols, we then assessed the performance of diverse secondary alcohols for this synthetic protocol.

Table 8. Three-component 2,4,6-trisubstituted pyridines: scope of secondary alcohols

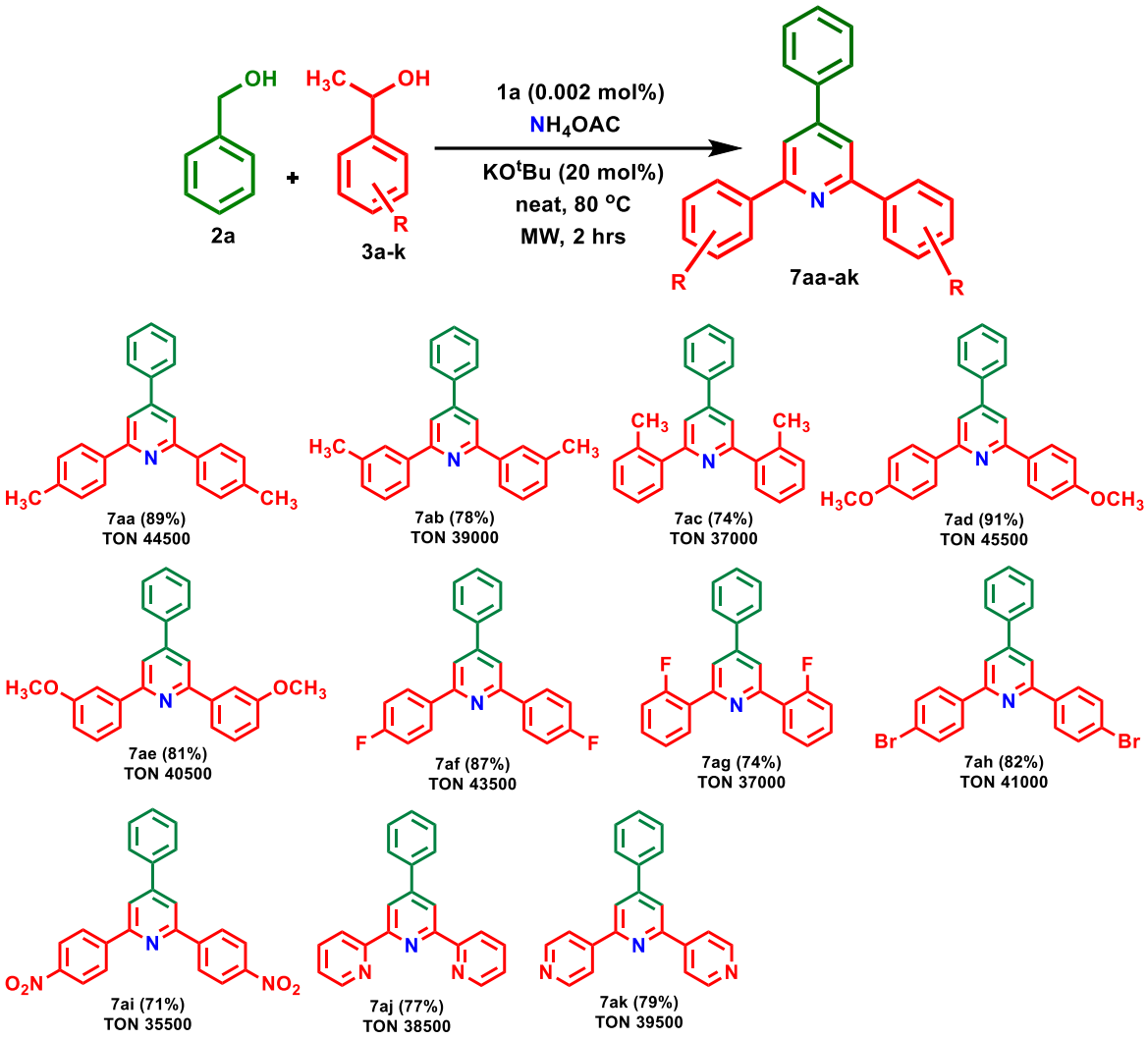

[a]Reaction conditions: benzyl alcohol **2a** (1.10 mmol); secondary alcohols **3a-k** (2.00 mmol); base (20 mol%), neat condition, microwave-assisted. [b]Isolated yields after column chromatography.

Aryl secondary alcohol featuring electron-withdrawing or electron-donating groups at the ortho-, para- or meta-position of the phenyl ring, underwent efficient conversion to the corresponding trisubstituted pyridines with moderate to high yields (Table 8). Electron-donating groups, such as *p*-Me and *p*-OMe substituted 1-phenyl ethanol, provided higher yields

compared to the unsubstituted 1-phenyl ethanol (Table 8, 7aa and 7ad), resulting in the corresponding trisubstituted pyridine with yields ranging from 89–91%. In contrast, electron-withdrawing groups, such as flouro, nitro group resulted in lower yields compared to the unsubstituted 1-phenyl ethanol (Table 8, 7af and 7ai), leading to the corresponding trisubstituted pyridine with yields ranging from 71–87%. Similarly, halogen derivatives yielded the desired product in good yields, with without impact on the halogen functionality (Table 8, 7ag and 7ah). Pyridines were obtained in relatively higher yields when electron-donating substituents were present, whereas a slight drop in yield was noted with electron-withdrawing substituents. Notably, heterocyclic moieties containing an ethan-1-ol group also performed well (Table 8, 7aj and 7ak), yielding the desired product with excellent efficiency. Catalyst **1a** demonstrated high functional group tolerance, facilitating the synthesis of tri-substituted products with simultaneous variations in the substituents on both the primary and secondary alcohols, achieving with good to excellent yields (Table 9).

The scope of various substituted primary and secondary alcohols was also examined, with NH_4OAc remaining unchanged. A diverse range of primary and secondary alcohols, including those bearing electron-donating, electron-withdrawing, and heteroaryl substituents, demonstrated compatibility under the optimized experimental conditions (Table 4).

Table 9: Three-component 2,4,6-trisubstituted pyridines: scope of both primary and secondary alcohols

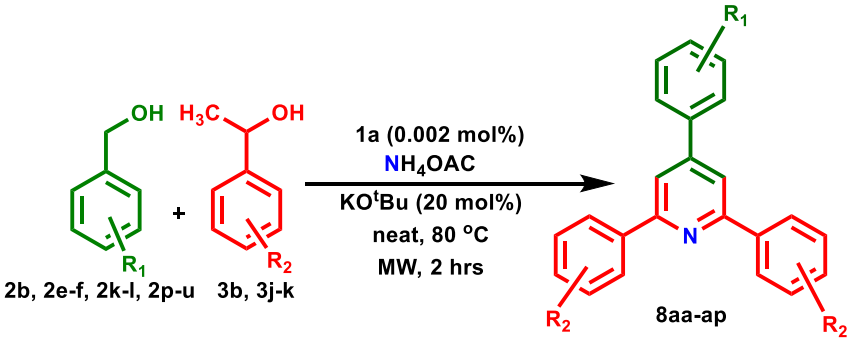

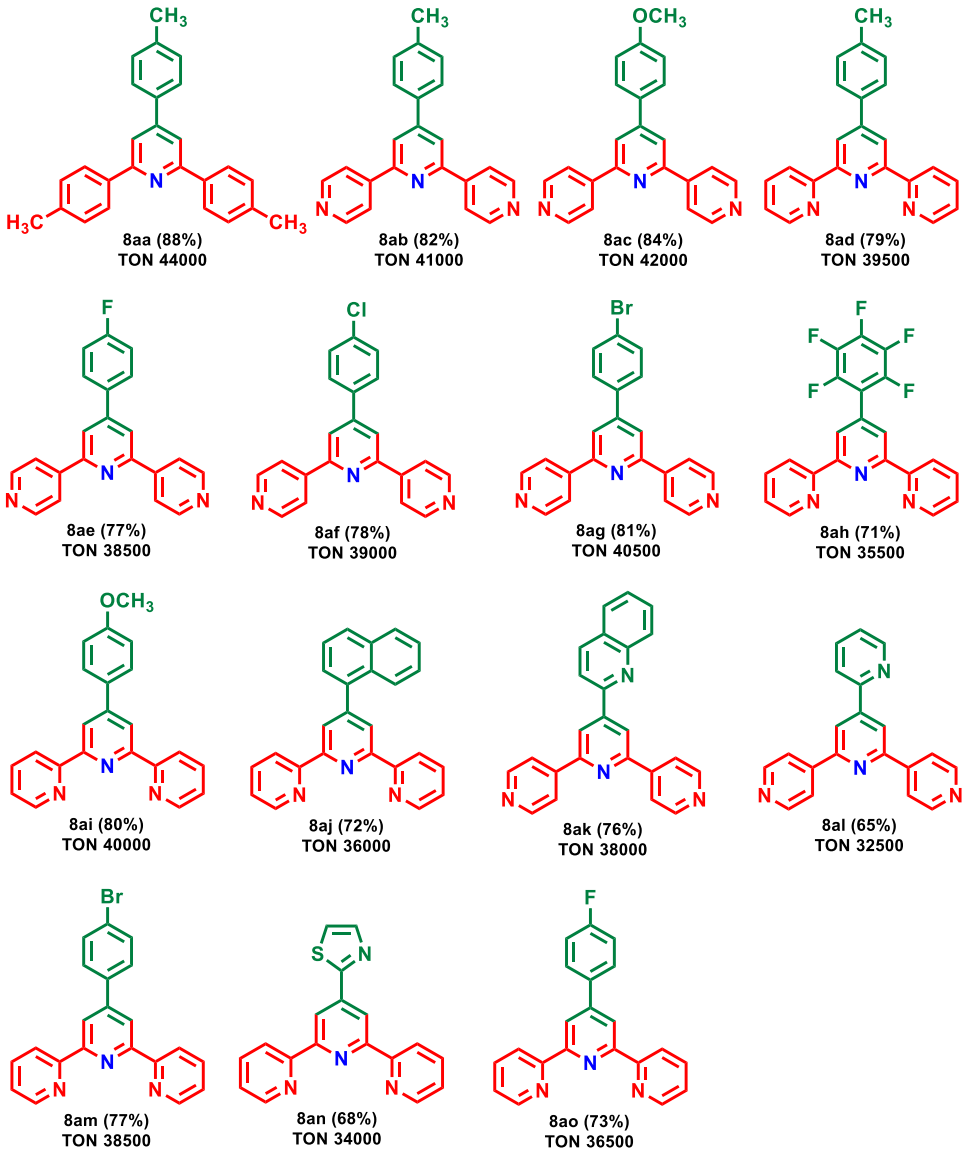

[a]Reaction conditions: primary alcohol **2b, 2e-f, 2k-l, 2p-u** (1.10 mmol); secondary alcohols **3b, 3j-k** (2.00 mmol); base (20 mol%), neat condition, microwave-assisted. [b]Isolated yields after column chromatography.

Pyridines were obtained in relatively higher yields when electron-donating substituents were present, whereas a slight reduction in yield was observed with halogen substituents (Table 9, entries 8ae-ah). In the presence of a penta-flouro group on the primary alcohol, compound **8ah** was obtained in a 71% yield. Heteroaryl secondary alcohols afforded the corresponding pyridines with yields ranging from 65% to 84% (Table 9, entries 8ab-ao).

We subsequently examined four-component reactions to synthesize unsymmetrical trisubstituted pyridines. In the presence of NH_4OAc, the reaction of primary alcohols with two differently substituted secondary alcohols proceeds efficiently yielding a diverse array of

Table 10: Four-component 2,4,6-trisubstituted pyridines: scope of both primary alcohols and secondary alcohols

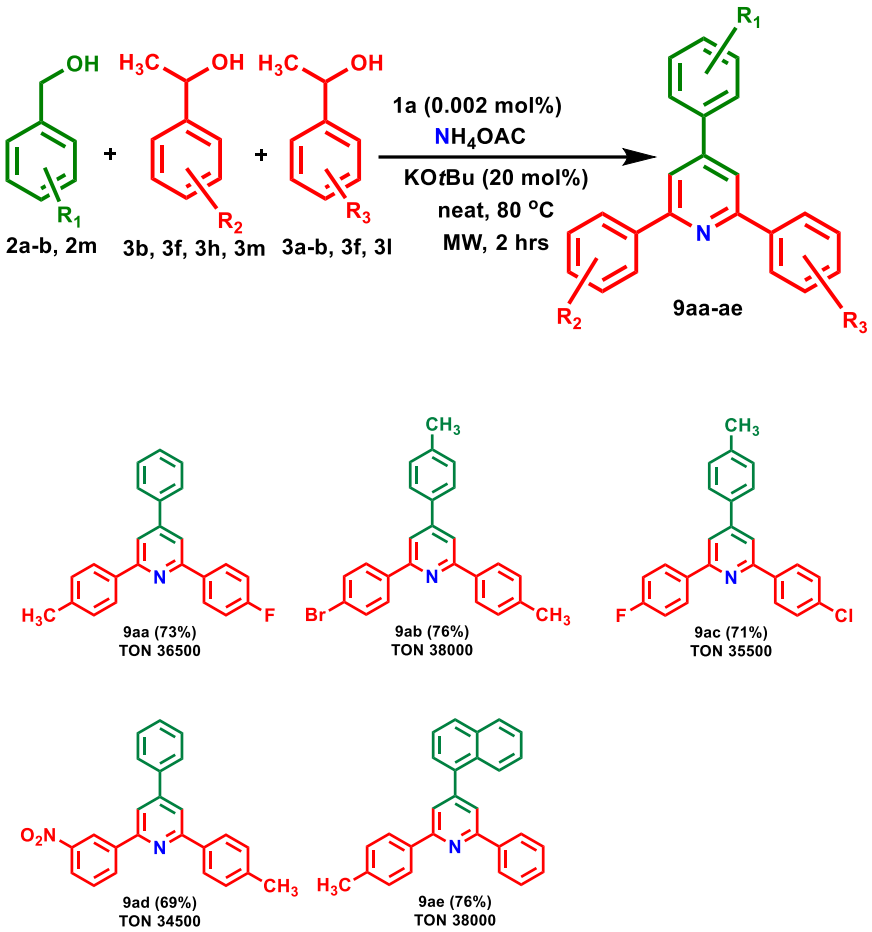

[a]Reaction conditions: primary alcohol **2a-b, 2m** (1.10 mmol); secondary alcohols(type1) **3b, 3f, 3h, 3m** (1.00 mmol); secondary alcohols(type2) **3a-b, 3f, 3l** (1.00 mmol); base (20 mol%), neat condition, microwave-assisted. [b]Isolated yields after column chromatography.

unsymmetrical trisubstituted pyridines in 69–76% yields. The reactions proceed efficiently with both electron-donating and electron-withdrawing groups, although a slightly lower yield when electron-withdrawing functionalities are present in the alcohol moiety (Table 10, 9aa-ae) Conspicuously, these reactions resulted in the regioselective formation of a single isomer, which can be attributed to the higher reactivity of one of the secondary alcohols, with the primary alcohol yielding only one α, β-unsaturated ketone as one the intermediates

To explore wide versatility of our catalyst, four-component coupling reactions were performed to synthesize unsymmetrical 2,3,4,6-tetrasubstituted pyridines (Table 11, 10aa-af). Compared to 2,4,6-trisubstituted pyridines, the synthesis of 2,3,4,6-tetrasubstituted pyridines resulted in slightly lower yields.

Table 11: Four-component 2,3,4,6-tetrasubstituted pyridines: scope of primary and secondary alcohols

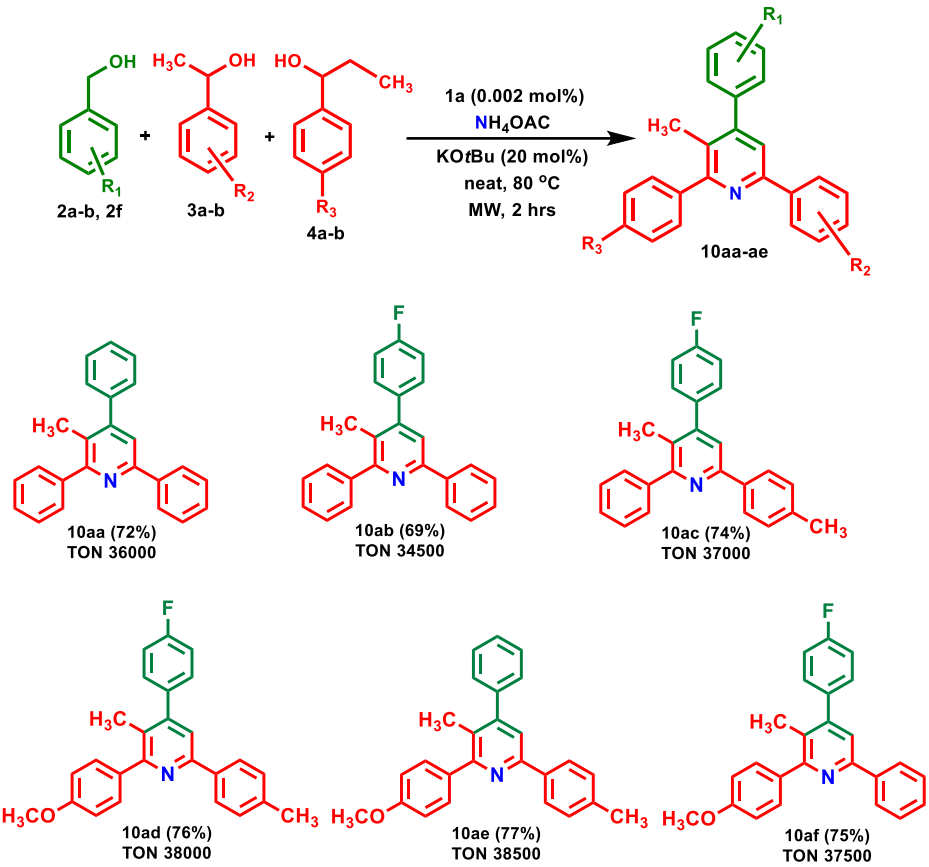

[a]Reaction conditions: primary alcohol **2a-b, 2f** (1.10 mmol); secondary alcohols(type1) **3a-b** (1.00 mmol); secondary alcohols(type2) **4a-b** (1.00 mmol); base (20 mol%), neat condition, microwave-assisted. [b]Isolated yields after column chromatography.

1-phenylpropanol and 1-(4-methoxyphenyl)propanol were employed as coupling partners with various primary and secondary alcohols, using NH_4OAc as the nitrogen source. 1-(4-methoxyphenyl)propanol afforded the desired tetrasubstituted pyridines in higher yields compared to 1-phenylpropanol (Table 11, entries 10ad–af). Both electron-donating and electron-withdrawing functionalities are compatible with the four-component coupling, providing 2,3,4,6-tetrasubstituted pyridines in isolated yields reaching from 69% to 77% (Table 11, 10aa--af).

Next, the coupling reactions were performed to synthesize 2,3,4,5,6-pentasubstituted pyridines (Table 12, 11aa-ad and 12aa-ad). 1-Phenylpropanol and 1-(4-methoxyphenyl)propanol

Table 12: 2,3,4,5,6-pentasubstituted pyridines: scope of primary and secondary alcohols

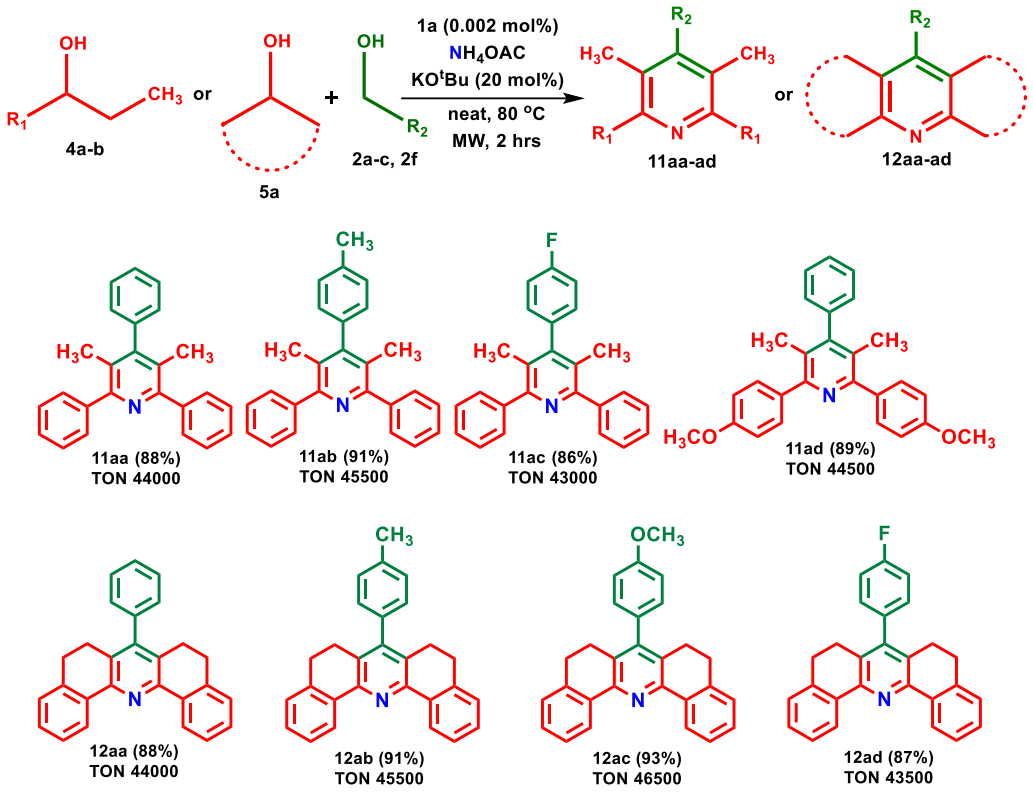

[a]Reaction conditions: primary alcohol **2a-c, 2f** (1.10 mmol); secondary alcohols(type1) **4a-b** (1.00 mmol); secondary alcohols(type2) **5a** (1.00 mmol); base (20 mol%), neat condition, microwave-assisted. [b]Isolated yields after column chromatography.

were used as coupling partners with both electron-releasing and electron-withdrawing primary alcohols to synthesize 2,3,4,5,6-pentasubstituted pyridine derivatives using standard reaction conditions. Pyridines were obtained in comparatively higher yields when electron-withdrawing substituents were present in primary alcohols, while a slight decrease in yield was observed with electron-releasing substituents. Furthermore, 1,2,3,4-tetrahydronaphthalen-1-ol was employed as coupling partner with various primary alcohols, using NH_4OAc as the nitrogen source. Electron-withdrawing and electron-donating functionalities are compatible with this reaction, resulting in the formation of 2,3,4,5,6-pentasubstituted pyridines in 87-93% isolated yields (Table 12).

To highlight the synthetic and industrial relevance of this methodology, the pyridine synthesis was performed on a gram scale (Scheme 2). Under standard conditions, pyridine derivatives were synthesized through the reaction of benzyl alcohol **2a** (10.20 mmol), 1-phenylethanol **3a** (20.00 mmol), and ammonium acetate (40.00 mmol), affording **6aa** in 81% yield (2.5 g) with high efficiency. Similarly, products **10aa** and **11aa** were obtained through scaled-up synthesis.

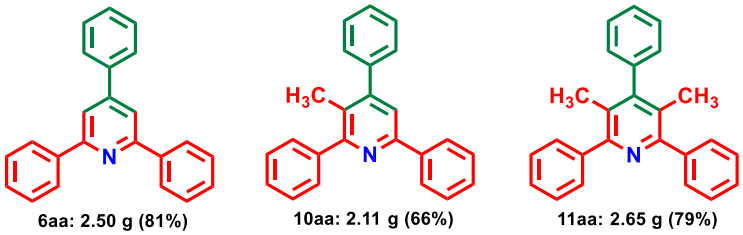

Scheme 2. Gram scale synthesis of pyridines.

IV.2.7.2. Mechanistic Investigation

After evaluating the substrate scope, we proceeded to study the plausible mechanism of the Ni-catalyzed multicomponent synthesis of substituted pyridine derivatives. To gain insights into the mechanism, we performed a series of controlled experiments (Scheme 3). When the reaction was conducted using only benzyl alcohol in the presence of **1a**, benzaldehyde was isolated, confirming that it is an intermediate in this coupling reaction, and

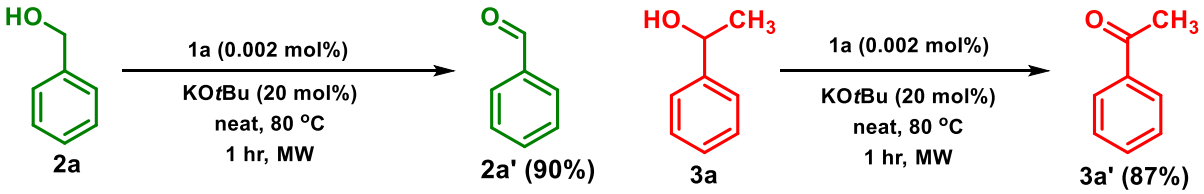

Scheme 3. Dehydrogenation of alcohols

hydrogen peroxide as a by-product was detected chromatographically. In the similar way, when the reaction was performed with 1-phenylethanol **3a**, the corresponding ketone was confirmed as sole product (Scheme 3). To identify possible intermediates, we reacted **2a** and **3a** under optimal conditions excluding NH_4OAc.

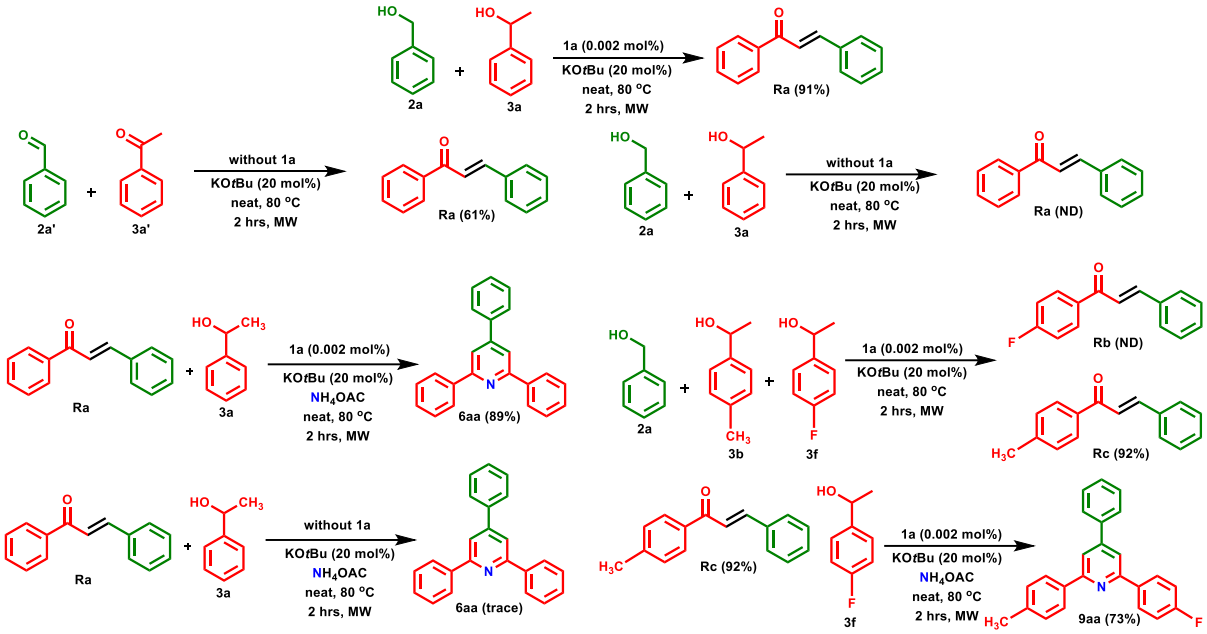

Scheme 4. Some control experiments performed for the synthesis of pyridines.

This led to the exclusive formation of a chalcone **Ra**, as evidenced by the product analysis in Scheme 4. To corroborate the intermediary of the chalcone, the synthesized chalcone was subjected to the same reaction conditions in the presence of NH_4OAc, leading to a quantitative conversion to the desired substituted pyridine (Scheme 4). Furthermore, analysis of the crude reaction mixture by ^1H NMR spectroscopy after 1 hr of reaction time revealed the formation of benzaldehyde and corresponding α, β unsaturated ketone as intermediates (Scheme 4). However, only trace amounts of **Ra** were obtained when the same reactions were repeated without **1a**. Conversely, when preformed benzaldehyde and acetophenone were reacted in the presence of 1.0 equiv. of KO*t*Bu, **Ra** was isolated in 61% yield. No **Ra** was obtained when benzaldehyde **2a′** and acetophenone **3a′** were reacted in the absence of catalyst and base (Scheme 4). This observation suggests that catalyst **1a** plays a crucial role in the oxidation of alcohols to the corresponding carbonyl compounds, which subsequently undergo in situ C-C coupling to generate intermediate **Ra**. Notably, **6aa** was isolated at only trace amount in the absence of catalyst **1a** under standard conditions starting from 3,4-dihydropyridine, indicating the significant role of catalyst **1a** in enhancing the yield of **6aa** during this aromatization step (Scheme 5). Thus, we concluded that catalyst **1a** is vital for the dehydrogenative aromatization of 3,4-dihydropyridine, demonstrating its effectiveness in facilitating these transformations.[15]

Based on these experimental results and literature examples, we propose plausible catalytic cycles for both the dehydrogenation of alcohols and dehydrogenative aromatization, as depicted in Scheme 5. Primarily, catalyst **1a** undergoes a single-electron reduction with

KO*t*Bu to form **[1a]**$^{\bullet-}$, which reacts with deprotonated alcohol in the presence of base to generate the alkoxy intermediate accompanied by the release of a chloride ligand.

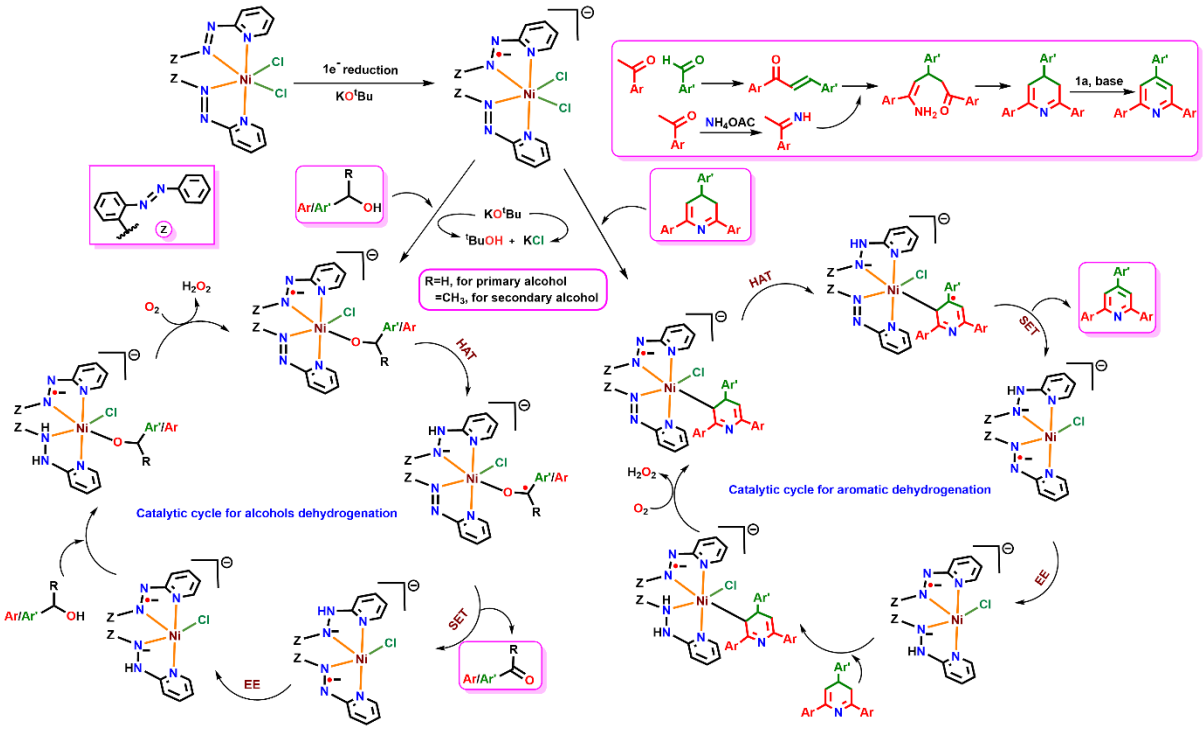

Scheme 5. Proposed reaction mechanism for Ni(II)-mediated annulation reactions.

Since, **[1a]**$^{\bullet-}$ comprises an organic azo-anion radical ligand bound to the Ni(II) center, we examined the dehydrogenation of the radical-clock substrate cyclobutanol. This reaction could proceed either through a one-electron hydrogen atom transfer (HAT) mechanism, where the β-hydrogen of the Ni-alkoxy intermediate is abstracted by the azo-anion radical ligand, or *via* a two-electron pathway involving the formation of a Ni-hydride intermediate. Cyclobutanol, used as a radical-clock substrate, was subjected to dehydrogenation under the optimized conditions. The generation of multiple ring-cleavage products aligns with the one-electron HAT mechanism, involving a ketyl radical intermediate.[15] A series of control experiments, complemented by EPR analysis, were performed to clarify the specific role of each reaction component. For example, the EPR signal observed in the presence of catalyst **1a** and the base KO*t*Bu indicates the formation of an azo-anion radical complex as an intermediate species. The experimental EPR spectrum and its simulation unequivocally support the formation of a ligand-centered azo-anion radical complex of **1a**, specifically $[Ni(L^{\bullet-})_2Cl_2]^-$ (Scheme 5). The EPR spectrum of the standard reaction showed no detectable signal in the absence of either catalyst **1a** or the base KO*t*Bu, or both, even in the presence of alcohols. To investigate the involvement of a radical pathway, we performed model reactions with radical inhibitors, TEMPO (2 equiv.)

or BHT (2 equiv.). The dehydrogenation reactions were completely inhibited in the presence of TEMPO. This further supports the HAT mechanism and confirms the presence of organic radical intermediates. Following this metalloradical pathway, primary alcohols and secondary alcohols are dehydrogenated to their corresponding carbonyl compounds and dihydropyridine derivatives aromatized to pyridine derivatives. Through base-mediated cross-aldol condensation, the aldehyde combines with a ketone to produce an α, β-unsaturated ketone **Ra**. Simultaneously, a second molecule of ketone reacts with ammonium acetate to form the corresponding imine. Subsequent condensation of this imine with the α, β-unsaturated ketone, followed by cyclization and dehydrogenative aromatized catalyzed by **1a** produced substituted pyridine derivatives (Scheme 5).

Mercury poisoning tests revealed that mercury did not affect the dehydrogenation of alcohol or subsequent coupling reactions, nor did it significantly impact the overall yield of the catalytic process.

IV.3. Conclusion

We synthesized a novel *cis*-[NiL_2Cl_2] complex featuring two bidentate, electron-deficient azo-pyridyl frameworks and two labile chlorides positioned adjacently. This arrangement leads to a unique metal-ligand cooperativity that enhances its potential as a pro-metalloradical catalyst. Herein, we demonstrate a nickel-mediated 4CRs cascade annulation strategy for the efficient and sustainable one-pot synthesis of biologically relevant poly-substituted pyridines. This domino strategy begins with catalytic dehydrogenative oxidation of primary and secondary aryl alcohols to generate α,β-unsaturated ketones. These intermediates react with in situ-generated imines, formed from ketones and ammonium acetate (‘N’ source), through sequential twofold C–C and C–N bond formations. The reaction culminates in catalytic dehydrogenative aromatization facilitated by the metalloradical catalyst. This catalyst orchestrates two distinct catalytic cycles, integrating in situ-generated carbonyl compounds to streamline the construction of complex pyridine frameworks. In both cycles, the reaction proceeds via a single-electron transfer (SET)-mediated radical pathway, ensuring high efficiency.

Key features of this approach include solvent-free conditions, minimal waste generation, and the use of cost-effective, less toxic nickel catalysts with a catalytic amount of base, catalytic amount of base, adhering to green chemistry principles. Conducted in a microwave reactor under mild, open-air condition, this four-component [2 + 2 + 1 + 1] domino methodology delivers high TON with excellent yields, operational simplicity, short residence time, and broad functional group tolerance, making it an attractive alternative for synthesizing

poly-substituted pyridines, including penta-substituted derivatives. Moreover, the approach is scalable for large-scale synthesis. Notably, the *cis*-[NiL_2Cl_2] catalyst outperforms the coordinatively-rigid and saturated bis-complex $[NiL_2]^{2+}$ under comparable oxidation conditions, demonstrating superior catalytic efficiency. These results underscore the promise of the nickel-metalloradical catalyst for further exploration in sustainable and efficient N-heterocycle synthesis in a strategically greener way.

IV.4. Experimental Section

IV.4.1. General Information

Solvent drying and purification were carried out following established literature procedures, and the solvents were distilled prior to use as needed. The required chemicals, including primary and secondary alcohols were procured from BLDpharm - Reliable research chemicals supplier, TCI Chemicals (India) Pvt. Ltd, Sisco Research Laboratories Pvt. Ltd. (SRL) – India, Sigma-Aldrich company. Ammonium acetate was purchased from Otto Chemie Pvt. Ltd. Supplementary solvents were purchased from Merck India and dried using standard procedures before use. Nickel(II) nitrate hexahydrate and dichlorobis(triphenylphosphine)nickel(II) were purchased from Sigma-Aldrich (India). Details of electro chemical details, physical measurements, computational studies and X-ray crystallography are provided in ESI.

IV.4.2. Synthesis

Synthesis of ligand:

The organic ligand **L** has been prepared using the previously reported procedure.[19]

Synthesis of complexes:

[Ni(L^H)$_2$Cl$_2$] 1a $NiCl_2(PPh_3)_2$ (654 mg, 1.00 mmol) was added to a solution of (**L^H**) (575 mg, 2.00 mmol) in toluene (30 mL) under open-air conditions, and the reaction mixture was refluxed for 5 hrs at elevated temperature. The solution turned dark in color and the solvent was evaporated under vacuum. An intense red color solution was eluted with 20:1 toluene: acetonitrile (v/v) and collected. The slow diffusion of a dichloromethane solution of the complex into n-hexane facilitated the formation of **1a** as block-shaped crystals. Yield and characterization data: Intense-red crystal, Yield 82% (536 mg) with respect to nickel. Anal. Calcd. for $C_{34}H_{26}N_{10}Cl_2Ni$: C 57.99, H 3.72, N 19.89; Found C 57.81, H 3.76, N 19.81%. UV/Vis spectrum (CH_2Cl_2): λ_{max} (nm) 236, 338, 370 nm. FT-IR (cm^{-1}): 1459, 1404 ($\nu_{N=N}$).

$[Ni(L^H)_2]^{2+}[PF_6]_2^-$ (**$[1b]^{2+}[PF_6]_2^-$**) A solution containing (575 mg, 2.00 mmol) **L^H** and (291 mg, 1.00 mmol) of $Ni(NO_3)_2.6H_2O$ in 30 mL of EtOH in 100 mL round bottom flask was kept in reflux condition for 5 hrs at elevated temperature. The dark red colored solution was evaporated in *vacuuo*. The crude product was purified using column chromatography. Complex **$[1b]^{2+}$** was eluted as a deep-red band with an acetonitrile/NH_4PF_6 mixture. The slow diffusion of a dichloromethane solution of the complex into n-hexane resulted in the crystallization of **$[1b]^{2+}$** as needle-shaped crystals. Yield and characterization data: Deep-red crystal, Yield 87% (253 mg) with respect to nickel. Anal. Calcd. for $C_{34}H_{26}N_{10}Ni$: C 64.48, H 4.14, N 22.12; Found C 64.29, H 4.09, N 22.21%. UV/Vis spectrum (CH_2Cl_2): λ_{max} (nm) 233, 331, 377, 504 nm. FT-IR (cm^{-1}): 1462, 1418 ($\nu_{N=N}$).

General procedure for the synthesis of substituted pyridine derivatives

- ***Under normal heating conditions***

An oven-dried 25 mL round-bottom flask was loaded with primary alcohol **2** (1.10 mmol), secondary alcohol **3** (2.00 mmol), NH_4OAC (4.00 mmol), KO*t*Bu (20 mol%), and **1a** (0.002 mol%) in 5 mL of toluene under open-air conditions. The mixture was stirred at 110 °C for 12 hrs. The reaction mixture was cooled to ambient temperature and concentrated in *vacuuo*. The crude product was subsequently purified by column chromatography on silica gel (100-200 mesh) using a hexane/ethyl acetate gradient elution to afford the desired compound. The desired product was characterized using ^1H, ^{13}C, and ^{19}F nuclear magnetic resonance (NMR) spectroscopy.

- ***Under microwave conditions***

The reaction was carried out in a sealed vessel under microwave reactor. A mixture of primary alcohol **2** (1.10 mmol), secondary alcohol **3** (2.00 mmol), NH_4OAC (4.00 mmol), KO*t*Bu (20 mol%), and **1a** (0.002 mol%) was prepared in solvent-free (neat) condition at room temperature. The reaction mixture was then subjected to microwave irradiation at 50 W and 80 °C for 2 hrs. After cooling, water was added to the reaction mixture. The organic layer was extracted with two 30 mL portions of ethyl acetate. The combined organic extracts were washed with brine and dried over anhydrous Na_2SO_4. The crude product was subsequently purified by column chromatography on silica gel (100-200 mesh) using a hexane/ethyl acetate gradient elution to afford the desired compound **6aa**–**12ad**. The desired product was characterized using ^1H, ^{13}C, and ^{19}F nuclear magnetic resonance (NMR) spectroscopy.

- ***Gram-scale synthesis***

A mixture of benzyl alcohol **2a** (1.1 g, 10.20 mmol), 1-phenyl ethanol **3a** (2.4 g, 20.00 mmol), NH_4OAC (3.0 g, 40.00 mmol), KO*t*Bu (50 mol%), and **1a** (0.002 mol%) was prepared in solvent-free (neat) condition at room temperature. The reaction mixture was then subjected to microwave irradiation at 50 W and 80 °C for 1 hr. After cooling, water was added to the reaction mixture. The organic layer was extracted with two 30 mL portions of ethyl acetate. The combined organic extracts were washed with brine and dried over anhydrous Na_2SO_4. The crude product was subsequently purified by column chromatography on silica gel (100-200 mesh) using a hexane/ethyl acetate gradient elution to afford the desired product **6aa** in 81% yield (2.5 g). Similar gram-scale reactions were also performed with **10aa** and **11aa**.

IV.4.3. Characterization data of Ni(II)-catalyzed compounds

2,4,6-triphenylpyridine (6aa):

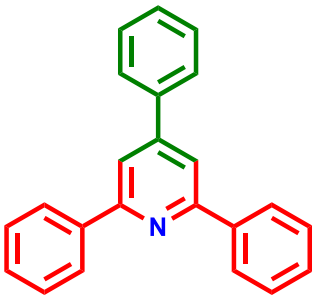

Eluent: Hexane/Ethyl acetate (50:1). White solid (yield = 89%, 274 mg). ^{1}H NMR (300 MHz, $CDCl_3$): δ (ppm) 8.25 – 8.22 (m, 4H), 7.93 (s, 2H), 7.80 – 7.77 (m, 2H), 7.59 – 7.47 (m, 9H). ^{13}C NMR (101 MHz, $CDCl_3$): δ (ppm) 157.50, 150.36, 139.44, 139.02, 129.16, 129.13, 129.06, 128.74, 128.27, 127.22, 117.25.

2,6-diphenyl-4-(*p*-tolyl)pyridine (6ab):

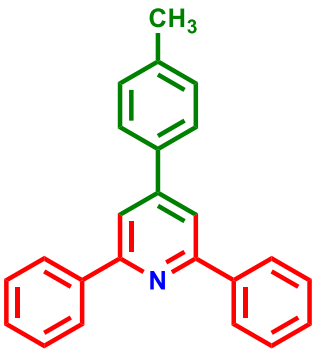

Eluent: Hexane/Ethyl acetate (50:1). White solid (yield = 91%, 292 mg). ^{1}H NMR (300 MHz, $CDCl_3$): δ (ppm) 8.24 (d, J = 6.9 Hz, 4H), 7.92 (s, 2H), 7.70 (d, J = 7.8 Hz, 2H), 7.58 – 7.45 (m, 6H), 7.37 (d, J = 7.5 Hz, 2H), 2.48 (s, 3H). ^{13}C NMR (75 MHz, $CDCl_3$): δ (ppm) 157.44, 150.29, 139.46, 139.24, 136.01, 129.94, 129.14, 128.79, 127.35, 127.22, 117.16, 21.32.

2,6-diphenyl-4-(*m*-tolyl)pyridine (6ac):

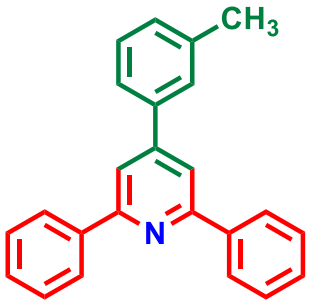

Eluent: Hexane/Ethyl acetate (50:1). White solid (yield = 86%, 276 mg). ^{1}H NMR (400 MHz, $CDCl_3$): δ (ppm) 8.23 (d, J = 7.6 Hz, 4H), 7.91 (s, 2H), 7.59 – 7.53 (m, 6H), 7.49 – 7.45 (m, 3H), 7.32 (d, J = 7.7 Hz, 1H), 2.51 (s, 3H). ^{13}C NMR (75 MHz, $CDCl_3$): δ (ppm) 157.48, 150.37, 139.67, 139.09, 138.86, 129.75, 129.05, 128.73, 127.92, 127.17, 124.32, 117.19, 21.57.

2,6-diphenyl-4-(*o*-tolyl)pyridine (6ad):

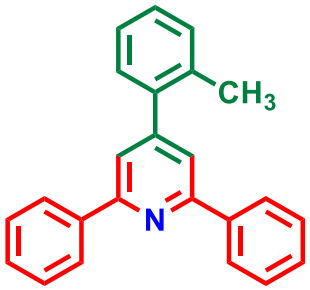

Eluent: Hexane/Ethyl acetate (50:1). White solid (yield = 79%, 254 mg). ^{1}H NMR (400 MHz, $CDCl_3$): δ (ppm) 8.24 (d, J = 7.8 Hz, 4H), 7.93 (s, 2H), 7.79 (d, J = 7.5 Hz, 2H), 7.58 – 7.54 (m, 7H), 7.35 (d, J = 7.5 Hz, 1H), 2.38 (s, 3H). ^{13}C NMR (101 MHz, $CDCl_3$): δ (ppm) 157.52, 150.31, 139.51, 130.40, 129.26, 129.16, 128.75, 128.57, 127.22, 117.23, 20.98.

4-(4-methoxyphenyl)-2,6-diphenylpyridine (6ae):

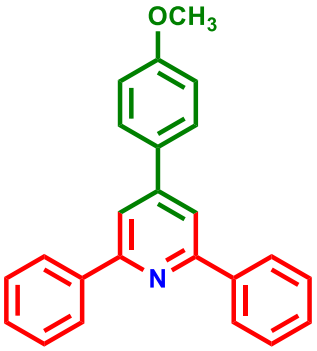

Eluent: Hexane/Ethyl acetate (50:1). White solid (yield = 93%, 314 mg). ^{1}H NMR (400 MHz, $CDCl_3$): δ (ppm) 8.23 (d, J = 7.6 Hz, 4H), 7.89 (s, 2H), 7.74 (d, J = 8.3 Hz, 2H), 7.55 (t, J = 7.5 Hz, 4H), 7.47 (t, J = 7.2 Hz, 2H), 7.08 (d, J = 8.2 Hz, 2H), 3.92 (s, 3H). ^{13}C NMR (75 MHz, $CDCl_3$): δ (ppm) 160.51, 157.47, 149.71, 139.67, 131.29, 129.02, 128.71, 128.37, 127.18, 116.68, 114.57, 55.46.

4-(4-fluorophenyl)-2,6-diphenylpyridine (6af):

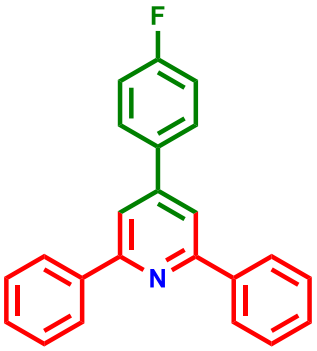

Eluent: Hexane/Ethyl acetate (50:1). White solid (yield = 83%, 270 mg). ^{1}H NMR (300 MHz, $CDCl_3$): δ (ppm) 8.25 – 8.22 (m, 4H), 7.95 – 7.91 (m, 1H), 7.87 (s, 1H), 7.80 – 7.73 (m, 2H), 7.61 – 7.46 (m, 8H), 7.28 – 7.21 (m, 2H). ^{13}C NMR (101 MHz, $CDCl_3$): δ (ppm) 157.62, 149.21, 139.43, 135.15, 129.17, 129.00, 128.93, 128.75, 127.17, 116.95, 116.26, 116.04. ^{19}F NMR (282 MHz, $CDCl_3$): δ = -112.67 (s, 1F).

4-(3-fluorophenyl)-2,6-diphenylpyridine (6ag):

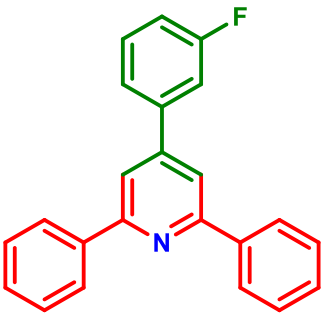

Eluent: Hexane/Ethyl acetate (50:1). White solid (yield = 78%, 254 mg). ^{1}H NMR (300 MHz, $CDCl_3$): δ (ppm) 8.25 – 8.21 (m, 4H), 7.93 (s, 1H), 7.89 (s, 1H), 7.55 – 7.48 (m, 9H), 7.24 – 7.14 (m, 1H). ^{13}C NMR (75 MHz, $CDCl_3$): δ (ppm) 163.37, 157.72, 148.92, 141.24, 139.34, 130.79, 130.67, 129.23, 128.77, 127.22, 127.17, 122.92, 117.24, 117.00, 116.01, 115.73, 114.37. ^{19}F NMR (282 MHz, $CDCl_3$): δ = -112.65 (s, 1F).

2,6-diphenyl-4-(4-(trifluoromethyl)phenyl)pyridine (6ah):

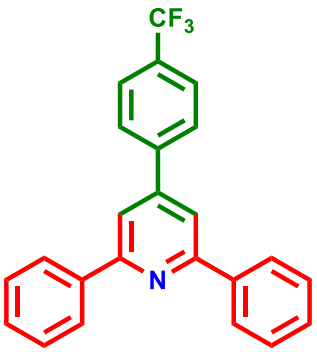

Eluent: Hexane/Ethyl acetate (50:1). White solid (yield = 77%, 289 mg). ^{1}H NMR (300 MHz, $CDCl_3$): δ (ppm) 8.25 (dd, J = 6.7, 1.7 Hz, 4H), 7.92 (d, J = 7.9 Hz, 2H), 7.84 – 7.77 (m, 3H), 7.58 – 7.49 (m, 7H). ^{13}C NMR (75 MHz, $CDCl_3$): δ (ppm) 157.81, 157.48, 148.85, 142.66, 139.23, 129.33, 128.82, 128.76, 127.66, 127.24, 127.17, 126.19, 126.14, 126.09, 126.04, 117.29, 117.12. ^{19}F NMR (282 MHz, $CDCl_3$): δ = -62.55 (s, 3F).

4-(4-nitrophenyl)-2,6-diphenylpyridine (6ai):

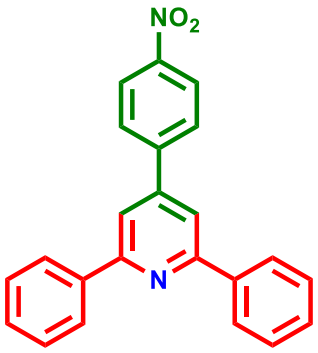

Eluent: Hexane/Ethyl acetate (50:1). White solid (yield = 74%, 261 mg). ^{1}H NMR (300 MHz, $CDCl_3$): δ (ppm) 8.43 – 8.40 (m, 2H), 8.25 – 8.20 (m, 4H), 8.01 – 7.91 (m, 4H), 7.59 – 7.50 (m, 6H). ^{13}C NMR (75 MHz, $CDCl_3$): δ (ppm) 157.99, 148.18, 147.86, 145.47, 139.03, 129.47, 128.86, 128.20, 127.16, 124.39, 116.97.

4-(3-nitrophenyl)-2,6-diphenylpyridine (6aj):

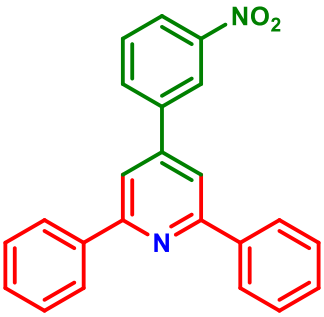

Eluent: Hexane/Ethyl acetate (50:1). White solid (yield = 71%, 250 mg). ^{1}H NMR (400 MHz, $CDCl_3$): δ (ppm) 8.64 (d, J = 2.2 Hz, 1H), 8.37 (dd, J = 8.2, 2.1 Hz, 1H), 8.24 (d, J = 7.3 Hz, 4H), 8.11 (d, J = 7.4 Hz, 1H), 7.93 (s, 2H), 7.76 (t, J = 7.4 Hz, 1H), 7.59 – 7.55 (m, 4H), 7.52 – 7.49 (m, 2H). ^{13}C NMR (75 MHz, $CDCl_3$): δ (ppm) 158.04, 147.84, 140.80, 138.93, 133.23, 130.26, 129.49, 128.86, 127.25, 127.19, 123.73, 122.19, 116.95.

4-(perfluorophenyl)-2,6-diphenylpyridine (6ak):

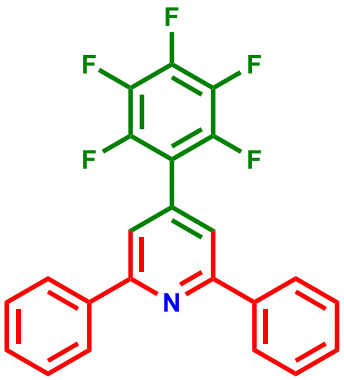

Eluent: Hexane/Ethyl acetate (50:1). White solid (yield = 72%, 286 mg). ^{1}H NMR (400 MHz, $CDCl_3$): δ (ppm) 8.20 – 8.17 (m, 4H), 7.76 (s, 2H), 7.57 – 7.53 (m, 4H), 7.51 – 7.47 (m, 2H). ^{13}C NMR (101 MHz, $CDCl_3$): δ (ppm) 157.73, 138.80, 129.49, 128.84, 127.14, 119.60. ^{19}F NMR (377 MHz, $CDCl_3$): δ = -141.90 – -143.98 (m, 2F), -152.87 (t, J = 21.1 Hz, 1F), -160.82 – -160.95 (m, 2F).

4-(naphthalen-1-yl)-2,6-diphenylpyridine (6al):

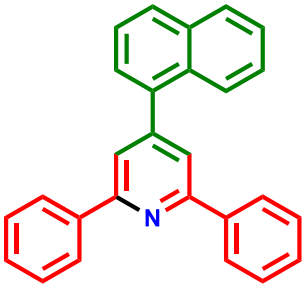

Eluent: Hexane/Ethyl acetate (50:1). White solid (yield = 84%, 300 mg). ^{1}H NMR (300 MHz, $CDCl_3$): δ (ppm) 8.29 – 8.26 (m, 5H), 8.05 (s, 2H), 8.01 – 7.88 (m, 4H), 7.61 – 7.46 (m, 8H). ^{13}C NMR (101 MHz, $CDCl_3$): δ (ppm) 157.00, 150.32, 139.44, 138.11, 133.86, 131.03, 129.14, 128.83, 128.77, 128.56, 127.18, 126.78, 126.73, 126.22, 125.44, 120.20, 118.66.

4-(naphthalen-2-yl)-2,6-diphenylpyridine (6am):

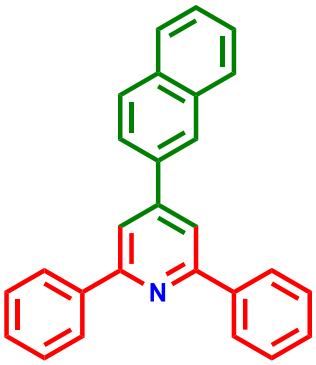

Eluent: Hexane/Ethyl acetate (50:1). White solid (yield = 81%, 289 mg). ^{1}H NMR (300 MHz, $CDCl_3$): δ (ppm) 8.28 – 8.24 (m, 4H), 8.02 – 7.98 (m, 3H), 7.89 (s, 2H), 7.63 – 7.49 (m, 10H). ^{13}C NMR (75 MHz, $CDCl_3$): δ (ppm) 157.00, 150.32, 139.44, 138.11, 133.86, 131.03, 129.14, 128.83, 128.77, 128.56, 127.18, 126.78, 126.73, 126.22, 125.44, 120.20, 118.66.

4-(anthracen-9-yl)-2,6-diphenylpyridine (6an):

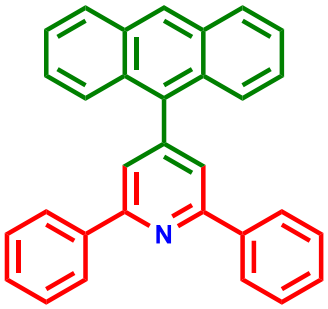

Eluent: Hexane/Ethyl acetate (50:1). White solid (yield = 78%, 318 mg). ^{1}H NMR (400 MHz, $CDCl_3$): δ (ppm) 8.61 (s, 1H), 8.29 (dt, J = 8.1, 1.2 Hz, 4H), 8.12 (d, J = 8.4 Hz, 2H), 7.88 (s, 2H), 7.79 (dt, J = 8.7, 1.1 Hz, 2H), 7.58 – 7.41 (m, 10H). ^{13}C NMR (101 MHz, $CDCl_3$): δ (ppm) 157.08, 149.03, 139.22, 134.34, 131.35, 129.60, 129.30, 128.82, 128.60, 127.58, 127.22, 126.20, 126.16, 125.42, 121.49.

4-([1,1'-biphenyl]-4-yl)-2,6-diphenylpyridine (6ao):

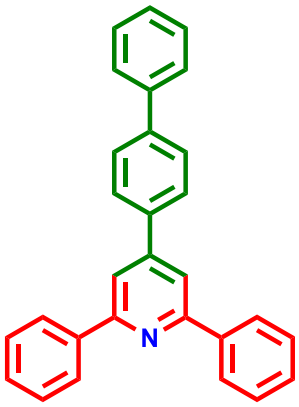

Eluent: Hexane/Ethyl acetate (50:1). White solid (yield = 86%, 330 mg). ^{1}H NMR (400 MHz, $CDCl_3$): δ (ppm) 8.26 (d, J = 7.5 Hz, 3H), 7.97 (s, 2H), 7.87 (d, J = 7.9 Hz, 2H), 7.80 (d, J = 7.6 Hz, 2H), 7.71 (d, J = 7.5 Hz, 2H), 7.59 – 7.42 (m, 10H). ^{13}C NMR (75 MHz, $CDCl_3$): δ (ppm) 157.60, 149.80, 141.99, 140.35, 139.54, 137.83, 129.12, 128.94, 128.75, 127.85, 127.75, 127.64, 127.25, 127.15, 117.01.

2-(2,6-diphenylpyridin-4-yl)quinoline (6ap):

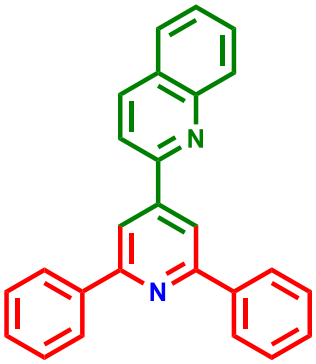

Eluent: Hexane/Ethyl acetate (50:1). White solid (yield = 82%, 294 mg). ^{1}H NMR (300 MHz, $CDCl_3$): δ (ppm) 8.49 (s, 2H), 8.37 (d, J = 8.5 Hz, 1H), 8.33 – 8.29 (m, 5H), 8.06 (d, J = 8.6 Hz, 1H), 7.92 (dd, J = 8.2, 1.5 Hz, 1H), 7.83 (ddd, J = 8.5, 6.9, 1.5 Hz, 1H), 7.64 (ddd, J = 8.1, 6.9, 1.2 Hz, 1H), 7.59 – 7.55 (m, 4H), 7.52 – 7.47 (m, 2H). ^{13}C NMR (101 MHz, $CDCl_3$): δ (ppm) 157.76, 155.20, 148.31 (d, J = 13.7 Hz), 139.54, 137.40, 130.18, 129.97, 129.13, 128.80, 128.73, 127.90, 127.25, 127.21, 118.82, 117.05.

4-phenyl-2,6-di-p-tolylpyridine (7aa):

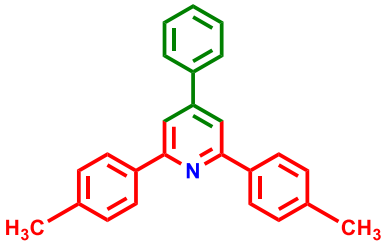

Eluent: Hexane/Ethyl acetate (50:1). White solid (yield = 89%, 298 mg). ^{1}H NMR (300 MHz, $CDCl_3$): δ (ppm) 8.14 (d, J = 8.2 Hz, 4H), 7.88 (s,2H), 7.79 – 7.75 (m, 2H), 7.59 – 7.52 (m, 3H), 7.36 (d, J = 8.0 Hz, 4H), 2.47 (s, 6H). ^{13}C NMR (75 MHz, $CDCl_3$): δ (ppm) 157.40, 150.13, 139.25, 139.04, 136.83, 129.45, 129.11, 128.93, 127.23, 127.07, 116.61, 21.37.

4-phenyl-2,6-di-m-tolylpyridine (7ab):

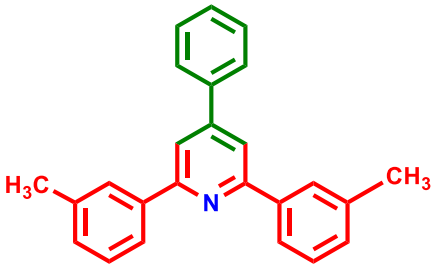

Eluent: Hexane/Ethyl acetate (50:1). White solid (yield = 78%, 262 mg). ^{1}H NMR (300 MHz, $CDCl_3$): δ (ppm) 8.04 – 7.99 (m, 4H), 7.90 (s, 2H), 7.80 – 7.76 (m, 2H), 7.59 – 7.52 (m, 5H), 7.46 – 7.40 (m, 2H), 2.51 (s, 6H). ^{13}C NMR (75 MHz, $CDCl_3$): δ (ppm) 157.77, 150.08, 139.68, 139.16, 138.34, 129.11, 128.63, 127.88, 127.22, 124.35, 117.23, 21.64.

4-phenyl-2,6-di-o-tolylpyridine (7ac):

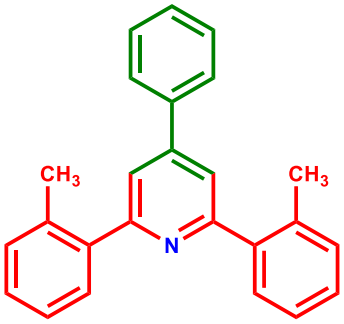

Eluent: Hexane/Ethyl acetate (50:1). White solid (yield = 74%, 248 mg). ^{1}H NMR (300 MHz, $CDCl_3$): δ (ppm) 7.60 – 7.58 (m, 2H), 7.54 – 7.50 (m, 2H), 7.44 – 7.40 (m, 6H), 7.33 – 7.28 (m, 5H), 2.48 (s, 6H). ^{13}C NMR (75 MHz, $CDCl_3$): δ (ppm) 160.37, 149.01, 140.96, 138.74, 136.10, 130.67, 129.31, 128.64, 128.59, 128.52, 128.19, 125.74, 120.31, 20.93.

2,6-bis(4-methoxyphenyl)-4-phenylpyridine (7ad):

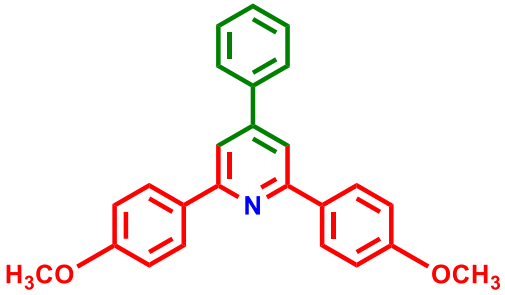

Eluent: Hexane/Ethyl acetate (50:1). White solid (yield = 91%, 334 mg). ^{1}H NMR (300 MHz, $CDCl_3$): δ (ppm) 8.33 – 8.30 (m, 6H), 7.98 (s, 2H), 7.61 – 7.58 (m, 3H), 7.12 – 7.07 (m, 4H), 3.94 (s, 6H). ^{13}C NMR (75 MHz, $CDCl_3$): δ (ppm) 164.24, 161.94, 150.12, 138.31, 130.62 (d, J = 11.4 Hz), 129.98, 128.86 (d, J = 9.3 Hz), 128.45, 127.28, 114.27, 55.48.

2,6-bis(3-methoxyphenyl)-4-phenylpyridine (7ae):

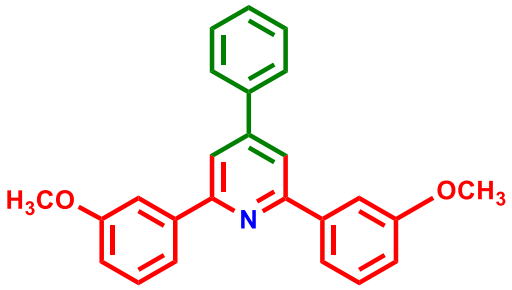

Eluent: Hexane/Ethyl acetate (50:1). White solid (yield = 81%, 298 mg). ^{1}H NMR (300 MHz, $CDCl_3$): δ (ppm) 8.19 (d, J = 7.0 Hz, 2H), 7.95 (s, 2H), 7.65 – 7.60 (m, 3H), 7.52 – 7.46 (m, 6H), 7.08 (ddd, J = 8.2, 2.6, 0.9 Hz, 2H), 3.96 (s, 6H). ^{13}C NMR (75 MHz, $CDCl_3$): δ (ppm) 160.14, 157.28, 150.25, 141.07, 138.89, 130.24, 129.23, 128.53, 127.27, 119.72, 117.49, 114.82, 112.93, 55.39.

2,6-bis(4-fluorophenyl)-4-phenylpyridine (7af):

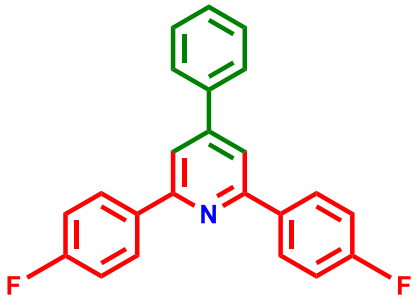

Eluent: Hexane/Ethyl acetate (50:1). White solid (yield = 87%, 299 mg). ^{1}H NMR (300 MHz, $CDCl_3$): δ (ppm) 8.24 – 8.17 (m, 4H), 7.84 (s, 2H), 7.77 – 7.71 (m, 2H), 7.58 – 7.50 (m, 3H), 7.25 – 7.19 (m, 4H). ^{13}C NMR (101 MHz, $CDCl_3$): δ (ppm) 164.91, 162.44, 156.49, 150.46, 138.85, 135.61, 135.58, 129.19, 129.15, 128.96, 128.88, 127.18, 116.71, 115.76, 115.55. ^{19}F NMR (282 MHz, $CDCl_3$): δ = -112.84 (s, 2F).

2,6-bis(2-fluorophenyl)-4-phenylpyridine (7ag):

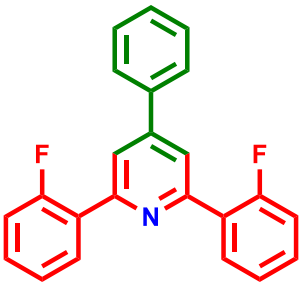

Eluent: Hexane/Ethyl acetate (50:1). White solid (yield = 74%, 254 mg). ^{1}H NMR (400 MHz, $CDCl_3$): δ (ppm) 8.43 (td, J = 7.9, 1.9 Hz, 2H), 8.19 (s, 2H), 7.59 – 7.55 (m, 7H), 7.39 (td, J = 7.6, 1.2 Hz, 2H), 7.27 – 7.22 (m, 2H). ^{13}C NMR (101 MHz, $CDCl_3$): δ (ppm) 162.22, 160.53, 158.07, 139.54, 138.94, 137.50, 132.91 (d, J = 9.4 Hz), 131.12 (d, J = 3.2 Hz), 130.81 (d, J = 8.3 Hz), 130.55, 129.07, 129.04, 128.46, 128.41, 128.36, 128.06 (d, J = 6.5 Hz), 125.84, 124.30 (d, J = 3.4 Hz), 115.71 (d, J = 21.6 Hz). ^{19}F NMR (377 MHz, $CDCl_3$): δ = -114.75 (s, 2F).

2,6-bis(4-bromophenyl)-4-phenylpyridine (7ah):

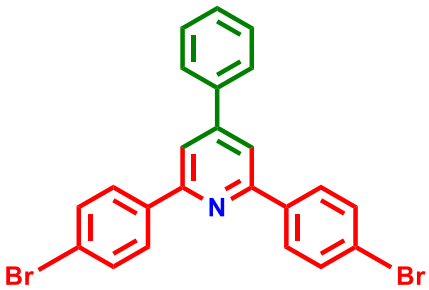

Eluent: Hexane/Ethyl acetate (50:1). White solid (yield = 82%, 381 mg). ^{1}H NMR (300 MHz, $CDCl_3$): δ (ppm) 8.08 (d, J = 8.6 Hz, 4H), 7.88 (s,2H), 7.76 – 7.72 (m, 2H), 7.66 (d, J = 8.6 Hz, 4H), 7.57 – 7.51 (m, 3H). ^{13}C NMR (75 MHz, $CDCl_3$): δ (ppm) 156.41, 150.67, 138.64, 138.15, 131.91, 129.23, 128.69, 127.20, 123.71, 117.19.

2,6-bis(4-nitrophenyl)-4-phenylpyridine (7ai):

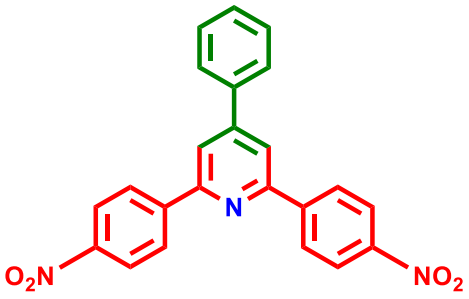

Eluent: Hexane/Ethyl acetate (50:1). White solid (yield = 71%, 282 mg). ^{1}H NMR (300 MHz, $CDCl_3$): δ (ppm) 8.44 – 8.39 (m, 4H), 8.34 – 8.31 (m, 3H), 8.07 (s, 2H), 7.59 – 7.57 (m, 6H). ^{13}C NMR (75 MHz, $CDCl_3$): δ (ppm) 165.56, 151.76, 147.63, 143.49, 137.60, 131.27, 129.43, 128.24, 127.46, 124.13, 121.33.

4'-phenyl-2,2':6',2''-terpyridine (7aj):

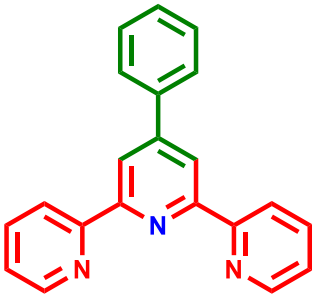

Eluent: Hexane/Ethyl acetate (50:1). White solid (yield = 77%, 238 mg). ^{1}H NMR (400 MHz, $CDCl_3$): δ (ppm) 9.05 (s, 2H), 8.78 (dd, J = 4.8, 1.7 Hz, 1H), 8.73 (dd, J = 4.7, 1.7 Hz, 2H), 8.66 – 8.64 (m, 2H), 8.09 (d, J = 7.8 Hz, 1H), 7.91 – 7.84 (m, 3H), 7.38 – 7.35 (m, 3H). ^{13}C NMR (101 MHz, $CDCl_3$): δ (ppm) 156.16, 156.09, 155.04, 149.95, 149.11, 148.60, 137.11, 137.02, 123.93, 123.83, 121.49, 118.71.

4'-phenyl-4,2':6',4''-terpyridine (7ak):

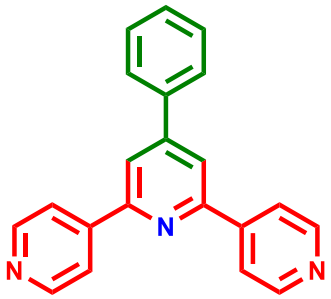

Eluent: Hexane/Ethyl acetate (50:1). White solid (yield = 79%, 244 mg). ^{1}H NMR (300 MHz, $CDCl_3$): δ (ppm) 8.82 – 8.80 (m, 4H), 8.12 – 8.10 (m, 4H), 8.07 (s, 2H), 7.79 – 7.76 (m, 2H), 7.62 – 7.52 (m, 3H). ^{13}C NMR (75 MHz, $CDCl_3$): δ (ppm) 155.29, 151.26, 150.54, 146.10, 137.97, 129.66, 129.40, 127.19, 121.24, 119.06.

2,4,6-tri-p-tolylpyridine (8aa):

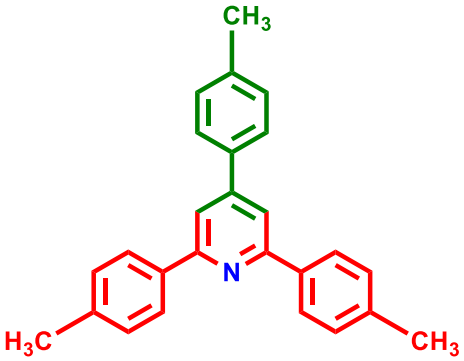

Eluent: Hexane/Ethyl acetate (50:1). White solid (yield = 88%, 307 mg). ^{1}H NMR (300 MHz, $CDCl_3$): δ (ppm) 8.22 (d, J = 8.2 Hz, 1H), 8.15 (d, J = 8.2 Hz, 3H), 7.87 (s, 2H), 7.69 (d, J = 8.2 Hz, 1H), 7.40 – 7.35 (m, 7H), 2.49 (s, 3H), 2.48 (s, 6H). ^{13}C NMR (75 MHz, $CDCl_3$): δ (ppm) 157.39, 149.90, 140.97, 138.92, 137.02, 136.31, 129.82, 129.43, 128.46, 127.04, 116.34, 21.37, 21.29.

4'-(p-tolyl)-4,2':6',4''-terpyridine (8ab):

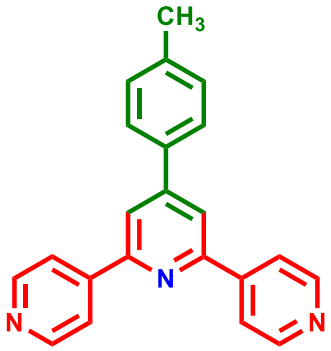

Eluent: Hexane/Ethyl acetate (50:1). White solid (yield = 82%, 265 mg). ^{1}H NMR (300 MHz, $CDCl_3$): δ (ppm) 8.78 – 8.72 (m, 8H), 8.01 (s, 2H), 7.63 (d, J = 7.9 Hz, 2H), 7.37 (d, J = 7.0 Hz, 2H), 2.43 (s, 3H). ^{13}C NMR (101 MHz, $CDCl_3$): δ (ppm) 155.03, 150.56, 150.23, 141.99, 139.95, 134.81, 131.53, 129.84, 128.78, 121.62, 121.30, 118.79, 21.57.

4'-(4-methoxyphenyl)-4,2':6',4''-terpyridine (8ac):

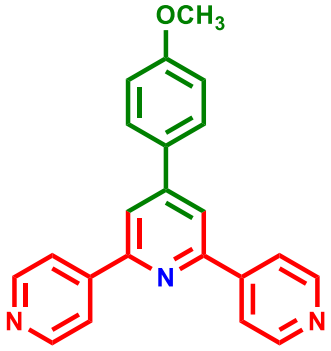

Eluent: Hexane/Ethyl acetate (50:1). White solid (yield = 84%, 285 mg). ^{1}H NMR (300 MHz, $CDCl_3$): δ (ppm) 8.78 (d, J = 6.2 Hz, 4H), 8.08 (d, J = 6.2 Hz, 4H), 8.00 (s, 2H), 7.72 (d, J = 8.8 Hz, 2H), 7.09 (d, J = 8.8 Hz, 2H), 3.91 (s, 3H). ^{13}C NMR (75 MHz, $CDCl_3$): δ (ppm) 160.98, 155.08, 150.58, 150.40, 146.21, 130.00, 128.36, 121.22, 118.39, 114.78, 55.49.

4'-(p-tolyl)-2,2':6',2''-terpyridine (8ad):

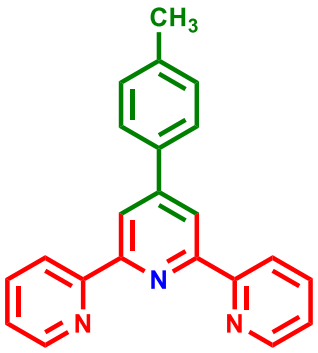

Eluent: Hexane/Ethyl acetate (50:1). White solid (yield = 79%, 255 mg). ^{1}H NMR (400 MHz, $CDCl_3$): δ (ppm) 8.75 – 8.67 (m, 6H), 7.92 – 7.84 (m, 4H), 7.38 – 7.33 (m, 4H), 2.45 (s, 3H). ^{13}C NMR (101 MHz, $CDCl_3$): δ (ppm) 156.38, 155.88, 149.12, 139.12, 136.89, 135.48, 129.67, 127.16, 123.79, 121.41, 118.66, 21.28.

4'-(4-fluorophenyl)-4,2':6',4''-terpyridine (8ae):

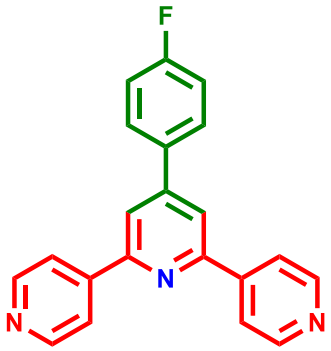

Eluent: Hexane/Ethyl acetate (50:1). White solid (yield = 77%, 252 mg). ^{1}H NMR (400 MHz, $CDCl_3$): δ (ppm) 8.79 – 8.76 (m, 4H), 8.09 – 8.07 (m, 4H), 8.00 (s, 2H), 7.82 – 7.69 (m, 4H). ^{13}C NMR (75 MHz, $CDCl_3$): δ (ppm) 165.42, 162.10, 155.31, 150.46, 145.98, 134.05, 134.01, 129.09, 128.97, 121.22, 118.82, 116.61, 116.32. ^{19}F NMR (377 MHz, $CDCl_3$): δ = -111.38 (s, 1F).

4'-(4-chlorophenyl)-4,2':6',4''-terpyridine (8af):

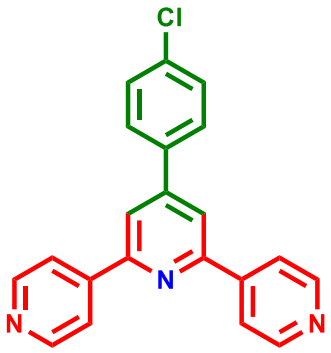

Eluent: Hexane/Ethyl acetate (50:1). White solid (yield = 78%, 268 mg). ^{1}H NMR (400 MHz, $CDCl_3$): δ (ppm) 8.81 (d, J = 5.1 Hz, 4H), 8.09 (d, J = 5.1 Hz, 4H), 8.02 (s, 2H), 7.70 (d, J = 8.1 Hz, 2H), 7.56 (d, J = 8.1 Hz, 2H). ^{13}C NMR (75 MHz, $CDCl_3$): δ (ppm) 155.47, 150.56, 149.99, 145.89, 136.37, 136.00, 129.64, 128.46, 121.21, 118.75.

4'-(4-bromophenyl)-4,2':6',4''-terpyridine (8ag):

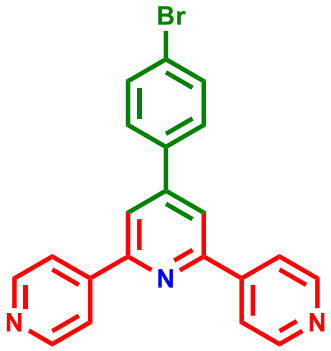

Eluent: Hexane/Ethyl acetate (50:1). White solid (yield = 81%, 314 mg). ^{1}H NMR (400 MHz, $CDCl_3$): δ (ppm) 8.80 – 8.78 (m, 4H), 8.10 – 8.08 (m, 4H), 8.01 (s, 2H), 7.73 – 7.70 (m, 2H), 7.65 – 7.62 (m, 2H). ^{13}C NMR (75 MHz, $CDCl_3$): δ (ppm) 155.47, 150.50, 150.05, 145.91, 136.82, 132.60, 128.72, 121.23, 120.97, 118.71.

4'-(perfluorophenyl)-2,2':6',2''-terpyridine (8ah):

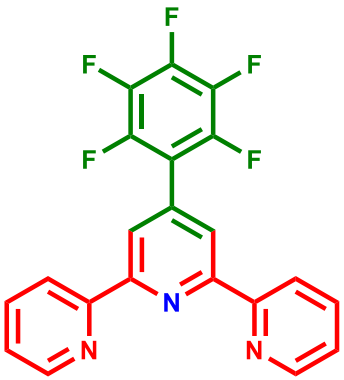

Eluent: Hexane/Ethyl acetate (50:1). White solid (yield = 71%, 283 mg). ^{1}H NMR (300 MHz, $CDCl_3$): δ (ppm) 8.73 – 8.67 (m, 4H), 8.58 (s, 2H), 7.94 – 7.87 (m, 2H), 7.41 – 7.35 (m, 2H). ^{13}C NMR (75 MHz, $CDCl_3$): δ (ppm) 155.96, 155.65, 149.27, 136.94, 124.21, 124.08, 122.06, 121.30. ^{19}F NMR (282 MHz, $CDCl_3$): δ = -143.64 – -143.76 (m, 2F), -156.87 – -157.71 (m, 1F), -161.25 – -161.37 (m, 2F).

4'-(4-methoxyphenyl)-2,2':6',2''-terpyridine (8ai):

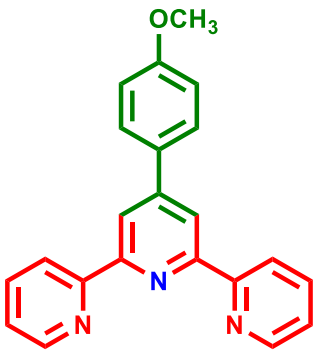

Eluent: Hexane/Ethyl acetate (50:1). White solid (yield = 80%, 271 mg). ^{1}H NMR (300 MHz, $CDCl_3$): δ (ppm) 8.69 – 8.59 (m, 6H), 7.89 – 7.82 (m, 4H), 7.35 – 7.30 (m, 2H), 7.01 (d, J = 8.8 Hz, 2H), 3.84 (s, 3H). ^{13}C NMR (75 MHz, $CDCl_3$): δ (ppm) 160.51, 156.22, 155.66, 149.74, 148.92, 137.06, 130.53, 128.45, 123.84, 121.56, 118.27, 114.35, 55.30.

4'-(naphthalen-1-yl)-2,2':6',2''-terpyridine (8aj):

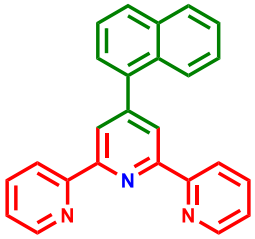

Eluent: Hexane/Ethyl acetate (50:1). White solid (yield = 72%, 258 mg). ^{1}H NMR (300 MHz, $CDCl_3$): δ (ppm) 8.76 – 8.66 (m, 6H), 7.99 – 7.8 (m, 5H), 7.68 – 7.61 (m, 4H), 7.39 – 7.34 (m, 2H). ^{13}C NMR (75 MHz, $CDCl_3$): δ (ppm) 156.26, 155.55, 150.87, 149.23, 137.95, 136.91, 133.76, 131.01, 128.74, 128.42, 127.06, 126.59, 126.01, 125.56, 125.32, 123.86, 122.45, 121.44.

2-([4,2':6',4''-terpyridin]-4'-yl)quinoline (8ak):

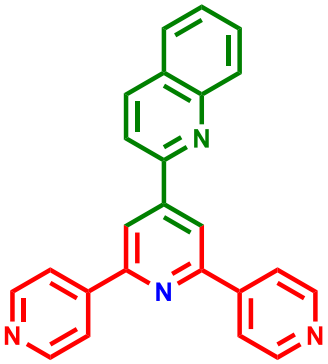

Eluent: Hexane/Ethyl acetate (50:1). White solid (yield = 76%, 274 mg). ^{1}H NMR (300 MHz, $CDCl_3$): δ (ppm) 8.86 – 8.82 (m, 4H), 8.67 (s, 2H), 8.41 (d, J = 8.4 Hz, 1H), 8.30 (dd, J = 8.5, 1.1 Hz, 1H), 8.21 – 8.16 (m, 4H), 8.08 (d, J = 8.5 Hz, 1H), 7.95 (dd, J = 8.1, 1.5 Hz, 1H), 7.86 (ddd, J = 8.5, 6.9, 1.5 Hz, 1H), 7.67 (ddd, J = 8.1, 6.9, 1.2 Hz, 1H). ^{13}C NMR (75 MHz, $CDCl_3$): δ (ppm) 155.51, 150.50, 149.37, 148.35, 146.11, 137.67, 130.48, 130.04, 128.07, 127.68, 121.33, 118.95, 118.42.

6'-(pyridin-4-yl)-2,4':2',4''-terpyridine (8al):

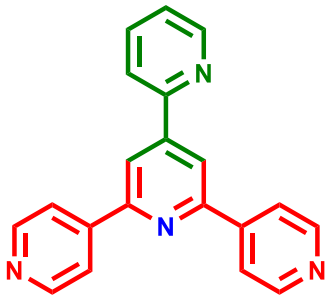

Eluent: Hexane/Ethyl acetate (50:1). White solid (yield = 65%, 201 mg). ^{1}H NMR (300 MHz, $CDCl_3$): δ (ppm) 8.84 – 8.78 (m, 5H), 8.47 (s, 2H), 8.13 – 8.11 (m, 4H), 7.98 – 7.88 (m, 2H), 7.46 – 7.41 (m, 1H). ^{13}C NMR (75 MHz, $CDCl_3$): δ (ppm) 155.39, 154.03, 150.51, 150.31, 149.01, 145.97, 137.34, 124.39, 121.23, 121.04, 118.30.

4'-(4-bromophenyl)-2,2':6',2''-terpyridine (8am):

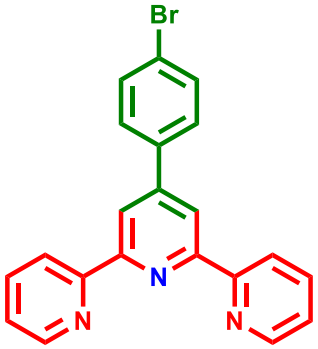

Eluent: Hexane/Ethyl acetate (50:1). White solid (yield = 77%, 299 mg). ^{1}H NMR (400 MHz, $CDCl_3$): δ (ppm) 8.74 – 8.65 (m, 6H), 7.90 (td, J = 7.7, 1.8 Hz, 2H), 7.79 (d, J = 8.5 Hz, 2H), 7.65 (d, J = 8.5 Hz, 2H), 7.38 (ddd, J = 7.5, 4.9, 1.3 Hz, 2H). ^{13}C NMR (101 MHz, $CDCl_3$): δ (ppm) 156.07, 156.04, 149.13, 137.38, 136.98, 132.13, 128.90, 123.98, 123.50, 121.50, 121.44, 121.38, 118.58.

2-([2,2':6',2''-terpyridin]-4'-yl)thiazole (8an):

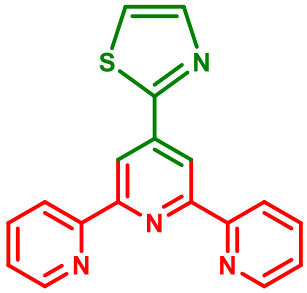

Eluent: Hexane/Ethyl acetate (50:1). White solid (yield = 68%, 215 mg). ^{1}H NMR (400 MHz, $CDCl_3$): δ (ppm) 9.03 (s, 2H), 8.76 (ddd, J = 4.9, 1.8, 0.9 Hz, 2H), 8.65 (dt, J = 8.0, 1.1 Hz, 2H), 8.03 (d, J = 3.2 Hz, 1H), 7.89 (td, J = 7.7, 1.8 Hz, 2H), 7.52 (d, J = 3.2 Hz, 1H), 7.37 (ddd, J = 7.5, 4.8, 1.3 Hz, 2H). ^{13}C NMR (75 MHz, $CDCl_3$): δ (ppm) 166.06, 156.52, 155.66, 149.24, 144.42, 142.42, 136.88, 124.06, 121.30, 120.69, 117.91.

4'-(4-fluorophenyl)-2,2':6',2''-terpyridine (8ao):

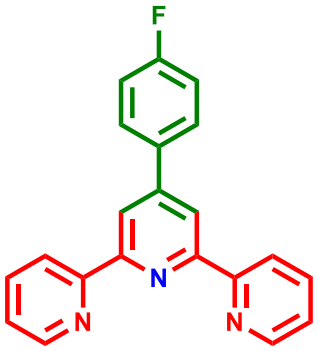

Eluent: Hexane/Ethyl acetate (50:1). White solid (yield = 73%, 239 mg). ^{1}H NMR (300 MHz, $CDCl_3$): δ (ppm) 8.82 – 8.66 (m, 6H), 7.92 – 7.82 (m, 4H), 7.38 – 7.33 (m, 2H), 7.24 – 7.16 (m, 2H). ^{13}C NMR (75 MHz, $CDCl_3$): δ (ppm) 165.13, 161.83, 1256.12, 155.97, 149.22, 149.13, 136.90, 135.50, 135.46, 134.63, 134.59, 129.17, 129.06, 123.90, 121.38, 118.67, 116.06, 115.77. ^{19}F NMR (282 MHz, $CDCl_3$): δ = -112.82 (s, 1F).

2-(4-fluorophenyl)-4-phenyl-6-(p-tolyl)pyridine (9aa):

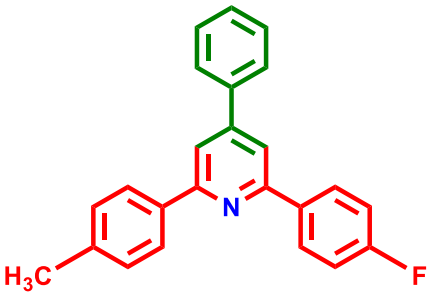

Eluent: Hexane/Ethyl acetate (50:1). White solid (yield = 73%, 247 mg). ^{1}H NMR (400 MHz, $CDCl_3$): δ (ppm) 8.24 – 8.18 (m, 2H), 8.14 – 8.11 (m, 2H), 7.89 – 7.83 (m, 2H), 7.78 – 7.75 (m, 2H), 7.58 – 7.51 (m, 2H), 7.36 – 7.34 (m, 3H), 7.25 – 7.20 (m, 2H), 2.46 (s, 3H). ^{13}C NMR (101 MHz, $CDCl_3$): δ (ppm) 157.43, 156.39, 150.26, 139.09, 138.98, 136.81 (d, J = 22.1 Hz), 129.48, 129.43, 129.13, 129.08, 128.97, 128.89, 127.19, 127.02, 116.64 (d, J = 21.5 Hz), 115.58 (d, J = 21.6 Hz), 21.34. ^{19}F NMR (282 MHz, $CDCl_3$): δ = -112.86 (s, 1F).

2-(4-bromophenyl)-4,6-di-p-tolylpyridine (9ab):

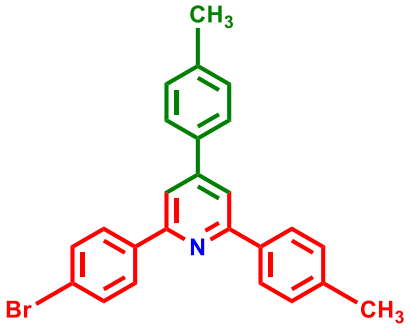

Eluent: Hexane/Ethyl acetate (50:1). White solid (yield = 76%, 315 mg). ^{1}H NMR (400 MHz, $CDCl_3$): δ (ppm) 8.15 – 8.06 (m, 4H), 7.88 – 7.82 (m, 2H), 7.69 – 7.63 (m, 4H), 7.36 (dd, J = 8.1, 2.3 Hz, 4H), 2.48 (s, 3H), 2.47 (s, 3H). ^{13}C NMR (101 MHz, $CDCl_3$): δ (ppm) 157.57, 157.34, 150.15, 139.16, 138.62, 138.31, 136.68, 135.96, 131.87, 131.81, 129.88, 129.44, 128.68, 127.02, 123.62, 116.85, 116.36, 21.38, 21.32.

2-(4-chlorophenyl)-6-(4-fluorophenyl)-4-(p-tolyl)pyridine (9ac):

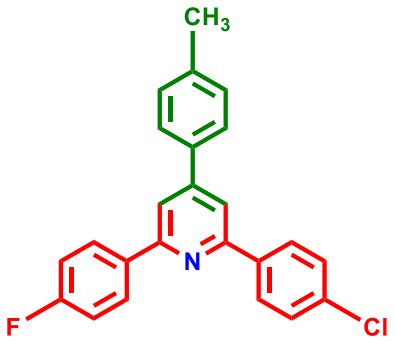

Eluent: Hexane/Ethyl acetate (50:1). White solid (yield = 71%, 265 mg). ^{1}H NMR (300 MHz, $CDCl_3$): δ (ppm) 8.22 – 8.11 (m, 4H), 7.82 – 7.76 (m, 2H), 7.68 (d, J = 8.2 Hz, 2H), 7.55 – 7.50 (m, 2H), 7.28 – 7.19 (m, 4H), 2.46 (s, 3H). ^{13}C NMR (75 MHz, $CDCl_3$): δ (ppm) 165.39, 162.10, 156.65, 156.51, 148.99, 139.31, 137.47, 136.46, 135.38, 135.24, 129.49, 129.33, 128.98, 128.87, 128.46, 127.00, 116.34, 116.15, 115.81, 115.53, 21.31. ^{19}F NMR (282 MHz, $CDCl_3$): δ = -112.57 (s, 1F).

2-(3-nitrophenyl)-4-phenyl-6-(p-tolyl)pyridine (9ad):

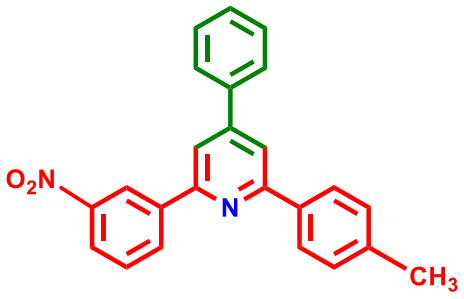

Eluent: Hexane/Ethyl acetate (50:1). White solid (yield = 69%, 252 mg). ^{1}H NMR (300 MHz, $CDCl_3$): δ (ppm) 8.85 (t, J = 2.0 Hz, 1H), 8.47 – 8.43 (m, 1H), 8.37 (dt, J = 7.8, 1.4 Hz, 1H), 7.96 (d, J = 8.3 Hz, 2H), 7.89 – 7.85 (m, 1H), 7.73 – 7.64 (m, 4H), 7.46 – 7.42 (m, 3H), 7.32 (d, J = 8.0 Hz, 2H), 2.46 (s, 3H). ^{13}C NMR (75 MHz, $CDCl_3$): δ (ppm) 157.91, 155.28, 150.68, 148.43, 139.50, 135.63, 135.01, 134.34, 134.12, 129.94, 129.34, 129.13, 128.96, 128.78, 128.68, 128.43, 127.07, 123.28, 122.09, 120.66, 21.70.

4-(naphthalen-1-yl)-2-phenyl-6-(p-tolyl)pyridine (9ae):

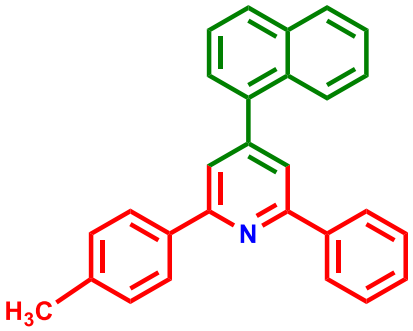

Eluent: Hexane/Ethyl acetate (50:1). White solid (yield = 76%, 282 mg). ^{1}H NMR (400 MHz, $CDCl_3$): δ (ppm) 8.26 (d, J = 7.4 Hz, 3H), 8.17 – 8.14 (m, 2H), 8.00 (d, J = 8.2 Hz, 3H), 7.89 – 7.85 (m, 2H), 7.61 – 7.50 (m, 6H), 7.35 (d, J = 7.7 Hz, 2H), 2.47 (s, 3H). ^{13}C NMR (75 MHz, $CDCl_3$): δ (ppm) 157.01, 156.91, 150.20, 139.46, 139.15, 138.22, 136.69, 133.86, 131.05, 129.50, 129.15, 129.09, 128.84, 128.78, 128.55, 127.19, 127.05, 126.75, 126.70, 126.22, 125.45, 120.20, 21.37.

3-methyl-2,4,6-triphenylpyridine (10aa):

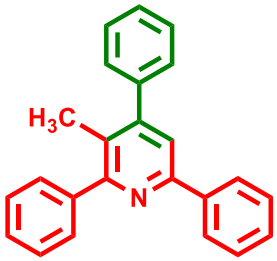

Eluent: Hexane/Ethyl acetate (50:1). White solid (yield = 72%, 231 mg). ^{1}H NMR (300 MHz, $CDCl_3$): δ (ppm) 8.16 – 8.13 (m, 2H), 7.75 – 7.72 (m, 2H), 7.67 (s, 1H), 7.57 – 7.46 (m, 11H), 2.31 (s, 3H). ^{13}C NMR (101 MHz, $CDCl_3$): δ (ppm) 159.46, 154.07, 151.73, 141.41, 14032, 139.32, 129.51, 128.83, 128.71, 128.67, 128.51, 128.12, 127.95, 126.97, 120.06, 18.01.

4-(4-fluorophenyl)-3-methyl-2,6-diphenylpyridine (10ab):

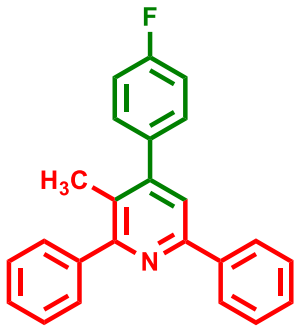

Eluent: Hexane/Ethyl acetate (50:1). White solid (yield = 69%, 234 mg). ^{1}H NMR (300 MHz, $CDCl_3$): δ (ppm) 8.13 – 8.09 (m, 2H), 7.71 – 7.68 (m, 2H), 7.61 (s, 1H), 7.52 – 7.44 (m, 8H), 7.25 – 7.19 (m, 2H), 2.27 (s, 3H). ^{13}C NMR (101 MHz, $CDCl_3$): δ (ppm) 159.59, 157.63, 154.16, 150.65, 149.18, 141.33, 139.23, 136.23 (d, J = 3.4 Hz), 130.56 (d, J = 8.1 Hz), 129.47, 128.78, 128.69, 128.14, 128.00, 127.17, 126.92, 119.99, 115.52 (d, J = 21.5 Hz), 18.01. ^{19}F NMR (282 MHz, $CDCl_3$): δ = -114.03 (s, 1F). HRMS (ESI) m/z calcd for $C_{24}H_{19}FN$ $[M + H]^+$ 340.1502, found 340.1499.

4-(4-fluorophenyl)-3-methyl-2-phenyl-6-(p-tolyl)pyridine (10ac):

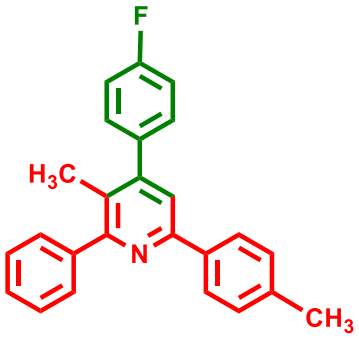

Eluent: Hexane/Ethyl acetate (50:1). White solid (yield = 74%, 261 mg). ^{1}H NMR (300 MHz, $CDCl_3$): δ (ppm) 8.01 (d, J = 8.2 Hz, 2H), 7.71 – 7.67 (m, 2H), 7.58 (s, 1H), 7.52 – 7.40 (m, 5H), 7.30 – 7.27 (m, 2H), 7.24 – 7.18 (m, 2H), 2.42 (s, 3H), 2.26 (s, 3H). ^{13}C NMR (75 MHz, $CDCl_3$): δ (ppm) 164.15, 160.87, 159.46, 154.15, 150.56, 141.42, 138.68, 136.43, 130.59, 130.48, 129.47, 129.39, 128.10, 127.92, 127.01, 126.77, 126.61, 119.64, 115.47 (d, J = 21.5 Hz), 21.30, 17.95. ^{19}F NMR (282 MHz, $CDCl_3$): δ = -114.14 (s, 1F). HRMS (ESI) m/z calcd for $C_{25}H_{21}FN$ $[M + H]^+$ 354.1658, found 354.1621.

4-(4-fluorophenyl)-2-(4-methoxyphenyl)-3-methyl-6-(p-tolyl)pyridine (10ad):

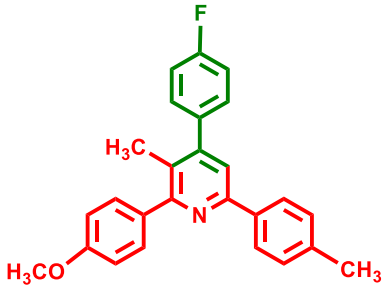

Eluent: Hexane/Ethyl acetate (50:1). White solid (yield = 76%, 291 mg). ^{1}H NMR (400 MHz, $CDCl_3$): δ (ppm) 8.09 (d, J = 8.1 Hz, 2H), 7.65 (d, J = 8.3 Hz, 2H), 7.57 (s, 1H), 7.49 – 7.39 (m, 5H), 7.20 (t, J = 8.5 Hz, 2H), 7.04 (d, J = 8.3 Hz, 2H), 3.90 (s, 3H), 2.28 (s, 3H). ^{13}C NMR (75 MHz, $CDCl_3$): δ (ppm) 164.19, 161.75, 160.91, 157.51, 154.17, 149.00, 138.74, 136.43, 136.32, 130.64, 130.54, 129.53, 129.50, 128.14, 127.06, 126.82, 119.66, 116.32, 115.51 (d, J = 21.6 Hz), 55.37, 21.34, 18.00. ^{19}F NMR (377 MHz, $CDCl_3$): δ = -114.14 (s, 1F). HRMS (ESI) m/z calcd for $C_{26}H_{23}FNO$ $[M + H]^+$ 384.1764, found 384.1755.

2-(4-methoxyphenyl)-3-methyl-4-phenyl-6-(p-tolyl)pyridine (10ae):

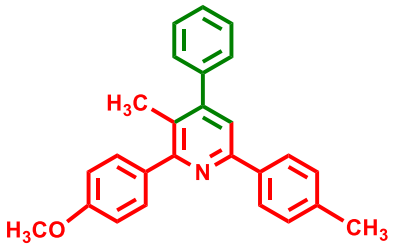

Eluent: Hexane/Ethyl acetate (50:1). White solid (yield = 77%, 281 mg). ^{1}H NMR (400 MHz, $CDCl_3$): δ (ppm) 8.02 (d, J = 7.9 Hz, 2H), 7.67 (d, J = 8.3 Hz, 2H), 7.59 (s, 1H), 7.54 – 7.44 (m, 5H), 7.29 (d, J = 8.2 Hz, 2H), 7.05 (d, J = 8.2 Hz, 2H), 3.91 (s, 3H), 2.43 (s, 3H), 2.30 (s, 3H). ^{13}C NMR (101 MHz, CDCl3): δ (ppm) 159.41, 158.93, 153.97, 151.59, 138.54, 136.62, 134.06, 130.86, 129.64, 129.36, 128.84, 128.45, 127.83, 126.76, 126.49, 119.35, 113.48, 55.38, 21.32, 18.19. HRMS (ESI) m/z calcd for $C_{26}H_{24}NO$ $[M + H]^+$ 366.1858, found 366.1845.

4-(4-fluorophenyl)-2-(4-methoxyphenyl)-3-methyl-6-phenylpyridine (10af):

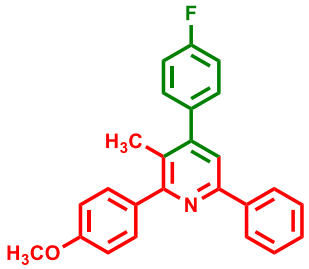

Eluent: Hexane/Ethyl acetate (50:1). White solid (yield = 75%, 277 mg). ^{1}H NMR (400 MHz, $CDCl_3$): δ (ppm) 8.09 (d, *J* = 8.1 Hz, 2H), 7.65 (d, *J* = 8.3 Hz, 2H), 7.57 (s, 1H), 7.49 – 7.40 (m, 5H), 7.20 (t, *J* = 8.5 Hz, 2H), 7.04 (d, *J* = 8.3 Hz, 2H), 3.90 (s, 3H), 2.28 (s, 3H). ^{13}C NMR (75 MHz, CDCl3): δ (ppm) 164.15, 160.87, 159.50, 159.18, 154.04, 150.65, 139.29, 136.35 (d, *J* = 3.4 Hz), 133.84, 130.82, 130.59, 130.48, 128.70, 128.64, 126.88, 119.60, 115.48 (d, *J* = 21.5 Hz), 113.53, 55.37, 18.17. ^{19}F NMR (377 MHz, $CDCl_3$): δ = -114.14 (s, 1F). HRMS (ESI) m/z calcd for $C_{25}H_{21}FNO$ $[M + H]^+$ 370.1607, found 370.1615.

3,5-dimethyl-2,4,6-triphenylpyridine (11aa):

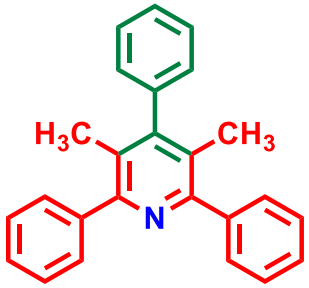

Eluent: Hexane/Ethyl acetate (50:1). White solid (yield = 88%, 295 mg). ^{1}H NMR (400 MHz, $CDCl_3$): *δ* (ppm) 7.78 (d, *J* = 7.4 Hz, 4H), 7.60 – 7.53 (m, 4H), 7.52 – 7.48 (m, 3H), 7.45 – 7.42 (m, 3H), 7.39 – 7.36 (m, 1H), 2.30 (s, 6H). ^{13}C NMR (101 MHz, $CDCl_3$): *δ* (ppm) 161.51, 142.26, 136.89, 135.82, 131.68, 129.71, 129.52, 129.39, 128.49, 128.31, 128.22, 123.19, 17.76.

3,5-dimethyl-2,6-diphenyl-4-(p-tolyl)pyridine (11ab):

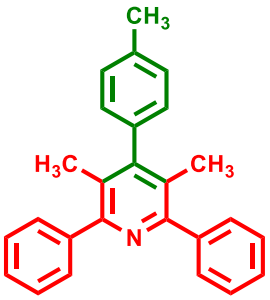

Eluent: Hexane/Ethyl acetate (50:1). White solid (yield = 91%, 318 mg). ^{1}H NMR (400 MHz, $CDCl_3$): δ (ppm) 7.61 (d, J = 7.5 Hz, 4H), 7.47 – 7.44 (m, 4H), 7.40 – 7.38 (m, 2H), 7.34 (d, J = 7.5 Hz, 2H), 7.15 – 7.13 (m, 2H), 2.47 (s, 3H), 2.06 (s, 6H). ^{13}C NMR (101 MHz, $CDCl_3$): δ (ppm) 156.15, 151.92, 141.49, 137.04, 136.79, 129.60, 129.44, 128.13, 128.09, 127.67, 127.59, 21.35, 18.30. HRMS (ESI) m/z calcd for $C_{26}H_{24}N$ $[M + H]^+$ 350.1909, found 396.1913.

4-(4-fluorophenyl)-3,5-dimethyl-2,6-diphenylpyridine (11ac):

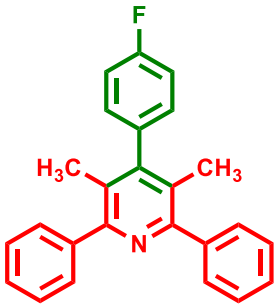

Eluent: Hexane/Ethyl acetate (50:1). White solid (yield = 86%, 304 mg). ^{1}H NMR (300 MHz, $CDCl_3$): δ (ppm) 7.61 – 7.57 (m, 4H), 7.48 – 7.35 (m, 6H), 7.22 (d, J = 7.0 Hz, 4H), 2.03 (s, 6H). ^{13}C NMR (75 MHz, $CDCl_3$): δ (ppm) 163.75, 156.27, 150.80, 141.27, 135.60 (d, J = 3.6 Hz), 129.94 (d, J = 7.8 Hz), 129.37, 128.09, 127.66, 127.59, 115.97 (d, J = 21.5 Hz), 18.22. ^{19}F NMR (282 MHz, $CDCl_3$): δ = -114.77 (s, 1F). HRMS (ESI) m/z calcd for $C_{25}H_{21}FN$ $[M + H]^+$ 354.1658, found 354.1652.

2,6-bis(4-methoxyphenyl)-3,5-dimethyl-4-phenylpyridine (11ad):

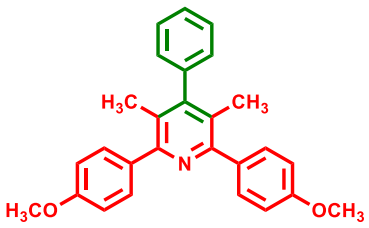

Eluent: Hexane/Ethyl acetate (50:1). White solid (yield = 89%, 352 mg). ^{1}H NMR (400 MHz, $CDCl_3$): δ (ppm) 7.84 – 7.82 (m, 4H), 7.77 (t, J = 6.5 Hz, 2H), 7.40 – 7.38 (m, 2H), 7.38 – 7.33 (m, 2H), 7.07 (d, J = 8.3 Hz, 1H), 6.97 (d, J = 9.3 Hz, 4H), 3.88 (s, 6H), 2.28 (s, 6H). ^{13}C NMR (101 MHz, $CDCl_3$): δ (ppm) 160.81, 151.09, 140.14, 136.96, 135.95, 132.02, 130.23, 129.63, 128.48, 128.38, 113.68, 55.45, 18.09. HRMS (ESI) m/z calcd for $C_{27}H_{26}NO_2$ $[M + H]^+$ 396.1964, found 396.1958.

7-phenyl-5,6,8,9-tetrahydrodibenzo[c,h]acridine (12aa):

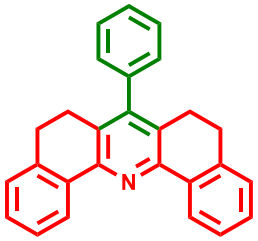

Eluent: Hexane/Ethyl acetate (50:1). White solid (yield = 88%, 316 mg). ^{1}H NMR (300 MHz, $CDCl_3$): δ (ppm) 8.61 (dd, J = 7.6, 1.5 Hz, 2H), 7.57 – 7.50 (m, 6H), 7.48 – 7.45 (m, 2H), 7.25 – 7.22 (m, 3H), 2.89 – 2.84 (m, 4H), 2.74 – 2.65 (m, 4H). ^{13}C NMR (75 MHz, $CDCl_3$): δ (ppm) 154.44, 150.06, 143.13, 140.57, 137.87, 136.72, 125.47, 133.57, 133.15, 131.83, 129.95, 129.21, 128.68, 128.42, 128.17, 127.01, 125.98, 125.66, 125.34, 28.81, 28.22, 27.27, 25.88.

7-(p-tolyl)-5,6,8,9-tetrahydrodibenzo[c,h]acridine (12ab):

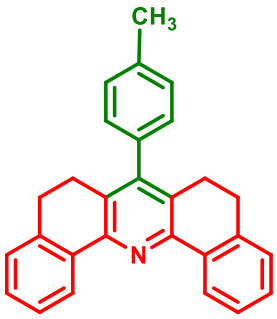

Eluent: Hexane/Ethyl acetate (50:1). White solid (yield = 91%, 339 mg). ^{1}H NMR (400 MHz, $CDCl_3$): δ (ppm) 8.61 (d, J = 7.8, 2H), 7.43 (d, J = 8.1 Hz, 2H), 7.33 (d, J = 7.5 Hz, 4H), 7.23 (d, J = 7.5 Hz, 2H), 7.13 (d, J = 7.5 Hz, 2H), 2.91 – 2.84 (m, 4H), 2.75 – 2.67 (m, 4H), 2.48 (s, 3H). ^{13}C NMR (101 MHz, $CDCl_3$): δ (ppm) 150.02, 147.54, 137.87, 137.34, 135.42, 134.86, 129.30, 129.00, 128.66, 128.63, 127.48, 127.01, 125.29, 28.18, 25.84, 21.37.

7-(4-methoxyphenyl)-5,6,8,9-tetrahydrodibenzo[c,h]acridine (12ac):

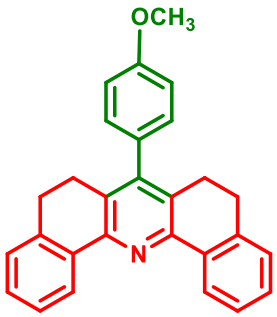

Eluent: Hexane/Ethyl acetate (50:1). White solid (yield = 93%, 362 mg). ^{1}H NMR (300 MHz, $CDCl_3$): δ (ppm) 8.62 (dd, J = 7.7, 1.4 Hz, 2H), 7.44 – 7.22 (m, 8H), 7.08 – 7.04 (m, 2H), 3.92 (s, 3H), 2.89 – 2.84 (m, 4H), 2.73 – 2.68 (m, 4H). ^{13}C NMR (75 MHz, $CDCl_3$): δ (ppm) 159.04, 150.06, 147.25, 137.85, 135.45, 130.00, 129.93, 129.20, 128.64, 127.46, 127.00, 125.32, 114.00, 55.32, 28.22, 25.87.

7-(4-fluorophenyl)-5,6,8,9-tetrahydrodibenzo[c,h]acridine (12ad):

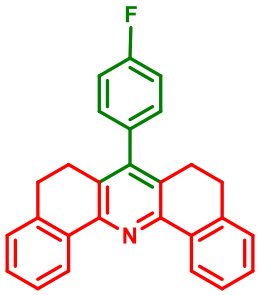

Eluent: Hexane/Ethyl acetate (50:1). White solid (yield = 87%, 328 mg). ^{1}H NMR (300 MHz, $CDCl_3$): δ (ppm) 8.62 (dd, J = 7.7, 1.5 Hz, 2H), 7.45 (td, J = 7.5, 1.4 Hz, 2H), 7.38 – 7.35 (m, 2H), 7.26 – 7.20 (m, 6H), 2.90 – 2.85 (m, 4H), 2.75 – 2.64 (m, 4H). ^{13}C NMR (101 MHz, $CDCl_3$): δ (ppm) 163.89, 149.14, 147.84, 137.80, 133.39, 130.77, 128.79, 128.51, 128.24, 127.10, 126.66, 124.59, 114.70, 28.79, 26.14. ^{19}F NMR (282 MHz, $CDCl_3$): δ = -114.30 (s, 1F).

IV.4.4. NMR spectra of selected compounds

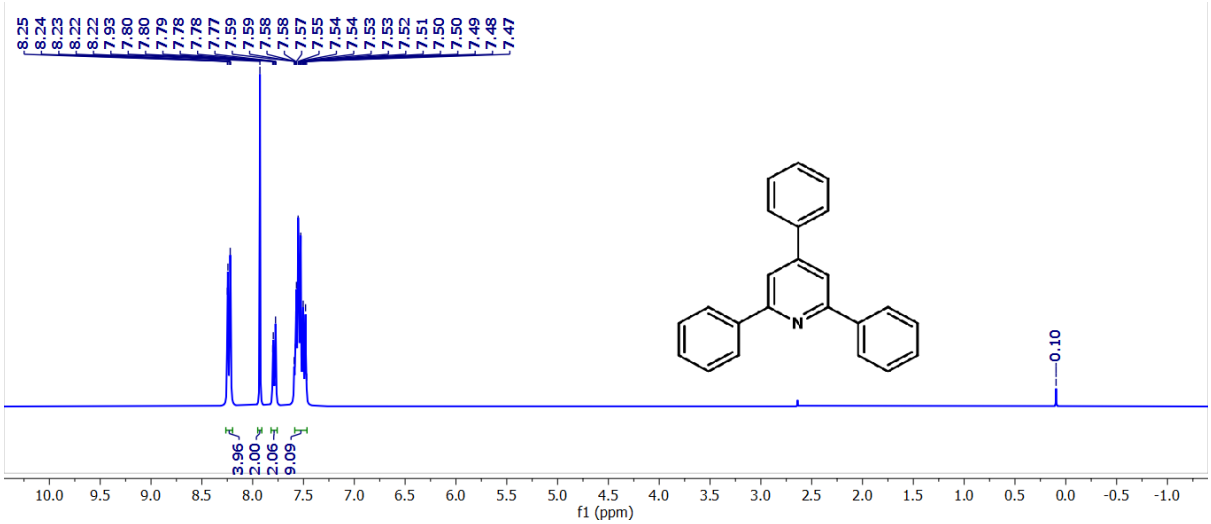

Figure 8. ^{1}H NMR spectrum of compound **6aa** (300 MHz, $CDCl_3$).

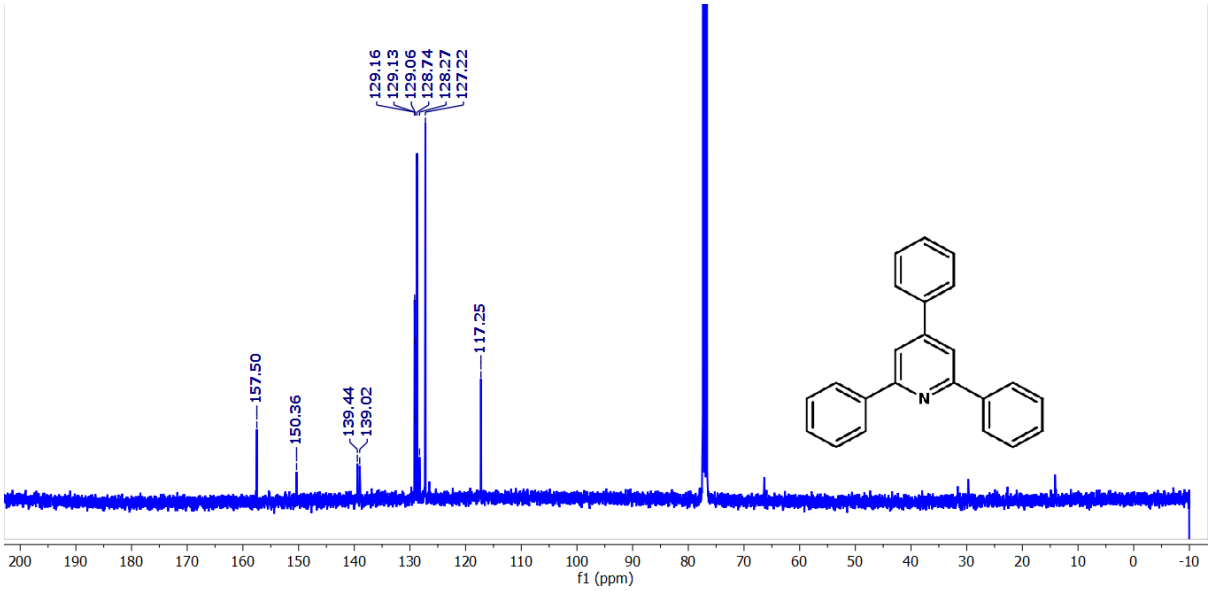

Figure 9. ^{13}C NMR spectrum of compound **6aa** (101 MHz, $CDCl_3$).

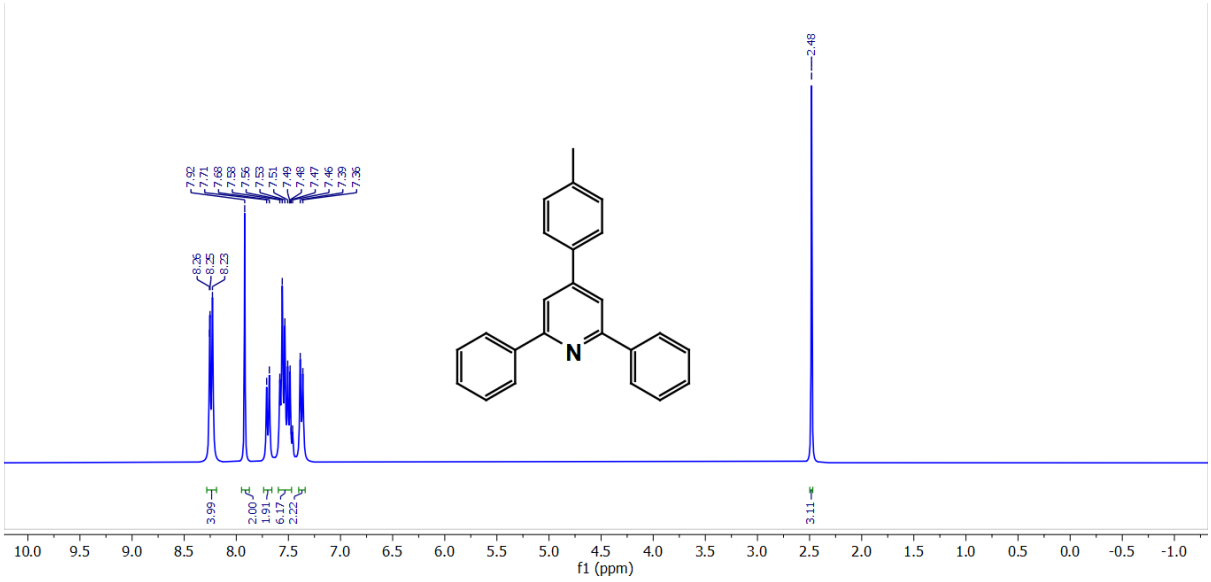

Figure 10. ^{1}H NMR spectrum of compound **6ab** (300 MHz, $CDCl_3$).

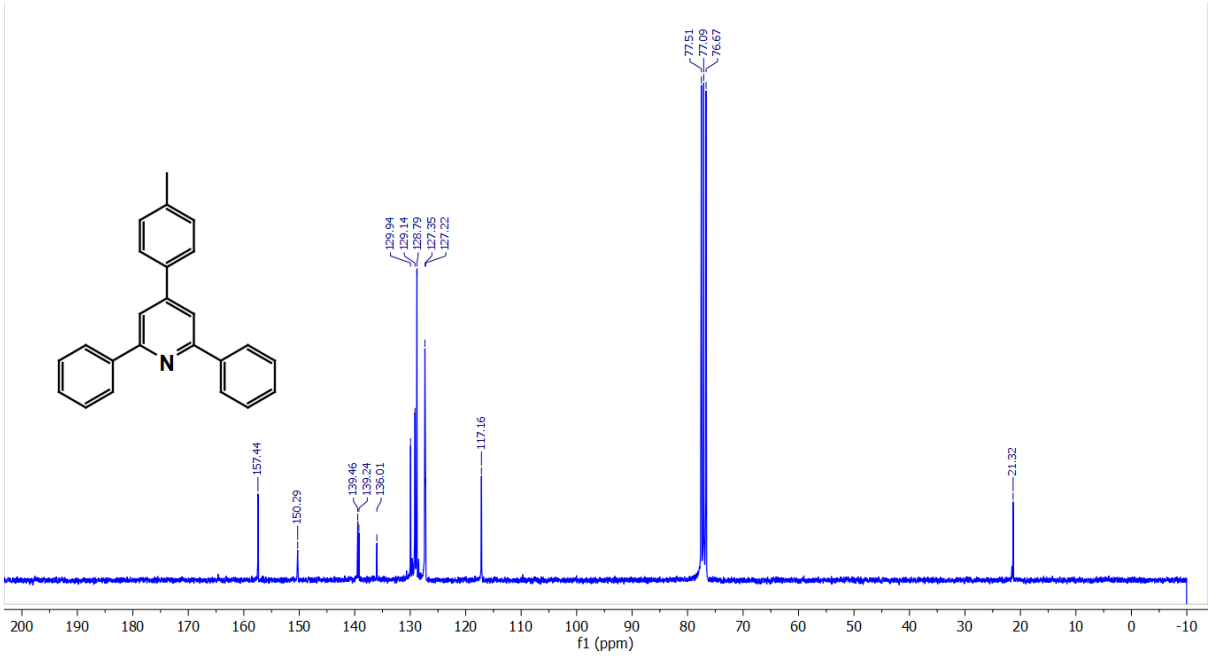

Figure 11. ^{13}C NMR spectrum of compound **6ab** (75 MHz, $CDCl_3$).

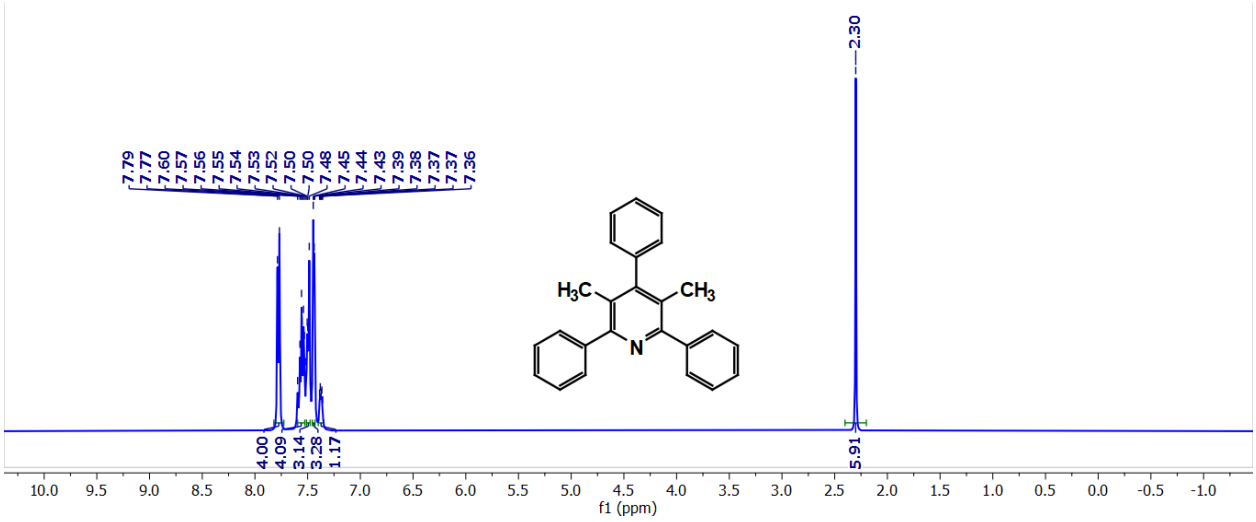

Figure 12. ^{1}H NMR spectrum of compound **11aa** (400 MHz, $CDCl_3$).

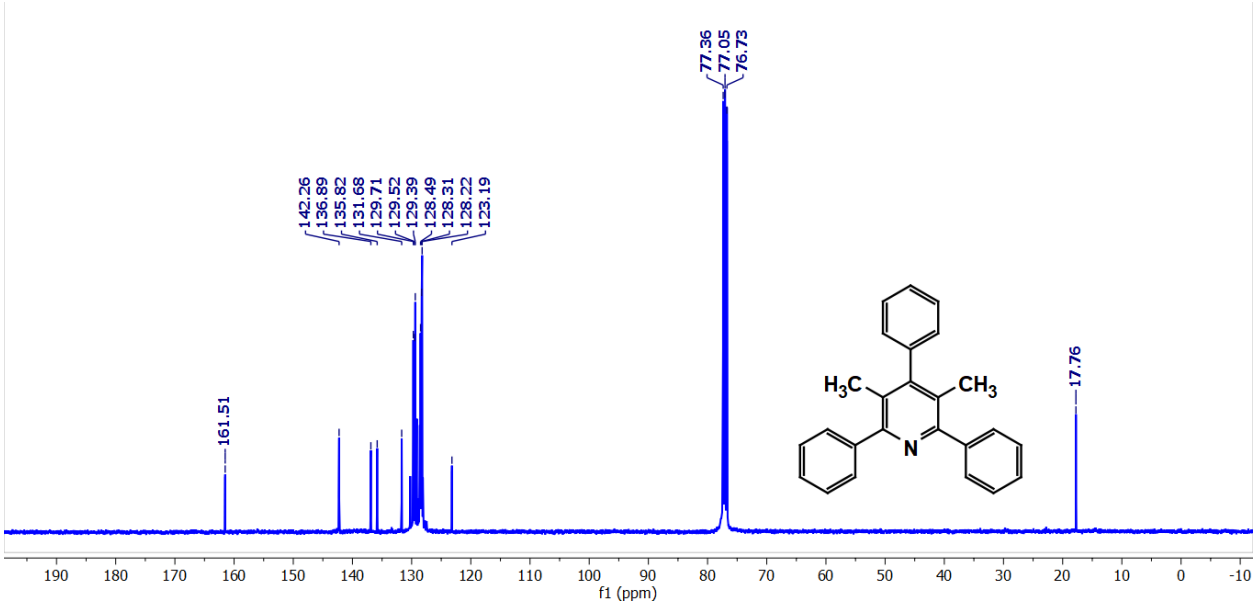

Figure 13. ^{13}C NMR spectrum of compound **11aa** (300 MHz, $CDCl_3$).

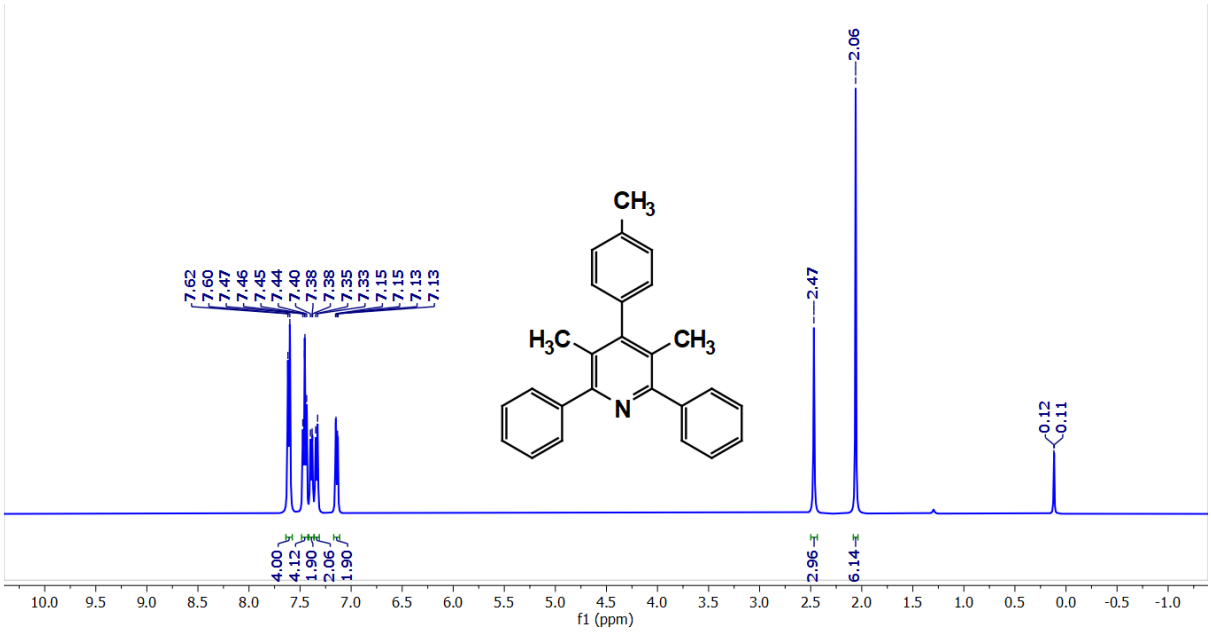

Figure 14. ^{1}H NMR spectrum of compound **11ab** (400 MHz, $CDCl_3$).

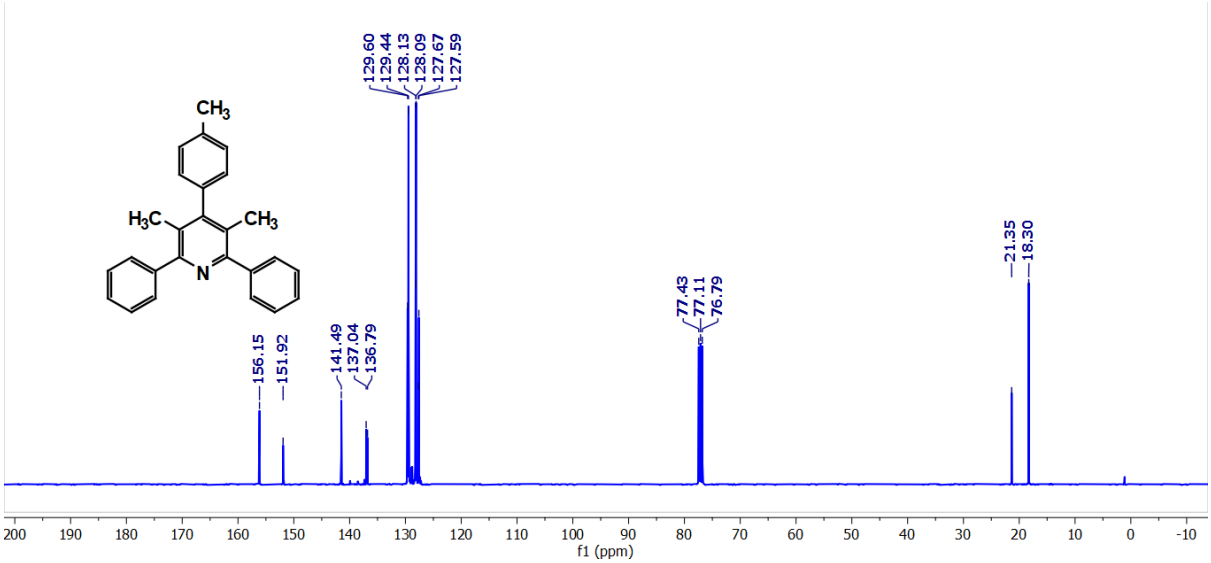

Figure 15. ^{13}C NMR spectrum of compound **11ab** (101 MHz, $CDCl_3$).

IV.5. References

1. (a) P. Bhutani; G. Joshi; N. Raja; N. Bachhav; P. K. Rajanna; H. Bhutani; A. T. Paul; R. Kumar. *J. Med. Chem*. **2021**, *64*, 2339−2381. (b) H. Chen; S. Deng; N. Albadari; M. K. Yun; S. Zhang; Y. Li; D. Ma; D. N. Parke; L. Yang; T. N. Seagroves; S. W. White; D. D. Miller; W. Li. *J. Med. Chem*. **2021**, *64*, 12049−12074 (c) Z. Guo; P. Zhou; H. Song; Y. Liu; J. Zhang; Y. Li; Q. Wang. *J. Agric. Food Chem*. **2021**, *69*, 15123−15135 (d) X. Song; X. Zhu; Ting. Li; C. Liang; M. Zhang; Y. Shao; J. Tao; R. Sun. *J. Agric. Food Chem*. **2019**, *67*, 11354−11363 (e) B. J. Wall; M. F. Will; G. K. Yawson; P. J. Bothwell; D. C. Platt; C. F. Apuzzo; M. A. Jones; G. M. Ferrence; M. I. Webb. *J. Med. Chem*. **2021**, *64*, 10124−10138 (f) T. Wang; S. Cai; M. Wang; W. Zhang; K. Zhang; D. Chen; Z. Li; S. Jiang. *J. Med. Chem*. **2021**, *64*, 7390−7403 (f) Y. Wang; S. Kou; J. Huo; S. Sun; Y. Wang; H. Yang; S. Zhao; L. Tang; L. Han; J. Zhang; L. Chen. *J. Agric. Food Chem.* **2022**, *70*, 9327−9336 (g) A. R. Dwivedi; S. Jaiswal; D. Kukkar; R. Kumar;T. G. Singh; M. P. Singh; A. M. Gaidhane; S. Lakhanpal; K. N. Prasad; B. Kumar. *RSC Med. Chem*., **2025**,*16*, 12-36 (h) M. M. Hammouda; K. M. Elattar. M. M. Rashedd; A. M. A. Osman. *RSC Med. Chem*., **2023**, *14*, 1934–1972 (i) A. G. Eissa; L. E. Powell; J. Gee; P. A. Foster; C. Simons. *RSC Med. Chem*., ***2023***, *14*, 356–366.
2. (a) A. Arcadi; V. Morlacci; L. Palombi. *Molecules* **2023**, *28*, 4725, (b) J. Li; J. Li, R. He; J. Liu; Y. Liu; L. Chen; Y. Huang; Y. Li. *Org. Lett*. **2022**, *24*, 1620−1625 (c) Y. Ding; R. Ma; X.Q. Xiao; L. Wang; Z. Wang; Y. Ma. *J. Org. Chem*. **2021**, *86*, 3897−3906 (d) R. Zhang; Y. Ding; R. Ma; X. Xiao; R. Chen; L. Wang; Y. Ma. *Org. Chem. Front*., **2023**, *10*, 780–785 (e) A. Kumar Patel; S. S. Rathor; S. Samanta. *Org. Biomol. Chem*., **2022**, *20*, 6759–6765
3. (a) T.N. Francisco; H.M.T. Albuquerque; A.M.S. Silva. *Chem. Eur. J.*, **2024**, *30*, e202401672 (b) J. H. Clark; A. Jardine; A. Matharu; C. Stevens. Greener Organic Transformations, ISBN: 978-1-78801-203-4, CHAPTER 16: Pyridine Synthesis, **2022**, 121–124. (c) S. K. Lokesh; S. Tabassum, K. S. Sagar; S. Govindaraju. Mini Review on the Multicomponent Synthesis of Pyridine Derivatives, *ChemistrySelect*, **2022**, *7*, e202203668.

4. (a) D. Srimani; Y. B. David; D. Milstein; *Chem*. *Commun*. **2013**, *49*, 6632−6634. (b) B. Pan; B. Liu; E. Yue; Q. Liu; X. Yang; Z. Wang; W. H. Sun. *ACS Catal*. **2016**, *6,* 1247−1253 (d) D. Deng; B. Hu; M. Yang; D. Chen; *Organometallics* **2018**, *37*, 2386−2394. (e) B. Guo; T. Q. Yu; H. X. Li; S.Q. Zhang; P. Braunstein; D. J. Young; H.Y. Li; J.-P. Lang; *Chem CatChem* **2019**, *11*, 2500−2510. (f) J. R. Manning; H. M. L. Davies. *J. Am. Chem. Soc.* **2008**, *130*, 8602−8603. (g) K.Parthasarathy; M. Jeganmohan; C. H .Cheng. *Org. Lett.* **2008**, *10*, 325−328. (h) T. K. Hyster; T. Rovis; *Chem. Commun.* **2011**, *47*, 11846−11848. (i) H. N. Dhara; S. Manna; B. K. Patel. *Chem. Eur. J.* 2025, *31*, e202403470 (j) Q. R. Zhang; J.R. Huang; W. Zhang; L. Dong. *Org*. *Lett*. **2014**, *16*, 1684−1687 (k) S. Chakraborty; R. Sikari; S. Chakraborty; M. Sharma; P. Brandão; N. D. Paul. *Adv. Synth. Catal.* **2024**, *366*, 5123– 5134 (l) T. Hille; T. Irrgang; R.Kempe. *Angew*. *Chem*. *Int*. *Ed*. **2017**, *56*, 371–374.

5. (a) Y. Yoshida; T. Kurahashi; S. Matsubara. *Chem. Lett.* **2012**, *41*, 1498−1499. (b) W. W. Tan; Y. J. Ong. N. Yoshikai. *Angew. Chem., Int. Ed.* **2017**, *56*, 8240−8244 (c) L. M. Kabadwal; S. Haldar; D. Banerjee. *Org. Lett.* **2024**, *26*, 9299−9304 (d) S. Gupta; A. Maji; D. Panja; M. Halder; S. Kundu; *Journal of Catalysis* **2022,** *413,* 1017–1027 (e), M.N. Zhao; L. Yu; N.F. Mo; Z.H. Ren; Y. Yu. Wang; Z.H. Guan; Org. Chem. Front., **2017**, *4*, 597-602 (f) Y. Yi; M.N. Zhao; Z. H. Ren; Yao; Y. Wang; Z. H. Guan; *Green Chem*., **2017**,*19*, 1023-1027 (g) A. Maji; S. Gupta; M. Maji; S. Kundu. *J. Org. Chem.* **2022**, *87*, 8351−8367 (h) C. Prakash; B. P. Tripathi. *J Heterocyclic Chem*. **2024**; *61*:407–420 (k) S. Pal; S. Das; S. Chakraborty; S. Khanra; N. D. Paul. *J. Org. Chem.* **2023**, *88*, 3650−3665 (l) J. Wang; D. Ba; M. Yang; G. Cheng; L. Wang. *J. Org. Chem.* **2021**, *86*, 6423−6432. (m) J. Han; X. Guo; Y. Liu; Y. Fu; R. Yan; B. Chen. *Adv. Synth. Catal.* **2017**, *359*, 2676−2681. (n) W. W. Tan; Y. J.Ong; N. Yoshikai. *Angew. Chem., Int. Ed.* **2017**, *56*, 8240−8244. (o) W. Wang; Q. Lin; N. Ma; S. Liu; M. Han; X. Yan; Q. Liu. G. A. Solan; W. H. Sun; W.H. *Catal. Sci. Technol*. **2021**, *11*, 8026−8036. (p) K. Gopalaiah; D. C. Rao; K. Mahiya; A. Tiwari. *Asian J. Org. Chem.* **2018**, *7,* 1872−1881.

6. (a) S. Varshney; N. Mishra. Recent Developments in the Synthesis and Applications of Pyridines, *Elsevier*, **2023**, Chapter 2, 43–69 (b) C. K. Chan; C.Y. Lai; C. C. Wang. *Catalysts*, **2021**, *11*, 877. (c) J. Chena; H. Menga; F. Zhanga; F. X. G.J. Denga. *Green Chem.,* **2019**, *21,* 5201-5206.

7. (a) S. M. He; Y.B. Yang; L.Y. Liu; N. Yu; Y.Q. Zhou; J. H. Zhou; M.J. Zheng; X. K. Jin; K. Jiang; Y. Wei. *Org*. *Lett*. **2025**, *27*, 1100−1105 (b) J. M. Neely; T. Rovis. *Org*. *Chem*. *Front*., **2014**, *1*, 1010–1015 (c)V.Bodala; R. L. Podugu; K. Yettula; P. Gollamudi. S. Vidavalur. S. Pulipaka. *Chem. Asian J.* **2023**, *18,* e202201004 (c) W. W. Tan; Y. J. Ong; N. Yoshikai. *Angew. Chem*. **2017**, *129*, 8352–8356. (d) X.J. Dai**;** P. Krolikowski; J. I. Murray; C. S. Wei; P. K. Dornan; A. R. Rötheli; S. Caille; O. R. Thiel; A. G. Smith; A.T. Parsons. *J. Org. Chem*. **2022**, *87*, 8437–8444 (e) D. Bai; X. Wang; G. Zheng; X. Li. *Angew. Chem*., **2018**, *130*, 6743–6747 () J.Duan; G. Xu; B. Rong; H. Yan; S. Zhang; Q. Wu; N. Zhu; K. Guo. *Green Synth. Catal.* **2021**, *2,* 237–240. (c) Q. Wu; G. Xu; Y. Li; L. Shen; Z. Fang; J. Duan; K. Guo; *Adv*. *Synth*. *Catal*. **2023**, *365,* 4310–4316.

8. (a) B. Heller; M. Hapke; *Chem. Soc. Rev*. **2007**, *36*, 1085– 1094 (b) T. Nagata; Y. Obora; *Asian J. Org. Chem.* **2020**, *9*, 1532–1547 (c) H. Jiang; J. Yang; X. Tang; J. Li; W. Wu; *J. Org. Chem*. **2015**, *80*, 17, 8763–8771. (d) Q. Gao; H. Yan; M. Wu; J. Sun; X. Yan; A. Wu. *Org*. *Biomol*. *Chem*., **2018**,*16*, 2342-2348 (e) H. Wang; S. Li; X. Wu; T. Chen; W. Liu; X. Liu; H.Cao. *Org.Lett*. **2024**, *26*, 45, 9648–9653, (f) C. Bai; H.

Guo; X. Liu; D. Liu; Z. Sun; A. Bao; M. Baiyin; T. Muschin; Y.S Bao. *J. Org. Chem*. **2021**, *86*, 18, 12664–12675.

9. (a) R. Vinodkumar, A. K. Nakate, R. K. Gamidi, R. Kontham**,** *Org. Lett.* **2024**, *26*, 7116–7121 (b) R. Echemendíaa, G. P. da Silva, M. Y. Kawamura, A. F. de la Torre, A. G. Corrêa, M. A. B. Ferreira, D. G. Rivera, M. W. Paixão, *Chem. Commun.*, **2019**, *55*, 286-289 (c) R. Vinodkumar, A. K. Nakate, R. Krishna, R. Kontham, *Chem. Commun.*, **2025**, *61*, 973-976 (d) Y. Tian, Z. Chen, K. Su, Y. Zheng, J. Liu, *Adv. Synth. Catal.* **2023**, *365*, 3909–3914 (e) S. Jamshaid, S. Mohandoss, Y. R. Lee, *Green Chem.*, **2021**, *23*, 5113-5119 (f) Q. Huang, R. Hua, *Chem. Eur. J.* **2007**, *13*, 8333 – 8337.
10. (a) Z. Song, X. Huang, W. Yi, W. Zhang, *Org. Lett*. **2016**, *18*, 5640−5643 (b) S. Chakraborty, A. S. Mohapatra, S. Saha, S. Mandal, N. D. Paul, *Chem Asian J.* **2025**, e202401038 (c) Y.-Y. Liu, Y.-T. Zhai, *J. Org. Chem.* **2024**, *89*, 17598−17608 (d) S. Kosuge, Y. Araki, K. Tsuge, K. Sugimoto, Y. Matsuya, *J. Org. Chem.* **2023**, *88*, 6973−6986.
11. (a) N. Vodnala, R. Gujjarappa, V. Satheesh, R. Gupta, D. Kaldhi, A. K. Kabi, C. C. Malakar, *ChemistrySelect* **2020**, *5*, 10144 – 10148. (b) H. Wang, S. Li, X. Wu, T. Chen, W. Liu, X. Liu, H. Cao, *Org. Lett.* **2024**, *26*, 9648–9653.
12. (a) A. A. Swatiputra, D. Mukherjee, S. Dinda, S. Roy, K. Pramanik, S. Ganguly, *Dalton Trans*., **2023**, *52*, 15627–15646 (b) L. Alig, M. Fritz, S. Schneider, *Chem. Rev.* **2019**, *119*, 2681−2751 (c) R. H. Crabtree, *Chem. Rev.* **2017**, *117*, 9228−9246 (d) Q. Yang, Q. Wanga, Z. Yu, *Chem. Soc. Rev.,* **2015**, *44*, 2305−2329.
13. (a) B. Heller, M. Hapke, *Chem. Soc. Rev.* **2007**, *36*, 1085–1094 (b) Q. Wu, G. Xu, Y. Li, L. Shen, Z. Fang, J. Duan, K. Guo, *Adv. Synth. Catal.* **2023**, *365*, 4310–4316 (c) J. M. Neely, T. Rovis, *Org. Chem. Front.*, **2014**, *1*, 1010–1015.
14. W. Yin, X. Pan, W. Leng, J. Chen, H. He, *Green Chem.*, **2019**, *21*, 4614-4618.
15. (a) D. Jana, S. Malik, G. Kanrar, S. Naskar, S. Halder, K. Pramanik, *ChemCatChem*, **2025**, *0*, e202401851 (b) D. Jana, S. Roy, S. Naskar, S. Halder, G. Kanrar, K. Pramanik, *Org. Biomol. Chem*., **2024**, *22*, 6393-6408.
16. S. Werkmeister, J. Neumann, K. Junge, M. Beller, *Chem. Eur. J.* **2015**, *21*, 12226 – 12250.
17. D. A. Colby, R. G. Bergman, J. A. Ellman, *J. Am. Chem. Soc.* **2008**, *130*, 3645–3651.
18. P. Hima, M. Vageesh, R. Dey, *RSC Adv.*, **2024**, *14*, 10761-10767.
19. S. Roy, S. Pramanik, S. C. Patra, B. Adhikari, A. Mondal, S. Ganguly, K. Pramanik, *Inorg. Chem.* **2017**, *56*, 12764-12774.

Chapter V

Effective Pincer-Copper Catalyzed Homogeneous Friedländer Quinoline Synthesis from Secondary Alcohols and Primary Alcohols/Ketones

V.1 Introduction

Quinolines constitute a key class of heterocyclic compounds with extensive applications in, agrochemical formulations, pharmaceutical development, and the design of functional materials (Figure 1).[1]

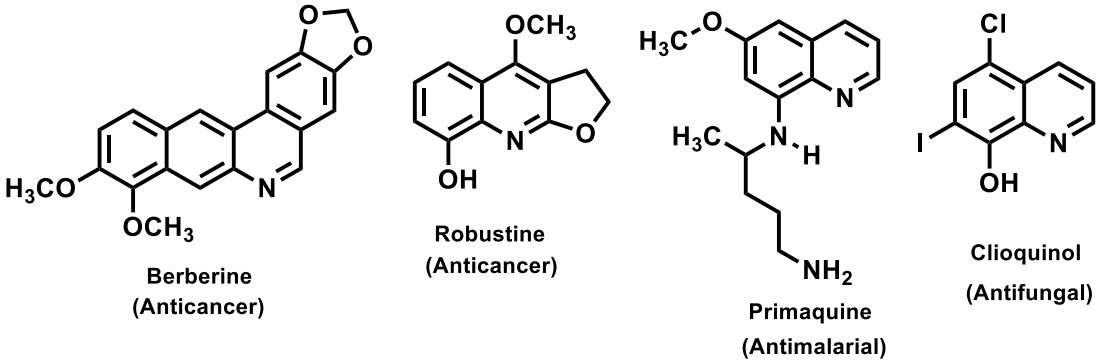

Figure 1. Examples of bio-active and drugs containing quinolines.

A wide range of synthetic strategies has been established for the construction of the quinoline core, including the Combes, Doebner–von Miller, Conrad-Limpach, Gould-Jacobs, Skraup and Povarov reactions.[2]

Nevertheless, the general applicability of these methods is constrained by harsh reaction conditions, multistep procedures, low stereoselectivity, and limited yields. Green and atom-economical acceptorless dehydrogenative coupling (ADC) reactions offer a competitive strategy for quinoline synthesis, serving as a variation of the Friedländer protocol.[3] These metal-catalyzed reactions proceed through a catalytic cycle involving the dehydrogenation of alcohols, followed by cyclo-condensation with amines. Among various homogeneous transition metal catalysts,[4] Copper complexes have also been reported as efficient systems to date.[5]

Consequently, the development of green, atom-economic synthetic methods for the preparation of highly functionalized N-heterocycles, such as quinolines, from readily available and cost-effective starting materials under mild conditions is still in demand.[6]

Over the past decade, significant advancements have been made in the design of synthetic strategies and novel catalysts aimed at achieving efficient dehydrogenative functionalization of inexpensive and environmentally friendly alcohols, leading to the production of various valuable products, including N-heterocycles.[7] The dehydrogenative synthesis of quinoline has been successfully achieved by Shim, Yus, Verpoort, Milstein, and Liu and Sun, through a Ru-catalyzed indirect Friedländer synthesis.[8]

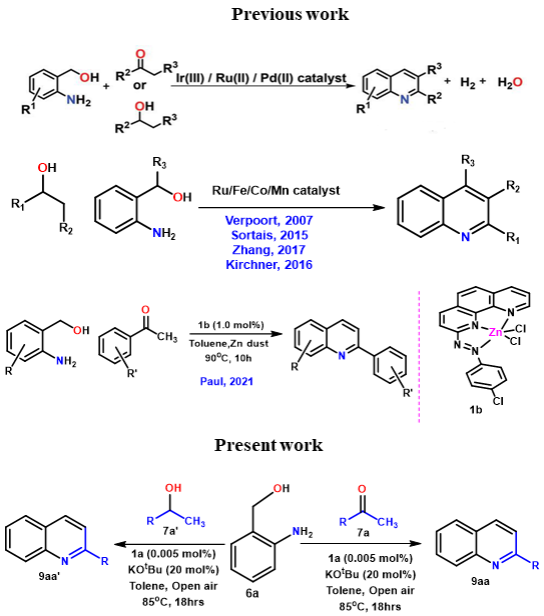

Scheme 1: synthesis of quinoline derivatives with various protocol.

Despite substantial advancements in N-heterocycle synthesis via direct dehydrogenative functionalization of alcohols, the process largely relies on costly and toxic noble metal catalysts, including Ru, Rh, and Ir.[9] To enhance the environmental sustainability and cost-effectiveness of dehydrogenative functionalization of alcohols, it is crucial to replace precious heavy metals with non-precious, earth-abundant alternatives such as Mn, Fe, Co, Cu, and Ni.[10] However, these methodologies commonly encounter several challenges, including difficulties in product separation, the generation of hazardous byproducts, the requirement of stoichiometric or excessive amounts of base, and low turnover numbers (TONs), necessitating high catalyst loadings. A significant limitation of homogeneous catalysts lies in their inherent difficulty in efficient recovery and recycling after the catalytic cycle. This limitation poses a substantial obstacle to achieving cost-effectiveness in industrial applications. It is noteworthy that copper catalysts generated *in-situ* from commercially available simple salts often need (over)stoichiometric loadings. This inherent limitation results in low TON[11] and consequently diminishes the sustainability of the process. Therefore, the development of more practical and environmentally benign catalytic systems for the synthesis of substituted quinolines from readily accessible starting materials is highly desirable.

Cooperative catalysis,[12] involving the synergistic interplay between metal centers and their ligands, offers a compelling strategy for enabling chemical transformations that are typically challenging to accomplish with first-row base metals under mild conditions.

In this chapter, we introduce a copper-catalyzed metal-ligand cooperative strategy for the dehydrogenative functionalization of alcohols into a range of substituted quinolines under

mild aerobic conditions. The catalytic system employs air-stable, cost-effective, and well-defined copper(II) complexes (**1a, 1b**) supported by tridentate bis-azo aromatic N^N^N pincer type ligands. Azo-chromophores, recognized for their redox activity, readily act as electron sinks[13] during the dehydrogenation of alcohols. We hypothesized that the synergistic interaction between copper and the bis-azo aromatic scaffold would facilitate these dehydrogenative functionalization reactions under such mild conditions.

V.2 Result and Discussion

V.2.1 Synthesis of ligands and complexes

Initially, two penta-coordinated Cu(II) complexes, $[Cu(L^{Cl})Cl_2]$ **1a** and $[Cu(L^{H})Cl_2]$ **1b**, along with a hexa-coordinated Cu(II) complex $[Cu(L^{H})_2]^{+}[(PF_6)_2^{-}]$ **1c**, were synthesized. The preparation of the penta-coordinated complexes involved the reaction of $CuCl_2{\cdot}4H_2O$, while the hexa-coordinated complex was synthesized by reacting $Cu(OAc)_2{\cdot}H_2O$ with 2-(2-pyridylazo)-4-chloroazobenzene (L^{Cl}) and 2-(2-pyridylazo)azobenzene (L^{H}).(Scheme 2). The use of a strongly electron-deficient organic template, L, is supported by its ability to promote the favorable initial attack of nucleophiles (primary or secondary alcohols) at the electron-rich copper center. This interaction, in turn, facilitates the overall catalytic pathway (Scheme 4). This work reports the exploration of these pincer complexes for their catalytic activity in cross-coupling reactions.

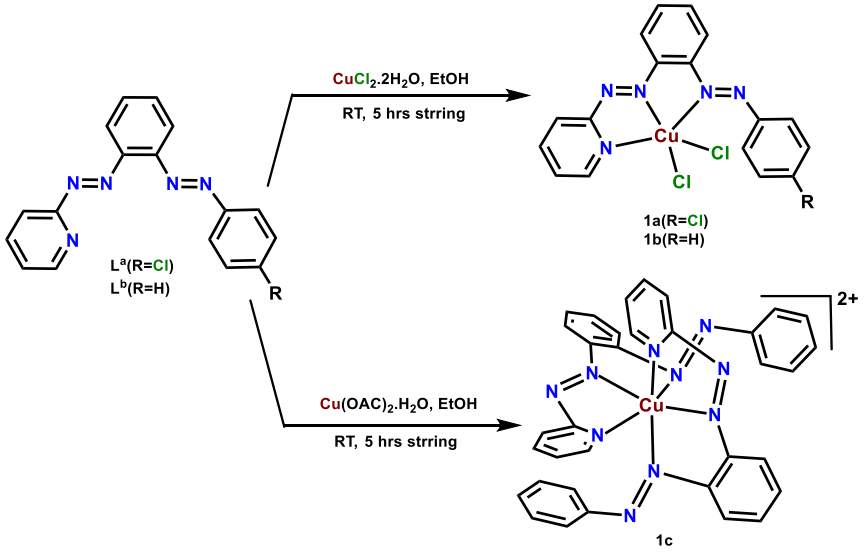

Scheme 2. synthetic strategy of the copper catalysts

The organic templates, L^{Cl} and L^{H}, containing two electron-deficient azo moieties and an aromatic heterocyclic group, were synthesized via the condensation of (E)-2-((4-chlorophenyl)azo)aniline or (E)-2-(phenylazo)aniline with 2-nitrosopyridine, following a

previously reported procedure.[14] The stoichiometric reaction of $CuCl_2.4H_2O$ with the respective organic template (L^{Cl} or L^{H}) in an ethanolic medium at room temperature for 6 hrs yielded two new deep brown complexes, **1a** and **1b**, with yields of 90% and 92%, respectively. A new brownish-red complex, **1c**, was obtained in 85% yield by reacting $Cu(OAc)_2 \cdot H_2O$ with L^{H} in an ethanolic medium at room temperature for 4 hrs. All the complexes are stable in air and moisture.

V.2.2 IR spectra

Sharp vibrations around 1456, 1395 cm^{-1}; 1459, 1397 cm^{-1} and 1448, 1389 cm^{-1} in the infrared spectra of complex **1a**; **1b** and **1c** were assigned to the $\nu_{N=N}$ stretching respectively (Figure 2).

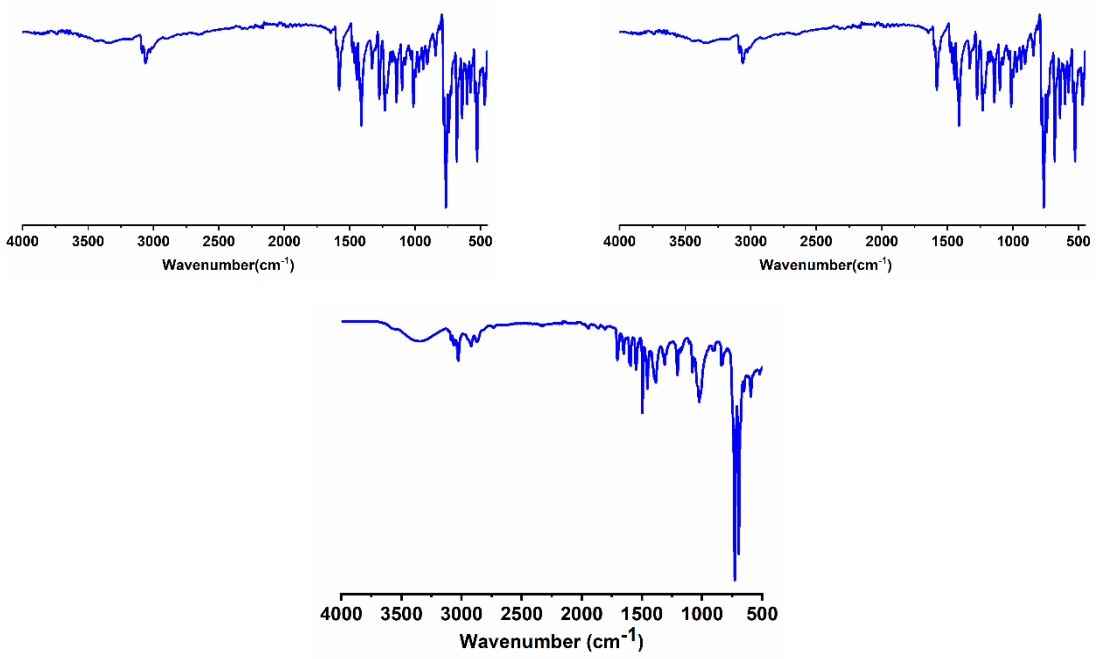

Figure 2. IR spectra of **1a** (upper left), **1b** (upper right) and **1c** (bottom).

V.2.3 Crystal Structures

Using the X-ray diffraction technique, the molecular structures of three copper complexes were determined by growing suitable X-ray quality single crystals from the slow diffusion of respective dichloromethane solutions into *n*-hexane at room temperature. ORTEP perspectives with selected bond parameters of **1a, 1b** and **1c** are given in Fig. 3-5 and additional

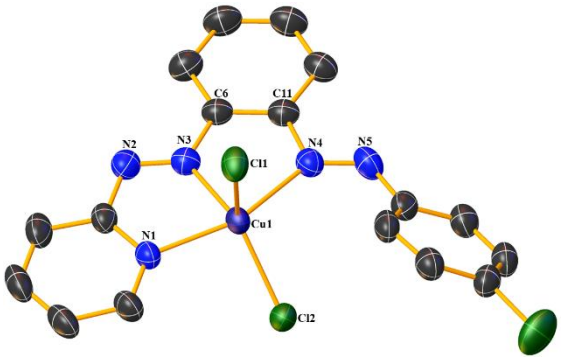

Figure 3. ORTEP view of **1a** (Solvent molecule and hydrogen atoms are omitted for clarity, and thermal ellipsoids are set at 50% probability). Selected bond lengths (Å) and bond angles (deg): Cu1–Cl1 2.239(6), Cu1–Cl2 2.371(7), Cu1–N1 2.017(2), Cu1–N3 2.002(3), Cu1–N4 2.119(3), N2–N3 1.256(5), N4–N5 1.252(4), N1–Cu1–N3 76.52(11), N3–Cu1–N4 78.17(12), N4–Cu1–Cl1 95.66(11), Cl1–Cu1–Cl2 122.10(10), Cl1–Cu1–N3 99.95(11), Cl1–Cu1–N1 94.45(12), N1–Cu1–Cl2 94.31(10), N3–Cu1–Cl2 137.68(11), N1–Cu1–N4 154.00(8).

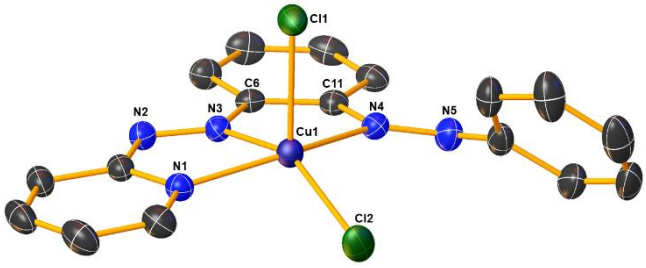

Figure 4. ORTEP view of **1b** (Solvent molecule and hydrogen atoms are omitted for clarity, and thermal ellipsoids are set at 50% probability). Selected bond lengths (Å) and bond angles (av) (deg): Cu1–Cl1 2.210(8), Cu1–Cl2 2.387(8), Cu1–N1 2.050(2), Cu1–N3 1.982(3), Cu1–N4 2.166(3), N2–N3 1.257(5), N4–N5 1.251(4), N1–Cu1–N3 76.52(11), N3–Cu1–N4 78.17(12), N4–Cu1–Cl1 95.66(11), Cl1–Cu1–Cl2 122.10(10), Cl1–Cu1–N3 99.95(11), Cl1–Cu1–N1 94.45(12), N1–Cu1–Cl2 94.31(10), N3–Cu1–Cl2 147.98(11), N1–Cu1–N4 153.02(11).

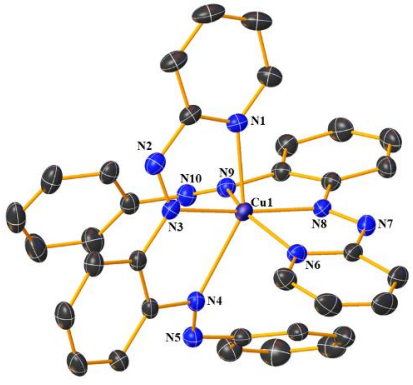

Figure 5. ORTEP view of **[1c]**$^{2+}$ (Solvent molecule and hydrogen atoms are omitted for clarity, and thermal ellipsoids are set at 50% probability). Selected bond lengths (Å) and bond angles (deg): Cu1–N1 2.103(3), Cu1–N3 1.972(3), Cu1–N4 2.374(3), Cu1–N6 2.103(3), Cu1–N8 1.972(3), Cu1–N9 2.374(3), N2–N3 1.254(5), N4–N5 1.262(5), N7–N8 1.254(5), N9–N10 1.262(5), N1–Cu1–N3 77.06(13), N3–Cu1–N4 75.15(12), N6–Cu1–N8 77.06(13), N8–Cu1–N9 75.15(12).

crystallographic information are provided in Table 1 and 2. Complexes **1a, 1b** and **1c** crystalize in monoclinic C12/c1, orthorhombic Pbca and monoclinic C12/c1 space group respectively.

The asymmetric unit of complex **1b** comprises two crystallographically independent molecules (Z' = 8), with all atoms occupying general positions. The unit cell contains a total of sixteen molecules. The primary valency of Cu(II) is satisfied by two chloride ligands positioned cis to each other, minimizing overall steric hindrance. In case of complex **1a** and **1b**, the ligand

Table 1. Crystallographic Details of complexes **1a** and **1b**.

	1a	**1b**	**$[1c]^{2+}.2PF_6^-$**
Empirical formula	$C_{17}H_{12}N_5Cl_3Cu$	$C_{17}H_{13}N_5Cl_2Cu$	$C_{34}H_{26}CuF_{12}N_{10}P_2$
T/K	298K	298K	298K
fw	456.21	421.77	928.13
Crystal system	Monoclinic	Orthorhombic	Monoclinic
Space Group	C12/c1	P b c a	C12/c1
a/Å	9.4407(7)	12.9783(3)	13.1384(5)
b/*Å*	14.0356(11)	12.8654(3)	21.2067(8)
c/ *Å*	14.0074(11)	41.2875(9)	14.6732(8)
α/deg	90	90	90
β/deg	98.164(2)	90	109.8600(10)
γ/deg	90	90	90
V/ *Å*^{3}	1837.3(2)	6893.8(3)	3845.1(3)
Z	4	16	4
D_c/Mgm^{-3}	1.649	1.625	1.603
μ/mm^{-1}	1.636	1.587	0.751
F(000)	916	3216	1868
cryst size/mm^3	0.5 × 0.3 × 0.2	0.5 × 0.3 × 0.2	0.51 × 0.43 × 0.31
θ/deg	2.847 – 29.591	2.28 – 22.85	2.42 – 25.43
Measured reflns	9941	9961	9354
Unique reflns	3912	10062	10516
[a]GOF on F^2	1.064	1.000	1.049
R1[b], wR2[c][$I>2\sigma(I)$]	0.0636, 0.1649	0.0405, 0.0830	0.0655, 0.0733
R1, wR2	0.0711, 0.1724	0.0748, 0.0956	0.1906, 0.1987
[a]GOF = $\{\Sigma[w(F_o{}^2-F_c{}^2)2]/(n-p)\}^{1/2}$. [b]R1 = $\Sigma\,[\lvert F_o\rvert-\lvert F_c\rvert]/\,\Sigma\,\lvert F_o\rvert$. [c]wR2 = $[\Sigma\,[w(F_o{}^2-F_c{}^2)^2]/\,\Sigma\,[w(F_o{}^2)^2]]^{1/2}$ where $w = 1/[\,\sigma^2(F_o{}^2)+(aP)^2+bP]$, $P = (F_o{}^2+2F_c{}^2)/3$.			

L and two Cl atoms furnish distorted penta-coordinated geometry around Cu(II), while tridentate coordination was found through $N_{pyridyl}$, $N_{azopyridyl}$ and and $N_{azophenyl}$ atoms to form two juxtaposed five-membered rings in due course of chelation. This typical class of ligand with appreciable π-acidity ensures strong coordination through back-bonding with the metal centre, and thus leads to a robust class of coordinatively unsaturated copper compounds. These two features are indispensable for a metal catalyst to be a good candidate in homogeneous

catalysis with sustainable character. For precise determination of geometry between square pyramid and trigonal bipyramid of penta-coordinated complexes, the largest (N1−Cu1−N4 154.02Å) and second-largest (N3−Cu1−Cl2 137.69Å) angles are used to calculate the τ value as 0.272 for **1a** and similar calculation for **1b** results τ value as 0.221.

Table 2. Selected Experimental and Theoretical Bond Parameters of **1a** and **1b** complex.

1a			**1b**		
Parameter	**Expt.**	**Theo.**	**Parameter**	**Expt.**	**Theo.**
Cu1–Cl1	2.2391(10)	2.501	Cu1–Cl1	2.3874(8)	2.498
Cu1–Cl2	2.3711(10)	2.325	Cu1–Cl2	2.2104(8)	2.328
Cu1–N1	2.015(3)	2.079	Cu1–N5	2.050(2)	2.080
Cu1–N3	2.002(2)	2.035	Cu1–N1	1.982(2)	2.040
Cu1–N4	2.118(3)	2.160	Cu1–N2	2.166(2)	2.156
N2–N3	1.253(4)	1.254	N4–N1	1.267(3)	1.254
N4–N5	1.232(5)	1.254	N2–N3	1.251(3)	1.254
Cl1Cu1Cl2	122.09(4)	118.52	Cl1Cu1Cl2	116.06(4)	119.73
Cl1Cu1N4	100.52(10)	101.24	Cl1Cu1N2	93.56(6)	96.43
Cl2Cu1N4	95.44(9)	95.96	Cl2Cu1N2	100.01(7)	101.27
N1Cu1Cl1	94.32(10)	95.41	N5Cu1Cl1	98.78(7)	95.07
N1Cu1Cl2	94.48(10)	93.16	N5Cu1Cl2	95.96(7)	92.08
N1Cu1N4	154.08(15)	154.19	N5Cu1N2	153.02(9)	154.04
N3Cu1Cl1	37.69(9)	142.43	N1Cu1Cl1	95.90(7)	98.41
N3Cu1Cl2	99.95(8)	98.60	N1Cu1Cl2	147.99(7)	141.31
N3Cu1N1	76.52(14)	75.84	N1Cu1N5	76.29(9)	75.72
N3Cu1N4	78.20(13)	78.94	N1Cu1N2	78.66(9)	78.92
C1N1Cu1	128.4(3)	128.77	C14N5Cu1	129.6(2)	128.66
C5N1Cu1	112.8(3)	111.94	C13N5Cu1	112.59(18)	112.05
N3N2C5	110.5(3)	112.44	N1N4C13	111.1(2)	112.39
C6N3Cu1	118.4(3)	117.66	C1N1Cu1	119.44(19)	117.57
N2N3C6	119.9(3)	121.38	N4N1C1	118.6(2)	121.43
N2N3Cu1	121.4(2)	120.92	N4N1Cu1	121.87(19)	120.94
C11N4Cu1	112.9(3)	110.44	C6N2Cu1	110.03(18)	110.56
N5N4C11	110.2(3)	113.99	N3N2C6	112.8(2)	114.04
N5N4Cu1	136.5(3)	134.74	N3N2Cu1	136.5(2)	134.51
N4N5C12	119.4(4)	121.96	N2N3C7	120.0(3)	121.89

So, they are best described as distorted square pyramid and not as trigonal bipyramid. The bond lengths Cu–N_{py} and Cu–N_{azopy} are 2.167(3) and 2.127(2) Å in **1a** and 2.170(2) and 2.126(2) Å in **1b** and these are quite expected for typical Cu–N bonding.[9b] In the contrary, Cu–N_{azoph} distances are significantly longer by 0.04 Å for the reported complexes and lie near 2.46 Å, indicating the natural preference of the Cu(II) centre towards the tetra-coordinated species. As a result, fascinating structural types have been achieved and these can be beneficial in catalysis

because the flexible-dentate nature of the organic scaffolds plays an important role towards the metal-substrate bond-making/breaking processes during catalysis.

Table 3. Selected Experimental and Theoretical Bond Parameters of **1c** complex.

1c		
Parameter	**Expt.**	**Theo.**
Cu1–N1	2.103(3)	2.205
Cu1–N3	1.972(3)	2.025
Cu1–N4	2.374(3)	2.400
Cu1–N6	2.103(3)	2.205
Cu1–N8	1.972(3)	2.025
Cu1–N9	2.374(3)	2.400
N2–N3	1.254(5)	1.256
N4–N5	1.262(5)	1.255
N1Cu1N6	99.93(18)	99.06
N1Cu1N4	148.31(12)	150.16
N1Cu1N9	90.76(12)	87.28
N3Cu1N1	77.05(13)	75.80
N1Cu1N6	97.84(13)	95.78
N3Cu1N8	171.45(18)	171.46
N3Cu1N4	75.16(12)	75.43
N3Cu1N9	111.44(12)	111.06

Single crystals of the $\mathbf{[1c]^{2+}}$ cation were obtained through vapor diffusion of hexane into a dichloromethane solution at ambient temperature. The resulting hexacoordinate complex crystallizes in the C12/c1 space group. Figure 5 presents the ORTEP plot, alongside key metrical parameters. Crystallographic analysis reveals a distorted octahedral geometry for this binary bis-complex. Two bis-azo ligands, oriented nearly perpendicular to each other, coordinate in a tridentate manner. This coordination occurs through the N_{py}, N_{azopy}, and N_{azoph} atoms, resulting in the formation of contiguous five-membered rings. This arrangement leads to the formation of an N6-coordinated copper(II) species. A pair of N_{azopy} atoms are oriented in a trans configuration relative to each other, while the N_{azoph} and N_{py} atoms are arranged in a cis configuration.

V.2.4 Absorption Spectra

The electronic spectra of compounds **1a, 1b** and **1c** were recorded in dichloromethane at room temperature and are presented in Figure 6. The bathochromically shifted structured profiles

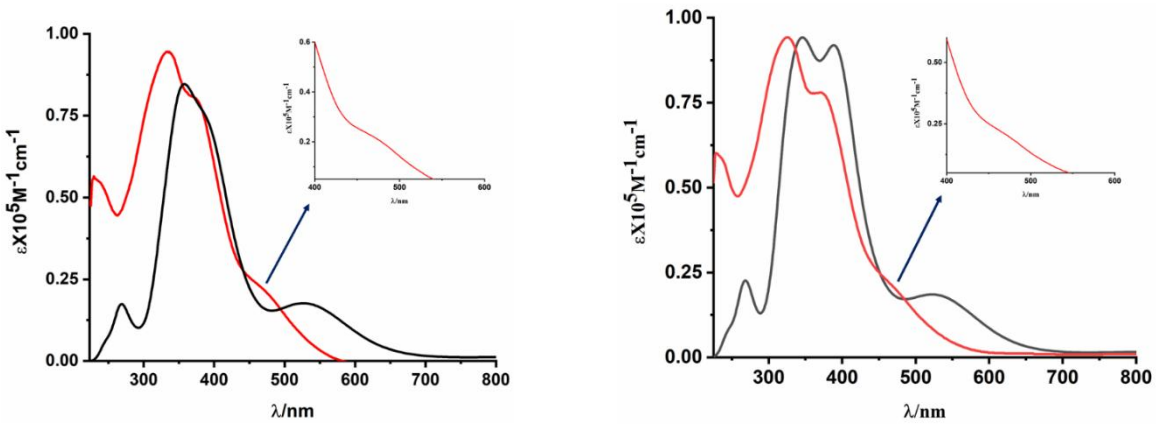

Figure 6. Experimental (red) and theoretical (black) absorption spectrum of **1a** (left) and **1b** (right) complex in CH_2Cl_2 solution at 298 K.

observed for the complexes may be attributed to the increased electronic asymmetry introduced by the electron-accepting bis-azo ligand. Multiple transitions, characteristic of these complexes, are primarily associated with charge-transfer transitions within the tri-coordinated bis-azo ligand. To investigate the origin of the redish-brown coloration, we conducted theoretical studies, which indicate that the lower energy bands are predominantly characterized by intraligand charge-transfer (ILCT) transitions of π to π* type. These transitions result in absorption within the blue-green region of the visible spectrum.[9a]

V.2.5 Electronic Structure and FMOs

The singlet ground state (S_0) and excited state molecular geometries of synthesised complex **1a, 1b** and **1c** were computed by DFT method by employing (R)B3LYP[15] in GAUSSIAN 09[16] programme package. The solution phase optimised geometries of the complexes were found without applying any geometry constraints. In order to verify all stationary points as the true minima in potential energy surface, frequency calculation was executed. The absence of any imaginary frequency (NImag = 0) indicates that all the obtained stationary points are indeed the true minima in potential energy surface. The X-Ray positional coordinates of complex **1a, 1b** and **1c** were directly used as the initial input for geometry optimisation calculation. By using these ground state optimised geometries as well as excited state geometries, we performed subsequent Single Point Energy and TD-DFT[17]calculation. In TD-DFT calculation we employ conductor like continuum model (CPCM)[18] and dichloromethane (CH_2Cl_2) as solvent to simulate absorption spectra in dichloromethane solvent. The lowest 100 singlet-singlet

transitions in absorption and emission processes for the complex **1a, 1b** and **1c** were evaluated gradually. The experimental results and the results obtained from TD calculations were qualitatively comparable. Presently the approach of TD-DFT is documented as a rigorous formalism for the electronic excitation energies among the DFT framework for calculating spectral properties of many transitions metal complexes[19]. In order to acquire the information and nature of absorption and emission processes natural transition orbital (NTO) analysis was executed. This method delivers the most accurate representation of the transition density between the ground and excited states in terms of an expansion into single-particle transitions (hole and electron states for each given excitation). we refer to the unoccupied and occupied NTOs as "electron" and "hole" transition orbitals. The computed vertical transitions were calculated at the equilibrium geometry of the S_0 state and described in terms of one-electron excitations of molecular orbitals of the corresponding S_0 geometry. The calculated transitions with moderate intensities ($f \geq 0.02$) can be envisaged going from the lower to the higher energy region of the spectrum. The zinc atom was described by a double-ζ basis set with the effective core potential of Hay and Wadt (LANL2DZ)[20a], and the 6-311++G(d,p)[20b] basis set was used for the other elements except hydrogen atom (6-31G) present in the complexes to optimize the ground state geometries. The calculated electronic density plots for frontier molecular orbitals were prepared by using the GaussView 6.0 software. GaussSum program, version 3.2[21], was used to calculate the molecular orbital contributions from groups or atoms.

Table 4. Frontier **α**-Molecular Orbital Composition (%) in the Ground State for **1a** complex.

Orbital	MO	Energy (eV)	Composition					
			Cu	Azo1	Azo2	Cl	Py	Ph
116	L+5	-0.89	1	0	2	0	0	97
115	L+4	-0.99	0	0	4	1	9	86
114	L+3	-1.33	1	3	1	0	50	45
113	L+2	-2.01	0	1	0	0	91	7
112	L+1	-3.37	1	7	42	3	4	43
111	LUMO	-4.10	1	39	8	3	23	26
110	HOMO	-6.15	2	0	1	97	0	0
109	H–1	-6.21	3	1	0	95	0	2
108	H–2	-6.37	11	1	3	79	3	3
107	H–3	-6.60	2	1	12	59	1	24
106	H–4	-6.93	8	2	7	80	2	2
105	H–5	-6.99	11	3	6	61	2	17

Table 5. Frontier **β**-Molecular Orbital Composition (%) in the Ground State for **1a** complex.

Orbital	MO	Energy (eV)	Composition					
			Cu	Azo1	Azo2	Cl	Py	Ph
115	L+5	-0.98	0	0	4	1	8	86
114	L+4	-1.33	1	3	1	0	51	43
113	L+3	-2.00	0	1	0	0	91	6
112	L+2	-3.30	3	7	39	4	5	42
111	L+1	-3.97	54	7	12	13	10	3
110	LUMO	-4.07	2	38	9	3	22	27
109	HOMO	-6.12	3	1	1	96	0	0
108	H–1	-6.18	3	1	1	94	0	2
107	H–2	-6.25	15	4	0	78	2	2
106	H–3	-6.57	3	0	8	67	2	20
105	H–4	-6.88	10	0	1	91	0	0
104	H–5	-7.02	5	2	6	36	1	50

V.2.6 Ligand Redox and EPR

The EPR spectrum of [Cu(L^{Cl})Cl_2] **1a** recorded from the solid crystalline sample exhibits three distinct g values, with the higher and lower values typically assigned to g_x and g_z, respectively, as illustrated in Figure 7. The presence of three g values is characteristic of a pentacoordinate geometry around the Cu(II) center, indicative of a structure intermediate between trigonal bipyramidal and square pyramidal geometries.[22] For compound **1a**, the geometry is more closely aligned with the square pyramidal limit, where the three nitrogen atoms from the $\mathbf{L^{Cl}}$ ligand and one labile chloride occupy the equatorial positions, while an additional labile chloride is situated at the axial site.

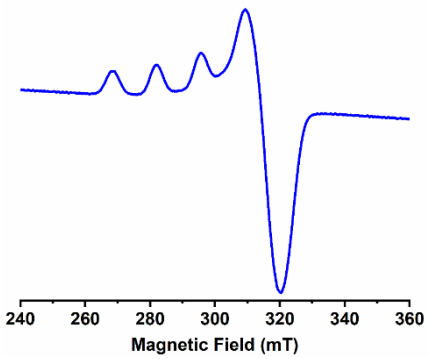

Figure 7. EPR spectrum of [Cu(L^{Cl})Cl_2] **1a**

The electron-transfer property of the complex **1a** was examined using cyclic voltammetry in an acetonitrile solution (0.1 M Bu_4NPF_6) with a platinum working electrode. Complex **1a** exhibited well-defined reductive responses at −0.49 V (ΔEp = 120 mV) and −1.52 V (ΔEp = 130 mV) vs. Ag/AgCl reference couple (Figure 8), indicating its strong electron-accepting

capability. The observed one reversible response at 0.51 V (ΔEp = 110 mV) is likely attributed to the Cu(II)/Cu(I) oxidation couple.

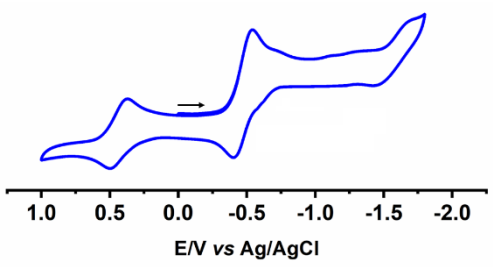

Figure 8. Cyclic voltammogram of **1a** in CH_3CN/0.1 M Bu_4NPF_6 with platinum as working electrode and saturated Ag/AgCl as reference electrode. Scan rate = 100 mV s^{-1}.

V.2.6 Catalytic Activity

Herein, we report the dehydrogenative coupling of secondary alcohols or ketones with 2-amino primary alcohol derivatives, catalyzed by the synthesized stable penta-coordinated Cu(II) complexes. The Cu(II)-based catalyst **1a** demonstrated efficient activity for the dehydrogenative coupling in a one-pot cascade synthesis of quinoline derivatives using 2-aminobenzyl alcohol **6a** as the coupling partner. Traditionally, Friedländer annulation reactions rely on the condensation of 2-aminobenzaldehydes with ketones in either basic or acidic environments.[23] However, these approaches often face challenges due to the limited stability of 2-aminobenzaldehydes, self-condensation, and related side reactions.[24] In this work, an eco-friendly synthesis of quinolines was developed through acceptorless dehydrogenative coupling (ADC), employing catalytic amounts of base and the more stable 2-aminobenzyl alcohol and its derivatives.

The reaction between 2-aminobenzyl alcohol **6a** and acetophenone **3a** was investigated as model substrates to optimize the conditions for mono-dehydrogenative cyclization to produce quinoline derivatives. Subsequently, the potential for double-dehydrogenative cyclization of secondary alcohols with 2-aminobenzyl alcohol was explored. Notably, the reaction using 1-phenylethanol **4a** and **6a** as benchmark substrates successfully yielded quinoline derivatives, as presented in Table 6.

Preliminary experiments were conducted using 1.00 mol% of catalyst **1a** and 100 mol% of KO*t*Bu under open-air conditions at 85 ºC, yielding 92% and 90% of **9aa** under condition **A** and condition **B**, respectively (Table 1, entry 1). The reactions were further optimized by decreasing the catalyst loading to as low as 0.005 mol%, which resulted in an almost unchanged yield of the desired product (Table 1, entries 2–4). However, when the catalyst loading was

Table 6. Optimization of the reaction conditions for the copper catalyzed acceptorless mono- and double-dehydrogenative coupling of 2-aminobenzylalcohol **6a** with acetophenone **3a** and 1-phenylethanol **4a**[a]

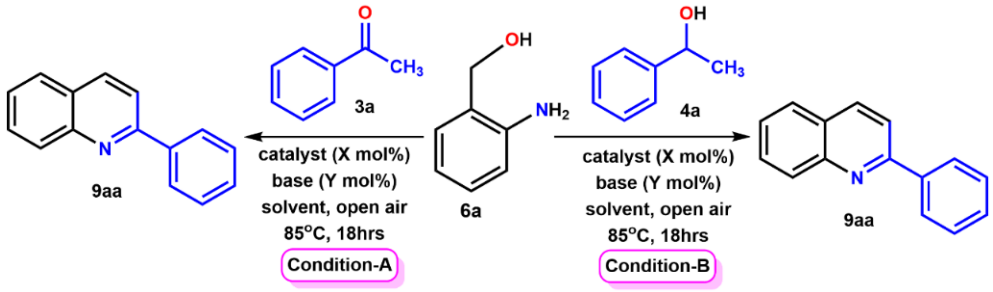

Entry	Catalyst (X mol%)	Solvent	Base (Y mol%)	Temp (°C)	Yield[b,f] (%)	Yield[b,g] (%)
1	**1a** (1.00 mol%)	Toluene	KO^{t}Bu (100)	85	92	90
2	**1a** (0.1 mol%)	Toluene	KO^{t}Bu (100)	85	91	90
3	**1a** (0.01 mol%)	Toluene	KO^{t}Bu (100)	85	92	91
4	**1a** (0.005 mol%)	Toluene	KO^{t}Bu (100)	85	92	87
5	**1a** (0.001 mol%)	Toluene	KO^{t}Bu (100)	85	53	47
6	**1a** (0.005 mol%)	Toluene	KO^{t}Bu (50)	85	92	87
7	**1a (0.005 mol%)**	**Toluene**	**KO^{t}Bu (20)**	**85**	**92**	**60**
8	**1a (0.005 mol%)**	**Toluene**	**KO^{t}Bu (40)**	**85**	**92**	**90**
9	**1a** (0.005 mol%)	Toluene	$NaBH_4$ (20)	85	74	42
10	**1a** (0.005 mol%)	Toluene	NaO^{t}Bu (20)	85	85	57
11	**1a** (0.005 mol%)	Toluene	NaOH (20)	85	90	59
12	**1a** (0.005 mol%)	Toluene	KOH (20)	85	90	57
13	**1a** (0.005 mol%)	Toluene	K_2CO_3 (20)	85	52	19
14	**1a** (0.005 mol%)	Xylene	KO^{t}Bu (20)	85	82	55
15	**1a** (0.005 mol%)	THF	KO^{t}Bu (20)	85	45	23
16	**1a** (0.005 mol%)	EtOH	KO^{t}Bu (20)	85	ND	ND
17[c]	**1a** (0.005 mol%)	Toluene	KO^{t}Bu (20)	RT	NR	ND
18	**1a** (0.005 mol%)	Toluene	KO^{t}Bu (20)	100	90	58
19	$CuCl_2$ + Ligand (1:1)	Toluene	KO^{t}Bu (20)	85	Trace	ND
20	$CuCl_2$ (0.005 & 1 mol%)	Toluene	KO^{t}Bu (20)	85	ND	ND
21	Ligand (1 mol%)	Toluene	KO^{t}Bu (20)	85	ND	ND
22		Toluene	KO^{t}Bu (20)	85	ND	ND
23[d]	**1a** (0.005 mol%)	Toluene	KO^{t}Bu (20)	85	trace	trace
24[e]	**1a** (0.005 mol%)	Toluene	KO^{t}Bu (20)	85	68	37
25	**1a** (0.005 mol%)	Neat	KO^{t}Bu (20)	85	45	trace
26	**1b** (0.005 mol%)	Toluene	KO^{t}Bu (20)	85	87	59
27	**1c** (0.005 mol%)	Toluene	KO^{t}Bu (20)	85	trace	trace

[a]Reaction Conditions: mono-dehydrogenation: condition **A**: 2-Amino benzyl alcohol **6a** (1.00 mmol), acetophenone **3a** (1.00 mmol). Double-dehydrogenation: condition **B**: 2-Amino benzyl alcohol **6a** (1.00 mmol), 1-phenylethanol **4a** (1.00 mmol), Base, 5.0 ml toluene, Reaction time 18 hrs, open air.
[b]Isolated yield after coloumn chromatography.
[c]RT = Room Temperature.
[d]Under an argon atmosphere.
[e]Reaction time 6 hrs, ND = Not Detected.
[f]represents the yield of the mono-dehydrogenative coupling reaction.
[g]represents the yield of the double-dehydrogenative coupling reaction.

reduced to 0.001 mol%, the yield of **9aa** dropped significantly to 53% with condition **A** and 47% with condition **B** (Table 6, entry 5). Hence, it was concluded that the optimum catalyst loading is 0.005 mol%. Upon reducing the base loading to 40 mol%, the yield of the desired products remained largely unaffected (Table 6, entries 5–6, 8). However, a further reduction to 20 mol% severely diminished the product yield (Table 6, entry 7). Among the various trial bases, including NaO*t*Bu, KOH, NaOH, K_2CO_3, $NaBH_4$, and KO*t*Bu, the highest yield of the desired **9aa** was achieved using 30 mol% of KO*t*Bu with 0.005 mol% catalyst (Table 6, entries 9–13). Notably, KO*t*Bu proved to be the most efficient base for this reaction, affording **9aa** in excellent yields. The reaction efficiency was maximized in aprotic solvents such as xylene, toluene, and THF, whereas the yield decreased drastically in protic solvents like ethanol (Table 6, entries 14–16). Additionally, the yield of **9aa** dropped significantly when the temperature was reduced from 85 ºC to room temperature. However, increasing the temperature beyond 85 ºC did not lead to a significant improvement in yield. Notably, the azo-chromophores play a crucial role in the catalytic activity, as no product formation was observed when commercially available $CuCl_2$ was used as the catalyst, even after prolonged reaction times (Table 6, entry 20). Furthermore, the ligand system alone produced no catalytic product, while only trace amounts of **9aa** were obtained when a 1:1 ligand-to-$CuCl_2$ ratio was employed (Table 6, entries 19, 21). No coupling occurred in the absence of copper catalyst **1a** or KO*t*Bu, or when the reaction was conducted under neat conditions (Table 6, entries 22, 24–25). Performing the reaction under an argon atmosphere yielded only trace amounts of the desired product (Table 6, entry 23). Additionally, reducing the reaction time to 6 hrs resulted in a decreased product yield of 68% (Table 6, entry 23). Remarkably, catalyst **1a** exhibited superior activity compared to **1b** and **1c** (Table 6, entry 26–27), likely due to the electron-withdrawing nature of the chlorine substituent (Cl *vs* H), which rendered complex **1a** more electron-deficient.

With the optimal conditions established, the scope of dehydrogenative cyclization between 2-aminobenzyl alcohol **6a** and various ketones was extensively investigated. A wide range of functional groups, including aryl, alkyl, and naphthyl substituents, were well tolerated.

Under the optimized condition **A**, acetophenones bearing both electron-withdrawing and electron-donating groups demonstrated compatibility with **6a** as coupling partners, yielding the desired quinoline derivatives efficiently. Superior yields of the corresponding quinolines were obtained when acetophenones containing electron-donating groups at the *para*-, *meta*-, and *ortho*- positions of the phenyl ring were utilized (Table 7, entries **9ab**–**ae**).

The corresponding quinolines **9ab**, **9ac**, and **9ad** were obtained in 94%, 90%, and 84% isolated yields, respectively, under condition **A** through the reaction of 1-(p-tolyl)ethan-1-one **3b**, 1-(m-tolyl)ethan-1-one **3c**, and 1-(o-tolyl)ethan-1-one **3d** with substrate **6a**. Additionally, acetophenones containing halogen substituents as electron-withdrawing groups afforded the corresponding quinolines in isolated yields ranging from 84% to 86% (Table 7, **9af**–**ag**). However, in the presence of strongly electron-withdrawing nitro substituents, the desired quinoline products were obtained in moderate yield (Table 7, **9ah**). Additionally, naphthyl ketones were examined as coupling partners. For instance, the reaction of 1-(naphthalen-2-

Table 7. Screening of various secondary alcohols and ketones for dehydrogenative coupling reaction with **1a**

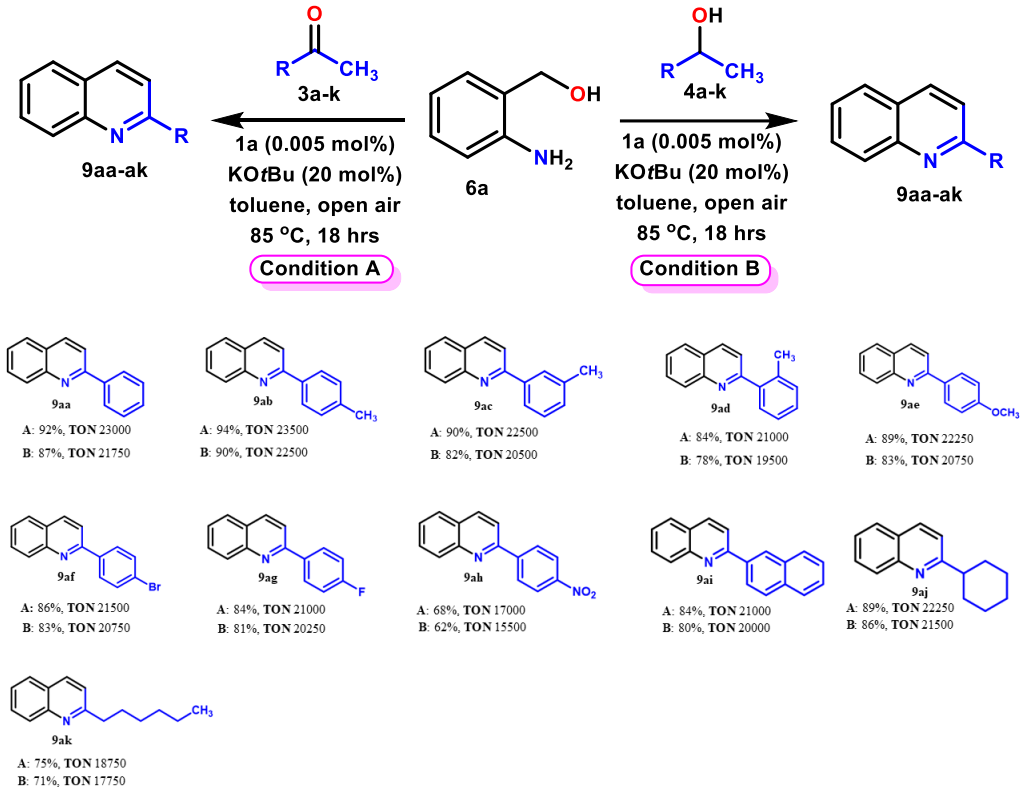

[a]Reaction Conditions: (mono-dehydrogenation reaction: condition **A**): 2-Aminobenzyl alcohol (**6a**) (1.00 mmol); ketone (**3a–k**) (1.00 mmol); base (20 mol%). (double-dehydrogenation reaction: condition **B**): 2-Aminobenzyl alcohol (**6a**) (1.00 mmol); secondary alcohols (**4a–k**) (2.00 mmol); base (40 mol%). [b]Isolated yields after column chromatography. 5.0 mL toluene. open air. [A]represents the yield of the mono-dehydrogenation reaction product i.e. the yield of the products between 2-Aminobenzyl alcohol (**6a**) (1.00 mmol) and ketones (**3a–k**) (1.00 mmol). [B]represents the yield of the double-dehydrogenation reaction product i.e. the yield of the products between 2-Aminobenzyl alcohol (**6a**) (1.00 mmol) and secondary alcohols (**4a–k**) (2.00 mmol).

yl)ethan-1-one **3o** with **6a** afforded quinoline **9ai** in 84% isolated yield. To further investigate the substrate scope, aliphatic ketones were employed as coupling partners. Notably, the corresponding quinolines **9aj** and **9ak** were obtained in 75% and 89% isolated yields, respectively (Table 7). This outcome contrasts significantly with the results reported by Sortais using a rhenium-based catalyst, where aliphatic alcohols failed to produce any quinoline products.[25]

To evaluate the versatility of the copper-catalyzed dehydrogenative cyclization process, the substrate scope of the double dehydrogenative coupling between 2-aminobenzyl alcohols and secondary alcohols was investigated. A range of substituted secondary alcohols **4a–o** was examined under reaction condition **B** using **6a** as the coupling partner (Table 7). The corresponding quinolines were obtained in moderate to high isolated yields when using 1-phenylethanol derivatives bearing electron-donating substituents at the *ortho*-, *meta*-, or *para*-positions of the phenyl ring. Reactions with 1-(p-tolyl)ethanol **4b**, 1-(m-tolyl)ethanol **4c**, and 1-(o-tolyl)ethanol **4d** afforded quinolines **9ab**, **9ac**, and **9ad** in 90%, 82%, and 78% yields, respectively. Secondary alcohols containing electron-withdrawing groups were also compatible, albeit requiring longer reaction times and yielding lower product amounts. Aliphatic alcohols proved to be suitable coupling partners, though they exhibited lower yields and required extended reaction times, likely due to their reduced reactivity in forming the corresponding ketones via acceptorless dehydrogenation.

Table 8. Screening of various secondary alcohols and ketones with 2-amino-5-chloro benzyl alcohol **6b** for dehydrogenative coupling reaction with zinc catalyst **1a**

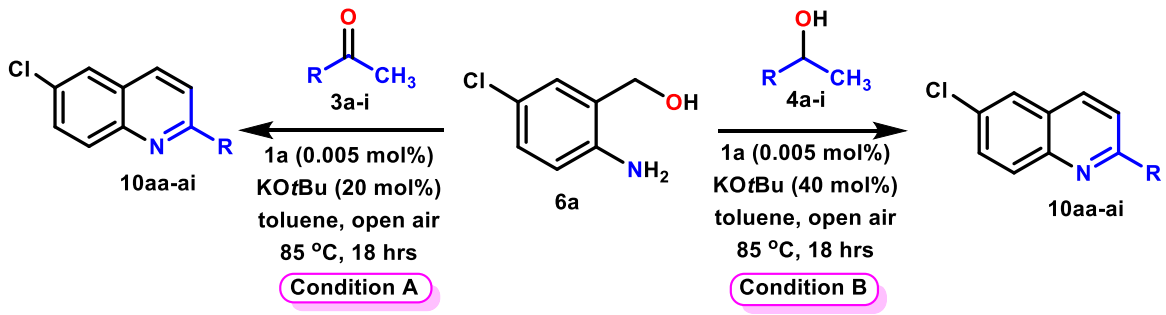

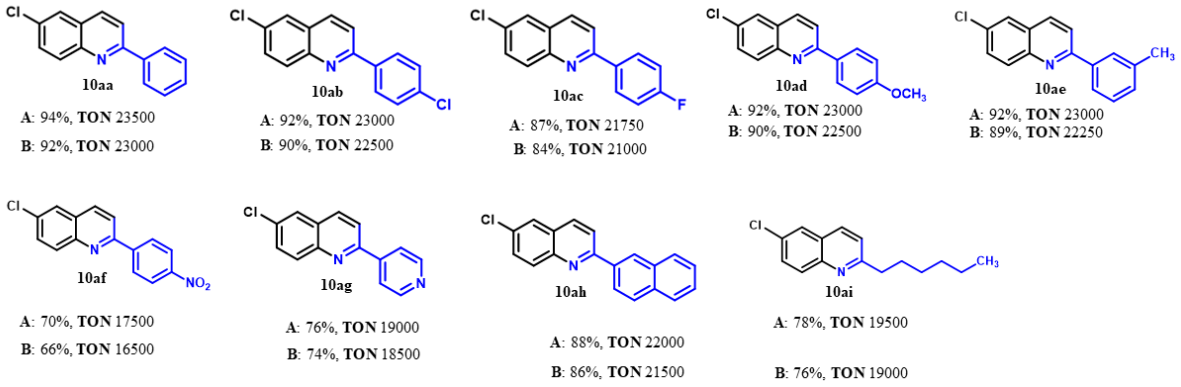

[a]Reaction Conditions: (mono-dehydrogenation reaction: condition **A**): 2-amino-5-chloro benzyl alcohol **6b** (1.00 mmol); ketone **3a–i** (1.00 mmol); base (20 mol%). (double-dehydrogenation reaction: condition **B**): 2-amino-5-chloro benzyl alcohol **6b** (1.00 mmol); secondary alcohols **4a–i** (2.00 mmol); base (40 mol%). [b]Isolated yields after column chromatography. 5.0 mL toluene. open air. [A]represents the yield of the mono-dehydrogenation reaction product i.e. the yield of the products between 2-amino-5-chloro benzyl alcohol **6a** (1.00 mmol) and ketones **3a–i** (1.00 mmol). [B]represents the yield of the double-dehydrogenation reaction product i.e. the yield of the products between 2-amino-5-chloro benzyl alcohol **6b** (1.00 mmol) and secondary alcohols **4a–i** (2.00 mmol).

To broaden the substrate scope, a substituted 2-aminobenzyl alcohol was evaluated as a potential coupling partner with acetophenone **3a** and 1-phenylethanol **4a**. Both electron-donating and electron-withdrawing substituents on **3a** and **4a** were well-tolerated, successfully coupling with 2-amino-5-chlorobenzyl alcohol **6b** to afford the corresponding quinolines in 66–92% isolated yields (Table 8).

Notably, the exclusive formation of quinoline-based derivatives, representing the desired cyclization products, was achieved under the optimized reaction conditions without the formation of self-condensed side products from 2-aminobenzaldehydes. Additionally, only trace amounts of unreacted alcohols or ketones were detected in all cases.

V.2.6 Mechanistic Investigation

A mercury poisoning test was conducted to assess the homogeneity of the catalytic system and evaluate the role of the catalyst. The presence of mercury did not affect either the dehydrogenation of alcohols or the subsequent coupling reactions. After exploring the substrate scope, investigations were directed toward elucidating the plausible mechanism of the Cu-catalyzed dehydrogenation of aromatic primary alcohols to their corresponding aromatic aldehydes.

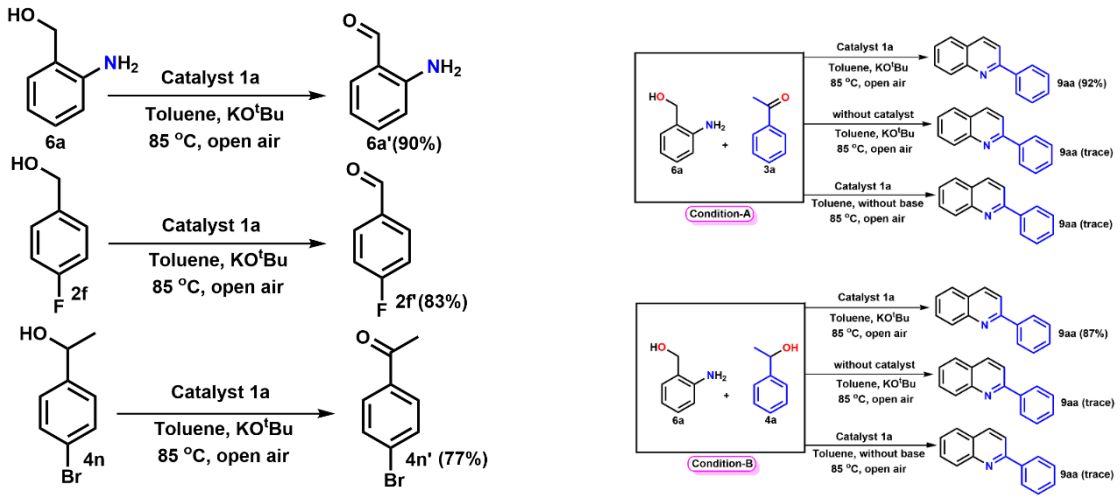

Figure 9. Some control experiments for both C–C and C–N catalytic reactions.

When **6a**, **2f**, and **4n** were subjected to the optimal reaction conditions in the absence of a coupling partner, the corresponding carbonyl compounds **6a'**, **2f'**, and **4n'** were obtained in 90%, 83%, and 77% yields, respectively (Figure 9), suggesting the probable conversion of both primary and secondary alcohols as intermediates. Notably, the reaction of **6a** with a base in the absence of catalyst **1a** yielded only trace amounts of **6a'**. To further elucidate the reaction mechanism, **6a** was reacted with **3a** and **4a** under both reaction conditions **A** and **B**, affording **9aa** in 92% and 87% yields, respectively. The target product **9aa** was not formed in the absence of either catalyst **1a** or base.

These findings demonstrated that alcohol oxidation to carbonyl compounds occurs exclusively in the presence of catalyst **1a** (Figure 9). To investigate the mechanistic pathway—specifically the feasibility of a one-electron hydrogen atom transfer (HAT) *vs* a two-electron hydride transfer (HT) process involving a transient copper hydride intermediate—the dehydrogenation of cyclobutanol (a radical clock substrate) was conducted under optimized conditions using catalyst **1a**. The formation of cyclobutanone as the dehydrogenated product strongly supports the involvement of a two-electron hydride transfer mechanism while excluding the possibility of a HAT pathway involving a ketyl radical intermediate (Scheme 3). The ^{1}H NMR spectrum confirmed the exclusive in situ formation of cyclobutanone as the final product in the presence of catalyst **1a**, further supporting the proposed two-electron hydride transfer mechanism. (Figure 10).[26]

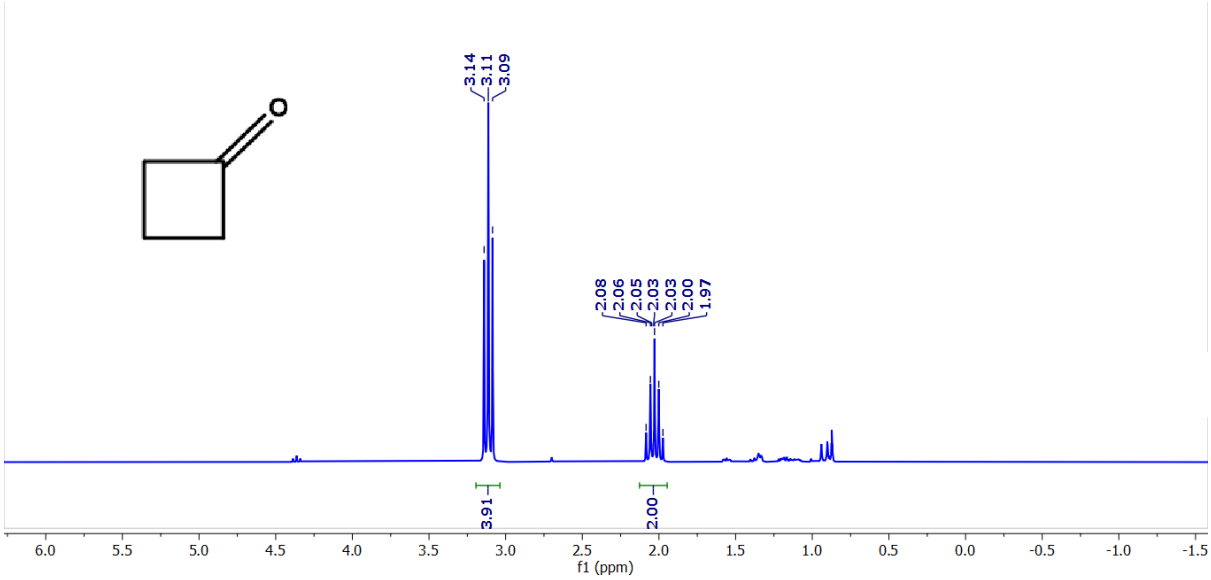

Figure 10. ^{1}H NMR spectrum of cyclobutanone (300 MHz, $CDCl_3$).

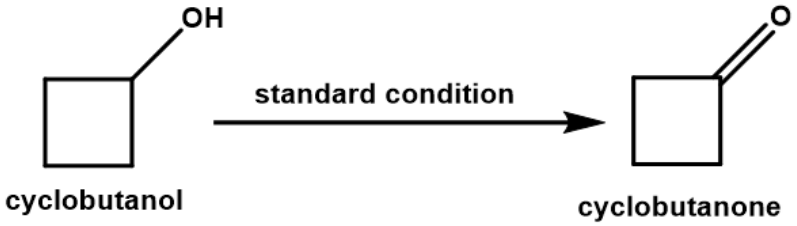

Scheme 3. Investigation of active participation of non-radical intermediate during catalytic transformation Dehydrogenation of cyclobutanol with catalyst **1a**

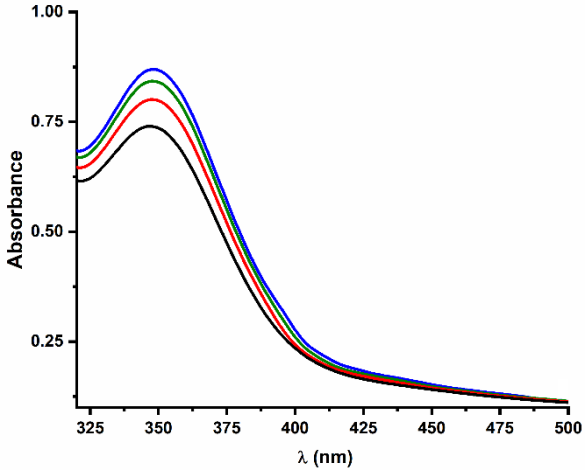

Figure 11. Electronic spectra of the formation of I_3^- ion in presence of H_2O_2 (detection of H_2O_2 was achieved as described in the experimental section).

Following the control experiments, a plausible catalytic cycle for the reaction mechanism is proposed, as illustrated in Scheme 3. These studies suggest the formation of α,β-unsaturated

ketones as intermediates through classical aldol condensation and subsequent dehydration to afford the corresponding quinoline derivatives, via the well-known borrowing-hydrogen (BH) mechanism.

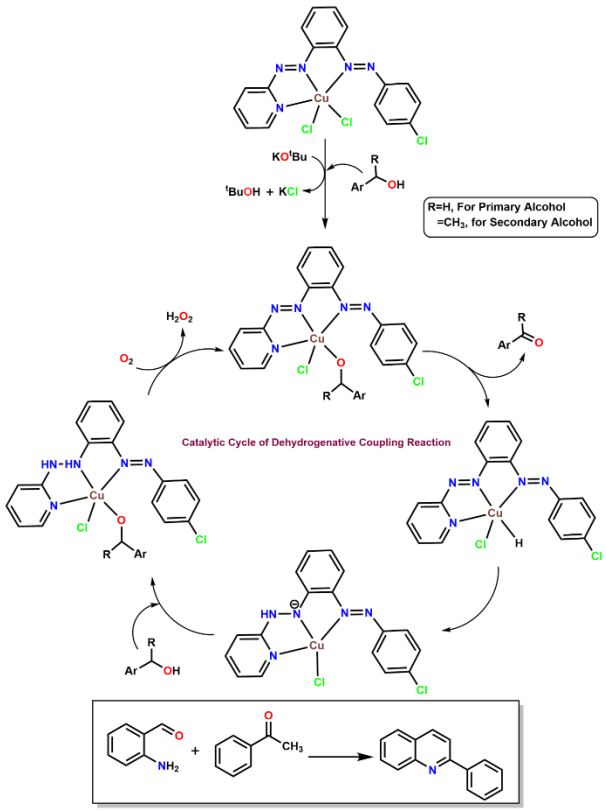

Scheme 4. Proposed reaction mechanism for Cu(II)-mediated catalytic reaction.

V.3 Conclusions

In summary, we have developed a straightforward, scalable, and sustainable dehydrogenative cross-coupling strategy utilizing a novel electron-deficient and robust N^N^N-pincer copper catalyst. The highly electron-deficient bisazo-pyridine framework likely enhances the overall catalytic cycle by promoting the initial nucleophilic coordination of alcohols during catalysis. This neutral, coordinatively unsaturated square-pyramidal [Cu^{II}(N^N^N)Cl_2] catalyst demonstrates excellent stability and in-situ recyclability, as evidenced by its remarkably high turnover numbers (up to 23,000 with a 0.005 mol% catalyst loading) and low base requirement (20 mol% KO*t*Bu) under homogeneous aerobic conditions. The C–N Friedländer annulation to quinoline derivatives proceeds *via* HT under open-air homogeneous reaction conditions in the presence of catalytic amounts (~20 mol%) of KO*t*Bu as a base. The production of quinoline derivatives is achieved through acceptorless dehydrogenative coupling followed by N-annulation in a one-pot process. Notably, the desired catalytic products are obtained without detectable self-condensed side products, and the reaction byproducts are inherently benign.

Lower metal catalyst and base loadings pose a challenge but are essential for green and sustainable chemistry, as they minimize the release of hazardous metal waste and toxic byproducts into the environment. A non-radical pathway involving a hydride transfer mechanism is proposed for the Cu(II)-mediated alcohol dehydrogenation reaction, supported by control studies. This advanced approach exhibits broad substrate tolerance, accommodating aliphatic, aromatic, and heteroaromatic alcohols to generate a diverse range of C–C and C–N cross-coupled products under mild conditions, achieving the highest TON reported to date among homogeneous copper catalysts.

V.4 Experimental Section

V.4.1 General Information

Except where stated otherwise, all manipulations were performed under an argon atmosphere. Solvents were dried using conventional techniques and subsequently distilled under argon before use. copper chloride dihydrate, benzyl alcohol and its derivatives, as well as ketones/secondary alcohols and its derivatives, were purchased from Sigma-Aldrich, BLD. Additional chemicals and solvents were obtained from Merck India, Ranchem Private Limited, TCI Chemicals (India) Pvt. Ltd., and Alfa Aesar, and were dried using standard methods before use. FT-IR spectra were recorded on a Perkin-Elmer L1600300 spectrometer. NMR spectra (^{1}H, ^{13}C, and ^{19}F) were measured using Bruker FT 300 and 400 MHz spectrometers, with TMS as the internal reference. Electronic spectra were obtained using a Perkin-Elmer LAMBDA 25 spectrophotometer in dichloromethane solutions at a solute concentration of approximately 10^{-5} M.

V.4.2 Synthesis

Synthesis of ligands

The organic ligands L^{Cl} and L^{H} comprising two electron-deficient azo moieties along with an aromatic heterocyclic group have been prepared by condensation of (*E*)-2-((4-chlorophenyl)azo)aniline or (*E*)-2-(phenylazo)aniline with 2-nitrosopyridine using the previously reported procedure.[14]

Synthesis of complexes

[Cu(L^{Cl})Cl_2] 1a $CuCl_2.2H_2O$ (170 mg, 1.00 mmol) was added to a solution of (L^{Cl}) (354 mg, 1.10 mmol) in ethanol (25 mL) under open air. The reaction mixture was stirred at room temperature for 4 hrs. The solvent was removed under reduced pressure. Slow diffusion of the dichloromethane solution of the complex into n-hexane led to the crystallisation of **1a** as block-

shaped crystals. Yield and characterization data: Brownish-red crystal, Yield 82% (356 mg). Anal. Calcd. for $C_{17}H_{12}N_5Cl_3Cu$: C 44.76, H 2.65, N 15.35; Found C 44.88, H 2.67, N 15.17%. FT-IR (cm^{-1}): 1452, 1392 ($\nu_{N=N}$). HRMS (ESI) m/z Calcd. for $C_{17}H_{12}N_5Cl_2Cu$ $[M - Cl]^+$ 418.9766, found 418.9716.

$[Cu(L^H)Cl_2]$ 1b The former procedure has been applied with same stoichiometrically amount to synthesised complex **1b**. Yield and characterization data: Brownish-red crystal, Yield 79% (318 mg). Anal. Calcd. for $C_{17}H_{13}N_5Cl_2Cu$: C 48.53, H 2.87, N 16.64; Found C 48.61, H 2.84, N 16.56%. FT-IR (cm^{-1}): 1448, 1391 ($\nu_{N=N}$). HRMS (ESI) m/z Calcd. for $C_{17}H_{12}N_5ClCu$ $[M - Cl]^+$ 384.0077, found 384.0045.

$[Cu(L^H)_2]$ 1c $Cu(OAC)_2.H_2O$ (200 mg, 1.00 mmol) was added to a solution of (L^H) (316 mg, 1.10 mmol) in ethanol (25 mL) under open air. The reaction mixture was stirred at room temperature for 4 hrs. The solvent was removed under reduced pressure. Subsequent brown solution was evaporated to dryness. The crude product was subjected to column chromatography. Complex **1c** was appeared as a brownish-red band when eluted with an acetonitrile/NH_4PF_6 mixture. Slow diffusion of the dichloromethane solution of the complex into n-hexane led to the crystallisation of **1c** as block-shaped crystals. Yield and characterization data: Brownish-red crystal, Yield 78% (510 mg). Anal. Calcd. for $C_{34}H_{24}N_{10}CuP_2F_{12}$: C 44.10, H 2.61, N 15.12; Found C 44.35, H 2.58, N 15.18%. FT-IR (cm^{-1}): 1456, 1389 ($\nu_{N=N}$). HRMS (ESI) m/z Calcd. for $C_{34}H_{24}N_{10}Cu$ $[M/2]^+$, 462.5382 found 462.5421.

General procedure for Friedländer quinoline synthesis

Catalyst 1a (0.005 mol%), KO*t*Bu (20 mol%), secondary alcohols/ketones (1.0 mmol), and 2-aminobenzyl alcohol derivatives (1.0 mmol) were added to a 50.0 mL round-bottom flask under ambient conditions. The reaction mixture was then placed in an oil bath preheated to 85 °C, followed by the addition of 5.0 mL of toluene. The reaction proceeded for 8 hours. After completion, the mixture was concentrated under vacuum and purified by column chromatography using silica gel (60–120 mesh) with a hexane/ethyl acetate eluent to obtain the desired product.

Detection of hydrogen peroxide in the catalytic reaction

The production of H_2O_2 as a byproduct during the catalytic process was monitored spectrophotometrically by detecting the characteristic absorption band of I_3^- (λ_{max} = 350 nm) upon reaction with KI.[27] Following our developed procedure, catalyst **1a** (0.005 mmol) and KO*t*Bu (20 mol%) were added to a round-bottom flask containing benzyl alcohol (1.00 mmol)

in 5 mL of dry toluene. After 2 hrs of reaction, the mixture was extracted using dichloromethane, and an equal volume of water was added. To prevent further oxidation, the aqueous layer was acidified with H_2SO_4 to pH 2, followed by the addition of 1 mL of a 10% KI solution and three drops of a 3% ammonium molybdate solution. The presence of hydrogen peroxide initiates the reaction: $H_2O_2 + 2I^- + 2H^+ \rightarrow 2H_2O + I_2$. Subsequently, in the presence of excess iodide ions, the following reaction occurs: I_2 (aq) + $I^- \rightarrow I_3^-$. Adding ammonium molybdate accelerates the reaction, which initially proceeds slowly but increases in rate as the acid concentration rises.

V.5 Characterization data of Cu catalyzed compounds:

All the reactions were carried out in 1.0 mmol scale of reactant and according to the general procedure for synthesis of quinoline derivatives.

2-phenyl quinoline (**9aa**): Eluent: Hexane/Ethyl acetate (20:1). white solid (yield = 92%, 189mg). ^{1}H NMR (300 MHz, $CDCl_3$): δ (ppm) 8.26-8.18 (m,4H), 7.92-7.84 (m, 2H), 7.78-7.73 (m,1H), 7.59-7.47 (m,4H). ^{13}C NMR (75 MHz, $CDCl_3$): δ (ppm) 157.4, 148.3, 139.7, 136.8, 129.8, 129.7, 129.4, 128.9, 127.6, 127.5, 127.2, 126.3, 119.1.

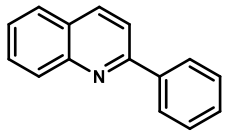

2-(p-tolyl)quinoline (9ab): Eluent: Hexane/Ethyl acetate (20:1). white solid (yield = 94%, 207mg). ^{1}H NMR (300 MHz, $CDCl_3$): δ (ppm) 8.21 (d, *J* = 8.5 Hz, 2H), 8.11 (d, *J* = 8.2 Hz, 2H), 7.89-7.82 (m,2H), 7.78-7.72 (m,1H), 7.57-7.51(m, 1H), 7.37(d, *J* = 7.8 Hz, 2H), 2.47 (s, 3H). ^{13}C NMR (75 MHz, $CDCl_3$): δ (ppm) 157.4, 148.3, 139.4, 136.8 (d, *J* = 16.6 Hz), 129.6 (d, *J* = 5.7 Hz), 129.3, 128.5, 127.5, 127.1, 126.1, 118.9, 21.4.

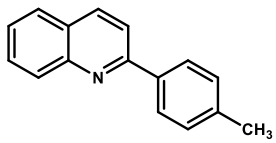

2-(m-tolyl)quinoline (**9ac**): Eluent: Hexane/Ethyl acetate (20:1). Yellowish Liquid (yield = 90%, 197mg). 1H NMR (300 MHz, $CDCl_3$): δ (ppm) 8.25-8.20 (m, 2H), 7.95 (d, *J* = 7.7 Hz, 1H), 7.85 (d, *J* = 6.6 Hz, 1H), 7.80-7.73 (m, 2H), 7.55 (t, *J* = 6.9 Hz, 1H), 7.47-7.37(m, 2H), 7.31 (d, *J* = 6.7 Hz, 1H), 2.51 (s, 3H). ^{13}C NMR (75 MHz, $CDCl_3$): δ (ppm) 157.6, 148.3, 138.5, 136.7, 133.8, 130.1, 129.7, 129.6, 128.7, 128.4, 128.3, 127.4, 126.2, 124.7, 119.1, 21.6.

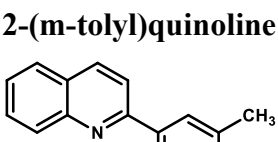

2-(o-tolyl)quinoline (9ad): Eluent: Hexane/Ethyl acetate (20:1). white solid (yield = 84%, 185mg). ^{1}H NMR (300 MHz, $CDCl_3$): δ (ppm) 8.22 (dd, J = 15.9, 8.5 Hz, 2H), 7.89 (dd, *J* = 8.2, 1.5 Hz, 1H), 7.77 (m,1H), 7.62-7.51 (m,3H), 7.40-7.31 (m, 3H), 2.44 (s, 3H). ^{13}C NMR (75 MHz, $CDCl_3$): δ (ppm) 160.3, 147.9, 140.8, 136.1, 136.0, 130.9, 129.7, 129.6, 128.5, 127.5, 126.8, 126.4, 126.0, 122.4, 20.4.

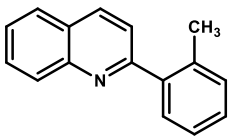

2-(4-methoxyphenyl)quinoline (9ae): Eluent: Hexane/Ethyl acetate (20:1). pastel orange solid (yield = 89%, 209mg). ^{1}H NMR (300 MHz, $CDCl_3$): δ (ppm) 8.22-8.15 (m, 4H), 7.88-7.82 (m, 2H), 7.73 (t, *J* = 6.9 Hz, 1H), 7.52 (t, *J* = 7.5 Hz, 1H),7.08 (d, *J* = 8.9 Hz, 2H), 3.92 (s, 3H). ^{13}C NMR (75 MHz, $CDCl_3$): δ (ppm) 160.8, 157.0, 148.3, 136.7, 132.3, 129.6, 129.5, 128.9, 127.4, 126.9, 125.9, 118.6, 114.2, 55.4.

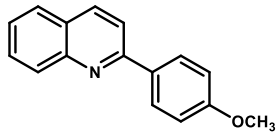

2-(4-bromophenyl)quinoline (9af): Eluent: Hexane/Ethyl acetate (20:1). fawn solid (yield = 86%, 245mg). ^{1}H NMR (300 MHz, $CDCl_3$): δ (ppm) 8.26 (d, *J* = 7.8 Hz, 1H), 8.18 (dd, *J* = 8.5, 1.0 Hz, 1H), 8.08 (d, *J* = 8.6 Hz,2H), 7.87 (d, *J* = 8.6 Hz,2H), 7.79-7.74(m, 1H), 7.68(d, *J* = 8.6 Hz, 2H), 7.57 (t, *J* = 6.9 Hz,1H). ^{13}C NMR (75 MHz, $CDCl_3$): δ (ppm) 156.1, 148.3, 138.5, 137.0, 132.0, 131.4, 129.9, 129.7, 129.1, 127.5, 127.3, 126.6, 123.9, 118.5.

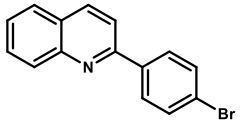

2-(4-fluorophenyl)quinoline (9ag): Eluent: Hexane/Ethyl acetate (20:1). white solid (yield = 84%, 188mg). ^{1}H NMR (300 MHz, $CDCl_3$): δ (ppm) 8.26-8.16 (m, 4H), 7.86 (d, *J* = 8.6 Hz, 2H), 7.76 (t, *J* = 6.9 Hz, 1H), 7.56 (t, *J* = 7.5 Hz, 1H), 7.27-7.21(m, 2H). ^{13}C-NMR (75 MHz, $CDCl_3$): δ (ppm) 165.5, 162.2, 156.3, 148.2, 136.9, 135.9, 129.8, 129.5, 129.4, 127.5, 126.4, 118.7, 115.9, 115.7. ^{19}F NMR (282 MHz, CDCl3): δ = -117.3 (s, 1F)

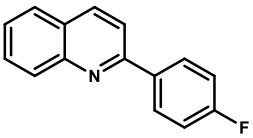

2-(4-nitrophenyl)quinoline (9ah): Eluent: Hexane/Ethyl acetate (20:1). beige solid (yield = 81%, 203mg). ^{1}H NMR (300 MHz, $CDCl_3$): δ (ppm) 8.43-8.36 (m, 4H), 8.35-8.32 (m, 1H), 8.24-8.20 (m, 1H), 7.96 (d, *J* = 8.6 Hz, 1H), 7.92-7.89 (m, 1H), 7.84-7.78 (m, 1H), 7.65-7.60 (m, 1H). ^{13}C NMR (75 MHz, $CDCl_3$): δ (ppm) 157.6, 148.4, 148.3, 145.5, 137.4, 130.3, 130.0, 128.4, 128.2, 127.6, 127.3, 124.1, 118.8.

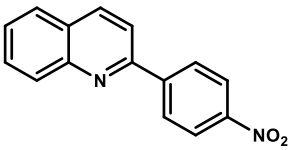

2-(naphthalen-2-yl)quinoline (9ai): Eluent: Hexane/Ethyl acetate (20:1). white solid (yield = 84%, 213mg). ^{1}H NMR (300 MHz, $CDCl_3$): δ (ppm) 8.65 (s, 1H), 8.41 (dd, *J* = 8.6, 1.8 Hz, 1H), 8.27 (dd, *J* = 8.5, 4.6 Hz, 2H), 8.07 – 8.02 (m, 3H), 7.94 – 7.92 (m, 1H), 7.87 (d, *J* = 6.7, Hz, 1H), 7.80 – 7.76 (m, 1H), 7.59 – 7.54 (m, 3H). ^{13}C NMR (75 MHz, $CDCl_3$): δ (ppm) 157.2, 148.4, 137.0, 136.8, 133.9, 133.5, 129.8, 129.7, 128.8, 128.6, 128.3, 127.7. 127.5, 127.3, 127.2, 126.7, 126.4, 125.1, 119.2.

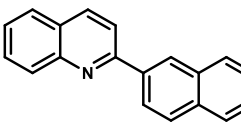

2-cyclohexylquinoline (9aj): Eluent: Hexane/Ethyl acetate (20:1). yellowish oil (yield = 89%, 188mg). ^{1}H NMR (300 MHz, $CDCl_3$): δ (ppm) 8.11 (d, *J* = 3.0 Hz, 1H), 8.08 (d, *J* = 3.4 Hz, 1H), 7.79 (dd, *J* = 8.1, 1.5 Hz, 1H), 7.70 (ddd, *J* = 8.5, 6.9, 1.5 Hz, 1H), 7.50 (ddd, *J* = 8.1, 6.9, 1.2 Hz, 1H), 7.36 (d, *J* = 8.6 Hz,

1H), 2.99-2.93 (m, 1H), 2.09-2.03 (m, 3H), 1.95-1.90 (m, 2H), 1.69-1.48 (m, 5H). ^{13}C NMR (75 MHz, $CDCl_3$): δ (ppm) 166.8, 147.9, 136.2, 129.2, 129.0, 128.2, 127.4, 125.6, 119.6, 47.62, 32.8, 28.5, 26.6, 26.2, 25.7.

2-hexylquinoline (9ak): Eluent: Hexane/Ethyl acetate (20:1). colorless oil (yield = 85%, 182mg). ^{1}H NMR (300 MHz, $CDCl_3$): δ (ppm) 8.06 (t, *J* = 8.1 Hz, 2H), 7.76 (dd, *J* = 8.1, 1.5 Hz, 1H), 7.68 (ddd, *J* = 8.5, 6.8, 1.5 Hz, 1H)), 7.47 (ddd, *J* = 8.1, 6.8, 1.2 Hz, 1H), 7.29 (d, *J* = 8.5 Hz, 1H), 3.00 – 2.95 (m, 2H), 1.87 – 1.77 (m, 2H), 1.37-1.27 (m, 6H), 0.93-0.87 (m, 3H). ^{13}C NMR (75 MHz, $CDCl_3$): δ (ppm) 163.1, 147.9, 136.1, 129.3, 128.8, 127.5, 126.7, 125.6, 121.3, 39.3, 31.7, 30.0, 29.2, 22.6, 14.1.

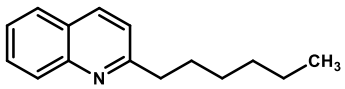

6-chloro-2-phenylquinoline (10aa): Eluent: Hexane/Ethyl acetate (20:1). white solid (yield = 94%, 225mg). ^{1}H NMR (300 MHz, $CDCl_3$): δ (ppm) 8.19-8.12(m, 4H), 7.92 (d, *J* = 8.7 Hz, 1H), 7.83 (d, *J* = 2.3 Hz, 1H), 7.68 (dd, *J* = 9.0, 2.3 Hz, 1H), 7.59-7.47 (m, 3H). ^{13}C NMR (75 MHz, $CDCl_3$): δ (ppm) 157.6, 146.7, 139.2, 135.9, 131.9, 131.3, 130.6, 129.6, 128.9, 127.7, 127.5, 126.2, 119.8.

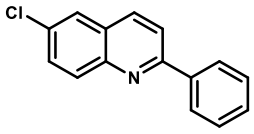

6-chloro-2-(4-chlorophenyl)quinoline (10ab): Eluent: Hexane/Ethyl acetate (20:1). white solid (yield = 92%, 252mg). ^{1}H NMR (300 MHz, $CDCl_3$): δ (ppm) 8.17-8.09 (m, 4H), 7.89-7.83 (m, 2H), 7.69 (dd, *J* = 9.0, 2.3 Hz, 1H), 7.54-7.50 (m, 2H). ^{13}C NMR (75 MHz, $CDCl_3$): δ (ppm) 156.2, 146.6, 137.6, 136.1, 135.8, 132.2, 131.3, 130.8, 129.1, 128.8, 127.8, 126.2, 119.4.

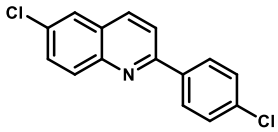

6-chloro-2-(4-fluorophenyl)quinoline (10ac): Eluent: Hexane/Ethyl acetate (20:1). white solid (yield = 87%, 224mg). ^{1}H NMR (300 MHz, $CDCl_3$): δ (ppm) 8.20-8.08 (m, 4H), 7.88-7.82 (m, 2H), 7.68 (dd, *J* = 9.0, 2.4 Hz, 1H), 7.26-7.20 (m, 2H). ^{13}C NMR (75 MHz, $CDCl_3$): δ (ppm) 165.6, 162.3, 156.4, 146.6, 135.9, 132.0, 131.2, 130.7, 129.5, 129.3, 127.6, 126.2, 119.4, 116.0, 115.7. ^{19}F NMR (282 MHz, $CDCl_3$): δ = -111.9 (s, 1F). MS (ESI+): $C_{15}H_{10}ClFN$ ([M+H]+); calculated: 258.04, found: 258.06.

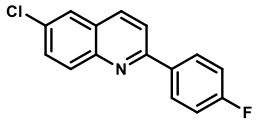

6-chloro-2-(4-methoxyphenyl)quinoline (10ad): Eluent: Hexane/Ethyl acetate (20:1). white solid (yield = 92%, 245mg). ^{1}H NMR (300 MHz, $CDCl_3$): δ (ppm) 8.17-8.07 (m, 4H), 7.87 (d, *J* = 8.7 Hz, 1H), 7.80 (d, *J* = 2.3 Hz, 1H), 7.66 (dd, *J* = 9.0, 2.4 Hz, 1H), 7.07 (d, *J* = 8.9 Hz, 2H), 3.91 (s, 1H). ^{13}C NMR (75 MHz, $CDCl_3$): δ (ppm) 161.0, 157.1, 146.7, 135.7, 131.8, 131.5, 131.1, 130.5,

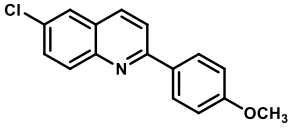

128.9, 127.5, 126.1, 119.4, 114.3, 55.4. MS (ESI+): $C_{16}H_{13}ClNO$ ([M+H]+); calculated: 270.06, found: 270.07.

6-chloro-2-(m-tolyl)quinoline (10ae): Eluent: Hexane/Ethyl acetate (20:1). white solid (yield = 92%, 233mg). 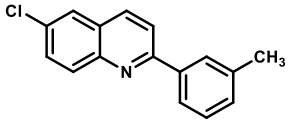 ^{1}H NMR (300 MHz, $CDCl_3$): δ (ppm) 8.12-8.06 (m, 4H), 7.88 (d, *J* = 8.7 Hz, 1H), 7.80 (d, *J* = 2.4 Hz, 1H), 7.66 (dd, *J* = 9.0, 2.4 Hz, 1H), 7.38-7.34 (m, 2H), 2.46 (s, 3H).^{13}C NMR (75 MHz, $CDCl_3$): δ (ppm) 157.5, 146.7 139.7, 136.4, 135.7, 131.7, 131.3, 130.5, 129.7, 129.3, 128.5, 127.6, 127.4, 126.1, 119.7, 21.4. MS (ESI+): $C_{16}H_{13}ClN$ ([M+H]+); calculated: 254.07, found: 254.09.

6-chloro-2-(4-nitrophenyl)quinoline (10af): Eluent: Hexane/Ethyl acetate (20:1). white solid (yield = 70%, 198mg). 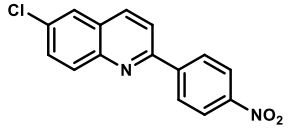 ^{1}H NMR (300 MHz, $CDCl_3$): δ (ppm) 8.23 (d, *J* = 8.7 Hz, 2H), 7.96 (d, *J* = 8.6 Hz, 2H), 7.86 (d, *J* = 2.3 Hz, 2H), 7.74 (d, *J* = 2.3 Hz, 1H), 7.45 (d, *J* = 2.5 Hz, 1H), 6.63 (d, *J* = 8.8 Hz, 1H). ^{13}C NMR (75 MHz, $CDCl_3$): δ (ppm) 154.7, 148.5, 146.4, 144.7, 136.6, 133.2, 131.4, 129.3, 128.4, 128.1, 126.3, 124.1, 119.7. MS (ESI+): $C_{15}H_9ClN_2O_2$ ([M]+); calculated: 284.03, found: 284.06.

6-chloro-2-(pyridin-4-yl)quinoline (10ag): Eluent: Hexane/Ethyl acetate (20:1). white solid (yield = 76%, 182mg). 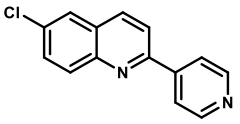 ^{1}H NMR (300 MHz, $CDCl_3$): δ (ppm) 8.73 (d, J = 5.1 Hz, 2H), 8.24 – 8.06 (m, 2H), 8.01 – 7.99 (m, 2H), 7.84 (dd, *J* = 8.7, 3.0 Hz, 1H), 7.78 – 7.72 (m, 1H), 7.67 – 7.63 (m, 1H). ^{13}C NMR (75 MHz, $CDCl_3$): δ (ppm) 154.5, 150.4, 146.6, 137.3, 136.3, 132.9, 131.5, 131.0, 130.1, 129.9. 128.3, 127.6, 126.2, 121.5, 119.2. MS (ESI+): $C_{14}H_9ClN_2$ ([M]+); calculated: 240.04, found: 240.07.

6-chloro-2-(naphthalen-2-yl)quinoline (10ah): Eluent: Hexane/Ethyl acetate (20:1). white solid (yield = 88%, 253mg). 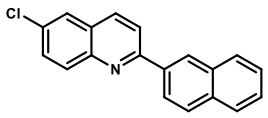 ^{1}H NMR (300 MHz, $CDCl_3$): δ (ppm) 8.61 (s, 1H), 8.37 (dd, *J* = 8.6, 1.8 Hz, 1H), 8.16 (dd, *J* = 8.8, 4.1 Hz, 2H), 8.06 – 7.98 (m, 3H), 7.95 – 7.89 (m, 1H), 7.83 (d, *J* = 2.4 Hz, 1H), 7.70 (dd, *J* = 9.0, 2.4 Hz, 1H), 7.59 – 7.54 (m, 2H). ^{13}C NMR (75 MHz, $CDCl_3$): δ (ppm) 157.4, 149.8, 136.5, 135.9, 133.9, 133.5, 131.9, 131.3, 130.7, 128.9, 128.7, 127.8. 127.2, 126.9, 126.5, 126.2, 124.9, 119.9. MS (ESI+): $C_{19}H_{12}ClN$ ([M]+); calculated: 289.06, found: 289.08.

6-chloro-2-hexylquinoline (10ai): Eluent: Hexane/Ethyl acetate (20:1). colorless oil (yield = 78%, 193mg). 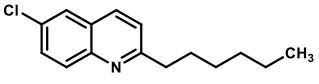 ^{1}H NMR (300 MHz, $CDCl_3$): δ (ppm) 8.00-7.92 (m, 2H), 7.77-7.71 (m, 1H), 7.64-7.53 (m, 1H), 7.34-7.28 (m, 1H), 2.97 (dd, *J* = 8.6, 7.2 Hz, 2H), 1.86-1.76 (m, 2H), 1.46-1.40 (m, 5H), 0.97-0.87 (m, 4H). ^{13}C NMR (75 MHz, $CDCl_3$): δ (ppm) 163.5, 146.2, 135.3, 131.2, 130.4, 130.2, 127.3, 126.1, 122.3, 39.3,

31.7, 29.9, 29.2, 22.6, 14.1. MS (ESI+): $C_{15}H_{19}ClN$ ([M+H]+); calculated: 248.120, found: 248.125.

V.6 NMR spectra of selected compounds

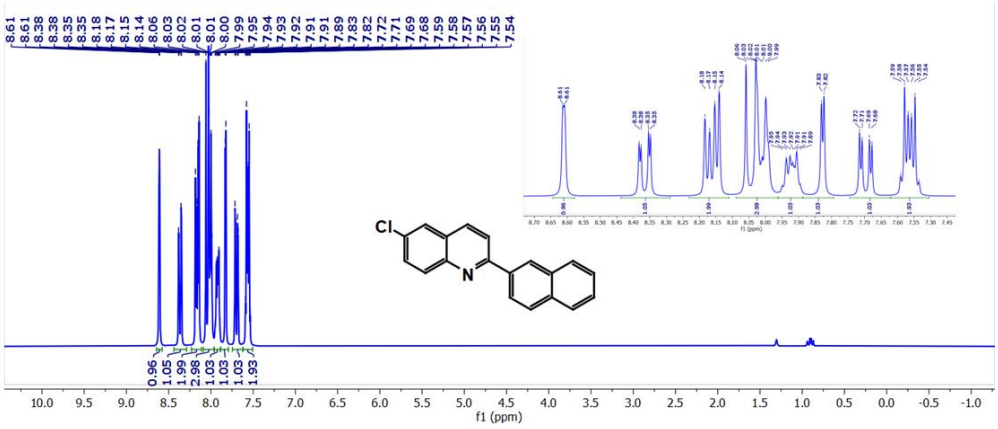

Figure 12. ^{1}H NMR spectrum of compound **10ah** (300 MHz, $CDCl_3$).

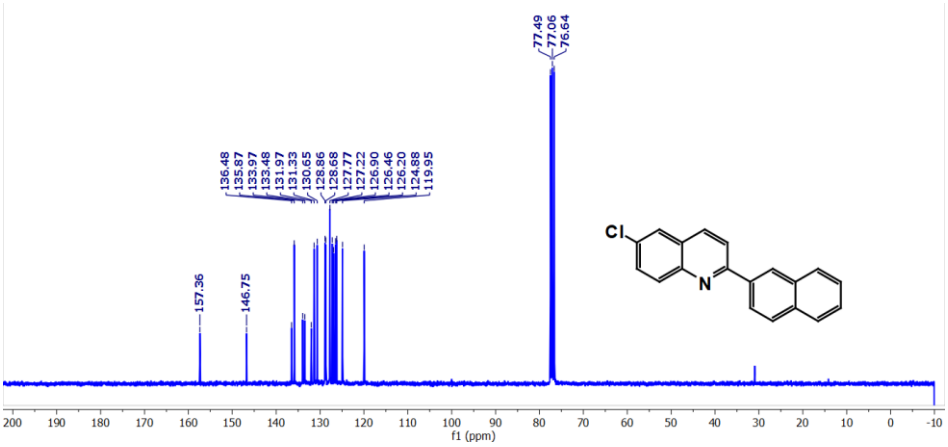

Figure 13. ^{13}C NMR spectrum of compound **10ah** (75 MHz, $CDCl_3$).

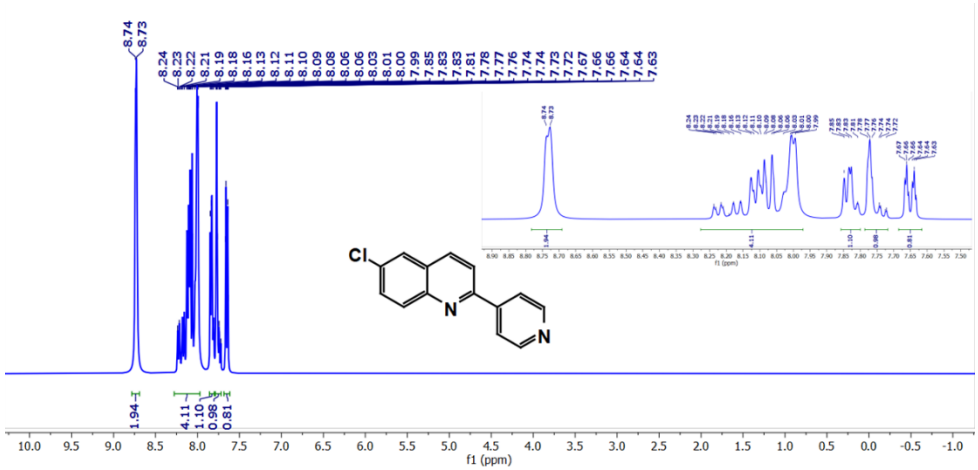

Figure 14. ^{1}H NMR spectrum of compound **10ag** (300 MHz, $CDCl_3$).

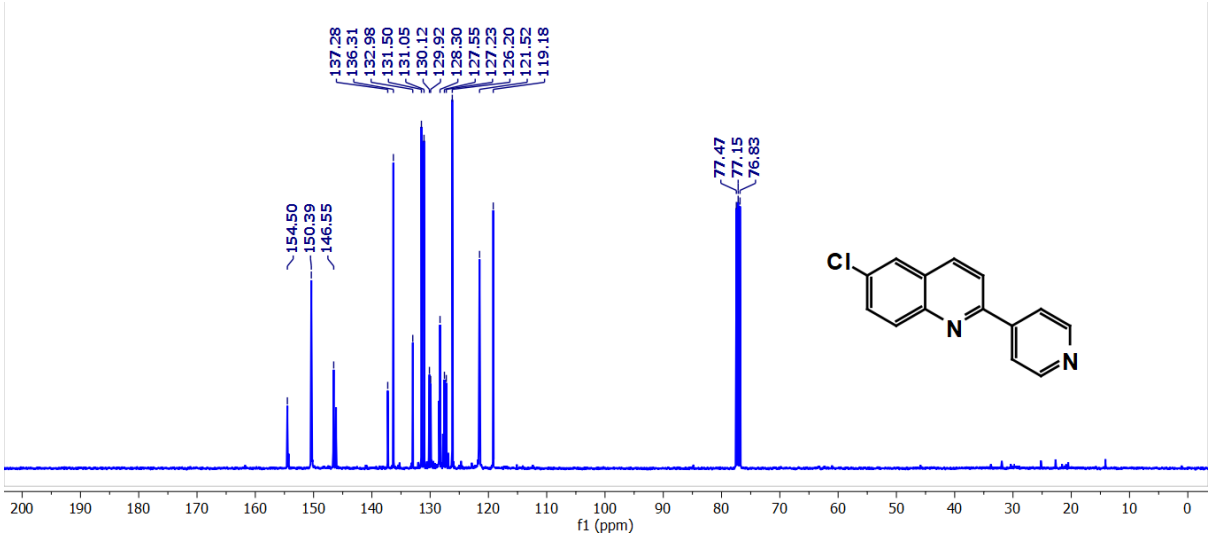

Figure 15. ^{13}C NMR spectrum of compound **10ag** (75 MHz, $CDCl_3$).

V.7 References

1. (a) O. Afzal; S. Kumar; M. R Haider; M. R Ali; R. Kumar; M. Jaggi; S. Bawa; Eur. J. Med. Chem. **2015**, *97*, 871−910. (b) J. P. Michael, *Nat. Prod. Rep.* **2008**, *25*, 166–187. (c) R. Musiol, *Expert Opin. Drug Discovery* **2017**, *12*, 583–597. (d) Gopaul, Kaalin; A. Shintre, Suhas; A. Koorbanally, Neil; *Anti-Cancer Agents Med. Chem.* **2015**, *15*, 631–646. (e) Y. Zhou, W. Li, L. Yu, Y. Liu, X. Wang, M. Zhou, *Dalton Trans.* **2015**, *44*, 1858–1865. (f) K. Nakatani, S. Sando, I. Saito, *J. Am. Chem. Soc.* **2000**, *122*, 2172–2177. (g) Jones, G. Comprehensive Heterocyclic Chemistry II; Rees, C. W., Scriven, E. F. V., Eds.; Pergamon: Oxford, **1996**; p 167.
2. (a) R. Sharma, P. Kour, A. Kumar, J. Chem. Sci. **2018**, *130*, 73–98. (b) G. Chelucci, A. Porcheddu, Chem. Rec. **2017**, *17*, 200–216. (c) M. E. Theclitou, L. A. Robinson, Tetrahedron Lett. **2002**, *43*, 3907–3910. (d) B. Jiang, Y. G. Si, J. Org. Chem. **2002**, *67*, 9449–9451. (e) G. Jones, Comprehensive Heterocyclic Chemistry, (Eds: A. R. Katritzky, C. W. Ress) Vol. 5, Pergamon, New York **1996**, 167. (f) R. J. Linderman, K. S. Kirollos, Tetrahedron Lett. **1990**, *31*, 2689–2692. (g) R. H. F. Mansake, M. Kulka, Org. React. **1953**, *7*, 59–98.
3. (a) F. Huang, Z. Q. Liu, Z. K. Yu, *Angew. Chem. Int.* Ed. **2016**, *55*, 862–875; *Angew. Chem.* **2016**, *128*, 872–885. (b) B. R. McNaughton, B. L. Miller, *Org. Lett.* **2003**, *5*, 4257–4259. (c) Y. Z. Hu, G. Zhang, R. P. Thummel, *Org. Lett.* **2003**, *5*, 2251–2253. (d) N. Anand, S. Koley, B. J. Ramulu, M. S. Singh, *Org. Biomol. Chem.* **2015**, *13*, 9570–9574. (e) S. Yao, K. J. Zhou, J. B. Wang, H. E. Cao, L. Yu, J. Z. Wu, P. H. Qiu, Q. Xu, *Green Chem.* **2017**, *19*, 2945–2951.
4. (a) M.-J. Zhang; H.-X. Li; D. J. Young; H.-Y. Li; J.-P. Lang. *Org. Biomol. Chem.* **2019**, *17*, 3567−3574. (b) K. Singh; M. Vellakkaran; D. Banerjee. *Green Chem.* **2018**, *20*, 2250−2256. (c) S. Parua; R. Sikari; S. Sinha; G. Chakraborty; R. Mondal; N. D. Paul. *J. Org. Chem.* **2018**, *83*, 11154−11166. (d) S. Parua; R. Sikari; S. Sinha; N. D. Paul. *J. Org. Chem.* **2017**, *82*, 7165−7175.

5. (a) G. Chakraborty; R. Sikari; S. Das; R. Mondal; S. Sinha; S. Banerjee; N. D. Paul. *J. Org. Chem.* **2019**, *84*, 2626−2641. (b) D.-W. Tan; H.-X. Li; D.-L. Zhu; H.-Y. Li; D. J. Young; J.-L. Yao; J.-P. Lang. *Org. Lett.* **2018**, *20*, 608−611. (d) D.-W. Tan; H.-X. Li; D.-L. Zhu; H.-Y. Li; D. J. Young; J.-L. Yao; J.-P. Lang. *ChemCatChem*, **2017**, *9*, 1113−1118.

6. (a) J. Wang; K. Sun; X. Chen; T. Chen; Y. Liu; L. Qu; Y. Zhao; B. Yu; *Org*. *Lett*. **2019**, *21*, 1863−1867. K. Sun; S. -J. Li; X.-L. Chen; Y. Liu; X.-Q. Huang; D.-H. Wei; L.-B. Qu; Y.-F Zhao; B. Yu; *Chem*. *Commun*. **2019**, *55*, 2861−2864. (b) Y. Liu; X.-L. Chen; K. Sun; X.-Y. Li; F.-L. Zeng; X.-C. Liu; L.-B. Qu; Y.-F. Zhao; B. Yu; *Org*. *Lett*. **2019**, *21*, 4019−4024.

7. (a) N. Deibl; R. Kempe; *Angew*. *Chem*., *Int*. *Ed*. **2017**, *56*, 1663−1666. (b) B. Pan; B. Liu; E. Yue; Q. Liu; X. Yang; Z. Wang; W.-H. Sun; *ACS Catal*. **2016**, *6,* 1247−1253. (c) M. Zhang; H. Neumann; M. Beller; *Angew*. *Chem*., *Int*. *Ed*. **2013**, *52*, 597−601. (d) S. Michlik; R. Kempe; *Nat*. *Chem*. **2013**, *5*, 140−144. (e) S. Michlik; R. Kempe; *Angew*. *Chem*., *Int*. *Ed*. **2013**, *52*, 6326−6329. (f) D. Srimani; Y. Ben-David; D. Milstein; *Angew*. *Chem*., *Int*. *Ed*. **2013**, *52*, 4012−4015. (g) D. Srimani; Y. Ben-David; D. Milstein, *Chem*. *Commun*. **2013**, *49*, 6632−6634. (h) K. Iida; T. Miura; J. Ando; S. Saito; *Org*. *Lett*. **2013**, *15*, 1436−1439. (j) R. Martínez; D. J. Ramon; M. Yus; *Eur*. *J. Org. Chem*. **2007**, *2007*, 1599−1605. (l) C. S. Cho; B. T. Kim; T.-J. Kim; S. C. Shim; *Chem*. *Commun*. **2001**, *0*, 2576−2577.

8. (a) C. S. Cho; B. T. Kim; T.-J. Kim; S. C. Shim; *Chem*. *Commun*. **2001**, *0*, 2576−2577, (b) R. Martínez; D. J. Ramon; M. Yus; *Eur*. *J. Org. Chem*. **2007**, 2007, 1599−1605, (c) H. V. Vander; Mierde, N. Ledoux; B. Allaert; P. V. D.Voort; R. Drozdzak; D. D. Vos; F. Verpoort; *New J. Chem.* **2007**, *31*, 1572−1574., (d) D. Srimani; Y .Ben-David; D. Milstein; *Chem. Commun*. ***2013***, *49*, 6632−6634, (e) B. Pan; B. Liu; E. Yue; Q. Liu; X. Yang; Z. Wang; W.-H. A. Sun; *ACS Catal*. **2016**, *6*, 1247−1253.

9. (a) F. Li; L. Lu; J. Ma; *Org. Chem. Front*. **2015**, *2*, 1589−1597. (b) J. Zhou; J. Fang; *J. Org. Chem*. **2011**, *76*,7730−7736. (c) H. V. Mierde; P. V. D. Voort; D. D. Vos; F. Verpoort; *Eur*. *J. Org. Chem*. **2008**, *2008*, 1625−1631. (d) H. V. Mierde; N. Ledoux; B. Allaert; P. V. D. Voort; R. Drozdzak; D. D. Vos; F. Verpoort, *New J*. *Chem*. **2007**, *31*, 1572−1574.

10. (a) P. Daw; A. Kumar; N. A. Espinosa-Jalapa; Y. Diskin-Posner; Y. Ben-David; D. Milstein. *ACS Catal.* **2018**, *8*, 7734−7741. (b) S. Shee; K. Ganguli; K. Jana; S. Kundu. *Chem. Commun.* **2018**, *54*, 6883−6886. (c) K. Das; A. Mondal; D. Srimani. *Chem. Commun.* **2018**, *54*, 10582−10585. (d) M.-J. Zhang; D.-W. Tan; H.-X. Li; D. J. Young; H.-F. Wang; H.-Y. Li; J.-P. Lang. *J. Org. Chem.* **2018**, *83*, 1204−1215. (e) B. Guo; J.-Y. Xue; H.-X. Li; D.-W. Tan; J.-P. Lang. *RSC Adv.* **2016**, *6*, 51687−51693. (f) P. Gandeepan; C. H. Cheng. *Asian J. Org. Chem.* **2014**, *3*, 303−308. (g) W. Yin; C. Wang; Y. Huang. *Org. Lett.* **2013**, *15*, 1850−1853.

11. (a) S. Parua; R. Sikari; S. Sinha; S. Das; G. Chakraborty; N.D. Paul. *Org. Biomol. Chem.* **2018**, *16*, 274−284. (b) G. Zhang; J. Wu; H. Zeng; S. Zhang; Z. Yin; S. Zheng. *Org. Lett.* **2017**, *19*, 1080−1083.

12. (a) K. Hindson; B. d. Bruin; *Eur*. *J. Inorg. Chem*.**2012**, *2012*, 340−342. (b) P.J.Chirik; *Inorg. Chem*. **2011**, *50*, 9737−9740. (c) P. J. Chirik; K. Wieghardt; *Science* **2010,** *327*, 794−795. (d) V. Lyaskovskyy; B. D. Bruin; *ACS Catal.* **2012,** *2*, 270−279.

13. (a) D. Sengupta; R. Bhattacharjee; R. Pramanick; S. P. Rath; N. S. Chowdhury; A. Datta; S Goswami; *Inorg*. *Chem*. **2016**, *55*, 9602−9610. (b) R. Pramanick; R. Bhattacharjee; D. Sengupta; A. Datta; S. Goswami; *Inorg*. *Chem*. **2018**, ***57***, 6816−6824. (c) S. Sinha; S. Das; R. Sikari; S. Parua; P. Brandaõ; S.

Demeshko; F. Meyer; N. D. Paul; *Inorg. Chem*. **2017**, *56*, 14084−14100. (b) S. P. Rath; D. Sengupta; P. Ghosh; R. Bhattacharjee; M.Chakraborty; S. Samanta,; A. Datta,; S. Goswami, *Inorg. Chem*. **2018**, *57*, 11995−12009.

14. S. Roy, S. Pramanik, S. C. Patra, B. Adhikari, A. Mondal, S. Ganguly, K. Pramanik, *Inorg. Chem.* **2017,** *56,* 12764–12774.
15. (a) A.D. Becke, *J. Chem. Phys.* **1993**, *98*, 5648-5652, (b) C. Lee, W. Yang, R.G. Parr, *Phys. Rev. B: Condens. Matter* **1988**, *37*, 785-789.
16. M. J. Frisch, G. W. Trucks, H. B. Schlegel, G. E. Scuseria, M. A. Robb, J. R. Cheeseman, G. Scalmani, V. Barone, B. Mennucci, G. A. Petersson, H. Nakatsuji, M. Caricato, X. Li, H. P. Hratchian, A. F. Izmaylov, J. Bloino, G. Zheng, J. L. Sonnenberg, M. Hada, M. Ehara, K. Toyota, R. Fukuda, J. Hasegawa, M. Ishida, T. Nakajima, Y. Honda, O. Kitao, H. Nakai, T. Vreven, J. A. Montgomery Jr., J. E. Peralta, F. Ogliaro, M. Bearpark, J. J. Heyd, E. Brothers, K. N. Kudin, V. N. Staroverov, R. Kobayashi, J. Normand, K. Raghavachari, A. Rendell, J. C. Burant, S. S. Iyengar, J. Tomasi, M. Cossi, N. Rega, J. M. Millam, M. Klene, J. E. Knox, J. B. Cross, V. Bakken, C. Adamo, J. Jaramillo, R. Gomperts, R. E. Stratmann, O. Yazyev, A. J. Austin, R. Cammi, C. Pomelli, J. W. Ochterski, R. L. Martin, K. Morokuma, V. G. Zakrzewski, G. A. Voth, P. Salvador, J. J. Dannenberg, S. Dapprich, A. D. Daniels, O. Farkas, J. B. Foresman, J. V. Ortiz, J. Cioslowski, D. J. Fox, GAUSSIAN 09 (Revision A.01), Gaussian, Inc., Wallingford, CT, (**2009**).
17. (a) J. Autschbach, T. Ziegler, S.J.A. Gisbergen, E.J. Baerends, *J. Chem. Phys.* **2002**, *116*, 6930-6940, (b) K.L. Bak, P. Jørgensen, T. Helgaker, K. Rund, H.J.A. Jenson, *J. Chem. Phys*. **1993**, *98*, 8873-8887. (c) T. Helgaker, P. Jørgensen, *J. Chem. Phys*. **1991**, *95*, 2595-2601. (d) E.K.U. Gross, W. Kohn, Adv. *Quantum Chem*. **1990**, *21*, 255-291.
18. (a) M. Cossi, V. Barone, *J. Chem. Phys*. **2001**, *115*, 4708-4717. (b) V. Barone, M. Cossi, *J. Phys. Chem.* **1998**, *102*, 1995-2001.
19. (a) T. Liu, H.X. Zhang, B.H. Xia, *J. Phys. Chem*. **2007**, *111*, 8724-8730. (b) A. Albertino, C. Garino, S. Ghiani, *J. Organomet. Chem*. **2007**, *692*, 1377-1391. (c) X. Zhou, H.X. Zhang, Q.J. Pan, B.H. Xia, *J. Phys. Chem*. **2005**, *109*, 8809-8818. (d) X. Zhou, A.M. Ren, J.K. Feng, *J. Organomet. Chem.* **2005**, *690*, 338-347.
20. (a) P.J. Hay, W.R. Wadt, *J. Chem. Phys*. **1985**, *82*, 299-310. (b) M.S. Gordon, J.S. Binkley, J.A. Pople, W.J. Pietro, W.J. Hehre, *J. Am. Chem. Soc*. **1982**, *104*, 2797-2803.
21. N.M. O'Boyle, A.L. Tenderholt, K.M. Langner, *J. Comput. Chem*. **2008**, *29*, 839-845.
22. Eugenio Garribba Giovanni Micera, J. Chem. Educ. **2006**, *83*, 8, 1229.
23. J. Marco-Contelles, E. Pérez-Mayoral, A. Samadi, M. C. Carreiras and E. Soriano, Chem. Rev., **2009**, *109*, 2652–2671.
24. In all cases, unreacted alcohols or ketones were identified during the TLC screening of the reaction mixture. Additionally, all yields listed here are isolated yields. Thus, it was likewise impossible to completely rule out the chance of product loss during workup and column chromatographic separation of the desired products from the reaction mixture.
25. D. Wei, V. Dorcet, C. Darcel and J. B. Sortais, ChemSusChem, **2019**, *12*, 3078–3082.

26. (a) Y. Ma, Z. Du, J. Liu, F. Xia and J. Xu, Green Chem., **2015**, *17*, 4968–4973; (b) R. Ray, S. Chandra, D. Maiti and G. K. Lahiri, Chem. – Eur. J., **2016**, *22*, 8814–8822; (c) W. Ai, R. Zhong, X. Liu and Q. Liu, Chem. Rev., **2019**, *119*, 2876–2953.
27. D. Sengupta, R. Bhattacharjee, R. Pramanick, S. P. Rath, N. Saha Chowdhury, A. Datta and S. Goswami, Inorg. Chem., **2016**, *55*, 9602–9610.

LIST OF PUBLICATIONS

1. S. Naskar, S. Halder, G. Kanrar, **D. Jana**, S. Dinda, K. Pramanik, S. Ganguly, Role of ligand disposition and oxime…oximato hydrogen bonding upon redox non-innocent character of rhodium(III) phenylazooximates, *Polyhedron*, 2023, **235**, 116342. (DOI: 10.1016/j.poly.2023.116342).

2. S. Dinda,[†] **D. Jana,**[†] R. M. Gomila, A. Frontera, S. Roy, S. C. Patra, K. Pramanik, S. Ganguly, Halogen Bonding in Stereoselective Metal Chloride (M–Cl) Bond Activation and Transformation to Metal Triiodide (M–I3), *Cryst. Growth Des.* 2024, **24**, 3342–3354 (DOI: 10.1021/acs.cgd.4c00066).

3. G. Kanrar, S. Halder, S. Naskar, **D. Jana**, A. Sarkar, B. K. Panda, S. Dinda, K. Pramanik, S. Ganguly, N–N hydrazonyl bond cleavage in benzothiazolyl-hydrazino-phenathrenequinone mediated by ruthenium(II) via an anion radical intermediate, *J. Mol. Struct.* 2024, **1314**, 138720 (DOI: 10.1016/j.molstruc.2024.138720).

4. S. Halder, S. Naskar, **D. Jana**, G. Kanrar, K. Pramanik and S. Ganguly, Ruthenium complexes of redox non-innocent aryl-azo-oximes for catalytic a-alkylation of ketones and synthesis of 2-substituted quinolines, *New J. Chem.* 2024, **48**, 8181-8194. (DOI: 10.1039/D4NJ00391H).

5. **D. Jana**, S. Roy, S. Naskar, S. Halder, G. Kanrar, K. Pramanik, Potent pincer-zinc catalyzed homogeneous α-alkylation and Friedländer quinoline synthesis reaction of secondary alcohols/ketones with primary alcohols, *Org. Biomol. Chem*., 2024, **22**, 6393-6408 (DOI: 10.1039/D4OB00988F).

6. S. Halder, S. Naskar, **D. Jana**, G. Kanrar, S. C. Mandal, S. Roy, N. Bharadwaj, K. Pramanik, S. Ganguly, Dehydrogenative Coupling for Synthesis of Quinazolin-4(3H)-ones *via* Tandem Reaction using Ruthenium(II)-Phenyl-Azo-Naphthaldoxime: An Experimental and Theoretical Investigation, *Chem. Asian J.*, 2025, **20**, e202401278 (DOI: 10.1002/chem.202401278).

7. **D. Jana**, S. Malik, G. Kanrar, S. Naskar, S. Halder, K. Pramanik, One-Pot Cascade [3+2+1] Annulation: Synthesis and Mechanistic Insight of s-Triazines and Pyrimidines Using Azo-Supported Metalloradical Nickel Catalyst, *ChemCatChem*, 2025, **0**, e202401851 (DOI: 10.1002/cctc.202401851).

8. S. Roy, T. Ghorui, **D. Jana**, S. C. Patra, S. Pramanik, S. Moorthy, S. K. Singh, S. Mehta, A. Mondal, K. Pramanik, Intramolecular Redox-Driven Synthesis of Mono- and Diradical Iridium(III) Complexes: Insights into Molecular and Electronic Structure, Electrochemistry, and Spin-Communication, *Chem. A – Eur. J.*, 2025, **31**, e202404027 (DOI: 10.1002/chem.202404027).
9. **D. Jana**, S. Malik, G. Kanrar, S. Naskar, S. Halder, K. Pramanik, Microwave-Driven Solvent-free [2 + 2 + 1 + 1] Cascade Annulation for Poly-Substituted Pyridine Synthesis Catalyzed by a Nickel Metalloradical (manuscript under revision).
10. Effective Pincer-Copper Catalyzed Homogeneous Friedländer Quinoline Synthesis from Secondary Alcohols and Primary Alcohols/Ketones (manuscript under preparation).

Polyhedron 235 (2023) 116342

Contents lists available at ScienceDirect

Polyhedron

journal homepage: www.elsevier.com/locate/poly

Role of ligand disposition and oxime…oximato hydrogen bonding upon redox non-innocent character of rhodium(III) phenylazooximates

Srijita Naskar [a], Supriyo Halder [a], Gopal Kanrar [b], Debashis Jana [a], Soumitra Dinda [b], Kausikisankar Pramanik [a,*], Sanjib Ganguly [b,*]

[a] Department of Chemistry, Jadavpur University, Kolkata 700032, India
[b] Department of Chemistry, St. Xavier's College (Autonomous), Kolkata 700016, India

ABSTRACT

The diaryl-azo-oxime ligands HL, **1** undergoes oxidative coordination reaction with Wilkinson's catalyst to form two isomeric complexes of type *cis*-[$Rh^{III}L_2Cl(PPh_3)$], **2a** (Cl and PPh_3 are *cis*) and *trans*-[$Rh^{III}L_2Cl(PPh_3)$], **2b** where they are *trans* with respect to each other. Unlike the case of **2a**, the complex **2b** upon treatment with sodium borohydride, can be transformed to *trans*-[$Rh^{III}(HL^{\bullet})(L^{-})Cl(PPh_3)$], **3** and the reaction appears to progress *via* PCET. The disposition of ligand frameworks as well as the formation of oxime…oximato hydrogen bond appears to have a significant function for phenylazooxime to exhibit redox non-innocent behaviour in presence of rhodium(III). The compounds were characterized by electrochemical analysis, different spectral methods, single crystal XRD and optoelectronic properties, particularly the nature of transitions in the chelates were scrutinized by TD-DFT.

1. Introduction

Redox non-innocent ligands are interesting owing to their inherent capacity to exhibit various ligand redox levels upon coordination [1–23] and such systems have the aptitude to embrace and reject electron(s) during the course of catalytic processes [24–30], in chemical and biochemical reactions [31–33]. Coordinated azo-aromatic systems have been found to act as apposite precursors for stabilizing ligand centered anion radical complexes since they possess low-lying azo-π* orbital [34–47]. It has been well understood that structure of the ligand skeleton and redox character of the metal centre has a significant role for controlling the stabilization of these type of complexes and ligand–metal π-interaction can further adjust the electronic structural features for maximum stabilization [48–50]. Moreover, ligand environment around the metal centre may also influence the aptitude of these chelated azo-ligands in conjunction with other moieties to receive or donate odd electron(s) and this may be attributed to electronic or steric factors. The impact of electronic environment of auxiliary ligands in supporting extra electron(s) within π* LUMO of these ligands have been much less reported [48,51]. As a continuation of our study on stabilization of odd electron in coordinated azooximes [51–53], we have tried to investigate the competence of these ligand to retain an unpaired electron over azo-oxime framework in presence of rhodium(III) and to stabilize the corresponding open shell complexes. In this regard, we have started with the diaryl-azo-oxime HL, **1** which possesses low lying π* LUMO, thereby having the aptitude to perform as an electron-sink upon ligation, and have successfully isolated two isomeric complexes of type *cis*-[$Rh^{III}L_2Cl(PPh_3)$] (**2a**), where Cl and PPh_3 are in *cis* positions and *trans*-[$Rh^{III}L_2Cl(PPh_3)$] (**2b**), where they are *trans* with respect to each other. The complex **2b** can be reduced to the azo-oxime radical anion complex of type *trans*-[$Rh^{III}(HL^{\bullet})(L^{-})Cl(PPh_3)$] (**3**) and the reaction appears to progress *via* PCET but the corresponding anion radical analog of the *cis* isomer could not be isolated. Thus, the *trans* isomer behaves as a superior electron carrier and this has been attributed to stereochemical control around the rhodium centre. In fact, in the *trans* isomer **2b**, there is scope for unpaired electron to be delocalized on both the ligands much more efficiently since they are practically coplanar. Furthermore, the stabilization of **3** may also be attributed to formation of oxime…oximato intramolecular hydrogen bonding during the course of electron acceptance in presence of protons and this is also consistent with theoretical scrutiny. (see Scheme 1.)

2. Experimental details

2.1. General information

Drying and purification of solvents were performed using literature procedure and distilled out before using as required. The required chemicals were purchased from following sources: Phenyl hydrazine and Benzaldehyde from TCI Chemical (India) Pvt. ltd. Wilkinson's

* Corresponding authors.
E-mail address: icsg@sxccal.edu (S. Ganguly).

https://doi.org/10.1016/j.poly.2023.116342
Received 21 December 2022; Accepted 14 February 2023
Available online 19 February 2023

CRYSTAL GROWTH & DESIGN

pubs.acs.org/crystal

Article

Halogen Bonding in Stereoselective Metal Chloride (M−Cl) Bond Activation and Transformation to Metal Triiodide (M−I_3)

Soumitra Dinda,[#] Debashis Jana,[#] Rosa M. Gomila, Antonio Frontera,* Subhadip Roy, Sarat Chandra Patra, Kausikisankar Pramanik,* and Sanjib Ganguly*

Cite This: *Cryst. Growth Des.* 2024, 24, 3342−3354

Read Online

ACCESS | Metrics & More | Article Recommendations | Supporting Information

ABSTRACT: The isolation of isomeric complexes *trans*-[$Ru^{II}L^{PyHPQ}$(CO)(PPh_3)Cl] **2** and *cis*-[$Ru^{II}L^{PyHPQ}$(CO)(PPh_3)Cl] **3**, (Cl and PPh_3 are trans in **2** and they are cis in **3** respectively) as well as [$Ru^{II}L^{PyHPQ}$(CO)(PPh_3)$_2$Cl] **4** and [$Rh^{III}L^{PyHPQ}$(PPh_3)Cl_2] **5** disclose the flexidentate nature of the multifunctional ligand, HL^{PyHPQ} 2-pyridylhydrazinophenanthrenequinone, **1**. These complexes are maneuvered as molecular templates for understanding the role of halogen bonds (XB) in M−Cl bond activation and subsequent cleavage processes. Both isomeric forms **2** and **3** furnish *trans*-[$Ru^{II}L^{PyHPQ}$(CO)(PPh_3)(I_3)] **6** (where PPh_3 and I_3^- in trans position) when they are treated separately with I_2 in a hydrocarbon solvent. Nonetheless, complex **5** is converted to **7** upon similar treatment but **4** remains unreacted. Crystal structure of **7** revealed that it is composed of 62% *trans*-[$Rh^{III}L^{PyHPQ}$(PPh_3)Cl(I_3)] and 38% *trans*-[$Rh^{III}L^{PyHPQ}$(PPh_3)Cl(ClI_2)] (where PPh_3 and I_3^-/ClI_2^- are trans). The I_3^-/ClI_2^- gets coordinated to metal centers exclusively in an end-on fashion in all cases. Since the valence state of metal centers remains unaltered in due course of the reaction, the emergence of M−I_3/M−ClI_2 from M−Cl in the absence of any reductant in solution is indicative of prior activation of M−Cl bond *via* the formation of Halogen Bond (XB) of type [M−Cl−I−I] in an intermediate step. The geometrical fluctuations around the coordination sphere during the transformation of *cis*-[$Ru^{II}L^{PyHPQ}$(CO)(PPh_3)Cl] **3** to *trans*-[$Ru^{II}L^{PyHPQ}$(CO)(PPh_3)(I_3)] **6** is reminiscent of the active influence of XB, triggering the isomerization of **3** to **2** owing to steric encumbrance, before it is being converted to **6**. Electrochemical behavior and optoelectronic properties of the complexes have been complimented by theoretical analysis and the structures were characterized by SCXRD. Repeated π-stacking motifs in the crystalline phase architecture of the complexes have been scrutinized using DFT calculations.

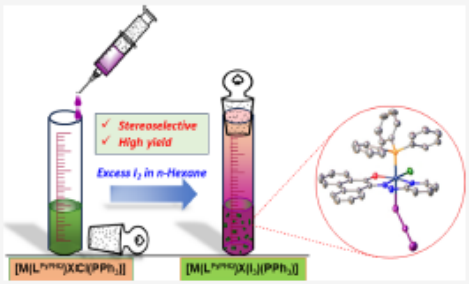

INTRODUCTION

It has been well understood that halogen bonds (XB)[1−19] are somewhat complementary to hydrogen bonds and their reasonably good directional as well as tunable characteristics led to wide-ranging applications in the rapidly growing field of catalysis and crystal engineering.[16,17,20−32] Halogen bonding has also been exploited in a few organocatalytic reactions[17,24−27] as well as in the synthesis of certain supramolecular entities.[28−30] Mother Nature employs iodine and XB for selective binding of thyroid hormones to their targets[31,32] and there are some reports of the formation of halogen bonds to coordinated halide[33−37] where certain other ligands may perform as Lewis bases in metal complexes.[31,32] Exchange of ligands *via* halogen bond formation has been observed only in very few cases[38−45] and this perception has triggered the development of innovative and fascinating insight into metal−halogen bond activation *via* the formation of halogen bonds.[45]

Our group has been striving to comprehend the role of ancillary ligands in influencing the stereoselectivity of C−H bond activation by using platinum group metal complexes.[46−49] In this article we have presented how judicious choice of coligands can induce selectivity in M−Cl (M = Ru^{II}, Rh^{III}) bond activation *via* the formation of halogen bond (XB). The ligand, 2-pyridylhydrazinophenanthrenequinone, HL^{PyHPQ} **1**[50] was used to synthesize two isomeric complexes *trans*- and *cis*-[$Ru^{II}L^{PyHPQ}$(CO)(PPh_3)Cl] **2** and **3** respectively and in both cases the ligand exhibits tridentate behavior. Additionally, another complex of composition [$Ru^{II}L^{PyHPQ}$(CO)(PPh_3)$_2$Cl] **4**, is formed where the ligand is bidentate, thereby revealing its flexidentate character. We have also synthesized [RhL^{PyHPQ}(PPh_3)Cl_2] **5** starting from Wilkinson's catalyst

Received: January 16, 2024
Revised: March 15, 2024
Accepted: March 15, 2024
Published: March 26, 2024

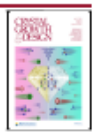

Journal of Molecular Structure 1314 (2024) 138720

Contents lists available at ScienceDirect

Journal of Molecular Structure

journal homepage: www.elsevier.com/locate/molstr

N–N hydrazonyl bond cleavage in benzothiazolyl-hydrazino-phenathrenequinone mediated by ruthenium(II) via an anion radical intermediate

Gopal Kanrar [a], Supriyo Halder [b], Srijita Naskar [b], Debashis Jana [b], Arup Sarkar [a], Bikash Kumar Panda [c], Soumitra Dinda [a], Kausikisankar Pramanik [b,*], Sanjib Ganguly [a,*]

[a] Department of Chemistry, St. Xavier's College (Autonomous), Kolkata 700016, India
[b] Department of Chemistry, Jadavpur University, Kolkata 700032, India
[c] Department of Chemistry, Jangipur College, Jangipur, Murshidabad, West Bengal 742213, India

ARTICLE INFO

Keywords:
Redox non-innocent ligand
Crystallography
DFT
NMR
Cyclic voltammetry

ABSTRACT

The complexes [Ru(L^{Benz})H(CO)(PPh$_3$)$_2$] **2**, [Ru(L^{Benz})Cl(CO)(PPh$_3$)$_2$] **3**, (ligand behaving as bidentate monoanionic) and [Ru(L^{Benz})Cl(CO)(PPh$_3$)] **4**, (ligand is tridentate monoanionic) have been synthesized starting from benzothiazolyl-hydrazino-phenathrenequinone (HL) **1** and [RuH(CO)Cl(PPh$_3$)$_3$]. These are characterized by electrochemical and spectral methods as well as single crystal X-ray diffractometry (SCXRD). Upon treating with NaBH$_4$, **3** accepts an electron within the coordinated ligand framework and the anionic hydrazonyl-*N* takes up a proton to be transformed to meta-stable hydrazinoquinone anion radical complex of ruthenium(II) [Ru(HL$^{Benz\bullet-}$)Cl(CO)(PPh$_3$)$_2$] **5**, possibly *via* concerted proton electron transfer process (CPET). Thus, the redox non-innocent character of the ligand upon complexation with ruthenium(II), has been disclosed and it is attributed to presence of low lying π* orbitals of almost entirely of phenanthraquinone and hydrazone character. In **5**, the π–acceptor ability of the ligand donor centres are reduced due to the existence of an odd electron in SOMO and hence the M-L distances around the coordination sphere are altered. The N–N (hydrazonyl bond length increases from 1.296 (6) Å in **3** to 1.429 Å in **5**, leading to lesser thermodynamic stability of the latter and upon standing, the N–N bond is cleaved to be transformed to **6**$^+$, possibly *via* the formation of iminoquinone anion radical complex, [6] (reported elsewhere). Also, it is *via* the dissociation of N–N (hydrazonyl) bond, the biologically important molecule 2-aminobenzothiazole is formed along with **6**$^+$, so as to provide a novel route for its synthesis.

1. Introduction

It has been well understood that concerted proton-electron transfer (CPET) has consequential roles in a diverse field of biological processes as well as in efficient energy conversions. [1–7] The most demanding and challenging illustration is the biological nitrogen fixation, which comprises of successive transfer and swapping of protons as well as electrons to coordinated nitrogen, [8–12] although the exact reaction pathway is still a matter of conjecture. In this regard, well-defined complexes having N–N bonds are good candidates to provide some illustrative clarification with respect to reduction sequences since they may be suitably engineered to comprehend the redox transformations accompanying the cleavage of N–N bonds. [13–24] Moreover, it has also been reported that metal–ligand synergy [25–27] is one of the significant aspects that regulate the activity of several redox metallo-enzymes like cytochrome P450, galactose oxidase and hydrogenases etc. [28–30] In these cases, both ligands (of the prosthetic group) and metal centres contribute to the redox events as well as in bond cleavage or activation. In fact, these types of ligands are often referred to as redox non-innocent [31–44] and they have the distinctive aptitude to confer unprecedented reactivity to the metal complexes by regulating loss or gain of electrons and protons.

We have been working with redox non-innocent ligands [45–56] and their roles in metal mediated redox transformations for a considerable period of time [57–61] and as an extension of our work in this field, we were motivated towards exploration of cooperative effect of metal along with redox active ligand comprising of hydrazone and iminoquinone moieties, to foster the cleavage of N–N bonds. [62–64] In the present

* Corresponding authors.
E-mail addresses: icsgxav@gmail.com, icsg@sxccal.edu (S. Ganguly).

https://doi.org/10.1016/j.molstruc.2024.138720
Received 19 March 2024; Received in revised form 17 May 2024; Accepted 21 May 2024
Available online 22 May 2024

NJC

PAPER

View Article Online
View Journal | View Issue

Cite this: *New J. Chem.*, 2024, 48, 8181

Ruthenium complexes of redox non-innocent aryl-azo-oximes for catalytic α-alkylation of ketones and synthesis of 2-substituted quinolines†

Supriyo Halder,‡[a] Srijita Naskar,‡[a] Debashis Jana,[a] Gopal Kanrar,[b] Kausikisankar Pramanik *[a] and Sanjib Ganguly *[b]

Ruthenium(II) complexes $[RuL(CO)Cl(PPh_3)_2]$, **1a–4a**, have been synthesized using ligands PhN=NC(Ar)NOH, HL **1–4**, respectively, by varying the pendant aryl (Ar) groups. The single crystal X-ray diffraction studies of complexes reveal that there are certain changes in Ru–N_{azo} and Ru–N_{oxime} bond lengths that may be explained primarily on the basis of electronic effects of pendant aryl groups. In **4a**, all Ru–N bond lengths are longer and this is attributed to oximato–O···O (hydroxyphenyl) interactions. Furthermore, there are weak intramolecular F···π interactions in **3a**. The complexes display multiple reductive responses ascribable to electron acceptance within the azo-oxime framework of the coordinated ligand and the corresponding one-electron reduced metastable anion radical complexes of type $[Ru(L^{\bullet-})(CO)Cl(PPh_3)_2]^-$ **[1]**$^{\bullet-}$ have been generated. This property of the complexes has been exploited in electron transfer catalysis *via* trapping of electrons in the azo-oxime skeleton in two types of reactions: (i) α-alkylation of ketones with primary alcohols and (ii) synthesis of 2-substituted quinoline derivatives from 2-aminobenzyl alcohols and substituted acetophenones/alkyl methyl ketones. The scope of catalysis has been studied and the probable catalytic pathway has been established from experimental results. The catalytic pathway is ligand-centric and redox-driven for the dehydrogenation process and the initial step involves formation of a coordinated anion radical. This leads to conversion of the starting 1° alcohol to the corresponding carbonyl *via* the HAT pathway, with the ruthenium(II) centre practically behaving as a template and remaining redox inactive. The catalytic reactions have been proven to be affected by the nature of pendant aryl (Ar) groups within the coordinated ligand.

Received 24th January 2024,
Accepted 3rd April 2024

DOI: 10.1039/d4nj00391h

rsc.li/njc

Introduction

The redox non-innocence[1] of coordinated ligands is gaining profound importance in the field of electron transfer catalysis since the metal center and the ligand skeleton have the ability to stimulate a process in a collaborative manner, with the catalyst switching from one spin isomeric state to another.[2–16] Such reactions may proceed *via* formation of a meta-stable ligand-centric coordinated radical and it is usually accompanied by proton coupled electron transfer (PCET)[17–22] or hydrogen atom transfer (HAT).[23–29] The chemistry of redox non-innocent ligands containing azo functions has developed over the past two and a half decades[30–43] and at present the catalytic role of their complexes is under intense investigation.[44–62] In the majority of the cases, ligands are of tridentate azo pincer type, where the ligated azo moieties have the ability to behave as electron pockets to store electron/s in the form of an azo anion-radical. In addition, the reserved electron/s may be transferred to suitable centres to bring about catalytic reduction and this concept has been widely employed to synthesize several value-added chemicals of pharmaceutical and industrial importance, in a cost effective and atom efficient manner.

We have been striving to explore and figure out the electron extracting ability of coordinated diaryl-azo-oximes in order to effectuate certain unusual redox transformations.[63–67] We are further motivated to synthesize suitable complexes of azo-oximes where the ligand skeleton may become redox active in the presence of ruthenium(II) and they may be skillfully employed to bring about electron-transfer catalysis for synthesis of useful organic compounds in an atom efficient manner. It is worth mentioning that there has been no report on

[a]*Department of Chemistry, Jadavpur University, Kolkata-700032, India. E-mail: kpramanik@hotmail.com; Tel: +91 33 2457 2781*
[b]*Department of Chemistry, St. Xavier's College (Autonomous), Kolkata-700016, India. E-mail: icsgxav@gmail.com, icsg@sxccal.edu; Tel: +91 33 2255 1266*

† Electronic supplementary information (ESI) available. CCDC 2303589, 2303590, 2303602, 2303603, 2303607 and 2303608. For ESI and crystallographic data in CIF or other electronic format see DOI: https://doi.org/10.1039/d4nj00391h

‡ Authors contributed equally to this work.

Organic & Biomolecular Chemistry

ROYAL SOCIETY OF CHEMISTRY

PAPER

View Article Online
View Journal | View Issue

Cite this: Org. Biomol. Chem., 2024, 22, 6393

Potent pincer-zinc catalyzed homogeneous α-alkylation and Friedländer quinoline synthesis reaction of secondary alcohols/ketones with primary alcohols†

Debashis Jana,[a] Sima Roy,[a] Srijita Naskar,[a] Supriyo Halder,[a] Gopal Kanrar[b] and Kausikisankar Pramanik*[a]

Received 12th June 2024,
Accepted 10th July 2024
DOI: 10.1039/d4ob00988f
rsc.li/obc

Herein, we describe an air- and moisture-stable, homogeneous zinc catalyst stabilised using an electron deficient N^N^N pincer-type ligand. This ternary, penta-coordinated neutral molecular catalyst [Zn(N^N^N)Cl_2] selectively produces α-alkylated ketone derivatives (14 examples) through a one-pot acceptorless dehydrogenative coupling (ADC) reaction between secondary and primary alcohols using the borrowing hydrogen (BH) approach in good to excellent isolated yields (up to 93%). It is worth noting that this catalyst also provides an eco-friendly route for the synthesis of quinoline derivatives (30 examples) using 2-aminobenzyl alcohols as alkylating agents *via* successive dehydrogenative coupling and N-annulation reactions. This cost effective, easy to synthesize and environmentally benign catalyst shows excellent stability in catalytic cycles under open-air conditions, as evident from its high turnover number (~10^4), and is activated by using a catalytic amount of base under milder conditions.

Introduction

The construction of molecules with diverse functional groups from commonly available small molecules/building blocks by C–C and C–heteroatom bond activation is one of the fundamental aspects of chemical and biochemical syntheses.[1] In reality, the majority of classical methods require expensive and environmentally toxic reagents and discharge hazardous waste even in (over)stoichiometric amounts.[2] Thus, the development of an efficient approach is desirable for selective C–C and C–heteroatom formation reactions. Accordingly, beneficial organic compounds with potential applications in the medical, agrochemical and pharmaceutical industries may be synthesized.[3] In this context, conversion of alcohols to C-alkylated derivatives and N-heterocycles *via* acceptorless dehydrogenation coupling (ADC) and borrowed hydrogen (BH)/N-annulation methodologies using homogeneous catalysts has received considerable attention in recent years.[4] Although such transformation reactions can be accomplished with 0.5–5 mol% platinum-group-metal catalysts (*e.g.*, Ru, Rh, Ir, Pd and Pt) in satisfactory yields.[5–9] In general, catalysis using non-precious first-row transition metals with good turnover numbers (TONs) under open-air conditions for α-alkylation and Friedländer annulation reactions remains challenging for gram-scale production of high-value bio-active molecules.[10] Nonetheless, continuous effort has been made with 3d metal catalysts (Mn, Fe, Co, Ni and Cu) with comparable catalyst loading (0.5–5 mol%), since they provide a more economically viable solution (Schemes 1 and 2).[11–15] A few examples have recently been reported where analogous reactions can be accomplished with 0.05% or less catalyst loading with Ni(II) and Mn(I), respectively.[16]

It is worth noting that the use of zinc(II) is less cited for homogeneous catalysis than other 3d metals plausibly due to its closed-shell, electron-rich, redox innocent nature. Only very recently molecular zinc-catalyzed dehydrogenation reactions of secondary alcohols have been documented.[17] Here, dehydrogenation of an alcohol occurs first to produce an aldehyde or ketone that undergoes an *in situ* condensation reaction with an enolate or amine to form an α,β-unsaturated ketone or imine, where the former is finally reduced to form a new C–C bond (Scheme 3) or the subsequent cyclization of aniline derivatives leads to quinolines because of the aromatization in the case of the C–N annulation reaction (Scheme 4).

In general, the catalytic performance of homogeneous catalysts is superior to that of heterogeneous catalysts.[18] Nonetheless, the disadvantage in the use of homogeneous cat-

[a]Department of Chemistry, Jadavpur University, Kolkata 700032, India. E-mail: kpramanik@hotmail.com; Tel: +91 94333 66013
[b]Department of Chemistry, St. Xavier's College (Autonomous), Kolkata-700016, India

†Electronic supplementary information (ESI) available. CCDC 2348683, 2348684, 2349095 and 2349099. For ESI and crystallographic data in CIF or other electronic format see DOI: https://doi.org/10.1039/d4ob00988f

ACES Asian Chemical Editorial Society
doi.org/10.1002/asia.202401278
Check for updates
CHEMISTRY AN ASIAN JOURNAL Research Article
www.chemasianj.org

Dehydrogenative Coupling for Synthesis of Quinazolin-4(3H)-ones *via* Tandem Reaction using Ruthenium(II)-Phenyl-Azo-Naphthaldoxime: An Experimental and Theoretical Investigation

Supriyo Halder+,[a] Srijita Naskar+,[a] Debashis Jana,[a] Gopal Kanrar,[b] Shyama Charan Mandal,[c] Subhadip Roy,[d] Nishchal Bharadwaj,[e] Kausikisankar Pramanik,*[a] and Sanjib Ganguly*[b]

The bidentate N, N, donor phenyl-azo-naphthaldoxime NpLH, **1** was used to synthesize the ruthenium(II) complex trans-[Ru(NpL)(CO)Cl(PPh_3)$_2$], **2**. It has been characterized by SCXRD, electrochemical and spectral studies. Computational analysis indicates that the low-lying π*-LUMO of the complex has substantial azo-character of coordinated ligand. This property has been exploited to form an efficient electron transfer pre-catalyst to effectuate dehydrogenative functionalization of a large number of benzyl alcohols to quinazolin-4(3H)-ones via condensation with diverse o-amino benzamides as well as N-substituted benzamides under aerobic conditions (57 entries). A reaction mechanism has been projected via isolation of intermediates and certain control experiments. Furthermore, it has been substantiated by theoretical scrutiny using density functional theory (DFT) calculation. The catalytic cycle involves stepwise hydrogen atom transfer (HAT) from benzyl alcohols to the N_{azo} atoms of the coordinated ligand with subsequent removal of the H-atoms from the N_{azo} atoms to regenerate the active catalyst.

Introduction

N-heterocycles have been found to be in plenitude in natural products due to their intimate biological relevance. This leads to extensive research towards the development of innovative, sustainable and greener methods for synthesis of aza-heterocycles.[1] The quinazolinone moiety is present as a building block in a wide range of naturally occurring alkaloids that have been sequestered from natural resources like micro-organisms, plants, and animals.[2,3] Quinazolin-4(3H)-ones and their substituted analogues have gained significant attention owing to various pharmacological activities, such as anti-inflammatory,[4] antimicrobial,[5] anticancer,[6,7] antihypertensive,[8] dihydrofolate reductase inhibition,[9] and Tyrosine Kinase inhibition.[10] Despite significant progress in this area, it has been found that in most cases multi-step synthesis is required. This creates unwanted byproducts and often needed hazardous chemicals for catalytic transformation. Furthermore, the precursor molecules are often expensive and less available.[11,12] Accordingly, it is always challenging to develop cost-effective and atom efficient production of substituted quinazolin-4(3H)-ones. There have been some reports of transition metal catalysed synthesis of substituted quinazolin-4(3H)-ones via dehydrogenative functionalization of aliphatic and aromatic alcohols and this strategy is quite promising since it is a single-step, economical, environment friendly synthesis starting from readily available precursors and generates hydrogen or water as the only byproducts (Scheme 1).[13–15]

We were inquisitive regarding the electron trapping aptitude of coordinated azooximes[16] for the past few years and this led us to explore their ability to bring about dehydrogenative functionalization of aliphatic and aromatic alcohols to form value added products.[17–19] As a continuation of our previous work, in this paper we have utilized phenyl-azo-naphthaldoxime NpLH, **1** to synthesize a ruthenium(II) complex trans-[Ru(NpL)(CO)Cl(PPh_3)$_2$], **2** (Scheme 2). The structural, electrochemical, and theoretical studies of **2** have been performed in order to have a comprehension of their competence to bring about electron transfer catalysis. The ruthenium(II) complex

[a] S. Halder,+ S. Naskar,+ D. Jana, K. Pramanik
Department of Chemistry, Jadavpur University, Kolkata 700032, India
Tel: +91 33 2457 2781
E-mail: kpramanik@hotmail.com
[b] G. Kanrar, S. Ganguly
Department of Chemistry, St. Xavier's College (Autonomous), Kolkata – 700016, India
Tel: +91 33 2255 1266
E-mail: icsgxav@gmail.com
icsg@sxccal.edu
[c] S. C. Mandal
SUNCAT Center for Interface Science and Catalysis, SLAC National Accelerator Laboratory
2575 Sand Hill Road, Menlo Park, CA 94025 (USA)
[d] S. Roy
Department of Chemistry, The ICFAI University Tripura, Agartala, Tripura 799210, India
[e] N. Bharadwaj
Department of Chemistry, Indian Institute of Technology (IIT) Indore, Indore, Madhya Pradesh 453552
[+] Authors contributed equally to this work
Supporting information for this article is available on the WWW under https://doi.org/10.1002/asia.202401278

Check for updates

ChemCatChem

Research Article
doi.org/10.1002/cctc.202401851

Chemistry Europe
European Chemical Societies Publishing

www.chemcatchem.org

One-Pot Cascade [3 + 2 + 1] Annulation: Synthesis and Mechanistic Insight of *s*-Triazines and Pyrimidines Using Azo-Supported Metalloradical Nickel Catalyst

Debashis Jana,[a] Sampad Malik,[a] Gopal Kanrar,[b] Supriyo Halder,[a] Srijita Naskar,[a] and Kausikisankar Pramanik*[a]

Highly efficient Ni-catalyzed C—N/C—C bond formation from amidines during the [3 + 2 + 1] annulation by primary alcohols alone or by primary alcohols with secondary alcohols/phenyl acetylenes has been successfully accomplished toward scaled synthesis of *s*-triazine and pyrimidines, respectively. A strongly π-acidic *bis*-azo NNN-pincer scaffold was successfully introduced for dual functionalization such as augmenting the sustainability of the molecular catalyst by enhancing the metal–ligand integrity and interposing a potent electron-sink chromophore. The high yield synthesis (up to 94%) of *poly*-azaheterocycles with merely 0.001 mol% catalyst loading demonstrates the potency of azo-anion radical assisted catalysis. A diverse range of primary and secondary alcohols are successfully used as substrates. Furthermore, use of methanol/ethanol as C1/C2 synthon (alkylating agents) enables the formation of challenging imine intermediates from amidines through dehydrogenation under mild conditions. This facilitates the synthesis of wide varieties of *s*-triazines, and pyrimidines driven by the auto-tandem catalyst. Mechanistic investigations reveal that the formation of C—C and C—N bonds proceed through a metalloradical catalysis (MRC) pathway instead of borrowing hydrogen (BH) method and thereby addresses the challenge of controlling stereoselection. This process is initiated by Ni-catalyzed acceptorless dehydrogenation (AD) of the alcohol substrate, followed by a series of sequential steps, including condensation, aza-Michael addition, cyclization, and subsequent dehydrogenation. The well-defined one-electron reductive response at −0.34 V (versus Fc^+/Fc) is indicative of the involvement of azo anion radical during catalytic annulation. The formation of the ligand radical intermediate was further substantiated by an electron paramagnetic resonance (EPR) study conducted both in the presence and absence of radical scavengers, specifically 2,2,6,6-tetramethyl-1-piperidinyloxy (TEMPO), and butylated hydroxytoluene (BHT).

1. Introduction

Metal-organic catalysts have played an important role in achieving numerous synthetically valuable organic and biomolecules that are otherwise challenging to achieve in realism. Remarkably, palladium continues to rule the field in fine organic synthesis when compared to other metals because it validates reliability and uniformity in metal-mediated catalysis and exhibits a wide substrate tolerance.[1] However, the substantial expense associated with palladium has limited its commercial adequacy, thereby motivating the exploration of catalysts based on earth-abundant, low-cost metals. Being the sibling, cost-effective nickel is the most viable option. Furthermore, they show striking resemblance in a number of organic catalytic transformation.[2] Nevertheless, they differ in many instances as well due to their innate physicochemical aspects. The recent development of homogeneous catalysis using 3d metals in organic synthesis is highly promising as it has only lately begun to challenge the abiding supremacy of late and mostly noble metals in this field and they hold the potency of being able to encompass large-scale synthesis with substantially high turnover number (TON).[3]

The synthesis of bio-active *poly*-azaheterocycles such as pyrroles, pyridines, imidazoles, pyrimidines, and triazines procured from common alcohols is a rapidly expanding area of interest for green sustainable chemistry.[4] Among these *N*-heterocycles, the pyrimidine and *s*-triazine are found in a wide range of bio-relevant molecules and are crucial structural motifs found in many pharmacological, enzyme inhibitor, antifungal, anticancer, antitubercular activity, argochemicals.[5,6] In fact, a variety of synthetic procedures have been cited in the literature depending on the substrates, reagents and reaction conditions; where metal-mediated homogeneous catalysis emerging as a versatile and valuable synthetic protocol due to their gradual improvising catalytic efficiency, sustainability and atom-economy (Scheme 1).[7] Nevertheless, such methods in general suffer from the complications of physical separation of product(s), formation of hazardous by-products, use of stoichiometric or high amounts of base and low TON, i.e., high catalyst loading. The primary drawback of homogeneous catalysts is that they cannot be efficiently reinstated after the reaction cycle, which makes cost reduction challenging in industrial

[a] D. Jana, S. Malik, S. Halder, S. Naskar, K. Pramanik
Department of Chemistry, Jadavpur University, Kolkata 700032, India
E-mail: kausikis.pramanik@jadavpuruniversity.in

[b] G. Kanrar
Department of Chemistry, St. Xavier's College (Autonomous), Kolkata 700016, India

Supporting information for this article is available on the WWW under https://doi.org/10.1002/cctc.202401851

Check for updates

Chemistry–A European Journal

Research Article
doi.org/10.1002/chem.202404027

Chemistry Europe
European Chemical Societies Publishing

www.chemeurj.org

Intramolecular Redox-Driven Synthesis of Mono- and Diradical Iridium(III) Complexes: Insights into Molecular and Electronic Structure, Electrochemistry, and Spin-Communication

Sima Roy[+],[a] Tapas Ghorui[+],[a] Debashis Jana,[a] Sarat Chandra Patra,[a] Shuvam Pramanik,[a] Shruti Moorthy,[b] Saurabh Kumar Singh,[b] Sakshi Mehta,[c] Abhishake Mondal,[c] and Kausikisankar Pramanik*[a]

Two π-radical complexes containing bisazo-aromatic-centered radical anion (**1**$^{\bullet-}$) were synthesized through *in-situ* electron transfer from metal-to-ligand using [Ir^{I}] and 2-(2-Pyridylazo)azobenzene (**1**) in inert hydrocarbon solvent. These are characterized as diradical [Ir^{III}(**1**$^{\bullet-}$)$_2$]$^+$ **[2]**$^+$ and monoradical [Ir^{III}(**1**$^{\bullet-}$)Cl$_2$(PPh$_3$)] **3**. In contrast, a rare metal-mediated hydrolytic cleavage of the C(sp^2)–N bond occurred in protic solvent resulting in quaternary radical complex [Ir^{III}(**1**$^{\bullet-}$)(**1'**)(PPh$_3$)]$^+$ **(4)**$^+$. This provides an easy way to synthesize stable unsubstituted pyridine-2-diazotate (**1'**), an otherwise unstable organic template. Theoretical scrutiny has been performed at (U)B3LYP/6–31G(d,p)/LANL2DZ level to explore the origin of redox and optical properties in radical complexes. Magnetic study of **[2]**$^+$ reveals that a weak antiferromagnetic (AF) spin-communication ($J = -4.39\ cm^{-1}$) exists between two radicals, leading to an open-shell singlet ground state. Broken symmetry density functional theory (BS-DFT) calculations were carried out to probe the nature of antiferromagnetic exchange interaction between the two radical centers in species **[2]**$^+$. This method has been employed with different basis functionals (BP86, BLYP, OLYP, TPSS0, TPSSh, ωb97D and B3LYP) to comprehend the nature of the exchange in **[2]**$^+$. The best result is obtained for pure functional OLYP with a *J* value $-8.4\ cm^{-1}$.

Introduction

Open-shell transition metal complexes featuring spin density localized on the ligand backbone are relatively less common compared to conventional metal-centered paramagnetism. Nevertheless, they have attracted significant attention in recent years due to their distinctive features and potential applications.[1] Certain organic scaffolds, by virtue of the presence of electron-poor or electron-excess domains, can exist in multiple oxidation states upon coordination with transition metals. The occurrence of such ligand-based variable valence in complexes is manifested from their well-defined electrochemical responses at the mild-to-moderate potential in solution.[2] However, it is not straightforward to isolate the *in-situ* generated corresponding radical anion [M(L$^{\bullet-}$)] or radical cation [M(L$^{\bullet+}$)] species starting from the corresponding neutral form *viz.* [M(L)] by chemical/electrochemical means since they typically exhibit limited stability. The sustainability of ligand-centered odd-electron species in both solid and solution can be augmented by suitable tuning of the energy of FMOs *vis-à-vis* redox potential values in the desired direction since the stability of π-radical complexes have been precisely related to the value of respective redox couples ($E_{L/L\bullet-}$ or $E_{L\bullet+/L}$). Indeed, remarkably stable radical anion (or radical cation) complexes can be accomplished by modifying the redox potential anodically (or cathodically).

It is worth mentioning that much thrust has been given to organic diradicals and diradicaloids recently due to their unique open-shell structure and physical properties with potential promising materials for bioelectronics, catalysis, and spintronics.[3] The development of a convenient synthetic procedure to isolate radical complexes in the crystalline state, more specifically, the ambient-stable open-shell system with multiple spin centers, is a challenge to a synthetic chemist. Since the discovery of intramolecular spin coupling by Guha, and Bleaney and Bowers in the early fifties for a two-spin system [(M•)(μ-L)(M•)],[4] immense impetuous has been given towards the design of new molecules with the desired value of coupling constant, *J*.[5] Exploration of an equivalent but alternative arrangement, *i.e.*, coordination of two radical ligands intervened by a closed-shell metal atom, [(L•)M(L•)], with magnetic state are sparse and has been started only recently.[6]

[a] S. Roy,[+] T. Ghorui,[+] D. Jana, S. Chandra Patra, S. Pramanik, K. Pramanik
Department of Chemistry, Inorganic Chemistry Section, Jadavpur University, Kolkata 700032, India
Tel: +91 89109 35661
E-mail: kpramanik@hotmail.com

[b] S. Moorthy, S. Kumar Singh
Department of Chemistry, Indian Institute of Technology, Hyderabad, Kandi, Telangana 502285, India

[c] S. Mehta, A. Mondal
Solid State and Structural Chemistry Unit, Indian Institute of Science, Sir C. V. Raman Road, 560012 Bangalore, India

[+] These authors contributed equally to this work

Supporting information for this article is available on the WWW under https://doi.org/10.1002/chem.202404027